91-02488/

Ontario
Ministry of
Northern Development
and Mines

Geoscience Research Grant Program
Summary of Research 1989–1990

Ontario Geological Survey
Miscellaneous Paper 150

edited by
V.G. Milne

1990

© Queens' Printer for Ontario, 1990
Printed in Ontario, Canada

ISSN 0704-2752 (Series)
ISSN 0225-5316 (Sub-series)

Publications of the Ontario Geological Survey and the Ministry of Northern Development and Mines are available from the following sources. Orders for publications should be accompanied by cheque or money order payable to the *Treasurer of Ontario.*

Reports, maps and price lists (personal shopping or mail order):

Public Information Centre, Ministry of Natural Resources
Room 1640, Whitney Block, Queen's Park
Toronto, Ontario, M7A 1W3

Reports and accompanying maps only (personal shopping):

Publications Ontario
Main Floor, 880 Bay Street
Toronto, Ontario M7A 1N8

Reports and accompanying maps (mail order or telephone orders):

Publications, Ontario, Ministry of Government Services
5th Floor, 880 Bay Street
Toronto, Ontario M7A 1N8
Telephone (local calls), 965-5300
Toll-free long distance, 1-800-668-9938

Every possible effort is made to ensure the accuracy of the information contained in this report, but the Ministry of Northern Development and Mines does not assume any liability for errors that may occur. Source references are included in the report, and users may wish to verify critical information.

If you wish to reproduce any of the text, tables or illustrations in this report, please write for permission to the Director, Ontario Geological Survey, Ministry of Northern Development and Mines, 11th Floor, 77 Grenville Street, Toronto, Ontario M7A 1W4.

Parts of this publication may be quoted if credit is given. It is recommended that reference be made in the following form:

Smith, L. and Charbonneau, S.L. 1990. Karst episodes and permeability development, Silurian reef reservoirs, Ontario; *in* Geoscience Research Grant Program, Summary of Research 1989–1990, Ontario Geological Survey, Miscellaneous Paper 150, p.4-12.

Scientific Editing: Nighthawk Editing/NTTPSproductions

Deyell-1000-90

Contents

Introductory Remarks, *V.G. Milne* 2

Grant 295 Karst Episodes and Permeability Development, Silurian Reef Reservoirs, Ontario, *Leigh Smith and Steven L. Charbonneau* 4

Grant 305 Geochemistry, Metamorphism, Skarn Development and Gold Mineralization of the White River Gold Prospect, Hemlo Area, *Y. Pan and M.E. Fleet* 13

Grant 319 Gypsum Deposits of Southern Ontario, *S.J. Haynes and J. Hughes-Pearl* 27

Grant 326 PGEs at Sudbury: their Concentration by Sulphide-liquid Fractionation, *C. Li and A. J. Naldrett* 37

Grant 328 Cyanobacterial Model System for the Biological Origin of Gypsum and Carbonate Minerals, *J.B. Thompson, S. Schultze, T.J. Beveridge and W.S. Fyfe* 47

Grant 329 Tectono-metamorphic Character of the Matachewan Area, Northeast Ontario, *W.G. Powell, C.J. Hodgson and D.M. Carmichael* 56

Grant 332 High-resolution Magnetic-susceptibility Probe for Mineral-exploration Boreholes: Design and Laboratory Prototype, *Alfred V. Dyck, Peter V. Auchincloss, Jane Rea and David L. Atherton* 66

Grant 340 Stratigraphy of the Middle Devonian Dundee Formation, Southwestern Ontario, *M.C. Birchard and M.J. Risk* 71

Grant 341 PGE Study: the MacRae and Marathon Copper-Precious Metal Deposits, Coldwell Complex, *D.J. Good and J.H. Crocket* 87

Grant 342 Paleomagnetic Analysis of Regional and Contact Strains, *C.J. Hale and P. Lloyd* 97

Grant 343 Structural Evolution of the Michipicoten (Wawa) Greenstone Belt, Superior Province: Evidence for an Archean Fold and Thrust Belt, *Z.G. Arias and H. Helmstaedt* 107

Grant 353 Diagenetic History of Dolomitized Ordovician and Devonian Oil and Gas Reservoirs in Southwestern Ontario. Part A: Styles of Reservoir Development in the Middle Devonian of Southwestern Ontario, *G.D. Hamilton and M. Coniglio* 115

Grant 353 Diagenetic History of Dolomitized Ordovician and Devonian Oil and Gas Reservoirs in Southwestern Ontario. Part B: Fracture-related Diagenesis of Middle Ordovician Carbonate Reservoirs, Southwestern Ontario, *K. Middleton, M. Coniglio and S.K. Frape* 131

Grant 357 Diagenetic Evolution of Cambro-Ordovician Clastic Sedimentary Rocks, Southwestern Ontario, *F.J. Longstaffe, M.A. Wadleigh, S.K. Frape and R.H. McNutt* 143

Grant 359 Structural Geology of the Midlothian Lake–Peterlong Lake Area, Abitibi Greenstone Belt, Superior Province, *R.B. Hrabi and H. Helmstaedt* 153

Grant 363 A Seismotectonic Study of the Western Lake Ontario Region. Phase 1: A Background-noise Survey and Further Testing of Two Microearthquake Recording Sites, *A.A. Mohajer and H.C. Halls* 164

Grant 364 The Kerr Addison–Chesterville Archean Gold-Quartz Vein System, Virginiatown: Time Sequence and Associated Mafic "Albitite" Dike Swarm, *J.P. Smith, E.T.C. Spooner, D.W. Broughton and F.R. Ploeger* 175

Grant 370 Tectonic Relations among Parry Sound Domain and Seguin and Rosseau Subdomains, *R.I. Macfie and J.M. Dixon* 200

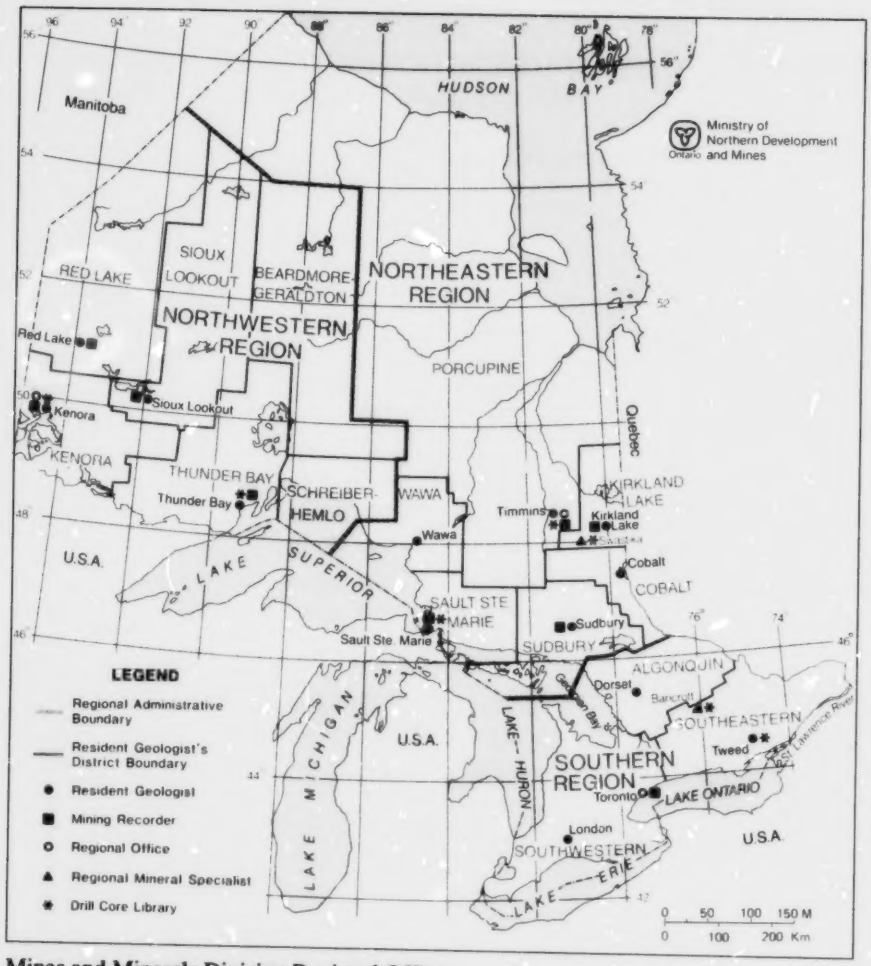

Mines and Minerals Division Regional Offices

CITY	OFFICE(S)	ADDRESS	TELEPHONE	FAX
Kenora	○	Box 5050, 12 Main St. S. P9N 3X9	(807) 468-3135	(807) 468-6298
	●	Box 5200, 808 Robertson St. P9N 3X9	(807) 468-3658	(807) 468-9451
	■	Box 5200, 808 Robertson St. P9N 3X9	(807) 468-8492	(807) 468-9451
	✱	860 Fourth Ave. S. P9N 2A1	(807) 468-3658	--
Red Lake	●	Box 324, Ont. Govt. Bldg. P0V 2M0	(807) 727-3272	(807) 727-3553
	■	Box 324, Ont. Govt. Bldg. P0V 2M0	(807) 727-3284	(870) 727-3553
Sioux Lookout	●	Box 3000, OPP Bldg. P0V 2T0	(807) 737-2039	(807) 737-1727
	■	Box 3000, OPP Bldg. P0V 2T0	(807) 737-2034	(807) 737-1727
Thunder Bay	● (3)	435 James St. S. P7E 6E3	(807) 475-1331	(807) 475-5312
	■	435 James St. S. P7E 6E3	(807) 475-1311	(807) 475-5312
	✱	335 Euclid Ave. P7E 6G6	(807) 475-1331	--
Wawa	●	Box 530, Mine Rd. P0S 1K0	(705) 856-4883	(705) 856-4282
Sault Ste. Marie	● ■	875 Queen St. E. P6A 2B3	(705) 949-1231	(705) 949-0014
	✱	64 Church St. P6A 5L5	(705) 949-1231	--
Timmins	○ ● ■	60 Wilson Ave. P4N 2S7	(705) 267-1401	(705) 264-8723
	✱	896 Riverside Dr. P4N 3W2	(705) 267-1401	--
Kirkland Lake	●	4 Government Rd. E. P2N 1A2	(705) 567-5242	(705) 567-5621
	■	4 Government Rd. E. P2N 1A2	(705) 567-9242	(705) 567-5621
Swastika	▲ ✱	Box 129 P0K 1T0	(705) 642-3222	(705) 642-3323
Cobalt	●	Box 230, Presley St. P0J 1C0	(705) 679-8558	(705) 679-5584
Sudbury	●	2nd floor, 159 Cedar St. P3E 6A5	(705) 670-7325	(705) 670-7223
	■	2nd floor, 159 Cedar St. P3E 6A5	(705) 670-7321	(705) 670-7223
Dorset	●	Box 190 P0A 1E0	(705) 766-2494	(705) 766-9976
Tweed	● ✱	B.S. 43, Old Troy Rd. K0K 3J0	(613) 478-2330	(613) 478-6247
Bancroft	▲ ✱	Box 3000, Highway 28 K0L 1C0	(613) 332-4875	(613) 332-1800
Toronto	■	1st floor, 10 Wellesley St. E. M4Y 1G2	(416) 965-1322	(416) 963-0257
	○	1st floor, 10 Wellesley St. E. M4Y 1G2	(416) 965-3611	(416) 963-0257
London	●	Box 5463, 659 Exeter Rd. N6A 4L6	(519) 661-2773	(519) 661-2819

CONVERSION FACTORS FOR MEASUREMENTS IN ONTARIO GEOLOGICAL SURVEY PUBLICATIONS

Conversion from SI to Imperial			Conversion from Imperial to SI		
SI unit	*Multiplied by*	*Gives*	*Imperial unit*	*Multiplied by*	*Gives*
			LENGTH		
1 mm	0.039 37	inches	1 inch	**25.4**	mm
1 cm	0.393 70	inches	1 inch	**2.54**	cm
1 m	3.280 84	feet	1 foot	**0.304 8**	m
1 m	0.049 709 7	chains	1 chain	20.116 8	m
1 km	0.621 371	miles (statute)	1 mile (statute)	**1.609 344**	km
			AREA		
1 cm^2	0.155 0	square inches	1 square inch	**6.451 6**	cm^2
1 m^2	10.763 9	square feet	1 square foot	**0.092 903 04**	m^2
1 km^2	0.386 10	square miles	1 square mile	2.589 988	km^2
1 ha	2.471 054	acres	1 acre	0.404 685 6	ha
			VOLUME		
1 cm^3	0.061 02	cubic inches	1 cubic inch	**16.387 064**	cm^3
1 m^3	35.314 7	cubic feet	1 cubic foot	0.028 316 85	m^3
1 m^3	1.308 0	cubic yards	1 cubic yard	0.764 555	m^3
			CAPACITY		
1 L	1.759 755	pints	1 pint	0.568 261	L
1 L	0.879 877	quarts	1 quart	1.136 522	L
1 L	0.219 969	gallons	1 gallon	**4.546 090**	L
			MASS		
1 g	0.035 273 96	ounces (avdp)	1 ounce (avdp)	28.349 523	g
1 g	0.032 150 75	ounces (troy)	1 ounce (troy)	**31.103 476 8**	g
1 kg	2.204 62	pounds (avdp)	1 pound (avdp)	**0.453 592 37**	kg
1 kg	0.001 102 3	tons (short)	1 ton (short)	**907.184 74**	kg
1 t	1.102 311	tons (short)	1 ton (short)	**0.907 184 74**	t
1 kg	0.000 984 21	tons (long)	1 ton (long)	**1 016.046 908 8**	kg
1 t	0.984 206 5	tons (long)	1 ton (long)	**1.016 046 908 8**	t
			CONCENTRATION		
1 g/t	0.029 166 6	ounce (troy)/ ton (short)	1 ounce (troy)/ ton (short)	34.285 714 2	g/t
1 g/t	0.583 333 33	pennyweights/ ton (short)	1 pennyweight/ ton (short)	1.714 285 7	g/t

OTHER USEFUL CONVERSION FACTORS

1 ounce (troy per ton) (short)	20.0	pennyweights per ton (short)
1 pennyweight per ton (short)	0.05	ounces (troy) per ton (short)

Note: Conversion factors that are in bold type are exact. The conversion factors have been taken from or have been derived from factors given in the Metric Practice Guide for the Canadian Mining and Metallurgical Industries, published by the Mining Association of Canada in cooperation with the Coal Association of Canada.

Geoscience Research Grant Program
Summary of Research 1989–1990

---

edited by V.G. Milne
Director, Ontario Geological Survey

Introductory Remarks

The Ontario Geoscience Research Grants Program was initiated in 1978 to support geoscience research at Ontario universities. By encouraging mission-oriented research, the program complements the work of the Ontario Geological Survey in carrying out its mandate:

> to build and maintain a comprehensive, up-to-date, publicly accessible geoscience information resource for Ontario as a stimulus to mineral exploration and development and as a basis for environmentally and economically sound planning and development of the land and groundwater resources of the Province

The program supports applied studies of up to 3 years duration towards the following: mineral deposit characterization studies of specific occurrences or groups of occurrences; petrology, rock geochemistry, structural geology, stratigraphy and geochronology studies; field and laboratory studies leading to the development of new geophysical and geochemical concepts and techniques; engineering and environmental geology studies; and methods for improving automated or manual processing to facilitate the interpretation of geoscience data.

To be eligible to receive funding, researchers must forward applications to the Ontario Geological Survey by November 15. Project proposals are subject to review by a committee reporting to the Director of the Ontario Geological Survey. This committee advises the Minister of Mines concerning geoscience research priorities at Ontario universities and of the scientific merit and relevance of the proposals submitted. The committee consists of 3 representatives from the minerals industry, 3 representatives from the university community, 4 representatives from the Ontario Geological Survey and a chairperson from either industry or a university. Members of the 1989–1990 committee are:

Dr. D.J. Misener, Chairperson; Paterson, Grant and Watson Limited

Dr. I.G.L. Sinclair; Minscan Consulting Ltd.

Dr. R. Lett; Barringer Magenta Ltd.

Dr. J.M. Morganti; Placer Dome Inc.

Dr. J. Legault; University of Waterloo

Dr. R. James; Laurentian University

Dr. H. Helmstaedt; Queen's University

Mr. C.L. Baker; Ontario Geological Survey

Mr. R.B. Barlow; Ontario Geological Survey

Dr. R.H. Sutcliffe; Ontario Geological Survey

Dr. J.A. Fyon; Ontario Geological Survey

Successful grant recipients are required to submit progress reports for publication in the annual Summary of Research and to participate in the Ontario Mines and Minerals Symposium held each December.

Publication in other scientific journals is encouraged, and a final report summarizing the research results will be released as an Ontario Geological Survey Open File Report. These reports are published periodically and are available at the Mines Library, 77 Grenville Street, Toronto, or at Ministry of Northern Development and Mines regional offices.

During 1989–1990, 20 projects were funded under this program; of these, 14 were renewal projects.

University	Value of grants	No. of grants
Carleton	$38 330.00	1
Guelph	$28 900.00	1
McMaster	$41 625.00	3
Queen's	$143 360.00	6
Toronto	$146 993.00	5
Waterloo	$18 970.00	1
Western	$55 375.00	2
Windsor	$26 552.00	1
Total	$500 105.00	20

I would like to thank Dr. D.J. Misener, Committee Chairperson, and the review committee members, all of whom gave freely of their time. The efforts of the researchers are of course fundamental and are acknowledged. The following are also acknowledged for their participation in producing this volume: P. Hinz, Grants Administrator and Secretary to the Committee; staff geologists who reviewed the papers; Sharon Stewart, who edited the volume; and Bojan Sifrer, who coordinated the production of this publication.

V.G. Milne

Director
Ontario Geological Survey

Grant 295 Karst Episodes and Permeability Development, Silurian Reef Reservoirs, Ontario

Leigh Smith[1] and Steven L. Charbonneau[2]

[1] Department of Geological Sciences, Queen's University, Kingston
[2] Shell Canada Ltd., 400-4th Ave. S.W., Calgary

ABSTRACT

The Rosedale, Warwick and Terminus pinnacle-reef bioherms and the Fletcher platform or bank bioherm, located in the southwestern Ontario subsurface, are part of the Guelph Formation of Middle Silurian age. Development of these subsurface hydrocarbon reservoirs was governed by cyclic sea-level fluctuations. Each rising sea level produced an episode of reef growth; each falling sea level caused an episode of exposure, with development of paleokarst features on and within the bioherms.

The bioherms consist of a succession of depositional facies that vary upward from regional platform, to local wackestone mound, to reef-core and reef-flank complex, to restricted algal cap, to algal mudstone and boundstone units.

There were 8 major episodes of subaerial exposure: thus, each pinnacle-reef bioherm is a vertical succession of up to 7 different biohermal units separated by erosional discontinuities. Notable exposure episodes produced karst breccia and severe leaching of the underlying units.

Such strong erosional episodes were followed by major changes in the bioherms' depositional facies; other such changes were caused by regional variations in salinity. Thus, major change in the reefs' organic communities was due to extrinsic factors.

Each episode of exposure created laterally extensive leached zones of enhanced permeability and increased porosity in the then upper portion of each bioherm. Paleosols and crusts were formed, which created vertical seals. This type of seal was enhanced by the formation of overlying impermeable limestones during the next sea-level rise.

There is abundant evidence of diagenesis—in early marine, meteoric vadose and phreatic, postkarstic marine and burial environments—resulting in different types and generations of pore-occluding calcite cements, especially in the lower portion of each bioherm.

Only major karstic episodes could have created the zones of laterally extensive permeability that constitute the hydrocarbon reservoirs in the middle and upper portions of each bioherm.

INTRODUCTION

Middle Silurian carbonate bioherms are present in the subsurface rocks of southwestern Ontario, within a broad area along the southeastern margin of the Michigan Basin. Over 70% of those that have been located contained hydrocarbon reserves. Some are now used for critical seasonal storage of natural gas. This project was a study of 7 of these bioherms.

Figure 295.1 shows the location of the Rosedale, Warwick and Terminus fields in Lambton County and the Fletcher field in Kent County. The first 3 reservoirs are contained within laterally extensive, permeable zones in limestone pinnacle-reef bioherms, and the Fletcher reservoir is within a dolomitized platform- or bank-reef complex. These reefs were chosen as examples of the 2 principal types of bioherm. All have continuous drill-core records. The stratigraphic sections of the Rosedale and the Fletcher bioherms were reported in Smith et al. (1988) and Grimes (1987), respectively. The Payne, Wilkesport and Bayfield pinnacle-reef reservoirs were studied in the last phase of the project, to further correlation of distinct lithic units and of permeable karstic zones between different pinnacle-reef bioherms. Their stratigraphic sections are reported in Charbonneau (1990).

These bioherms are in the Guelph Formation (Table 295.1). They rest on the regional carbonate platform of the Lockport Formation, which in turn unconformably overlies the regionally extensive Rochester Formation. These reefal bioherms are sealed, overlain and laterally surrounded by impermeable carbonate and evaporite units of the lower part of the Salina Formation. Most of the 13 drill cores studied are continuous from the upper portions of the Rochester Formation to the lower units of the overlying Salina Formation, and all penetrate the key reservoirs in the middle and upper portions of each bioherm.

Tectonic and Environmental Controls

Southwestern Ontario in the mid–Silurian was within the North American Bank—a large region with decreasing tectonic activity. Within this region was an oval area of very slightly differential downsinking, the incipient Michigan Basin. This basinal differential produced only very slight differences in seawater depth, but these were enough to have profound effects on reef location and development.

At the end of a long episode of subaerial exposure, community-reef growth was made possible by overall sea-level rise and the end of the westward dispersal of the substantial amounts of fine, terrigenous sediment that had formed the Rochester Formation.

However, as with the type Wenlockian (Middle Silurian) of Shropshire, being in the midst of a huge regional bank was not ecologically optimal. The very slightly

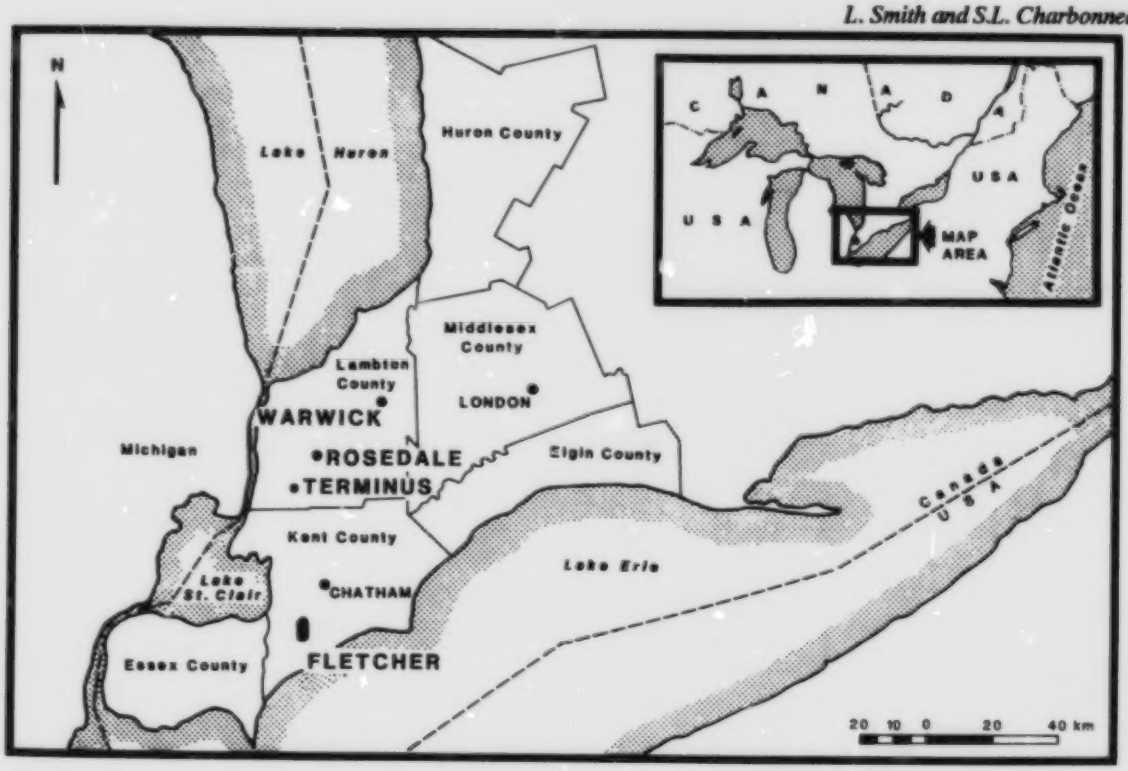

Figure 295.1. Location of reef bioherm reservoirs in southwestern Ontario.

Table 295.1. Lithic units in cores from pinnacle-reef bioherms.

Stratigraphic unit	Facies unit: Terminus (m)	Rosedale (m)	Warwick (m)
Salina Formation			
Regional carbonates and evaporites			
Shallow-marine and leached	21	22	22
Guelph Formation			
Karst breccia	4	5-6	6
Restricted cap	1	4	5
Reef mass*	59	77	103
Silt mound	5	21	29
Lockport Formation			
Regional platform dolostone	15+	28	13
Rochester Formation			
Regional dolomitic shale			

**Reef-core and reef-flank complex.*

elevated salinities caused the production of the smaller brachiopods and crinoids dominant in the sediment of the Lockport Formation. In contrast, in the Gotland region of the Baltic, reef bioherms developed at once after a marine transgression and produced large skeletal sizes, evidence of an optimal environment for reef growth (Smith 1990).

Deposition of the regionally extensive Lockport carbonate platform provided a base for later reef development. Slight freshening of seawater was signalled by an end to dolomitization and by initiation of biohermal reef growth. Broad areas of bank-reef platforms developed over most of North America.

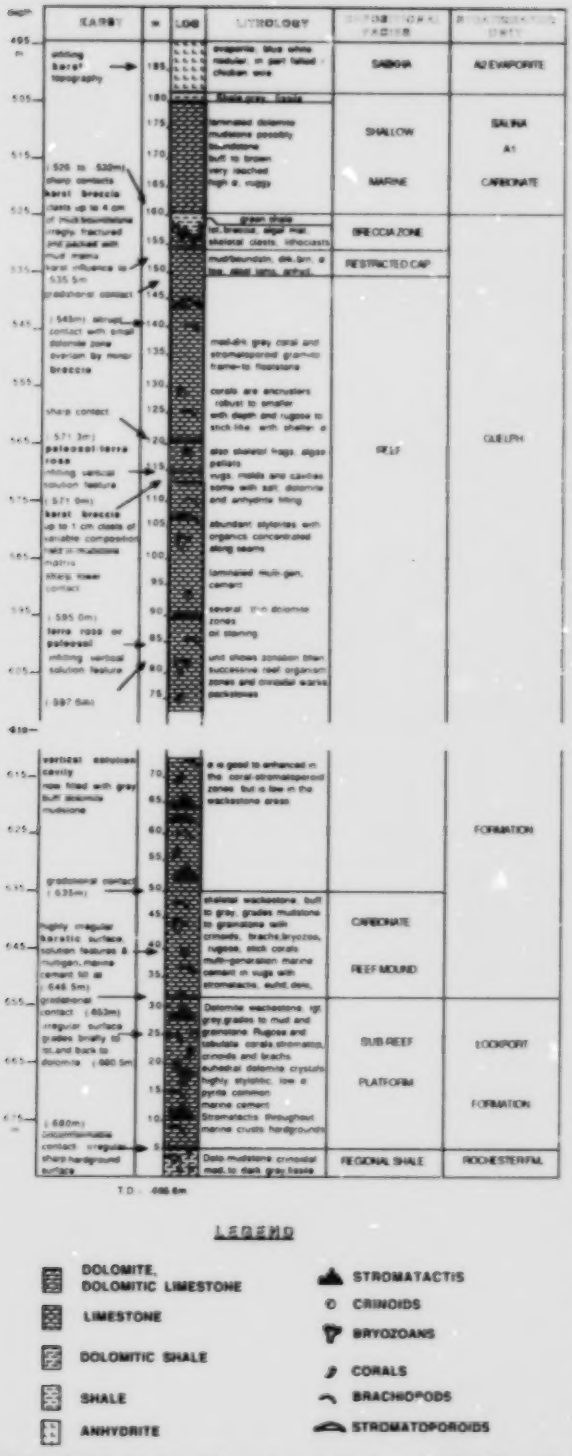

Figure 295.2. Stratigraphic section of the Imperial 399, Warwick 4-12-IIISER core showing depositional, organic and karstic features (Charbonneau).

Slightly more rapid downwarping caused deposition of a thin section of the Lockport Formation in the incipient Michigan Basin, and the resulting very gentle slope around its margin allowed only patch-reef development on top of slight and very local crinoidal sand mounds, initiating pinnacle bioherm growth (Trevail and Smith 1987).

The combined effect of this slightly differential tectonism and the differential bioherm growth that resulted caused the regional thickness variations in the Lockport and Guelph formations shown by Bailey (1986) and, in great detail, by Bailey Geological Services Ltd. and Cochrane (1990). Sanford et al. (1985) suggested that rejuvenation of basement fault blocks controlled both the origin and the development of these reservoir units, and this seems to be responsible for some of the platform- and bank-reef geometries. Prouty (1983) interpreted a fault-block influence throughout southern Michigan. Effects on the pinnacle reefs are analyzed and discussed in Charbonneau (1990).

Objectives

The major objective of this study was to delineate the internal nature and three-dimensional geometry of the permeable zones in the Silurian pinnacle-, platform- and bank-reef reservoirs of southwestern Ontario. This study also tested our concept that there were several subaerial, karstic episodes during the development of these bioherms and that each episode formed a zone of increased permeability and enhanced porosity in the then upper portion of each bioherm. Detailed knowledge of these zones and of the extent to which they are sealed by karstic crusts and fills, by evaporite plugging or by overlying impermeable marine limestones will greatly aid enhanced hydrocarbon recovery and their proper use as gas storage reservoirs or waste-fluid disposal reservoirs.

Methods

Detailed sedimentologic description of slabs from the Rosedale, Warwick, Terminus, Wilkesport, Payne, Bayfield and Fletcher drill cores identified the original organic components and depositional features in the bioherms. The erosional (karstic) aspects were separately identified. Thin section, scanning electron microscope and cathodoluminescence techniques were used to identify the growth patterns and zoning of pore-occluding cements. Thin section study and cathodoluminescence revealed patterns of rock, grain and cement truncation along pore walls and showed the complex succession of erosional and precipitational events that altered rock porosity. Thin section staining and minor use of X-ray diffraction analysis identified carbonate mineral species and variations in iron content. Variations in $\delta^{13}C$ and $\delta^{18}O$ isotope signatures in calcite pore cements allowed the identification of freshwater and mixed-water signatures in crusts, soils and phreatic and marine cements. They also showed the effect on the ^{13}C isotope of the presence of hydrocarbons.

Correlations using well logs have helped to identify the major porous zones, in contrast to those that are substantial in a particular core but may have little lateral extent. Data reports and production information from the files of the Petroleum Resources Section, Ministry of Natural Resources, were used to delineate permeable zones.

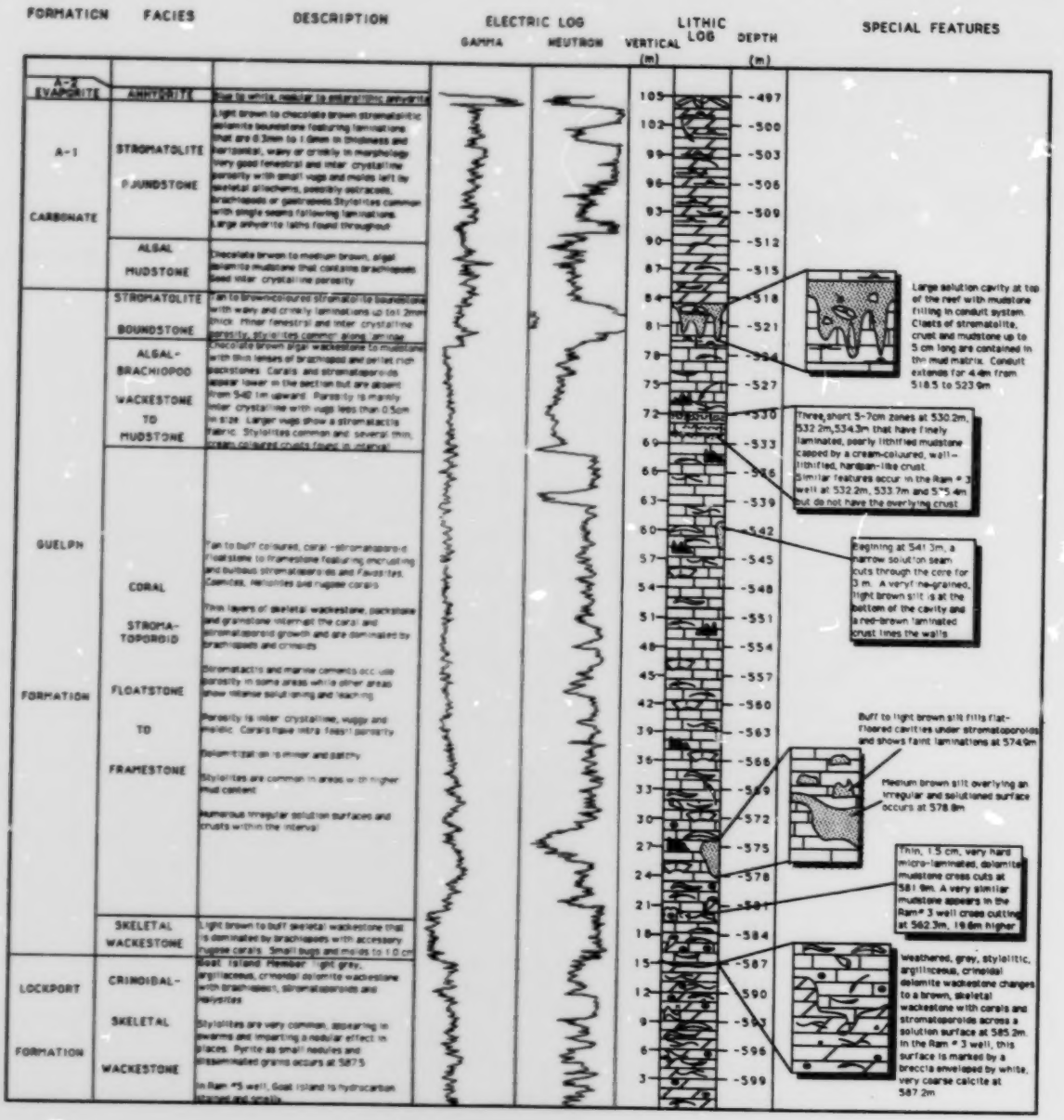
FORMATION
FACIES
DESCRIPTION
ELECTRIC LOG
GAMMA
NEUTRON
LITHIC LOG
VERTICAL (m)
DEPTH (m)
SPECIAL FEATURES
A-2 EVAPORITE
ANHYDRITE
A-1 CARBONATE
STROMATOLITE BOUNDSTONE
ALGAL MUDSTONE
GUELPH FORMATION
STROMATOLITE BOUNDSTONE
ALGAL-BRACHIOPOD WACKESTONE TO MUDSTONE
CORAL
STROMATOPOROID FLOATSTONE TO FRAMESTONE
SKELETAL WACKESTONE
LOCKPORT FORMATION
CRINOIDAL-SKELETAL WACKESTONE
Large solution cavity at top of the reef with mudstone filling in conduit system. Clasts of stromatolite, crust and mudstone up to 5 cm long are contained in the mud matrix. Conduit extends for 4.4m from 518.5 to 523.9m
Three short 5-7cm zones at 530.2m, 532.2m,534.3m that have finely laminated, poorly lithified mudstone capped by a cream-coloured, well-lithified, hardpan-like crust. Similar features occur in the Ram # 3 well at 532.2m, 533.7m and 5**5.4m but do not have the overlying crust
Beginning at 541.3m, a narrow solution seam cuts through the core for 3 m. A very fine-grained, light brown silt is at the bottom of the cavity and a red-brown laminated crust lines the walls
Buff to light brown silt fills flat-floored cavities under stromatoporoids and shows faint laminations at 574.9m
Medium brown silt overlying an irregular and solutioned surface occurs at 578.8m
Thin, 1.5 cm, very hard micro-laminated, dolomite mudstone cross cuts at 581.9m. A very similar mudstone appears in the Ram# 3 well cross cutting at 582.3m, 19.6m higher
Weathered, grey, stylolitic, argillaceous, crinoidal dolomite wackestone changes to a brown, skeletal wackestone with corals and stromatoporoids across a solution surface at 585.2m. In the Ram # 3 well, this surface is marked by a breccia enveloped by white, very coarse calcite at 587.2m

Figure 295.3. Stratigraphic section of the Ram 5, Sombra 2-24-IX (Terminus) core showing depositional, organic and karstic features (*from* Charbonneau 1990). Lower 7 m and some karstic features are from the Ram 3, Sombra 4-23-IX core.

DEPOSITIONAL HISTORY

Once begun, the development of these bioherms was governed by cyclical sea-level fluctuations. Rising sea level allowed organic growth on the bioherms and deposition off reef of fine carbonate interbedded with storm layers of reef skeletal debris (Smith 1989).

Pinnacle-reef Facies

The first detailed description of the Rosedale bioherm was made by Bainbridge (1973). The fauna of the Warwick reef was studied by Pearson (1980). Our study used an analysis of specific and inclusive descriptions of cores from these and other Guelph bioherms. On this basis, we divided the

bioherms into the 5 discrete depositional facies and the 2 most distinct karstic facies that overlie the regional Lockport platform (Table 295.1). The Warwick core section is described in Figure 295.2; the Terminus core section, in Figure 295.3. The Rosedale bioherm core section was detailed in Smith et al. (1988).

The Lockport Formation platform facies consists of coalesced mounds and sand waves of abundant crinoid and brachiopod remains. This wackestone unit was regionally dolomitized.

In most instances, the Guelph Formation pinnacle bioherms initially developed on this platform as the carbonate-silt wackestones and packstones of the crinoid-bryozoan mound facies. The overlying reef mass proper is composed of a complex of core-facies wackestones, packstones and floatstones, with corals, bryozoans, algae and stromatoporoids, intermingled with flank-facies bedded, bioclastic floatstones. This reef-mass complex is topped by an algae-brachiopod-dominated wackestone unit, followed by a thin unit of laminated mudstone and algal boundstone, the upper part of which was subaerially (karstically) altered and brecciated. Above this major erosional discontinuity is the uppermost biohermal unit, a restricted cap facies of layered algal mudstone and boundstone, followed by stromatolite boundstone. This unit was severely leached just after deposition. Although there are other intervals in these bioherms showing karstic alteration, these last 2 units are the most conspicuous examples.

Platform-reef Facies

The structure of the Fletcher bioherm was first described by Chalkley (1983). This study found that the platform reef was deposited as a series of adjacent and superimposed patch reefs. As a result, only 3 biohermal facies were recognized above the Lockport Formation platform: reef-core wackestone or floatstone with corals and stromatoporoids; reef-flank beds of bioclastic floatstone; and a thin algal unit overlying both. The silt-mound facies is absent (Grimes 1987).

SUBAERIAL EXPOSURE

Most early workers thought that the Lockport and Guelph carbonate units and the succeeding Salina evaporite units accumulated during one long, submarine episode. Mesolella et al. (1974) interpreted 2 episodes caused by sea-level fluctuations but thought a period of subaerial exposure was only "possible". Sarg (1982) thought that the development of all reef porosity was due to salinity variation, without exposure. Huh et al. (1977), Sears and Lucia (1979), Petta (1980) and Cercone and Lohmann (1986) identified one exposure episode, mainly because of the general duality of off-reef Salina units. Bay (1983) saw 2 subaerial exposure episodes. Kahle (1974) identified the many karstic features in a reef in northern Ohio. However, the idea that there was only one karstic episode at most and that it occurred after the growth of the entire bioherm has been a persistent misconception.

Karst Facies

This study found that during cyclic sea-level fluctuations, lowering sea level caused reef exposure, creating soils, crusts and laterally extensive zones of enhanced porosity; and off-reef exposure, with sabkha formation and deposition of evaporites and reef lithic debris. As a result, each growth phase of these Silurian bioherms was delineated by a period of major subaerial exposure (Smith 1984, 1990). There were 8 such episodes of subaerial exposure during the development of the Guelph Formation bioherms (Figures 295.2 and 295.3; *see also* Smith et al. 1988). Each episode created a new beginning for subsequent reef growth, so that each bioherm is a vertical succession of up to 7 individual and different reefal units, separated by erosional discontinuites.

During subaerial exposure, all of these units were internally altered in part or in whole by rainwater, creating very distinct karstic features. Besides forming the karst breccias, soils and crusts and causing the severe leaching of the underlying depositional facies, these waters enlarged any residual depositional porosity in the then upper portion of each bioherm and enlarged any joints or available conduits, producing small caves or grikes. Charbonneau (1990) places the top of the Lockport Formation at the erosional surface found in each bioherm a few metres above the dolomitized portion of the unit (Figures 295.2 and 295.3).

In this way, each karstic episode formed a zone of notably increased permeability and enhanced porosity that has extensive lateral interconnection but is vertically sealed by subaerial or later submarine cementation. Because of the original heterogeneity of the calcareous sediment and the different responses of the resulting limestones to the freshwater and mixed-water subaerial environment, each of these leached, once-vadose zones is complex in internal detail. They are separated vertically from one another by impermeable intervals of karstically unaltered (nonporous) carbonate, by karstic crusts and soils, by fills in karstic conduits and by intervals plugged with precipitated anhydrite or halite. They possess, therefore, the best reservoir characteristics in each bioherm. These zones of enhanced porosity and permeability in the Rosedale pinnacle bioherm have been delineated and described by Grimes (1987); those in the Warwick and Terminus bioherms, by Charbonneau (1990) (Figures 295.2 and 295.3). Equivalent porosity zones in the Wilkesport, Payne and Bayfield reefs are also delineated by Charbonneau.

These pinnacle bioherms are thus very similar to Holocene bioherms such as Enewetok Atoll, where Buddemeier and Oberdorfer (1986) found several "solution unconformities" in cores showing abundant karstic features.

FACIES CHANGES—CAUSES

The development of Middle Silurian bioherms is the result of a series of subaerial exposures, each followed by reef-growth episodes. Therefore, each bioherm is a vertical succession of at least 7 individual reefal units separated by erosional discontinuites. Within this framework is a pattern of changes in the bioherm's depositional facies; this pattern only coincides with the erosional pattern in some places.

Each karstic facies is directly related to the overlying erosional surface, as both are due to eustatic sea-level change. Some of the changes in depositional facies, however, appear to be due to interregional variation in salinity, apparently independent of sea-level change.

The change from platform to silt-mound deposition followed a slight salinity decrease; that from silt mound to reef-mass complex occurred after subaerial exposures. Deposition of the reef complex ended because of a distinct salinity increase, well before the prolonged subaerial exposure that produced the main karst breccia facies. This higher salinity remained afterward, to cause deposition of the algal shallow-marine facies.

Organic-reef biohermal development would have continued indefinitely if outside factors had not interfered. Thus, the apparent linear pattern of reef development was due to factors extrinsic to the reef's organic communities.

Overall, Middle Silurian bioherm growth was terminated by a general trend of lowering of sea level, causing more frequent and longer subaerial exposures. The reef communites were unable to re-establish themselves in the Late Silurian because of an interregional rise in salinities over the North American Bank caused by the development of barrier reefs.

DIAGENETIC HISTORY

The pinnacle-reef bioherms have undergone a complex and varied diagenesis. Considerable physical and chemical alteration of the original sediments was caused by submarine diagenesis and by changes during and just after subaerial exposure and the subsequent marine flooding. Petrographical and chemical studies show that there were stages in the development of these diagenetic changes that were caused by variations in the chemistry of the pore fluids. Data on carbon and oxygen stable isotopes are being used to evaluate conclusions derived from the petrographical and chemical data.

The results of each diagenetic stage are unevenly distributed throughout the bioherms. Some diagenetic effects were found to be spatially restricted and facies specific. This results from variations in the original carbonate sediment and its primary depositional porosity, from a resulting variability in karstic porosity enhancement and from the variable residence times of any particular fluid in the pores. Original shelter porosities have partially survived in some places within the lower and middle portions of the bioherms and are associated with bryozoa and stromatoporoids. Karstically enhanced, vuggy porosities are more important in the reef-complex portions, with fenestral porosities in the leached algal facies of the "A-1 Carbonate" unit.

Pinnacle Bioherms

The Rosedale, Warwick and Terminus reservoirs underwent early marine, meteoric vadose and phreatic, postkarstic marine and burial diagenetic stages. Early marine cement in the form of isopachous, pore-lining, fibrous calcite is mainly restricted to the silt-mound wackestone facies. It lines primary shelter porosity, initially associated with fenestrate bryozoan fragments but later enhanced, commonly, by vadose solution. Marine and/or later vadose silt deposition in each pore gave it the characteristic flat base below a very irregular top surface. Many karstically enhanced pores have an initial, nonluminescent vadose cement. In others, marine cements were formed first. A solution event interrupted the precipitation of these fibrous calcites, truncated the crystals, and left a pyrite concentration on the lower surface of the pore. Return of marine waters caused precipitation of a second fibrous calcite layer on the truncation surface. Many of these pores were not filled with isopachous calcite but were infilled later by iron-poor blocky calcite of probable meteoric phreatic origin. This produced one of the characteristic types of "stromatactis" and caused most of the porosity loss in the lower portion of the bioherm. In the upper portions, cementation was less efficient. Burial cements are not volumetrically significant. Euhedral white dolomite and euhedral calcite are found in a few vugs and fractures. Cercone and Lohmann (1986) found hydrocarbon inclusions in both the dolomite and the calcite in a northern Michigan bioherm, which emphasizes their burial environment genesis. Simo and Lehmann (1988), however, found that hydrocarbon migration postdated such cements in central Indiana.

Platform Bioherms

The Fletcher bioherm also contains much isopachous, pore-lining cement, but this cement has been thoroughly dolomitized along with the surrounding rocks. These cements are also present in karstically altered zones, partially or fully occluding the enhanced porosity. A burial phase of pore-lining, euhedral white dolomite postdates the pervasive dolomitization of the bioherm (Grimes and Smith 1987).

Dolomitization

The original tectonic background appears to have predetermined the lack of pervasive dolomitization in isolated pinnacle bioherms, whereas platform and bank bioherms were thoroughly dolomitized. The regionally extensive Lockport Formation platform was also well dolomitized. At those times when the region's marine waters were sufficiently enriched in magnesium to dolomitize the bioherms, the more widespread platform masses constricted seawater flow. This forced the magnesium-rich marine waters through the pores of the platforms and banks, especially if these had just been karstically enhanced. The less-constrained water currents in the basin-slope environment flowed around the relatively small pinnacles, leaving them undolomitized except around their margins.

Mixed-water dolomitization, if it occurred at all, did not produce this pervasive dolomitization. It may have operated locally during a few of the exposure episodes, at 2 levels in the Fletcher bioherm and at one level in the Warwick bioherm. The Rosedale bioherm was not affected at those times, even though it was also exposed.

Isotope Analysis

The results of analysis for the stable isotope ratios of $\delta^{18}O$ and $\delta^{13}C$ were given in Smith et al. (1988). The basic assumption behind this analysis is that the composition of the oxygen and carbon isotopes in the cements will reflect

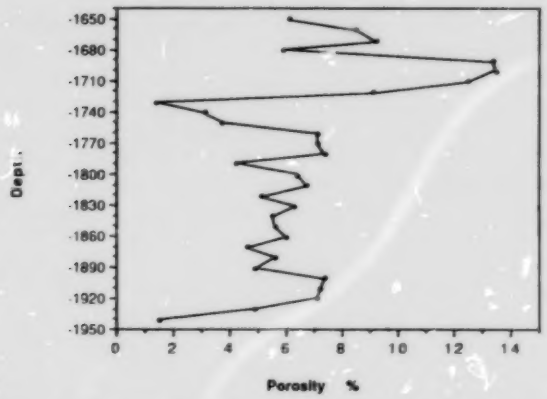

Figure 295.4. Higher porosity values in Union Enniskillen 8-9-IIA (Rosedale) core (depth in feet) indicate leached or vuggy karstic zones in gas-bearing portion of bioherm (Guelph Formation).

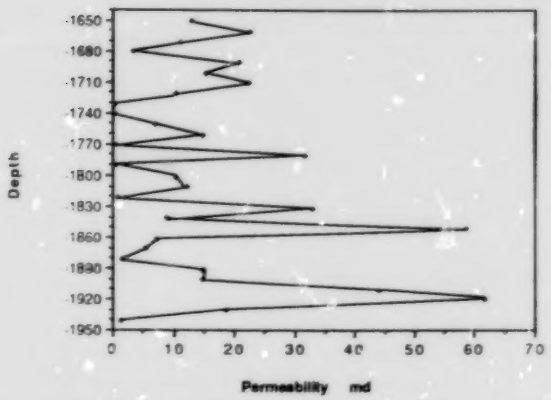

Figure 295.5. Higher permeability values (millidarcys) in Union Enniskillen 8-9-IIA (Rosedale) core (depth in feet) also indicate karstic zones.

the composition of the pore fluids from which they precipitated and/or with which they later reacted. However, oxygen isotopic composition varies with temperature, salinity and biological activity, whereas the carbon isotopic composition varies with organic matter content and any sediment or rock source of the bicarbonate ion. The isotope values indicated the different cement phases in the pores of the bioherms and delineated the sequence of events in their history (*see, for example,* Dickson and Coleman 1980).

It appears that some of the signatures obtained from fossil skeletal grains in the Rosedale bioherm give a close indication of normal seawater composition during Middle Silurian time. Comparison with the other signatures emphasizes how much the pore waters varied in other environments. The signature shift from the first-phase isopachous cement (slightly mixed water?), to the second phase (closer to normal seawater), to the blocky cement (meteoric phreatic water) shows that these cements were precipitated from different pore waters. This is significant, as the 3 cement types in each case were sampled from the same pore.

Very different signatures from calcites in laminated crusts and paleosols are important indicators of the more variable subaerial environments. The coarse, euhedral calcites clearly show a burial environment.

The effect of the natural gas in enriching the ^{13}C of cements in the upper portion of the Rosedale pinnacle is noticeable. This can also be seen in a reef on the northern margin of the Michigan Basin (Cercone and Lohmann 1986).

HYDROCARBON OR STORAGE RESERVOIRS

This research has shown the presence of 8 major subaerial, karstic episodes during development of the Rosedale, Warwick and Terminus bioherms. Each episode formed a laterally extensive zone of increased permeability and vuggy or leached porosity. This permeability is laterally connected but is vertically restricted beneath a zone of subaerial cementation or evaporite plugging and between sections of impermeable, marine-cemented rock not affected by karstic processes. Some early zones of enhanced permeability were formed in the silt-mound facies, lower in the bioherm. As these were later sealed by marine and phreatic cementation, their karstic affinity has not been recognized. The reservoir zones in the pinnacle bioherms are laterally extensive and vertically separate, occur in the middle and upper portions and are laterally enclosed by the impermeable carbonates and evaporites of the Salina Formation. Each zone can be expected to act as a separate reservoir.

Porosity and Permeability

Figures 295.4 and 295.5 show the variation in porosity and permeability, respectively, in the central reef-mass complex and upper restricted or leached facies units in the Rosedale bioherm (analyses by Maness Petroleum Laboratories 1971). Both figures show the pre-eminent role of karstic processes in creating the reservoir zones. Figure 295.4 shows karstic vuggy zones peaking at –1900, –1880, –1860 and –1830 feet. Figure 295.5 shows the associated permeability peaks at –1920, –1890, –1850 and –1830 feet. Leached porosity peaks occur in the upper portion of the reef mass at –1810 and –1780 feet; in the restricted cap, at –1760 feet. The equivalent permeabilities are at –1810, –1780 and –1760 feet. Peaks in the upper leached unit are, for porosity, at –1710 and –1670 feet and, for permeability, at –1710, –1690 and –1660 feet.

The seals to permeability that effectively separate the reservoir zones are well shown in Figure 295.5. Evaporites caused the plugging at –1880 feet; submarine cements, at –1940 and –1840 feet; karstic crusts and paleosols, at –1820, –1790, –1770 and –1730 to –1740 feet; a tight stromatolite unit, at –1680 feet; and nodular anhydrite, above –1650 feet.

Thus, the base of the reef-complex mass is the base of the effective porosity and permeability in the Rosedale bioherm and is the base of the original gas-bearing interval. The base of the overlying nodular anhydrite of the Salina Formation forms the top.

Figures 295.6 and 295.7 show the effect of fracturing on permeability in a shale that does not contain the mobile

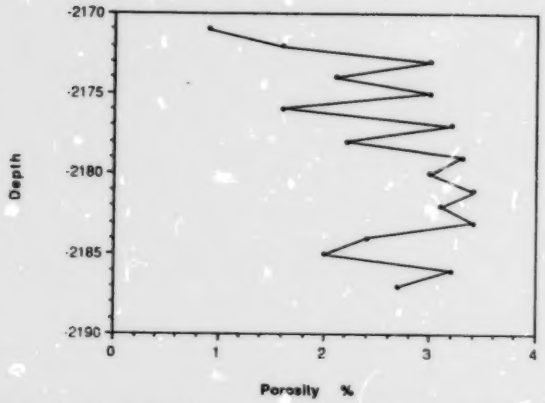

Figure 295.6. Typical low porosity values of dolomitic shale (depth in feet; Rochester Formation).

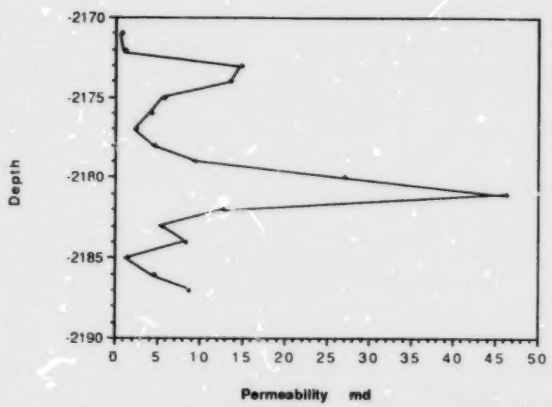

Figure 295.7. Typical low permeability (millidarcys) of dolomitic shale (depth in feet), except in upper karstic leached zone and across a fracture (Rochester Formation).

carbonate or evaporite minerals to seal the fracture. Figure 295.6 shows the low porosity of dolomitic shales typical of those in the upper part of the Rochester Formation. Figure 295.7 shows the sharp increase in permeability at a fracture. Both figures show a strong decrease into the paleosol at the top of the formation.

The persistent concept that there was only one karst episode at the end of bioherm construction has led to the assumption that the major permeability interconnections in the Guelph reefal bioherms are vertical. Instead, there are laterally extensive and separate zones of enhanced permeability within these bioherms. This has a major impact on exploration procedures, formation testing, well completions, recovery techniques, gas storage and retrieval methods, and techniques of subsurface waste disposal.

CONCLUSIONS

1. Development of the subsurface Silurian bioherm reservoirs in southwestern Ontario was governed by cyclic sea-level fluctuations.
2. The succession of growth stages and depositional facies was identified in the Rosedale, Warwick and Terminus pinnacle bioherms and in the Fletcher platform-bank bioherm.
3. There were 8 major episodes of subaerial exposure during development of the pinnacle bioherms.
4. Each bioherm is a vertical succession of up to 7 individual reefal units separated by erosional discontinuities.
5. The appearance of a linear pattern of reef development was not intrinsic to the reef communities but was caused by the external controls of sea-level change and salinity variation.
6. Each karst episode produced a zone of enhanced porosity and permeability; this zone is laterally extensive and is vertically restricted by karstic crusts, paleosols and evaporite pluggings.
7. Marine, meteoric vadose and phreatic, and burial environments created pore-occluding cements, especially in the lower portions of each bioherm.
8. Only major karstic episodes, probably followed by relatively rapid sea-level rise, seemed able to create lasting zones of enhanced permeability.

ACKNOWLEDGMENTS

The Rosedale cores were given by Union Gas Limited, with the assistance of Thomas Bainbridge. The Fletcher cores and cuttings from Lake Erie were given by Consumers' Gas Co. Limited. We thank Steven Colquhoun of Telesis Oil and Gas for initiating the Fletcher study. The cores were slabbed by the Petroleum Resources Section Laboratory of the Ministry of Natural Resources. Other cores have been made available for study at the Core Library Facility of the laboratory. We wish to thank P.A. Palonen and T. Carter of the Ministry and R.A. Trevail of Telesis Oil and Gas for their considerable assistance to the project. We also thank Canterra Energy Limited for supplying thin sections; and K.C. Lohmann and his laboratory for stable isotope analyses. Field study of quarries in Ohio, Indiana and Illinois was funded by the Advisory Research Committee of Queen's University. Sarmistha Dey assisted with petrographic analysis. Linda Anderson typed the manuscript.

REFERENCES

Bailey, S.M.B. 1986. A new look at the development, configuration and trapping mechanisms of the Silurian Guelph reefs of southwestern Ontario; Ontario Petroleum Institute, 25th Annual Conference, London, Ontario, October 19–21, Paper 14, 28p.

Bailey Geological Services Ltd. and Cochrane, R.O. 1990. Geology of selected oil and gas pools in the Silurian carbonates of southern Ontario; Ontario Geological Survey, Open File Report 5722, 50 p.

Bainbridge, T.W. 1973. The sedimentology of a Silurian pinnacle reef in the Michigan Basin; unpublished BSc thesis, Queen's University, Kingston, Ontario, 62p.

Bay, T.A. 1983. The Silurian of the northern Michigan Basin; *in* Carbonate buildups, edited by P.M. Harris, Society of Economic Paleontologists and Mineralogists, Core Workshop 4, Dallas, Texas, April 16–17, p.53-72.

Buddemeier, R.W. and Oberdorfer, J.A. 1986. Internal hydrology and geochemistry of coral reefs and atoll islands; key to diagenetic variations; p.94-111 *in* Reef diagenesis, edited by J.H. Schroeder and B.H. Purser, Springer-Verlag, Berlin, 455p.

Cercone, K.R. and Lohmann, K.C. 1986. Diagenetic history of the Union 8 pinnacle reef (middle Silurian), northern Michigan, U.S.A.; p.381-398 *in* Reef diagenesis, edited by J.H. Schroeder and B.H. Purser, Springer-Verlag, Berlin, 455p.

Chalkley, P. 1983. The sedimentologic correlation and history of the Fletcher Silurian pinnacle reef, eastern Michigan Basin; unpublished BSc thesis, Queen's University, Kingston, Ontario, 54p.

Charbonneau, S.L. 1990. Subaerial exposure and meteoric diagenesis in Guelph Formation (Niagaran) pinnacle reef bioherms of the Michigan Basin, southwestern Ontario; unpublished MSc thesis, Queen's University, Kingston, Ontario, 215p.

Dickson, J.A.D. and Coleman, M.L. 1980. Changes in carbon and oxygen isotope composition during limestone diagenesis; Sedimentology, v.27, p.107-118.

Grimes, D.J. 1987. Depositional models, subaerial facies, and diagenetic histories of the Rosedale and Fletcher reefs, southwestern Ontario; unpublished MSc thesis, Queen's University, Kingston, Ontario, 120p.

Grimes, D.J. and Smith, L. 1987. Depositional and diagenetic history of the Fletcher reservoir, a platform reef in southwestern Ontario; *in* Abstracts volume, Canadian Society of Petroleum Geologists, Reef Research Symposium, Banff, Alberta, January 27–30. p.86.

Huh, J.M., Briggs, L.I. and Gill, D. 1977. Depositional environments of pinnacle reefs, Niagara and Salina groups, northern shelf, Michigan Basin; *in* Reefs and evaporites, edited by J.H. Fisher, American Association of Petroleum Geologists, Studies in Geology 5, p. 1-21.

Kahle, C.F. 1974. Nature and significance of Silurian rocks at Maumee quarry, Ohio; *in* Silurian reef-evaporite relationships, edited by R.V Kesling, Michigan Basin Geological Society, p.31-54.

Maness Petroleum Laboratories 1971. Core analysis report; Union Gas Company, Enniskillen no.8-9-IIA, 29p.

Mesolella, K.J., Robinson, J.D., McCormick, L.M. and Ormiston, A.R. 1974. Cyclic deposition of Silurian carbonates and evaporites in Michigan Basin; American Association of Petroleum Geologists Bulletin, v.58, p.34-62.

Pearson, E.M. 1980. Sedimentology and diagenesis of the Warwick reef (Silurian), Lambton County, southwestern Ontario; unpublished MSc thesis, University of Waterloo, Windsor, Ontario, 250p.

Petta, T.J. 1980. Silurian pinnacle reef diagenesis—northern Michigan: effects of evaporites on pore space distribution; *in* Carbonate reservoir rocks, edited by R.B. Halley and R.G. Loucks, Society of Economic Paleontologists and Mineralogists, Core Workshop no.1, Denver, Colorado, June 8–12, p.32-42.

Prouty, C.E. 1983. The tectonic development of the Michigan Basin intrastructures; *in* Tectonics, structure, and karst in northern lower Michigan, edited by R.E. Kimmel, Michigan Basin Geological Society, Field Conference, August, p.36-81.

Sanford, B.V., Thompson, F.J. and McFall, G.H. 1985. Plate tectonics—a possible controlling mechanism in the development of hydrocarbon traps in southwestern Ontario; Bulletin of Canadian Petroleum Geology, v.33, p.52-71.

Sarg, J.F. 1982. Off-reef Salina deposition (Silurian), southern Michigan Basin—implications for reef genesis; *in* Deposition and diagenetic spectra of evaporites, edited by C.R. Handford, R.G. Loucks and G.R. Davies, Society of Economic Paleontologists and Mineralogists, Core Workshop no.3, Calgary, Alberta, June 26–27, p.354-384.

Sears, S.O. and Lucia, F.J. 1979. Reef growth model for Silurian pinnacle reefs, northern Michigan reef trend; Geology, v.7, p.299-302.

Simo, A. and Lehmann, P. 1988. Deposition and diagenesis of a cratonic Silurian platform reef, Pipe Creek Jr., Indiana; American Association of Petroleum Geologists Bulletin, v.72, p.248-249.

Smith, L. 1984. The Guelph–lower Salina in southwestern Ontario: subaerial exposure and episodic reef growth in a syn-erosional basin; Geological Association of Canada, Program with Abstracts, v.9, p.107.

———1989. Middle Silurian platform and pinnacle reefs, southwestern Ontario: initiation, development and termination; Geological Association of Canada, Program with Abstracts, v.14, p.63–64.

———1990. Karst episodes during cyclic development of Silurian reef reservoirs, southwestern Ontario; Core Workshop volume, edited by T.R. Carter, American Association of Petroleum Geologists, Eastern Section, London, Ontario, September 9, p.69-88.

Smith, L., Grimes, D.J. and Charbonneau, S.L. 1988. Karst episodes and permeability development, Silurian reef reservoirs, Ontario; *in* Geoscience Research Grant Program, summary of research 1987–1988, Ontario Geological Survey, Miscellaneous Paper 140, p.124-132.

Trevail, R.A. and Smith, L. 1987. Cratonic tectonism as control of spatial distribution and form of Silurian pinnacle and platform reefs, southwestern Ontario; *in* Abstracts volume, Canadian Society of Petroleum Geologists, Reef Research Symposium, Banff, Alberta, January 27–30, p.61.

Grant 305 Geochemistry, Metamorphism, Skarn Development and Gold Mineralization of the White River Gold Prospect, Hemlo Area

Y. Pan and M.E. Fleet

Department of Geology, The University of Western Ontario, London

ABSTRACT

At the White River exploration property of LAC Minerals Ltd. and in the vicinity of the Hemlo gold deposit, the Hemlo–Heron Bay greenstone belt comprises mainly sequences of highly deformed and metamorphosed volcanic and volcaniclastic sedimentary rocks. From the Hemlo area to the White River property there is no systematic variation in geochemistry of fine-grained clastic metasedimentary rocks in corresponding stratigraphic units, despite an apparent facies change. Locally developed cordierite-anthophyllite rocks are restricted to a thick sedimentary sequence and most likely represent metamorphosed magnesian- and iron-rich sediment, which was derived mainly from ultramafic volcanic sources. The gold contents of most of the unaltered supracrustal rocks, with the exception of a few ultramafic occurrences, are generally lower than 10 ppb in this highly gold-mineralized greenstone-belt terrane.

In the study area, the Hemlo–Heron Bay greenstone belt has been subjected to a complicated history of deposition, magmatism, deformation, metamorphism and alteration. Polymetamorphism is characterized by an earlier Barrovian-type metamorphism that peaked at a temperature of about 500°C and a pressure of 6.0 to 6.5 kbars (1 kbar = 100 MPa) and by a regional thermal metamorphism that was generally low grade (475° to 500°C and 3 kbars) in most areas but reached middle amphibolite facies (580° ± 20°C and 4 kbars) in 2 narrow zones associated with regional structures. Immediately after the peak of the regional thermal metamorphism, a protracted episode of skarn development resulted from extensive rock-fluid interaction along major dilatant structures. It commenced with the formation of 2 skarn occurrences, continued with a limited retrograde alteration and terminated with a late, low- to very low-grade calc-silicate alteration.

Metallogenesis in the study area did not occur during the regional thermal metamorphism but was related to rock-fluid interaction along dilatant structures. The metallic associations in earlier skarns strongly correlate with their respective host lithologies. Gold mineralization, in spatial and temporal association with rare earth element (REE)-enriched calc-silicates in the Anomalous zone from the study area, resembles Proterozoic auriferous skarn deposits but is clearly differentiated from typical Archean lode gold deposits by fluid inclusions of a moderate salinity. Although the brittle-ductile shear zone almost certainly provided necessary permeability for the fluid responsible for gold mineralization and the REE-enriched calc-silicates, gold precipitation was largely controlled by a pre-existing pyritic zone.

INTRODUCTION

The White River exploration property of LAC Minerals Ltd. is adjacent to the Hemlo mining district in the Hemlo–Heron Bay greenstone belt (Figures 305.1 and 305.2), which, in turn, is part of the large Schreiber–White River belt in the Wawa subprovince of the Superior Province (Muir 1982a, 1982b). The greenstone belt comprises mainly sequences of highly deformed and metamorphosed volcanic rocks and volcaniclastic sedimentary rocks, sandwiched between 2 major granitoid complexes, the Pukaskwa gneissic complex to the south and the Gowan Lake pluton to the north (Figure 305.1).

This report is a continuation of 4 previous papers (Pan and Fleet 1988, 1989a, 1989b, 1990) that dealt with various aspects of the geological, mineralogical and geochemical characteristics of all principal lithologies in the Hemlo–Heron Bay greenstone belt on the White River property (Table 305.1). The main objectives of this report are the following:

1. To present and discuss new textural evidence and calculated temperature-pressure conditions for metapelites and metabasites of the study area in order to improve our understanding of the metamorphic evolution of the Hemlo–Heron Bay greenstone belt.
2. To document and generalize geochemical characteristics of all principal lithologies, with emphasis on the fine-grained clastic metasedimentary rocks on the White River property and in the vicinity of the Hemlo deposit and the locally developed cordierite-anthophyllite rocks on the White River property, and to report the gold contents of all principal lithologies of this highly gold-mineralized section of the greenstone belt.
3. To present and discuss physicochemical conditions for calc-silicate crystallization in three prominent occurrences and abundant epidote-prehnite veins on the White River property, along with observed textural evidence, in order to elucidate the rock-fluid interaction history in the greenstone-belt terrane.

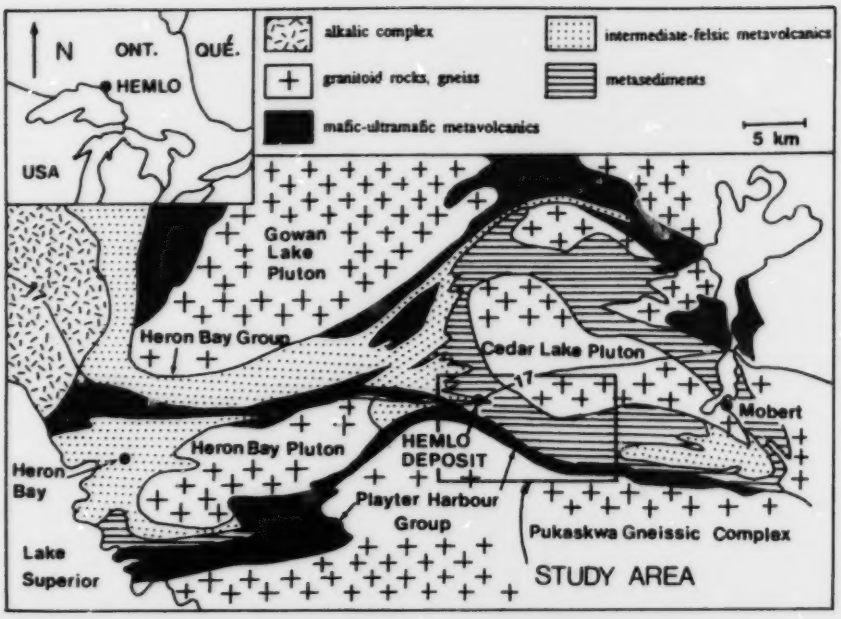

Figure 305.1. Geological map of the Hemlo–Heron Bay greenstone belt (*after* Robinson and McMillan 1985). Study area is outlined.

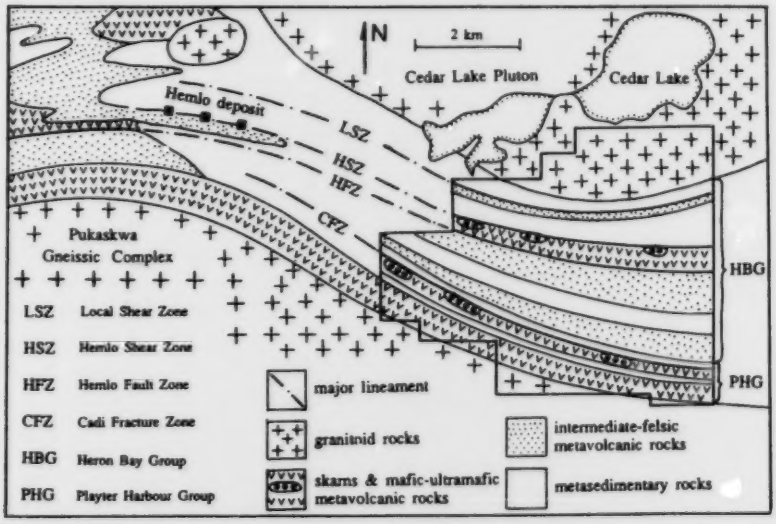

Figure 305.2. Geology of the White River exploration property of LAC Minerals Ltd. (outlined) and the Hemlo gold deposit (*after* Robinson and McMillan 1985; Hugon 1986; Pan and Fleet 1988).

4. To discuss correlations between metallogenesis of the Cr-rich and Fe-rich skarns and REE-enriched calc-silicates and host lithology and to establish their relative timing in the evolution of the greenstone belt.

METAMORPHISM

Preliminary results of a detailed documentation of mineral assemblages, including chemical compositions of major

Table 305.1. Lithostratigraphy of the Hemlo–Heron Bay greenstone belt on the White River property.

Group	Unit	Description	Sedimentary sequence
Heron Bay	9	Greywackes, mafic volcanics	Upper
	8	Pelites	
	7	Intermediate-felsic volcanics	
	6	Pelites, greywackes, BIF, CARs	Middle
	5	Greywackes, pelites, BIF, CARs	
	4	Pillowed mafic volcanics	
	3	Intermediate-felsic volcanics	
Playter Harbour	2	Greywackes, mafic-ultramafic volcanics	
	1	Mafic volcanics, greywackes, pelites	Lower

Note: Sedimentary sequence has been established for apparent lithostratigraphic relationships and most probably represents southern limb of a synclinal fold that was obliterated by later plutonism.

rock-forming minerals, in all principal lithologies of the White River property indicate a polymetamorphic history for the Hemlo–Heron Bay greenstone belt (Pan and Fleet 1988, 1989a; Pan 1990; Burk et al. 1986). An earlier metamorphic event has been delineated from the presence of relict kyanite and staurolite porphyroblasts in some metapelitic rocks. All supracrustal rocks of the study area have also been subjected to a regional thermal (typical andalusite-sillimanite series) metamorphism that is generally of low grade (as indicated by mineral assemblages of quartz + oligoclase + biotite + chlorite ± andalusite ± garnet in metapelitic rocks and of actinolitic hornblende + oligoclase + quartz ± biotite ± chlorite ± epidote in metabasites). The thermal metamorphism climaxed at middle amphibolite facies (as indicated by mineral assemblages of quartz + andesine + biotite + muscovite ± garnet ± sillimanite ± cordierite ± orthoamphiboles in metapelitic rocks and of hornblende + andesine + quartz ± garnet in metabasites) in 2 narrow zones associated with regional structures: a lower zone consisting of the lower portion of unit 1 mafic metavolcanic rocks of the Playter Harbour Group and structurally overlying the migmatized margin of the Pukaskwa gneissic complex; and an upper zone consisting of lithologic units 4, 5 and 6 enclosing the Hemlo shear zone and bounded to the south by the Hemlo fault zone (Table 305.1; Figure 305.2).

The zone of medium-grade metamorphism in the lower portion of lithologic unit 1 mafic metavolcanic rocks of the Playter Harbour Group was delineated on the basis of textures and mineral compositions (tschermakitic hornblende and andesine) in metabasites (Pan and Fleet 1989a). This has been confirmed by a mineral assemblage of quartz + bytownite + biotite + sillimanite + almandine garnet in samples collected from intercalated metasedimentary layers of this unit.

We estimated metamorphic conditions by using various published geothermometers and geobarometers (Ganguly and Saxena 1987; Indares and Martingnole 1985; Graham and Powell 1984; Ghent et al. 1979; Koziol 1989; Kohn and Spear 1990) for mineral assemblages in metapelites and metabasites from the study area. The results are summarized here: 1) 6.0 to 6.5 kbars and 456° to 520°C for the earlier metamorphic event associated with kyanite and staurolite in the upper zone of medium grade; 2) 4.2 to 4.5 kbars and 580° ± 20°C for the peak of the regional thermal metamorphism in zones of medium grade (units 1, 4, 5 and 6); and 3) 3.2 kbars and 476° to 503°C for the peak of the regional thermal metamorphism in zones of low grade.

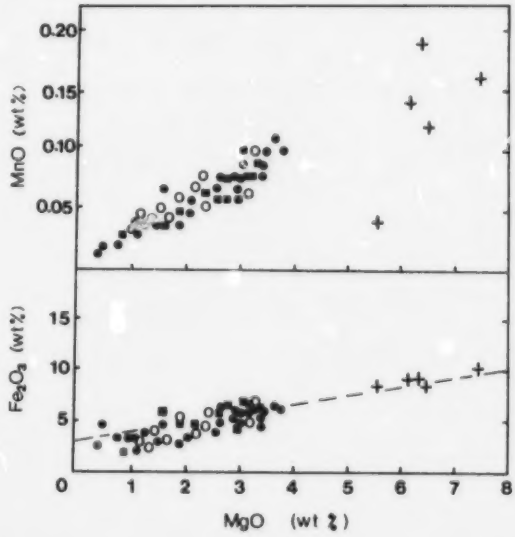

Figure 305.3. Plots of Fe_2O_3* and MnO versus MgO for fine-grained clastic metasediments from the Hemlo area (open circles), compared with data for pelites (solid squares), greywackes (solid circles) and cordierite-anthophyllite rocks (crosses) from the White River property. Dashed line represents the Fe_2O_3*-MgO mantle curve (cf. Naqvi et al. 1988).

The estimated pressure for the earlier metamorphic event at the White River property (6.0 to 6.5 kbars) is slightly lower than that at the Hemlo deposit (up to 7.3 kbars) calculated by Burk et al. (1986). The regional peak metamorphism is typically low in calculated pressure (3 to

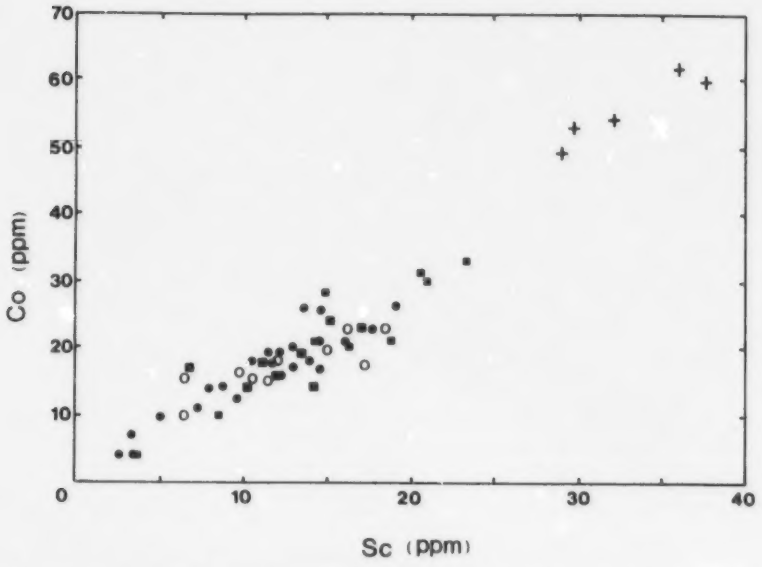

Figure 305.4. Plot of Co versus Sc for clastic metasedimentary rocks and CARs from the study area: symbols as in Figure 305.3.

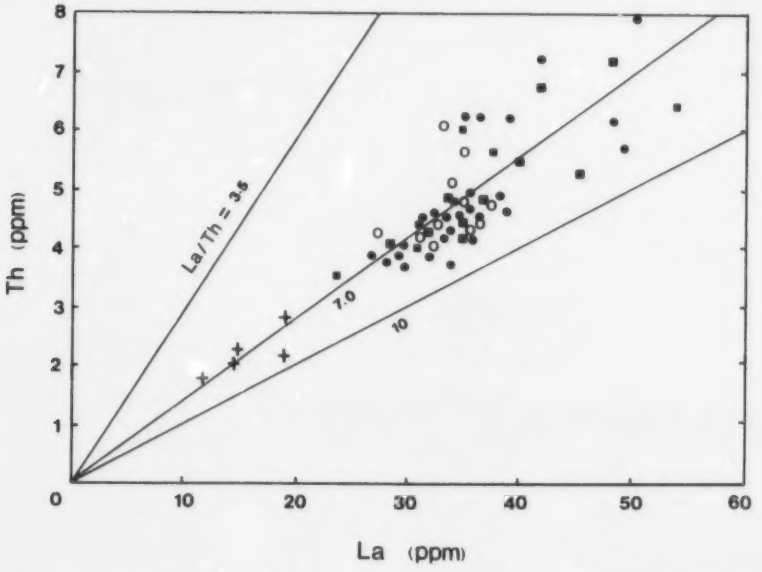

Figure 305.5. Plot of Th versus La for all clastic metasedimentary rocks and CARs from the study area: symbols as in Figure 305.3.

4 kbars), corresponding to the presence of sillimanite and andalusite in metapelitic rocks at, respectively, medium and low grade.

GEOCHEMISTRY

The geochemical characteristics of the clastic metasedimentary rocks on the White River property have been given in Pan and Fleet (1989a). These rocks are highly immature and in some geochemical respects, such as low Al_2O_3/Na_2O ratio, low chemical index of alteration (CIA), K_2O/Na_2O of <1.0, uniform Th/U ratio (3.6) and strong correlations between transition metals and MgO and Fe_2O_3*(total Fe), they are similar to typical Archean sediments. However, their REE patterns, particularly the high contents of light REEs, and their steep chondrite-normalized REE patterns are similar to those of more mature Proterozoic sediments. These geochemical characteristics, especially the REE compositions, indicate that the clastic metasedimentary rocks of the White River property were derived mainly from local intermediate to felsic volcanic sources, admixed with variable amounts of mafic-ultramafic volcanic components and continental weathering products, and were deposited rapidly as turbidites in an island-arc environment (cf. Pan and Fleet 1989a).

Fine-grained Clastic Metasedimentary Rocks

There is an overall decrease in grain and fragment size eastward from the Hemlo gold deposit to the White River property. This trend is exemplified by the presence of conglomerates in the major clastic unit of Walford et al. (1986) at Hemlo and by their typical absence at the White River property. It is worth noting that conglomerates are also present in the Hemlo–Heron Bay greenstone belt farther to the east, south of Mobert (Figure 305.1). In addition, banded iron formation (BIF) appears to be more abundant at the White River property than at the Hemlo deposit, although it is volumetrically insignificant at both localities (Muir and Elliott 1987; Pan and Fleet 1988).

In this study, fine-grained banded sedimentary rocks from the vicinity of the Hemlo deposit were collected from outcrops along Trans-Canada Highway 17, east of the Cedar Creek bridge, because they are remote from the ore zones of the Hemlo deposit and are therefore less affected by late alteration. They are interpreted as representing a lateral extension of unit 9 greywackes from the White River property.

Fine-grained banded sedimentary rocks from the Hemlo deposit area are generally intermediate to felsic in major-element composition, are characterized by the K_2O/Na_2O weight ratio of <1.0 and steep chondrite-normalized REE patterns without a pronounced Eu anomaly, and are similar to all clastic sedimentary rocks on the White River property (Pan and Fleet 1989a). However, their other geochemical parameters, such as a wide range of the Al_2O_3/TiO_2 weight ratio (34 to 42), a low Al_2O_3/Na_2O weight ratio (3.6 to 3.7) and a low CIA (50.7 to 54.6), are similar to those of metagreywackes from the White River property but differ from those of metapelites from the White River property (Pan and Fleet 1989a).

Fine-grained banded sedimentary rocks from the Hemlo deposit area are also characterized by good positive correlations in MnO and Fe_2O_3* versus MgO and in Sc versus Co, similar to those of all clastic metasedimentary rocks on the White River property (Figures 305.3 and 305.4). The geochemical coherence of Th and light REEs is apparent in clastic metasedimentary rocks from the White River property and the Hemlo area (Figure 305.5). The La/Th ratio (6 to 7, with a few values of ≤9), however, is considerably higher than the average estimate (3.5 ± 0.3) for most Archean sediments (McLennan and Taylor 1984).

Cordierite-Anthophyllite Rocks

Within the middle metasedimentary sequence (units 5 and 6 of the Heron Bay Group; Figure 305.2; Table 305.1), a few rock samples with mineral assemblages consisting mainly of Fe-Mg-Mn amphiboles (mainly anthophyllite with minor gedrite and cummingtonite) and cordierite are particularly distinctive and are referred to as cordierite-anthophyllite rock (CAR). CARs are generally very coarse grained and are commonly spatially associated with BIFs and coarse-grained metapelites.

Table 305.2. Whole-rock data for cordierite-anthophyllite rocks.

Samples	I812/345	I813/368	I815/510	I91/131	I92/110
SiO_2 (wt.%)	55.90	63.00	57.40	58.30	57.00
TiO_2	0.80	0.62	0.90	0.74	0.80
Al_2O_3	17.90	13.40	19.10	16.50	15.40
Fe_2O_3*	9.20	8.67	10.20	8.41	9.32
MnO	0.19	0.12	0.16	0.04	0.19
MgO	6.35	6.51	7.46	5.59	6.35
CaO	3.15	2.51	1.38	3.33	3.13
Na_2O	2.60	2.30	1.04	3.16	3.65
K_2O	2.37	1.57	0.83	1.78	1.47
P_2O_5	0.12	0.08	0.12	0.11	0.11
LOI	1.30	1.50	1.10	2.00	1.80
Total	99.64	100.3	99.69	99.96	99.22
Au (ppb)	0.7	–	11.0	4.5	7.5
Co (ppm)	62	49	54	60	53
Cr	480	770	670	550	680
Hf	3	2	2	2	3
Ni	370	370	500	300	300
Sc	36.1	29.0	32.1	37.7	29.7
Ta	–	1	–	–	–
Th	3.5	1.8	2.2	2.9	2.2
U	–	0.7	0.8	1.4	0.6
V	210	180	210	220	200
Zr	90	60	90	70	90
La	23.7	11.5	15.4	19.0	18.9
Ce	46	28	35	25	35
Nd	17	–	18	9	21
Sm	4.0	2.4	3.6	2.7	2.9
Eu	2.2	0.6	0.4	–	1.3
Yb	2.2	1.3	1.9	1.7	1.6
Lu	0.46	0.22	0.31	0.22	0.30
Al_2O_3/TiO_2	22.4	21.6	21.2	22.3	19.3
Al_2O_3/Na_2O	6.88	5.83	18.47	5.22	4.22
K_2O/Na_2O	0.91	0.68	0.80	0.56	0.40
FM/A	0.87	1.13	0.92	0.85	1.02
CIA	64.8	63.3	83.2	61.9	59.6
Zr/Hf	30.0	30.0	45.0	35.0	30.0
Th/U	–	2.57	2.75	2.07	3.67
La_N/Yb_N	7.0	5.8	5.3	7.3	7.7

Notes: Fe_2O_3 is total iron content; FM/A is $(Fe_2O_3^* + MgO)/Al_2O_3$ weight ratio.*

CARs are distinguished from the clastic metasedimentary rocks by their low contents of SiO_2 and high concentrations of Mg and Fe (5.6 to 7.5 weight % MgO and 8.4 to 10.2 weight % Fe_2O_3*; Table 305.2) and from BIF by their lower contents of Fe_2O_3*. The $(Fe_2O_3^* + MgO)/Al_2O_3$ whole-rock weight ratio (Table 305.2) is characteristically greater than that of cordierite (0.48 and 0.47 in samples I812/345 and I815/510, respectively). The values of Al_2O_3/Na_2O (4.22 to 6.88, with the exception of one sample, which is 18.47) and K_2O/Na_2O (0.40 to 0.91) are similar to or slightly higher than corresponding values in greywackes. Although the Al_2O_3 and TiO_2 contents of CARs show even wider variation than those of clastic metasedimentary rocks, the Al_2O_3/TiO_2 weight ratio is fairly constant at an average of 21 ($\sigma = 0.6$, $n = 5$) and is close to

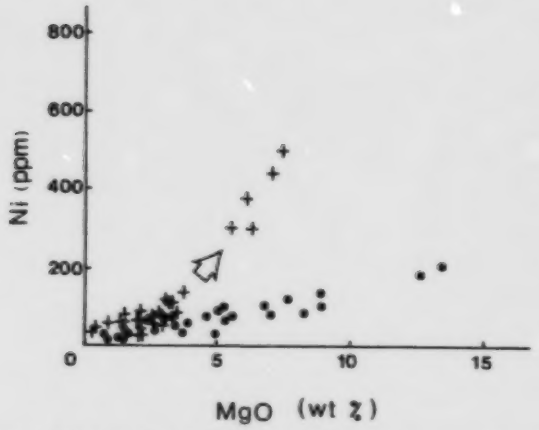

Figure 305.6. A plot of Ni versus MgO for all supracrustal rocks (except for BIF and komatiite) from the study area: crosses represent metasedimentary rocks; circles represent metavolcanic rocks.

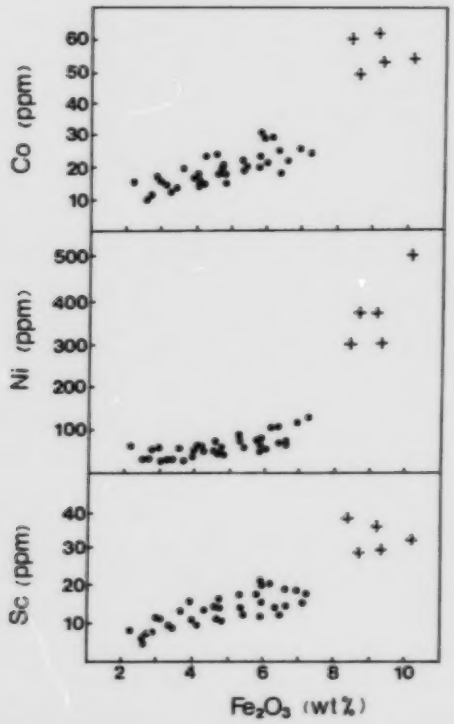

Figure 305.7. Plots of transition metals (Co, Ni and Sc) versus $Fe_2O_3^*$ for all clastic metasedimentary rocks (circles) and CARs (crosses) from the study area.

the chondrite and komatiitic values (Sun and Nesbitt 1978; Condie 1981). The abundances of transition metals, especially Cr (480 to 770 ppm) and Ni (300 to 500 ppm), are significantly higher than in clastic metasedimentary rocks but are similar to those of komatiitic basalt and komatiite from the study area. The large, less-mobile incompatible elements, such as Ta, Hf and Th, in CARs are also lower than in host clastic metasedimentary rocks. An average value of the Zr/Hf ratio at 34.0 ($\sigma = 3.26$, $n = 5$) in the White River CARs is also similar to that in komatiites. The chondrite-normalized REE patterns of the CARs ($La_n/Yb_n < 10$) are flatter than those of clastic metasedimentary rocks and do not have a pronounced Eu anomaly.

CARs have attracted much attention since the beginning of this century because of their common spatial association with volcanogenic massive sulphide (VMS) deposits and their unusual whole-rock composition, which is without equivalents amongst common igneous and sedimentary rocks. Reinhardt (1987) tabulated all genetic models for CAR origin and proposed his own model of isochemical metamorphism of sediment. This model rests on both field observations and major-element composition of Proterozoic CARs (highly magnesian metamorphic rocks) from Queensland, Australia, and on similarities to clays and shales associated with evaporites. The White River CARs occur in spatial association with BIF and metapelites and extend eastwards and westwards exclusively within the middle sedimentary sequence. Therefore, the CARs in the Hemlo–Heron Bay greenstone belt are most likely sedimentary in origin.

Clastic metasedimentary rocks in the Hemlo–Heron Bay greenstone belt on the White River property show strong correlations between many transition metals and MgO (and $Fe_2O_3^*$), and their elevated abundances at given MgO (or $Fe_2O_3^*$) contents distinguish them from intermediate to felsic metavolcanic rocks. This is illustrated on a plot of Ni versus MgO for all supracrustal rocks (Figure 305.6), with the exception of ultramafic rocks, from the White River property. It is apparent that there is a good positive correlation between Ni and MgO in CARs; in particular, their Ni-MgO trend appears to coincide with that for the clastic metasedimentary rocks; such relationships also can be observed in many other plots (Figures 305.3, 305.4 and 305.7). This further supports a sedimentary origin for CARs.

The features of the geochemistry of the White River CARs, such as uniform Al_2O_3/TiO_2 weight ratio and Zr/Hf ratio close to chondrite value, extremely high Cr and Ni abundances, good positive correlation between Ni and MgO, low concentrations of the less-mobile incompatible elements (Hf, Ta and Th), and low total REE abundance, collectively favour an ultramafic precursor. Sedimentary rocks that are highly magnesian and extremely enriched in Cr and Ni are not uncommon in Archean terranes worldwide, including the Fig Tree formation, South Africa (Danchin 1967), the Pilbara Block, Australia (McLennan et al. 1983) and the Chitradurga belt, India (Naqvi et al. 1988). Furthermore, sedimentary rocks of ultramafic compositions with well-preserved turbidite sequences have been reported in the Lac Guyer greenstone belt, James Bay region of Quebec (Stamatelopoulou-Seymour and Francis 1980), and are interpreted as having been derived from the transported degradation products of associated komatiitic volcanic rocks or as representing contemporaneous reworked ultramafic tuffs or ash flows. Therefore, it is possible that

Table 305.3. Representative compositions of epidote-group minerals.

	1	2	3	4	5	6
SiO_2 (wt.%)	33.37	38.69	38.44	37.67	37.55	35.82
TiO_2	0.15	0.05	0.04	nd	nd	0.03
Al_2O_3	20.60	28.29	26.46	21.26	21.36	16.04
Cr_2O_3	nd	nd	nd	nd	nd	11.77
$\sum RE_2O_3$	19.58	nd	nd	nd	nd	nd
FeO*	7.93	5.94	6.95	14.75	14.96	9.29
MgO	1.20	nd	0.02	nd	nd	0.06
MnO	1.29	0.12	0.40	nd	0.11	0.23
CaO	13.12	24.31	23.91	23.08	22.10	22.52
Na_2O	0.12	nd	nd	0.05	nd	nd
Total	96.95	97.21	96.41	96.81	96.08	95.76
Si	3.030	3.044	2.962	3.048	3.146	2.940
Ti	0.010	0.003	0.002	0.000	0.000	0.002
Al	2.204	2.623	2.402	2.026	2.069	1.552
Cr	0.000	0.000	0.000	0.000	0.000	0.764
Fe^{3+}	0.066	0.391	0.448	0.901	1.046	0.638
Fe^{2+}	0.536	–	–	–	–	–
Mg	0.099	0.000	0.002	0.000	0.000	0.007
Mn	0.163	0.008	0.026	0.000	0.008	0.016
Ca	1.278	2.049	1.974	2.004	1.987	1.981
∑RE	0.654	0.000	0.000	0.000	0.000	0.000
Na	0.018	0.000	0.000	0.008	0.000	0.000

Notes: 1) Allanite from the REE-enriched calc-silicate (analysis also contains 0.50 and 0.86 wt % F and Cl, respectively); 2, 3) epidote from the REE-enriched calc-silicate; 4) epidote from a crosscutting vein in mafic metavolcanic rocks; 5) epidote from the Fe-rich skarn; 6) epidote from the Cr-rich skarn. FeO is total iron content; $\sum RE_2O_3$ and ∑RE are total REE contents in oxide and atomic proportion (on the basis of 12.5 oxygens), respectively; nd is not detectable.*

the White River CAR is a metamorphic equivalent of magnesium- and iron-rich sediment, which was derived from ultramafic sources.

Gold Abundances

The Hemlo–Heron Bay greenstone belt is a highly gold-mineralized terrane: the Hemlo deposit alone contains >80 Mt of gold ore with an average grade of 7.7 g/t Au (Harris 1989), making it the largest gold reserve in Canada, and numerous subeconomic gold occurrences are also present throughout the belt (Patterson 1984; Pan and Fleet 1989a). Although some authors have suggested that no favourable source rock is required for gold mineralization (e.g., Phillips et al. 1987), gold in Archean terranes is generally believed to be derived ultimately from mafic-ultramafic volcanic rocks, because most Archean gold deposits worldwide occur generally in spatial association with thick mafic-ultramafic volcanic sequences (Hodgson and MacGeehan 1982). However, the Hemlo gold deposit and occurrences of anomalous gold values on the White River property are all located in a volcaniclastic sedimentary basin, with only subordinate volcanic rocks.

Analyses of all principal lithologies on the White River property revealed that the gold contents in the majority of the supracrustal rocks are only slightly above the background gold values (1 to 2 ppb; Keays 1984). At the White River property, the following rock types are conspicuously enriched in gold: a thin layer of komatiite (interpreted as representing the Hemlo fault zone; Muir 1982a) within unit 4 mafic metavolcanic rocks with 11 to 62 ppb Au (cf. Keays 1984); metagreywackes of unit 5 from the middle sedimentary sequence with 11 to 56 ppb Au; and metapelites of unit 8 from the upper sedimentary sequence with 2.8 to 39 ppb Au. The metapelites of unit 8 host a laterally extensive zone of anomalous gold values (Pan and Fleet 1988, 1989a). However, the gold abundances of other principal lithologies are close to the Clark value (4 ppb). Meyer and Saager (1985) suggested that Fe-rich sediments are commonly enriched in gold. However, BIF and CARs from the study area show no significant concentrations of gold (<11 ppb).

At the Hemlo gold deposit, the Au abundances of hanging-wall clastic metasedimentary rocks are also generally lower than 6 ppb. We did, however, obtain high concentrations of both Au and V (up to 370 ppb and 220 ppm, respectively) in a small mafic volcanic lens (chlorite schist). The significance of this sample lies not only in its high concentration of Au but also in its abundance of V, which is characteristically high within the Hemlo gold deposit itself (associated mainly with green vanadium muscovite; Harris 1989).

CALC-SILICATES

Three prominent ore-mineral calc-silicate occurrences, differing widely in both scale of development and salient mineralogical and geochemical characteristics, are present in close association with major dilatant structures on the White River property (Figure 305.2; *see also* Fleet and Pan

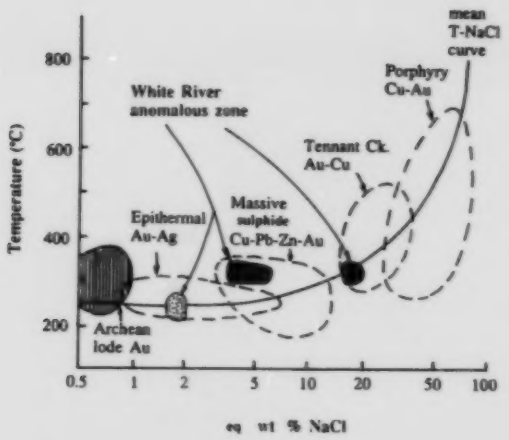

Figure 305.8. Temperature-salinity diagram illustrating physicochemical conditions estimated from fluid inclusions (primary, black; secondary, stippled) in quartz grains of the REE-enriched calc-silicates and comparison with literature data of common gold deposits (cf. Large et al. 1988).

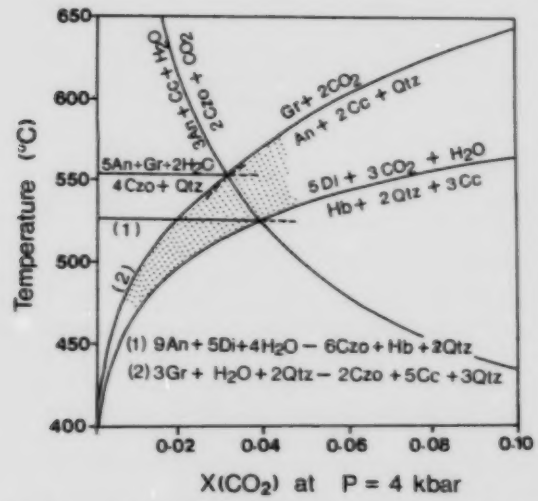

Figure 305.9. Calculated T-$X(CO_2)$ phase diagram section for the Fe-rich skarn at a pressure of 4 kbars. The shaded area represents stable conditions for main assemblages of the Fe-rich skarn; An, anorthite; Cc, calcite; Czo, clinozoisite; Di, diopside; Gr, grossular; Hb, hornblende.

1990). Cr-rich skarn is present within the Cadi fracture zone of the Playter Harbour Group and is characterized by the unusual mineral association of zincian chromite (≤6.6 weight % ZnO) and uvarovite (Pan and Fleet 1989b); Fe-rich skarn occurs within unit 4 metabasites of the Heron Bay Group, at or near the Hemlo shear zone (Figure 305.2), and is characterized by coarse-grained Fe-rich clinopyroxene ($Hd_{80}Di_{20}$) and Mn-rich grandite garnet (≤8.4 weight % MnO); and REE-enriched calc-silicates occur within the Local shear zone (Figure 305.2) and are characterized by abundant epidote and prehnite veins and minor REE-rich minerals, including an unusual halogen-bearing allanite (Table 305.3), REE-bearing clinozoisite and monazite on a thin-section scale (Pan and Fleet 1990). In addition, epidote-prehnite crosscutting veins are also widespread in the study area, being particularly abundant in mafic metavolcanic rocks in close association with lithologic boundaries or major dilatant structures (Pan and Fleet 1988, 1989a, 1989b).

Conditions of Calc-silicate Crystallization

A fluid-inclusion study was attempted to quantify the physicochemical conditions for the formation of the 3 calc-silicate occurrences and epidote-prehnite crosscutting veins in the study area. Unfortunately, no usable fluid inclusions were found in the Cr-rich skarn. In the Fe-rich skarn, fluid inclusions are generally rare and rather small (<12 μm in diameter) in clinopyroxene and garnet grains. They appear to be irregular in shape and are commonly two-phase, with a volume ratio of liquid to vapour of >9. Homogenization temperatures show a very limited range of variation at about 520° ± 14°C. The range of the freezing points, from −1.2° to −1.7°C, indicates that the ambient fluid responsible for the Fe-rich skarn was very low in salinity, <2.9 equivalent weight % NaCl (cf. Potter et al. 1978).

Quartz grains in the REE-enriched calc-silicates from the Local shear zone (Figure 305.2) contain abundant fluid inclusions. However, the majority of these fluid inclusions are apparently secondary, as indicated by their elongated shapes and preferential occurrence in trails along resealed grain fractures. Primary inclusions are less abundant, isolated and ellipsoidal and generally contain a single liquid phase. Occasionally, a gas phase and, rarely, a cubic halite daughter crystal are present in some primary fluid inclusions.

Homogenization temperatures of 35 primary fluid inclusions vary from 340° to 368°C. Estimated salinities of primary inclusions range from 3.9 to 20 equivalent weight % NaCl (Figure 305.8; cf. Potter et al. 1978; Keevil 1942). However, there are no values between 6.5 and 17.4 equivalent weight % NaCl (Figure 305.8), and the higher salinities (from 17.4 to 20 weight % NaCl) correspond to halite-bearing fluid inclusions that were probably metastable (cf. Roedder 1984). The average homogenization temperature and salinity for undersaturated primary fluid inclusions of 350°C and 4.5 equivalent weight % NaCl, respectively, yielded a pressure of about 1.2 kbars according to the calibration of Potter and Brown (1977).

Pan and Fleet (1989b) calculated the physicochemical conditions for the calc-silicate crystallization in the Cr-rich skarn by using the GEO-CALC programs of Perkins et al. (1986) with internally consistent thermodynamic data of Berman et al. (1985). A similar approach applied to the main assemblage of clinopyroxene + garnet + ferro-tschermakitic hornblende + epidote + plagioclase + quartz + calcite yielded a crystallization temperature of 500° to 560°C with $X(CO_2)$ of <0.05 at a pressure of 4 kbars (Figure 305.9). This is in good agreement with the homogenization temperatures of fluid inclusions in clinopyroxene and garnet grains.

Table 305.4. Physicochemical conditions of calc-silicate crystallization and maximum temperatures of the regional thermal metamorphism in their host rocks.

Occurrence	*T* (°C)	*P* (kbars)	Fluid compositions X_{CO_2}	NaCl (wt. %)	Metamorphic *T* (°C)
Cr-rich skarn	400 ± 50	3	<0.03	NA	500
Fe-rich skarn	500–560	4	<0.05	<2.9	580 ± 20
REE-enriched calc-silicates	340–368	1.2	Very low	3.9–20	500
Epidote-prehnite veins	320	1.7	Very low	<2.0	NA

Notes: NaCl is salinity (equivalent weight % NaCl); NA is not applicable.

The mineral assemblages of the epidote-prehnite veins are similar to those of metabasites in low- to very low-grade (prehnite-pumpellyite to greenschist transition facies) metamorphic terranes (Liou et al. 1985; Cho and Liou 1987). Although most epidote-prehnite veins from the study area are mono- or bimineralic in nature, a low-variance assemblage (which is useful for pressure-temperature estimation) consisting of epidote + prehnite + pumpellyite + actinolite + chlorite + quartz is observed in small vesicles and veins within metavolcanic rocks of komatiitic basalt composition. Equilibration of this assemblage (albeit on a very small scale; Cho and Liou 1987) indicates a crystallization temperature of 320°C and a pressure of 1.7 kbars for an average epidote composition of Ps_{30} (cf. Liou et al. 1985). This is similar to the pressure-temperature conditions (350°C and 1.2 kbars) estimated from primary fluid inclusions in quartz grains of the REE-enriched calc-silicates.

Skarn Development

The estimated maximum temperatures for calc-silicate crystallization in the Cr-rich and Fe-rich skarns are slightly lower than the peak temperatures for the regional thermal metamorphism of their respective host rocks (Table 305.4). This is consistent with structural and textural evidence (Pan and Fleet 1989b) that these two skarn occurrences were broadly contemporaneous with the regional thermal metamorphism and, probably, formed immediately after the peak metamorphic conditions had been attained.

Retrograde alteration after the regional thermal metamorphism is generally poorly developed or only of local significance in metapelites and metabasites of the greenstone belt (Burk et al. 1986; Pan and Fleet 1988, 1989a). Hydration is a characteristic retrogression in skarn deposits (Einaudi et al. 1981), and there is some evidence for this in the Fe-rich skarn. In the Cr-rich skarn, uvarovite and Cr-rich epidote, both replacing zincian chromite, clearly crystallized after the main assemblage of clinopyroxene + grandite garnet (Pan and Fleet 1989b). However, it is not certain whether they represent a retrograde alteration, similar to that in the Fe-rich skarn, or a late calc-silicate alteration, as indicated by the presence of other Cr-rich silicate minerals in crosscutting veins.

REE-enriched calc-silicates from the Local shear zone are similar mineralogically to the crosscutting epidote-prehnite veins, except for their association with REE-rich minerals. Pan and Fleet (1990) suggested that the presence of REE-rich minerals in the Local shear zone (Figure 305.2) resulted from a high water/rock ratio and consequently local remobilization of light REEs. It is most likely, then, that this occurrence was an exceptional development of the late calc-silicate alteration within a dilatant structure (Local shear zone). This is strongly supported by the agreement of estimated temperature-pressure conditions for epidote-prehnite veins and REE-enriched calc-silicates (Table 305.4). Corfu and Muir (1989) obtained U-Pb dates of about 2632 to 2645 Ma on monazite in microcline-rich ores from the Hemlo gold deposit. On the White River property, monazite, which is confined to the Local shear zone, is a characteristic mineral phase of the REE-enriched calc-silicate and is almost identical in both absolute abundances and chondrite-normalized patterns of REEs to the occurrence at Hemlo (Pan 1990). This indicates that the late, low- to very low-grade calc-silicate alteration of the study area also occurred at about 2632 to 2645 Ma.

The Cr-rich skarn appears to extend laterally in the Hemlo–Heron Bay greenstone belt and is confined to the Cadi fracture zone (Siragusa 1983; Holding 1987; Pan and Fleet 1989b). The distribution of Fe-rich skarn is unknown, largely because of its limited scale of development. However, Muir (1988) reported skarn-like assemblages in mafic metavolcanic rocks of the Heron Bay Group at Hemlo. Our field observations have also recognized calc-silicate rocks of Fe-rich skarn-like mineral assemblages in mafic metavolcanic rocks of the Heron Bay Group farther to the east of the study area. It is likely, then, that the Fe-rich skarn occurs within the mafic metavolcanic rocks of the Heron Bay Group throughout the Hemlo–Heron Bay greenstone belt. It is interesting that there is a layer of Fe-rich skarn-like rocks within the mafic metavolcanic rocks (unit 1 of Pan and Fleet 1989a) of the Playter Harbour Group (on the structural footwall of the Cr-rich skarn) farther to the east of the study area. Again, this skarn-like layer occurs in close association with a lithological boundary between mafic metavolcanic rocks (high-iron tholeiitic basalt in composition; cf. Pan 1990) and intercalated clastic metasedimentary rocks. The regional distribution of the late, low- to very low-grade calc-silicate alteration is more obvious, as crosscutting veins of epidote and prehnite have been reported in various lithologies at a number of localities (Muir 1982a, 1982b; Pan and Fleet

Table 305.5. Transition-metal contents in skarns and their host metavolcanic rocks.

	Cr-rich skarn						Fe-rich skarn			
	1	2	3	4	5	6	7	8	9	10
Ti	2400	2600	3100	1500	1500	2700	5900	7400	7200	9200
V	90	92	170	180	78	180	260	300	310	340
Cr	4200	5100	3300	2700	2300	2900	460	360	230	270
Mn	2400	3400	2300	4300	3700	3200	1900	7800	6600	2600
Fe	9.62	10.7	13.6	9.34	7.78	11.3	12.8	22.7	20.6	17.6
Co	130	93	58	110	120	63	62	100	43	46
Ni	920	790	440	1300	1600	680	250	310	64	85
Cu	0.5	12	29	38	86	19	62	670	260	150
Zn	210	260	160	270	69	70	130	2100	220	130
Au	5.0	8.9	0.9	0.6	34	<0.1	35	<0.1	150	7.6
Ag	<0.5	<0.5	<0.5	<0.5	<0.5	<0.5	<0.5	<0.5	<0.5	<0.5
Ni/Co	7.1	8.5	7.6	11.8	13.3	10.8	4.0	3.1	1.5	1.9

Notes: The abundances of all elements are in parts per million, except for Fe (in weight % Fe_2O_3) and Au (in parts per billion); 1–5) representative analyses of Cr-rich skarn from the Cadi fracture zone; 6, 7) representative analyses of komatiite and komatiitic basalt associated with the Cr-rich skarn, respectively; 8, 9) representative analyses of Fe-rich skarn; 10) representative analysis of high-iron tholeiitic basalt associated with the Fe-rich skarn.

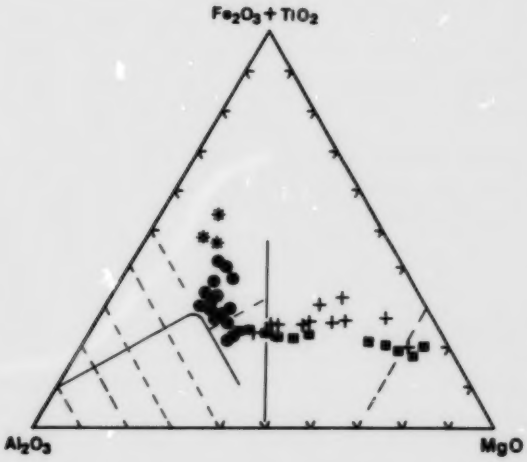

Figure 305.10. A Jensen cation plot (Jensen 1976) for Cr-rich skarn (crosses) and for Fe-rich skarn (stars) and their respective host metavolcanic rocks. Squares represent komatiitic basalt and komatiite associated with Cr-rich skarn; circles represent tholeiitic basalt associated with Fe-rich skarn.

1988, 1989a, 1989b). Also at Hemlo, Walford et al. (1986) reported a pervasive late calc-silicate alteration in the hanging-wall metasedimentary rocks.

We can conclude that the Hemlo–Heron Bay greenstone belt has been subjected to a protracted episode of skarn development after the regional thermal metamorphism. This skarn development reflected extensive rock-fluid interaction along dilatant structures and commenced immediately after the peak of the regional thermal metamorphism, continued with a limited retrograde alteration and terminated with a late, low- to very low-grade calc-silicate alteration.

Polymetallic Sulphides in Cr-rich and Fe-rich Skarns

Pan and Fleet (1989a) reported mineralogical and geochemical characteristics of sulphides in the Cr-rich skarn and suggested its metallic association is Fe-Ni-Co-Zn-Cu-Mo, similar to the well-known Outokumpu-type ores. The Fe-rich skarn from the study area also contains a subeconomic sulphide occurrence consisting of pyrite, pyrrhotite, sphalerite, chalcopyrite, pentlandite and Fe-rich siegenite, but its metallic association is best expressed as Fe-Zn-Cu-Ni-Co and is similar to that of sulphide ores in calcic iron skarn deposits (Einaudi et al. 1981; Meinert 1984; Kaneda et al. 1986).

The characteristic sulphide mineral assemblages in both the Cr-rich and Fe-rich skarns largely reflect sporadic local concentrations of transition metals. Inspection of Table 305.5 reveals that the abundances of transition metals in the skarns strongly correlate with their contents in the respective host lithologies: komatiitic basalt and komatiite for the Cr-rich skarn and high-iron tholeiitic basalt for the Fe-rich skarn. However, the maximum Ni and Cr contents in the Cr-rich skarn are significantly higher than in the unaltered (or less-altered) host lithologies (Table 305.3). Analogously, Mn, Fe, Co, Ni, Cu and Zn are enriched in the Fe-rich skarn compared with its host lithology. Therefore, local remobilization and secondary enrichment of these transition metals must have occurred during the formation of these 2 skarns.

In both Cr-rich and Fe-rich skarns, most polymetallic sulphides are disseminated and appear to coexist with earlier anhydrous calc-silicate minerals, such as clinopyroxene and garnet. Therefore, the main sulphide mineralization occurred during the earlier stages of the skarn development.

Other sulphide minerals, such as pyrite in the Fe-rich skarn, occur in close association with hydrous silicate minerals (actinolite and chlorite) and occupy grain fractures and cleavages of earlier anhydrous minerals. They most likely crystallized during the retrograde event. Additionally, some sulphide minerals are restricted to the crosscutting veins. In the Cr-rich skarn, for example, molybdenite is restricted to veins and was almost certainly introduced during the late, low- to very low-grade calc-silicate alteration.

A genetic link between the Cr-rich and Fe-rich skarns and their respective metavolcanic host rocks is obvious in temporal stratigraphic relationships (Figure 305.2) and textural evidence (e.g., relict mafic metavolcanic fragments within the Cr-rich skarn; Pan and Fleet 1989b) and can be demonstrated further by strong correlations in major-element and REE geochemistry. Figure 305.10 shows that most whole-rock compositions of the Cr-rich skarn are in the komatiitic basalt field and one falls in the komatiitic field, whereas whole-rock compositions of the Fe-rich skarn plot in the high-iron tholeiitic field. Therefore, the composition fields of both Cr-rich and Fe-rich skarns broadly correspond to those of their unaltered metavolcanic host rocks. In respect to REE geochemistry, most samples of Cr-rich and Fe-rich skarns are also similar in both absolute abundances and chondrite-normalized patterns, which are generally flat, to their respective unaltered ultramafic and mafic metavolcanic host rocks. However, a few samples do show a considerable variation in REE abundances accompanied by a fluctuation in La_N/Yb_N ratio. One Fe-rich skarn sample, in particular, is significantly enriched in light REEs (La and Ce at 110 and 240 ppm, respectively), whereas its heavy REE abundances are only slightly higher than those of other Fe-rich skarn samples and host metamorphosed high-iron tholeiitic basalt. This points to local remobilization of light REEs in association with extensive rock-fluid interaction as observed in the REE-enriched calc-silicate (Pan and Fleet 1990). It is noteworthy, however, that REE-rich minerals are typically absent even in the Fe-rich skarn sample of the highest REE concentration.

Gold Mineralization

The White River property, approximately 5 km east of the world-class Hemlo gold deposit, is one of the leading gold prospects in the greenstone belt. Assays on core samples from the study area indicate several locations with anomalous gold concentrations. Among these locations, a narrow but laterally extensive zone with sporadic high values (≤27 ppm) of gold and occurring within a brittle-ductile shear zone is of most interest and is referred to as the "Anomalous zone" (Pan and Fleet 1988, 1989a). It is marked by a footwall pyritic zone and hanging-wall sericitic zone, and maximum gold values have been obtained where the 3 zones coalesce (Figure 305.11). A detailed description including geological setting and mineralogical and geochemical characteristics of this Anomalous zone from the study area has been given in Pan and Fleet (1988, 1989a, 1990).

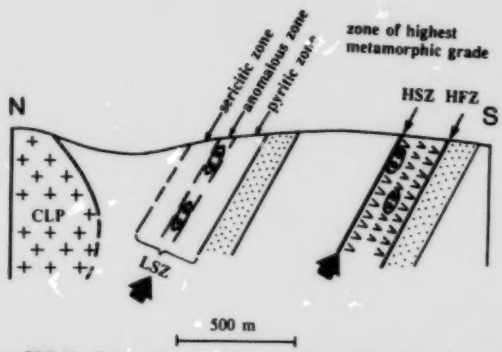

Figure 305.11. Schematic cross section of the Heron Bay Group on the White River property (lateral extent of the Local shear zone is exaggerated). Labels and stratigraphic legends as in Figure 305.2.

The close spatial and temporal association with the REE-enriched calc-silicates (Pan and Fleet 1989a, 1990; Fleet and Pan 1990) indicates the gold mineralization in the Anomalous zone from the study area is similar to that of many auriferous skarn deposits (Ray and Ettlinger 1989; Meinert 1989). However, most auriferous skarn deposits, similar to skarn deposits in general (Einaudi et al. 1981), are situated in Phanerozoic terranes and occur in spatial association with carbonate strata and granitoid intrusions. The White River gold occurrence is located within a brittle-ductile shear zone and is associated with both intermediate to felsic metavolcanic rocks and metapelitic rocks (Pan and Fleet 1989a). Recently, Mueller (1988, 1990) reported gold-silver and gold-copper skarn deposits in the Southern Cross belt, Yilgarn Block, Western Australia, and recognized that geological settings in shear zones and association with carbonate-free host rocks are indeed characteristic features of these Australian Archean auriferous skarn deposits.

The hydrothermal fluid responsible for the REE-enriched calc-silicates and gold mineralization was predominantly aqueous (low in $X(CO_2)$; cf. Liou et al. 1985). However, concentrations of other anions, such as F^-, Cl^- and HS^-, must have been elevated, as indicated by fluid inclusions of moderate salinity (Table 305.4; Figure 305.8) and the crystallization of halogen-bearing (F and Cl) allanite (Pan and Fleet 1990) and sulphide minerals. In this respect, the White River gold occurrence is, again, similar to some Phanerozoic auriferous skarn deposits (Theodore and Blake 1978; Ewers and Sun 1989) but is clearly differentiated from typical Archean lode gold deposits, which generally involved H_2O-CO_2-predominant fluids with very low salinities (<2 equivalent weight % NaCl; Figure 305.8; *see also* Ho 1987; Large et al. 1988).

It is apparent that the localization of the anomalous zone and REE-enriched calc-silicate within the brittle-ductile shear zone is attributable to the necessary permeability for the fluids during periods of dilatancy. However, the gold precipitation itself was apparently controlled largely by the pre-existing footwall pyritic zone (Figure 305.11).

Pan and Fleet (1990) recognized that the halogen-bearing allanite is lower in ferric iron content than any other allanite reported to date. The iron content in epidote from the Anomalous zone and the footwall pyritic zone (12 to 15 mol % pistacite) is also considerably lower than that stratigraphically below and above (28 to 34 mol % pistacite; Table 305.3). Experimental studies of Holdaway (1972) and Liou (1973) suggested that the pistacite content in epidote-group minerals is a function of host-rock composition, oxygen fugacity and temperature. No evidence for a dramatic change in physicochemical conditions within the brittle-ductile shear zone (relative to rocks stratigraphically below and above) during the late calc-silicate alteration was found in studies of fluid inclusions and mineral equilibria. The most reasonable explanation, then, is that a pre-existing pyritic zone controlled the composition of epidote-group minerals during the REE-enriched calc-silicate event by a sulphur-buffering reaction of the type given in reaction (1) below. This type of reaction is also favoured by the presence of pyrrhotite as the dominant sulphide associated with the late calc-silicate alteration in the Anomalous zone and pyritic zone.

There are at least 2 mechanisms by which the pre-existing pyrite could have exerted a significant control on the localization of gold deposition. Firstly, experimental studies (Sakharova and Lobacheva 1978; Mironov et al. 1981; Bancroft and Jean 1982) have demonstrated that gold is plated onto sulphides because of the piezoelectric properties of these minerals, even if the fluid is undersaturated in respect to gold. Secondly, if chloride complexes are important carriers of gold, a decrease in oxygen fugacity associated with the pre-existing pyrite would destabilize them and cause gold precipitation (Huston and Large 1989).

SUMMARY

1. The existence of a lower metamorphic zone of medium grade in the Playter Harbour Group has been confirmed.
2. The earlier Barrovian-type metamorphism peaked at a temperature of 500°C and a pressure of 6.0 to 6.5 kbars. The peak metamorphic conditions of the regional thermal metamorphism are estimated to have been 475° to 500°C and about 3 kbars in most areas and 580° ± 20°C and 4 kbars in zones of medium grade.
3. There is no systematic change in the geochemistry of fine-grained clastic metasedimentary rocks from the vicinity of the Hemlo gold deposit to the White River property.
4. Locally developed cordierite-anthophyllite rocks are restricted to a wide sedimentary sequence and most likely represent metamorphosed magnesian and iron-rich sediment that was derived mainly from ultramafic sources.
5. With the exception of a few ultramafic volcanic occurrences, the gold contents in most supracrustal rocks of this highly gold-mineralized greenstone belt are generally <10 ppb.
6. A protracted episode of skarn development has been delineated in relation to the formation of Cr-rich skarn, Fe-rich skarn, REE-enriched calc-silicates and some epidote-prehnite veins. It reflects extensive rock-fluid interaction along major dilatant structures and commenced during the waning stages of the regional thermal metamorphism, continued with a limited retrograde alteration and terminated with a late, low- to very low-grade calc-silicate alteration.
7. Polymetallic sulphides in Cr-rich and Fe-rich skarns largely reflect the sporadic high concentrations of transition metals in host lithologies. Although most sulphides in these two skarns formed during the earlier stages of the skarn development, additional crystallization also occurred during the retrograde alteration and late calc-silicate alteration.
8. Gold mineralization in the Anomalous zone resembles Proterozoic auriferous skarn deposits in respect to its spatial and temporal association with abundant calc-silicates but is clearly differentiated from typical Archean lode gold deposits by fluid inclusions of a moderate salinity. Although the brittle-ductile shear zone almost certainly provided necessary permeability for the fluid responsible for gold mineralization and the REE-enriched calc-silicates during phases of dilatation, the gold precipitation itself was largely controlled by a pre-existing pyritic zone.

ACKNOWLEDGMENTS

We thank L.D. Meinert, R.W. Hodder, R.L. Barnett, N.D. MacRae and A.G. Mueller for discussions and helpful suggestions; and LAC Minerals Ltd. for access to the White River property and provision of drill-core materials and mapping information, especially R.A. Campbell for his contribution to the field work. We also wish to thank J.A. Forth for preparation of polished thin section, R.L. Barnett and D.M. Kingston for assistance with microprobe analyses and D.M. Kingston and D.W. McDonald for assistance with fluid-inclusion techniques.

$$Fe^{3+}\text{-silicate} + 0.5S_2 + Al^{3+} + 1.5H_2O = Al^{3+}\text{-silicate} + FeS + 3H^+ + 0.75O_2 \qquad (1)$$

REFERENCES

Bancroft, G.M. and Jean, G. 1982. Gold deposition at low temperature on sulphide minerals; Nature (London), v.298, p.730-731.

Berman, R.G., Brown, T.H. and Greenwood, H.J. 1985. An internally consistent thermodynamic data set for minerals in the system Na_2O-K_2O-CaO-MgO-FeO-Fe_2O_3-Al_2O_3-SiO_2-TiO_2-H_2O-CO_2; Atomic Energy of Canada Ltd., Technical Report 377, 62p.

Burk, R., Hodgson, C.J. and Quartermain, R.A. 1986. The geological setting of the Teck-Corona Au-Mo-Ba deposit, Hemlo, Ontario, Canada; *in* Proceedings of Gold'86, an International Symposium on the Geology of Gold, Toronto, Ontario, edited by A.J. Macdonald, Konsult International Inc., Willowdale, p.311-326.

Cho, M. and Liou, J.G. 1987. Prehnite-pumpellyite to greenschist facies transition in the Karmutsen metabasites, Vancouver Island, B.C.; Journal of Petrology, v.28, p.417-443.

Condie, K.C. 1981. The Archean greenstone belts; *in* Developments in Precambrian geology, v.3, edited by B.F. Windley, Elsevier, Amsterdam, 434p.

Corfu, F. and Muir, T.L. 1989. The Hemlo–Heron Bay greenstone belt and Hemlo Au-Mo deposit, Superior Province, Ontario, Canada. 2. Timing of metamorphism, alteration and Au mineralization from titanite, rutile and monazite U-Pb geochronology; Chemical Geology, v.79, p.201-223.

Danchin, R.V. 1967. Chromium and nickel in the Fig Tree shale from South Africa; Science, v.158, p.261-262.

Einaudi, M.T., Meinert, L.D. and Newberry, R.J. 1981. Skarn deposits; Economic Geology, 75th Anniversary Volume, p.317-391.

Ewers, G.R. and Sun, S-S. 1989. Genesis of the Red Dome skarn deposit, northeast Queensland; *in* The geology of gold deposits: the perspective in 1988, edited by R.R. Keays, W.R.H. Ramsay and D.I Groves, Economic Geology, Monograph 6, p.218-232.

Fleet, M.E. and Pan, Y. 1990. Cr-rich, Fe-rich and REE-enriched skarns in gold-mineralized greenstone belt terrane, Hemlo area, Ontario: correlation of metallogenic association with host lithology [abstract]; *in* Gold'90, Salt Lake City, Utah, February 26–March 1.

Ganguly, J. and Saxena, S. 1987. Mixtures and mineral reactions. Minerals and rocks; v.19, Springer-Verlag, Berlin, 291p.

Ghent, E.D., Robbins, D.B. and Stout, M.Z. 1979. Geothermometry, geobarometry and fluid compositions of metamorphosed calc-silicates and pelites, Mica Creek, British Columbia; The American Mineralogist, v.64, p.874-885.

Graham, C.M. and Powell, R. 1984. A garnet-hornblende geothermometer: calibration, testing and application to the Pelona Schist, southern California; Journal of Metamorphic Geology, v.2, p.13-22.

Harris, D.C. 1989. Mineralogy and geochemistry of the Hemlo gold deposit, Hemlo, Ontario; Geological Survey of Canada, Economic Geology Report 38, 88p.

Ho, S.E. 1987. Fluid inclusions: their potential as an exploration tool for Archean gold deposits; *in* Recent advances in understanding Precambrian gold deposits, edited by S.E. Ho and D.I. Groves, Geology Department and University Extension, The University of Western Australia, Perth, Western Australia, Publication no.11, p.239-263.

Hodgson, C.J. and MacGeehan, P.J. 1982. Geological characteristics of gold deposits in the Superior Province of the Canadian Shield; *in* Geology of Canadian gold deposits, edited by R.W. Hodder and W. Petruk, Canadian Institute of Mining and Metallurgy, Special Volume 24, p.211-229.

Holdaway, M.J. 1972. Thermal stability of Al-Fe epidote as a function of fO_2 and Fe content; Contributions to Mineralogy and Petrology, v.37, p.307-340.

Holding, D.C. 1987. The LAC Minerals Ltd. Cadi zone: a petrographic-geochemical study; unpublished BSc thesis, The University of Western Ontario, London, Ontario, 46p.

Hugon, H. 1986. The Hemlo gold deposit, Ontario, Canada: a central portion of a large scale, wide zone of heterogeneous ductile shear; *in* Proceedings of Gold'86, an International Symposium on the Geology of Gold, Toronto, Ontario, edited by A.J. Macdonald, Konsult International Inc., Willowdale, p.379-387.

Huston, D.L. and Large, R.R. 1989. A chemical model for the concentration of gold in volcanogenic sulphide deposits; Ore Geology Reviews, v.4, p.171-200.

Indares, A. and Martingnole, J. 1985. Biotite-garnet geothermometry in the granulite facies: the influence of Ti and Al in biotite; The American Mineralogist, v.70, p.272-278.

Jensen, L.S. 1976. A new cation plot for classifying subalkalic volcanic rocks; Ontario Geological Survey, Miscellaneous Paper 66, 22p.

Kaneda, H., Takenouchi, S. and Shoji, T. 1986. Stability of pentlandite in the Fe-Ni-Co-S system; Mineralium Deposita, v.21, p.169-180.

Keays, R.R. 1984. Archean gold deposits and their source rocks: the upper mantle connection; *in* Gold'82, Zimbabwe, edited by R.P. Foster, A.A. Balkema, Rotterdam, p.17-51.

Keevil, N.D. 1942. Vapour pressure of aqueous solutions at high temperatures; Journal of the American Chemical Society, v.64, p.823-830.

Kohn, M.J. and Spear, F.S. 1990. Two new geobarometers for garnet amphibolites and applications to southern Vermont; American Mineralogist, v.75, p.89-96.

Koziol, A.M. 1989. Recalibration of the plagioclase-garnet-Al_2SiO_5-quartz (GASP) geobarometry and applications for natural assemblages; Eos, v.70, p.493.

Large, R.R., Huston, D.L. and McGoldrick, P.J. 1988. Gold distribution and genesis in Paleozoic volcanogenic massive sulphide systems, eastern Australia; *in* Bicentennial Gold'88, Melbourne, Victoria, edited by A.D.T. Goode and L.I. Bosma, Geological Society of Australia, p.121-126.

Liou, J.G. 1973. Synthesis and stability relations of epidote, $Ca_2Al_2FeSi_3O_{10}(OH)$; Journal of Petrology, v.4, p.381-413.

Liou, J.G., Maruyama, S. and Cho, M. 1985. Phase equilibria and mixed parageneses of metabasites in low-grade metamorphism; Mineralogical Magazine, v.49, p.345-356.

McLennan, S.M. and Taylor, S.R. 1984. Archean sedimentary rocks and their relation to the composition of the Archean continental crust; p.47-72 *in* Archean geochemistry, edited by A. Kroner, G.N. Hanson and A.M. Goodwin, Springer-Verlag, Berlin.

McLennan, S.M., Taylor, S.R. and Eriksson, K.A. 1983. Geochemistry of Archean shales from the Pilbara Supergroup, Western Australia; Geochimica et Cosmochimica Acta, v.47, p.1211-1222.

Meinert, L.D. 1984. Mineralogy and petrology of iron skarns in western British Columbia, Canada; Economic Geology, v.79, p.869-882.

———1989. Gold skarn deposits and exploration criteria; *in* The geology of gold deposits: the perspective in 1988, edited by R.R. Keays, W.R.H. Ramsay and D.I. Groves, Economic Geology, Monograph 6, p.537-552.

Meyer, M. and Saager, R. 1985. The gold content of some Archean rocks and their possible relationship to epigenetic gold-quartz vein deposits; Mineralium Deposita, v.20, p.284-289.

Mironov, A.G., Zhmodik, S.M. and Maksimova, E.A. 1981. An experimental investigation of the absorption of gold by pyrites with different thermoelectric properties; Geochemistry International, v.18, p.153-160.

Mueller, A.G. 1988. Archean gold-silver deposits with prominent calc-silicate alteration in the Southern Cross greenstone belt, Western Australia: analogues of Phanerozoic skarn deposits; Geology Department and University Extension, The University of Western Australia, Perth, Western Australia, Publication no.12, p.141-163.

———1990. Archean Cu-Au and Au-Ag deposits in the Yilgarn Block, Western Australia: greenstone-hosted and shear-zone-controlled skarns; *in* Gold'90, Salt Lake City, Utah, February 26–March 1.

Muir, T.L. 1982a. Geology of the Hemlo area, District of Thunder Bay; Ontario Geological Survey, Geological Report 217, 65p.

———1982b. Geology of the Heron Bay area, District of Thunder Bay; Ontario Geological Survey, Geological Report 218, 89p.

———1988. Hemlo tectonic-stratigraphic study, District of Thunder Bay; Ontario Geological Survey, Miscellaneous Paper 141, p.226-239.

Muir, T.L. and Elliott, A.G. 1987. Hemlo tectonic-stratigraphic study, District of Thunder Bay; Ontario Geological Survey, Miscellaneous Paper 137, p.117-129.

Naqvi, S.M., Sawkar, R.h., Subba Rao, D.V., Govil, P.K. and Gnaneswar Rao, T. 1988. Geology, geochemistry and tectonic setting of Archean greywackes from Karnataka nucleus, India; Precambrian Research, v.39, p.193-216.

Pan, Y. 1990. Metamorphic petrology and gold mineralization of the White River gold prospect, Hemlo area, Ontario; unpublished PhD thesis, The University of Western Ontario, London, Ontario, 256p.

Pan, Y. and Fleet, M.E. 1988. Metamorphic petrology of the White River gold prospect, Hemlo area; *in* Geoscience Research Grant Program, summary of research, 1987–1988, Ontario Geological Survey, Miscellaneous Paper 140, p.65-176.

———1989a. Metamorphic petrology and gold mineralization of the White River gold prospect, Hemlo area; *in* Geoscience Research Grant Program, summary of research, 1988–1989, Ontario Geological Survey, Miscellaneous Paper 143, p.42-52.

———1989b. Cr-rich calc-silicates from the Hemlo area, Ontario; The Canadian Mineralogist, v.27, p.565-577.

———1990. Halogen-bearing allanite from the White River gold occurrence, Hemlo area, Ontario; The Canadian Mineralogist, v.28, p.67-75.

Patterson, G.C. 1984. Field trip guidebook to the Hemlo area; Ontario Geological Survey, Miscellaneous Paper 118, 33p.

Perkins, E.H., Brown, T.H. and Berman, R.G. 1986. PTX-SYSTEM: three programs for calculation of pressure-temperature-composition phase diagrams; Computers and Geosciences, v.12, p.949-755.

Phillips, G.N., Groves, D.I. and Brown, I.J. 1987. Source requirements for the Golden Mile, Kalgoorlie: significance to the metamorphic replacement model for Archean gold deposits; Canadian Journal of Earth Sciences, v.24, p.1643-1651.

Potter, R.W. and Brown, D.L. 1977. The volumetric properties of aqueous sodium chloride solutions from 0 to 500°C at pressures up to 2000 bars based on a regression of available data in literature; United States Geological Survey, Bulletin 1421-C, 36p.

Potter, R.W., Clynne, M.A. and Brown, D.L. 1978. Freezing point depression of aqueous sodium chloride solutions; Economic Geology, v.73, p.284-285.

Ray, G.E. and Ettlinger, A.D. 1989. Precious metal enriched skarns in British Columbia: an overview and geological study; Geological Survey Branch, British Columbia Ministry of Mines and Petroleum Resources, Paper 1989-3, 128p.

Reinhardt, J. 1987. Cordierite-anthophyllite rocks from north-west Queensland, Australia: metamorphosed magnesian pelites; Journal of Metamorphic Geology, v.8, p.451-472.

Robinson, D.J. and McMillan, R.H. 1985. Introduction and overview metallogenesis of the Hemlo–Manitouwadge–Winston Lake greenstone belt; *in* Gold and copper-zinc metallogeny within metamorphosed greenstone belt terrane, Hemlo–Manitouwadge–Winston Lake, Ontario, Canada, edited by R.H. McMillan and D.J. Robinson, Geological Association of Canada–Canadian Institute of Mining and Metallurgy, p.1-5.

Roedder, E. 1984. Fluid inclusions; Mineralogical Society of America, Reviews in Mineralogy, v.12, 644p.

Sakharova, M.S. and Lobacheva, I.K. 1978. Microgalvanic systems involving sulfides and gold-bearing solutions, and characteristics of gold deposition; Geochemistry International, v.15, p.152-157.

Siragusa, G.M. 1983. White River area, District of Thunder Bay; *in* Summary of field work and other activities 1983, Ontario Geological Survey, Miscellaneous Paper 116, p.41-44.

Stamatelopoulou-Seymour, K. and Francis, D.M. 1980. An Archean ultramafic turbidite from Lac Guyer, James Bay area, Quebec, Canada. Canadian Journal of Earth Sciences, v.17, p.1576-1582.

Sun, S-S. and Nesbitt, R.W. 1978. Petrogenesis of Archean ultrabasic and basic rocks: evidence from rare earth elements; Contributions to Mineralogy and Petrology, v.65, p.301-325.

Theodore, T.G. and Blake, D.W. 1978. Geology and geochemistry of the west ore body and associated skarns, Copper Canyon porphyry copper deposits, Lander County, Nevada; United States Geological Survey, Professional Paper 748-C.

Walford, P., Stephens, J., Skrecky, G. and Barnett, R. 1986. The geology of the 'A' zone, Page-Williams Mine, Hemlo, Ontario, Canada; *in* Proceedings of Gold'86, an International Symposium on the Geology of Gold, Toronto, Ontario, edited by A.J. Macdonald, Konsult International Inc., Willowdale, p.362-378.

Grant 319 Gypsum Deposits of Southern Ontario

S.J. Haynes and J. Hughes-Pearl

Department of Geological Sciences, Brock University, St. Catharines

ABSTRACT

This paper details the geology of the mined gypsum bed and enclosing strata at the Canadian Gypsum Company Ltd. Mine at Hagersville (Canadian Gypsum). From comparison with known stratigraphy across the Algonquin Arch, from holes drilled near Drumbo and Welland, the Canadian Gypsum sequence appears to correlate with the Upper Silurian Salina Formation E unit. Although vertical exposure is limited to 6 m at Canadian Gypsum, 4 sedimentary cycles were recognized, each (with the exception of the upper, incomplete cycle) capped by gypsum. Although each cycle changes vertically upward from shale and mudstone, through dolostone to gypsum, each displays significant differences in sedimentary structures and textures that are directly related to changes in depositional environment: from a subtidal, through intertidal, to supratidal sabkha deposition in the first cycle; to deposition in tidal mud flats, through carbonate-gypsum crystal mushes of the intertidal-supratidal interface, to the thick gypsum (mined gypsum bed) characteristic of the lower part of a coastal salina in the second cycle; to carbonate boxworks (capped by desiccation features) overlain by stromatolites, algal and boundstone veneers and terminal evaporites in the third cycle. The fourth, incomplete cycle consists of gypsiferous laminated shales that represent deposition as either terrestrial (playa) or marine (mud flat) sedimentation.

The mined bed has been severely deformed by ductile shear fabrics and both small and large thrusts, one of which has displaced the bed 4 m vertically. This deformation obliterated most of the original sedimentary textures and enriched the ore by pressure-solution dissolution of dolomite. This accounts for the higher grade of ore at Canadian Gypsum compared with the Westroc deposit, which displays nodular textures similar to those present in the areas of low strain at Canadian Gypsum.

The previously proposed modern analogue (invoked to explain differences in the Salina A between the Westroc and Domtar deposits) of the semiarid coastal zone of northern Egypt—where gypsum is depositing in sabkha-fringed lagoons and coastal salinas, as well as continental salinas and playas—can be extended to the Salina E to explain the rapid lateral and vertical facies changes.

INTRODUCTION

This paper is the third in a series concerning the gypsum deposits of southwestern Ontario. All the deposits are hosted by the Upper Silurian Salina Formation and are located on the eastern flank of the Algonquin Arch, which separates the Michigan and Appalachian basins (Figure 319.1). In 1988, these deposits produced 1 458 800 t of gypsum, valued at $19 712 000 (McKnight and Fell 1989). The Domtar Construction Materials (Domtar), Caledonia, and the Westroc Industries Ltd. (Westroc), Drumbo, deposits were described in previous publications (Haynes et al. 1988, 1989; Haynes and Hughes-Pearl 1989).

This paper describes the geology of the Canadian Gypsum Company Ltd. deposit ("Canada Gypsum", Figure 319.1) at Hagersville, where production commenced in 1931. Annual production in 1985 was about 500 000 t (Fowler and Adams 1988). The deposit is located about 20 m below surface and is accessed via a decline. Information on the early operations and a brief description of the geology were given in Guillet (1964), the only published report on the deposit. The present study characterizes the geology of the deposit in terms of both the enclosing host rocks and the vertical and lateral variation of the mined gypsum bed. An additional objective of this study was to determine the stratigraphic position of the mined gypsum bed, its relationship to facies variations in the Salina Formation, and the likely environment of deposition from comparison with both modern evaporites and the previously described Domtar and Westroc deposits.

REGIONAL STRATIGRAPHIC SETTING OF THE CANADIAN GYPSUM MINE

The Niagara Peninsula, the area east of the Algonquin Arch, contains mixed Upper Silurian facies of both the Michigan and Appalachian basins. Stratigraphic correlation across the Algonquin Arch is difficult because of the lack of reliable stratigraphic time lines and controversy over facies relationships and diachroneity. Geophysical logs, in particular gamma-ray logs, have been used successfully to correlate the major Upper Silurian units across the Michigan and Appalachian basins (Carter 1987). All the gypsum deposits are hosted by the Salina Formation. Recent descriptions of the Salina Formation were given in Haynes et al. (1988, 1989) and Haynes and Hughes-Pearl (1989), from which the following has been condensed.

Within the Niagara Peninsula, the Salina A unit is divided into the A-1 and A-2 subunits. Halite, limestone and anhydrite of the A-1 and A-2 subunits in the Michigan Basin change progressively eastwards to dolostone, dolomitic shales and anhydrite (gypsum) in the Niagara Peninsula and to shale and anhydrite in the Appalachian Basin. Over the Algonquin Arch, the basal A-2 anhydrite unit is the mined gypsum bed at the Westroc Industries Mine at Drumbo. The Salina B unit consists of dolomitic shales in the Niagara Peninsula that can be correlated from the Algonquin Arch eastwards to the Appalachian Basin. The base of the B unit throughout southeastern Ontario is characterized by an

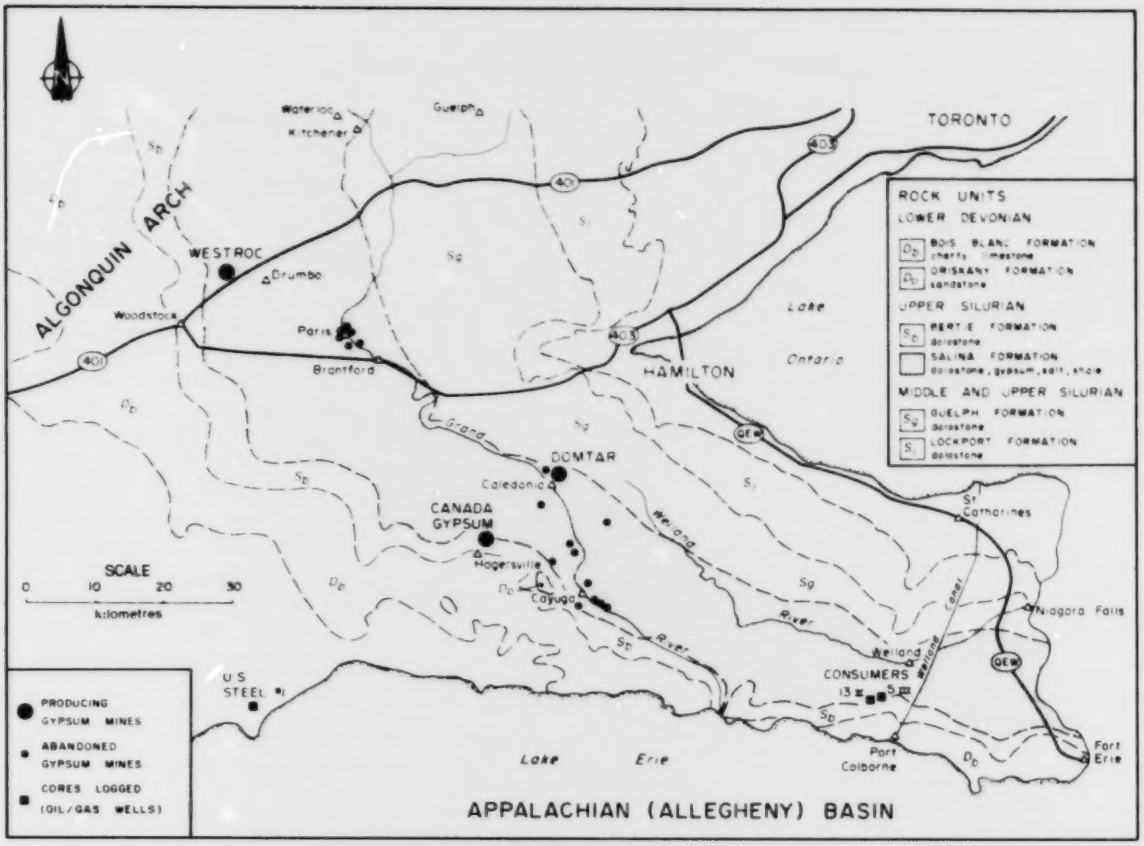

Figure 319.1. Gypsum deposits and geology, Niagara Peninsula, Ontario.

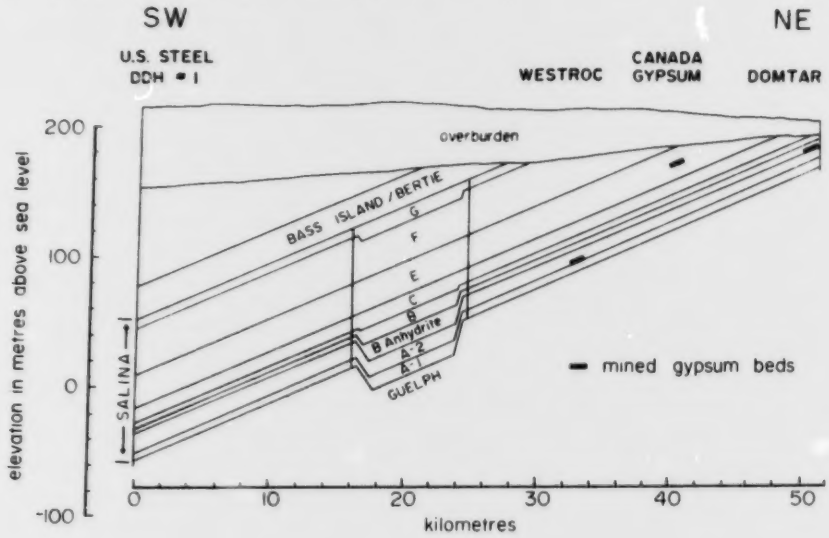

Figure 319.2. Plot of position and elevation of the Canadian Gypsum deposit on a downdip section, suggesting it forms part of the Salina E unit.

extensive anhydrite unit called the "B anhydrite", which constitutes the mined gypsum bed at the Domtar Ltd. property at Caledonia. The Salina C unit appears as a consistent sequence of shales throughout the Michigan and Appalachian basins and the Algonquin Arch. The Salina D unit is present as halite-rich evaporites in both the Michigan and Appalachian basins. Carter (1987) considered the D unit as essentially absent in the Niagara Peninsula. However, recent comparison of the geophysical logs of holes drilled in the Niagara Peninsula indicates that the D unit is often

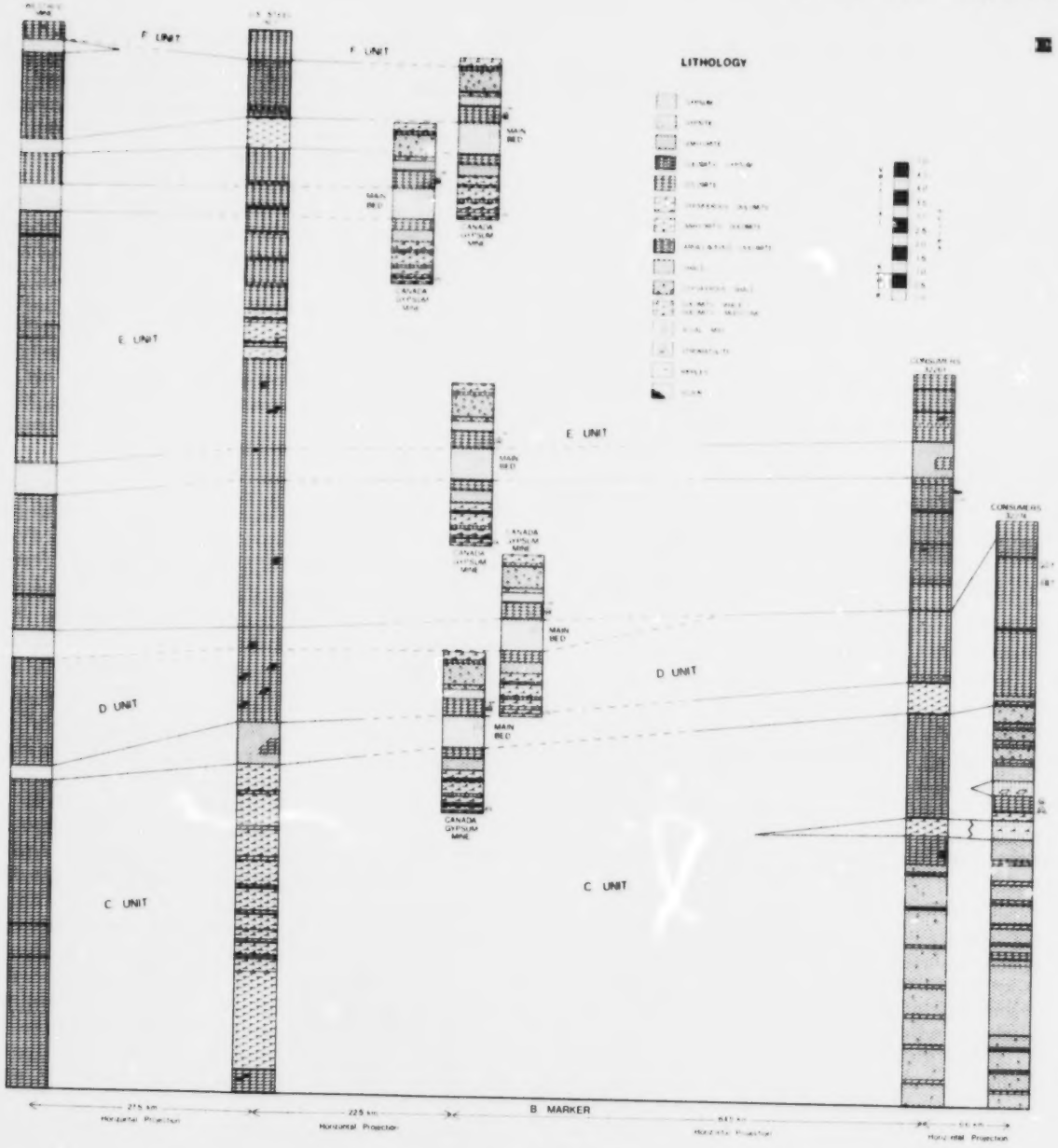

Figure 319.3. Along-strike regional correlation of the upper Salina Formation from the Westroc deposit to the Welland area, showing possible positions of the Canadian Gypsum deposit.

present as a thin, anhydrite- or gypsum-rich unit (unpublished work in conjunction with T. Carter, 1989). In southwestern Ontario, the Salina E unit consists of dolostone and argillaceous dolostone with local anhydrite beds. These facies become more argillaceous in both the Michigan and Appalachian basins. The Canadian Gypsum deposit at Hagersville is probably hosted by either the Salina D or E unit. The lower Salina F unit comprises a sequence of halite and dolostone in the Michigan Basin and a thick sequence of halite, dolomitic shales and thin anhydrite beds in the Appalachian Basin. These sequences are absent over the Algonquin Arch and the Niagara Peninsula. The upper F unit is present as shale in the Michigan Basin. This changes over the Algonquin Arch to dolostone overlain by shale, with thin anhydrite beds in the Niagara Peninsula and Appalachian Basin. The Salina G unit changes from argillaceous dolostone, with anhydrite, in the Michigan Basin to dolostone in the Appalachian Basin.

At the Canadian Gypsum Mine, Hagersville ("Canada Gypsum", Figure 319.1), only a limited stratigraphic section is exposed. Also, no oil or gas company holes have been cored to the Salina–Guelph contact in the vicinity of the

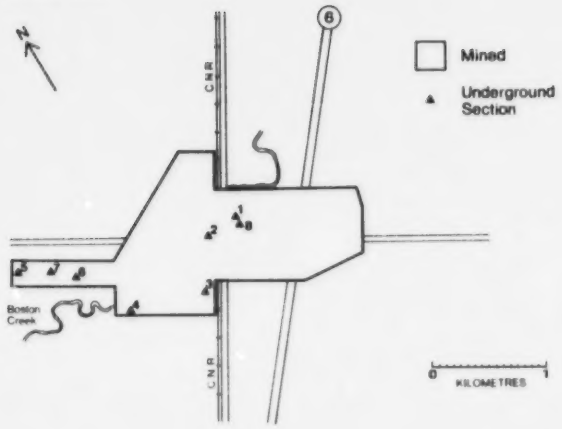

Figure 319.4. Plan of the Canadian Gypsum Company Ltd. Mine at Hagersville. Highway 6 is also shown.

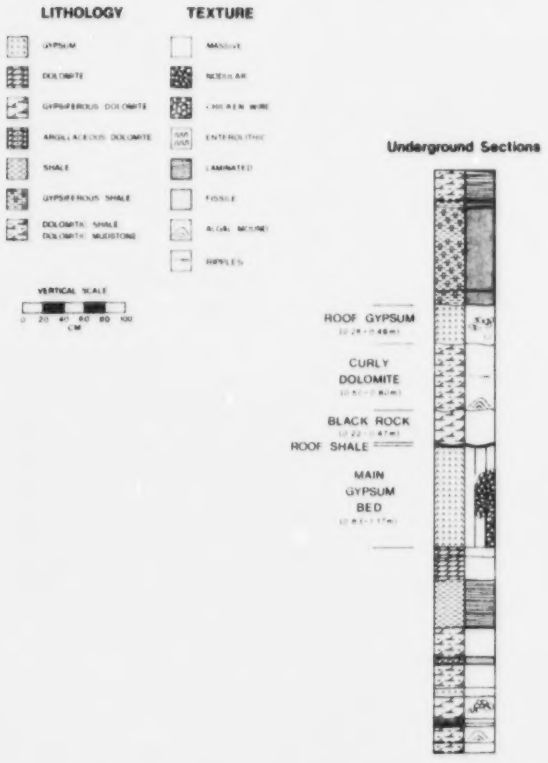

Figure 319.5. Geologic compilation of the Canadian Gypsum Company Ltd. Mine at Hagersville.

mine. In an attempt to determine the stratigraphic position of the Canadian Gypsum deposit, an approximately downdip section was constructed from the Domtar deposit, to the northeast, to the U.S. Steel Company hole #1 at Charlotteville, to the southwest (*see* Figure 319.1 for locations). At both localities the stratigraphy and elevations are known. Plotting the position and elevation of the Canadian Gypsum deposit with an assumed uniform dip of the units suggests that the Canadian Gypsum sequence forms part of the Salina E unit (Figure 319.2). Approximately along-strike correlation of the stratigraphy determined by Haynes (1989) from cores and geophysical logs of oil and gas company holes located between Drumbo and Welland (northwest to southeast across the Niagara Peninsula) indicates that there are rapid facies variations and that the Canadian Gypsum Mine sequence (detailed below) may correlate with several evaporite units (gypsum and anhydrite) in either the Salina D or E unit, and possibly even the Salina C and F units (Figure 319.3). Unfortunately, cores of holes drilled at, or in, the vicinity of the Westroc Mine (by both Westroc Industries Ltd. and various oil and gas companies) are not available, and geophysical logs are not available for either the Westroc Mine or the U.S. Steel Company drill hole at Charlotteville. Thus, until holes are drilled to the Guelph Formation in the vicinity of Hagersville, the exact stratigraphic position of the Canadian Gypsum sequence cannot be accurately determined.

GEOLOGY OF THE CANADIAN GYPSUM DEPOSIT

Mine Stratigraphy and Lithologies

The Canadian Gypsum deposit is a room and pillar operation accessed by a decline from surface. Mining operations extend about 3.5 km west-northwest and about 1.5 km north-northeast (Figure 319.4). No drill core was available for examination, and vertical exposure of the mined bed and enclosing units is limited to 6 m (Figure 319.5). Significant exposure of enclosing units is limited to a 2.3 m section, below the mined gypsum bed (here termed the "Main gypsum bed"), in the mine sump (section 6, Figure 319.4); and a 2.8 m section, above the Main gypsum bed, exposed in the decline (section 8, Figure 319.4) and in the ore-conveyor haulageway (section 2, Figure 319.4). Unlike the other producing gypsum mines (Domtar and Westroc, Figure 319.1), where the stratigraphic position can be determined by direct measurement from the contact of the Salina and Guelph formations (Haynes et al. 1988, 1989; Haynes and Hughes-Pearl 1989), no reliable stratigraphic datum horizon is available for the Canadian Gypsum deposit. However, from regional compilation and comparison, the stratigraphic position of the Canadian Gypsum sequence is constrained between the upper part of the Salina C unit and the lower part of the Salina F unit and is probably part of the Salina E unit (Figures 319.2 and 319.3). Guillet (1964, p.88) quoted company officials as saying, "...the Hagersville seam corresponds stratigraphically with that mined in Genesee County, New York, in the vicinity of Oakfield...". The U.S. Gypsum Company, which operates the Oakfield Mine and is the parent of Canadian Gypsum, retains this view (personal communications, 1987–1989). However, both Cole (1925) and Dyer (1925) pointed out that no economic gypsum beds had been drilled in Welland County, Ontario (Welland, Figure 319.1). Stratigraphic analysis (Haynes 1989) of Consumers Gas Co. holes, cored recently in Welland County (Consumers, Figure 319.1), confirms Cole's and Dyer's information but also illustrates that facies change rapidly

over distances as small as 6.6 km (*see* stratigraphy of Consumers 32261 and 32274, Figure 319.3). Thus, caution should be used in direct correlation of the Canadian Gypsum and Oakfield sequences, although it is entirely possible that both Canadian Gypsum and Oakfield correlate with the 1.2 m thick anhydrite layer near the top of Consumers hole 32261 and with the third gypsum bed above the Salina Formation B marker at the Westroc Mine (compiled from Westroc Industries Ltd. company core logs). If so, this would place the Canadian Gypsum sequence in the lower third of the Salina E unit (middle of the 5 possible correlations in Figure 319.3). The stratigraphy, lithology and textures of the Canadian Gypsum sequence were determined from 1:10 scale mapping of vertical exposures in the sump, decline and conveyor haulageway. A compilation of this is presented in Figure 319.5.

The lowermost unit exposed in the mine sump is 0.1+ m (base not exposed) of massive, brown, dolomitic mudstone. This is overlain by 0.16 m of finely laminated, brown dolomite, containing numerous carbonaceous partings, that commonly forms mound structures. This is capped by a 3 mm satin spar layer, then a 3 cm layer of broken and thin-bedded, brown, dolomitic mudstone with selenite eyes; both of these continue, without thinning, over underlying mounds. These layers are overlain by a 5 to 8 cm bed of brown dolomite, containing numerous 2 mm discoid selenite eyes, that thins over underlying mound structures such that its upper surface is essentially horizontal, with only a slight doming over the mounds. This is followed by 0.22 m of gypsiferous dolomite to dolomitic gypsum, consisting of a complex mixture of brown, finely laminated dolomite (layers, clasts and wisps) and white gypsum (displaying enterolith, nodular and chicken-wire mosaic textures). Locally, areas of enterolith and nodular gypsum exhibit recumbent folds. Vertical gypsum-filled fractures are present in the top 4 cm. The upper contact with an overlying 0.05 to 0.10 m layer of massive gypsum is undulatory and varies from sharp to gradational. Above the massive gypsum layer the lithology changes abruptly to shales (*see* below). The lithologies, textures and structures of this basal 0.65 m sequence are consistent with similar features observed at the intertidal-supratidal interface of modern sabkhas: the brown colour of the dolomites and dolomitic mudstones indicates oxidizing supratidal to intertidal conditions; the finely laminated dolomite, interlayered with carbonaceous material and forming mounds, is indicative of an intertidal algal mat; the overlying dolomite with crowded selenite disks is identical to the gypsum-carbonate crystal mushes of the supratidal-intertidal interface described from Persian Gulf sabkhas by Warren and Kendall (1985) and Scholle et al. (1987); the upper part of the sequence, comprising thin-bedded gypsiferous dolomite to gypsum, with abundant enteroliths and folded nodular layers, is identical to the supratidal evaporite sequences overlying the selenite crystal mushes of the Persian Gulf (Warren and Kendall 1985; Scholle et al. 1987; Warren 1989). Similar ancient sequences containing ~2 mm crowded disks of selenite or anhydrite have been described by West (1975, 1979) in the Jurassic Purbeck beds of southern England and by Shinn (1983) in the Permian Grayburg and Queen formations of west Texas. Both authors considered this texture as having developed as early diagenetic crystals in a supratidal to intertidal environment.

This basal sequence is overlain by a 1.29 m sequence of argillaceous units (Figure 319.5). The argillaceous sequence commences with 0.46 m of black (passing upward to grey), thin-bedded, laminated, dolomitic shale that exhibits a sharp, carbonaceous lower contact. The upper contact with 0.07 m of grey, highly fissile, argillaceous dolomite is also sharp. This dolomite is overlain by 0.29 m of grey brown, dolomitic shale displaying undulatory, fine laminations. The upper unit of the sequence comprises 0.47 m of finely laminated brown shale, with gradational contacts. The upward colour variation of this sequence, from black to brown, suggests that deposition started with anaerobic subaqueous conditions but changed to an oxidizing environment that may have been either intertidal or subaerial (wind-blown clays). Consideration of the postulated supratidal environment of the underlying lithologies suggests that this argillaceous sequence was deposited as mud either in an ephemeral coastal lake (playa or salina) or in a sabkha tidal flat (subtidal to intertidal) during marine incursion.

The argillaceous sequence is overlain by 0.34 m of brown to buff dolostones (2 units) that underlie the Main gypsum bed (Figure 319.5). The basal dolostone unit consists of 0.24 m of brown dolomite. The lower contact of this unit is gradational with the underlying brown shale: the basal 4.5 cm of the dolomite contains 4 to 15 mm thick patches of dark mud. The lower 0.15 m contains 9 undulatory carbonaceous partings spaced 1 to 4 cm apart. The upper 0.09 m, above a carbonaceous parting, is more massive and is marked by randomly oriented discoid selenite eyes, 0.25–2 mm thick (average 0.5 mm). Gypsum nodules (2 to 15 mm in diameter) and 0.05 to 1.5 mm thick satin spar seams (occasionally bifurcating) are spaced irregularly throughout the unit. The basal dolostone is overlain, with a sharp, undulatory, carbonaceous-coated contact, by 0.10 m of massive dolomite distinguished by 1 to 5 mm colour bands and dispersed, randomly oriented, 2 to 5 mm (average 2 mm) discoid selenite eyes. This dolostone sequence is interpreted as a gypsum-carbonate mush (*see* above). With reference to the possible depositional environments of the underlying argillaceous sequence, it is likely that the dolostones were deposited either at the subaqueous-subaerial interface of an ephemeral coastal lake or at the intertidal-supratidal interface of a marine sabkha mud flat.

In places, the dolostone sequence is separated from the overlying Main gypsum bed by a 1 cm thick satin spar veinlet. Although details of the Main gypsum bed are described below, a summary of its main characteristics is included here. It varies in thickness from 0.83 to 1.17 m. Lithologically, it consists of gypsum rock (>85% gypsum) with minor dolomite as wisps and matrix to nodular and chicken-wire mosaic textures. Although upper and lower contacts are nearly horizontal and usually display large-scale undulation, deformation of the bed is clearly evident. This is present as ductile shear arrays that have significantly distorted the original sedimentary fabric. Usually, shear deformation is constrained by the upper and lower contacts of the bed: it is more intense in the central

parts. However, locally, the bed is displaced vertically along small thrusts. At 2 localities in the mine, large-scale duplex ramps have elevated and displaced the bed vertically by several metres. Nodular and chicken-wire mosaic textures are common, and enterolithic textures are minor, in areas of low strain (often close to the upper and lower contacts). The ductile shear stress has caused plastic flow and concentration of the gypsum; this has resulted in a lithologically massive gypsum (albeit with an apparent shear fabric) as the dominant texture. This is in marked contrast to the gypsum beds at the Domtar mines, where shear is essentially absent, and the Westroc Mine, where shear is local (Haynes et al. 1988, 1989; Haynes and Hughes-Pearl 1989). As the shear deformation has often obliterated the original sedimentary fabrics and textures, it is impossible to postulate a depositional environment with any certainty. However, on the basis of locally preserved textures in the mined bed and the likely depositional environments of the enclosing lithologies, we suggest that the Main gypsum bed formed in a coastal salina.

The Main gypsum bed is capped irregularly by a thin, fissile, dolomitic shale (0 to 12 cm thick) that is called the "Roof shale" (mine term). It is composed of 1 to 4 cm bands distinguished by marked differences in colour (across sharp contacts) from black, to grey to light grey. The black bands are carbonaceous. The shale probably represents fluvial incursion (during annual rainy seasons) as the salina lake became infilled and its hydraulic head with marine waters diminished, as with the coastal salina lakes of South Australia (Warren 1982a, 1982b; Warren and Kendall 1985). However, deposition as a sabkha tidal mud flat during a marine incursion cannot be ruled out.

Overlying the Roof shale (or the Main gypsum bed where the Roof shale is absent) is the "Black rock" (mine term). This was examined at sections 1, 2, 5 and 8. It is a thin-bedded, massive, dark grey dolomite (0.22 to 0.47 m thick) that exhibits fine colour banding and, locally, fine laminations. Its lower contact with the Roof shale varies from sharp to gradational. The upper part becomes browner grey, and the top is marked by small teepee structures (approximately 10 cm high and 30 cm wide) and brecciation. Its upper contact is highly irregular. It is overlain by the "Curly dolomite" (mine term), a 0.5 to 0.8 m thick reddish brown dolomite to dolomitic mudstone, characterized by fine, wavy laminae. The lower part of the Curly dolomite is marked by algal mounds. These are usually small (about 10 cm high), coalesced and bounded by subhorizontally laminated algal laminae. However, larger isolated stromatolite mounds, enclosed by massive dolomite, are present locally (e.g., at section 3, an isolated mound is 20 cm high and 50 cm wide). The upper half of the Curly dolomite comprises thin beds of finely laminated, brown dolomites and dolomitic mudstones, interspaced with millimetre-thick beds and elongated lenses of gypsum. Ripple-mark casts often occur at the contact of dolomitic mudstones with overlying dolomites. The Curly dolomite is overlain, with an undulating contact, by a 0.28 to 0.46 m thick bed of nodular to massive gypsum ("Roof gypsum", mine term). The nodules are large (up to 20 cm in diameter) and commonly form a mosaic texture. The entire sequence from the Main gypsum bed to the Roof gypsum is similar to the upper parts of the coastal salinas of South Australia described by Warren (1982a, 1982b) and satisfies the criteria for distinguishing coastal salinas from sabkhas given by Warren and Kendall (1985). The Black rock dolostones are interpreted as the subaqueous carbonate boxwork that forms around the margins of a coastal salina (*see* Warren 1982b). As the coastal salina infilled, subaerial desiccation resulted in the teepee structures and brecciation at the top of the Black rock, whereas the large isolated stromatolitic mounds at the base of the Curly dolomite could have formed in areas of groundwater resurgence; such subaerial features and domal stromatolites are characteristic of coastal salinas (Warren and Kendall 1985). The algal mounds and laminations that form much of the Curly dolomite are identical to the algal veneers that form at the margins of salina lakes and extend toward the lake centre when the lake salinity is lowered by an increase of the ratio of fresh to marine waters (*see* Warren 1982b; Warren and Kendall 1985). The thin-bedded, rippled mudstones and laminated dolostones that form the top of the Curly dolomite probably represent the veneer boundstones and algal veneers that form in the continuously subaqueous, but very shallow, parts of salina lakes during their latter stages (Warren 1982b). The thin Roof gypsum is interpreted as representing the final stages of infilling and evaporation of the salina. Warren (1982a, 1982b) and Warren and Kendall (1985) noted that the final stages of modern South Australian coastal salinas are often marked by lunettes of wind-blown gypsum. However, such ephemeral features would be easily destroyed by erosion. Also, such lunettes appear to be absent from the coastal salinas (e.g., El Alamein lagoons) along the semiarid coast of northern Egypt (West et al. 1983). Although it is possible that the large coalesced nodules of the Roof gypsum formed by burial diagenesis of subaerial gypsum lunettes, it is more likely that they formed at the subaerial-subaqueous interface of a receding salina lake; domes of gypsum are exposed at the margins of the El Alamein lagoon (West et al. 1983), which is considered a coastal salina by Warren (1989).

The Roof gypsum is overlain, with a gradational contact, by 0.97 m of grey, fissile, gypsiferous shales. The lower 11 to 17 cm contains abundant small, rounded gypsum nodules (about 1 cm in diameter). The remaining 80 to 86 cm contains only a few small nodules, but elongated gypsum lenses (up to 5 cm thick and 34 cm wide) are present locally. Both units contain numerous, locally crosscutting, horizontal satin spar seams. These gypsiferous shales probably represent mixing of residual salina evaporites with subaerial clays brought into the salina lake either by runoff (during the annual rainy seasons) or by dust storms; both events are typical of the coastal regions of South Australia and northern Egypt. As desiccation and dune features (e.g., climbing ripples) are not present, subaerial eolian sedimentation is less likely, although possible.

The gypsiferous shales are overlain by 0.07 m of grey, very finely laminated, fissile shale that is softer than the enclosing units. Upper and lower contacts are horizontal. The shale is overlain by the highest unit exposed in the decline. This consists of ≥0.3 m of light grey, very finely laminated, dolomitic shale containing 0.5 cm partings of dark grey shale similar to the underlying unit. Satin spar seams are evident along bedding planes. The cyclic nature

of these grey shale to light grey dolomitic shale packages and the varve-like nature of their fine laminations suggest seasonal sedimentation. Such lithologies and textures are consistent with the ephemeral terrestrial sedimentation of the final stages of a salina, where the salina lake is fed by sediments from either surface runoff during the rainy season or dust storms during the dry season. The dolomite fraction (dolomitic shales) would have formed during the rainy season as either a subaqueous lake precipitate on evaporation or fluvial clastic material. However, marine incursion and deposition of this argillaceous package as a sabkha tidal flat may be an alternative explanation.

Main Gypsum Bed

The general description of lithologies and textures of the Main gypsum bed, presented above, was derived from examination of the bed at sections 1 to 8 (Figure 319.4). As time allowed for underground work was restricted, the Main gypsum bed was mapped in detail at only 3 locations (sections 3, 4 and 8). Results from these are presented as a fence diagram in Figure 319.6. The Main gypsum bed is remarkably similar throughout the mine (sections 3 and 8 being typical of the local variations of textures), with the exception of section 4. At sections 3 and 8 the bed is about 1.0 m thick (varying from 0.83 to 1.17 m at section 3 and from 1.00 to 1.10 m at section 8) and is composed essentially of "massive" gypsum that generally lacks sedimentary textures but displays obvious shear fabrics. Nodular gypsum and wisps of dolomite are presently preserved only in local areas of low strain; their distribution is controlled by structural deformation. The upper 30 cm at the 3 sections is marked by the presence of structural stylolites that formed from the deformational pressure solution of dolomite. This dissolution of dolomite has resulted in a thin residue of brown shaly material as the stylolite and concentration of the gypsum ore (structural enrichment). Such stylolites are absent from the Westroc and Domtar mined beds, and the lack of pressure solution of dolomite is an explanation for their lower grades of gypsum ore.

At section 4 (Figure 319.6), the upper stylolitic unit is underlain by 0.22 m of blue anhydrite, with large nodular to massive texture. Dark brown gypsum surrounds, or is incorporated in, the anhydrite nodules. The anhydrite is underlain by 0.55 m of chicken-wire mosaic to large nodular gypsum that is light blue in nodules and dark brown in the matrix of the mosaic. Patches of purer gypsum and anhydrite are present in the larger nodules. The contacts are marked by a change to smaller size of chicken-wire mosaic (upper contact) and nodules (lower contact). The basal unit is 0.10 m of white gypsum nodules set in dark brown matrix. Brecciated dolomite is present at the contact with the dolostones underlying the Main gypsum bed. The nodules have been considerably modified by ductile shear, which in thin section is present as several generations of shear fabrics. Thus, it is impossible to ascertain whether the nodular textures are original sedimentary features or structural features. As shear is less intense in the anhydrite unit, it is reasonable to postulate that the shear deformation resulted from the hydration expansion of anhydrite to gypsum during postglacial uplift. This expansion was contained by the bed contact and directed horizontally. This resulted in small reverse faults at many locations (e.g., section 13, Figure 319.6) and 2 large, circular duplex thrust ramps. At section 7, gypsum has plastically flowed from the downthrown block into the ramp thrust, along which the gypsum bed has been ramped 4 m above its normal stratigraphic position.

DISCUSSION AND CONCLUSIONS

The succession exposed underground at Canadian Gypsum is only 6 m high, and drill-hole logs were not available in the vicinity of the mine. Regional correlation with Salina Formation stratigraphy present in oil and gas company holes and Westroc Industries Ltd. logs suggest that the Canadian Gypsum succession can be assigned to the Salina E unit. However, lack of measurement to a known stratigraphic marker horizon precludes definition of its exact stratigraphic position; in fact, it could form the Salina D unit or the lower part of the Salina F unit.

The succession at Canadian Gypsum forms 4 separate cycles capped by gypsum (the upper cycle is incomplete). In each cycle, basal shales and mudstones pass upward into dolostones; these are in turn capped by gypsum. The lowermost cycle is only 0.65 m thick. Basal dolomitic mudstones are overlain by mudstones with algal dolomite layers, followed by dolostones containing abundant small discoid selenite eyes, then by a sequence of thin-bedded gypsiferous dolomite and gypsum layers that display enterolith, nodular and mosaic textures. This cycle is interpreted as having formed in a coastal sabkha environment: the basal mudstones as subtidal to intertidal sabkha mud flats; the dolomitic algal mounds layers as intertidal algal mats; the selenite-eye dolostones as carbonate-gypsum crystal mushes characteristic of the intertidal-supratidal interface (*see* Scholle et al. 1987); and the uppermost unit of gypsiferous dolomite and gypsum as supratidal, early diagenetic precipitates. In modern sabkhas, the supratidal area can be subdivided into a zone of anhydrite precipitation above the high water mark (the middle sabkha) and a zone of gypsum precipitation farther inland (the upper sabkha). In both middle and upper sabkhas, calcium sulphate precipitates in response to upward transpiration of groundwaters, forming caliche-like layers.

The second cycle, which is capped by the Main gypsum bed, is about 2.6 m thick. It commences with 1.29 m of shales deposited as mud in an ephemeral coastal lake or a sabkha tidal mud flat. This is followed by 0.34 m of selenite-eye dolostones, indicative of a sabkha intertidal-supratidal interface. The cycle is capped by the ~1 m thick Main gypsum bed. As postdepositional ductile shear has largely obliterated or distorted original sedimentary fabrics, it is difficult to deduce its sedimentary depositional environment from internal features, in contrast to the gypsum beds at the Westroc and Domtar deposits (Haynes and Hughes-Pearl 1989; Haynes et al. 1989). The textures preserved in areas of low strain are mainly nodular and chicken-wire mosaic, with a matrix of dolomite; the rock constitutes a dolomitic gypsum (70 to 85% gypsum). With reference to the underlying intertidal-supratidal interface unit, it could be suggested that the Main gypsum bed is a supratidal middle or upper sabkha sequence.

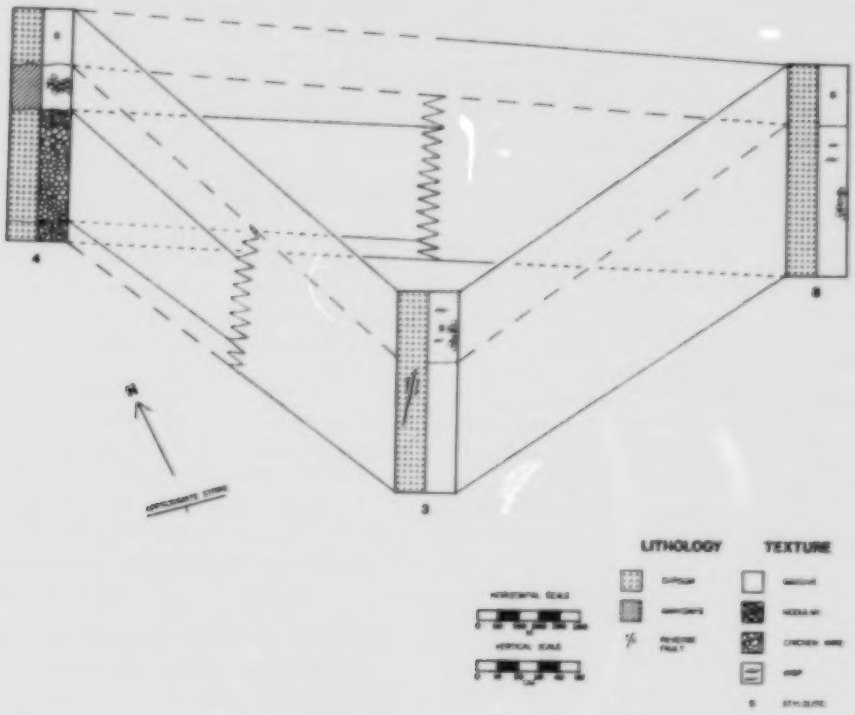

Figure 319.6. Fence diagram showing lithologies and textures in the Main gypsum bed at sections 3, 4 and 8.

However, the overlying cycle 3 sequence displays features typical of the upper part of a coastal salina (*see* below), indicating that the Main gypsum bed is more likely to represent the lower part of a coastal salina. Coastal salinas can form on a variety of substrates, especially an intertidal-supratidal sabkha interface, as the salina must be fed by marine groundwater percolating through a permeable, seaward barrier (Warren 1982b, 1989; Warren and Kendall 1985). Also, supratidal sabkha sequences are characterized by thin gypsum layers interbedded with gypsum (Scholle et al. 1987; Warren 1989; Warren and Kendall 1985), similar to the gypsiferous unit forming the upper part of cycle 1 (described above); no thick, high-purity gypsum beds have been reported from modern sabkhas. In contrast, modern coastal salinas are characterized by basal sequences of thick, high-purity gypsum that are of mineable grades, e.g., South Australia (Warren 1982a, 1982b) and northern Egypt (West et al. 1983).

Cycle 3 comprises the ~1.3 m thick sequence of the Roof shale, Black rock, Curly dolomite and Roof gypsum. The lithologies and textures displayed by these units, as well as the order that they appear in the sequence, are identical to those in the upper part (above thick basal gypsum units) of coastal salinas (Warren 1982b, 1989; Warren and Kendall 1985). The Black rock represents the boxwork carbonates, capped by teepees and breccias, that grow inward from the margins of a salina lake as it infills and dries. The Curly dolomite represents the stromatolite mounds and the thin algal and veneer boundstones that develop in areas of groundwater resurgence and seasonal influx of freshwater (rainy seasons) during the terminal stages of a salina. The Roof gypsum represents the final stages of salina lake evaporation, either at the subaerial-subaqueous interface (like the gypsum domes at El Alamein, Egypt) or as eolian lunettes derived from a desiccated lake surface (like the gypsum lunettes of South Australian salinas).

Only the basal argillaceous units of cycle 4 are exposed. This gypsiferous shale sequence formed either by influx of terrestial sediment (eolian and/or fluvial) into the infilled coastal salina (now an ephemeral playa lake) or by marine incursion and sedimentation as a sabkha tidal mud flat.

The intense ductile-shear deformation of the Main gypsum bed resulted in features not present in the 2 other Ontario deposits (Westroc and Domtar) producing gypsum from the Salina Formation. At the large scale, this deformation is present as 2 large ramp thrusts that at the one locality examined (section 7) formed a 4 m thick duplex of the Main gypsum bed. At the intermediate scale, reverse thrusts and shear zones resulted in plastic flow of gypsum, and even displacement of the upper and lower contacts of the bed. At smaller scales, a complex array of progressive ductile bands severely distorted the original sedimentary fabrics. Also, throughout much of the mine the upper part

of the Main gypsum bed exhibits large-amplitude structural stylolites; these are accompanied by high-grade gypsum ore. These stylolites appear to have formed by pressure-solution processes (during the postdepositional shear event) that involved dissolution of the dolomite originally present as the matrix to the nodules, now preserved only in local areas of low strain. Dolomite was similarly dissolved and removed from much of the gypsum bed along macro- and microshear arrays. The dissolution and removal of dolomite by a deformational, rather than diagenetic, process have important economic implications: enrichment of the orebody to average grades greater than 90% gypsum. This is significantly different from the Domtar deposit (average grade at Mine 2 is 74%), where deformation is absent, but less different from the Westroc deposit (average grade 88%), where deformation is confined to local internal distortion of nodules by microshears and plastic bending and displacement of layers. However, this deformational enrichment of ore grades by dissolution has a negative impact on bed thickness. At Canadian Gypsum, the least-strained areas tend to be thicker and contain anhydrite (e.g., section 4 is 1.15 m thick), whereas highly strained areas (away from reverse faults) are the thinnest (e.g., 0.83 m at section 3). Although average grades at Canadian Gypsum, Westroc and Domtar Mine 2 are inversely related to bed thickness (79% over 1 m, 88% over 2 m and 74% over 4 m, respectively), they are controlled essentially by the original sedimentological conditions of the depositional environment. The ductile shear deformation was most likely due to expansion on the hydration of anhydrite to gypsum during postglacial uplift in the Quaternary.

All 3 deposits contain shale, through dolostone, to gypsum cycles and display evidence that the mined beds formed in coastal salinas. However, details of the lithologies and textures of both the mined beds and their host rocks are different, and the cycles at Canadian Gypsum are considerably thinner (*see* Haynes and Hughes-Pearl 1989; Haynes et al. 1989). Notwithstanding a lack of exposure above the bed at Domtar, the Canadian Gypsum deposit is similar to the Westroc deposit: the mined bed is nodular and overlain by stromatolites, desiccation features, algal and boundstone veneers and terminal evaporites—a characteristic coastal salina sequence. In contrast, the Canadian Gypsum deposit formed on a sabkha substrate, the Westroc deposit on an interreef or lagoonal substrate and the Domtar deposit on a mesosaline to hypersaline lagoonal substrate. Also, the sequences overlying the coastal salina succession at Canadian Gypsum (above the Roof gypsum) are different from those at Westroc (above the Upper gypsum). At Canadian Gypsum, these are finely laminated, "varved" shales of possible playa lake, eolian or tidal mud-flat origin, whereas at Westroc these are a sabkha sequence of mud flats passing upward, through intertidal-supratidal carbonate-gypsum mush, to supratidal, thin-bedded dolomites and enterolithic anhydrite (middle sabkha).

The rapid vertical change in the depositional environments of the Canadian Gypsum sequence and the significant lateral facies changes of the Salina E unit over the 60 km between Westroc and Canadian Gypsum are similar to the distribution of coastal salinas, sabkhas and playas of northern Egypt described by West et al. (1983). Thus, the previous suggestion by Haynes et al. (1989) and Haynes and Hughes-Pearl (1989) that the modern analogue of the Salina A unit (across the Algonquin Arch) is the semiarid coastal zone of northern Egypt can now be extended to the Salina E unit.

ACKNOWLEDGMENTS

We are indebted to Rick Webber, Manager, Canadian Gypsum Company Ltd., Hagersville, for permission to conduct underground mapping and for assistance with staff and underground travel. We are particularly grateful to Tim Schoffer, Canadian Gypsum Company Ltd. Staff Geologist, for taking time from his operations schedule to be with us and for his invaluable knowledge of mine geology. Kirk Scheifele, Operations Manager, Westroc Industries Ltd., generously gave us access to company drill logs. Special thanks go to Reinhart Boland for assistance with underground mapping; Mike Lozon for drafting the diagrams; and Anne Sawchuk and Penny Kent for word processing.

REFERENCES

Carter, T. 1987. A comparison of the Middle Proterozoic Balmat evaporite sequence with Niagaran and Cayugan strata in the Michigan–Appalachian Basin; Proceedings of the Ontario Petroleum Institute, 26th Annual Conference, Toronto, Ontario, Proceedings Technical Paper 13, p.1-42.

Cole, G.E. 1925. Gypsum in Ontario; Ontario Department of Mines, Annual Report, v.34, pt.2, p.1-34.

Dyer, W.S. 1925. Geology of the gypsum deposits of southwestern Ontario; Ontario Department of Mines, Annual Report, v.34, pt.2, p.35-58.

Fowler, J.H. and Adams, G.C. 1988. Gypsum in Canada—present status and future developments; Mining Engineering, v.40, no.2, p.120-123.

Guillet, G.R. 1964. Gypsum in Ontario; Ontario Department of Mines, Industrial Mineral Report 18, 126p.

Haynes, S.J. 1989. Lithologies of the Salina Formation, Niagara Peninsula area: core log data file; Petroleum Resources Section, Ontario Ministry of Natural Resources, Open File Report, 205p.

Haynes, S.J. and Hughes-Pearl, J. 1989. Gypsum deposits of southern Ontario; *in* Geoscience Research Grant Program, summary of research 1988–1989, Ontario Geological Survey, Miscellaneous Paper 143, p.68-82.

Haynes, S.J., Boland,R. and Hughes-Pearl, J. 1988. Gypsum deposits of southern Ontario; *in* Geoscience Research Grant Program, summary of research 1987–1988, Ontario Geological Survey, Miscellaneous Paper 140, p.217-230.

———1989. Depositional setting of gypsum deposits, southwestern Ontario: the Domtar Mine; Economic Geology, v.84, p.857-870.

McKnight, R. and Fell, V. 1989. Mineral production in Ontario; Communications Branch, Energy, Mines and Resources Canada–Ontario Ministry of Northern Development and Mines, COMDA Review, v.2, no.2, 2p.

Scholle, P.A., Shinn, E.A., Halley, R.B. and Harris, P.M. 1987. Arid carbonate coastlines; American Association of Petroleum Geologists, Film.

Shinn, E.A. 1983. Tidal flat environment; *in* Carbonate depositional environments, edited by P.A. Scholle, D.G. Bebout and C.H. Moore, American Association of Petroleum Geologists, Memoir 33, p.172-210.

Warren, J.K. 1982a. The hydrological setting, occurrence and significance of gypsum in late Quaternary salt lakes in South Australia; Sedimentology, v.129, p.608-637.

———1982b. The hydrological significance of Holocene teepees, stromatolites, and boxwork limestones in coastal salinas in South Australia; Journal of Sedimentary Petrology, v.52, p.1171-1201.

———1989. Evaporite sedimentology; Prentice-Hall, Englewood Cliffs, New Jersey, 285p.

Warren, J.K. and Kendall, C.G.St.C. 1985. Comparison of sequences formed in marine sabkha (subaerial) and salina (subaqueous) settings—modern and ancient; American Association of Petroleum Geologists Bulletin, v.69, p.1023-1023.

West, I.M. 1975. Evaporites and associated sediments of the basal Purbeck Formation (Upper Jurassic) of Dorset; Geological Society of London Proceedings, v.86, p.205-225.

———1979. Review of evaporite diagenesis in the Purbeck Formation of southern England; *in* Sédimentation jurassique européen, Association de sédimentologie du France, publication spéciale n°1, p.407-416.

West, I.M., Ali, Y.A. and Hilmy, M. . 1983. Facies associated with primary gypsum nodules of northern Egyptian sabkhas; *in* 6th Symposium on Salt, edited by B.C. Schreiber and H.L. Harner, Northern Ohio Geological Society, Cleveland, Ohio, v.1, p.171-183.

Grant 326 PGEs at Sudbury: their Concentration by Sulphide-liquid Fractionation

C. Li and A. J. Naldrett

Department of Geology, University of Toronto, Toronto

ABSTRACT

Platinum-group elements (PGEs) occur throughout the ore zones of the Strathcona deposit on the North Range of the Sudbury igneous complex (SIC), but individual PGEs are fractionated from each other. Platinum, palladium and gold increase progressively, along with copper, away from the basal contact of the sublayer norite towards the footwall, and rhodium, ruthenium, iridium and osmium show the reverse trend.

The deep copper zone, which is the farthest from the contact in the deposit, falls at one extremity of the compositional variation. It is marked by the highest abundances of PGEs and ratios of Cu/(Cu + Ni) and (Pt + Pd)/(Os + Ir + Ru). PGEs are not distributed uniformly within this zone. Generally, Pt and Pd increase in areas where Os, Ir, Ru and Rh decrease in abundance. This zonation is visible across the vein system as a whole, with platinum and palladium increasing and osmium, iridium, ruthenium and rhodium decreasing away from the contact of the SIC. The same trend of increasing platinum and palladium is also observed on passing from the main veins (>20 cm) to some small branching veins (<20 cm)—which are usually associated with hydrothermal minerals and have more-intensive alteration than the main veins—and at the terminations of the veins.

Accelerator mass spectrometry (AMS) analysis of individual minerals indicates that sulphide minerals such as pentlandite, chalcopyrite, millerite, cubanite and bornite contain much lower platinum, gold and iridium than the ore as a whole (parts per billion versus parts per million, respectively), whereas magnetite contains slightly higher iridium than the bulk ores.

It is suggested that the fractional crystallization of sulphide liquid followed by hydrothermal fluids during the closing stages of crystallization can account for these observations: the early crystallization of monosulphide solid solution (MSS) and magnetite concentrated iron, cobalt, ruthenium, rhodium, iridium and osmium and led to an enrichment in copper, platimum, palladium and gold in the residual sulphide liquid. The progressive expulsion of the fractionated liquid into the footwall during its cooling gave rise to the observed compositional variations in the different zones.

INTRODUCTION

The Strathcona Mine at Sudbury, renowned for its PGE zoning, which has been regarded as being the result of sulphide-liquid fractionation (Naldrett et al. 1982; Naldrett 1984), is located on the North Range of the SIC (Figure 326.1). The ore lies at the contact of the complex and in the footwall (Figure 326.2). The geology of this deposit has been described by Naldrett and Kullerud (1967), Cowan (1968), Abel et al. (1979) and Coats and Snajdr (1984). Four ore types are observed. Disseminated sulphides of the hanging-wall zone occur within the sublayer norite. The norite is underlain by the main zone ore, which consists of massive and disseminated ores within the footwall breccia (which is composed of fragments of footwall gneiss), and by the deep zone, which consists of stringers of massive sulphides emplaced in fractures within the gneisses forming the footwall. Pyrrhotite, chalcopyrite, magnetite and pyrite are the main minerals in each of the preceding ore zones. Very rich stringers of massive chalcopyrite (copper zone) with minor magnetite, pyrite, pentlandite and sphalerite occur 100 to 200 m into the footwall (Abel et al. 1979). In 1979, 15 years after mining commenced, a second, more-extensive zone of copper-rich stringers, the deep copper zone, was discovered up to 500 m from the contact into the footwall.

From the available Pt, Pd and Au analyses at the mine, it is known that the concentrations of these noble metals in the deep copper zone are much higher than in other zones and that they are not uniformly distributed in the deep copper zone (Li and Naldrett 1989). The objective of this project is to investigate the distribution of PGEs within, adjacent to and at the extremities of ore veins in the deep copper zone at the Strathcona Mine, in order to understand the behaviour of PGEs during the formation of this ore deposit.

This paper is the second in a continuing study of the project. The PGE analytical technique developed in the first year was reported in Li and Naldrett (1989). This report details the geological features of the deep copper zone and includes more PGE data on different types of the ores and the trace quantities of Pt, Au and Ir in the major minerals determined *in situ* by AMS.

ANALYTICAL TECHNIQUES

The principal of using AMS for trace-element analyses has been discussed by Rucklidge et al. (1987). Here we present only a brief description of the procedure. Small cores of ore enriched in particular sulphide minerals are removed from polished sections with a diamond-edged core drill of 4 mm internal diameter. Sets of 12 such cores, including the appropriate standards, are loaded in turn into a sample-changing system linked to a high-intensity cesium ion source. The samples are optically aligned, and the negative secondary ions sputtered from the selected sample surface are extracted from a target area of about 0.3 mm in

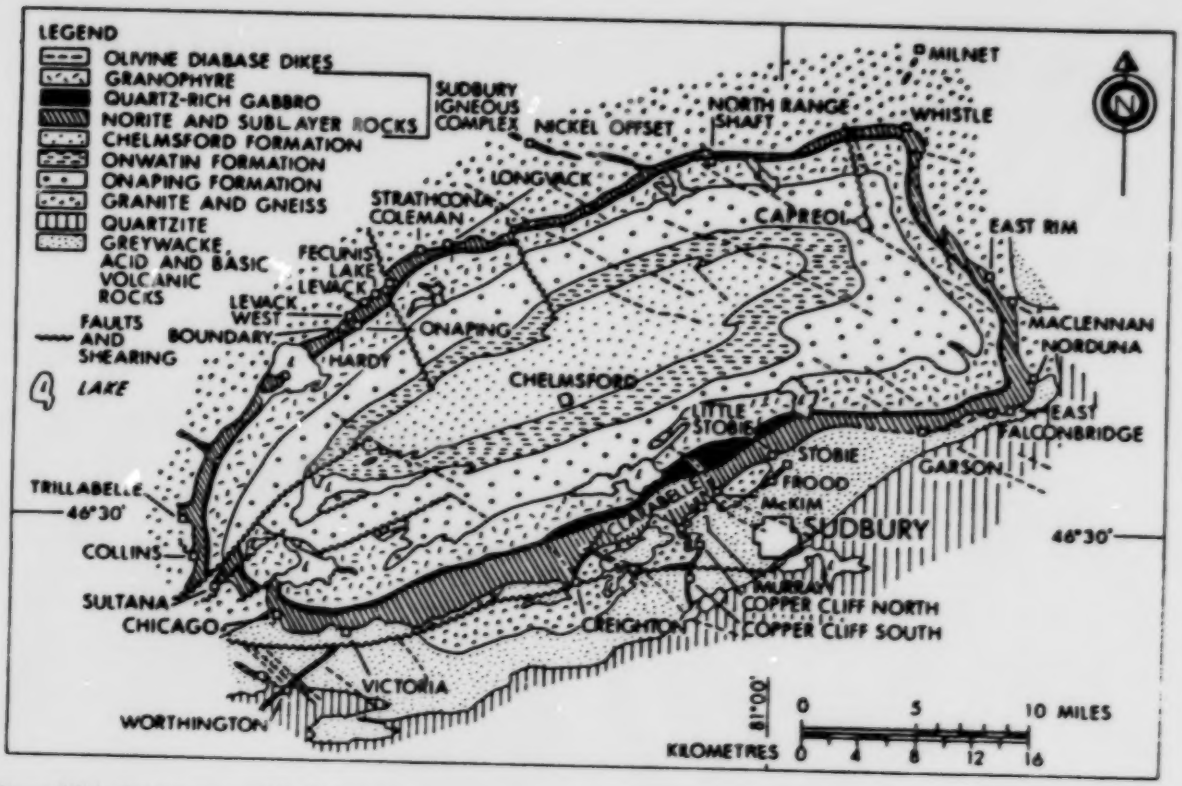

Figure 326.1. Geological map of the Sudbury area.

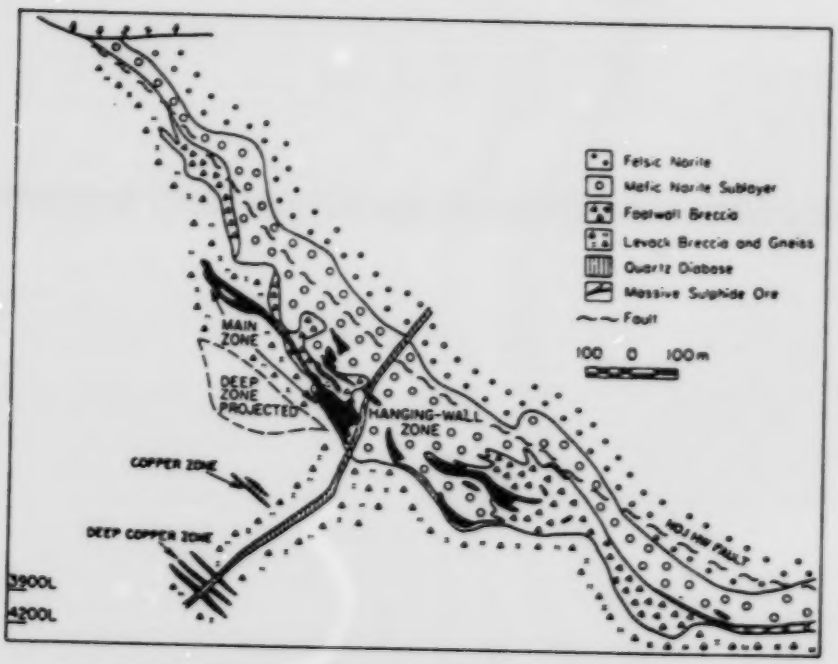

Figure 326.2. Vertical cross section (6280E) through the Strathcona Mine, looking east.

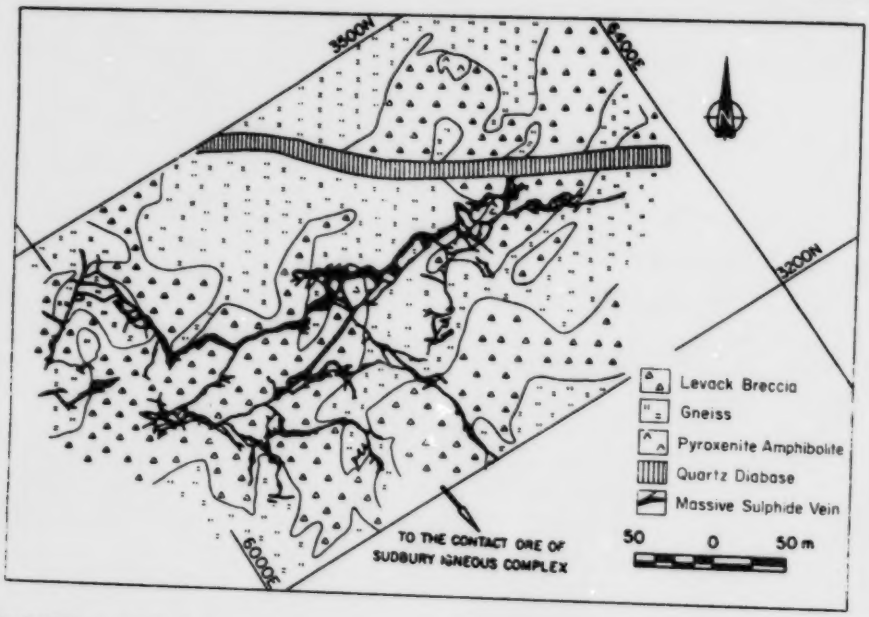

Figure 326.3. a) Geological map of the deep copper zone at Strathcona Mine (3900-foot level).

diameter. The 20 kV ions are energy and mass filtered and then introduced into the Tandem accelerator, which has the terminal set at 1.6 MV. Following charge changing (electron stripping) at the accelerator terminal, electrostatic selection of ions of charge state +6 is employed prior to final high-resolution mass and energy analysis. The filtered beam of chosen ions is displayed on an energy spectrum collected with a silicon surface-barrier detector, which serves to resolve completely the desired ion from potential interference.

The detection limits by AMS of Pt is estimated to be 1.5 ppb; of Ir, 30 ppb; and of Au, 0.1 ppb (Wilson et al., in press).

GEOLOGICAL FEATURES OF THE DEEP COPPER ZONE

The host rocks of the deep copper zone are Archean footwall gneisses, which were extensively brecciated prior to the intrusion of SIC to form the Sudbury breccia (Levack breccia) (Figures 326.3a and 326.3b). The footwall gneisses consist of rocks ranging from feldspathic gneiss through intermediate gneiss to mafic gneiss. Pyroxenite-amphibolite rocks occur as irregular masses or layers in the gneiss complex and are usually altered to serpentine and tremolite.

Quartz diabase bodies cut the Archean gneiss complex and the massive sulphide vein system. They occur as irregular masses or sharply defined sills or dikes. Principal minerals in quartz diabase are hornblende, orthopyroxene or clinopyroxene, andesine and quartz.

The Sudbury breccia is the dominant host rock of the ore of the deep copper zone. Underground observation indicates that approximately 60 to 70% of the rock mass in the vicinity of sulphide veins is Sudbury breccia. This

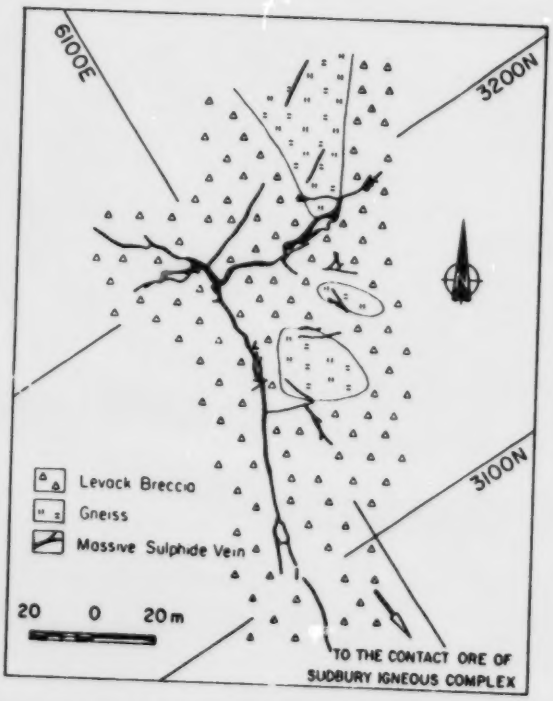

Figure 326.3 (concluded). b) Geological map of the deep copper zone at Strathcona Mine (4200-foot level).

breccia appears to be the fine-grained matrix of a "megabreccia": huge fragments up to 10 to 15 m in diameter are set in the Sudbury breccia. On both the 3900- and 4200-foot levels, the "megabreccia" increases away from

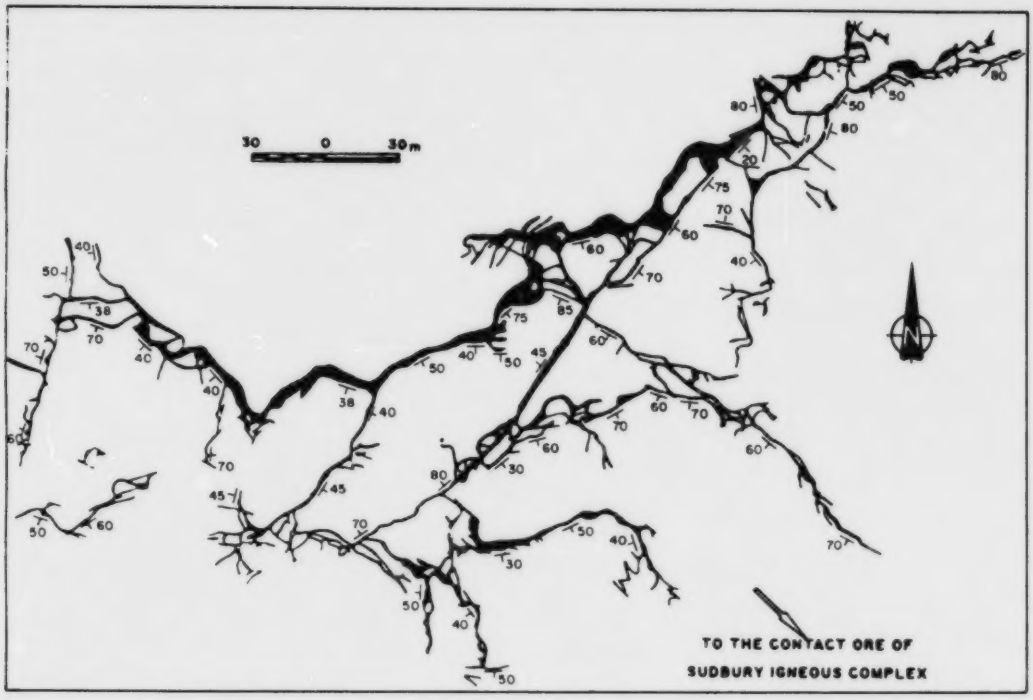

Figure 326.4. Vein structure of the deep copper zone at Strathcona Mine (3900-foot level).

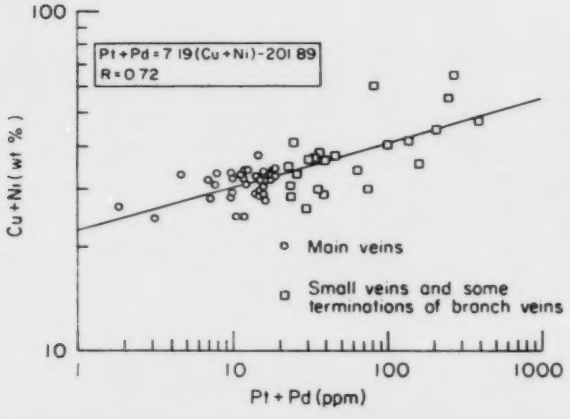

Figure 326.5. Metal content in 100% sulphides in different ore types in the deep copper zone at Strathcona Mine.

the SIC, that is, from southeast to northwest. The entire deep copper zone appears to be located in a transitional zone between the Sudbury breccia and the "megabreccia". The Sudbury breccia occurs as irregular masses, veins and veinlets.

The deep copper zone has an arcuate form in section, parallel to the contact of the SIC and 400 to 500 m below it (Figure 326.2). It occurs between the 4600- and 3300-foot levels, approximately 1000 to 1400 m below the surface. The zone consists of a complex, twisted, composite, interconnecting vein system. The veins range in width from very thin (<1 cm) to a maximum of about 6 m. The principal orientations are northeasterly, northwesterly and easterly, with individual veins dipping northwesterly, southwesterly, southeasterly and south (Figure 326.4); however, the vein system as a whole plunges southeasterly, that is, in a direction towards the contact of the SIC (see Figure 326.2). Although there is some apparent continuity of the veins in dip length, individual veins are not easy to trace to different levels. The vein system appears to have a root below the 4200-foot level and branches and spreads out upwards. There is no evidence of the replacement of wall rocks along the vein. It appears that the vein system occupies a complex series of fractures.

The veins of the deep copper zone are composed of chalcopyrite, cubanite, pentlandite, millerite, pyrrhotite, magnetite and bornite. Additional accessory minerals include galena, mackinawite and sphalerite. According to Snajdr (1985), a number of platinum-group minerals, mostly bismuthides and tellurides, are present as extremely small grains (5 to 10 μm). Although the contacts of the veins are sharp, the chalcopyrite is dispersed a distance of several millimetres to several centimetres into the wall rocks, to form a fabric along the margins. The dispersal is often accompanied by chlorite, epidote, amphibole and silicates, which give rise to visible dark selvage bands along the sulphide veins. Hydrothermally deposited minerals, such as quartz, calcite, amphibole and epidote, occasionally occur along with sulphides at the margins or the terminations of veins. Veins of this type tend to be thinner and less straight than those containing massive sulphides. Typically, they are <20 cm thick and contain chalcopyrite or millerite along

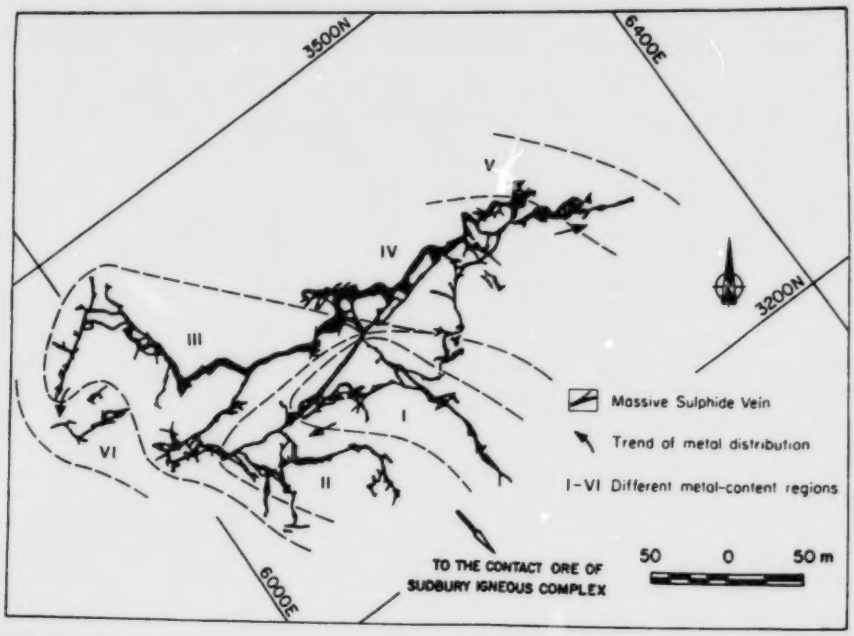

Figure 326.6. Metal distribution in the deep copper zone at Strathcona Mine (3900-foot level).

Table 326.1. Metal contents (in 100% sulphides) of different regions in Figure 326.6.

Regions	Number of Samples	Ni	Cu	Co	Pt	Pd	Au	Ag	Pb	(Cu+Ni)	(Pt+Pd)
I	135	1.95	27.27	0.04	4.01	6.56	0.41	167.2	0.08	29.22	10.57
II	49	1.94	26.91	0.03	4.93	6.72	0.45	186.4	0.06	28.85	11.65
III	137	2.19	28.19	0.03	4.5	7.62	0.31	154.5	0.05	30.38	12.12
IV	57	1.64	29.01	0.02	5.57	7.89	0.59	131.2	0.04	30.65	13.46
V	55	1.7	31.21	0.01	6.69	9.25	0.59	113.4	0.09	32.91	15.92
VI	6	3.19	29.49	<0.01	7.9	9.32	0.62	155.7	0.06	32.68	17.22
Average	439	1.97	28.27	0.03	4.86	7.47	0.43	138.5	0.06	30.24	12.32

Notes: Ni, Cu, Co and (Cu + Ni) are in weight percent; Pt, Pd, Au, Ag, Pb and (Pt + Pd) are in parts per million.

with the quartz, calcite and amphibole and are associated with much thicker alteration zones of epidote and chlorite (≤50 cm on each side) than the massive sulphide veins.

PGE CONCENTRATION AND DISTRIBUTION

PGE Distribution from Main Veins to Small Branching Veins

Three thousand analyses for Ni, Co, Cu, Pt, Pd and S from the 3900-10 horizontal drilling level have been composited in terms of width of the veins intersected by drill holes. Veins with widths of >20 cm are described as main veins; those with widths of <20 cm, as small veins. The results indicate that disseminated sulphides occurring within some small veins and terminations of veins branching off main veins are richer in (Pt + Pd) and to a lesser extent in (Cu + Ni) than sulphides within the main veins. This is illustrated in Figure 326.5, where it is seen that (Cu + Ni) varies between 24 and 36% in the main veins and between 25 and 60% in the small veins and branches. The values of (Pt + Pd) on going from the main veins to some of the small veins increase with (Cu + Ni) with a correlation coefficient of 0.72. The extreme enrichment in PGEs toward what appear to be the terminations of veins is important from the point of view that these may be the end product of sulphide-liquid fractionation.

PGE Distribution within the Vein System

The Ni, Cu, Co, Au, Pt, Pd, Ag and Pb contents of 439 analyses of massive sulphide ore, collected by the mine geologists at the 3900-foot level of the deep copper zone,

Table 326.2. Composition of deep copper zone ores.

Samples	Os	Ir	Ru	Rh	Pt	Pd	Au	Ni	Cu	Co	S	Recalc. factor	Mineral composition
R-2a	nd	0.07	nd	nd	3949	1356	1323	4.85	1.15	0.022	3.39	9.6	Mill, Cp
R-2b	nd	0.1	nd	nd	4248	1202	1442						
R-3a	nd	0.08	nd	14.38	744	9137	7	49	0.16	0.37	30.8	1	Pn, Cp, Mt
R-3b	nd	0.07	nd	nd	676	8767	58						
R-4	nd	nd	nd	nd	2670	740	151	0.42	36	0.028	32	1	Cp, Mt, Pn
R-6	nd	nd	nd	nd	1102	3202.7	36	1.43	36	0.038	30.9	1	Cp, Mt, Pn
R-8	nd	0.1	nd	nd	3219	4879	202	0.32	31.8	0.028	29.9	1	Cub, Cp, Mt, Pn
R-10	nd	0.11	nd	nd	5607	9214	159	1.06	32.5	0.03	30.3	1	Cp, Cub, Mt
R-11	nd	0.31	nd	52.5	3467	8167	244	0.44	29.3	0.033	31	1	Cp, Cub, Pn, Mt
R-12a	nd	0.05	nd	nd	3573	3475	2221	5.05	11.2	0.047	18.3	2	Cp, Cub, Pn, Mt
R-12b	nd	nd	nd	nd	2968	3591	2882						
R-14	nd	0.24	nd	44.9	2052	4402	20	0.47	32.8	0.032	33	1	Cp, Cub, Pn
R-16	nd	nd	nd	nd	5298	7446	483	2.64	23.4	0.041	26.6	1	Cp, Cub, Pn, Mt
R-17	nd	nd	nd	nd	4131	6785	242	1.06	21.4	0.029	29.1	1	Cub, Cp, Pn, Mt
R-18	nd	0.12	nd	nd	4139	4704	187	0.4	25.9	0.028	31.9	1	Cp, Cub, Pn
R-19a	nd	0.07	nd	2.77	9490	4988	258	6.84	19.3	0.05	30.8	1	Cp, Pn, Cub, Mt
R-19a	nd	nd	nd	3.57	10 554	5208	274						
R-20	nd	0.17	nd	nd	2214	4151	166	0.64	24.9	0.032	30.4	1	Cp, Cub, Mt
R-21	nd	nd	nd	nd	3261	5169	46	0.45	25.2	0.031	30.1	1	Cp, Cub, Mt
L89-1a	nd	nd	nd	nd	9151	4666	1302	0.06	29.7	0.024	29.5	1	Cp, Cub
L89-b	nd	nd	nd	nd	9102	4756	1324						
L89-2a	nd	nd	nd	nd	16 637	6020	1441	48.4	0.32	0.47	30	1	Pn, Mill, Cp
L89-2b	nd	nd	nd	nd	17 127	5794	1824						
L89-3a	nd	nd	nd	nd	7579	8696	1563	7.32	17.5	0.072	25.6	1.3	Cp, Pn
L89-3b	nd	nd	nd	nd	7847	8353	1114						
L89-4a	nd	nd	nd	nd	8053	12 079	754	0.67	10.7	0.11	11.6	3	Cp, Pn
L89-4b	nd	nd	nd	nd	7896	11 282	623						
L89-5a	nd	0.04	nd	nd	3874	3000	639	0.2	6.64	0.011	6.41	5.2	Cp, Pn
L89-5b	nd	nd	nd	nd	3523	3019	649						
L89-6a	nd	nd	nd	nd	8992	10 840	360	0.98	24.4	0.034	32.3	1	Cp, Cub, Pn
L89-6b	nd	nd	nd	nd	9766	10 475	264						
L89-7a	nd	nd	nd	nd	5122	6049	79	0.47	25	0.032	31.3	1	Cp, Cub, Pn
L89-7b	nd	nd	nd	nd	5161	5971	94						
L89-8a	nd	0.03	nd	nd	3483	2416	5344	1.32	4.89	0.013	6.67	5.5	Cp, Pn
L89-9a	nd	nd	nd	nd	5391	5835	1393	14.2	5.14	0.41	22.1	1.6	Cp, Pn, Cub
L89-9b	nd	nd	nd	nd	5637	5955	1370						
L89-10a	nd	0.04	nd	nd	52	73	90	0.07	0.08	0.003	0.31		
L89-10b	nd	0.03	nd	nd	66	88	87						
L89-11a	nd	0.04	nd	nd	223	48	58	0.02	0.1	0.002	0.26		
L89-11b	nd	0.03	nd	nd	202	43	45						
L89-12a	nd	0.05	nd	nd	2776	831	187	0.64	4.97	0.014	6.44	5.5	Cp, Pn
L89-12b	nd	0.06	nd	nd	2995	813	214						
L89-13a	nd	0.24	nd	nd	4648	3630	3004	0.68	7.49	0.011	8.81	3.4	Cub, Cp, Pn
L89-13b	nd	0.15	nd	nd	4858	3295	3007						
L89-14a	nd	nd	nd	nd	14 854	5010	492	9.64	17.6	0.094	31	1	Cp, Cub, Pn
L89-14b	nd	nd	nd	nd	14 879	5016	523						
L89-15a	nd	0.24	nd	nd	2989	3898	2134	0.58	1.79	0.002	3.76	10	Cub, Pn, Cp
L89-15b	nd	nd	nd	nd	2912	3826	2257						
L89-16a	nd	nd	nd	nd		4072		0.46	14.5	0.022	18	1.8	Cub, Cp, Pn
L89-16b	nd	nd	nd	nd	9270	3882	1297						
L89-17a	nd	nd	nd	nd	3052	1150	235	18.5	0.5	0.071	17.3	1.89	Pn, Cp
L89-17b	nd	0.15	nd	nd	2882	1135	240						
L89-18a	nd	0.04	nd	nd	6403	5950	3175	6.85	1.86	0.019	5.43	5.88	Mill, Cp, Cub
L89-18b	nd	0.04	nd	nd	6274	6094	3127						
L89-19a	nd	nd	nd	nd	7719		126	0.28	29.6	0.018	31.6	1	Cp, Cub, Mt
L89-19b	nd	nd	nd	nd	6907		120						
L89-20a	nd	nd	nd	nd	1302		18	0.47	30.9	0.021	31.9	1	Cp, Pn
L89-20b	nd	nd	nd	nd	1336		19						
L89-21a	nd	nd	nd	nd	1373	13 613	382	0.32	26.9	0.026	32.5	1	Cp, Cub, Mt
L89-22a	nd	0.42	nd	nd	12 637	951	508	6.65	26.3	0.042	30.7	1	Cp, Pn
L89-23a	nd	nd	nd	nd	10 723	3568	817	30.9	1.45	0.36	19	1.88	Mill, Cp
L89-23b	nd	nd	nd	1.5	11 584	3159	1000						
L89-24a	nd	nd	nd	nd	5950		421	0.41	31.9	0.018	33	1	Cp, Mt
L89-25a	nd	0.03	nd	nd	8880	7887	3936	6.74	12.1	0.038	19.2	1.67	Cp, Pn, Cub
L89-25b	nd	nd	nd	nd	9049	7863	4206						

Notes: Sample numbers ending with a "b" are duplicates. Os, Ir, Ru, Rh, Pt, Pd and Au are in parts per billion; Ni, Cu, Co and S are in weight percent; nd, not detected. Cp, chalcopyrite; Cub, cubanite; Mill, millerite; Mt, magnetite; Pn, pentlandite.

have been composited and examined in terms of the variations that they display across the zone. The regions within which composites were calculated are numbered I to VI in Figure 326.6. PGE concentrations of the different regions are listed in Table 326.1. The data indicate that Co decreases and that (Cu + Ni), Pt, Pd and Au increase in a

Table 326.3. Metal contents (in 100% sulphides) in different ore zones at Strathcona.

Ore types	Number of samples	Ni	Cu	Co	Pt	Pd	Rh	Ru	Ir	Os	Au	$\frac{Cu}{Cu+Ni}$	$\frac{Pt}{Pt+Pd}$	$\frac{Pt+Pd}{Ru+Ir+Os}$
Hanging-wall ore*	10	3.1	0.37	0.21	114	105	60	52	29	20	19	0.11	0.52	1.2
Breccia ore*	18	3.4	1.2	0.14	413	380	20	12	7	4	78	0.26	0.52	3.4x10
Footwall ore*	8	4	2.3	0.13	750	701	16	4	4	3	112	0.37	0.52	1.3x100
Copper zone*	1	0.39	29.6	0.02	2551	890	4	3	0.2	2	189	0.99	0.74	6.6x100
Deep copper zone†	40	1.97	28.3	0.03	4860	7470	<3.8	<3	<0.1	<2	430	0.93	0.4	2.5x1000
Chondrites (C1)‡					1020	545	200	690	540	514	152			

Notes: Ni, Cu and Co are in weight percent; Pt, Pd, Rh, Ru, Ir, Os and Au are in parts per billion.
**Naldrett et al. (1982).*
†This study. Ni, Cu, Co, Pt, Pd and Au are calculated from the mine data of 439 massive sulphide ores.
‡C1 chondrite values after *Naldrett and Duke (1980).*

direction directly away from the contact of the SIC and then in a northwesterly and southeasterly direction along the vein system. These compositional variations are consistent with the progressive fractional crystallization of a sulphide liquid (Naldrett et al. 1982) and may therefore indicate the direction in which the sulphide liquid entered and moved along the system.

PGE Distribution within Strathcona Mine

Forty full-spectrum PGE analyses are given in Table 326.2. The average value of PGE concentration in 100% sulphides of the deep copper zone is given with the data of other ore zones in Table 326.3. The recalculation factors for 100% sulphides listed in Table 326.2 are based on the observed mineral compositions. The data indicate that the contents of Os, Ir, Ru and Rh in the deep copper zone are extremely low: Os is <2 ppb, Ir is <0.1 ppb, Ru is <3 ppb and Rh is <3.8 ppb. On the other hand, Pt, Pd and Au values are extremely high. In comparison with other zones of the Strathcona deposit, the deep copper zone shows significant Pt and Pd enrichment and Os, Ir, Ru and Rh depletion and high ratios of Cu/(Cu + Ni) and (Pt + Pd)/(Os + Ir + Ru). This trend is well illustrated in Figure 326.7. It can be seen that the deep copper zone falls at one extremity of the compositional variation shown by the deposit.

PGE Contents of Base Metal Minerals

Trace quantities of Pt, Au and Ir in the major minerals have been determined *in situ* by AMS down to less than parts per billion levels. The concentrations of these PGEs in the individual minerals are variable (Table 326.4, 326.5, 326.6 and 326.7), with 2.43 ppb Pt, 12.57 ppb Au and <0.08 ppb Ir in pentlandite; 1.55 ppb Pt, 7.67 ppb Au and 1.2 ppb Ir in magnetite; 1.24 ppb Pt, 0.09 ppb Au and <0.08 ppb Ir in bornite; 1.19 ppb Pt, 7.48 ppb Au and 0.08 ppb Ir in chalcopyrite; 0.59 ppb Pt, 23.91 ppb Au and <0.08 ppb Ir in cubanite; and 0.14 ppb Pt, 7.21 ppb Au and 0.08 ppb Ir in millerite. These levels for Pt and Au are much lower than those in the bulk ores (parts per billion versus parts per million). This indicates that the sulphide minerals are not significant carriers of platinum, gold and iridium. Thus these PGEs must occur mainly as discrete minerals in this environment. Higher PGE values (up to 52.13 ppb Pt and 181.28 ppb Au) have been encountered in the cracks and boundaries of individual grains and may indicate that micrograins of separate PGE minerals are distributed in these areas.

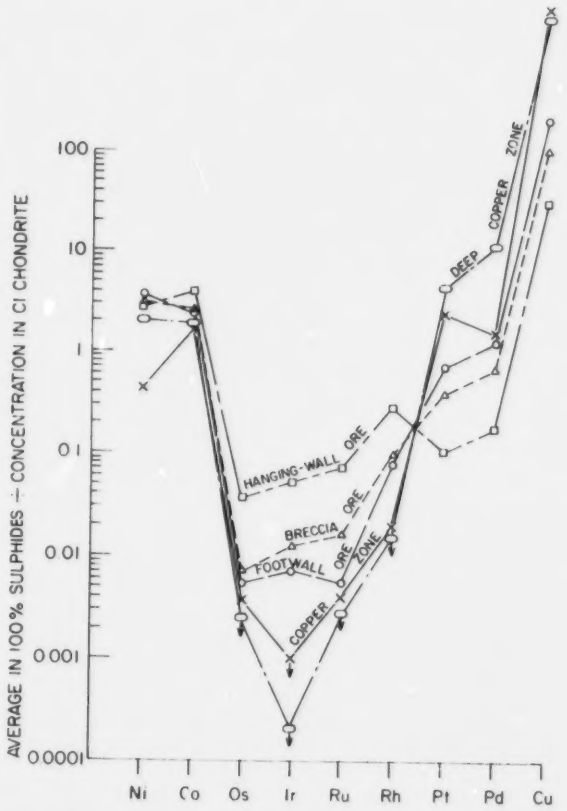

Figure 326.7. Average metal content (chondrite normalized) in 100% sulphides in different ore types at Strathcona Mine.

DISCUSSION AND CONCLUSIONS

Naldrett et al. (1982) considered a number of models to explain the compositional variations of the Strathcona

Table 326.4. Pt contents in minerals.

Sample no.	Mineral	Analysis time	Mean (ppb)	sd
898-3-1	Born	2	1.24	0.06
898-3-2	Born*	1	3.74	
R-3-1	Pn	3	3.12	1.31
R-3-2	Pn†	1	52.13	
L-17	Pn	3	1.64	0.3
R-1-1	Mill	2	0.11	0.04
R-1-2	Mill†	1	2.5	
P-1	Cp	3	1.91	0.38
MT-1-1	Cub	4	0.35	0.18
MT-1-2	Cp	4	0.58	0.2
MT-1-3	Pn	1	2.52	
MT-1-4	Cub	3	0.82	0.29
MT-1-5	Cp*	2	6.47	1.05
MT-1-6	Mt	2	1.55	0.07
MT-1-7	Cp	3	1.07	0.28
P-4	Mill	3	0.16	0.02

Notes: 100 s integration on samples; 20 s on SARM7 standard; Pt of SARM = 5681 ppb; Born, bornite; other mineral abbreviations as in Table 326.2; sd, standard deviation.
**Mineral boundary.*
†Crack.

Table 326.5. Average Pt contents in minerals.

Mineral	Number of grains	Mean (ppb)	sd
Born	1	1.24	
Pn	3	2.43	0.61
Mill	2	0.14	0.03
Cp	3	1.19	0.55
Cub	2	0.59	0.24
Mt	1	1.55	

Note: Mineral abbreviations as in Tables 326.2 and 326.3.

Table 326.6. Au contents in minerals.

Sample no.	Mineral	Au (ppb)	
MT-1-1	Cp	7.04	
MT-1-1	Cp	7.48	
Average	Cp	7.27	(0.21)
MT-1-1	Cp*	181.28	
MT-1-1	Cp*	50.27	
MT-1-2	Cub	19.23	
MT-1-2	Cub	28.59	
Average	Cub	23.91	(4.68)
MT-1-3	Mt	7.67	
P-1	Cp	79.5	
P-4	Mill	7.21	
R-3	Pn	95.92	
R-17	Pn	12.57	
898-3	Born	0.09	

Notes: 100 s integration on samples; 20 s on SARM; Au of SARM = 471 ppb; mineral abbreviations as in Tables 326.2 and 326.3.
**Mineral boundary.*

Table 326.7. Ir contents in minerals.

Sample no.	Mineral	Ir (ppb)	
MT-1-1	Mt	1.36	
MT-1-1	Mt	1.04	
Average	Mt	1.2	(0.16)
MT-1-2	Cp	0.08	
P-4	Mill	0.08	
R-17	Pn	<0.08	

Notes: 100 s integration on samples; 20 s on SARM; Ir of SARM = 112 ppb; mineral abbreviations as in Table 326.2.

Mine. These include 1) successive segregation of sulphides from the magma reservoir; 2) progressive partial melting of MSS; 3) redistribution of metal by diffusion in response to the thermal gradients; and 4) fractional crystallization of MSS from a sulphide melt.

The first process cannot account for the zoning of the Strathcona ores because it cannot explain the progressive increase in the Cu/(Cu + Ni) ratio, since the partition coefficients for these metals between a sulphide melt and a silicate magma of basaltic composition are approximately equal (Rajamani and Naldrett 1978). A far more serious objection stems from the fact that all the metals in question, Ni, Cu, Co, PGEs and Au, are highly chalcophile and should, therefore, show a depletion in successive sulphides rather than the enrichment that is shown at Strathcona.

In the case of the model calling upon fractional melting of an already solidified ore zone to cause redistribution of the metals, it is to be said that net texture of hanging-wall ore shows no sign of having had sulphides removed from it once the ore and its enclosing host rock solidified. This rules out the sulphide-remelting model.

Thermal diffusion models have difficulty in explaining how rhodium, ruthenium, iridium, osmium and cobalt could diffuse against the thermal gradient, as required by the enrichment of these metals in the hanging-wall ore. Different diffusion speeds for rhodium, ruthenium, iridium, osmium, cobalt and others may account for the zoning but, as calculated by Naldrett et al. (1982), would require more than 50% of iron sulphide diffusion from hanging wall to footwall. Massive diffusion on this scale is incompatible with net texture of the hanging-wall ore. Therefore, thermal diffusion is unable to explain the differences between the concentrations of cobalt, rhodium, ruthenium and osmium in the 3 observed ore types at Strathcona.

Therefore, Naldrett et al. (1982) concluded that fractional crystallization of an MSS from a sulphide melt, with continuous expulsion of the progressively more fractionated sulphide liquid downward, away from the hanging wall and into the footwall, provides the best explanation for the gross zoning of metals in the deposits. Hawley (1965) first suggested the model to explain the Fe-Cu-Ni zoning at Frood deposit, and it was subsequently favoured by Keays and Crocket (1970) and Chyi and Crocket (1976) to account for the zoning at the Strathcona Mine.

This model is supported by the experimental data in the Fe-Ni-S system (Naldrett et al. 1967) and Fe-Cu-S system

(Kullerud et al. 1969). MSS is continuous across the Fe-Ni-S system from a solidus temperature of about 1100°C to below 300°C. The bulk composition of Strathcona ore plots with and toward the sulphur-rich side of the MSS (see Naldrett 1984) as it occurs at 600°C. With cooling, MSS would be the first to crystallize. Liquidus relations in the Fe-Ni-S and Cu-Fe-S systems (Kullerud et al. 1969) indicate that, although Ni and Cu would substitute in the MSS, both would be more concentrated in the liquid. Fractional crystallization of the initial sulphide melt would, therefore, give rise to a liquid significantly enriched in these metals. The increase in the Cu/(Cu + Ni) ratio toward the footwall requires that copper favour the liquid over the MSS to a greater degree than nickel. This is consistent with data on the Fe-Cu-Ni-S system (Craig and Kullerud 1969). The depletion in the absolute Ni content with very high Cu content in the copper zone and deep copper zone requires that as the residual liquids become richer in copper, there is a reversal in the tendency for nickel to favour the liquid: it begins to favour MSS. This is again consistent with the Craig and Kullerud (1969) study. They reported that at 850°C, the sulphide liquid contained much more copper and less nickel than the coexisting MSS.

The fractional crystallization model carries implications with respect to the preference of other metals for the sulphide liquid over the MSS structure. Apart from nickel and copper, the observed zoning indicates that platinum, palladium and gold should also prefer the sulphide liquid, and copper, rhodium, ruthenium, iridium and osmium should prefer the Mss structure. Studies by Skinner et al. (1976) on the Fe-Pt-S and Fe-Pd-S systems are consistent with the requirement that palladium and platinum should become enriched in the residual liquid.

In work on PGEs in the Fe-Ni-S system, Distler et al. (1977) studied the distribution of palladium, rhodium and ruthenium between MSS and a Ni-rich residual liquid lying on the sulphide-deficient side of the MSS. Their data provide evidence that palladium is progressively concentrated in the liquid; rhodium and ruthenium, in the MSS.

Makovicky et al. (1986) have studied the solubilities of PGEs in base metal sulphides in the Fe-PGE-S and Cu-Fe-PGE-S systems. They found that platinum, palladium, rhodium and ruthenium solubilities in pyrrhotite decrease dramatically from 900°C to 500°C, and the consequent quenching or cooling can cause exsolution of almost all the PGEs in pyrrhotite. They also found that neither intermediate Cu-Fe-S solid solution (Iss) nor chalcopyrite dissolves PGEs at 500°C, while the coexisting pyrrhotite dissolves small amounts of Pt (1.2%), and a sulphide liquid concentrates Pt up to 6 to 15 weight %, which is a six-fold enrichment over pyrrhotite. The results indicate that platinum will concentrate in the coexisting liquid during the crystallization of a sulphide melt. In addition, on slow cooling, additional PGEs will be rejected from an originally PGE-saturated pyrrhotite structure and diffuse into the coexisting liquid. The composition of the sulphide liquid is close to that of bornite and is of interest with respect to the Cu-rich stringers at Strathcona.

A fifth model for PGE enrichment is also a possibility. The fractionation of a sulphide liquid may involve a hydrothermal fluid that dissolves PGEs and other elements such as arsenic, tellurium, thallium and bismuth during the final stage of crystallization. These latter elements could control PGE transportation and deposition. Orlova et al. (1987) obtained the platinum solubility of 0.2 to 0.3 g/kg H_2O in a 1 *M* solution of (Na,K)Cl at 600°C and 1.5 kbars (1.5 kbar = 1 MPa). The solubilities of PGEs in iron sulphides decrease significantly as the temperature is reduced (Makovicky et al. 1986). These data suggest that platinum and possibly other PGEs may be enriched in a coexisting hydrothermal fluid during sulphide-liquid fractionation.

ACKNOWLEDGMENTS

The authors would like to thank R.G.V. Hancock (SLOWPOKE Laboratory, University of Toronto) for the use of the reactor and counting facilities and M.J. Gorton (Department of Geology, University of Toronto) for access to instrumental neutron activation analysis counting equipment in the Department of Geology Laboratory. J.C. Rucklidge, G.C. Wilson and L.R. Kilius (Isotrace Laboratory, University of Toronto) are thanked for their technical support of AMS analyses. We are most grateful to C.J.A. Coats, P. Johannessen, M.K. Abel and S.B. Nikolic (Falconbridge Limited, Sudbury Operations) and other staff at Strathcona Mine for the support during field work.

REFERENCES

Abel, M.K., Buchan, R., Coats, C.J.A. and Penstone, M.E. 1979. Copper mineralization in the footwall complex, Strathcona Mine, Sudbury, Ontario; The Canadian Mineralogist, v.17, p.275-286.

Chyi, L.L. and Crocket, J.H. 1976. Partition of platinum, palladium, iridium, and gold among coexisting minerals from the Deep ore zone, Strathcona Mine, Sudbury, Ontario; Economic Geology, v.71, p.1196-1205.

Coats, C.J.A. and Snajdr, P. 1984. Ore deposits of the North Range, Onaping–Levack area, Sudbury; *in* The geology and ore deposits of the Sudbury Structure, edited by E.G. Pye, A.J. Naldrett and P.E. Giblin, Ontario Geological Survey, Special Volume 1, p.327-346.

Cowan, J.C. 1968. The geology of the Strathcona ore deposit, Sudbury District, Ontario; CIM Bulletin, v.61, p.38-54.

Craig, J.R. and Kullerud, G. 1969. Phase relations in the Cu-Fe-Ni-S system and their application to magmatic ore deposits; *in* Magmatic ore deposits, edited by H.D.B. Wilson, Economic Geology, Monograph 4, p.344-358.

Distler, V.V., Malevsky, A.Yu and Laputina, P.P. 1977. Distribution of platinoids between pyrrhotite and pentlandite in crystallization of a sulfide melt; Geochemistry International, v.14, no.6, p.30-40.

Hawley, J.E. 1965. Upside-down zoning at Frood, Sudbury, Ontario; Economic Geology, v.60, p.529-575.

Keays, R.R. and Crocket, J.H. 1970. A study of precious metals in the Sudbury nickel irruptive ores; Economic Geology, v.65, p.438-450.

Kullerud, G., Yund, R.A. and Moh, G. 1969. Phase relations in the Fe-Ni-S, Cu-Fe-S and Cu-Ni-S systems; Economic Geology, Monograph 4, p.323-343.

Li, C. and Naldrett, A.J. 1989. PGE study in the footwall at Sudbury; *in* Geoscience Research Grant Program, summary of research 1988–1989, Ontario Geological Survey, Miscellaneous Paper 143, p.104-113.

Makovicky, M., Makovicky, E. and Rose-Hansen, J. 1986. Experimental studies on the solubility and distribution of platinum group elements in base-metal sulfides in platinum deposits; *in* Metallogeny of basic and ultrabasic rocks, edited by M.J. Gallagher, R.A. Ixer, C.R. Neary and F.M. Pritchard, Institute of Mining and Metallurgy, Special Publication, p.415-426.

Naldrett, A. J. 1984. Summary, discussion and synthesis; *in* The geology and ore deposits of the Sudbury Structure, edited by E.G. Pye, A.J. Naldrett and P.E. Giblin, Ontario Geological Survey, Special Volume 1, p.533.

Naldrett, A.J. and Duke, J.M. 1980. Platinum metals in magmatic sulfide ores; Science, v.208, p.1417-1428.

Naldrett, A.J. and Kullerud, G. 1967. A study of the Strathcona Mine and its bearing on the origin of the nickel-copper ores of the Sudbury District, Ontario; Journal of Petrology, v.8, p.453-531.

Naldrett, A.J., Craig, J. and Kullerud, G. 1967. The central portion of the Fe-Ni-S system and its bearing on pentlandite solution in iron-nickel sulfide ores; Economic Geology, v.62, p.826-847.

Naldrett, A.J., Innes, D.G., Sowa, J. and Gorton, M. 1982. Compositional variation within and between 5 Sudbury ore deposits; Economic Geology, v.77, p.1519-1534.

Orlova, G.P., Ryabchikov, I.D., Distler, V.V. and Gladyshev, G.D. 1987. Platinum migration in fluids during the formation of magmatic sulfides; International Geology Review, v.29, p.360-362.

Rajamani, V. and Naldrett, A.J. 1978. Partitioning of Fe, Co, Ni, and Cu between sulfide liquid and basaltic melts and the composition of Ni-Cu sulfide deposits; Economic Geology, v.73, p.82-93.

Rucklidge, J.C., Litherland, A.E. and Lillius, L.R. 1987. The promise of trace element analyses by accelerator mass spectrometry; Journal of Trace and Microprobe Techniques, v.5, no.1, p.23-52.

Skinner, B.J., Luce, F.D., Dill, J.A., Ellis, D.E., Hagan, H.A., Lewis, D.M., Odell, D.A., Sverjensky, D.A. and Williams, N. 1976. Phase relations in the ternary portion of the system Pt-Pd-Fe-As-S; Economic Geology, v.71, p.1469-1475.

Snajdr, P. 1985. Mineralogy and petrology of the Strathcona deep copper zone; Falconbridge Ltd. Sudbury Operation, interoffice memo.

Wilson, G.C., Rucklidge, J.C. and Kilius, L.R, in press. *In situ* parts-per-billion analysis of precious metal in polished minerals samples and sulphide "standards" by accelerator mass spectrometry; Geochimica et Cosmochimica Acta.

Grant 328 Cyanobacterial Model System for the Biological Origin of Gypsum and Carbonate Minerals

J.B. Thompson[1], S. Schultze[1], T.J. Beveridge[1] and W.S. Fyfe[2]

[1]Department of Microbiology, College of Biological Science, University of Guelph, Guelph
[2]Department of Geology, The University of Western Ontario, London

ABSTRACT

Synechococcus, a ubiquitous unicellular cyanobacterium, was investigated as a model system for the biological origin of some gypsum and fine-grain carbonate mud deposits. Transmission electron microscopy of the *Synechococcus* model system provided direct evidence for unicellular cyanobacterial precipitation of gypsum, calcite and magnesite. Laboratory simulations using *Synechococcus* and filter-sterilized alkaline lake water revealed the precipitation of gypsum (within 4 h), calcite (within 24 h) and magnesite (after 72 h). Experimental evidence indicates that because of its abundance and wide distribution over time *Synechococcus* or similar microorganisms may be responsible for a large proportion of the fine-grain carbonate mud within both marine and freshwater environments since the Neoarchean.

INTRODUCTION

The role of cyanobacteria in precipitation of calcium carbonate in natural aquatic environments has long been a subject of controversy (Davis 1903; Hale 1903; Lane 1903; Pollock 1918; Krumbein 1974, 1979; Pentecost 1985; Pentecost and Bauld 1988). Natural marl deposits are often up to 95% pure $CaCO_3$, and they commonly furnish the raw materials to the cement industry throughout North America. Although cyanobacteria have been linked to the origin of marl deposits in North America (Pollock 1918), direct experimental evidence for cyanobacterial calcification in natural waters is lacking. Previously, the best direct evidence for bacterial calcification has come from transmission electron microscopy (TEM) of heterotrophic bacteria from the human oral cavity (dental calculi; Ennever 1963; Ennever and Takazoe 1973) and urinary tract (kidney stones; McLean et al. 1985; Nickel et al. 1987). Therefore, the present study presents direct experimental data for the precipitation of gypsum, calcite and magnesite by a small, unicellular, photosynthetic cyanobacterium of the genus *Synechococcus* in a simulated natural setting.

METHODS

To experimentally investigate the role of small, unicellular cyanobacteria in calcite precipitation in nature we isolated a pure culture of *Synechococcus* sp. (Photo 328.1) from Fayetteville Green Lake, a marl-rich lake in New York. We isolated *Synechococcus* sp. by using serial dilutions on BG-11 agar (a cyanobacterial growth medium). We tested the ability of *Synechococcus* to calcify in natural alkaline waters by inoculating test tubes with 9.0 mL of filter-sterilized (0.22 μm nylon filters) Fayetteville Green Lake water with 1.0 mL of standard suspension of *Synechococcus* containing 10^3 colony-forming units per millilitre. The cultures were incubated under fluorescent light (24 h/day) at 20°C for periods of up to 72 h. At sampling times of 4, 24, 48 and 72 h, a test tube was removed for experimental analysis. We harvested the cells and/or precipitates by centrifugation and initially analyzed them using whole-mount preparations in the TEM. The remaining material was fixed in 1% glutaraldehyde and embedded in an epoxy resin for thin sectioning and detailed electron microscopy. All whole mounts and thin sections were examined on a Philips EM300 or a Philips EM400T equipped with an energy-dispersive X-ray spectrometer (EDS). The supernatant was analyzed for changes in water chemistry including pH, Ca^{2+}, Mg^{2+} and SO_4^{2-}. Calcium and magnesium concentrations were determined via inductively coupled plasma emission spectroscopy (ICP); and sulphate concentrations were determined by liquid chromatography. The carbonate-ion concentration was estimated with an assumed open system ($PCO_2 = 3 \times 10^{-4}$ atm (1 atm = 101.325 kPa); Stumm and Morgan 1981). Alkalinity was determined from acid titration to a pH 4.30 end point. Ion-activity coefficients were calculated with the extended Debye-Hückel equation. Apparent dissociation constants for carbonic acid were calculated with the Güntelberg approximation and saturation indices according to $SI = \log IAP/K_{sp}$, where SI is the saturation index; IAP is the ion-activity product; and K_{sp} is the solubility product. Ionic strength was calculated according to Stumm and Morgan (1981), and we measured pH using standard combination electrodes and National Bureau of Standards buffers. Controls consisted of test tubes with no inoculum, inoculated tubes kept in constant darkness and tubes containing only bacterial cell walls.

RESULTS

The alkaline lake water used in the laboratory simulations was rich in calcium, magnesium and sulphate and was derived from the local Silurian bedrock (Table 328.1). TEM results of the experimental time course indicated a progressive epicellular biomineralization of gypsum, calcite and magnesite from the alkaline lake water. Epicellular mineralization of gypsum, on the surface of *Synechococcus*, occurred within 4 h (Photo 328.2; Figure 328.1). The role of cyanobacteria in gypsum precipitation has never before been reported, except as an indirect physical control on the evaporation of seawater (Braithwaite and Whitton 1987). Calcite precipitation was first recognized after 24 h had

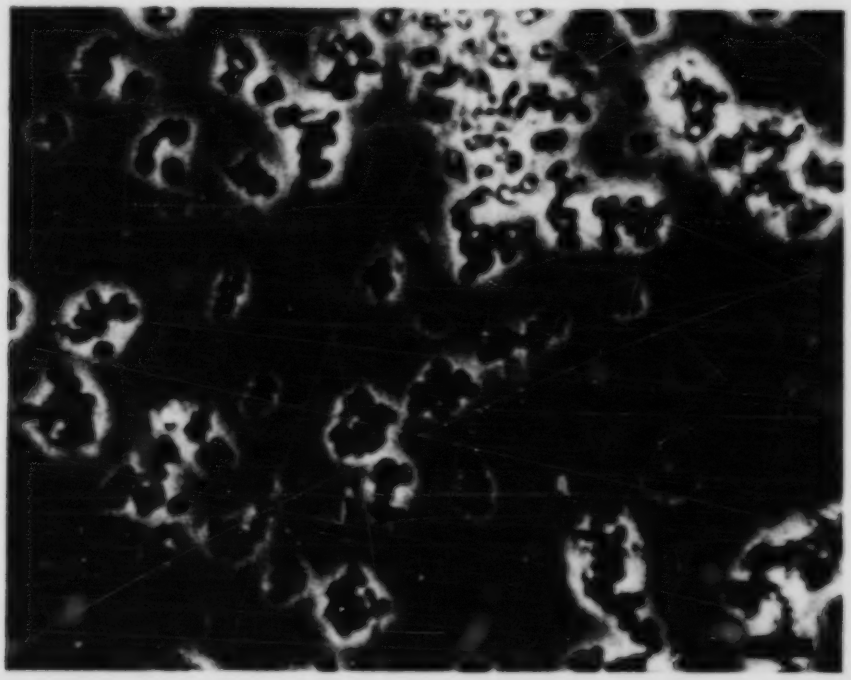

Photo 328.1. Photomicrograph of *Synechococcus* sp. isolated from Fayetteville Green Lake and used in the current experimental laboratory simulations (bar scale = 5 μm).

Table 328.1. Chemistry of Fayetteville Green Lake water used in laboratory simulations.

Components	Values for water collected at 5 m depth (mmol/L)
Ca^{2+}	11.39
Mg^{2+}	2.67
SO_4^{2-}	9.30
Alkalinity	3.20
Ionic strength	55.20
pH	7.97

Table 328.2. Results of the chemical analysis of supernatant from the experimental time course (0, 4, 24, 48 and 72 h).

	Concentrations (mmol/L)				
Components	0 h	4 h	24 h	48 h	72 h
Ca^{2+}	11.39	11.28	11.20	10.19	9.37
Mg^{2+}	2.67	2.67	2.67	2.61	2.65
SO_4^{2-}	9.30	8.81	8.34	8.27	8.38
CO_3^{2-}	$10^{-2.35}$	$10^{-2.35}$	$10^{-1.73}$	$10^{-1.61}$	$10^{-1.13}$
pH	7.97	7.97	8.28	8.34	8.57

elapsed. Epicellular calcite precipitation was more massive and disruptive to the *Synechococcus* cells than the fibrous gypsum precipitation (Photos 328.3A and 328.3B).

Calcification directly coincided with a small increase in pH that occurred between the 4 and 24 h sampling periods (Table 328.2). The photosynthetic metabolism of *Synechococcus* was directly responsible for the alkalization of the microenvironment because of its ability to use HCO_3^- as its primary source of inorganic carbon (Miller and Colman 1980; Badger et al. 1985). Miller and Colman (1980) reported a similar alkalization during photosynthesis by *Synechococcus*. They suggested that *Synechococcus* conducts an HCO_3^-/OH^- exchange process across the cell membrane and that the hydroxyl ions were produced as a result of HCO_3^- fixation in photosynthesis. The present experimental results support such an exchange process: the pH of the experimental microenvironment continued to increase throughout the experiment (Table 328.2).

Measured changes in water chemistry from the natural simulations were consistent with the progressive biomineralization inferred from TEM (Table 328.2). Calcium concentration decreased throughout the entire experiment, coinciding with the precipitation of $CaSO_4$ and $CaCO_3$. Magnesium concentration was unaltered during the 72 h course, although electron microscopic and EDS results obtained after 72 h suggest some precipitation of magnesite as pH continued to increase (Photo 328.4). Sulphate concentrations decreased during the first 48 h but showed a slight increase thereafter. Carbonate-ion concentration increased after 4 h because of the corresponding increase in pH (Table 328.2). Gypsum and calcite mineralization was verified by EDS and electron diffraction, whereas the

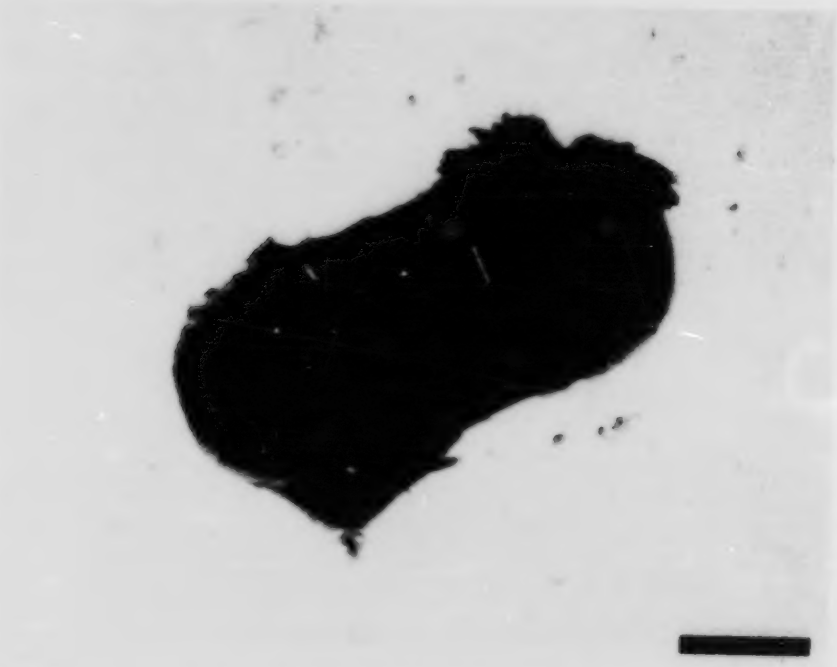

Photo 328.2. Whole-mount transmission electron micrograph showing epicellular gypsum precipitation on *Synechococcus* (bar scale = 500 nm).

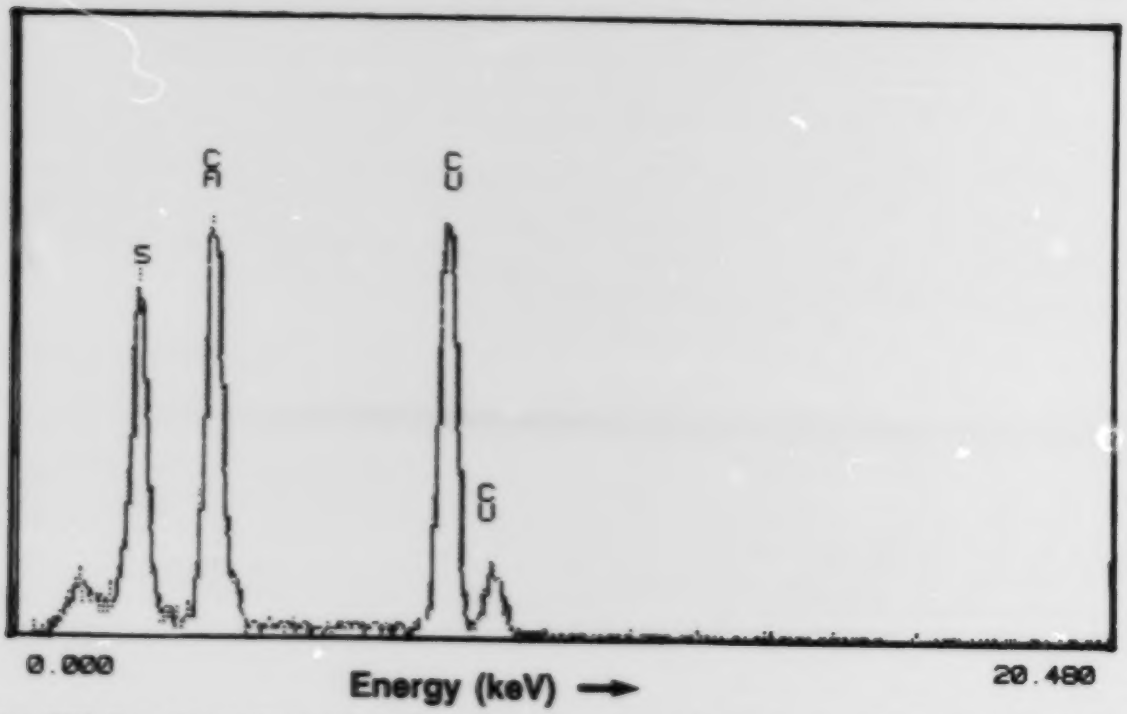

Figure 328.1. Energy-dispersive X-ray spectrum from gypsum precipitates associated with *Synechococcus* (*see* Photo 328.2). Calcium (Ca) and sulphur (S) peaks are from the gypsum, whereas copper (Cu) peaks are from the supporting grid.

magnesite precipitation was suggested by a single, strong magnesium peak shown by EDS (Figure 328.2). No precipitation or alkalization was evident in the sterile controls. Also, no calcite precipitation or alkalization took place in inoculated controls kept in the dark, which suggests that the calcite precipitation was directly related to photosynthesis by *Synechococcus*. However, gypsum was observed in the dark controls, and therefore its formation appears related to the cell surface and is independent of *Synechococcus*'s photosynthetic alkalization process.

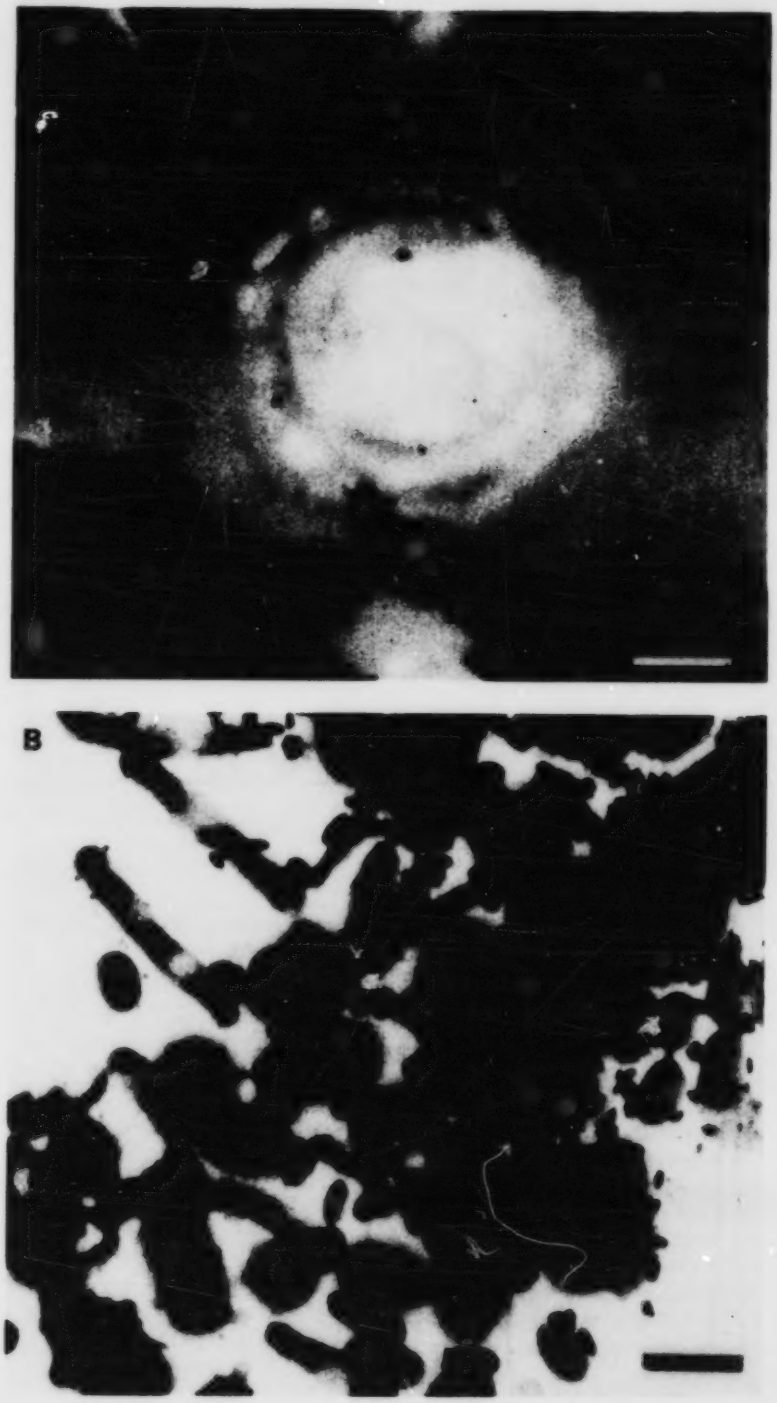

Photo 328.3. Transmission electron micrographs. A) Thin section of *Synechococcus* from 72 h culture showing extensive calcite precipitation on and around the cell surface (arrows). Cells are unstained because of the dissolution of calcite by acidic heavy-metal stains used to provide contrast. Therefore, *Synechococcus* cell is represented by white oval area in centre of the micrograph (bar scale = 250 nm). B) Whole-mount preparation of the same 72 h culture showing the precipitation of calcite within the microcolony and on the surface of the cells (bar scale = 1 μm).

Solubility products and mineral-saturation indices, calculated from the experimental results in Table 328.2, agree with the observed precipitation trends (Figures 328.3 and 328.4). Initially, the lake water plotted in the solid field with respect to gypsum and in the solution field with respect to calcite because of the metal concentrations and pH of the natural lake water (Figure 328.3; Table 328.2). However, according to the calculated saturation indices the lake water

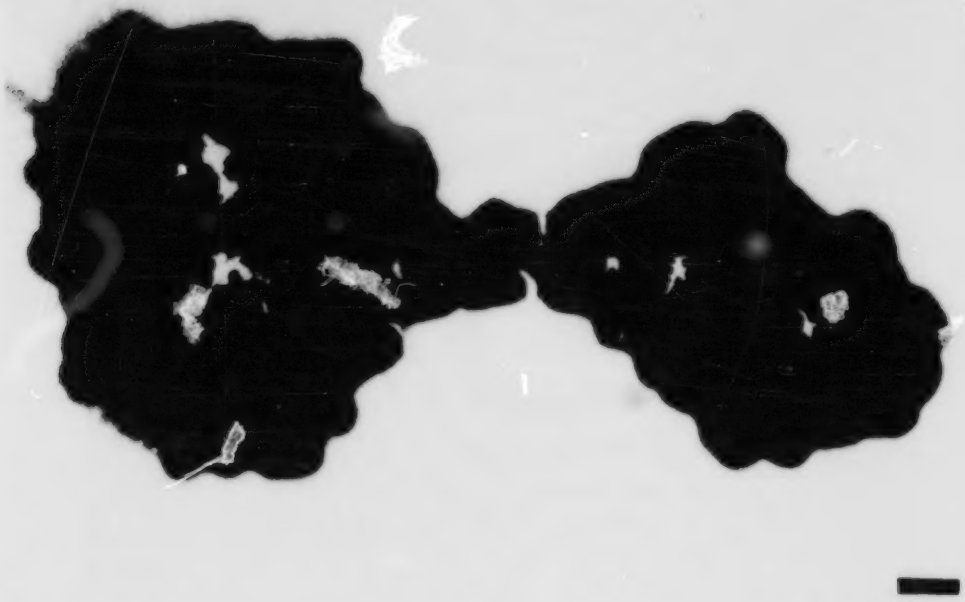

Photo 328.4. Whole-mount transmission electron micrograph of microcolonies of *Synechococcus* with magnesite precipitation in the centre of the colonies (bar scale = 1 μm).

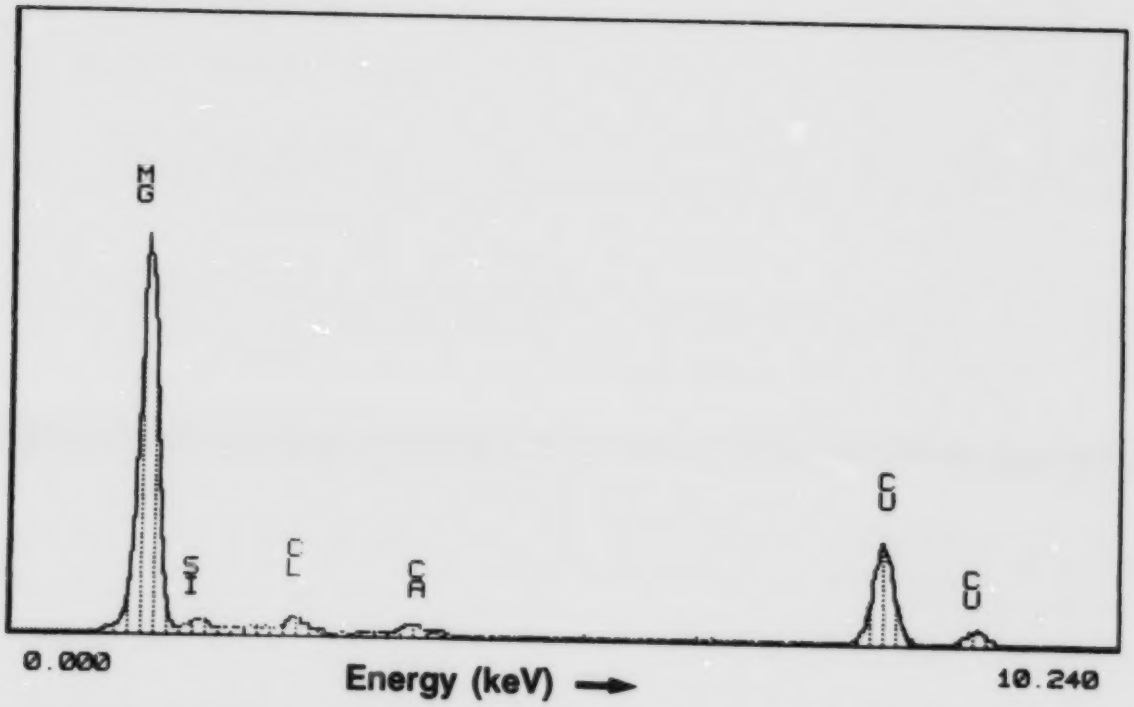

Figure 328.2. Energy-dispersive X-ray spectrum from magnesite precipitates (*see* Photo 328.4). Magnesium (Mg) peak is from the magnesite, whereas copper (Cu) peaks are from the supporting grid.

was oversaturated with respect to gypsum (SI = 1.16) and calcite (SI = 2.73) (Figure 328.4). Photosynthetic alkalization by *Synechococcus* perturbed water chemistry by increasing conditions of oversaturation with respect to calcium solubility (Figure 328.4A). During a 24 to 48 h period the calcification process had so reduced Ca^{2+} activity that solutions were no longer oversaturated with respect to soluble gypsum (Figure 328.4A). Experimental evidence

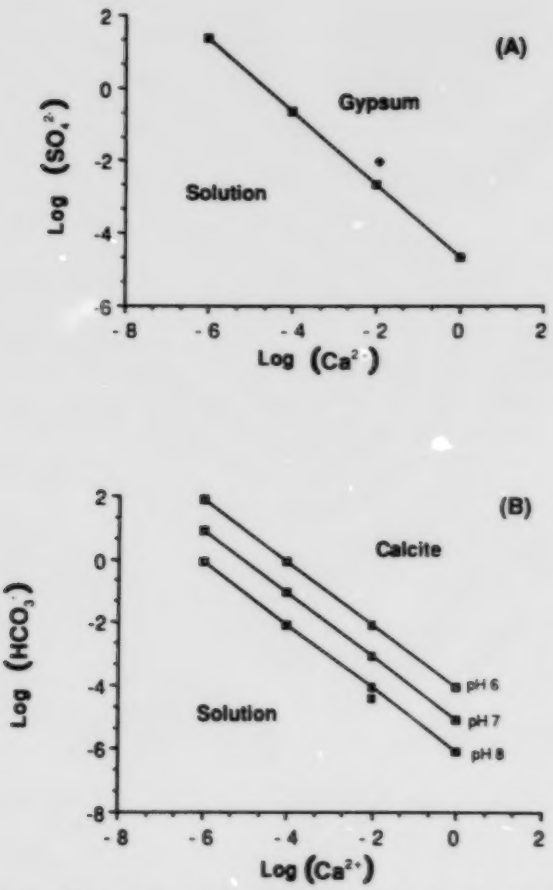

Figure 328.3. A) Plot of calcium versus sulphate concentration with the lake water at time zero plotted as a black dot. Note that the lake water plots within the gypsum field. B) Calcium versus bicarbonate concentration with the lake water at time zero plotted as black dot. Note that at the starting pH (7.97) the lake water plots slightly within the solution field for calcite.

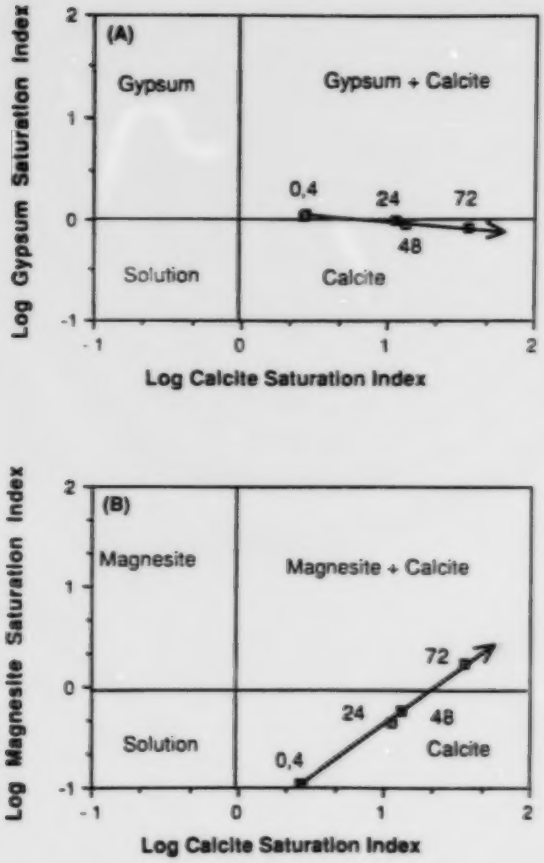

Figure 328.4. Mineral saturation indices determined from results of water chemistry (Table 328.2). Numbers represent sampling time intervals (0, 4, 24, 48 and 72 h). A) Gypsum versus calcite saturation; notice that the alkalization of the microenvironment by *Synechococcus* has raised the level of oversaturation with respect to calcite solubility to 35 times by 72 h. The saturation index with respect to gypsum has dropped, becoming undersaturated between approximately 24 and 48 h. B) Magnesite versus calcite saturation; note that the experimental microenvironment actually became oversaturated with respect to magnesite by 72 h. Saturation index for magnesite at 72 h was 1.71.

indicates that some gypsum may have redissolved as the system became undersaturated with respect to soluble gypsum after 48 h; this is shown by the increasing sulphate concentration recorded at 72 h (Table 328.2).

The experimental system was oversaturated with respect to soluble magnesite after approximately 72 h (Figure 328.4B). Magnesite was found to be associated with large *Synechococcus* aggregates (Photo 328.4). The pH associated with large cell aggregates was possibly higher than the experimentally recorded pH (Table 328.2) resulting in magnesite precipitation.

DISCUSSION AND CONCLUSIONS

Our results clearly indicate that the small cyanobacterium *Synechococcus* is capable of epicellular biomineralization (Mann 1986) of gypsum and calcite in natural alkaline aquatic environments. It is well known that many microorganisms can bind cations, including calcium, to their cell surface and extracellular glycocalyx (a polyanionic polysaccharide matrix; Costerton et al. 1981; Beveridge and Fyfe 1985; Ferris 1989). Calcium cations concentrated on the cell surface act as nucleation centres for both gypsum and calcite precipitation (Figure 328.5). *Synechococcus* acts as a natural biomineralization nucleation site because of 1) its very high surface/volume ratio and 2) its ability to concentrate cations on the cell surface.

Synechococcus also strongly induces calcification in natural alkaline environments because of its photosynthetic alkalization process (HCO_3^-/OH^- exchange system) (Figure 328.5). Gypsum precipitated on the surface of *Synechococcus* because of the naturally high sulphate concentrations in the lake water and the tendency of the bacterial wall to bind calcium cations, which results in a calcium-enriched microenvironment at the cell surface. Subsequently, *Synechococcus* induced calcification in the presence of light by increasing the pH of the microenvironment. These small, unicellular cyanobacteria are ubiquitous within most freshwater and marine environments (Bailey-Watts et al. 1968; Whitton 1973;

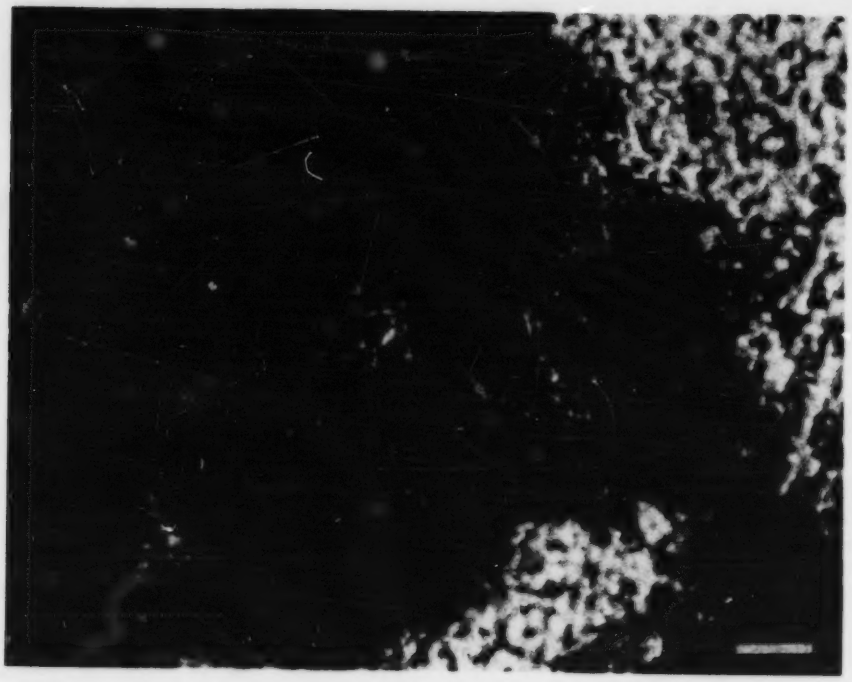

Photo 328.5. Thin-section photomicrograph of a marl grain from Fayetteville Green Lake showing numerous occluded *Synechococcus* cells within the calcite grain (arrows) (bar scale = 5 μm).

Waterbury et al. 1979; Li et al. 1983; Murphy and Haugen 1985; Wyman et al. 1985; Guillard et al. 1985; Stockner 1988). Present data show that *Synechococcus* is responsible for the predominant calcification (marl formation) in Fayetteville Green Lake and that *Synechococcus* cells are continually entombed within growing calcite crystals (Photo 328.5). Moreover, the *Synechococcus* sp. used in these experiments possesses an S layer or paracrystalline surface array as its outermost boundary layer (Photos 328.6 and 328.7). This S layer may act as a template that captures and orders Ca^{2+} to promote mineral development. To protect the cells from the epicellular calcification, the old S layer may be shed and replaced by a new S layer when it becomes calcified, which would allow for the growth and survival of *Synechococcus* in alkaline environments. *Synechococcus*' direct role in calcification, along with its antiquity and ubiquity in aquatic environments, has widespread implications for both modern and ancient marl or carbonate mud deposits that are important to the cement and other industries. Finally, these results suggest that some gypsum and magnesite deposits may be of unicellular cyanobacterial origin. Further investigations are needed to determine the extent and importance of these processes.

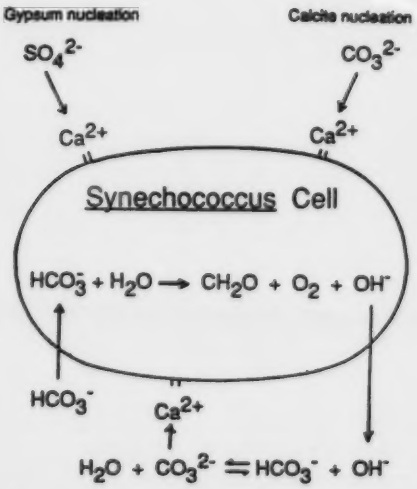

Figure 328.5. Schematic model for *Synechococcus* calcification. *Synechococcus* is responsible for the direct alkalization of its surrounding microenvironment because of an HCO_3^-/OH^- exchange process across its cell membrane. This exchange process is the result of HCO_3^- fixation in photosynthesis (Miller and Colman 1980). *Synechococcus* also provides an ideal nucleation site for calcification within this microenvironment because of its high surface/volume ratio and its ability to bind calcium cations to the cell surface.

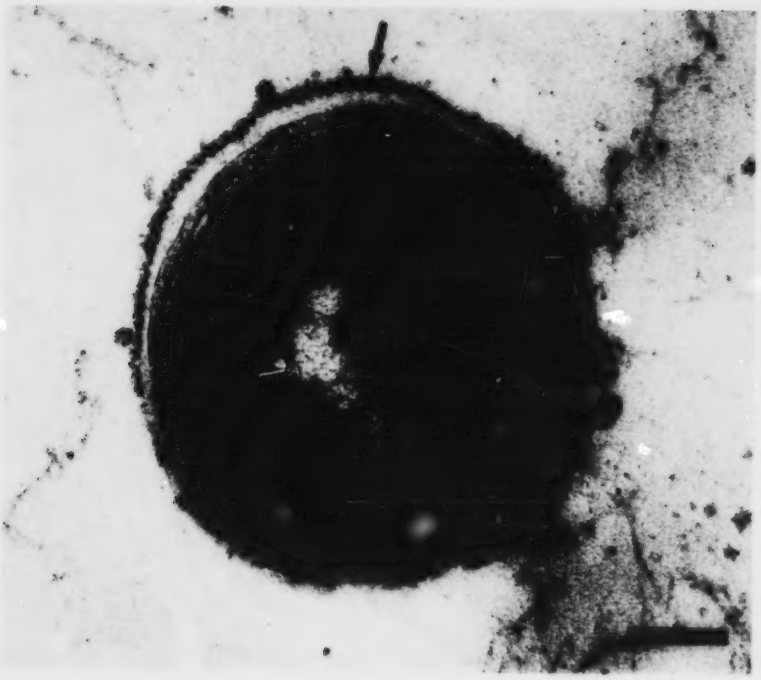

Photo 328.6. Stained thin-section electron micrograph of *Synechococcus* showing the S layer surrounding the cell (arrow) (bar scale = 200 nm).

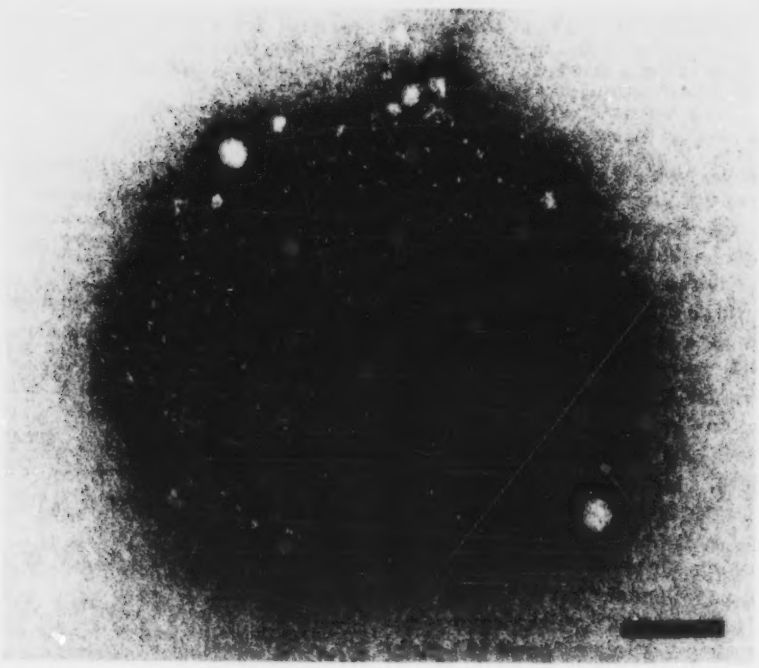

Photo 328.7. Negative-stained whole-mount transmission electron micrograph showing the outer surface of the hexagonal paracrystalline S layer (bar scale = 100 nm).

REFERENCES

Badger, M.R., Bassett, M. and Comins, H.N. 1985. A model for HCO_3^- accumulation and photosynthesis in the cyanobacterium *Synechococcus* sp.; Plant Physiology, v.77, p.465-471.

Bailey-Watts, A.E., Bindloss, M.E. and Belcher, J.H. 1968. Freshwater primary production by a blue-green alga of bacterial size; Nature (London), v.220, p.1344-1345.

Beveridge, T.J. and Fyfe, W.S. 1985. Metal fixation by bacterial cell walls; Canadian Journal of Earth Sciences, v.22, p.1893-1898.

Braithwaite, C.J.R. and Whitton, B.A. 1987. Gypsum and halite associated with the cyanobacterium *Entophysalis*; Geomicrobiology Journal, v.5, p.43-55.

Costerton, J.W., Irvin, R.T. and Cheng, K.J. 1981. The bacterial glycocalyx in nature and disease; Annual Review of Microbiology, v.35, p.299-324.

Davis, C.A. 1903. A contribution to the natural history of marl; Geological Survey of Michigan, Annual Report, v.8, p.65-102.

Ennever, J. 1963. Microbiologic calcification; Annals of the New York Academy of Sciences, v.109, p.4-13.

Ennever, J. and Takazoe, I. 1973. Bacterial calcification; p.629-648 *in* Biological mineralization, edited by I. Zipkin, Wiley Interscience, New York, 899p.

Ferris, F.G. 1989. Metallic ion interactions with the outer membrane of gram-negative bacteria; p.295-323 *in* Metal ions and bacteria, edited by T.J. Beveridge and R.J. Doyle, Wiley Interscience, New York, 461p.

Guillard, R.R.L., Murphy, L.S., Foss, P. and Liaaen-Jensen, S. 1985. *Synechococcus* spp. as likely zeaxanthin-dominant ultraphytoplankton in the North Atlantic; Limnology and Oceanography, v.30, p.412-414.

Hale, D.J. 1903. Theories of origin of bog lime or marl; Geological Survey of Michigan, Annual Report, v.8, p.41-64.

Krumbein, W.E. 1974. On the precipitation of aragonite on the surface of marine bacteria; Naturwissenschaften, v.61, p.167.

———1979. Calcification by bacteria and algae; p.47-68 *in* Biogeochemical cycling of mineral-forming elements, edited by P.A. Trudinger and D.J. Swaine, Elsevier, Amsterdam, 612p.

Lane, A.C. 1903. Notes on the origin of Michigan bog limes; Geological Survey of Michigan, Annual Report, v.8, p.199-223.

Li, W.K.W., Subba Rao, D.V., Harrison, W.G., Smith, J.C., Cullen, J.J., Irwin, B. and Platt, T. 1983. Autotrophic picoplankton in the tropical ocean; Science, v.219, p.292-295.

Mann, S. 1986. Biomineralization in lower plants and animals: chemical perspectives; p.39-54 *in* Biomineralization in lower plants and animals, edited by B.S.C Leadbeater and R. Riding, Clarendon Press, Oxford, 401p.

McLean, R.J.C., Nickel, J.C., Noakes, V.C. and Costerton, J.W. 1985. An in vitro ultrastructural study of infectious kidney stone genesis; Infection and Immunity, v.49, p.805-811.

Miller, A.G. and Colman, B. 1980. Evidence for HCO_3^- transport by the blue-green alga (cyanobacterium) *Coccochloris peniocystis*; Plant Physiology, v.65, p.397-402.

Murphy, L.S. and Haugen, E.M. 1985. The distribution and abundance of phototrophic ultraplankton in the North Atlantic; Limnology and Oceanography, v.30, p.47-58.

Nickel, J.C., Olson, M., McLean, R.J.C., Grant, S.K. and Costerton, J.W. 1987. An ecological study of infected urinary stone genesis in an animal model; British Journal of Urology, v.59, p.21-30.

Pentecost, A. 1985. Association of cyanobacteria with tufa deposits: identity, enumeration, and nature of the sheath material revealed by histochemistry; Geomicrobiology Journal, v.4, p.285-299.

Pentecost, A. and Bauld, J. 1988. Nucleation of calcite on the sheaths of cyanobacteria using a simple diffusion cell; Geomicrobiology Journal, v.6, p.129-135.

Pollock, J.B. 1918. Blue-green algae as agents in the deposition of marl in Michigan lakes; Michigan Academy of Science, Annual Report, v.20, p.247-261.

Stockner, J.G. 1988. Phototrophic picoplankton: an overview from marine and freshwater ecosystems; Limnology and Oceanography, v.33, p.765-775.

Stumm, W. and Morgan, J.J. 1981. Aquatic chemistry: an introduction emphasizing chemical equilibria in natural waters; Wiley Interscience, New York, 780p.

Waterbury, J.B., Watson, S.W., Guillard, R.R.L. and Brand, L.E. 1979. Widespread occurrence of a unicellular, marine, planktonic cyanobacterium; Nature (London), v.277, p.293-294.

Whitton, B.A. 1973. Freshwater plankton; p.353-367 *in* The biology of blue-green algae, edited by N.G. Carr and B.A Whitton, University of California Press, Berkeley.

Wyman, M., Gregory, R.P.F. and Carr, N.G. 1985. Novel role for phycoerythrin in a marine cyanobacterium, *Synechococcus* strain DC2; Science, v.230, p.818-820.

Grant 329 Tectono-metamorphic Character of the Matachewan Area, Northeast Ontario

W.G. Powell, C.J. Hodgson and D.M. Carmichael

Department of Geological Sciences, Queen's University, Kingston

ABSTRACT

Examination of both the Archean and Proterozoic rocks of the Matachewan area has revealed a complex tectonic history. Structures have been divided into 2 groups: those observed in the Archean rocks (D_A), and those postdating the overlying Proterozoic age Gowganda Formation (D_P). The groups have been subdivided as follows:

D_A1. Folds without an associated foliation, predating the deposition of the Timiskaming Group

D_A2. Strong schistosity and/or gneissosity adjacent to the Round Lake batholith, formed by the diapiric rise of the pluton after it had crystallized

D_A3. Discrete east-southeast-trending domainal zones of "banded" cleavage associated with extensive carbonatization

D_A4. Domainal zones of spaced cleavage to schistosity, generally superimposed on the D_A3 zones, trending east-northeast; one of these zones hosts the mineralization of the Young–Davidson and Matachewan Consolidated gold mines; another is the extension of the Kirkland Lake–Larder Lake break (KLLB)

D_A5. Open, moderate to steeply plunging folds trending north to northeast

D_P1. Reactivation of D_A4 faults, forming local upright open folds with an axial-planar cleavage in fine-grained sedimentary rocks of the Gowganda Formation

D_P2. North-trending normal faults with associated north-trending pressure-solution cleavage (e.g., the Mistinikon Lake fault)

D_P3. Northwest-trending normal faults postdating the Silurian carbonate rocks of the Earlton area (eg. the Cross Lake fault)

The rocks of the Matachewan area have been affected by 2 aerially extensive metamorphic episodes: a regional metamorphic event ranging in grade from prehnite-pumpellyite to greenschist; and a greenschist-grade contact-metamorphic event associated with the diapiric emplacement of the Round Lake batholith. Mineral assemblages and metamorphic sequences in the subgreenschist-greenschist transition zone provide constraints on conditions of peak metamorphism for the regional event. Based on the generalized *P-T* diagram of Liou et al. (1987), with corrections for rock composition, pressures at peak regional metamorphism just north of the KLLB were of the order of 1.8 kbars (1 kbar = 100 MPa).

INTRODUCTION

The large gold deposits of the southern Abitibi belt occur within a few kilometres of 2 major "breaks", the Kirkland–Larder Lake–Cadillac break and the Destor–Porcupine break. This spatial association makes the tracing of these breaks a priority in gold exploration. The objective of this project was to trace the KLLB west from Kenogami Lake (approximately 15 km southwest of Kirkland Lake), through Matachewan, to the Halliday dome area (Figure 329.1).

This project involved detailed structural analysis, reconnaissance mapping and detailed mapping in areas where strong airphoto lineaments and/or deformation zones had been recognized in the reconnaissance mapping. Mapping of the Archean basement clarified the distribution and nature of the Archean deformation. Mapping within the Proterozoic sedimentary Gowganda Formation revealed that late reactivation of underlying Archean basement faults had affected the Gowganda Formation, allowing the tracing of Archean structures through the overlying cover rocks.

During the 1989 field season samples were collected for study of the metamorphic petrology of the Archean volcanic rocks. Earlier studies of the metamorphic history of the Abitibi belt (Jolly 1980; Dimroth et al. 1983) indicated that the KLLB may define a transition in metamorphic conditions, with metamorphic grade increasing southwards across the break. If this applies to the Matachewan area, then the metamorphic facies of the Archean rocks could provide a further constraint to the position of the KLLB within the study area. Documentation and understanding of the metamorphic history of the Abitibi greenstone belt are also required before a comprehensive tectonic history can be developed. With recent advances in the understanding of the subgreenschist facies (e.g., Liou et al. 1987), limits to pressure and temperature of peak metamorphism of mafic rocks at very low grade can be determined.

GENERAL GEOLOGY

Parts of the study area were previously mapped by Lovell (1967, 1972), Moore (1966), Junnila (1989) and Bright (1970) (Figure 329.2). Tholeiitic basalt and andesite flows (MERQ–OGS 1983) with minor iron formation and interflow sediments constitute the majority of the Archean supracrustal rocks. A sequence of sedimentary and alkalic volcanic rocks of the Timiskaming Group unconformably overlies the volcanic rocks (Thomson 1946). The Timiskaming Group contains distinctive fluvial conglomerates and greywackes and is spatially associated with the Kirkland–Larder Lake–Cadillac break, a major

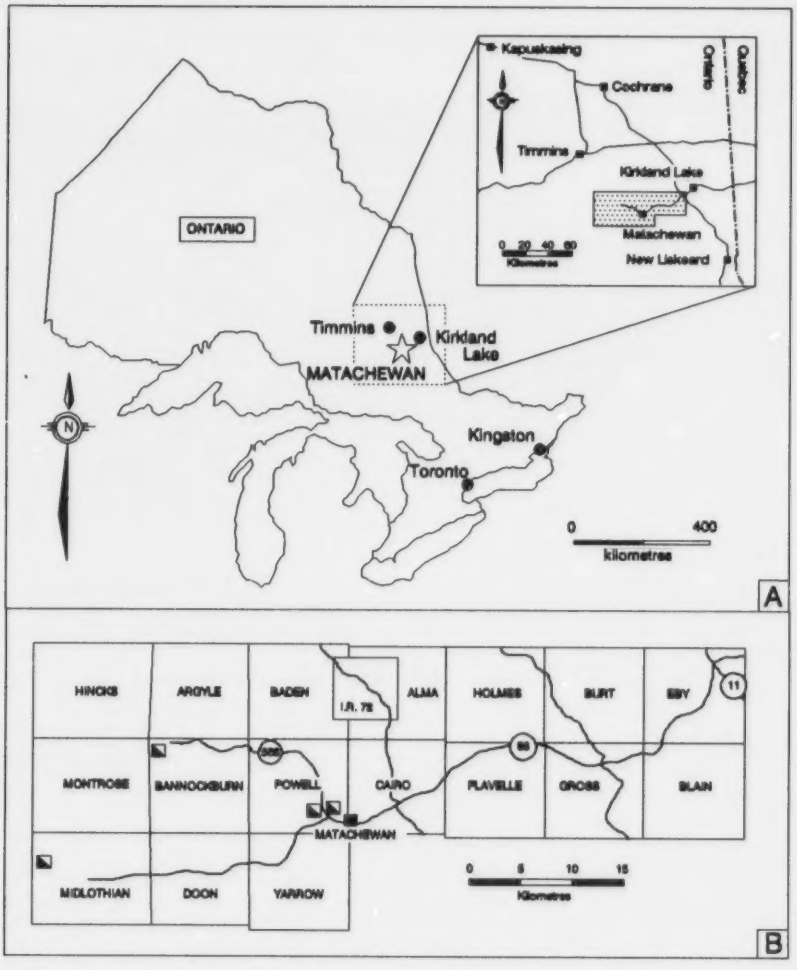

Figure 329.1. A) Location map of the study area; B) townships located within the study area.

structural zone controlling the distribution of gold mineralization along its strike length from Val-d'Or in Quebec through to the Matachewan area in Ontario.

Several phases of intrusive activity have been documented in the study area. The earliest intrusives are small diorite bodies. A period of felsic intrusive activity followed in which the Round Lake batholith was emplaced on the south side of the study area. The batholith is a composite intrusion, dominantly trondhjemite and tonalite, but younger granodiorites have intruded along its margins and interior (Jensen 1985). The latest felsic intrusive bodies are syenites. These include the Otto, Cairo, Holmes and Dixon Lake stocks.

Deformation associated with the Larder Lake–Cadillac break is recorded in all of the Archean lithologies listed above.

Proterozoic rocks within the map area include diabase dikes of the Matachewan dike swarm, which cut the Archean rocks but are overlain by the glacigenic sediments of the Coleman Member of the Gowganda Formation (Cobalt Group, Huronian Supergroup) (2288 ± 87 Ma) (Fairbairn et al. 1969). The youngest intrusive rocks in the area are the Nipissing diabase (2219.4$^{+3.3}_{-3.3}$ Ma) (Corfu and Andrews 1986) and the Sudbury diabase (1238 ± 4 Ma) (Krough et al. 1987).

STRUCTURAL GEOLOGY

The sequence of deformation events outlined below is based on observations from the Matachewan area only. A suggested correlation with deformational events recognized elsewhere in the Abitibi belt is given in Table 329.1.

Deformational events in the Matachewan area have been divided into 2 groups: those that predate the Gowganda Formation (D_A), and those that postdate the Gowganda Formation (D_P).

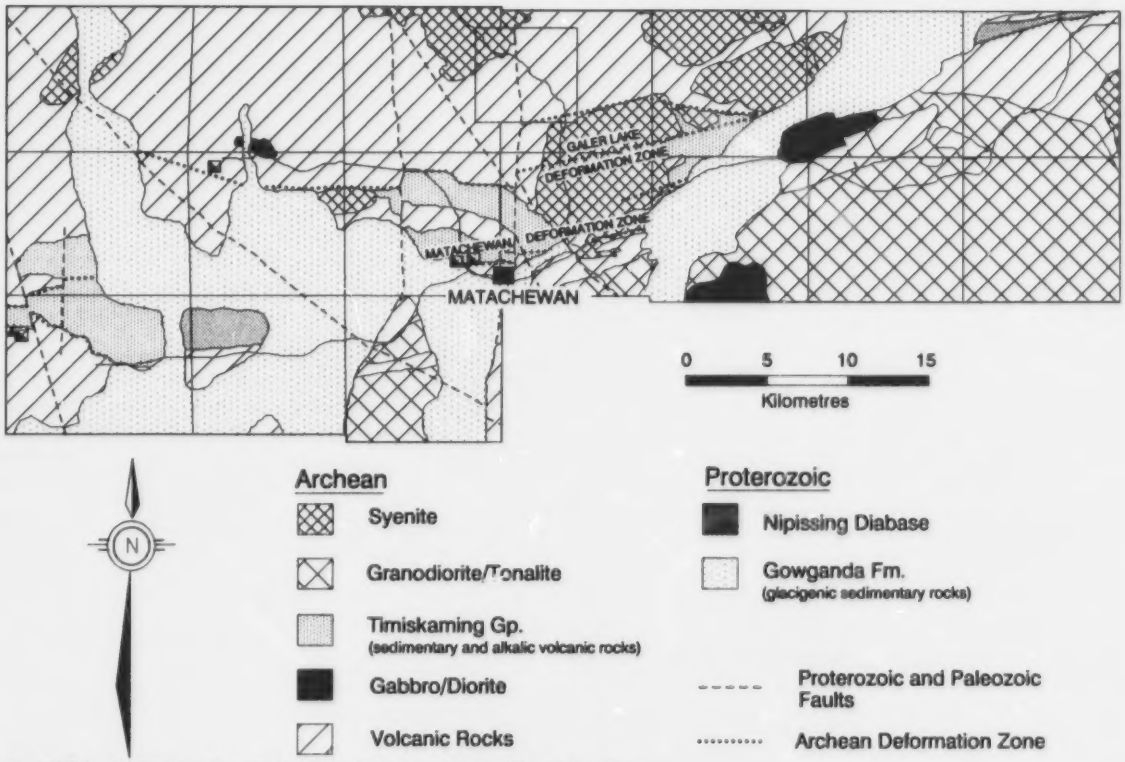

Figure 329.2. General geology of the Matachewan area (*after* Pyke et al. 1973).

Archean Structures: D_A

D_A1

These structures consist of large-scale folds in the Archean volcanic strata without an associated axial-planar foliation. The trace of the fold-axial planes trends approximately 070° to 080°. These folds are confined to the volcanic rocks but do not appear to be present in the Timiskaming Group. Therefore, this deformation event preceded deposition of the Timiskaming Group sediments. The D_A1 folds are likely correlative with the Porcupine syncline and North Tisdale anticline in the Timmins area, as described by Piroscho and Kettles (1988).

D_A2

These structures consist of L-S fabrics in supracrustal rocks and the margin of the Round Lake batholith formed during the solid-state diapiric rise of the batholith. The fabric is dominated by steeply plunging stretching and mineral lineations (Figure 329.3E). The associated schistosity, oriented subparallel to the contact of the pluton, is well developed in xenoliths and volcanic rocks near the margin of the Round Lake batholith but is generally weak in the granodiorite. Asymmetric folds in mafic mylonites indicate south-side-up motion along the northern margin of the batholith.

The D_A2 zones, which grade from weakly foliated to mylonitic, are distinguished from the younger deformation zones related to the regional breaks on the basis of the higher metamorphic grade of the deformed rocks and the lack of associated carbonate and pyrite alteration. The orientations of D_A2 fabrics and foliations related to the breaks are similar in the Matachewan area because of the subparallelism of the breaks and the contact of the batholith.

The mylonites related to the D_A2 event lack the carbonate and pyritic alteration associated with the younger structures. The higher metamorphic grade near the batholith and the low CO_2 of the environment of formation of D_A2 structures resulted in the fabrics being characterized by amphibole (actinolite or hornblende) rather than chlorite and muscovite as found in D_A3 or D_A4 structures. As a result, D_A2 mylonites are much more resistant to erosion and therefore commonly form high ground rather than the swampy valleys of the D_A3 and D_A4 zones.

D_A3

These structures consist of domainal, moderately plunging, closed folds and a "banded" cleavage of alternating quartz-carbonate and chlorite-muscovite bands. These bands appear to develop initially as chloritic alteration along permeable horizons, such as bedding planes. With continued development, these chloritic seams grow while the country rock is carbonatized. This same distinctive form of cleavage is observed in volcanic, sedimentary and felsic intrusive rocks. In general the foliation trends east-southeast except where it is affected by later deformational events. Extensive carbonatization accompanied the D_A3 event.

Pebbles within an outcrop of Timiskaming conglomerate within a D_A3 zone are oblate (Figure 329.4).

Table 329.1. A suggested correlation of deformational events recognized across the Abitibi greenstone belt.

Current study	Hodgson and Hamilton (1989)	Piroscho and Kettles (1988)	Hubert et al. (1984)	Dimroth et al. (1983)
D_A1	D0	D0	–	–
D_A2	–	–	–	–
D_A3	D1	D2	D1	D1
D_A4	D2	D3a	D2	D2
D_A5	–	D3b	–	–

Average aspect ratios of felsic intrusive clasts are $x:y:z$ = 1.9:2.5:1, where xy is the foliation plane and y is the vertical component.

The D_A3 zones are typically located at the contact of the Timiskaming sedimentary rocks with the older volcanic rocks. Deformation is most intense in the sedimentary rocks and increases in intensity toward the contact. Where bedding parallels the contact, foliations are parallel to bedding. Where bedding is oblique to the Timiskaming-volcanic contact, the foliation is oblique to bedding and parallel to the inferred contact. These relationships suggest that the Timiskaming Group is, at least locally, in fault contact with the older volcanic rocks.

D_A4

This structure is a subvertical, planar spaced cleavage to schistosity generally trending 060° to 090°. This foliation is highly domainal; within 100 m of a D_A4 zone the micas and amphiboles, which define the cleavage in the deformation zone, have no preferred orientation. Without exception the D_A4 zones are superimposed on the earlier D_A3 zones.

Pebbles within the Timiskaming conglomerate at the Young–Davidson Mine (a zone of superimposed D_A3 and D_A4 structures) are more prolate than those in the D_A3 zone described above. However, the direction of elongation of the pebbles is always parallel to the intersection of S_A3 and S_A4 (Figure 329.3F). This suggests that the vertical stretching observed within D_A4 zones may be the result of superimposed flattening events at high angles to each other.

The steep plunge of elongation lineations and the common occurrence of subhorizontal tension veins, which often contain subvertical mineral fibres, indicate that D_A4 zones are reverse faults.

A number of D_A4 faults are present in the study area, including the KLLB and the deformation zone hosting the Young–Davidson and Matachewan Consolidated gold mines. These mines have been described by Dyer (1936), Derry et al. (1948) and Sinclair (1982).

D_A5

These structures are moderately to steeply plunging open folds with a locally developed axial-planar spaced cleavage. The axial-planar cleavage is subvertical, but the strike is variable, generally lying between 000° and 040°. Intensity of cleavage development increases and fold wavelength decreases within schistose zones formed during the D_A3 and D_A4 events.

Poles to bedding of the Timiskaming sediments of the Midlothian Lake area are dispersed about a great circle whose pole is oriented at 043°/78° (Figure 329.3A). The S_A2 cleavage shows a similar variation in orientation, about an axis oriented 046°/76° (Figure 329.3B). These patterns of bedding and cleavage orientation are attributed to D_A5 folding. The S_A4 schistosity at the Young–Davidson Mine, near Matachewan, appears to be folded about an F_A5 axis oriented at 218°/64° (Figure 329.3C). The fact that these fold axes plunge in opposite directions is likely due to the pre-D_A5 orientation of the surface that was folded during the D_A5 event: bedding in the Midlothian Lake area and S_A2 generally dip to the north, whereas S_A4 is south dipping at the Young–Davidson Mine.

Proterozoic and Paleozoic Structures: D_P

The glacigenic sedimentary rocks of the Gowganda Formation in the Matachewan area have been affected by several periods of deformation.

D_P1

These structures consist of linear zones of upright folds with associated wavy slaty cleavage and growth of white micas in the cleavage planes. The orientation of the cleavage varies across the linear deformation zones. In the centre, where cleavage is most intensely developed, foliations strike 060° to 070° with subvertical dips. Within 50 to 150 m of the centre, the cleavages rotate into a northeast orientation (045° to 055°). The intensity of cleavage development diminishes from the centre of the zone, and cleavage is not observed in either outcrop or thin section more than 400 m from the centre of the deformation zone.

The D_P1 zones lie along strike from D_A3 zones in the Archean basement. The folding and probable faulting of the Gowganda Formation are likely due to minor strike-slip or transpressive reactivation of the underlying D_A3 faults. The rotation of the foliation within these zones indicates a dextral horizontal displacement.

Development of S_P1 is highly dependent on the grain size and composition of the sedimentary rocks. Cleavage is only evident in siliceous mudstones and siltstones. Sandstone beds within cleaved siltstone units exhibit no foliation but are folded. A vertical outcrop within a D_P1 zone in southern Holmes Township comprises mainly siliceous siltstones but contains several >10 cm thick arkose beds. The siltstones contain a well-developed D_P1 cleavage, but the arkose is massive; however, the arkose beds have been steepened and disjointed, with each segment onlapping the adjacent segments (see Photo 329.1).

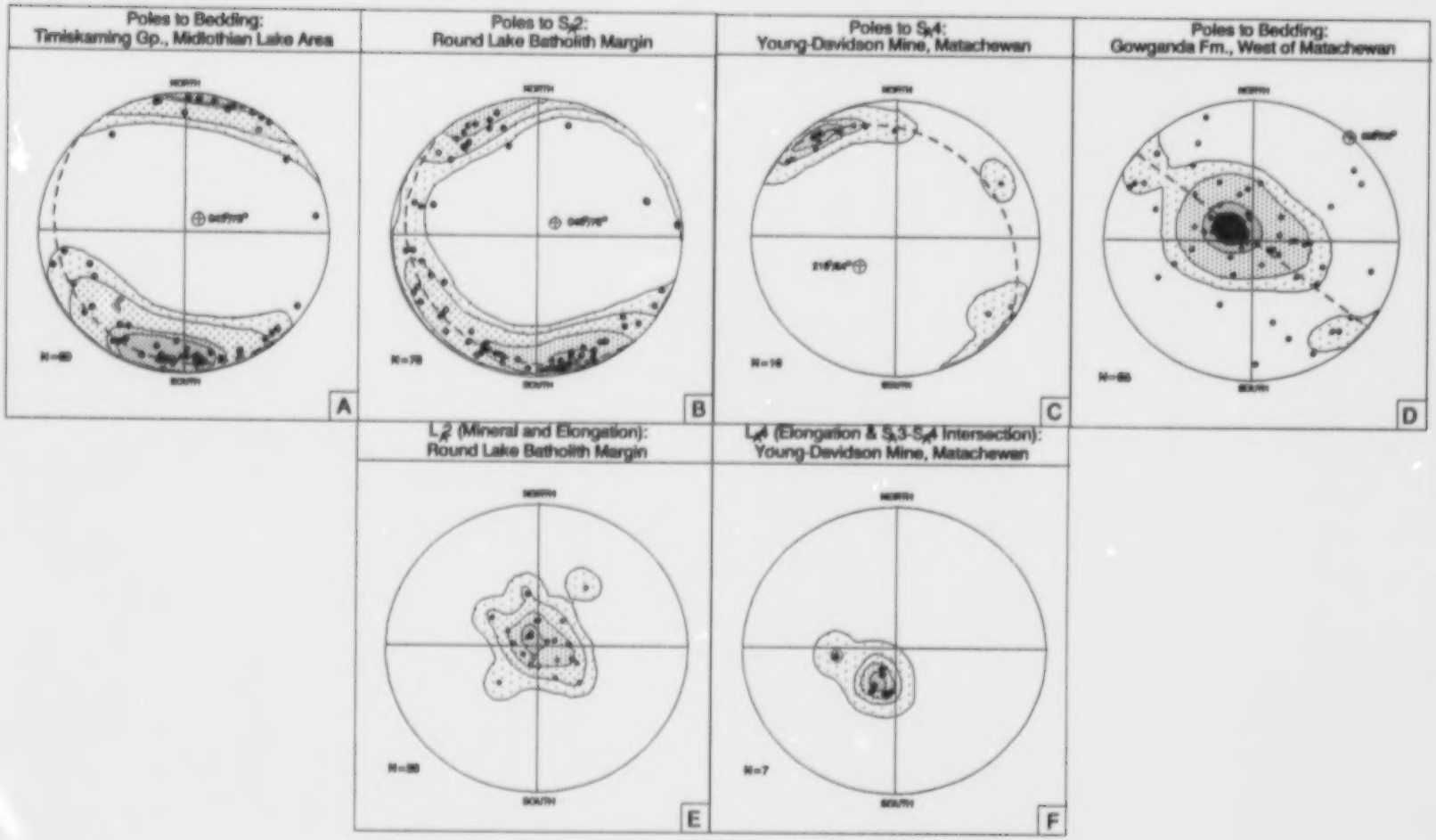

Figure 329.3. Stereographic projection of selected structural elements from the Matachewan area. (The circle with cross hairs on the planar-element plots mark the pole to the best-fit great circle.)

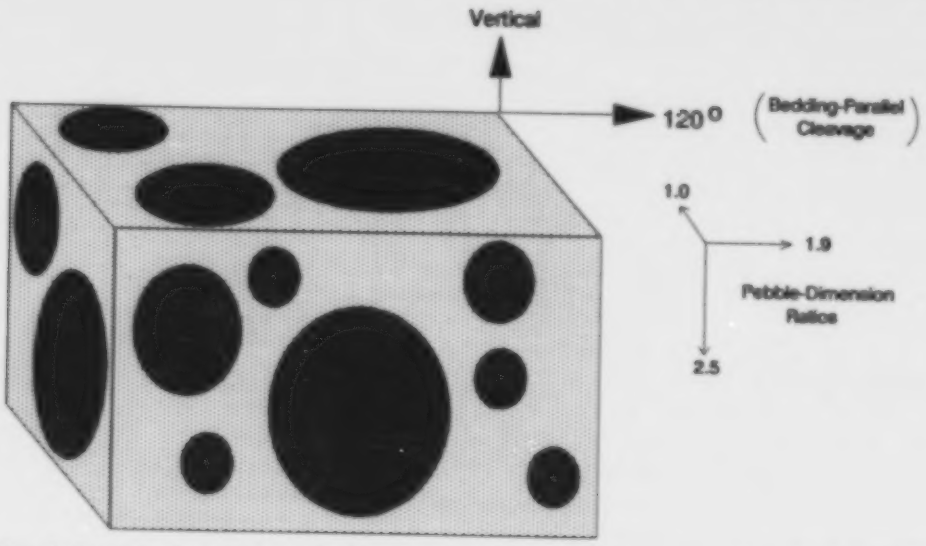

Figure 329.4. Schematic diagram of the dimensions of felsic intrusive clasts in Timiskaming conglomerate within a D_A3 zone in Midlothian Township, illustrating the oblate form of the clasts. Number of measurements used in average: horizontal plane, 12; vertical in the plane of flattening, 24; vertical perpendicular to the plane of flattening, 19.)

Photo 329. 1. D_P1 zone within a siliceous siltstone unit of the Gowganda Formation, southern Holmes Township. A subvertical slaty pressure-solution cleavage developed in the siltstone while the more competent arkose bed buckled and fractured to accommodate the strain.

The cleavage associated with this period of deformation has only been observed east of Mistinikon Lake (central Powell Township). This may be a function of the stratigraphic level exposed within the Cobalt Group on either side of the Mistinikon Lake normal fault (west-side down), since a relatively high structural level is present on the west side of the lake and a relatively low structural level is present on the east side of the lake.

Within the Gowganda Formation, the same compressional event formed regional north- to northeast-trending horizontal flexures and gentle folds, which lack a corresponding axial-planar cleavage. Poles to bedding of Gowganda sedimentary rocks are dispersed about a great circle whose pole is oriented at 038°/00° (Figure 329.3D). This dispersion is interpreted as being the result of D_P1 folding: the pole of the great circle is roughly coincident with the axis of flexures observed in the Gowganda Formation of Doon Township.

Although the trend of the D_P1 folds is similar to that of the D_A5 folds, it is considered unlikely that the D_A5

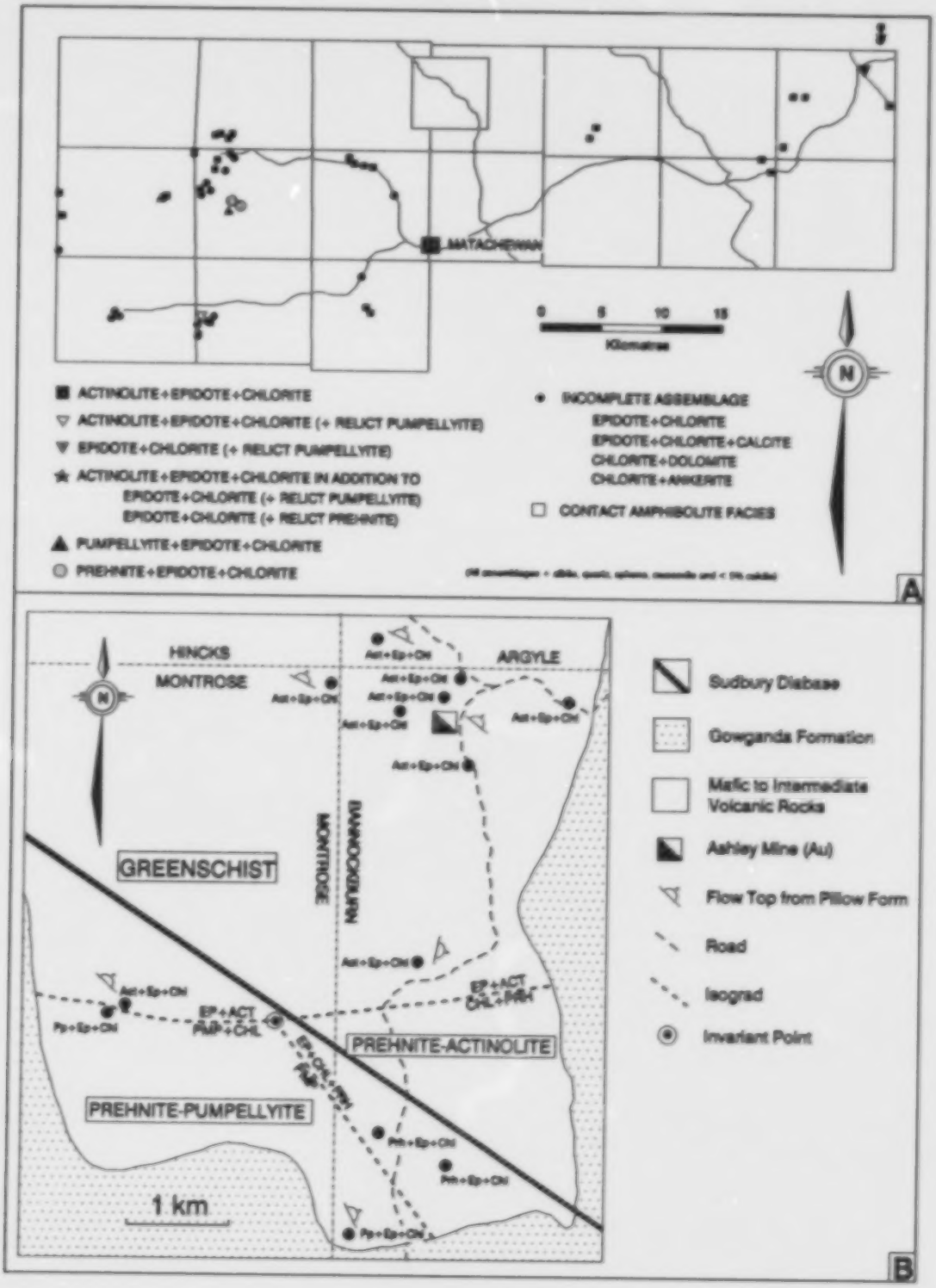

Figure 329.5. A) Distribution of metamorphic mineral assemblages in the Matachewan area. B) Map of subgreenschist-greenschist isograds in northern Bannockburn and Montrose townships. Isograds are placed to maximize the width of the pumpellyite-actinolite facies.

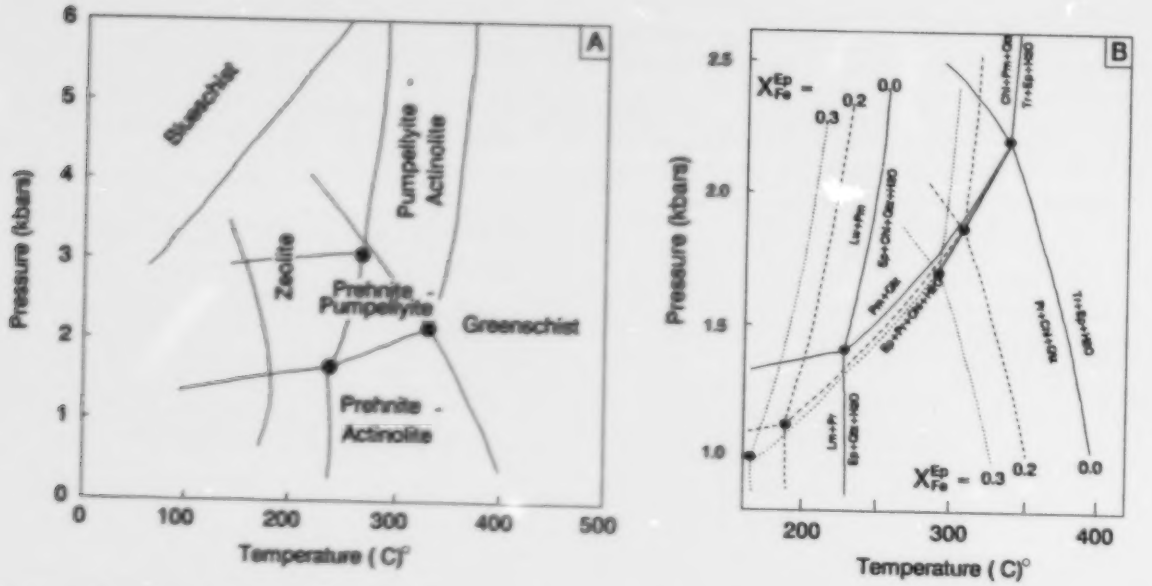

Figure 329.6. Petrogenetic grid for various low-grade metamorphic facies in rocks of basaltic composition. A) Idealized *P-T* system with Fe^{3+} assumed absent (*from* Liou et al. 1987). B) *P-T-*$X_{Fe^{3+}}$ for the subgreenschist basaltic system, illustrating the displacement of the invariant points with increasing Fe^{3+} as determined from epidote compositions (*from* Liou et al. 1987).

structures are related to a post–Gowganda event. The absence of a related cleavage, the very low amplitude of the folds and the very gentle interlimb angles all distinguish the regional F_n2 folds from the F_n5 folds.

D_P2

These structures consist of normal faults and associated local folding. Pressure-solution cleavage at 020°/60° is present in Gowganda siliceous mudstones along major north-south lineaments (e.g., Montreal River, Mistinikon River). A D_P2 fault, oriented at 000°/60° and containing coarse, silicified fault breccia, was noted along the west shore of Mistinikon Lake.

D_P3

These are normal faults of post–Silurian age trending northwest (e.g., Englehardt River fault). No exposure of this fault was observed because of extensive overburden cover.

METAMORPHISM

Two distinct, aerially extensive metamorphic events were documented in the area around Matachewan: 1) a regional metamorphic event ranging from prehnite-pumpellyite to greenschist facies and 2) a contact-metamorphic event associated with the emplacement of the Round Lake batholith. It is difficult to determine, with certainty, the relative timing of the 2 metamorphic events because of the overlapping metamorphic facies.

Pillow selvages, hyaloclastite, volcanic breccias and amygdaloidal flows of basaltic to andesitic composition were sampled across the study area. These rocks have higher permeabilities, a factor that substantially facilitates the development of prehnite and pumpellyite in rocks of very low grade (Jolly 1978).

Regional Metamorphism

SUBGREENSCHIST FACIES

Subgreenschist assemblages were found in 3 isolated windows of basaltic volcanic rocks: 1) northeast Eby–southwest Grenfell townships, 2) east-central Bannockburn–west-central Montrose townships and 3) western Doon Township (Figure 329.5A).

In all localities the prehnite and pumpellyite are restricted to fractures and fragments of devitrified glass within pillow selvages and hyaloclastite or as fill components of amygdules. No prehnite or pumpellyite was found replacing relict igneous minerals. The crystals are anhedral to subhedral and never define a fabric.

In addition to pumpellyite, prehnite, epidote and chlorite, the observed subgreenschist assemblages may also contain quartz, albite, calcite, sphene and stilpnomelane.

The area south of the Ashley Mine, in Bannockburn Township, was the only region in which textures indicate that prehnite- or pumpellyite-bearing assemblages are stable. Isograds between the greenschist, prehnite-actinolite and prehnite-pumpellyite facies were mapped in this area (Figure 329.5B). Grade decreases southward, while pillow facings indicate a northeast younging direction. Therefore, these subgreenschist metamorphic assemblages must be a product of a syn- or posttectonic regional metamorphic event rather than a synvolcanic metamorphic event. The arrangement of isograds in the Ashley Mine area indicates

a northerly increase in temperature and a westward increase in pressure. The presence of the invariant point as a mappable feature allows the interpretation of local pressure attending peak metamorphism; with corrections for ferric iron content of the rocks the invariant point lies in the vicinity of 1.8 kbars, based on the petrogenetic grid of Liou et al. (1987). Recent thermodynamic data for subgreenschist minerals may increase the pressure value for the invariant point (D.M.C.). Therefore, the value of 1.8 kbars should be considered a minimum. Further work will be done to constrain the peak pressure value.

A sample from a basaltic pillow selvage located 1.5 km north of the KLLB, within Grenfell Township (Figure 329.5A: most northeast sample sites) contains the stable assemblage actinolite + epidote + chlorite as well as the relict assemblages pumpellyite + epidote + chlorite and prehnite + epidote + chlorite. The presence of both prehnite and pumpellyite in the greenschist facies suggests that pressure conditions must have been nearly coincident with the value of the greenschist-subgreenschist invariant point (Figure 329.6A). After correction for the ferric iron content of the host rock, this point corresponds to 1.75 kbars, with a temperature of approximately 300°C (Figure 329.6B). Similar pressure values are indicated for the Bannockburn area.

South of the KLLB, no prehnite was found. However, relict pumpellyite is present in pillow selvages from northern Eby and central Doon townships. This distribution of subgreenschist minerals in relation to the KLLB is similar to that observed by Jolly (1980) in the Kirkland Lake area. The general distribution of prehnite-absent subgreenschist assemblages suggests that the rocks south of the KLLB were metamorphosed under a lower geothermal gradient than the rocks located north of the KLLB. This implies that the regional metamorphism predated the breaks, since the isograds are cut by the KLLB, and is consistent with the rocks south of the break having been uplifted, relative to those north of the break, after regional metamorphism.

GREENSCHIST FACIES

With the exception of the subgreenschist domain in Bannockburn Township, all other volcanic rocks record peak metamorphic conditions of greenschist grade. The diagnostic assemblage for greenschist grade metabasites is actinolite + epidote + chlorite in the absence of prehnite or pumpellyite (Liou et al. 1987). In addition, albite, sphene, quartz and stilpnomelane or biotite are also common minerals that are stable at greenschist grade (Winkler 1979).

The textures of the secondary minerals in the greenschist-grade metabasites are variable. In most areas the minerals define no tectonic fabric; locally, however, alignment of chlorite, epidote or actinolite defines a foliation. Aligned growth of greenschist-facies minerals is only evident near and within narrow, discrete linear deformation zones and within 1.5 km of the Round Lake batholith.

Contact Metamorphism

Although an amphibolite-grade aureole is absent from the margins of the Round Lake batholith, there is an extensive zone of greenschist facies enveloping the pluton. Xenoliths and roof pendants are amphibolite or epidote-amphibolite facies, which indicates that the blocks within the batholith were metamorphosed at higher temperature and pressure than the highly deformed volcanic rocks in the contact aureole. This pattern of metamorphism indicates relatively cold emplacement of the batholith after crystallization.

THE KIRKLAND LAKE–LARDER LAKE BREAK

The KLLB is one of a number of deformation corridors within the Abitibi greenstone belt (Daignault and Archambault 1990). Several features characterize this set of deformation zones, which includes the KLLB: 1) strongly schistose fabric; 2) steeply plunging elongation lineations (Daignault and Archambault 1990); 3) roughly east trend of the deformation zone (Daignault and Archambault 1990); 4) intense carbonatization, commonly ankeritic; and 5) association with linear sedimentary rock belts (MERQ–OGS 1983).

In the Matachewan area 2 regionally extensive zones satisfy the above criteria: 1) the Matachewan deformation zone, which hosts the mineralization of the Young–Davidson and Matachewan Consolidated mines, south Powell Township (Figure 329.2); and 2) the Galer Lake deformation zone, south Holmes Township (Figure 329.2). Although no economic gold deposits are associated with the Galer Lake deformation zone, a number of gold showings occur in the area of the fault.

Both deformation zones can be traced eastward to the Proterozoic cover rocks in Flavelle and Holmes townships, underneath which the 2 zones may join. Westward the Matachewan deformation zone can be traced underneath the Gowganda sediments by mapping zones of D_P1 cleavage, to the east shore of Mistinikon Lake. The deformation zone located near the Halliday–Montrose township line is likely correlative with the Matachewan deformation zone. The Galer fault zone can be traced west through Bannockburn and Hincks townships.

Either of these faults is a candidate for the extension of the KLLB; in fact, they likely merge below the Proterozoic rocks in Burt Township, and both are potential gold exploration targets.

FUTURE WORK

In 1990–1991, work will be concentrated on the Proterozoic deformation zones overlying the reactivated D_A3 zones.

A lithogeochemical survey will be undertaken over these areas to determine if trace-element signatures of Archean rocks below the D_P1 zones were transferred to the overlying Gowganda Formation during deformation, thus providing a prospecting tool for areas of Huronian cover. Surveys previously conducted in the Gowganda sediments of western Quebec (Hines 1982, 1983) suggest this approach has considerable potential.

ACKNOWLEDGMENTS

We would like to thank our field assistant Evan Trickey, as well as Dr. S.L. Jackson (Ontario Geological Survey) and Blair Hrabi (Queen's University).

REFERENCES

Bright, E.G. 1970. Geology of Halliday and Midlothian townships; Ontario Department of Mines, Geological Report 79, 33p.

Corfu, F. and Andrews, A.J. 1986. A U-Pb age for mineralized Nipissing diabase, Gowganda, Ontario; Canadian Journal of Earth Sciences, v.23, p.107-109.

Daignault, R. and Archambault, G. 1990. Les grands couloirs de déformation de la sous-province de l'Abitibi; *in* The northwest Quebec polymetallic belt, edited by M. Rive, P. Verpaest, Y. Gagnon, J.-M. Lulin, G. Riverin and A. Simard, Canadian Institute of Mining and Metallurgy, Special Volume 43, p.43-64.

Derry, D.R., Hopper, C.H. and McGowan, H.S. 1948. Matachewan Consolidated Mine; *in* Structural geology of Canadian ore deposits, Canadian Institute of Mining and Metallurgy, Special Volume 1, p.638-643.

Dimroth, E., Imreh, L., Goulet, N. and Rocheleau, M. 1983. Evolution of the south-central segment of the Archean Abitibi belt, Quebec. Part II: Tectonic evolution and geomechanical model; Canadian Journal of Earth Sciences, v.20, p.1355-1373.

Dyer, W.S. 1936. Geology and ore deposits of the Matachewan–Kenogami area; Ontario Department of Mines, Annual Report, v.44, pt.2, p.1-55.

Fairbairn, H.W., Hurley, P.M., Card, K.D. and Knight, C.J. 1969. Correlation of radiometric ages of Nipissing diabase and Huronian metasediments with Proterozoic orogenic events in Ontario; Canadian Journal of Earth Sciences, v.6, p.489-497

Hines, G.J. 1982. Report on a rock geochemical survey done on a claim group located in Dassérat Township, northwestern Quebec; unpublished company report.

———1983. Levé Géochimique Propriété Léo-Paul Bégin, canton Dasséral, Québec; unpublished company report.

Hodgson, C.J. and Hamilton, J.V. 1989. Gold mineralization in the Abitibi greenstone belt: end-stage results of Archean collisional tectonics?; *in* The geology of gold deposits: the perspectives in 1988, edited by R.R. Keays, W.R.H. Ramsay and D.I. Groves, Economic Geology, Monograph 6, p.86-100.

Hubert, C., Trudel, P. and Gélinas, L. 1984. Archean wrench fault tectonics and structural evolution of the Blake River Group, Abitibi belt, Quebec; Canadian Journal of Earth Sciences, v.12, p.1024-1032.

Jensen, L.S. 1985. Stratigraphy and petrogenesis of Archean metavolcanic sequences, southwestern Abitibi Subprovince, Ontario; *in* Evolution of Archean supracrustal sequences, edited by L.D. Ayres, P.C. Thurston, K.D. Card and W. Weber, Geological Association of Canada, Special Paper 28, p.65-86.

Jolly, W.T. 1978. Metamorphic history of the Archean Abitibi belt; *in* Metamorphism in the Canadian Shield, edited by J.A. Fraser and W.W. Heywood, Geological Survey of Canada, Paper 78-10, p.63-78.

———1980. Development and degradation of Archean lavas, Abitibi area, Canada, in light of major element geochemistry; Journal of Petrology, v.21, p.323-363.

Junnila, R.M. 1989. Reconnaissance investigation of the geology of Yarrow and Doon townships, District of Timiskaming, with emphasis on the Huronian Supergroup; Ontario Geological Survey, Open File Report 5696, 75p.

Krough, T.E., Corfu, F., Davis, D.W., Dunning, G.R., Heaman, L.M., Kamo, S.L., Machado. N., Greenhough, J.D. and Nakamura, E. 1987. Precise U-Pb isotope ages of diabase dykes and mafic to ultramafic rocks using trace amounts of baddeleyite and zircon; *in* Mafic dyke swarms, edited by H.C. Halls and W.F. Fahrig, Geological Association of Canada, Special Paper 34, p.147-152.

Liou, J.G., Maruyama, S. and Cho, M. 1987. Very low-grade metamorphism of volcanic and volcaniclastic rocks — mineral assemblages and mineral facies; p.59-113 *in* Low temperature metamorphism, edited by M. Frey, Blackie & Son, London.

Lovell, H.L. 1967. Geology of the Matachewan area, District of Timiskaming; Ontario Department of Mines, Geological Report 51, 61p.

———1972. Geology of the Eby and Otto area, District of Timiskaming; Ontario Department of Mines, Geological Report 99, 34p.

MERQ–OGS 1983. Lithostratigraphic map of the Abitibi Subprovince; Ontario Geological Survey–Ministère de l'Énergie et des Ressources du Québec, MERQ DV 83-16 and OGS Map 2484, scale 1:500 000.

Moore, J.C.G. 1966. Geology of Holmes–Burt area, District of Timiskaming; Ontario Department of Mines, Geological Report 44, 20p.

Piroshco, D.W. and Kettles, K. 1988. Geology of Tisdale and northern Whitney townships; *in* Summary of field work and other activities 1988, Ontario Geological Survey, Miscellaneous Paper 141, p.197-205.

Pyke, D.R., Ayers, L.D. and Innes, D.G. 1973. Timmins–Kirkland Lake; Ontario Department of Mines, Geological Compilation Series, Map 2205.

Sinclair, W.D. 1982. Gold deposits of the Matachewan area; *in* Geology of Canadian gold deposits, edited by R.W. Hodder and W. Petruk, Canadian Institute of Mining and Metallurgy, Special Volume 24, p.83-93.

Thomson, J.E. 1946. Kenogami Lake area; Ontario Department of Mines, Map 1946-1.

Winkler, H.G.F. 1979. Petrogenesis of metamorphic rocks, 5th ed.; Springer-Verlag, Berlin, 348p.

Grant 332 High-resolution Magnetic-susceptibility Probe for Mineral-exploration Boreholes: Design and Laboratory prototype

Alfred V. Dyck[1], Peter V. Auchincloss[1], Jane Rea[1] and David L. Atherton[2]

[1]Department of Geological Sciences, Queen's University, Kingston
[2]Department of Physics, Queen's University, Kingston

ABSTRACT

A high-resolution magnetic-susceptibility logger is under development. It will have permanent magnets and miniature Hall probes. By facilitating continuous measurements in exploration drill holes or on diamond-drill core, it will provide the means to study detailed magnetic signatures of mineral deposits and their environments, including structural features. The project includes design, laboratory testing, and field testing of the instrument. This report presents the design arrived at through the process of finite-element modelling of the desired characteristics of the probe and the results of a preliminary experiment to verify the computer-aided design.

The design of the tool has become substantially more intricate than could have been anticipated at the outset. The benefit of the design approach using finite-element modelling has clearly been substantiated. The value of signal/background ratio of ≥5 predicted by the computer modelling exceeds the minimum required for functioning of the Hall probes by a factor of 250 for detection of the worst-case situation set as the initial design criterion. This considerable margin in performance characteristics gives us margin for error in actual fabrication of the prototype and/or additional sensitivity in detection of weakly magnetic rocks. The experimental verification included here demonstrates that the original design specifications can be met on a practical basis and that a working prototype for field use is realizable in the next phase of the project.

INTRODUCTION

Concept

The objective of this project is to develop a new method of susceptibility mapping using a high-resolution magnetic-susceptibility logger and 3-arm dipmeter for use in exploration drill holes and on diamond-drill cores.

The project has 3 phases: 1) initial-design phase (computer study) to be completed before the end of the first year; 2) construction of a prototype for laboratory testing); and 3) design, fabrication and field testing of the drill-hole probe in mineral exploration environments (Sudbury and Timmins). The concept of this device and previous progress have been presented by Dyck et al. (1989) but are reviewed briefly here as background to the current state of the project. This report focusses on phase 2 of the project.

The high spatial resolution of the susceptibility measurement will be achieved using powerful permanent magnets and miniature Hall-effect probes. Sensitivity of the device to magnetic-susceptibility variations, comparable to that of conventional susceptibility probes, will render it useful in a wide range of rocks of interest in mineral exploration. The design target is to achieve a sensitivity to susceptibility values as small as 1.2×10^{-4} SI units, with a spatial resolution as small as 5 mm.

This method will provide the means to search systematically for and to study characteristic magnetic signatures of mineral deposits and their environments. The orientation of planar magnetic features intersected by the drill hole can be determined with respect to the hole by means of the three-point measurement illustrated in Figure 332.1. Of ultimate interest is the potential of yielding quantitative mineral-exploration data on the distribution and orientation of small but structurally important features like dikes and veins. Two such possibilities are mafic dike orientations and magnetite-bearing or magnetite-destructive alteration, both important in gold exploration.

Review of Previous Progress

TOOL DESIGN

A large number of finite-element calculations were carried out for the purpose of evaluating variations of 3 basic designs, the simple design in the initial proposal and 2 more complicated designs. Sensitivity was found to be as good as or better than expected from the original calculations. One problem was identified: measurement of anomalous field (signal) must be made in a region of high background flux. Reduction of the amount of background flux in the measurement zone, to improve signal/background ratio, became the primary design approach to achieving the required resolution and sensitivity.

DESIGN

The practical challenge is that of achieving the necessary resolution through miniaturization. The design of the tool has become substantially more intricate than could have been anticipated at the outset. However, the original specifications have been exceeded so as to provide a significant margin on the desired performance

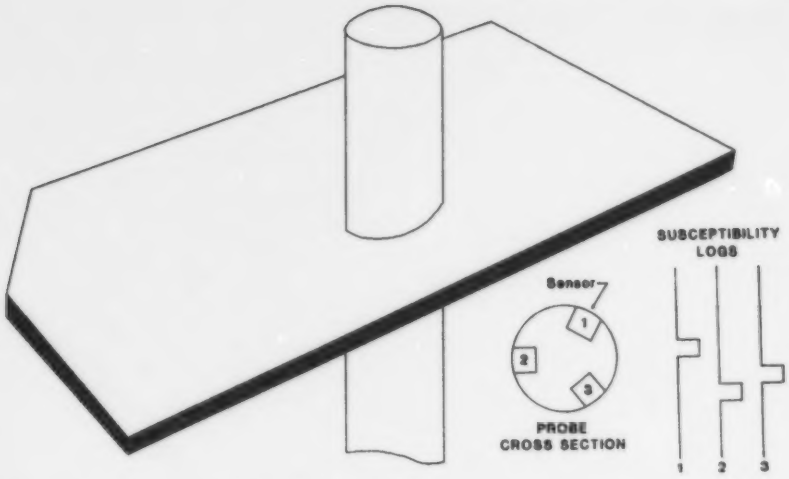

Figure 332.1. Schematic illustration of the concept of 3-point orientation measurements using a 3-sensor, high-resolution magnetic-susceptibility borehole probe.

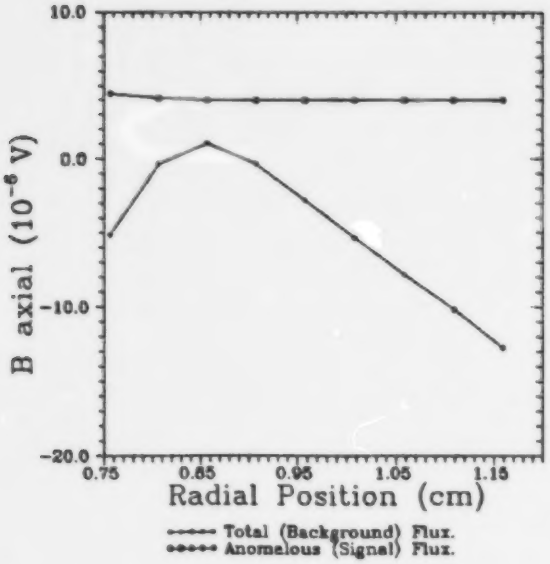

Figure 332.2. Profiles of background flux and primary flux (radial profile of the axial component) in the measurement region. A signal/background value of ≥5 is predicted by this final-design model.

characteristics. Calculations have been carried out with the INFOLYTICA finite-element package, MAGNET (*see* Atherton and Daly 1987).

The signal/background ratio must be increased to ≥0.02 in the measurement region to allow use of Hall probes as flux detectors. Profiles of the background and anomalous flux in the measurement region are shown in Figure 332.2. The value of signal/background of ≥5 predicted by the computer modelling exceeds the minimum required for functioning of the Hall probes by a factor of 250 for detection of our minimum (i.e., most difficult case) target layer. This provides considerable margin in performance characteristics, giving us margin for error in actual fabrication of the prototype and/or additional sensitivity in detection of weakly magnetic rocks. We have also performed computer tests of the effect of standoff distance (variable distance between the borehole tool and the wall of the hole). Tests using our target layer as a model predict that variable standoff distance will not be a problem.

The final computer-aided design is shown in exploded view in Figure 332.3 (approximate scale 1:2) and in axial section in Figure 332.4 (approximate scale 1:1). The design is an elaboration and combination of 2 of the preliminary designs discussed previously. It features the use of a pair of opposing pole magnets and extensive flux shaping and shielding in the central region of the tool, especially in the neighbourhood of the measurement region. All components except the head and Hall-probe sensors have axial symmetry. Details of the design include the following:

1. Primary-field magnets: opposing pole, machined, high-strength (B_{max} = 2 T) NeFeB alloy.
2. Flux concentrator: machined from mild steel, relative permeability ≥ 100. The purpose of this component is to shape the source field, that is, to direct flux into the target region.
3. Shield: machined from mild steel, relative permeability ≥ 100. The purpose of the shield is reduce the background field in the measurement region and to improve resolution by acting as a secondary path for anomalous flux originating from rock adjacent to the target layer.
4. Head: machined from Armco steel, relative permeability ≥ 500. The purpose of the head is to optimize flux in the measurement region by providing a primary path for the anomalous flux of the target layer. The measurement region is at the midpoint of the tool, surrounded by the 2 halves of the head.

(Of course, the magnets, flux concentrator, shield and head interact magnetically with each other, and together they shape the flux that is projected into the surrounding rock and ultimately is detected as an anomalous flux indicative of nearby magnetic material.)

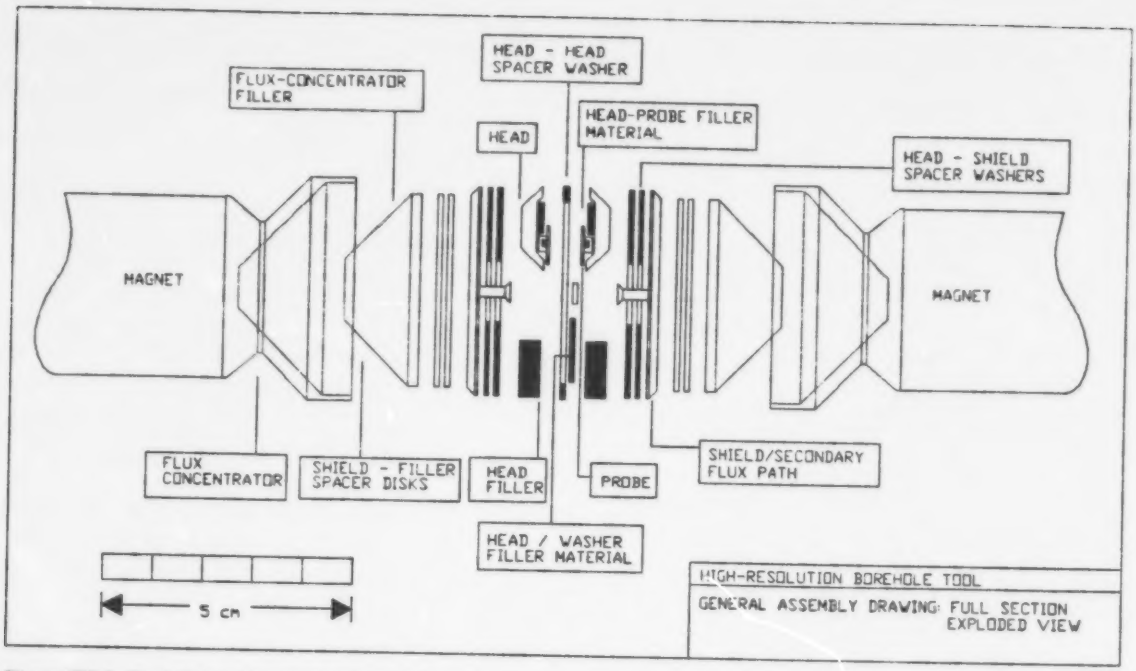

Figure 332.3. Final design of magnetic-susceptibility tool.

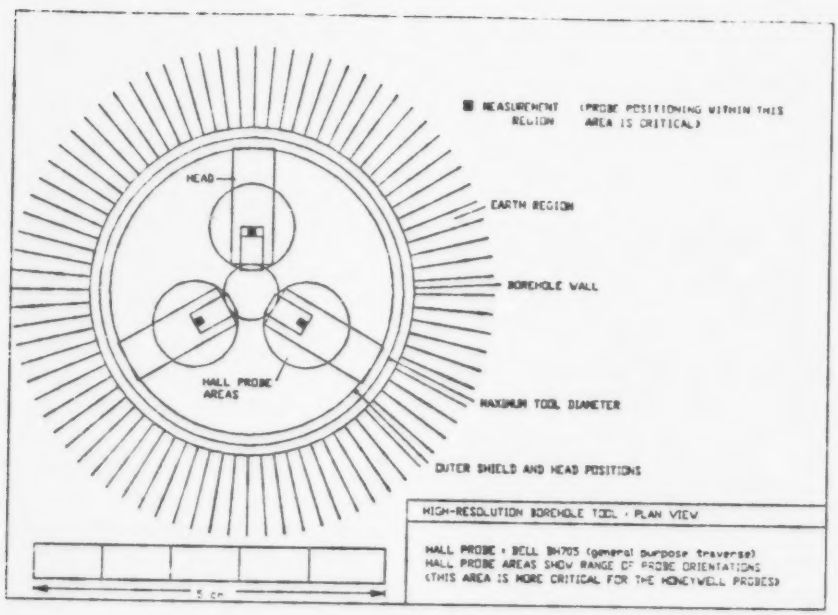
MEASUREMENT REGION (PROBE POSITIONING WITHIN THIS AREA IS CRITICAL)
HEAD
EARTH REGION
BOREHOLE WALL
HALL PROBE AREAS
MAXIMUM TOOL DIAMETER
OUTER SHIELD AND HEAD POSITIONS
HIGH-RESOLUTION BOREHOLE TOOL - PLAN VIEW
HALL PROBE - BELL BH705 (general purpose traverse)
HALL PROBE AREAS SHOW RANGE OF PROBE ORIENTATIONS
(THIS AREA IS MORE CRITICAL FOR THE HONEYWELL PROBES)
5 cm

Figure 332.4. Axial view of measurement region of the tool, showing the 3 positions of the sensors necessary for dipmeter measurements.

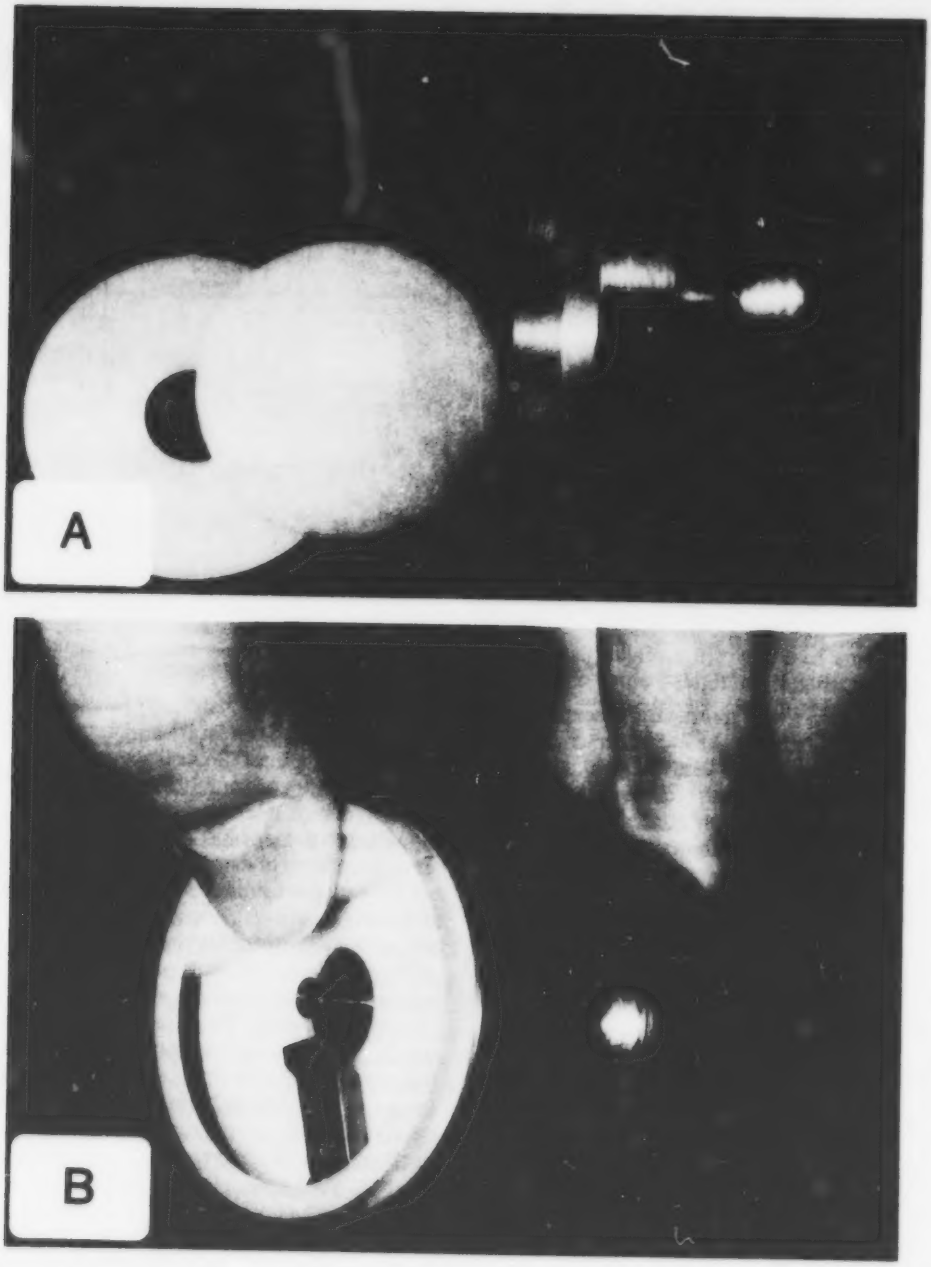

Photo 332.1. Machined components of the magnetic susceptibility probe. **A)** The permanent magnet (on the right) attached to the flux concentrator; nylon spacers. **B)** One half of the magnetic probe assembled, showing, in addition, the shield projecting through the nylon spacer and the head, lying off centre near the perimeter of the probe.

5. Sensors: Hall-effect probes situated in measurement region, differential pickup (each probe area shown in Figures 332.3 and 332.4 contains a pair of Hall probes, displaced in axial direction and measuring axial component). Honeywell 9SS12-2 probes have been chosen for their miniature size, linearity and improved temperature coefficient (cf. other models).

6. Spacers: machined from nonmagnetic, nonconductive material (nylon). The spacers will allow precise alignment of various magnetic components and sensors in the tool; precise adjustment of air gaps can be made by changing the number and thickness of spacers.

LABORATORY PROTOTYPE

Photograph 332.1 shows some of the machined components of the probe. The tool has been assembled and a preliminary experiment carried out to record a magnetic signature for a layer perpendicular to the tool. The layer had the following

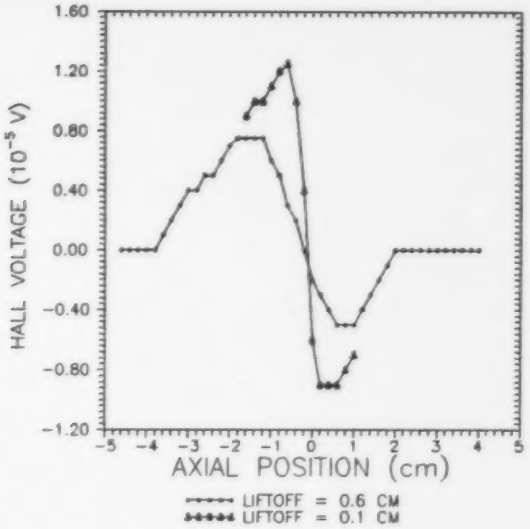

Figure 332.5. Laboratory simulation of the probe's response to a radially oriented magnetic layer; $k = (1.3 \pm 0.5) \times 10^{-5}$ SI; thickness, 4 mm; tool stationary during measurement interval; Hall current, 125 mA; probe sensitivity, 2.96 V/T•A.

parameters: 4 mm thick, with a magnetic susceptibility of $(1.3 \pm 0.5) \times 10^{-3}$ SI, slightly thinner and with a susceptibility approximately 10 times larger than the minimum layer (representing target resolution and sensitivity as originally specified). Two values of liftoff (or standoff) distance were used, 1 and 6 mm. Figure 332.5 shows the results.

The purpose of this experiment was to obtain preliminary verification of the calculations of the computer-aided design phase. The position of the crossover corresponds to the axial position (to within 1 mm) at which the Hall probe passes by the middle of the layer. The measured peak value of the layer signature for 1 mm liftoff corresponds (using the manufacturer-specified Hall-probe sensitivity) to a field of about 32×10^{-6} T. The calculated prediction is about a factor of 2 larger. Given the uncertainty of positioning of the tool components for this preliminary experiment (plus the error in susceptibility of the hand-mixed layer), we consider these 2 values as being in rough agreement. The slight skewness of the profile is probably a result of a small offset in position of the Hall probe, but the general shape is what we expect for the axial component of the anomalous field.

CONCLUSIONS

We must emphasize that the results from this initial laboratory simulation were obtained with a rather crude measurement of Hall-effect voltage. Increased sensitivity is to be achieved using an alternating-current source and

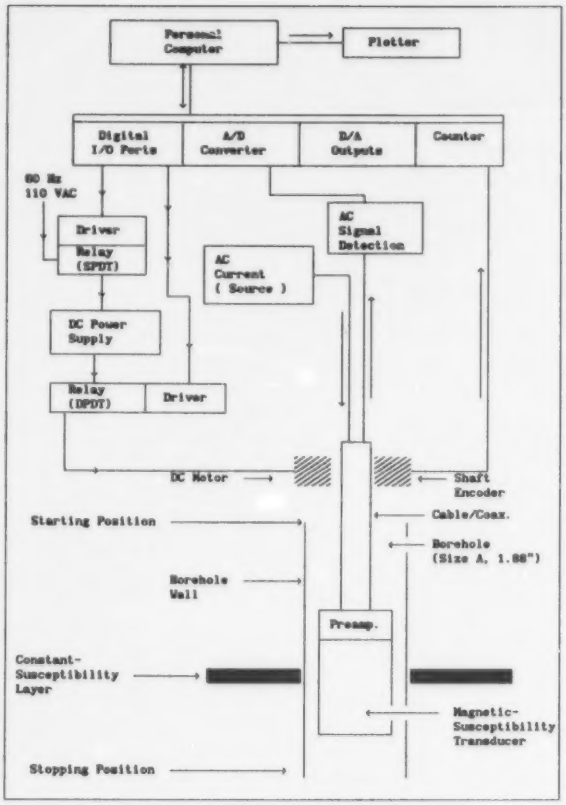

Figure 332.6. Revised schematic of the measurement system.

synchronous detection techniques, as indicated in the revised schematic of the complete measurement system shown in Figure 332.6. This will allow us to exceed the originally specified target sensitivity. The measurement system is presently being used to test the design under tightly controlled experimental conditions and to carry out additional tests under simulated operating conditions (such as motion of the probe) and, of course, forms the basis for the field-worthy system required for the field tests during the final phase of the project.

REFERENCES

Atherton, D.L. and Daly, M.G. 1987. Finite element calculation of magnetic flux leakage detector signals; NDT International, v.20, p.235-238.

Dyck, A.V., Auchincloss, P.V. and Atherton, D.L. 1989. High-resolution magnetic-susceptibility logger and dipmeter for mineral exploration boreholes: concept and initial progress; *in* Geoscience Research Grant Program, summary of research 1988–1989, Ontario Geological Survey, Miscellaneous Paper 143, p.146-159.

Grant 340 Stratigraphy of the Middle Devonian Dundee Formation, Southwestern Ontario

M.C. Birchard and M.J. Risk

Department of Geology, McMaster University, Hamilton

ABSTRACT

The Middle Devonian Dundee limestones of southwestern Ontario accumulated in the Michigan and Appalachian basins, with deposition in part being controlled by the proximity to the Findlay and Algonquin arches. Six lithofacies were recognized in the Dundee Formation during detailed core and outcrop studies. Stratigraphic relations indicate that prior to deposition of Dundee carbonates, a major regression exposed underlying Detroit River Group sediments, and up to 10 m of sediment may have been eroded. Subsequent transgression deposited reworked sands and shallow-shelf bioclastic limestones in most areas of the adjoining basins while in westernmost regions of the Appalachian Basin, stratigraphically equivalent Columbus Formation sediments were accumulating adjacent to the Findlay arch.

Evidence of relative sea-level fluctuations in middle Dundee time are preserved as 1) repetitions of lagoonal and open-shelf facies in Appalachian Basin regions, 2) firm-ground developments and 3) coarse, reworked packstone to grainstone pulses. Dundee facies show that the 2 basins responded differently to sea-level fluctuations and that pre-existing topography on underlying Detroit River Group sediments may have influenced deposition. Uppermost Dundee strata in the Appalachian Basin suggest a final transgressive episode with deposition of deep-water argillaceous mudstones; however, uppermost Dundee strata in the Michigan Basin may suggest sea-level stillstand, winnowing and reworking.

INTRODUCTION

In southwestern Ontario, Dundee Formation and underlying Detroit River Group carbonates have produced nearly 6.3 × 10^6 m^3 of oil from a variety of traps (Bailey Geological Services Ltd. and Cochrane 1985). Some traps in Kent, Elgin and Middlesex counties are in uppermost Detroit River and lower Dundee limestones, whereas many wells in Lambton County produce from intervals in uppermost Dundee strata. All of these traps are found within different lithofacies.

Previous workers (Best 1953; Diffendal 1971) have proposed depositional models for the Dundee Formation based primarily on outcrop studies; others have attempted to make depositional interpretations using limited subsurface data from a number of small pools (Dutton 1985). This project describes lithofacies of the Dundee Formation that have been identified from core and outcrop information and interprets the stratigraphy of the formation as observed in the Michigan and Appalachian basins of southwestern Ontario. More detailed coverage of stratigraphy and facies is given in Birchard (1990).

REGIONAL SETTING AND STRATIGRAPHY

In most of southwestern Ontario, the Dundee Formation disconformably overlies Lucas Formation carbonates (Figure 340.1), which include sparsely fossiliferous laminated dolomites, sandy limestones and fossiliferous coral-stromatoporoid bioclastic limestones. In the northwestern region of the Appalachian Basin, however, fossiliferous bioclastic dolomitic limestones of the Columbus Formation conformably overlie Lucas strata (Sparling 1988). Although it is presently not recognized in Ontario, we propose using the term "Columbus Formation" to describe those rocks occurring between the Detroit River Group and Dundee Formation in that area as defined by this study and as presently used to describe similar rocks in Ohio (Sparling 1988; Rickard 1984). In the past, the term "Columbus" has been incorrectly applied to thick sands near the base of the Dundee Formation. In Ontario, the top of the Columbus is diastemic and, as suggested by Sparling (1988), probably becomes younger northward. Black shales of the Marcellus Formation disconformably overlie Dundee limestones in all localities in this region (Uyeno et al. 1982).

Middle Devonian carbonates of southwestern Ontario occur within and between the Michigan and Appalachian basins on the flanks of 2 major structural highs (Figure 340.2). The Algonquin Arch trends northeast, and the Findlay Arch trends north; they are separated by a topographic low called the "Chatham Sag". These structural features appear to have played an important role in the deposition of carbonates during the Middle Devonian. Both arches had been partially exposed in early Dundee time, and

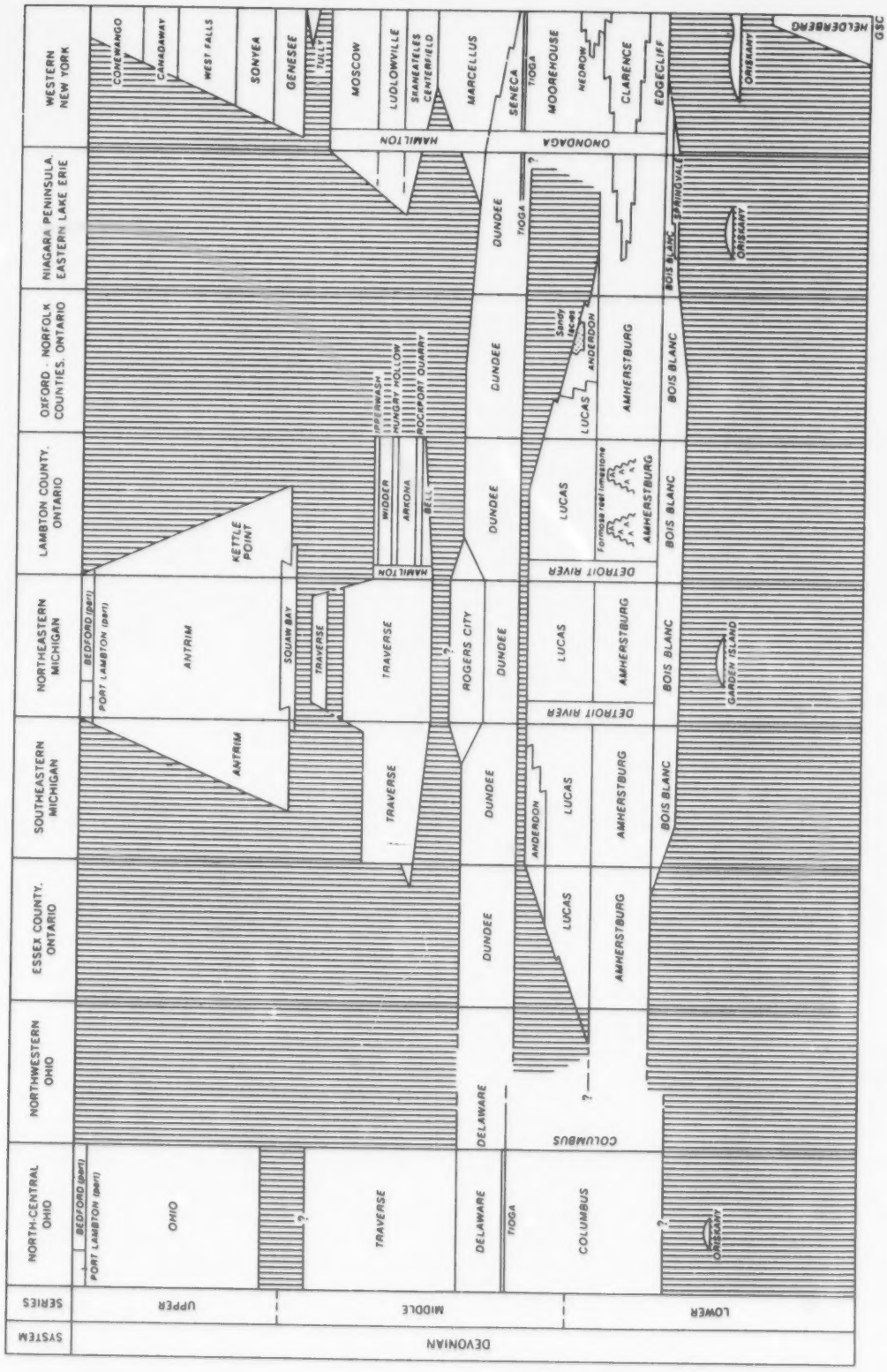

Figure 340.1. Stratigraphy and correlation of the Devonian succession in southwestern Ontario and adjoining areas (*after* Uyeno et al. 1982).

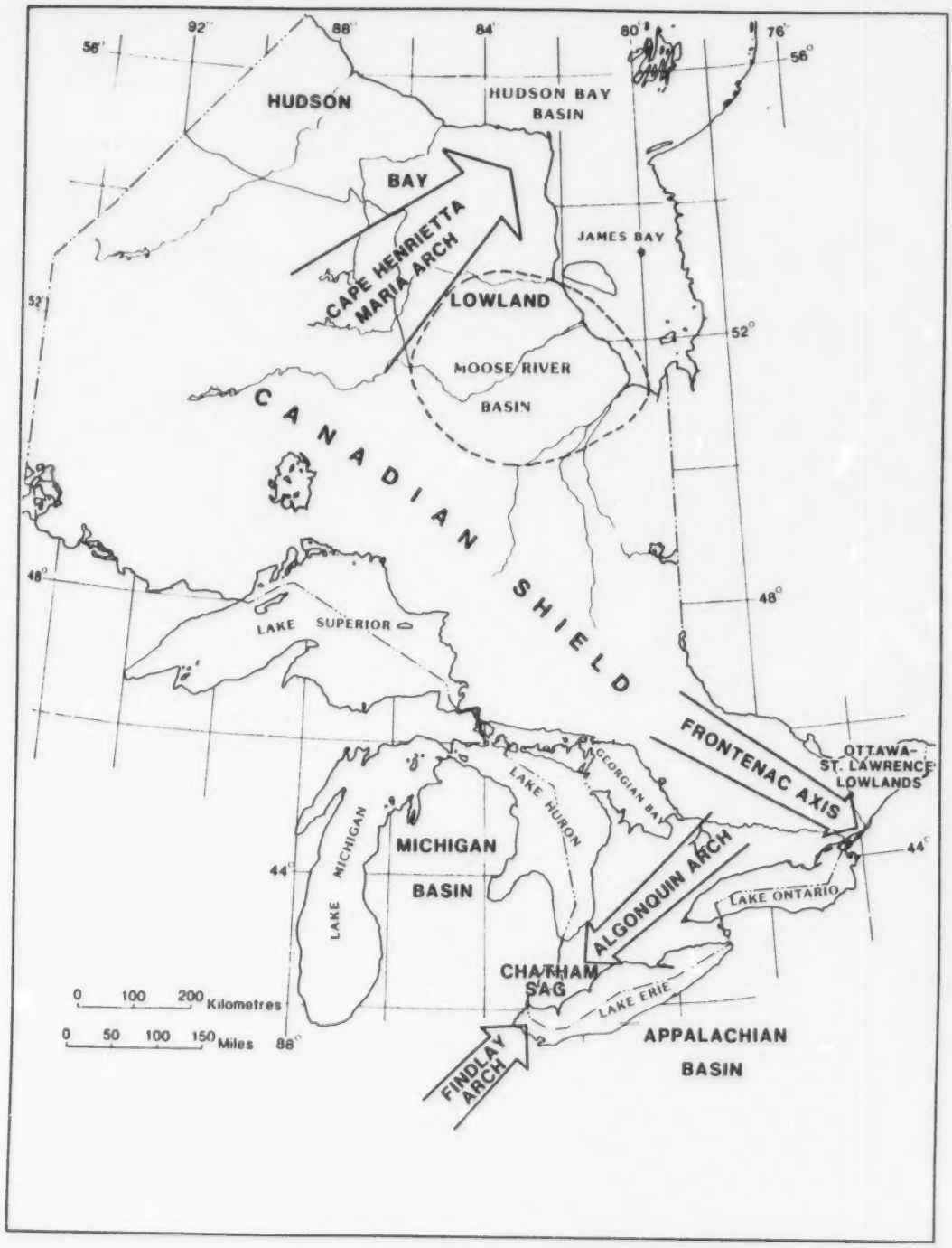

Figure 340.2. Major structural features of Paleozoic rocks in Ontario.

the Chatham Sag may have acted as a trap for lower Dundee sediments. Later in Dundee time, waters may have become somewhat restricted in parts of this structural low. In the past, placement of the formation contact at the base of the Dundee has been a problem. The present study attempts to define this contact in order to help delineate reservoirs within lower Dundee strata.

DUNDEE LITHOFACIES AND DEPOSITIONAL ENVIRONMENTS

Six distinct lithofacies can be recognized within Dundee strata. Only 3 of these lithofacies (facies 2, 4 and 5) are common to both the Michigan and Appalachian basins. The remaining lithofacies are in part topographically controlled

Photo 340.1. Facies 1: bioturbated dolomitic sandy limestones. Core width = 6 cm.

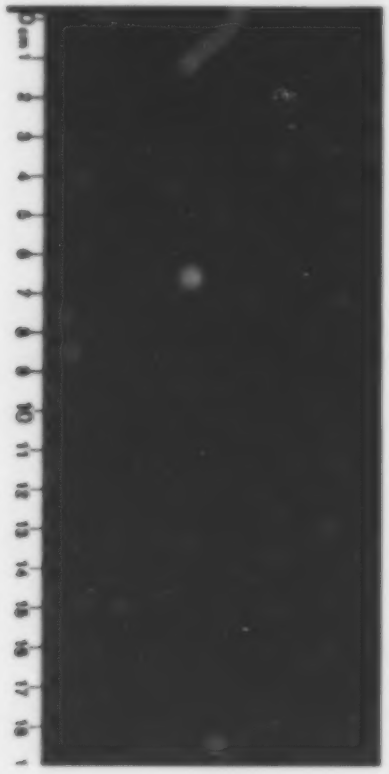

Photo 340.2. Facies 2: cherty bioclastic facies showing pseudonodular texture of wackestones. Core width = 8 cm.

and represent different depositional conditions during the development of the 2 basins during this episode of the Middle Devonian.

Lithofacies 1: Bioturbated, Dolomitic Sandy Wackestones

This facies is composed dominantly of slightly argillaceous, moderately bioturbated, dolomitic sandy wackestones (Photo 340.1) and makes up the prominent reservoir of the Rodney pool, Elgin County. Well-rounded, very fine- to fine-grained quartz sands generally make up 20 to 50% of this facies, with sand content decreasing upwards. The proportion of crinoidal material increases upwards through this facies, and sandy 0.5 to 2.0 cm diameter subhorizontal burrows are commonly found.

This facies represents marginal marine conditions above fair-weather wave base where sands became well sorted. The best-preserved record of *in situ* fauna is the horizontal burrows. Reworking of upper Detroit River Group sediments is the most likely origin of lower Dundee sands.

Lithofacies 2: Cherty Bioclastic Facies

Thin crinoidal-brachiopod-bryozoan packstones occur in a bioturbated, cherty wackestone matrix. Light brown wackestones commonly have a pseudonodular texture and are finer grained and contain fewer fossils than packstone pulses (Photo 340.2). Chert nodules make up less than 10% of sediments and are light tan to whitish with diffuse, often bioturbated edges. Reworked quartz grains and Detroit River Group clasts are common at the base of this facies, which becomes more argillaceous upwards.

Common, thin bioclastic pulses composed of partially broken bryozoan colonies set in a crinoidal wackestone matrix, as well as the bioturbated texture of wackestones, suggest that these sediments were deposited in an open-shelf environment near or below storm wave base.

Lithofacies 3: Cherty Mudstone Facies

Dark brown, thinly bedded to massive, bioturbated mudstones with thin, black, argillaceous seams make up this facies (Photo 340.3), which is distinct both lithologically and also because of the scarcity of fossils. *Tentaculites* and *Tasmanites* are common and well preserved. Sharp-edged chert nodules may be laminated, massive or bioturbated and were consolidated prior to lithification of surrounding sediments.

The abundance of well-preserved sporecases (*Tasmanites*) in dark brown mudstones suggests a quiet-water, possibly dysaerobic, restricted lagoonal environment. The lack of marine suspension and filter-feeding organisms, commonly found in adjacent facies, supports this interpretation.

Photo 340.3. Facies 3: cherty mudstone facies with common conical *Tentaculites*. Core width = 8 cm.

Photo 340.4. Facies 4: well-developed firm ground with common mud-filled subvertical burrows. Polished core slab. Core width = 6 cm.

Lithofacies 4: Crinoid-Brachiopod Grainstone to Wackestone Firm-ground Facies

Coarse grainstones grading upward to dark grey crinoidal wackestones with well-developed firm grounds characterize this facies. Grainstones commonly found at the base of this facies are 5 to 15 cm thick and consist primarily of reworked brachiopods, corals and crinoid fragments. Above these grainstones are sparsely fossiliferous wackestones with well-developed firm grounds that are commonly capped by thin packstone pulses (Photo 340.4). Coarse, crinoidal wackestones may be found at the top of this facies. Unlike facies 2 this facies does not exhibit a pseudonodular texture and can further be distinguished from facies 2 by a sudden increasing thickness of packstone and grainstone beds, an absence of chert and a higher mud content upwards.

This facies was deposited in a time of deeper water, open-shelf conditions, during which periodic minor sea-level fluctuations and stillstands occurred. Coarse basal grainstones overlain by sparsely fossiliferous wackestones with well-developed firm grounds represent a period of initial reworking that was followed by quieter water and nondepositional conditions. These firm grounds are important markers in Dundee strata.

Photo 340.5. Facies 5: argillaceous pulse in muddy wackestones. Scale bar = 3 cm.

Photo 340.6. Facies 6: muddy, bioturbated packstones at top of Dundee Formation, Lambton County area, Michigan Basin. Note diagnostic mud-lined subvertical burrows.

Lithofacies 5: Argillaceous, Bioturbated Brachiopod Mudstone to Wackestone Facies

Massive to medium-bedded, pervasively bioturbated (mottled), argillaceous mudstones to wackestones with common, small disarticulated brachiopods, uncommon Rugosa and uncommon crinoidal debris make up this facies (Photo 340.5). *Planolites*-like horizontal burrows are common in argillaceous seams, and rare, well-developed firm grounds can be found. Marcellus Formation shale precursory sediments can also be seen in the uppermost parts of this facies.

The occurrence of sparse crinoidal debris, uncommon small rugosans, rare laminar stromatoporoids (generally capping firm grounds) and abundant horizontal burrows suggests middle-shelf deep-water deposition and soft substrates.

Lithofacies 6: Muddy, Bioturbated Wacke-Packstone Facies

Capping the Dundee succession in the Michigan Basin are fine-grained, relatively well-sorted, dominantly crinoidal, "clean" wackestones with occasional thick packstone pulses. Vertical mud-lined burrows are common and are diagnostic of this facies (Photo 340.6).

The lack of argillaceous material in this facies and the degree of sorting of fine crinoidal material suggest that these sediments may represent an episode of reworking, winnowing and transport of nearby shallow-shoal sediments.

DISCONTINUITY SURFACES IN DUNDEE SEDIMENTS

Two types of discontinuity surfaces have been identified in Dundee sediments: lithified horizons and firm grounds. The first type, lithified horizons, are commonly found in medium- to coarse-grained packstones and grainstones with similar sediments found overlying the surfaces. Sharp, smooth upper contacts commonly have been indurated and exhibit a rind of opaque minerals and/or dolomite. Some lithified horizons that are slightly undercut and may be overlain by lithified clasts have unquestionably been eroded. Well-sorted allochems, rare, rounded quartz grains and rare glauconite may also be found above these surfaces.

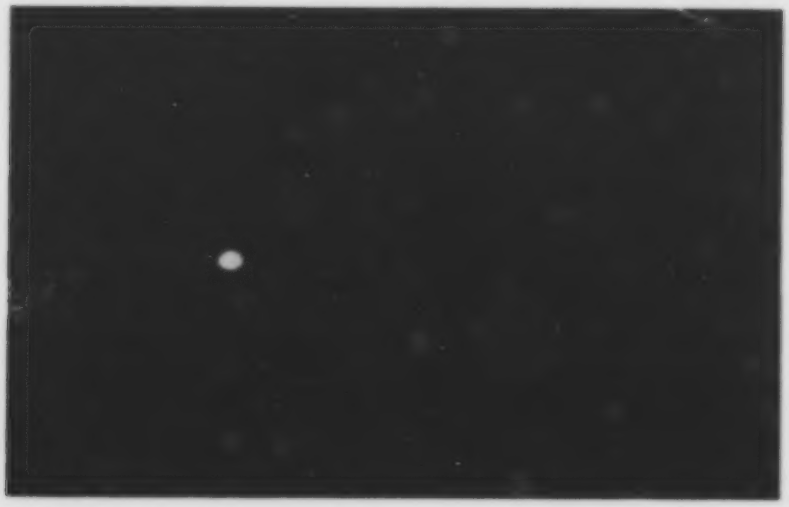

Photo 340.7. Outcrop photo of indurated lithified horizon with U-shaped burrows in upper Columbus Formation strata, Parkertown quarry, Parkertown, Ohio.

Photo 340.8. Thin-section internegative of lithified horizon with dolomite-filled fracture penetrating upper surface (left centre). From OGS 82-3 well, Elgin County. Width of section = 3 cm.

Commonly, 2 to 3 cm diameter by 5 to 10 cm deep burrows penetrate these surfaces (Photo 340.7). These burrows are generally vertical and most likely represent a dwelling structure. Dolomite-filled fractures penetrate downward from the upper surface (Photo 340.8), and rare, thin, encrusting stromatoporoids were found. These horizons are laterally discontinuous features that have been interpreted as representing episodes of nondeposition, winnowing and reworking followed by submarine lithification. Continued reworking blanketed the lithified surface with a thin layer of well-sorted, usually crinoidal grainstone.

The term "firm ground" is used here to describe the second, more common type of discontinuity surface found within Dundee sediments. These surfaces have been divided into poorly, moderately and well-developed firm grounds based on the degree of development of these horizons with regard to the following described characteristics. Firm grounds most commonly occur in fine-grained, slightly argillaceous mudstones and wackestones and have a sharp, irregular upper surface that may be undercut. Upper surfaces are commonly pyritized and/or dolomitized. The key distinguishing characteristic of firm grounds in Dundee strata is the presence of thin (2 to 3 mm diameter), often pyritized, vertical burrows that penetrate the upper surface to a depth of 10 cm.

True hardground development was rarely achieved: only a few examples were observed where grains were cut at the margins of borings. Sediment grain size may have been too fine for cut grains to be observed. Twenty-seven thin sections or acetate peels representing more than half of all firm grounds identified were made in order that these surfaces could be distinguished and classified. Burrows commonly are infilled by overlying sediments, which are either fine-grained, dark, carbonate muds or coarse, well-sorted crinoidal packstones and grainstones. Phosphatic fish fragments, approximately 1 to 3 mm in size, were commonly found overlying well-developed firm-ground surfaces and infilling burrows. Eroded clasts are occasionally seen above firm grounds. Rarely, thin, tabular stromatoporoids encrust moderately to well-developed surfaces. The term "hardground" has not been used to describe these surfaces mainly because of the absence of distinct *Trypanites* borings and encrusting organisms.

In Dundee strata, firm grounds were found to be rare in facies 2 and 6, uncommon in facies 5 and common in facies 4. These firm grounds appear to have developed proximal to topographically high areas and are useful for intra- and interbasin correlations as evidence of sea-level stillstands and regressions during Dundee deposition. Correlation of individual firm grounds may be difficult, although "packages" of firm-ground surfaces may be correlatable. Stratigraphic section A–A′ (Figures 340.3, 340.4 and 340.5) shows that within a relatively small area firm-ground packages in facies 4 are readily identifiable and locally correlatable in what otherwise appears to be a relatively conformable succession of strata of Columbus Formation to overlying Dundee limestones. Identification of firm-ground surfaces as potentially correlatable packages and mapping of diagnostic facies have been key elements in helping to clarify regional facies relationships.

FACIES DISTRIBUTIONS

The Columbus Problem

In the past, sands present near the base of the Dundee Formation have been called "Columbus sands". In the last decade it has been shown that in many cases this designation has been incorrectly applied and that many of the sands

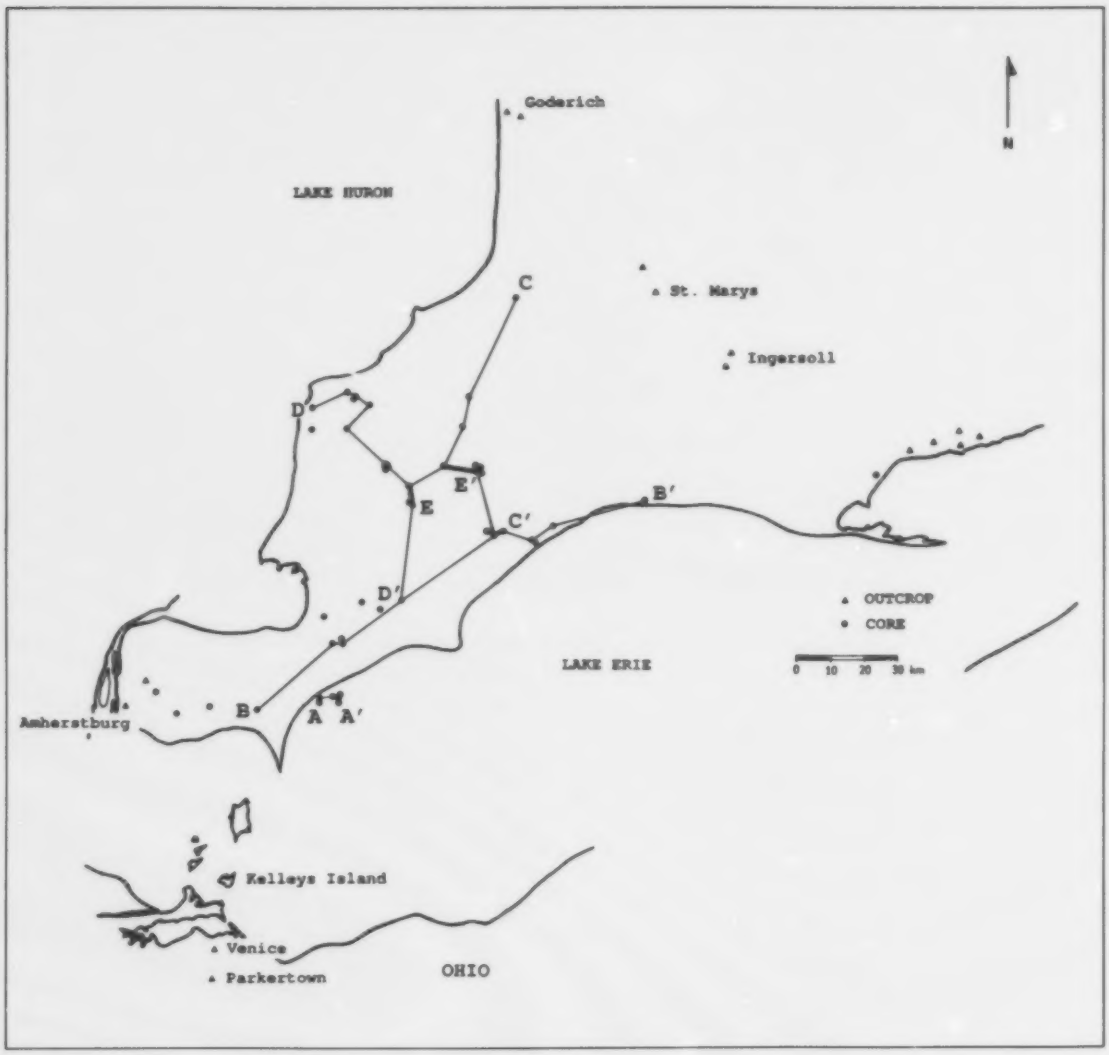

Figure 340.3. Location of stratigraphic sections.

actually belong within Detroit River Group strata (Uyeno et al. 1982; Dutton 1985). In parts of Ohio and western New York, Columbus Formation carbonates have been mapped underlying what have been interpreted as Delaware Formation (= Dundee equivalent) sediments. This problem has been compounded by the fact that outcroppings on Pelee Island have recently been mapped by American geologists as Columbus Formation (Bjerstedt and Feldmann 1985) and by Canadian geologists as Dundee Formation (Sanford 1969).

A number of outcrop sections were examined on Pelee (Ontario) and Kelleys (Ohio) islands in western Lake Erie; on the Marblehead peninsula, at Venice and Parkertown (Ohio); and in the area of Amherstburg (Ontario). Many of the carbonate sediments mapped in these areas have completely different lithologies than Dundee Formation sediments mapped in other parts of southwestern Ontario. On Pelee Island, dolomitic bioclastic limestones are biostromal, having an abundant and diverse fossil assemblage. Uyeno et al. (1982) described the lower part of the formation on Pelee Island as "...massive, light brown, medium to coarse grained bioclastic limestone. Lenses of pseudo-oolitic limestone enclosing coarse bioclastic debris are occasionally present". The pseudo-oolitic material described is actually an abundance of calcitic charophyte oogonia. Conkin et al. (1970) identified similar prominent and readily recognizable fossil material from central Ohio as *Moellerina greenei* (Photo 340.9) and proposed a thin biostratigraphic zone consisting of an abundance of *Moellerina* in upper Columbus strata that can be correlated from the Columbus area of Ohio to parts of Kentucky and southern Indiana.

At quarries near Venice and Parkertown, *Moellerina* occurs only within upper Columbus strata and not within lower Dundee sediments. The abundance of charophyte material in Pelee Island sediments, along with other facies

Figure 340.4. Legend for stratigraphic sections.

evidence, supports a correlation with the upper portions of the Columbus Formation in Ohio. Abundant *Moellerina* from subsurface cores in the Lake Erie area have enabled the recognition of Columbus and Dundee formations and may in places be correlatable with the *Moellerina greenei* biostratigraphic zone as proposed by Conkin et al. (1970). Stratigraphic section A–A′ shows that in western Lake Erie the Columbus and Dundee formations can be differentiated in part on the basis of common to abundant charophyte material near the top of the Columbus Formation.

Regional Facies Relationships

Using the lithofacies scheme proposed for the Dundee, *Moellerina* as a possible marker of upper Columbus strata and firm grounds as possible stratigraphic markers, one can construct a number of regional stratigraphic sections. As previously discussed, the cherty mudstone facies (facies 3) is readily recognizable within Dundee strata of the Appalachian Basin. Stratigraphic section B–B′ is constructed across the northern edge of the Appalachian Basin and uses the top of facies 3 as a datum (Figure 340.6). The contact of facies 3 with overlying facies 4 is commonly a distinctive firm ground. Facies 3 only occurs over a relatively thin interval near the middle of the Dundee and apparently records a basinwide change in depositional and environmental conditions. Using this marker facies as a regional datum, it is possible to trace firm-ground packages in the Appalachian Basin within facies 4. These traceable firm-ground packages may also be used as a regional datum.

The most obvious feature observed in section B–B′ is the erosive topography at the Detroit River–Dundee contact. Approximately 10 m of Detroit River Group sediments may

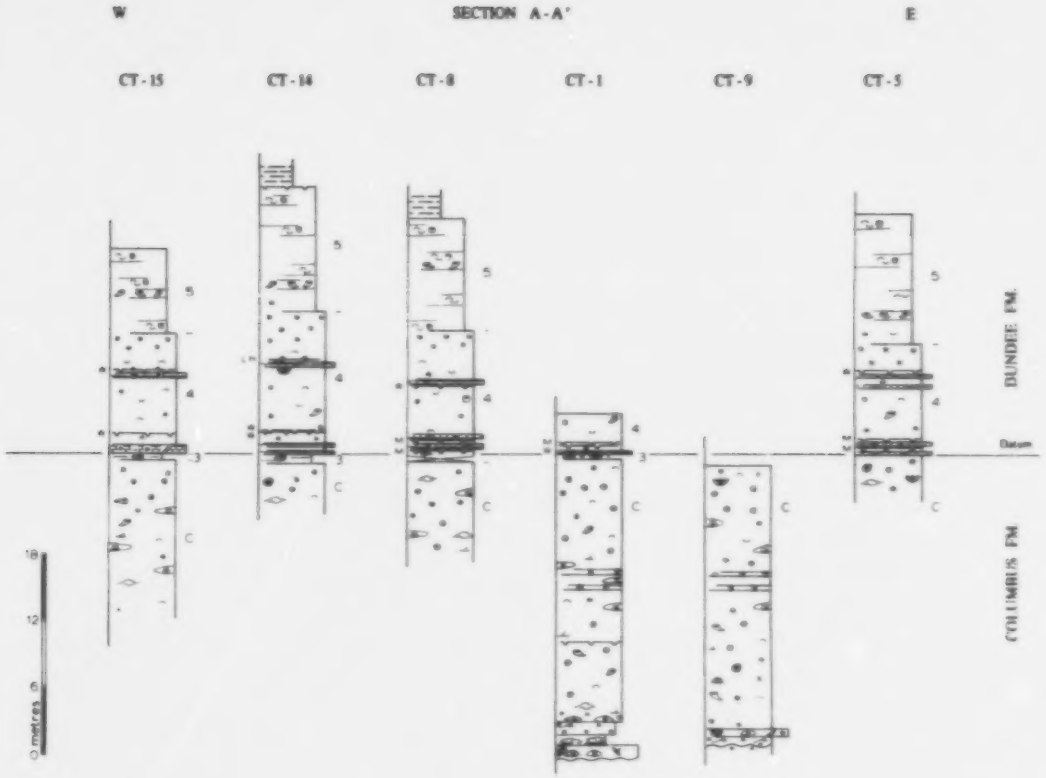

Figure 340.5. Stratigraphic section A–A'.

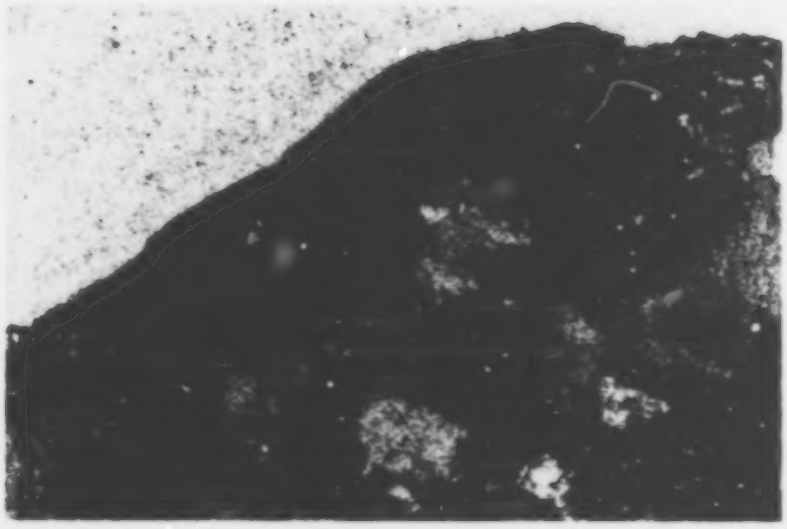

Photo 340.9. Calcified charophyte oogonia (*Moellerina*? sp.). Unstained thin-section photomicrograph under plane-polarized light. Magnification 25×. Columbus Formation sediments, Pelee Island, Ontario.

have been eroded in the area of the Chatham Sag. Dolomitic sands of facies 1 fill the lowest part of the erosive cut and are overlain by the cherty bioclastic facies 2. A somewhat cyclic repetition of facies 2 and 3 is also evident and may record relative sea-level changes. In the southwestern part of Lake Erie and in wells from Essex County, Columbus Formation sediments are gradationally overlain by the cherty bioclastic facies. As noted by Sparling (1988), Columbus Formation sediments pinch out towards the northeast, away from the Findlay Arch.

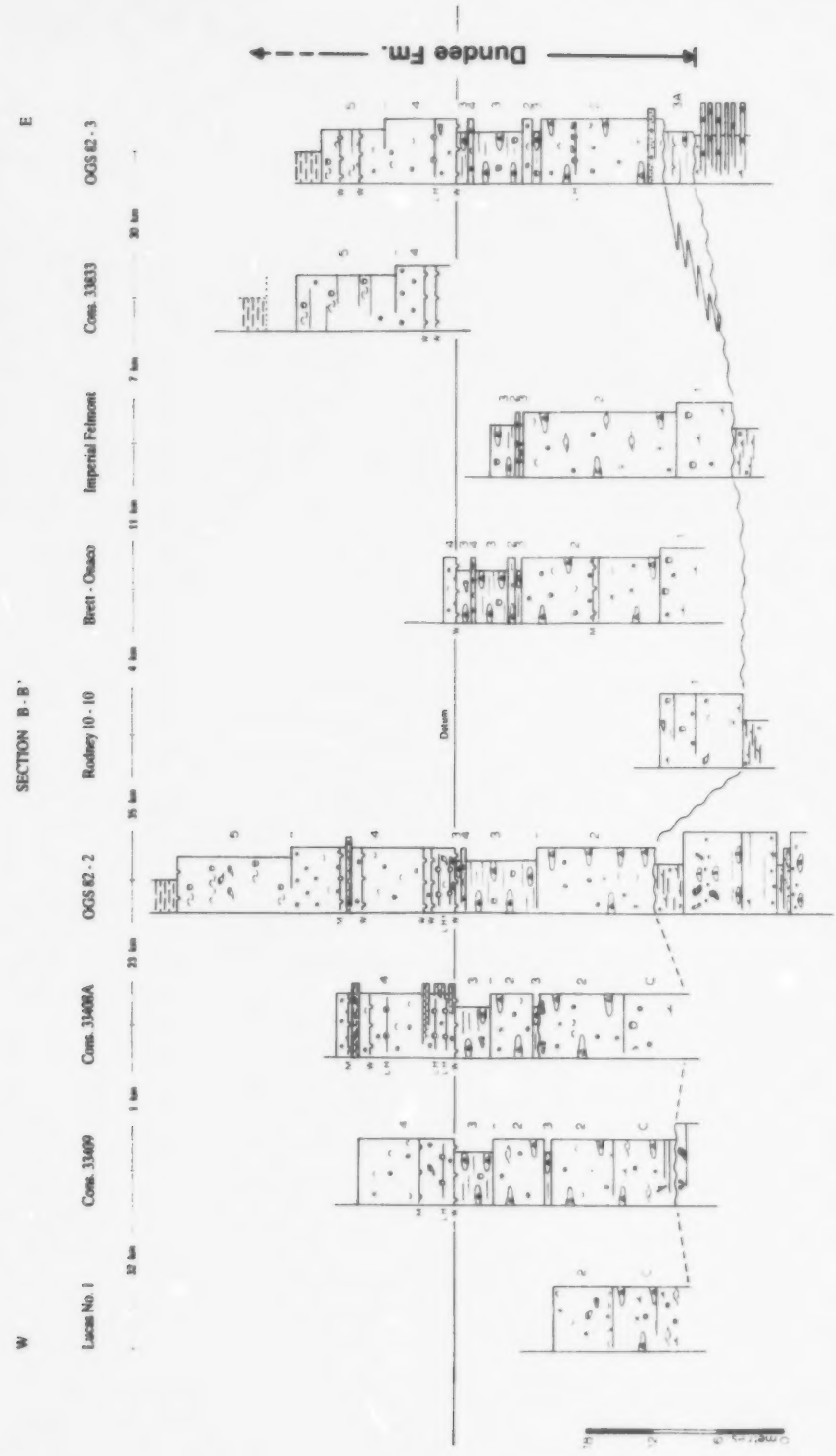

Figure 340.6. Stratigraphic section B–B'.

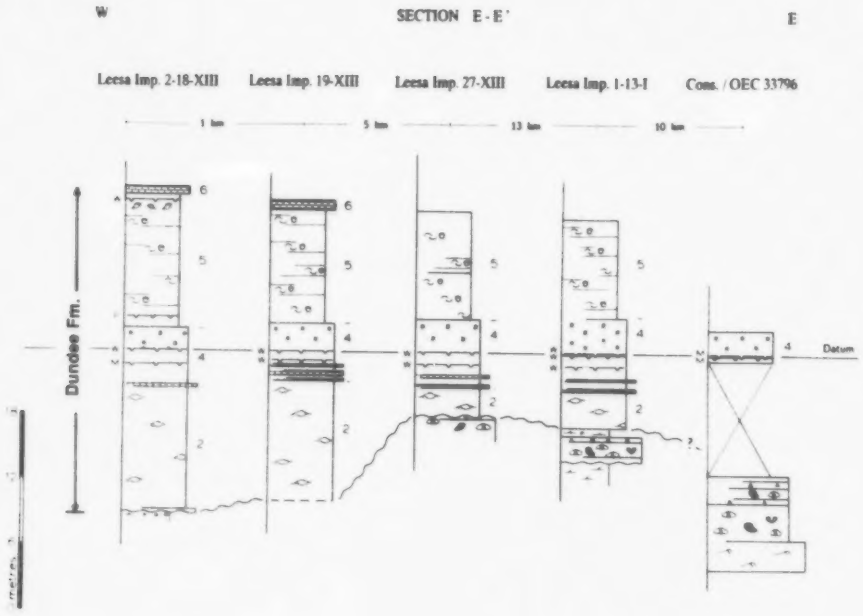

Figure 340.7. Stratigraphic section E–E'.

Section E–E' is between the Michigan and Appalachian basins and uses a firm-ground package within facies 4 as a datum, since no other internal markers are present (Figure 340.7). This section shows topography at the lower contact that separates sandy fossiliferous Detroit River Group carbonates from overlying bioclastic limestones of the Dundee Formation. A thinning of facies 2 over the paleotopographic high is also noted.

Section C–C' is a north-south cross section beginning in the Michigan Basin, cutting across the western pinchout of the Algonquin Arch and ending in the Appalachian Basin (Figure 340.8). This section uses the traceable firm-ground package near the base of facies 4 as a datum and shows the erosive formation contact overlain by dolomitic sands within the Appalachian Basin. Also evident in this cross section are the northward pinchout of facies 3, the thinning of facies 2 over the topographic high and the discontinuous nature of firm grounds into deeper portions of the Michigan Basin. In all wells, firm grounds in facies 4 appear to be best developed proximal to the topographic high at the Dundee–Detroit River contact where the record of sea-level falls and stillstands would be most amplified.

Section D–D' across the northwestern edge of the study area (Figure 340.9) shows features similar to those described for previous stratigraphic sections and also a possible thickening of facies 6 towards the northwest. The paleotopographic highs shown in sections D–D' and E–E' may be a result of thickening caused by dissolution of Silurian salts, as modelled by Brigham (1972).

DEPOSITIONAL MODEL

Based upon information derived from outcrop and subsurface cores it can be postulated that evidence of a number of sea-level fluctuations has been preserved within Dundee and equivalent sediments. Firm grounds and diagnostic marker facies can be recognized within cores, but recognition of these markers on geophysical logs is virtually impossible. Diffendal (1971) proposed that the Dundee Formation in Ontario represents a single time-transgressive package. The present study suggests that the lower Dundee is time transgressive and that minor relative sea-level falls interrupted transgression during middle Dundee time. Upper Dundee strata seem to reflect a time-stratigraphic deposition in which the Michigan and Appalachian basins were beginning to respond to separate depositional controls.

By mid–Eifelian time, evaporites and sandy limestones characteristic of the Detroit River Group were prevalent throughout the northwestern part of the Appalachian Basin. A significant relative sea-level fall caused subaerial exposure and erosion of Detroit River facies along the northern margin of the basin (section C–C'). Up to 10 m of Detroit River Group sediments may have been eroded, with the greatest amount of erosion taking place in an area coincidental with the Chatham Sag. This region of maximum erosion is the area where the greatest influx of waters from the Appalachian Basin mixed with those of the Michigan Basin.

Subsequent transgression of Dundee seas may have mixed reworked Detroit River Group sands with eolian sands (Summerson and Swann 1970) supplied from the Algonquin Arch, depositing them preferentially in topographic lows created by erosion between the two basins. In the westernmost region of the Appalachian Basin adjacent to the Findlay Arch, Columbus Formation limestones were being deposited (section B–B'). With continued transgression, a return to normal marine conditions is reflected by deposition of a cherty bioclastic facies.

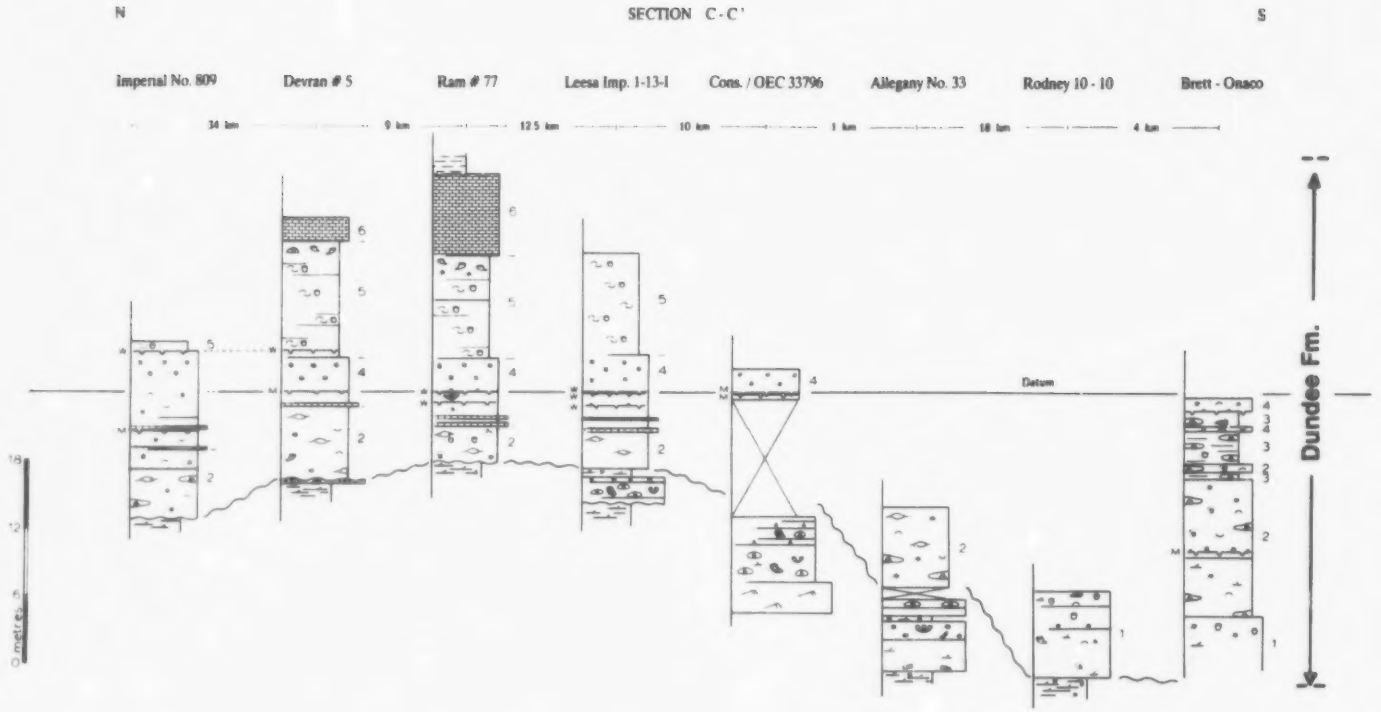

Figure 340.8. Stratigraphic section C–C'.

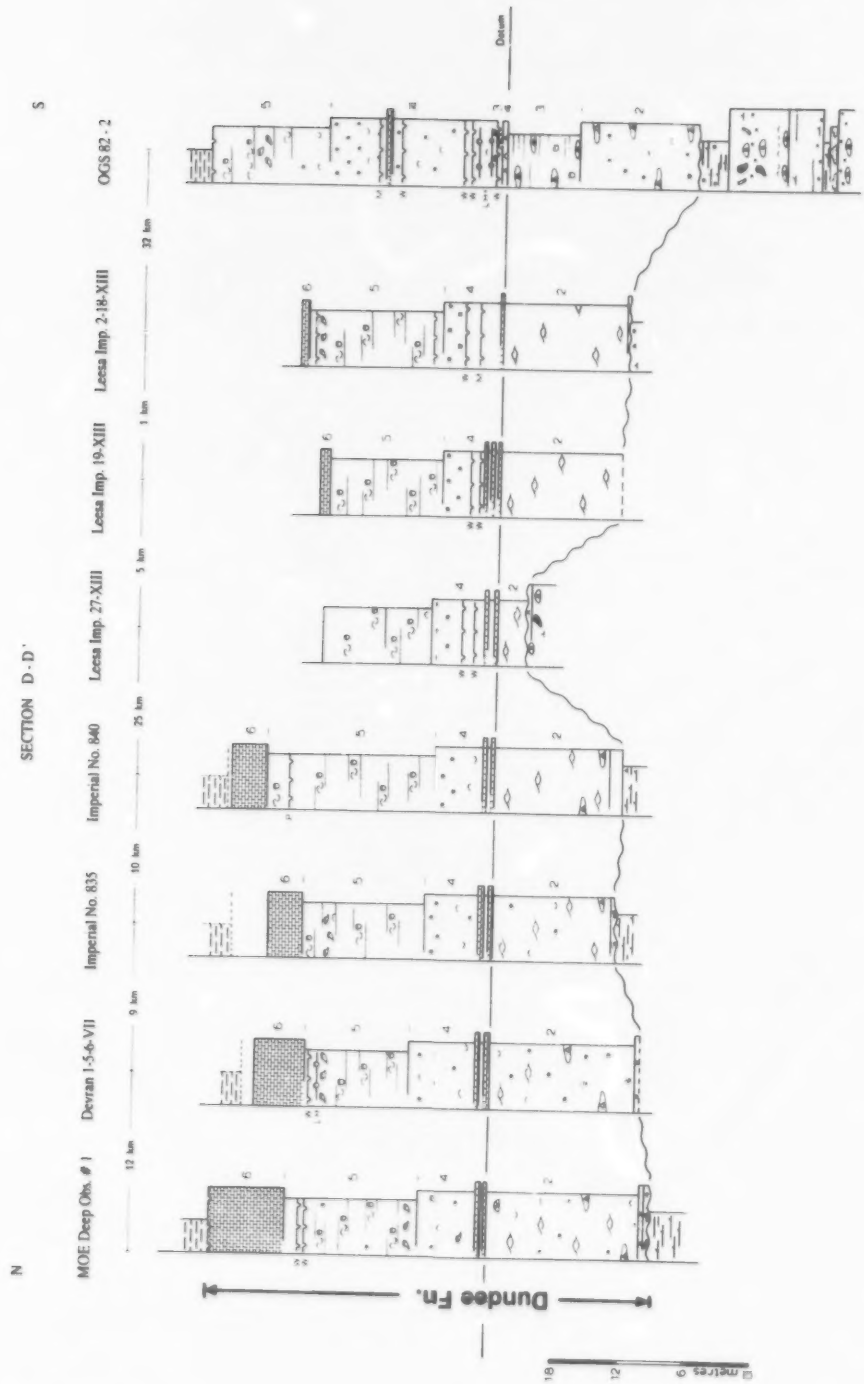

Figure 340.9. Stratigraphic section D–D'.

Transgressive conditions were interrupted towards middle Dundee time when minor sea-level fluctuations occurred; these relative sea-level changes are preserved as thin repetitions of facies 2 and 3. Facies 3 represents a pause in transgression or a relative sea-level fall during which restricted, possibly dysaerobic lagoonal conditions prevailed in nearshore waters of the Appalachian Basin. A minor transgressive-regressive cycle reflected by thin pulses of facies 4 and 3 preceded transgressive deposition of facies 4 and 5 in the Appalachian Basin. Facies 3 is not present within the Michigan Basin, possibly indicating the onset of independent basinal responses to sedimentation and deposition.

The final piece of evidence suggesting possible sea-level fluctuations during middle Dundee time is the laterally persistent firm grounds developed at the top of facies 3 and in the lower part of facies 4. The laterally persistent, well-developed firm ground located at the top of facies 3 may record a maximum relative sea-level lowstand. Coarse-grained, 10 to 20 cm thick packstones and grainstones are commonly observed capping firm grounds within facies 4, therefore suggesting that 2 to 3 episodes of nondeposition followed by winnowing and reworking must have occurred. The firm-ground surfaces within facies 4 may record brief episodes of sea-level stillstand and nondeposition within a final step-like transgression.

Open-shelf, argillaceous mudstones and wackestones of facies 5 were the last sediments to be deposited at the end of Dundee time in the Appalachian Basin. Thin, precursory Marcellus Formation shale pulses exist in uppermost Dundee strata towards the east in the Appalachian Basin (OGS 82-3, Figure 340.6), suggesting that the disconformity between the Dundee and overlying shales there may not represent a significant period of time. In contrast to upper Dundee strata in the Appalachian Basin, facies 6 is identified only within the Michigan Basin. This muddy, bioturbated wackestone to packstone facies suggests pervasive, shallow-shoal sediments occasionally blanketed by thin carbonaceous muds. It appears that at this time waters in the Michigan Basin were less argillaceous than those of the Appalachian Basin, thereby allowing a burrowing and filter-feeding fauna to proliferate. The thickest development of facies 6 occurs in the northwestern part of Lambton County, therefore suggesting that a laterally extensive shallow shoal may have been close by. Precursor Marcellus Shale pulses are not observed within the Michigan Basin; therefore, the time represented by the disconformity at the top of the Dundee is likely greater in the Michigan Basin than in the Appalachian Basin.

CONCLUSIONS

In summary, core data from the Dundee Formation of southwestern Ontario document changes in sea level as reflected in shallow-shelf carbonate facies. Sea-level fall and subsequent rise following Detroit River deposition resulted in erosion, reworking and deposition of nearshore-marine sandy and bioclastic limestones. Structural highs partially separating the 2 basins and erosive topography at the base of the Dundee controlled lithofacies character and distribution. Continuing sea-level rise was interrupted in middle Dundee time by minor episodes of sea-level fluctuation, as reflected by marker facies and laterally persistent firm-ground packages. Transgression continued but at a decreasing rate until the end of Dundee time, at which point depositional responses of the Michigan and Appalachian basins were quite different.

This overall interpretation agrees quite well with regional biostratigraphic and lithostratigraphic interpretations for surrounding areas in Ohio and Michigan (Gardner 1974; Montgomery 1986; Sparling 1988) and also agrees in the global context with eustatic sea-level changes proposed for the Devonian (Johnson et al. 1985).

REFERENCES

Bailey Geological Services Ltd. and R.O. Cochrane, 1985. Evaluation of the conventional and potential oil and gas reserves of the Devonian of Ontario; Ontario Geological Survey, Open File Report 5555, 178p.

Best, E.W. 1953. Pre-Hamilton Devonian stratigraphy, southwestern Ontario, Canada; unpublished PhD thesis, University of Wisconsin, Madison, Wisconsin, 222p.

Birchard, M.C. 1990. Stratigraphy and facies of the Middle Devonian Dundee Formation, southwestern Ontario; unpublished MSc thesis, McMaster University, Hamilton, Ontario, 136p.

Bjersted, T.W. and Feldmann, R.M. 1985. Stromatoporoid paleosynecology in the Lucas dolostone (Middle Devonian) on Kelleys Island, Ohio; Journal of Paleontology. v.59, p.1033-1061.

Brigham, R.J. 1972. Structural geology of southwestern Ontario and Michigan; Ontario Department of Mines and Northern Affairs, Paper 71-2.

Conkin, J.E., Conkin, B.M., Sawa, T. and Kern, J.M. 1970. Middle Devonian *Moellerina greenei* zone and suppression of the genus *Weikkoella* Summerson, 1958; Micropaleontology, v.16, no.4, p.399-406.

Diffendal, R.F., Jr. 1971. The biostratigraphy of the Delaware limestone (Middle Devonian) of southwestern Ontario; unpublished PhD thesis, University of Nebraska, Lincoln, Nebraska, 208p.

Dutton, B.C. 1985. Sedimentology and diagenesis of the Middle Devonian Dundee Formation in south Lambton and west Middlesex counties, southwestern Ontario, Canada; unpublished MSc thesis, University of Toronto, Toronto, Ontario, 193p.

Gardner, W.C. 1974. Middle Devonian stratigraphy and depositional environments in the Michigan Basin; Michigan Basin Geological Society, Special Paper 1, 132p.

Johnson, J.G., Klapper, G. and Sandberg, C.A. 1985. Devonian eustatic fluctuations in Euramerica; Geological Society of America Bulletin, v.96, p.567-587.

Montgomery, E.L. 1986. Facies development and porosity relationships in the Dundee limestone of Gladwin County, Michigan; unpublished MSc thesis, Western Michigan University, Kalamazoo, Michigan, 82p.

Rickard, L.V. 1984. Correlation of the subsurface Lower and Middle Devonian of the Lake Erie region; Geological Society of America Bulletin, v.95, p.814-828.

Sanford, B.V. 1969. Geology, Toronto–Windsor area, Ontario; Geological Survey of Canada, Map 1263A, scale 1:250 000.

Sparling, D.R. 1988. Middle Devonian stratigraphy and conodont biostratigraphy, north-central Ohio; Ohio Journal of Science, v.88, no.1, p.2-18.

Summerson, C.H. and Swann, D.H. 1970. Patterns of Devonian sand on the North American craton and their interpretation; Geological Society of America Bulletin, v.81, p.469-490.

Uyeno, T.T., Telford, P.G. and Sanford, B.V. 1982. Devonian conodonts and stratigraphy of southwestern Ontario; Geological Survey of Canada, Bulletin 332, 55p.

Grant 341 PGE Study: the MacRae and Marathon Copper-Precious Metal Deposits, Coldwell Complex

D.J. Good and J.H. Crocket

Geology Department, McMaster University, Hamilton

ABSTRACT

The MacRae occurrence and Marathon deposit are located within and at the intrusive margin, respectively, of the Coldwell Complex, near Marathon, Ontario. Both of the deposits are unusual in that they have very high concentrations of Cu and Pd with respect to Ni and the other platinum group elements (PGEs). Evidence suggests that the dominant process responsible for the precipitation of PGEs in these deposits is magmatic and not hydrothermal, although the MacRae deposit possibly formed under magmatic conditions that evolved to a hydrothermal system.

At the Marathon deposit, sulphides occur in both magmatic and apparent hydrothermal settings. However, the PGE abundances, recalculated to the amount in 100% chalcopyrite, do not exhibit the interelement fractionation expected in a hydrothermal system. The PGE distribution for samples of pegmatite overlie the range of PGEs in homogeneous, coarse-grained gabbro. It is likely that the sulphides and PGEs precipitated in association with hydrothermal fluids and were not transported in and deposited from them.

At the MacRae occurrence, sulphides and PGEs are associated with secondary minerals introduced into the Geordie Lake gabbro from feldspathic dikelets. The dikelets apparently intruded the magma chamber prior to the complete solidification of the crystal pile. The PGE patterns pivot about the abundance of Ir. Pd/Rh ratios in weakly mineralized samples are consistent, but in the strongly mineralized samples the ratio increases with the increasing abundance of Pd. As the system evolved the PGEs continued to migrate into the gabbro, possibly by a hydrothermal fluid that acted to fractionate palladium from the other PGEs.

INTRODUCTION

There are 2 large-tonnage, low-grade copper-precious metal deposits in the Coldwell Complex (Figure 341.1). The first is the Marathon deposit (Fleck Resources Ltd.) in the Two Duck Lake gabbro on the eastern contact of the complex. The second is the MacRae occurrence in the Geordie Lake gabbro located well within the complex.

The dominant precious metals found in both deposits are silver and palladium, with lesser amounts of gold, platinum and rhodium. These elements are found in a number of platinum group minerals (PGMs), several of which are common to both deposits, associated with Cu-rich sulphides, predominantly chalcopyrite. These minerals have been documented by Ohnenstetter et al. (1989) in the Marathon deposit and by Mulja and Mitchell (in press) in the MacRae occurrence.

These 2 deposits are unusual in that they have very high abundances of Cu and Pd with respect to Ni and the rest of the PGEs. There are 2 possible processes that can account for these highly fractionated base and precious metal signatures. The first possibility involves crystal fractionation in the magma chamber and assumes that copper and palladium are more incompatible than nickel and the other PGEs and therefore accumulate in the residual magma. The second possibility is that the fractionation occurred during the transport and deposition of the metals by hydrothermal fluids.

This report is focussed on petrographic and geochemical evidence, including PGE concentrations, that support either a magmatic or hydrothermal origin for these deposits. Some work along this line has already been completed for these deposits.

At the Marathon deposit, Watkinson et al. (1986) suggested that high F and Cl concentrations in biotite as well as the common association of pegmatites and hydrous minerals with PGMs and sulphides are consistent with a hydrothermal origin for the mineralization. However, it has not yet been shown whether the PGEs were deposited in association with hydrothermal fluids, i.e., fluids and sulphides exsolved from the melt at the same time, or were actually transported and deposited from these fluids. Some evidence presented here suggests that the former is more likely.

At the MacRae occurrence, Good and Crocket (1989) and Mulja and Mitchell (in press) suggested that the PGEs and sulphides exsolved from a highly evolved melt. This interpretation is now believed to be unlikely. The sulphides are probably not of primary magmatic origin, since there is an absence of pyrrhotite and the sulphides are only associated with what are apparently secondary silicate minerals. A reinterpretation of data presented by Good and Crocket (1989) and a possible model for the MacRae mineralization are presented here.

GEOLOGY OF THE MARATHON DEPOSIT

A simplified plan view of the geology of the Marathon property is presented in Figure 341.2. The Marathon deposit is hosted within and near the base of the Two Duck Lake gabbro.

The Two Duck Lake gabbro intruded along the contact between an older gabbroic body and the Archean basement. The Two Duck Lake gabbro was in turn cut by a leucogabbroic dike and later syenitic dikelets. The

Table 341.1. Representative analyses for the Two Duck Lake gabbro and xenoliths from the Marathon Property.

Sample	F1	F2	F3	F4	F5	F6
Rock type*	TDL	TDL	TDL	TDL	TDL	TDL
SiO_2	47.36	47.68	46.76	44.58	48.21	47.55
Al_2O_3	15.56	15.27	14.92	15.26	15.73	15.83
Fe_2O_3	12.96	11.96	13.36	13.34	11.00	11.02
MgO	8.06	7.87	7.85	7.80	7.98	7.54
CaO	12.36	13.00	12.88	13.67	13.77	12.87
Na_2O	2.01	1.95	2.30	1.92	1.96	1.87
K_2O	0.37	0.41	0.35	0.25	0.29	0.47
TiO_2	0.65	0.73	0.68	0.57	0.51	0.46
P_2O_5	0.16	0.19	0.14	0.22	0.26	0.13
MnO	0.16	0.16	0.14	0.15	0.15	0.12
Total	99.67	99.22	99.38	97.78	99.87	97.86
S	0.02	0.03	1.96	2.40	0.10	2.44
Cu	239	398	8897	17 172	1297	13 551
Ni	117	114	325	464	189	342
V	237	282	282	197	166	130
Nb	6.7	9.6	3.6	0.4	3.3	4.3
Rb	8.6	12	5.4	3.9	2.2	13
Sr	694	670	665	688	697	664
Y	12	12.7	8.5	7.2	12	10.3
Zr	53	60	46	34	39	57

Sample	F7	F8	F8c	F9	F18	F15
Rock type*	TDL	TDL	TDL	TDL	TDL	TDL
SiO_2	47.06	45.32	48.21	47.79	46.00	47.86
Al_2O_3	15.48	13.75	15.24	16.81	15.02	15.67
Fe_2O_3	10.43	13.98	11.17	10.84	14.12	12.14
MgO	8.48	8.48	8.59	7.53	8.61	6.73
CaO	13.53	13.06	12.74	12.72	12.09	12.66
Na_2O	2.03	1.97	1.50	2.41	2.00	2.42
K_2O	0.40	0.41	0.28	0.36	0.33	0.42
TiO_2	0.54	0.81	0.51	0.55	0.66	1.48
P_2O_5	0.19	0.23	0.18	0.17	0.18	0.35
MnO	0.15	0.16	0.17	0.14	0.15	0.14
Total	98.40	99.57	98.59	99.34	99.09	99.86
S	1.03	2.76	n.a.	0.10	1.35	0.01
Cu	5522	15 173	1.18p	1092	4763	131
Ni	240	308	406	147	211	77
V	145	228	149	213	202	288
Nb	5.8	9.0	10.1	3.9	5.7	5.1
Rb	15	18	9.1	5.0	4.9	6.8
Sr	635	517	599	735	637	625
Y	12.4	15	13.3	9.9	9.0	14.9
Zr	47	65	37	46	55	59

Table 341.1 (continued).

Sample	F19	F30	F200d	F8p	F21	F22
Rock type*	TDL	TDL	TDL	Peg	Peg	Peg
SiO_2	47.04	44.97	48.14	48.03	47.86	43.71
Al_2O_3	13.23	12.13	14.87	12.92	17.96	13.38
Fe_2O_3	14.12	17.70	11.25	11.49	10.56	19.07
MgO	9.05	7.40	9.00	10.30	5.09	11.06
CaO	11.47	11.54	12.90	13.93	12.21	8.98
Na_2O	1.91	1.72	1.53	1.06	2.34	1.82
K_2O	0.51	0.43	0.22	0.26	0.55	0.30
TiO_2	0.92	0.77	0.58	0.52	1.05	0.42
P_2O_5	0.30	0.37	0.28	0.13	0.23	0.19
MnO	0.20	0.22	0.17	0.18	0.13	0.25
Total	100.07	97.26	98.94	98.82	97.97	99.18
S	0.13	2.57	n.a.	n.a.	1.39	0.90
Cu	392	5323	0.76	1.26p	7885	3838
Ni	110	248	298	458	184	162
V	262	309	148	204	299	166
Nb	9.8	3.6	11	5.3	7.4	3.8
Rb	15	14	13.7	14.5	11	11
Sr	568	580	617	445	770	575
Y	12.2	14.3	14.7	12.3	14.3	5.6
Zr	74	54	44	40	63	43

Sample	F23	F24	F26	F25	F27	F200W
Rock type*	Peg	Peg	Peg	Gran	Gran	Gran
SiO_2	46.81	45.81	45.72	56.04	56.36	66.47
Al_2O_3	11.64	14.20	12.66	8.34	14.00	13.45
Fe_2O_3	15.01	16.30	16.22	10.73	7.46	4.67
MgO	8.84	6.61	6.81	6.60	4.60	2.47
CaO	13.43	11.72	12.95	10.92	10.45	4.24
Na_2O	1.60	2.05	1.99	1.89	3.28	2.86
K_2O	0.33	0.52	0.42	1.71	1.50	3.33
TiO_2	1.13	1.73	1.94	1.02	0.58	0.66
P_2O_5	0.18	0.29	0.30	0.14	0.17	0.63
MnO	0.18	0.19	0.19	0.17	0.14	0.13
Total	99.04	99.41	99.73	97.46	98.69	98.91
S	0.32	0.14	0.15	0.02	0.03	n.a.
Cu	1915	718	472	293	203	0.32
Ni	141	73	70	52	70	45
V	438	629	728	428	215	79
Nb	6.1	14	11	15	16	45
Rb	10	14	13	63	58	112
Sr	476	639	575	144	533	293
Y	14.9	12.7	17.3	18.6	19.5	22
Zr	57	79	67	213	100	321

Table 341.1 (concluded).

Sample Rock type*	F11 X gn	F37 X gn	F13 X oph-g	F14 X ol-g	F36 X ol-g
SiO_2	50.85	51.48	46.20	42.15	45.37
Al_2O_3	15.30	16.14	17.34	9.10	9.40
Fe_2O_3	10.51	9.99	13.54	22.07	16.01
MgO	7.09	8.07	10.10	16.11	16.44
CaO	11.75	8.54	9.92	8.19	8.53
Na_2O	2.57	2.77	2.06	1.23	2.13
K_2O	0.19	0.19	0.30	0.24	0.26
TiO_2	1.04	1.68	0.14	0.44	0.75
P_2O_5	0.08	0.05	0.12	0.20	0.15
MnO	0.11	0.21	0.16	0.29	0.26
Total	99.50	99.10	99.88	100.01	99.36
S	0.01	0.01	0.01	0.01	0.01
Cu	68	165	36	95	151
Ni	161	147	132	203	365
V	216	24	59	182	167
Nb	2.1	3.3	0.9	2.5	3.2
Rb	3.6	2.2	4.5	4.5	9
Sr	527	448	823	434	336
Y	10.5	11	3.6	6.1	13
Zr	29	77	30	30	45

Notes: Major elements are in weight percent; trace elements are in parts per million; n.a., not analyzed; p, percent.
**Rock types: TDL, coarse-grained Two Duck Lake gabbro; PEG, pegmatitic Two Duck Lake gabbro; GRAN, granophyre-bearing, pegmatitic TDL gabbro; X oph-g, xenolith of fine-grained, ophitic olivine gabbro that underlies the next unit in 2 places; X ol-g, xenolith of medium- to coarse-grained, allotriomorphic, biotite-bearing olivine gabbro; X gn, xenolith of fine- to medium-grained, ophitic gabbronorite.*

mineralized zone and rare layering in the Two Duck Lake gabbro strike approximately north-northeast and dip moderately west parallel to the intrusive contact.

The Two Duck Lake gabbro is divided into an upper and a lower zone. The upper zone is west of the long, thin xenolith that strikes northerly across the map area (Figure 341.2) and was not previously recognized as being part of the Two Duck Lake gabbro.

The lower zone of the Two Duck Lake intrusion consists of coarse-grained, relatively homogeneous gabbro and sporadic pegmatitic pods that may contain granophyric patches. The homogeneous gabbro consists of subhedral plagioclase and olivine, ophitic clinopyroxene and interstitial biotite, magnetite and sulphides. Accessory phases such as apatite and zircon occur sporadically.

Pegmatitic pods are unevenly distributed in the lower zone of the Two Duck Lake gabbro and are associated with the sulphide mineralization. The pegmatite consists of plagioclase, clinopyroxene, amphibole, magnetite, biotite, calcite and sulphides. Some pegmatites have granophyric patches that contain intergrowths of orthoclase and quartz.

The upper zone consists of layered, ophitic to very coarse-grained gabbro. Layers are a few to several metres thick, and their contacts are gradational. The ophitic-textured gabbro consists of medium- to coarse-grained subhedral plagioclase and ophitic clinopyroxene, olivine and magnetite. The oikocrysts of clinopyroxene and olivine range in size from 1 to several centimetres.

The sequence of major mineral crystallization in both the upper and lower zones is plagioclase, followed by olivine, then clinopyroxene and finally the interstitial minerals. The textures in the Two Duck Lake gabbro are different from those in the xenoliths.

There are at least 4 types of gabbro represented in the xenoliths. These are ophitic gabbronorite, allotriomorphic, biotite-bearing olivine gabbro, fine-grained, ophitic olivine gabbro and glomeroporphyritic gabbro. The first 2 types make up the majority of xenoliths.

The gabbronorite xenoliths are fine to medium grained and consist of ophitic, inverted pigeonite and anhedral plagioclase and clinopyroxene.

The biotite-bearing olivine gabbro xenoliths are medium to coarse grained and consist of anhedral olivine and plagioclase, subophitic to ophitic clinopyroxene and ophitic magnetite. Biotite is associated with the magnetite. In 2 locations this unit is underlain by a fine-grained ophitic olivine gabbro distinguished by its thin layering (2 to 10 cm), 0.5 to 1 cm black clinopyroxene oikocrysts and smaller ophitic magnetite crystals.

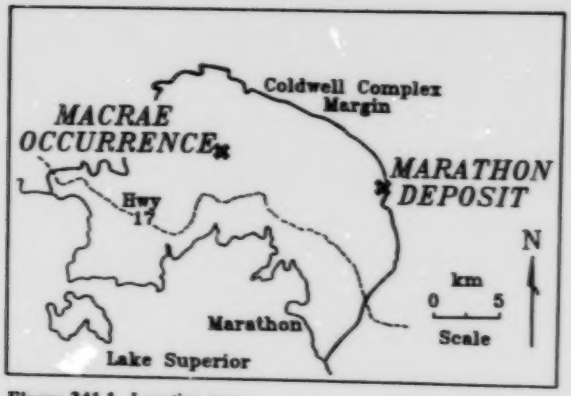

Figure 341.1. Location map.

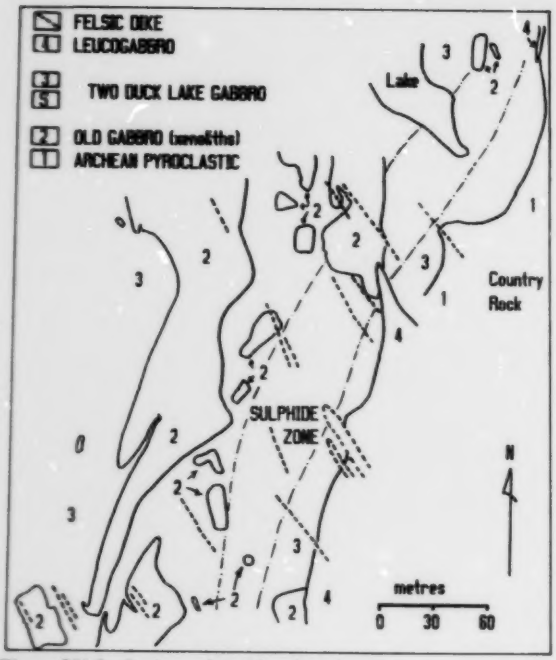

Figure 341.2. Geology of the Marathon deposit.

The glomeroporhyritic gabbro xenoliths are fine grained and contain 1 to 2 cm accumulations of medium- to coarse-grained plagioclase laths.

The old gabbro and Two Duck Lake gabbro have been intruded by a leucogabbroic body close to the contact with the Archean country rock. The leucogabbro consists of numerous rounded fragments of old gabbro and rare angular fragments of Two Duck Lake gabbro.

All of the above units have been cut by late north-northwest-trending syenite dikes. The dikes range in thickness from less than 1 to several metres. The thicker dikes are commonly zoned and contain cores with graphic intergrowths of quartz and feldspar.

ASSIMILATION OF XENOLITHS

Xenoliths are ubiquitous in the Two Duck Lake gabbro. They range in size from a few centimetres to tens of metres across. A long slice of old gabbro occurs in the centre of the map area. The xenoliths are typically angular in form.

It is not possible to assess the extent of assimilation by mass-balance techniques. This is primarily due to the variety of xenoliths and the similarity in the ranges of trace-element abundances and interelement ratios for the xenoliths and the Two Duck Lake gabbro. The actual process of assimilation is also complex because mass is apparently transferred both ways between the magma and the xenolith, and when the xenolith is actually assimilated the clinopyroxene apparently dissolves first. This is expected, if one considers the order of crystallization of the Two Duck Lake magma; clinopyroxene was not on the liquidus at the time of intrusion, so it was resorbed.

GEOCHEMISTRY OF THE GABBROS

The compositions of Two Duck Lake gabbro and old gabbro xenoliths for samples analyzed are listed in Table 341.1.

Samples of Two Duck Lake gabbro and the associated pegmatite have similar trace-and major-element concentrations. Although each sample group does show a wide variation in the abundance of individual trace elements, the range of concentrations for each group does overlap. This observation seems to indicate that the pegmatite pods are not accumulations of intercumulus melt or end products of local crystal fractionation, as might be the case if the pegmatite samples were enriched in the incompatible elements. It is likely, therefore, that the pegmatite formed in response to local enrichments in volatiles in the Two Duck Lake magma.

The granophyric pods are enriched in incompatible elements with respect to the pegmatitic and homogeneous Two Duck Lake gabbro. These pods are considered the result of crystallization of the Two Duck Lake residual melt. Granophyre is also commonly devoid of sulphides and so will not be considered further.

The composition of xenoliths is similar to that of the Two Duck Lake gabbro. There is a wide range of trace-element concentrations in the xenoliths, due in part to the 4 distinct types of xenoliths. The range for individual elements and interelement ratios of the xenoliths overlaps, in most cases, the range for samples of the Two Duck Lake gabbro.

The degree to which assimilation of the old gabbro has affected the chemistry of the Two Duck Lake gabbro is difficult to assess because the Two Duck Lake gabbro and old gabbro are similar in composition and because the assimilation undoubtedly favours the dissolution of specific minerals, e.g., clinopyroxene, in the old gabbro. The effects of assimilation might also be masked by the loss of material from the Two Duck Lake melt into the xenoliths as zoned dikelets.

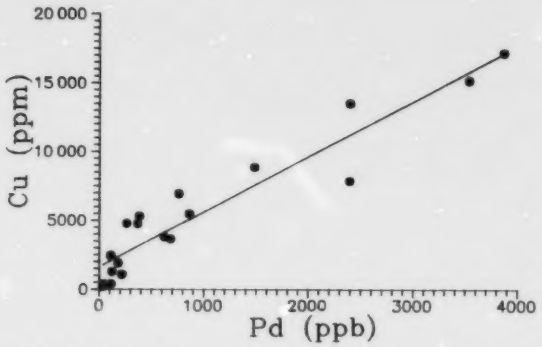

Figure 341.3. Plot of Cu versus Pd for homogeneous coarse-grained Two Duck Lake gabbro.

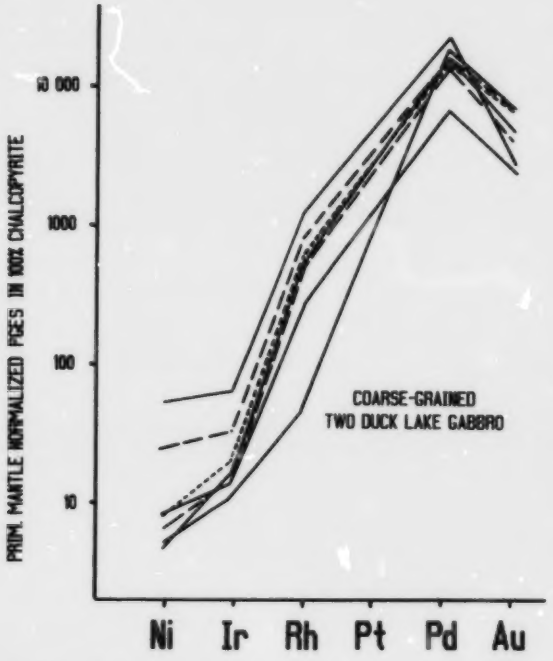

Figure 341.4. PGE abundances in the homogeneous coarse-grained Two Duck Lake gabbro in 100% chalcopyrite and normalized to mantle abundances (*after* Barnes et al. 1987).

SULPHIDE MINERALIZATION

The sulphide minerals consist of chalcopyrite, cubanite, pyrrhotite, pentlandite and pyrite. In large blebs of sulphide, pyrrhotite typically forms the core and chalcopyrite the rim. The PGMs are associated with the Cu-rich sulphides (Ohnenstetter et al. 1989).

There are several common sulphide-silicate associations in the Two Duck Lake gabbro. They can be divided on the basis of their association with either hydrous or nonhydrous minerals. The former group includes sulphides within both coarse-grained and pegmatitic gabbro. The hydrous minerals include biotite, chlorite and amphibole and are usually associated with altered plagioclase and calcite.

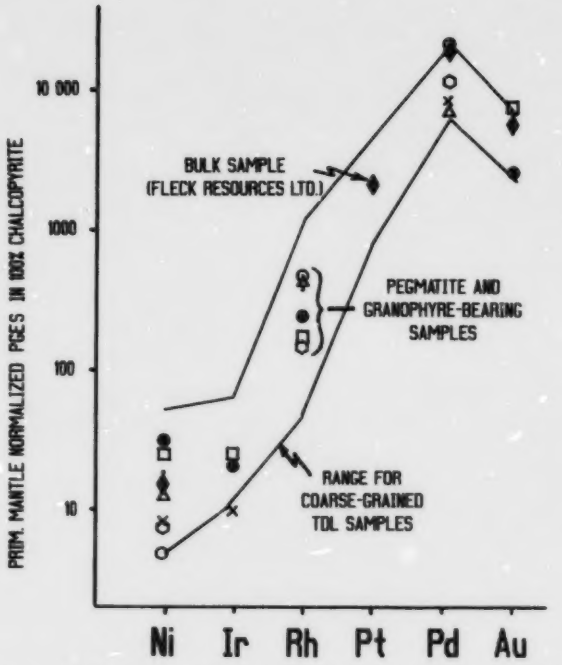

Figure 341.5. PGE abundances in pegmatite- and granophyre-bearing samples of the Two Duck Lake (TDL) gabbro plotted over the range of samples plotted in Figure 341.4. Samples are normalized as in Figure 341.4.

The second common occurrence of sulphides is interstitial to fresh silicates. These sulphides are interpreted as primary disseminated sulphides.

There are therefore 2 apparent origins for the sulphides. The first possibility is that they are of hydrothermal origin; the second, magmatic. If both of these processes occurred, then there should be notable differences in the PGE abundances between the 2 sulphide settings. The differences related to fractionation caused by transport in, and deposition from, a hydrothermal fluid are discussed in the next section.

PGE DISTRIBUTION

In order to test the possible hydrothermal origin for the sulphides the abundance of PGEs in the 2 settings must be compared. To test the hypothesis the values are normalized to 100% chalcopyrite. This normalization is deemed acceptable because there is a good correlation between the abundances of Pd and Cu (Figure 341.3) in the Two Duck Lake gabbro samples and there is a well-documented association between the Cu-rich sulphides and the PGMs (Smyk 1986; Ohnenstetter et al. 1989). The values are also normalized to the mantle abundances of Barnes et al. (1987).

The normalized abundances of PGEs in samples of coarse-grained gabbro with both interstitial and hydrous mineral associated sulphides are plotted in Figure 341.4 and do not show any evidence of fractionation. There is a tight grouping of PGE patterns in Figure 341.4, and except for a few samples, the patterns are parallel. The lack of fractionation shown here is expected in a suite of samples that contain sulphides precipitated from the magma and not from a hydrothermal fluid.

The normalized abundances of PGEs in samples of pegmatite that have an obvious hydrous mineral association are plotted in Figure 341.5. These samples clearly plot above the range of values obtained from the coarse-grained gabbro with interstitial sulphides. Also plotted is the abundance in a bulk sample analyzed by Fleck Resources Ltd. It is evident that the tenor of PGEs in the mineralized samples is remarkably consistent. The lack of fractionation of the PGEs exhibited in these diagrams does not support a hydrothermal origin for the sulphides.

GEOLOGY OF THE GEORDIE LAKE PROPERTY

A plan view of the geology of the Geordie Lake Property (*after* Bond Gold Canada Inc., Private Company Report, Assessment File Review Office, Thunder Bay) with sample locations was presented in Figure 341.2 *in* Good and Crocket (1989).

The following is a summary of the geology, petrography and geochemistry of the Geordie Lake gabbro, which was described in more detail by Good and Crocket (1989). Some of the data in the earlier publication are reinterpreted here, and a model for the mineralization is presented.

The MacRae occurrence is located within the Geordie Lake gabbro. The Geordie Lake gabbro strikes north and dips moderately west. It has been cut by a north-trending quartz syenite sill.

The mineralized zone consists of several lenticular zones of disseminated chalcopyrite that trend roughly north, parallel to the syenite. The gabbro is mineralized on both sides of the syenite. Some stringer sulphide occurs in the syenite.

The gabbro consists of subhedral plagioclase, subhedral olivine, subhedral to skeletal magnetite, euhedral apatite and ophitic clinopyroxene. The composition of the gabbro varies according to the abundance of these phases, but in general most are present in any sample.

Mulja (1989) determined that major-mineral compositions in the mineralized zone vary only slightly; olivine and plagioclase compositions were close to Fo_{50} and An_{52}, respectively.

The gabbro in the mineralized zone is heterogeneous. Variations in the composition and grain size are chaotic and occur on a scale of centimetres to metres. The variations are apparently zoned about irregular, discontinuous dikelets and pods of fine- to medium-grained granular feldspar. The sulphides are also closely associated with these feldspathic pods.

The gabbro above the mineralized zone is relatively homogeneous. This homogeneous nature contrasts sharply with that of gabbro in the mineralized zone, although the mineralogy and geochemical trends are similar.

GEOCHEMISTRY

The range of compositions for samples analyzed and their locations in the Geordie Lake gabbro are shown in Figures 341.4 and 341.2, respectively, of Good and Crocket (1989).

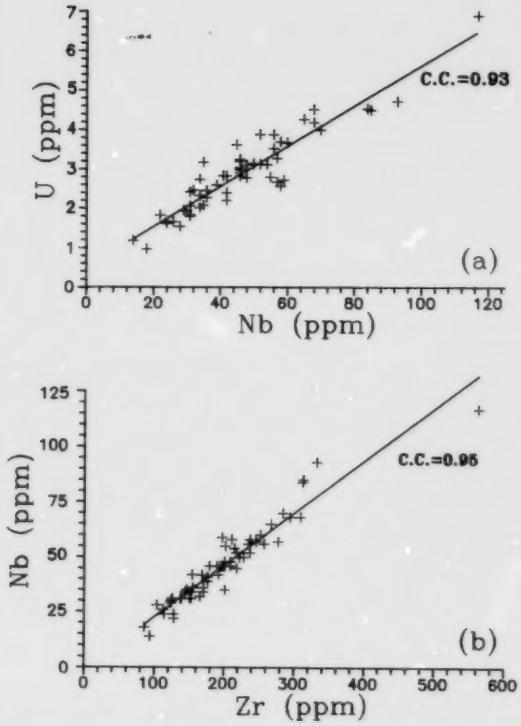

Figure 341.6. Samples of gabbro from the Geordie Lake Property: **a)** U versus Nb; **b)** Nb versus Zr; c.c., correlation coefficient.

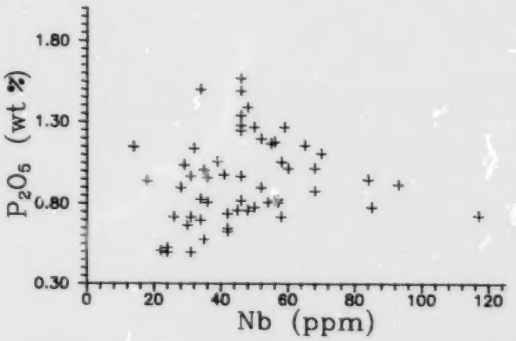

Figure 341.7. P_2O_5 versus Nb plot for the Geordie Lake gabbro, showing a lack of correlation between trace elements and the abundance of apatite.

Plots of U versus Nb and Nb versus Zr (Figures 341.6a and 431.6b, respectively) show straight-line trends for all of the gabbro samples. This relationship holds for the rare earth element (REE) data obtained by Mulja (1989).

There is a relationship between the major- and trace-element compositions. Although it is not indicated in Figure 341.6, samples at the lower end of the trend are olivine rich and at the upper end are olivine poor.

The wide range for trace-element abundances in the Geordie Lake gabbro samples shown in Figure 341.6 is unusual. There are 4 possible mechanisms that can account for the variations in trace-element abundances: crystal

Table 341.2. Geordie Lake gabbro cross section samples.

Sample Rock type*	g47 Gab	g48 Gab	g49 Dike	g49a Gab	g50 Gab
SiO_2	40.57	42.23	52.05	45.85	45.36
Al_2O_3	11.21	12.95	15.42	13.22	13.12
Fe_2O_3	24.62	21.60	12.32	19.52	18.97
MgO	7.30	6.12	2.92	4.18	4.62
CaO	9.14	8.95	7.63	8.88	9.42
Na_2O	1.75	2.01	5.35	3.01	2.81
K_2O	1.42	1.97	0.85	0.93	1.26
TiO_2	2.45	2.01	1.91	2.05	2.13
P_2O_5	0.94	0.90	0.73	1.27	1.50
MnO	0.30	0.26	0.21	0.24	0.25
Total	97.75	99.00	99.39	99.14	99.44
S	<0.01	0.01	0.53	0.02	0.02
Cu	54	106	6165	250	211
Ni	95	83	48	68.5	49
V	792	615	259	515	476
Nb	19	28	117	59	34
Rb	38	62	13	35	44
Sr	463	612	433	674	659
Y	20	28	60	43	36
Zr	86	104	564	198	154

Notes: Major elements are in weight percents; trace elements are in parts per million; the samples were selected from a 0.5 m section of diamond drill core (borehole 2); the dikelet sample (g49) contains granular feldspar, magnetite, sulphides and some of the Geordie Lake gabbro.
*Rock type: Gab, gabbro.

fractionation, variations in the abundance of intercumulus melt, control by an accessory phase and mixing of 2 components.

Crystal fractionation as a cause for the trace-element trends is unlikely. During crystal fractionation there are 2 possible ways to change the trace-element composition in the crystal pile. The first involves fractional crystallization of one or more minerals; the resultant trend for each element will depend on the bulk partition coefficient. The second is to change the group of minerals, thereby changing the bulk partition coefficient. Neither of these processes could have been responsible for the trends in the Geordie Lake gabbro. In the first case, the narrow range for mineral compositions determined by Mulja (1989) suggests that only minor *in situ* fractionation occurred. For the second case, in order to obtain the straight-line relationship from olivine-rich to olivine-poor samples, the bulk partition coefficients for all 3 elements would have to change proportionately from one rock type to another, and this is highly unlikely.

Variations in the amount of intercumulus melt cannot account for the trace-element trends. As stated above there is a relationship between rock type and trace-element abundance, but there is no reason for the trapping of intercumulus melt to be dependent on the phases present.

There are no obvious accessory minerals present that could account for the large spread in the trace-element abundances. In Figure 341.7, P_2O_5 is plotted versus Nb, showing that there is no correlation between apatite and the trace elements.

The last mechanism to explain the trace-element trends is the mixing of 2 components.

EVIDENCE FOR MIXING

In the mineralized zone there are numerous feldspathic pods and dikelets associated with the heterogeneous gabbro and sulphide mineralization. A cross section of one of these dikelets was studied in detail. The analyses for 5 samples collected from a section (0.5 m long) of drill core that intersects one of these feldspathic dikelets are listed in Table 341.2.

The 5 cross section samples are plotted on the Nb versus Zr diagram (Figure 341.8), along with all of the Geordie Lake gabbro samples. Note that the dikelet has the highest abundance of trace elements; those samples farthest from the dikelet, the lowest. Those samples with the lowest values also have the highest proportion of olivine.

There is macroscopic and microscopic petrographic evidence for a mixing event. The macroscopic evidence includes the systematic change in silicate assemblages and the coarsening of plagioclase and clinopyroxene approaching the dikelets. The microscopic evidence

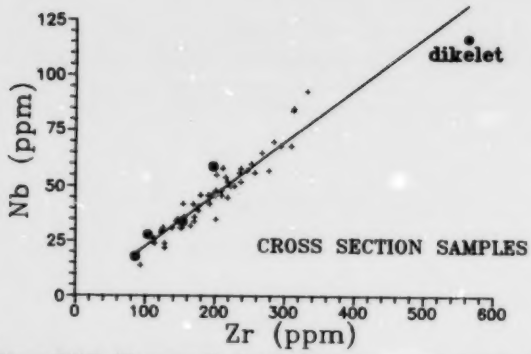

Figure 341.8. Nb versus Zr plot showing cross section samples g47 to g50 from Table 341.2 on top of the entire suite of Geordie Lake gabbro samples.

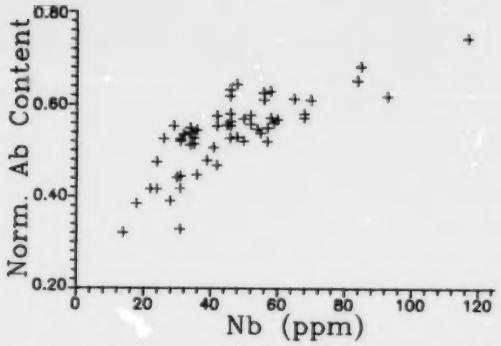

Figure 341.9. CIPW-normative plagioclase compositions plotted against Nb for all of the Geordie Lake gabbro samples.

includes the addition of secondary plagioclase rims to the primary plagioclase laths and the partial alteration of the clinopyroxene to amphibole. Examples of the plagioclase mantles are shown in Photos 341.2 and 341.4 in Good and Crocket (1989). This mantling is evident to some extent in most of the gabbro samples.

There is a correlation between the trace-element abundance and the amount of secondary plagioclase. Mulja (1989) investigated the plagioclase rims and determined they have a much higher albite content than the cores. It is assumed, therefore, that the CIPW-normative plagioclase composition for the rock is representative of the amount of secondary plagioclase. In Figure 341.9 the plot of CIPW-normative plagioclase composition versus Nb shows a straight-line correlation. A similar plot using the core plagioclase compositions instead of the CIPW value would be a horizontal line.

SULPHIDES

The mineralized zones are lenticular, strike near north and dip moderately west parallel to the contact with the syenite. The sulphides consist predominantly of disseminated chalcopyrite and exsolved bornite.

There are 3 common silicate-sulphide associations: within cloudy plagioclase rims, within the secondary amphibole rims on clinopyroxene and with amphibole interstitial to primary silicates. In samples with low concentrations of sulphide the chalcopyrite typically occurs as very fine disseminations in the secondary plagioclase and amphibole rims. As the concentration of sulphide increases, interstitial amphibole becomes the dominant sulphide-associated silicate.

The deposition of sulphides in the Geordie Lake gabbro is believed to be related to the intrusion of the feldspathic dikelets. The macroscopic association of sulphides with the feldspathic dikelets is confirmed by the microscopic association of the sulphides and the secondary minerals.

PGE DISTRIBUTION

The PGE abundances for representative Geordie Lake gabbro samples are normalized to mantle values (*after* Barnes et al. 1987) and plotted in Figure 341.10. The sample

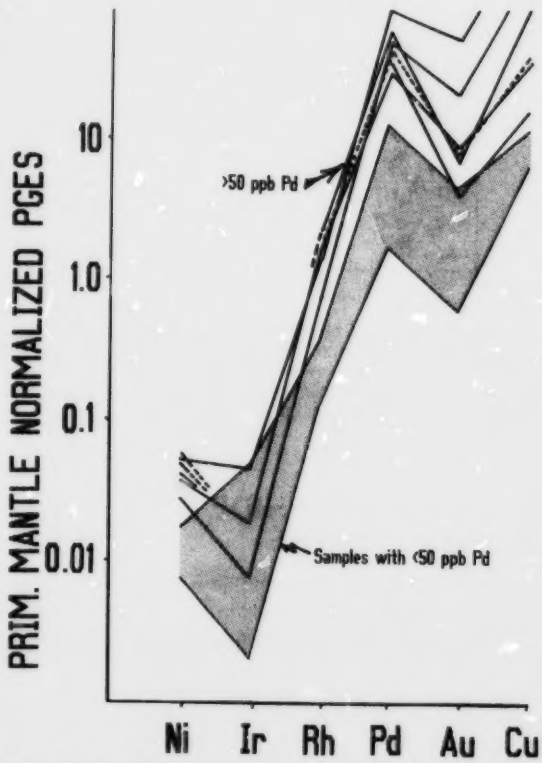

Figure 341.10. PGE abundances in the Geordie Lake gabbro samples of the MacRae occurrence normalized to mantle values (*after* Barnes et al. 1987). The samples are divided into weakly mineralized (<50 ppb Pd) and mineralized (>50 ppb Pd). There is an increase in the Pd/Ir ratio with increasing Pd, typical of hydrothermal processes.

set is divided into 2 groups: the weakly mineralized (<50 ppb Pd) and mineralized samples (>50 ppb Pd). Only the range for the former group is shown in Figure 341.10.

The fractionation of the PGEs is evident in Figure 341.10. The Ir concentration is similar in both groups of samples, and the Pd/Rh ratio increases with increasing Pd. The variation in the Pd/Rh ratio in the 2 groups of samples is shown in Figure 341.11.

Grant 341

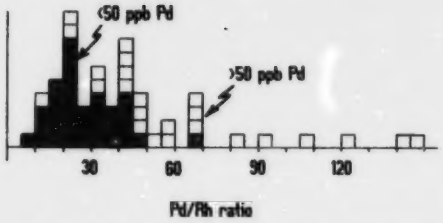

Figure 341.11. Pd/Rh ratios for the 2 groups of samples outlined in Figure 341.10.

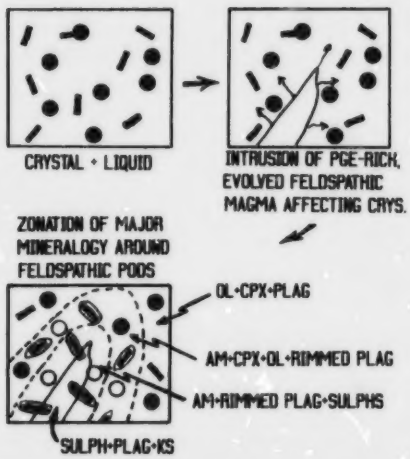

Figure 341.12. Proposed model to account for the zoned silicate assemblages in the mineralized zone of the Geordie Lake gabbro. The solid rectangles and circles represent plagioclase and mafic minerals, except amphibole, respectively. The open circles and margins on the plagioclase represent the amphibole and plagioclase rims, respectively.

ORIGIN OF SULPHIDE MINERALIZATION

A proposed model for the sulphide mineralization in the Geordie Lake gabbro is presented in cartoon form in Figure 341.12. The model involves the intrusion of a PGE-enriched feldspathic magma into a crystal pile that has a considerable amount of interstitial melt. At the contact between the 2 the plagioclase and clinopyroxene grow much larger than normal. Amphibole becomes the stable ferromagnesian mineral displacing clinopyroxene and olivine. The localized effects of the interaction could account for the heterogeneity in the mineralized zone. It is conccivable that the system changed as it evolved, becoming dominantly hydrothermal in nature. A hydrothermal system could account for the fractionation of palladium from iridium and the higher proportion of sulphides associated with amphibole in sulphide-rich samples compared with sulphide-poor samples.

ACKNOWLEDGMENTS

We thank Mr. John McGoran, Fleck Resources Ltd., and Mr. Mel Joa, prospector, for access to their properties, accumulated geological information and diamond drill core. We also thank Bernie Schnieders, Resident Geologist, and Mark Smyk, Staff Geologist, Schreiber–Hemlo District, Ontario Ministry of Northern Development and Mines, for introducing us to the Geordie Lake property and for their logistical support.

REFERENCES

Barnes, S-J., Boyd, R., Kornelliussen, A., Peter-Nilsen, L., Often, M., Pedersen, R-B. and Robins, B. 1987. The use of noble and base metal ratios in the interpretation of ultramafic and mafic rocks; examples from Norway; *in* Geo-platinum 1987 Symposium abstracts, The Open University, Milton Keynes, Buckinghamshire, England, April 1987, Paper F4.

Good, D.J. and Crocket, J.H. 1989. PGE study of the MacRae and Marathon Cu-precious metal deposits, Coldwell Complex; *in* Geoscience Research Grant Program, summary of research 1988–1989, Ontario Geological Survey, Miscellaneous Paper 143, p.186-198.

Mulja, T. 1989. Petrology, geochemistry and platinum-group element mineralization of the Geordie Lake intrusion, Coldwell Complex, Ontario; unpublished MSc thesis, Lakehead University, Thunder Bay, Ontario.

Mulja, T. and Mitchell R.H., in press. Platinum-group minerals and tellurides from the Geordie Lake intrusion, Coldwell Complex, northwestern Ontario, Canada; The Canadian Mineralogist.

Ohnenstetter, D., Watkinson, D.H. and Dahl, R. 1989. Platinum group minerals from the Two Duck Lake intrusion, Coldwell Complex, Canada; Bulletin of the Geological Society of Finland, no.61, pt.1.

Smyk, M.C. 1986. Macroscopic petrography of sulphide mineralization at the Marathon Pt-Pd-Cu property, Coldwell alkaline complex, northwestern Ontario; unpublished study, Department of Geology, Carleton University, Ottawa, Ontario, 36p.

Watkinson, D.H., Dahl, R. and McGoran, J. 1986. The Coldwell Complex platinum-group-element deposit: 2. Relationships of platinum-group elements to pegmatitic biotite-bearing gabbro and the role of a fluid phase; Geological Association of Canada–Mineralogical Association of Canada, Joint Annual Meeting, Programs with Abstracts, v.11.

Grant 342 Paleomagnetic Analysis of Regional and Contact Strains

C.J. Hale and P. Lloyd

Department of Geology, University of Toronto

ABSTRACT

We have carried out alternating-field demagnetization and thermal demagnetization studies on samples from 11 sites in the Kawashe Lake gabbro and 6 sites in the neighbouring Dobie Lake batholith. Both of these units have ages near 2.74 Ga and both lie in or near the Meen Lake–Dempster Lake (ML–DL) greenstone belt. The Kawashe Lake gabbro yields a characteristic magnetization with a southwesterly, steeply upwards direction that implies a paleopole near 47.2°N, 42.4°W. The Dobie Lake characteristic magnetization is southerly, with a similar steep inclination implying a paleopole at 87.3°N, 52.9°W. The discrepancy between these pole positions apparently results from rotation of the Kawashe Lake gabbro in response to northwesterly transpression between 2.74 and 2.72 Ga. Samples from the Dempster Lake gabbro carry only a modern, viscous magnetization. We have also obtained preliminary paleomagnetic results for the 2.87 Ga North Caribou Lake batholith from the Sachigo Subprovince. This batholith also yields a steep southerly remanence ($D = 216°$, $I = -78°$, $\kappa = 58$, $\alpha_{95} = 16.2°$) implying a paleopole at 66.9°N, 55.8°W (dm = 31.6°, dp = 28.8°). This lone Sachigo Subprovince paleopole lies outside the cluster of Uchi Subprovince poles. Attempts to define an apparent polar wander path (APWP) from posttectonic plutons from the central Uchi Subprovince have met with little success, as samples from these plutons tend to be magnetically unstable.

INTRODUCTION

In 1989 we presented the first paleomagnetic results from the central Uchi Subprovince (Hale and Lloyd 1989). Paleomagnetic studies carried out on the Kawashe Lake gabbro, the Dobie Lake batholith and neighbouring metavolcanic and plutonic rocks enabled us to conclude that much of the deformation in the ML–DL greenstone belt occurred in a narrow time window between 2.74 and 2.72 Ga. We were surprised to discover that none of the Archean paleomagnetic directions determined during these studies could be reconciled with the generally accepted Archean APWP for the Superior craton, track 6 of Irving (1979).

Our attempt to use paleomagnetism to show the timing and sense of rotations in the Archean depends on the comparison of locally obtained directions with a reference APWP. Recent work in the Abitibi greenstone belt (Buchan et al., in press; Amin 1990) and Red Lake (Constanzo-Alverez and Dunlop 1989) and our own work (Hale and Lloyd 1989) have forced us to abandon track 6 and to begin the redefinition of a reference APWP for use in tectonic syntheses.

Gold mineralization has been linked to the tectonic history of the Uchi Subprovince, with prospecting targets provided by both the contact shear zones of late-stage plutons and the regional shear zones resulting from northwesterly directed transpression. It seems likely, therefore, that the re-establishment of a reference Archean APWP and careful interpretation of its tectonic consequences will be of long-term benefit to the exploration sector.

We have begun this process by further sampling of the Kawashe Lake gabbro and the Dobie Lake batholith in an attempt to clarify the chronology of the remanences reported in 1989 and to determine their relationship within the history of regional shear. We have also carried out reconnaissance paleomagnetic studies on a number of dated plutons in the Uchi and Sachigo subprovinces. To date, only the North Caribou Lake batholith has yielded reliable paleomagnetic data.

GEOLOGICAL SETTING

The ML–DL greenstone belt contains several bimodal cycles of mafic to felsic volcanic rocks. These have been multiply intruded by the Dobie Lake batholith ($2.747^{+0.003}_{-0.002}$ Ga), the Kawashe Lake gabbro, the Kawashe Lake stock ($2.720^{+0.006}_{-0.004}$ Ga) and the Graniteboss Lake stock (2.699 ± 0.002 Ga) (T. Corfu, Royal Ontario Museum (ROM), personal communication, 1989).

The northern boundary of the greenstone belt is a zone of intense shearing at the margin of the Dobie Lake batholith. This zone is an extension of the northwesterly trending, transcurrent Bear Head fault. The southern margin of the greenstone belt is also intensely sheared. This system of parallel shear zones bounding comparatively weakly strained rocks suggested a cordilleran collage analogy for the tectonism, and this led us (Hale and Lloyd 1989) to test for block rotations paleomagnetically.

Stable magnetizations were recovered from the Kawashe Lake gabbro, the Dobie Lake batholith and the Graniteboss Lake stock, suggesting that a block containing the Kawashe Lake gabbro underwent a clockwise rotation with respect to the Dobie Lake batholith sometime between 2.74 and 2.72 Ga.

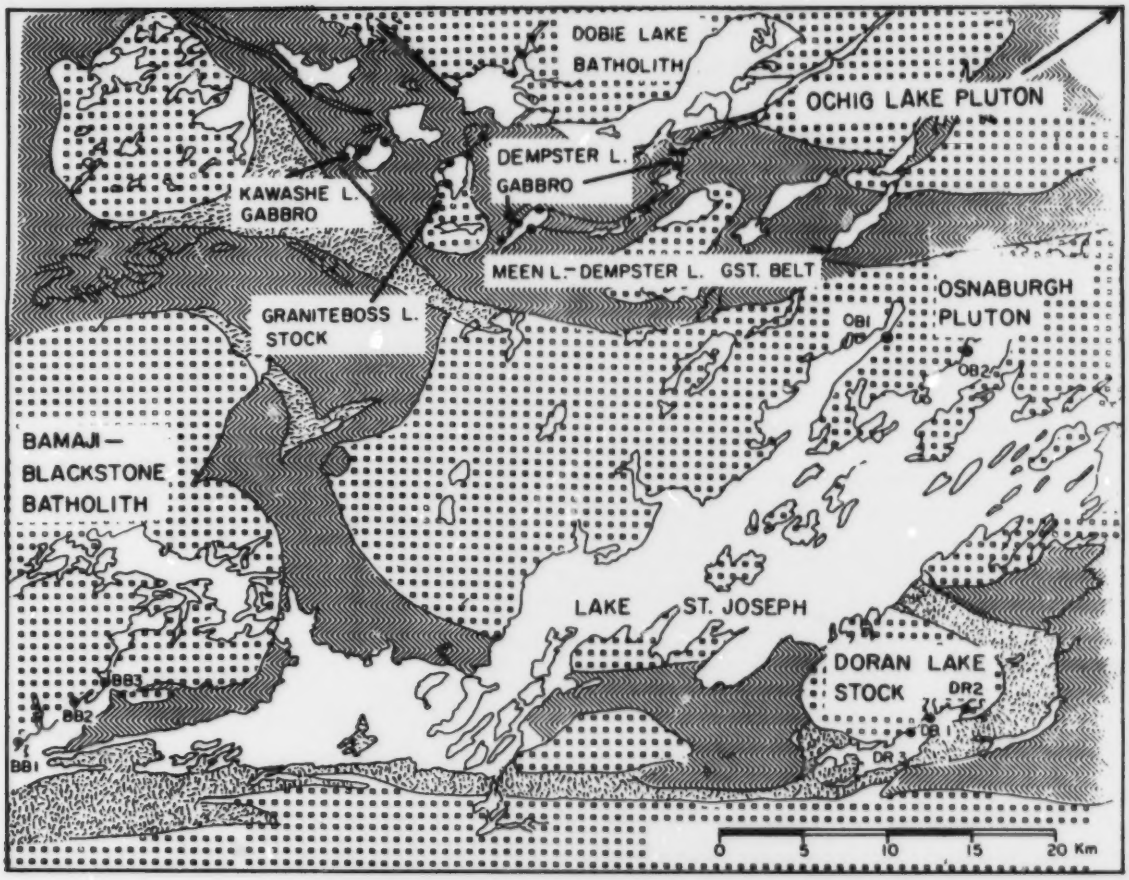

Figure 342.1. Location of sampling sites in the Lake St. Joseph–Dobie Lake region showing the Meen Lake–Dempster Lake greenstone belt and its marginal plutons. The geology is simplified *after* Stott et al. (1987) and Stott and Wilson (1986).

PALEOMAGNETIC SAMPLING

We have carried out additional paleomagnetic sampling in the Kawashe Lake gabbro and the neighbouring Dempster Lake gabbro (Figure 342.1) for two reasons. Firstly, we wanted to augment the collection from the interior of the Kawashe Lake gabbro and from a second gabbroic pluton within the fault-bounded region. This concentration on the gabbro plutons was prompted by the recognition that the magnetization of metabasalts of the ML–JL volcanic cycle is dominated by a viscous overprint. Secondly, we wished to see how the paleomagnetic remanence of the Kawashe Lake gabbro is affected by local shearing in outcrop-scale zones that cut across comparatively massive gabbro. Preliminary measurements (Hale and Lloyd 1989) showed that severe shearing tends to scramble the paleomagnetic remanence in the gabbro. This raises the possibility that comparison of the paleomagnetism in strained and massive parts of an outcrop can provide a relative chronology for the tectonism, setting an upper age limit for the tectonism by reference to an APWP.

In addition, we have collected representative samples for preliminary paleomagnetic assessment of a number of posttectonic plutons. These span a considerable north-south distance centred on the ML–DL greenstone belt. Because of the generally southward younging of tectonism in the Sachigo and Uchi subprovinces (G. Stott, Ontario Geological Survey, personal communication, 1990), this geographic spread provides a range of ages for the posttectonic plutons from >2.8 to <2.7 Ga. To date, the plutons that we have sampled include the North Caribou Lake batholith (2.87 ± 0.003 Ga, D. Davis, ROM, personal communication, 1990), the Dobie Lake batholith ($2.747^{+0.003}_{-0.002}$ Ga, U-Pb zircon, Corfu and Stott 1989), the Kawashe Lake gabbro, the Kawashe Lake stock ($2.720^{+0.005}_{-0.004}$ Ga, U-Pb zircon, Corfu and Stott 1989), the Graniteboss Lake stock (2.699 ± 0.002 Ga, F. Corfu, ROM, personal communication, 1989), the Osnaburgh pluton, the Ochig Lake pluton, the Doran Lake stock and the Bamaji–Blackstone batholith.

At each site, 3 to 5 samples were oriented with magnetic compasses, and at least 2 specimens were cored from each in the laboratory. These were used in thermal and alternating-field demagnetization experiments. Experimental details were the same as those reported by Hale and Lloyd (1989).

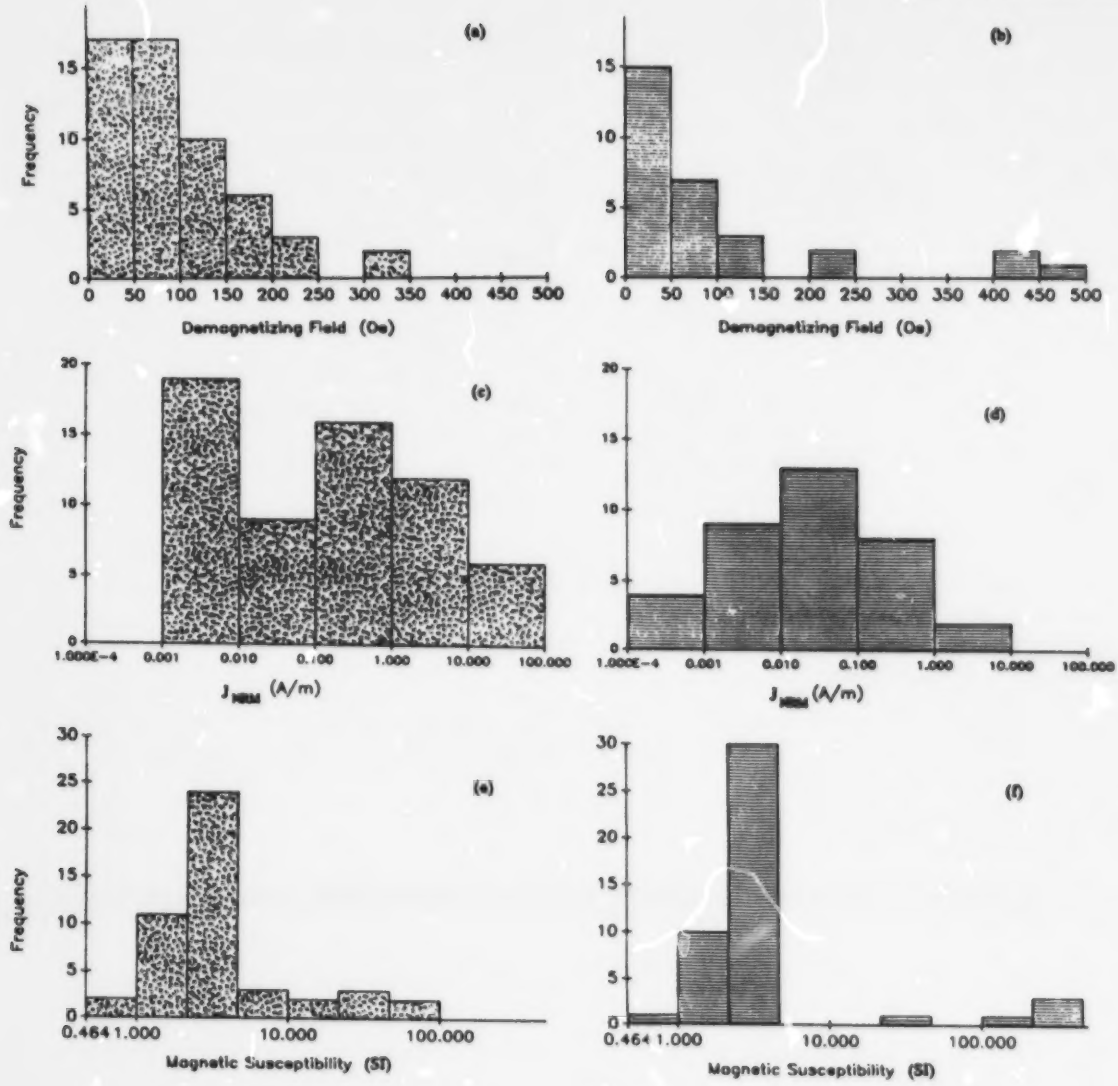

Figure 342.2. Magnetic characteristics of samples collected from the Meen Lake–Dempster Lake greenstone belt: intensity of natural remanent magnetization in **a)** gabbro and **b)** basalt; stability of remanence (J_{NRM}) characterized by the median demagnetizing field in **c)** gabbro and **d)** basalt; and initial magnetic susceptibility of **e)** gabbro and **f)** basalt.

PALEOMAGNETIC RESULTS

Meen Lake–Dempster Lake Greenstone Belt

MAGNETIC CHARACTERISTICS OF THE GABBRO AND METABASALT

Figure 342.2 shows histograms of the intensity of remanence (J_{NRM}), the stability of remanence (as median demagnetizing field (MDF)) and low-field magnetic susceptibility (in SI units) for all samples collected from the ML–DL greenstone belt. The natural remanent magnetization (NRM) intensities span several orders of magnitude in both lithologies, but the peak in the distribution occurs in an intensity range that is about an order of magnitude higher in the gabbro samples than in the metabasalts. The second peak in the intensity histogram for gabbroic samples, lying between 0.001 and 0.01 A/m, reflects the comparatively low intensities recovered from strained gabbro samples.

The remanence-stability histograms indicate a clear distinction between the gabbro and metabasalt samples. Although the gabbro samples tend to be relatively soft, MDFs up to 200 Oe (20 mT) were reasonably common in the collection. The metabasalt samples, on the other hand, typically had MDFs as low as 25 Oe (2.5 mT), and very few of them had MDFs over 100 Oe (10 mT). The comparative

Table 342.1. Site averages of paleomagnetic directions and their implied paleomagnetic poles.

A) Site average directions

Site	Avg value	*D* (°)	*I* (°)	κ	α_{95} (°)
		Kawashe Lake gabbro			
Kg1	5	297.5	-56.3	16.5	19.3
Kg2	4	15.1	-80.2	11.4	28.4
Kg3	4	250.7	-76.6	34.4	15.8
Kg4	3	216.5	-83.2	12.1	37.1
Kg5	5	199.1	-72.2	6.5	32.2
Kg6	5	263.9	-51.6	15.5	20.0
Kg7	4	268.9	-77.3	43.4	18.9
Kg17	5	207.5	-76.0	11.1	23.9
Kg18	–	–	–	–	–
Kg19	4	253.6	-49.9	7.1	36.8
Kg20	–	–	–	–	–
		Dobie Lake batholith			
Db1	–	–	–	–	–
Db2	5	172.8	-63.7	7.4	30.0
Db3	4	194.8	-56.0	15.8	23.7
Db4	3	208.0	-68.1	390.0	6.2
Db5	–	–	–	–	–
Db6	5	176.3	-71.0	21.6	16.8
		North Caribou Lake pluton			
NC508	5	283.0	-86.0	37.0	12.7
NC509	5	226.5	-72.0	25.0	15.7
NC510	5	192.3	-73.0	45.0	11.5
		Dempster/Kawinogan Lake gabbro			
Dl1	3	354.0	38.4	12.7	36.0
Dl2	5	271.8	56.7	1.6	23.3
Dl4	4	295.8	52.7	41.3	14.4
Dg1	3	309.9	73.7	17.7	30.2
Dg3	4	253.5	6.3	5.9	41.0

B) Overall averages and their implied paleomagnetic pole positions

Formation	Avg *D* (°)	Avg *I* (°)	κ	α_{95} (°)	Lat. (°)	Long. (°)	dp (°)	dm (°)
Kawashe Lake gabbro	258.1	-73.4	19.4	11.9	47.2	-42.4	15.7	28.4
Dobie Lake batholith	182.4	-66.4	56.6	12.3	87.3	52.9	24.6	31.4
North Caribou Lake pluton	216.0	-78.0	58.0	16.2	66.9	-55.8	28.8	31.6

Notes: D, declination; I, inclination; κ, Fisher's precision parameter; α_{95}, radius of the 95% circle of confidence; dp and dm, semiangles of the oval of confidence about the pole position.

instability of the metabasalt samples, combined with their tendency to yield paleomagnetic directions lying near the present geomagnetic field at the sampling site, suggests that their magnetization is dominated by a modern, viscous component.

The histograms of magnetic susceptibility show that a wider range of susceptibilities is found for the gabbro samples than for the metabasalts, but both lithologies show a peak in the distribution at values between 2 and 5 SI susceptibility units.

PALEODIRECTIONAL RESULTS

Kawashe Lake Gabbro

Demagnetization characteristics of representative samples from the Kawashe Lake gabbro were presented in the *Geoscience Research Grant Program, Summary of Research 1988–1989* and will not be reproduced here. The addition of new sites 17 to 20 brings the total of sites within the gabbro to 11. Further, the completion of demagnetization experiments on additional specimens from all sites permits us to carry out a three-tier averaging: at sample, site and global levels. A characteristic southwesterly, upwardly inclined magnetization is recovered from all sites within the pluton (Table 342.1; Figure 342.3). This magnetization is directionally distinct from the Dobie Lake batholith characteristic magnetization. We have thus strengthened our earlier conclusion (Hale and Lloyd 1969) that there has been a rotation of the Kawashe Lake gabbro body with respect to the Dobie Lake batholith. The difference in declination between the Dobie Lake batholith magnetization and the Kawashe Lake gabbro magnetization has been reduced by the three-tier averaging to 76°. This discrepancy can be explained by a rotation about a local vertical Euler pole; alternatively, it may result from northwesterly tilting of the Kawashe Lake gabbro by as little as 25° in response to regional transpression, after emplacement of the gabbro but prior to 2.72 Ga (Hale and Lloyd 1989).

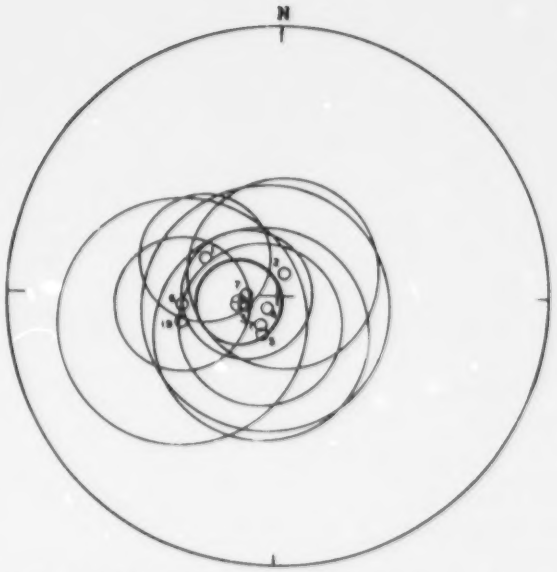

Figure 342.3. Magnetization directions calculated as a three-tier average for sites in the Kawashe Lake gabbro pluton at which the characteristic reversed magnetization was recovered. The open circles indicate a point on the upper hemisphere, and each is surrounded by its α_{95} circle of confidence. The heavier circle indicates the cone of confidence drawn around the global average, indicated by an encircled cross.

It is clear from comparison of the directional statistics given in Table 342.1 that dispersion of the paleomagnetic vectors is greatest at the site level. Site averages have fairly large associated uncertainties, but the average directions group quite well.

At least 2 possibilities exist to explain this dispersion of the magnetizations recorded in a single outcrop. Secular variation of the geomagnetic field during the slow cooling of the pluton and recording of a primary thermal remanence can produce such dispersions, but we favour an alternative explanation based on the modification of primary magnetization during strain.

Four new sites (17 to 20) were collected from outcrops at which there was an obvious strain gradient (sites 17, 20), a well-developed schistosity (site 18) or evidence of carbonate alteration and deformed veining (site 19).

The 11 hand samples collected at site 17 range from essentially unsheared to the highly schistose representatives of a 2.5 m wide zone of sinistral shear trending 250°. The characteristic Kawashe Lake gabbro direction can be isolated in 5 of the comparatively unstrained samples. Sheared samples carry weak ($<10^{-3}$ A/m) magnetizations. Several of these are directionally unstable during demagnetization, whereas the remainder yield apparently stable magnetizations. These show little or no directional agreement between samples. We thus suppose that low levels of strain have contributed to the dispersion of paleomagnetic remanences apparent in averages calculated at the outcrop scale.

Of the 8 samples collected at site 19, only 4 carry stable magnetizations. These can be averaged to give a direction that is shallower than the Kawashe Lake gabbro characteristic magnetization, but the large uncertainty associated with this average renders the distinction of a shallower and possibly younger magnetization moot. The sheared samples from sites 18 and 20 failed to show any directional agreement among the sample magnetizations, and averaging therefore has not been attempted.

In summary, the major result of shear in the Kawashe Lake gabbro appears to be an obliteration of the primary magnetization rather than its replacement by a magnetization dating from the time of the tectonism. A clean slate may thus be left on which to record magnetizations associated with hydrothermal activity. We are currently investigating this possibility using sheared gabbros from the extension of the Bear Head fault that occurs as a mineralized shear zone along the southeastern margin of Hour Lake. This work will combine paleomagnetic, susceptibility anisotropy and petrofabric studies.

Dempster Lake Gabbro

Samples of the Dempster Lake gabbro were collected from 8 sites shown in Figure 342.1, for comparison with the Kawashe Lake gabbro. Six oriented samples were collected at each site, but in all cases some of the samples proved to be directionally unstable. In comparison with the Kawashe Lake gabbro samples, the Dempster Lake gabbro carries magnetizations that are less intense, typically less than 10^{-3} A/m. Median demagnetizing fields range up to 200 Oe (20 mT) in a few samples but are typically 50 Oe (5 mT) or less.

Directional consistency was disappointing in the weakly magnetized Dempster Lake gabbro samples. A few samples from the western end of Dempster Lake carry a magnetization that appears to have been acquired during reheating in the contact aureole of the Graniteboss Lake

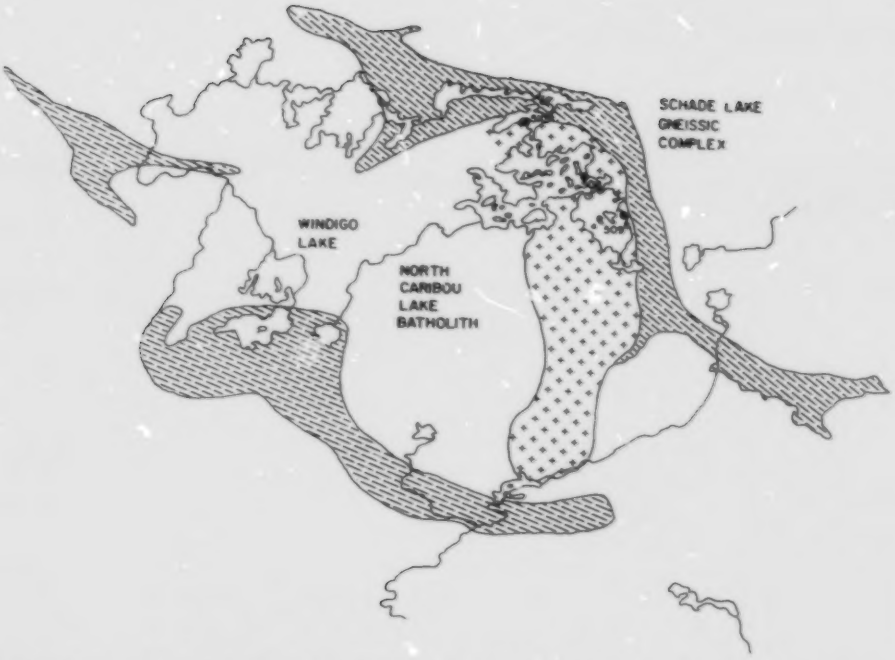

Figure 342.4. Sampling locations in the North Caribou Lake batholith, *after* a sketch provided by G. Stott, Ontario Geological Survey.

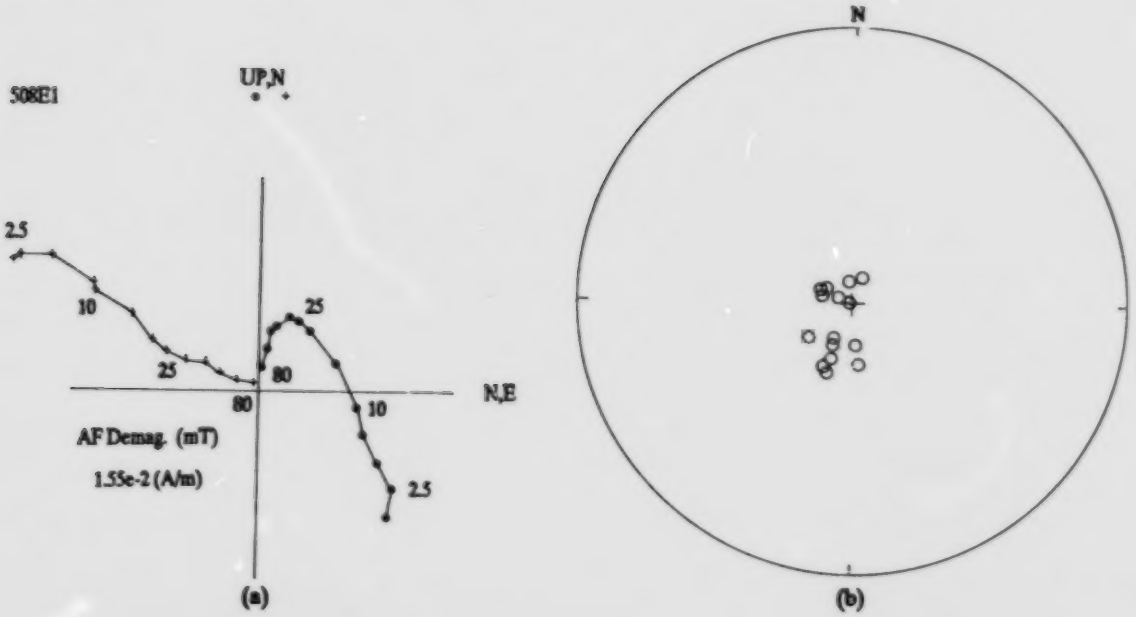

Figure 342.5. a) Orthogonal vector plot indicating the demagnetization characteristics of a typical North Caribou Lake batholith sample. Linear segments on these plots are evidence of high directional stability. b) Sample average directions from the North Caribou Lake batholith show the excellent directional agreement between samples.

stock. Alternatively, this magnetization may be interpreted as having a modern, viscous origin. Directional consistency at other sites is poor, and there is no agreement amongst the site averages. A global average for the Dempster Lake gabbro cannot therefore be calculated with any confidence.

Preliminary Paleomagnetic Data from Granitic Plutons

NORTH CARIBOU LAKE BATHOLITH

The North Caribou Lake batholith outcrops along the northern shore of North Caribou Lake (52.5°N, 91°W). The batholith is composed of a white-weathering, grey tonalite with associated granodiorite. The tonalite ranges from massive to foliated.

A preliminary suite of paleomagnetic samples, consisting of 6 samples from each of three sites, was collected by G. Stott. The sampling locations are shown in Figure 342.4.

All of the samples collected from site 508 show a steeply inclined, upwardly directed magnetization that remains directionally stable during demagnetization or becomes apparent after an oppositely directed, modern, viscous component is removed (e.g., 508E1, Figure 342.5a). The MDFs are very high, typically 600 to 800 Oe (60 to 80 mT). Thermal demagnetization data show high directional stability and blocking temperatures well above 500°C.

Several of the samples collected from site 510 show the same type of nearly ideal paleomagnetic behaviour as those from site 508. Directional consistency is good both within the site and between the 2 sites.

Samples from site 509 tend to be directionally less stable than samples from the other 2 sites. The steep, upwardly directed magnetization was recovered from 2 of the samples, but the demagnetization behaviour of the others tended to be somewhat erratic.

Figure 342.5b shows the sample average directions obtained from North Caribou Lake batholith samples. Each point represents the average of at least 2 specimens from a sample. Averages were not calculated for samples in which the specimen directions differed by 40° or more. Site averages and a global average are given in Table 342.1 and and Figure 342.6. A preliminary paleomagnetic pole for the North Caribou Lake batholith is shown in Figure 342.9.

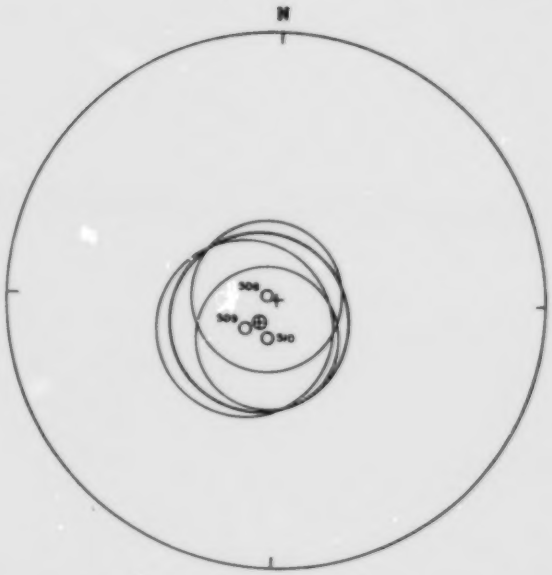

Figure 342.6. Site average directions from the North Caribou Lake batholith calculated as a three-tier average. Open circles indicate points on the upper hemisphere. The global average, characteristic of the North Caribou Lake batholith, is shown by an encircled cross, and its confidence limit is shown by the heavier circle.

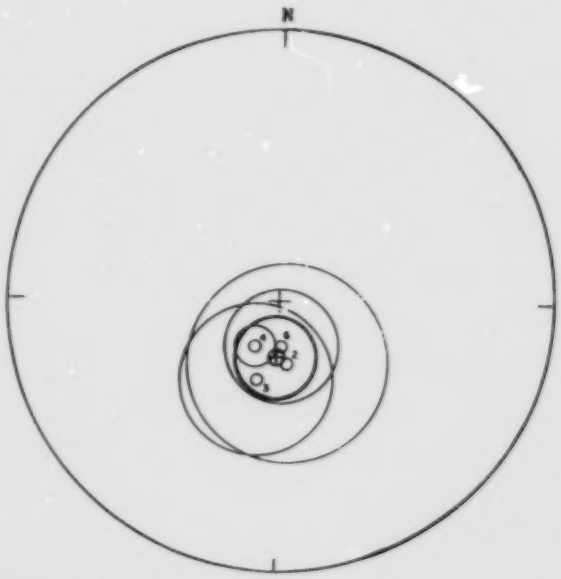

Figure 342.7. Site average directions from Dobie Lake batholith samples calculated as a three-tier average. The characteristic Dobie Lake batholith direction is indicated by an encircled cross, and its confidence interval is shown by the heavier circle.

DOBIE LAKE BATHOLITH

Preliminary paleomagnetic data have been reported for the Dobie Lake batholith (Hale and Lloyd 1989). We have augmented our collection of Dobie Lake samples with 3 new sites, located along and north of Wright Lake. In addition, we have collected samples from the highly deformed margin of the batholith where the extension of the Bear Head fault cuts across Wright Lake.

The southerly, upwardly directed magnetization characteristic of the Dobie Lake batholith is recorded in samples from site DB6 and in a single sample from site DB5. The remainder of site DB5 samples carry a steep, positive magnetization with a northerly to northwesterly declination. This direction is difficult to interpret: it may represent either the antipole of the southerly magnetization or a modern, viscous magnetization.

Samples from the sheared margin of the batholith (DB1) invariably carry steep positive magnetizations with MDFs near 50 Oe (5 Mt), and these are probably viscous overprints. There is no evidence of a component of magnetization that can be related to either the shearing or mineralization in the contact zone.

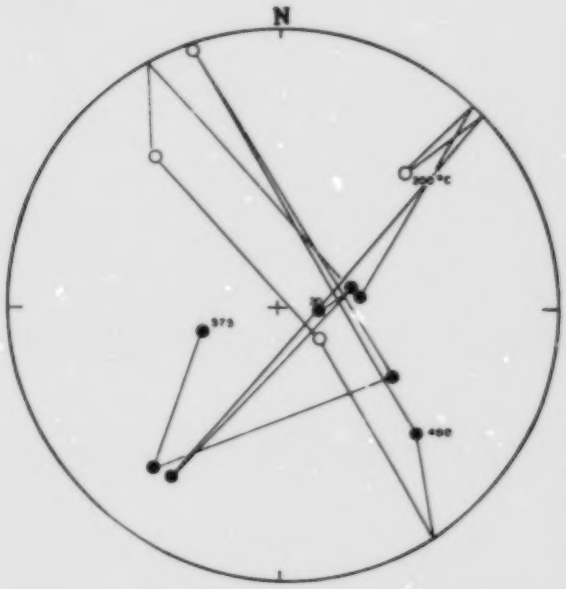

Figure 342.8. The erratic behaviour of Osnaburgh pluton sample OB1A is typical of the disappointing instability of many posttectonic pluton samples in both thermal and alternating-field demagnetization experiments. Paleomagnetically, these plutons provide no useful information.

Figure 342.7 and Table 342.1 present site averages for the Dobie Lake batholith and provide a preliminary paleomagnetic pole position for the batholith based on all of the southerly magnetizations recovered to date.

POSTTECTONIC PLUTONS

Preliminary sampling was carried out in the Ochig Lake pluton, the Osnaburgh pluton, the Doran Lake stock and the Bamaji–Blackstone batholith.

Ochig Lake Pluton

Samples were obtained from 2 sites in the Ochig Lake pluton at the localities along the highway between Central Patricia and New Osnaburgh House. All of the Ochig Lake pluton samples were magnetically weak, with initial intensities of $<10^{-3}$ A/m. In both alternating-field and thermal demagnetization experiments these samples behaved erratically, and no useful paleomagnetic information was recovered.

Osnaburgh Pluton

The Osnaburgh Pluton samples produced no useful paleomagnetic results in either alternating-field or thermal demagnetization experiments. Figure 342.8 shows their typical erratic demagnetization behaviour. Initial intensities were moderately weak (10^{-3} A/m).

Doran Lake Stock

The Doran Lake stock is the only pluton in which reconnaissance sampling suggests that further collection may be warranted. Five samples from site DR1 carry an easterly, positive magnetization with an intermediate inclination. The initial intensity of remanence is moderate (10^{-3} to 10^{-2} A/m).

Site DR2 shows a classic assemblage of very strong, highly stable remanences in unrelated directions, characteristic of lightning contamination. Site 3 only included 2 samples, but both of these carried a northwesterly, positive magnetization with steep inclination, resembling the magnetization of the Graniteboss Lake stock (Hale and Lloyd 1989).

Bamaji–Blackstone Batholith

Eighteen samples were collected from 3 sites in the Bamaji–Blackstone batholith. Although the initial intensities were moderate (10^{-3} to 10^{-2} A/m), all of the samples from this batholith behaved erratically during both alternating-field and thermal demagnetization. No useful data were obtained from the Bamaji–Blackstone batholith.

In summary, reconnaissance sampling of posttectonic plutons has met with little success.

SIGNIFICANCE OF THE NEW PALEOMAGNETIC DATA

Only the North Caribou Lake batholith has yielded data that can be added to our previously determined Dobie Lake batholith and Graniteboss Lake stock poles (Hale and Lloyd 1989) to begin construction of a preliminary Archean APWP for the northwestern Superior craton. These poles are shown in Figure 342.9, along with the recently determined paleomagnetic pole for the Red Lake reversed magnetization of Constanzo-Alverez and Dunlop (1989) and the reordered Matachewan and Otto stock poles of Buchan et al. (in press).

It is premature to construct an APWP from these few data, but we sketch one possible interpretation to emphasize the fact that none of these poles is consistent with the conventional path (Irving 1979).

The Kawashe Lake gabbro pole position lies well away from the rest of the population. We continue to believe that this displacement results from postemplacement rotation of the Kawashe Lake gabbro in response to regional transpression between 2.74 and 2.72 Ga.

We have chosen to include the North Caribou Lake batholith pole with the younger poles to construct a single APWP, but it is far from clear that this is appropriate. The North Caribou Lake batholith paleopole lies well away from the poles from the Uchi Subprovince. Although this discrepancy is not unreasonable in view of the age difference between the North Caribou Lake batholith pole at 2.87 Ga and the next oldest pole, that of the Dobie Lake batholith at 2.74 Ga, it raises the intriguing speculation that there may have been a separation between the Sachigo and Uchi subprovinces in space as well as time. This question can only be resolved by further paleomagnetic studies on younger posttectonic plutons from the Sachigo Subprovince having ages between 2.7 and 2.75 Ga.

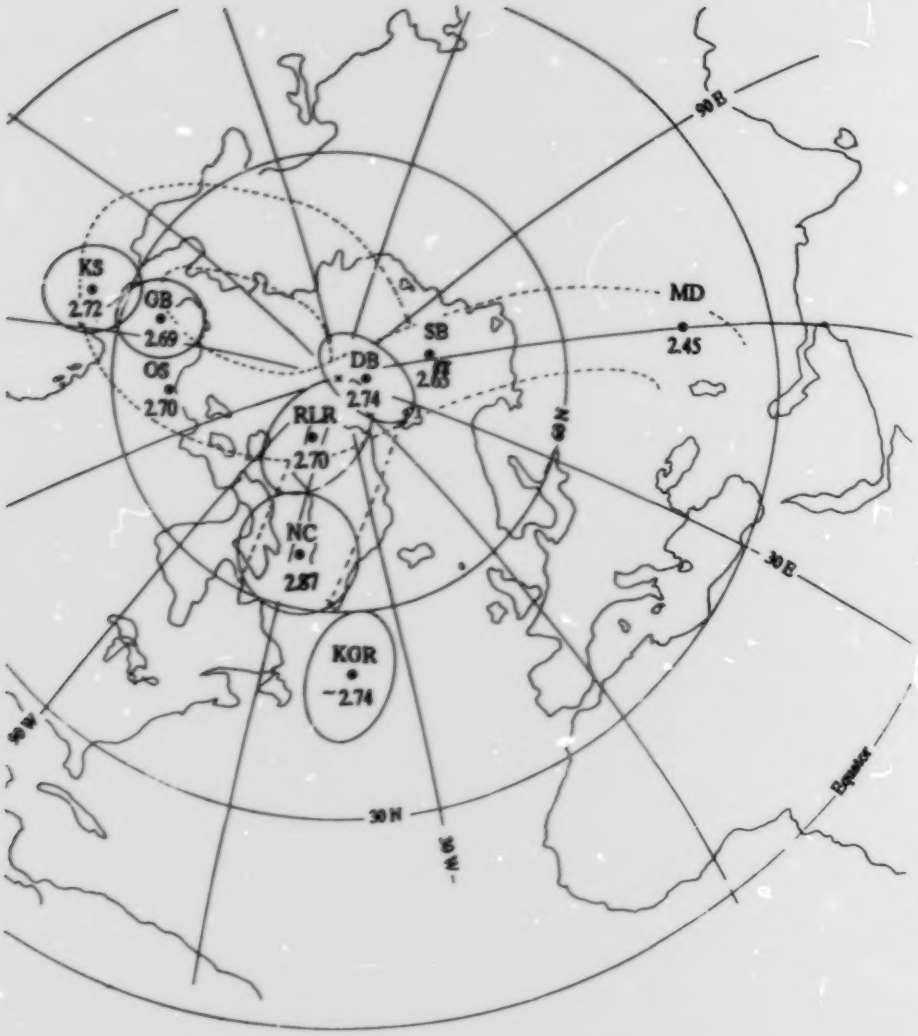

Figure 342.9. Paleomagnetic pole positions obtained from the these and recent studies show that poles between 2.74 and 2.65 Ga in age cluster at high latitudes. The Kawashe Lake gabbro reversed pole (KGR) lies outside this cluster as a result of its local rotation (Hale and Lloyd 1989). One possibility of an APWP has been sketched through the data, but this path is highly tentative. Additional poles RLR (Red Lake reversed, Constanzo-Alverez and Dunlop 1989), SB (Shelley Lake B, Dunlop 1984), OS and MD (Otto stock and Matachewan dikes, Buchan et al., in press) have been included, as these provide a younging direction for the tentative path. DB, Dobie Lake batholith; GB, Graniteboss Lake stock; KS, Kawashe Lake stock; NC, North Caribou Lake batholith.

CONCLUSIONS

1. Additional data from the Kawashe Lake gabbro and the Dobie Lake batholith are consistent with our earlier interpretation of a rotation of the Kawashe Lake block relative to the Dobie Lake batholith after 2.74 Ga but before 2.72 Ga. This rotation may have been a simple northwesterly tilting by about 25°).

2. Preliminary samples from the North Caribou Lake batholith carry a stable magnetization with a steep negative inclination. This appears to be the oldest paleomagnetic pole obtained to date from the Superior Province. It lies outside the main cluster of northwest Superior Province poles.

3. Posttectonic plutons from the Uchi Subprovince are unrewarding subjects for paleomagnetic study.

4. Preliminary reconnaissance studies can eliminate many unfruitful plutons while rapidly assessing potentially significant targets, such as the North Caribou Lake batholith.

5. Only the most tentative of APWPs can now be advanced for the Archean of the northwest Superior Province. More data will be required before constraints can be placed on tectonic reconstructions.

ACKNOWLEDGMENTS

Greg Stott has been a key participant in this project since its inception. In addition to suggesting the field localities he has participated in the collecting, and in the case of the North Caribou Lake batholith he is solely responsible for assembling the preliminary collection.

We thank Don Davis of the Jack Satterly Geochronology Laboratory, Royal Ontario Museum, for permission to use his unpublished date for the North Caribou Lake batholith. As well, we thank Fernando Corfu for the use of his unpublished Graniteboss Lake stock age.

REFERENCES

Amin, M.T. 1990. Paleomagnetic demonstration of block rotations in the Rouyn–Noranda area, Abitibi greenstone belt, Quebec; unpublished MSc thesis, McMaster University, Hamilton, Ontario.

Buchan, K.L., Neilson, D. and Hale, C.J. in press. Relative ages of Otto stock and the Matachewan dykes from paleomagnetism and implications for the Precambrian polar wander path; Canadian Journal of Earth Sciences, v.27.

Constanzo-Alverez, V. and Dunlop, D.J. 1989. Paleomagnetism of Archean formations from the Red Lake greenstone belt, northwestern Ontario—North America's oldest $^{40}Ar/^{39}Ar$-dated paleopoles; poster, American Geophysical Union, Fall Meeting, San Francisco, California.

Corfu, F. and Stott, G.M. 1989. U-Pb geochronology of the central Uchi Subprovince, NW Ontario; Geological Association of Canada, Program with Abstracts, p.A55.

Dunlop, D.J. 1984. Paleomagnetism of Archean rocks from northwestern Ontario: II. Shelley Lake granite, Quetico Subprovince; Canadian Journal of Earth Sciences, v.21, p.869-878.

Hale C.J. and Lloyd, P. 1989. Paleomagnetic analysis of regional and contact strains; *in* Geoscience Research Grant Program, summary of research 1988–1989, Ontario Geological Survey, Miscellaneous Paper 143, p.199-209.

Irving, E. 1979. Paleopoles and paleolatitudes of North America and speculations about displaced terrains; Canadian Journal of Earth Sciences, v.16, p.669-694.

Stott, G.M. and Wilson, A.C. 1986. Precambrian geology of the Muskegsagagen–Bancroft lakes area, District of Kenora (Patricia Portion); Ontario Geological Survey, Geological Series, Preliminary Map P.3049, scale 1:50 000.

Stott, G.M., Kay, S.V. and Sanborn, M.M. 1987. Precambrian geology of the Lake St. Joseph area, districts of Thunder Bay and Kenora (Patricia Portion); Ontario Geological Survey, Geological Series, Preliminary Map P.3051, scale 1:50 000.

Grant 343 Structural Evolution of the Michipicoten (Wawa) Greenstone Belt, Superior Province: Evidence for an Archean Fold and Thrust Belt

Z.G. Arias and H. Helmstaedt

Department of Geological Sciences, Queen's University, Kingston

ABSTRACT

Structural studies in the Archean Michipicoten greenstone belt suggest that the youngest supracrustal rocks formerly interpreted as a thick stratigraphic sequence consisting of 2 volcanic cycles represent a single lithologic package that was highly deformed and thickened by structural repetition.

Field observations show that the sedimentary rocks in the central part of the belt unconformably overlie intermediate to mafic volcanic rocks and represent the youngest rocks in the section. The depositional angular unconformity is structurally overturned up to 45° in the northern part of the area, and the upside-down, volcanic-sedimentary panel appears to represent the inverted limb of a major nappe fold (F_1). Repetition of rock units within this overturned panel can be attributed to structural discontinuities that, on the basis of kinematic analyses in mylonitic zones along the contacts, are interpreted as thrust faults, suggesting that the inverted limb of the early nappe fold has been imbricated by subsequent south-verging thrusting.

To the south, a major thrust fault separates the inverted, southward-younging, imbricated sequence from a geologically similar, inverted, northward-younging sequence of rocks. This configuration suggests the presence of a regional, faulted, inverted syncline (F_2).

On the local scale, in volcanic and sedimentary rocks underlying the central part of the belt, the regional strike of the rock units is approximately parallel to the axial surfaces of prominent F_2 folds. The limbs of these folds are typically sheared off parallel to their axial surfaces and represent folds on the limbs of the regional inverted F_2 folds related to the imbricate thrusts.

Younging reversals along the F_2 axial surfaces (S_2) indicate the presence of earlier folds (F_1), only locally associated with an S_1 cleavage. These folds may represent minor folds in the overturned limb of the recumbent nappe structure.

INTRODUCTION

The ca. 2.7 to 2.9 Ga Michipicoten (Wawa) greenstone belt, located within the Superior Province of the Canadian Shield, extends northeast from Michipicoten Bay in northeastern Lake Superior (Figure 343.1).

As for most greenstone belts in this and other shield areas, lithologic contacts within the belt were traditionally interpreted as primary depositional contacts juxtaposing continuous "cycles" of volcanism and sedimentation (Goodwin 1962; Attoh 1980; Sage et al. 1987). The original "homoclinal layer-cake" sequence was thought to have been folded into broad synclines and anticlines, probably related to diapiric emplacement of the surrounding granitoids (Gledhill 1927; Frohberg 1935; Moore 1931, 1948; Bruce 1940; Goodwin 1962; Sage et al. 1987).

Recent detailed structural studies by McGill and Shrady (1986) in the southwestern part of the belt first led them to the conclusion that no dependable belt-wide stratigraphic correlation was possible because several different lithologic packages, inferred to be bounded by early thrust faults, were mapped within a single belt of clastic sedimentary rocks. They suggested that such a configuration could be the product of tectonic juxtaposition of allochthonous terranes (Shrady 1988; G. McGill, University of Massachusetts, personal communications, 1987, 1989). A second alternative assumed a correlative stratigraphic section across the faults, suggestive of structural juxtaposition by folding and related thrusting (Shrady 1988). The latter interpretation is supported by the regional and local field relationships examined in the central part of the belt (this study, Figure 343.1, area A).

During the 1988 field season, several areas underlain by clastic sedimentary rocks in the central part of the belt were mapped in detail to establish the local structural style and deformation history (Arias and Helmstaedt 1989). During the field season of 1989, the structural interpretations were reaffirmed, and attention was focused on the nature of the lithologic contacts within and between the areas mapped in 1988. It was found that the youngest supracrustal rocks, formerly interpreted as a thick stratigraphic sequence consisting of 2 volcanic cycles (Goodwin 1962; Attoh 1980; Sage et al. 1987), represent a single volcano-sedimentary depositional sequence that was complexly deformed and repeated along imbricate thrust faults (Arias and Helmstaedt 1990). This deformation was imposed upon a belt-scale recumbent nappe structure, the inverted limb of which is exposed at the present level of erosion.

In this paper, the field relationships are described and our interpretation of the early structural evolution of the Michipicoten greenstone belt is presented on a preliminary basis. The proposal, essentially a refinement of the local deformation sequence established from detailed work (McGill and Shrady 1986; Arias and Helmstaedt 1989), defines the regional structural geometry across the breadth of the belt, as illustrated by an *admissible* cross section (Marshak and Woodward 1988).

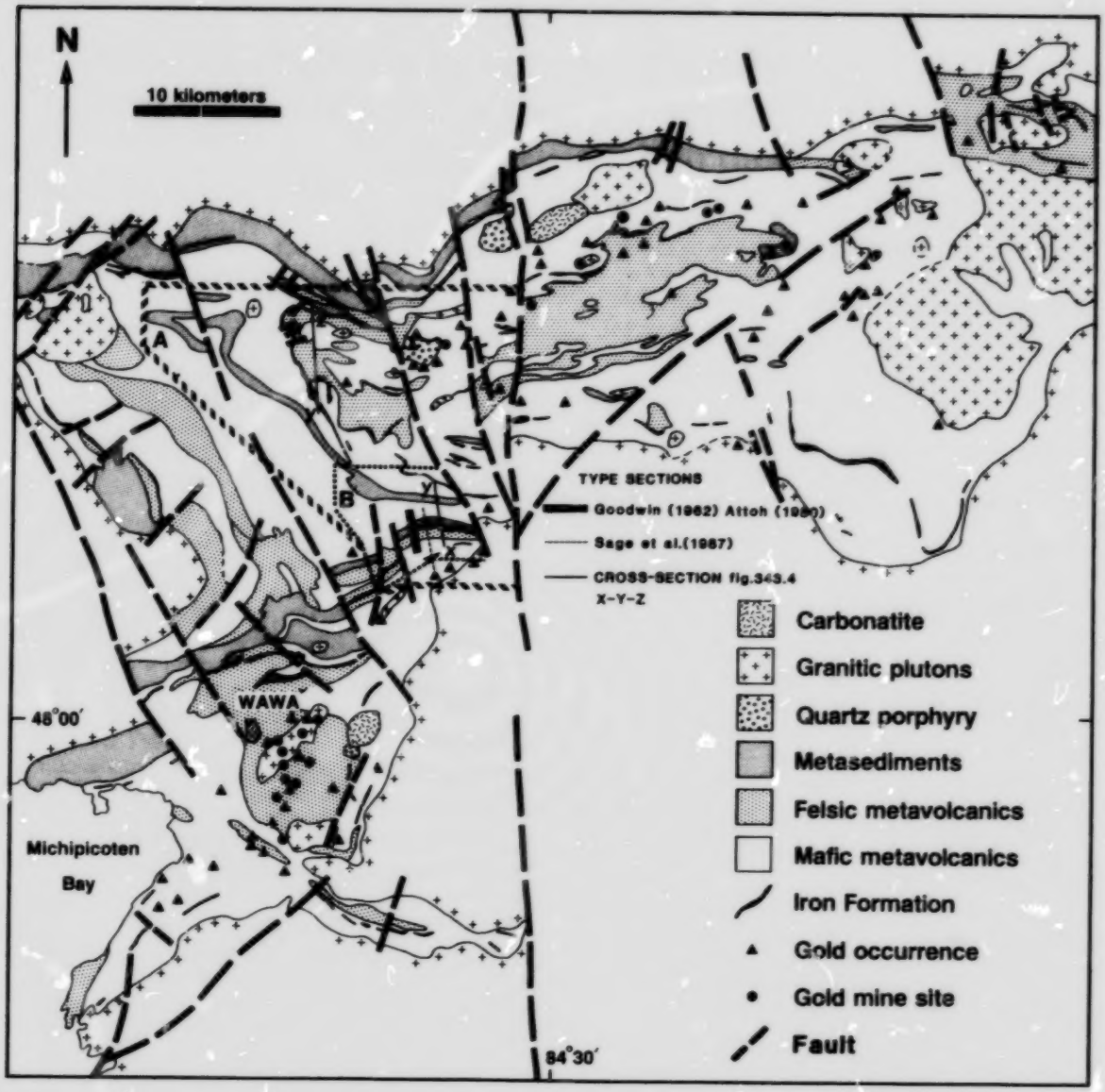

Figure 343.1. General geology of the Michipicoten greenstone belt (compilation *after* Milne et al. 1971). A, Central belt area; B, area of Figure 343.3, showing type sections of Goodwin (1962), Attoh (1980) and Sage et al. (1987) illustrated on Figure 343.2. Sections marked X–Y and Y–Z correspond to the structural cross section on Figure 343.4.

The extensive geologic map base for the Michipicoten greenstone belt (Goodwin 1962; Milne et al. 1971; Sage et al. 1982a–1982e, 1984; Sage 1985, in press) has been a critical part of this attempt to reconstruct the structural development of the belt, providing an opportunity to focus on the deformation sequence of a large area and the nature of various lithologic contacts.

STRATIGRAPHY—MICHIPICOTEN GREENSTONE BELT[1]

As our structural interpretation changes part of the established stratigraphic definitions, a review of previous stratigraphic interpretations for the Michipicoten greenstone belt is necessary.

1 The prefix "meta" has been dropped from all rock names but is implied, as all rocks (diabase excluded) have been metamorphosed.

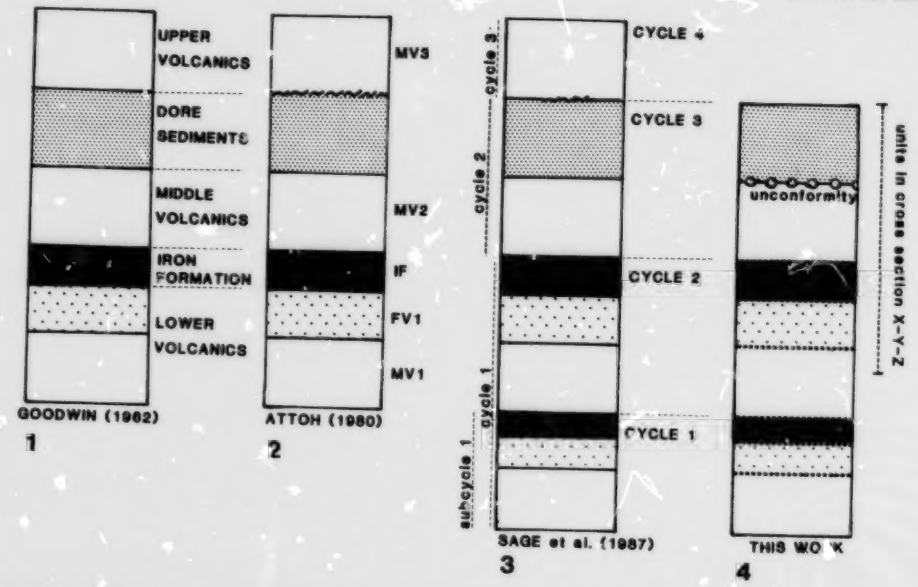

Figure 343.2. Stratigraphic columns for the Michipicoten greenstone belt (columns 1, 2 and 3) and lithologic column (4) used in present study. In this column, Dore sediments are interpreted as representing the youngest rocks, and the mafic volcanic unit above the Dore is a structural repetition of the mafic volcanic unit below the Dore sedimentary rocks. The dashed lines in column 4 indicate that lithologic boundaries of the lower units may not represent conformable contacts. See Figure 343.3 for legend.

Stratigraphic sequences established for the belt by Goodwin (1962), Attoh (1980) and Sage et al. (1987) are illustrated on Figure 343.2. The location of sections by Goodwin (1962) and Sage et al. (1987) was chosen within area B of Figure 343.1 because the complete sections are more easily observed here. This area is also the site of one of Attoh's (1980) type sections.

A cyclic evolution of volcanism within the belt was identified by Goodwin (1962) (column 1, Figure 343.2). The "Lower" volcanic rocks, at the base of his first cycle, comprise intermediate to mafic flows. These are followed by felsic pyroclastic rocks and iron formation, composed of chert with siderite and/or pyrite, pyrrhotite, magnetite and hematite, forming the top of the first cycle. The "Middle" volcanic rocks, forming the second cycle, consist of intermediate to mafic flows and pyroclastic rocks. These grade upward into the Dore clastic sedimentary rocks, composed of greywacke, shale, argillite or conglomerate. The "Upper" volcanic rocks also consist of intermediate to mafic flows and tuffs, with minor felsic pyroclastic rocks, and were thought to represent the youngest supracrustal rocks in the belt.

Column 2 on Figure 343.2 is one of the type sections by Attoh (1980), who attempted a stratigraphic correlation of several sections throughout the Michipicoten (Wawa) greenstone belt. This stratigraphic column essentially corresponds to that of Goodwin (1962), with the exception of a structural break between the youngest mafic volcanic unit (MV3) and the underlying sedimentary unit that was inferred on the basis of truncation of bedding in the mafic volcanic unit (MV3) of supposed younger age. Not shown on the section, the sedimentary rocks along the northern margin of the belt (Figure 343.1) were considered as the oldest, basal rocks in the sequence, and the felsic volcanic rocks at the western margin of the belt, northwest of Wawa, were interpreted as the youngest in the belt (Attoh 1980).

On the basis of geological mapping (Sage et al. 1982a–1982e, 1984; Sage 1985, in press), U-Pb zircon geochronology of felsic igneous rocks (Turek et al. 1982, 1984; Sullivan et al. 1985; Frarey and Krogh 1986) and whole-rock geochemical analyses (*see* Sage et al. 1987), Sage (1986) reaffirmed the existence of the 3 volcanic cycles documented by Goodwin (1962) and Attoh (1980) (Figure 343.2). As shown in column 3, these were originally referred to as "cycle 1" (ca. 2750 Ma), "cycle 2" (ca. 2700 Ma) and "cycle 3" (age unknown), until an older cycle at ca. 2900 Ma (Turek et al. 1988) was discovered and referred to as "subcycle 1" (Sage et al. 1987). The cycle nomenclature was subsequently revised for clarity: cycle 1 is now ca. 2900 Ma; cycle 2 is now ca. 2750 Ma; cycle 3 is now ca. 2700 Ma; and cycle 4 is of unknown age (R.P. Sage, Ontario Geological Survey, oral communication, 1987).

The base of the section established by Sage et al. (1987), defined as cycle 1 (column 3, Figure 343.2), consists of massive and pillowed basaltic to peridotitic komatiite, overlain by minor rhyolite and dacite flows and pyroclastics of calc-alkalic affinity and iron formation. The felsic rocks of cycle 1 yielded a maximum age of 2889 ± 9 Ma (Turek et al. 1988). Cycle 2 is similar to the first cycle, except that the basal mafic volcanic rocks are tholeiitic and the overlying intermediate to felsic volcanic rocks yielded a maximum age of 2749 ± 2 Ma (Turek et al. 1982). Cycle 3 consists of massive and pillowed tholeiitic basalts overlain by the Dore clastic sedimentary rocks, which were thought to be correlative with felsic volcanic rocks 10 km north of Wawa that yielded a minimum age of 2696 ± 2 Ma (Turek et al. 1982). Cycle 4 was considered an incomplete cycle

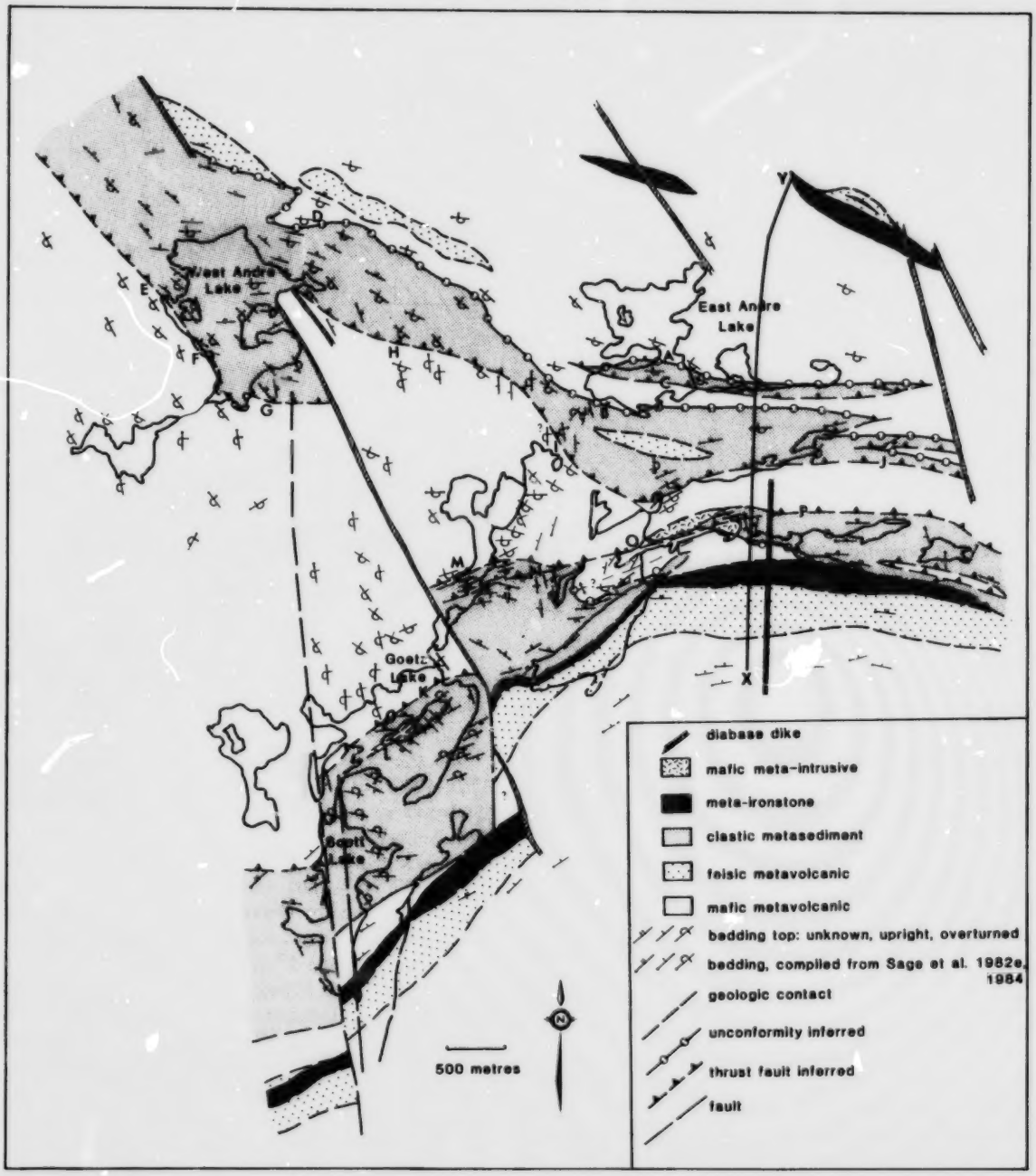

Figure 343.3. Structural interpretation and distribution of stratigraphic younging within the southern part of the Central belt area (Figure 343.1, area B). Field relationships at localities A to P are described in the text. Section X–Y corresponds to the southern part of the structural cross section on Figure 343.4. Shaded bar beside X–Y shows the location of the stratigraphic sections of Goodwin (1962), Attoh (1980) and Sage et al. (1987). Distribution of rock types *after* Sage et al. (1982b, 1982e, 1984).

that consists of massive and pillowed mafic volcanic rocks, thought to be the youngest Archean supracrustal rocks in the belt.

In all stratigraphic sections, the Dore clastic sedimentary rocks were postulated as older than the overlying mafic volcanic "cycle". Our detailed work in the southern part of the central belt area (Figure 343.1, area B, and Figure 343.3) has shown both depositional and structural juxtapositions, as well as tectonic repetition, of the mafic volcanic and sedimentary units in the upper part of the "succession". The field relationships presented below imply that the clastic sedimentary rocks are the youngest in the section (column 4, Figure 343.2) and that the "Middle" and "Upper" volcanic rocks of Goodwin (1962), the MV2 and MV3 of Attoh (1980) and cycles 3 and 4 of Sage et al. (1987) are tectonic repetitions of the same unit. Below this

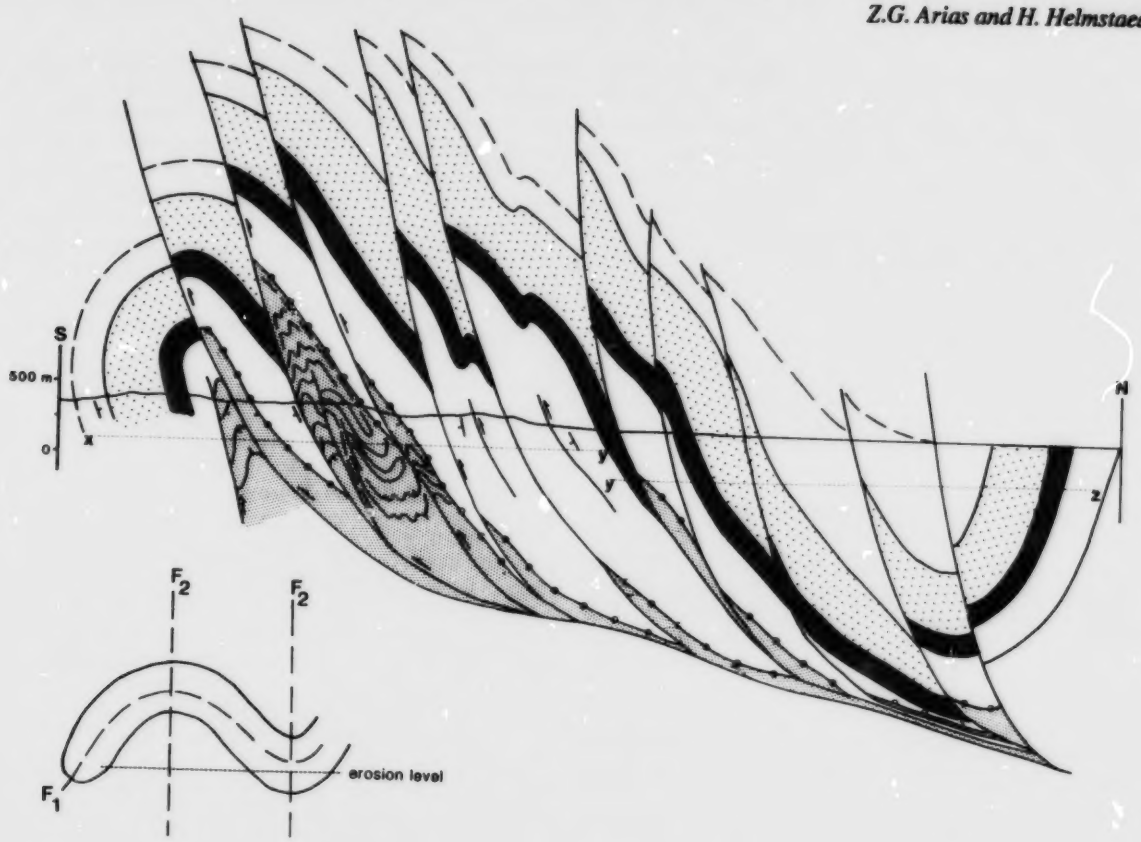

Figure 343.4. Composite structural section through the central part of the Michipicoten greenstone belt (section X–Y–Z on Figure 343.1). Section X–Y is an admissible section based on the present work. Section Y–Z is a schematic section based on compilation (Goodwin 1963; Sage 1985). *See* Figure 343.3 for legend. The sketch (lower left) explains the present configuration of the belt as a regional nappe fold (F_1) refolded about F_2. Imbricate thrusts are considered related to F_2.

mafic volcanic unit, the section shown on Figure 343.2 (column 4) is not intended to imply the presence of a continuous conformable succession. The rock units are considered mappable packages, but the nature of the lithologic contacts between them has not been ascertained. No cyclic, genetic relationship should be assumed between the mafic and felsic volcanic rocks within the lower "cycles" of Sage et al. (1987), especially as only felsic volcanic and subvolcanic intrusive rocks have been dated. The regional map pattern (Figures 343.1 and 343.3) and present structural interpretation (Figure 343.4) suggest that the package as a whole was folded into a very large recumbent structure and subsequently refolded and displaced along imbricate thrusts.

FIELD RELATIONSHIPS

The local structural geometry and the deformation sequence within clastic sedimentary rocks in the vicinity of Scott, Goetz and West Andre lakes (Figure 343.3) were presented by Arias and Helmstaedt (1989). The regional strike of the rock units in the area is approximately parallel to the axial surfaces of prominent F_2 folds. Limbs and sections of fold closures are commonly sheared off subparallel to their axial surfaces. Younging reversals of beds along the F_2 axial surfaces (S_2) prove the presence of earlier folds (F_1), locally associated with an S_1 cleavage. A structural discontinuity parallel to S_2 (i.e., the trend of the rock units) separates overturned beds with opposed younging directions over a strike of 500 m, suggesting the presence of a faulted, upside-down fold, indicative of pre-F_2 overturning. A northeast-striking crenulation cleavage (S_3) overprints the early structures but does not regionally alter the dominant D_2 map pattern.

Our recent field work shows that the deformation history recognized in the clastic sedimentary rocks in the central part of the belt corresponds to that in the felsic and mafic volcanic rocks with the exception that the earliest cleavage and fold set (F_1) preserved in the sedimentary rocks are not recognized in the volcanic rocks. The structural style differs in that cleavages (S_2), axial planar to well-preserved F_2 folds in sedimentary rocks, are only related to minor crenulation folds within felsic volcanic rocks and only the cleavage is usually preserved in the mafic volcanic rocks.

From the detailed work conducted in the Goetz Lake–Scott Lake area and the West Andre Lake area (Arias and Helmstaedt 1989), it was suspected that a deciphering of the structural relationship between these areas could lead to a better understanding of the regional geometry of the belt. Toward this end, it was necessary to establish the relative age of the mafic volcanic unit that separates the 2 areas underlain by clastic sedimentary rocks.

The stratigraphic sections of Goodwin (1962) and Attoh (1980) and the section above cycle 1 of Sage et al. (1987) are marked on Figure 343.3 as a single section line. Goodwin (1962) and Attoh (1980) interpreted the presence of a major syncline within the mafic volcanic unit (top of the section) that separates the sedimentary rocks along Goetz Lake and West Andre Lake, further supporting their interpretation that these mafic volcanic rocks are younger than the enclosing clastic sedimentary rocks. However, no younging reversal was observed within the mafic volcanic unit to support the synclinal geometry.

The locations at which critical geological relationships have been observed are labelled A to P on Figure 343.3.

Locality A

The northern mafic volcanic-sedimentary contact at East Andre Lake represents a north-dipping angular unconformity that is structurally overturned up to 45° and is locally tectonically modified. Southwest-younging pillow forms with brecciated cores grade southward into forms with fissures and interstices infilled with fine-grained sedimentary rock. Just west of locality A, the contact is marked by a conglomerate unit comprising subangular mafic volcanic clasts in a silty matrix and grading into folded turbidites. Near the contact, flame structures and graded bedding indicate younging to the south; hence, the section is overturned. These observations show that the sedimentary rocks unconformably overlie the mafic volcanic rocks.

Locally, strong deformation and alteration within pillowed mafic volcanic rocks are coincident with the contact zone, as shown by highly stretched pillows along strike from locality A. East of locality A, the volcaniclastic conglomerate exhibits deformed clasts stretched parallel to the contact. Steep elongation of clasts and a well-developed, north-dipping tectonic planar fabric, with a possible north-side up, reverse sense of displacement on planar shear fabrics, are observed in the vertical cross section. The contact west of locality A is marked by a linear topographic depression, or a thin, iron-rich gossan zone where exposed.

Locality B

The volcanic-sedimentary contact south of locality A (at locality B) is also marked by a volcaniclastic conglomerate unit. Similarities to features observed at the locality A contact support a similar interpretation for this contact. However, the rock units are more strongly deformed.

The tectonically modified, depositional unconformities at localities A and B are interpreted as faulted versions of the same contact. Repetition of the mafic volcanic-sedimentary package at localities A and B may be accommodated along a north-dipping fault (locality C). Deformation associated with minor thrusting may be responsible for modification of the depositional contacts, particularly at locality B.

Locality D

The unconformity interpreted at locality B was identified along strike in the West Andre Lake area at locality D. A gossan zone marks the geologic contact, similar to that at locality A. Weakly to moderately deformed, overturned pillows young southwestward, toward a coarse polymictic pebble conglomerate unit composed of subrounded clasts of felsic and mafic volcanic composition and, rarely, black chert and vein quartz. The conglomerate grades southward into coarse psammites with distinctive sericitized pelitic interbeds. These appear to grade into finer turbidites. Planar fabric elements are moderately developed, and pillows and clasts are steeply elongated. The various sedimentary packages may represent a primary normal gradation, probably modified by minor tectonic imbrication. Outcrop-scale contraction faults are commonly observed in psammites and finer turbidites.

Localities E to J

The mafic volcanic rocks south of the contact at localities E through J have previously been interpreted as the youngest rocks in the area (Attoh 1980; Sage et al. 1984, 1987). Mafic pillowed flows everywhere young away from the sedimentary rocks and are overturned. The nature of the mafic volcanic-sedimentary contact is difficult to identify at any single locality. However, field evidence, described below, shows that it is a structural, rather than a stratigraphic, contact.

The contact at locality E is marked by a linear topographic depression, coincident with the southwest shoreline of West Andre Lake. To the east, sedimentary rocks between localities E and F are highly deformed turbidites. Granule to pebble conglomerate consists of volcanic, chert and mudstone clasts. Observed rootless, tight folds with limbs or noses sheared off subparallel to their northwest-striking axial surfaces (subparallel to the geologic contact) are typical of rocks that outcrop elsewhere in the West Andre Lake area. Within mafic volcanic rocks to the west, intensity of deformation and of iron-carbonate alteration increases toward the contact. At locality F, conglomeratic rocks near the contact are strongly sheared and mylonitized, and clasts are steeply extended down the shallow northeastward dip of the tectonic planar fabric. A few metres away from the contact to the northeast, coarse conglomeratic, psammitic and pelitic units are relatively undeformed. The conglomerate unit consists of rounded pebbles and cobbles of various mafic volcanic, felsic volcanic, chert, vein quartz and wacke compositions. Erosional surfaces and truncation of bedding indicate younging toward the northeast, opposite to the southwest younging of pillows. The strong deformation, steep tectonic lineation and younging reversal across the contact at locality F suggest structural rather than depositional juxtaposition of the volcanic and sedimentary units.

At locality G (southeast West Andre Lake), the contact is also coincident with a narrow topographic depression. Pillowed mafic volcanics are sheared, and folded bedding in the turbidite unit is discordant to the contact. Although these features appear to be consistent with an older age for the sedimentary rocks, mapping by Sage et al. (1984) at locality H clearly shows that pillows are also truncated at the mapped geologic contact. This is inconsistent with a southward-younging depositional contact and suggests the presence of a fault.

North of locality I, along strike of the same contact, bedding within sedimentary rocks is practically perpendicular to the strike of the geologic contact. As the contact is approached, bedding is parallel to it, and younging appears to be to the southwest, i.e., overturned. A similar geometry exists within mafic pillowed volcanics. The contact is marked by a narrow, linear depression along which iron-rich mudstone is intensely deformed. Pillows are steeply elongated and may be truncated at the contact.

Based on these observations, the contact at localities E through J may represent a dip-slip fault similar to that inferred at locality C. Such an interpretation requires that the mafic volcanic rocks south of the contact be equivalent to, and a faulted version of, the mafic volcanic rocks north of the sedimentary unit at West and East Andre lakes. This further implies that the volcanic rocks are older than the enclosing sedimentary rocks. If the dominant structural regime involves imbricate stacking of the overturned limb of a nappe, such contractional structures (thrust faults) offer a reinterpretation of the mapped interdigitation between mafic volcanic and sedimentary rocks north of locality J.

Localities K to P

High-angle truncation of bedding in both mafic volcanic and sedimentary rocks at locality K along Goetz Lake is indicative of a fault, dipping moderately to the northwest. Reworked volcanic clasts in a conglomerate unit truncated at the contact show a steeply plunging elongation. The volcaniclastic conglomerate is strongly sheared parallel to the contact and is cut by rare pseudotachylite. Shear fabrics suggest reverse, northwest-side up displacement. All observed features support the interpretation of a thrust fault along this contact, also observed on the northeast shore of Goetz Lake.

A northwest-dipping, highly deformed sliver of mafic volcanic rock has been structurally juxtaposed against a polymictic pebble conglomerate and psammite with shallow south- and southeast-dipping bedding near locality L, at Goetz Lake. Clasts consist of felsic and mafic volcanic rocks, chert and quartz porphyry.

Along the same contact, offset along a late northwest-striking fault zone, at locality M, an otherwise relatively undeformed polymictic pebble to cobble conglomerate with psammite interbeds is highly sheared. Pillowed volcanic rocks at the contact are overturned, younging toward the sedimentary rocks in the south and dipping toward the northwest. These observations suggest that older mafic volcanic rocks were unconformably overlain by conglomerate and finer grained turbidites, and evidence of the unconformity has largely been obliterated by the major thrust postulated for this contact at Goetz Lake. All previous workers have considered the 2 major sedimentary packages that outcrop at West Andre Lake and at Goetz Lake as the same unit. As mafic volcanic rocks at locality M are older than the sedimentary rocks, it follows that the same volcanic unit at localities E through J is also older than the sedimentary unit to the north, consistent with a thrust along this contact.

Field work during 1988 resulted in the recognition of a lineament at locality N, across which overturned beds exhibit opposed younging directions and dips. This lineament is on strike with the Magpie River fault (localities O and P) recognized by Sage et al. (1984), which dominantly separates northward-younging sedimentary rocks from overturned, southward-younging volcanic and sedimentary rocks. The iron-carbonatized fault zone was interpreted as being dominantly strike slip (Sage et al. 1984); however, the steeply plunging striations on the northwest-dipping mylonitic fabric indicating a reverse sense of displacement (observed at locality O) strongly suggest the presence of a thrust fault. This thrust separates the inverted, southward-younging, imbricated sequence in the north from a similar, inverted, northward-younging sequence in the south. The configuration suggests the presence of a regional, faulted, upside-down syncline (section X–Y, Figures 343.3 and 343.4).

STRUCTURAL CROSS SECTION

The fieldrelationships described above have been incorporated in a structural section across the central part of the Michipicoten greenstone belt (Figures 343.1 and 343.4). The southern part of the section (X–Y, Figures 343.1 and 343.3) is an admissible section based on the present work. The northern part (Y–Z, Figure 343.1) is a schematic section based on the regional map pattern (Goodwin 1963; Sage 1985). The units in the section are shown in column 4, Figure 343.2.

The following major features of the structural cross section illustrate the overall geometry of the belt:

1. The entire section is upside down and represents the overturned limb of a belt-scale recumbent nappe fold (F_1).
2. The inverted limb of the nappe fold has been refolded and imbricated by subsequent south-verging thrusts (F_2); the geometry of the southern part of the section (X–Y) is that of a thrust-faulted inverted syncline (F_2); and the geometry of the northern part of the section (Y–Z) is that of an inverted anticline (F_2) (see Figure 343.1 for map view).
3. The thrust imbrication was responsible for repetition of lithologic units, suggesting that rocks formerly interpreted as a thick stratigraphic sequence of volcanic cycles 3 and 4 (Sage et al. 1987) represent a single, structurally repeated sequence.

REFERENCES

Arias, Z.G. and Helmstaedt, H. 1989. Structural evolution of central and east-central Michipicoten (Wawa) greenstone belt, Superior Province; *in* Summary of research 1988–1989 by the Ontario Geological Survey, Ontario Geological Survey, Miscellaneous Paper 143, p.210-226.

———1990. Early thrust faults in the Archean Michipicoten greenstone belt, Superior Province, central Ontario; Geological Association of Canada–Mineralogical Association of Canada, Joint Annual Meeting, Program with Abstracts; v.15, p.4.

Attoh, K. 1980. Stratigraphic relations of the volcanic-sedimentary successions in the Wawa greenstone belt, Ontario; *in* Current research, pt.A, Geological Survey of Canada, Paper 80-1A, p.101-106.

Bruce, E.L. 1940. Geology of the Goudreau–Lochalsh area; Ontario Department of Mines, Annual Report, v.49, pt.3, p.1–50.

Frarey, M.J. and Krough, T.E. 1986. U-Pb zircon ages of late internal plutons of the Abitibi and eastern Wawa subprovinces, Ontario and Quebec; *in* Current research, pt.A, Geological Survey of Canada, Paper 86-1A, p.43-48.

Frohberg, M.H. 1935. The gold deposits of the Michipicoten area; Ontario Department of Mines, Annual Report, v.44, pt.8, p.39-83.

Gledhill, T.L. 1927. Michipicoten gold area, District of Algoma; Ontario Department of Mines, Annual Report, v.36, pt.2, p.1-49.

Goodwin, A.M. 1962. Structure, stratigraphy and origin of iron formations, Michipicoten area, Algoma District, Ontario, Canada; Geological Association of America Bulletin, v.73, p.561-586.

———1963. Michipicoten area compilation sheet; Ontario Department of Mines, Geological Series, Preliminary Map P.184, scale 1:126 720.

Marshak, S. and Woodward, N. 1988. Introduction to cross-section balancing; *in* Basic methods of structural geology, by S. Marshak and G. Mitra, Prentice-Hall, Inc., Engelwood Cliffs, New Jersey.

McGill, G.E. and Shrady, C.H. 1986. Evidence for a complex Archean deformational history; southwestern Michipicoten greenstone belt, Ontario; Journal of Geophysical Research, v.91, no.B13, p.E281-E289.

Milne, V.G., Giblin, P.E., Bennett, G., Thurston, P.C., Wolfe, W.J., Giguere, J.F., Leahy, E.J. and Rupert, R.J. 1971. Manitouwadge–Wawa sheet, Ontario Department of Mines, Geological Compilation Series, Map 2220, scale 1:253 440.

Moore, E.S. 1931. Goudreau and Michipicoten gold areas, District of Algoma; Ontario Department of Mines, Annual Report, v.40, pt.4, p.1-54.

———1948. Structure of the Michipicoten–Goudreau area; p.414-419 *in* Structural geology of Canadian ore deposits, Geology Division, Canadian Institute of Mining and Metallurgy, 948p.

Sage, R.P. 1985. Precambrian geology of Leclaire Township, District of Algoma; Ontario Geological Survey, Geological Series, Preliminary Map P.2636, scale 1:15 840.

———1986. Stratigraphic correlation in the Wawa area; *in* Volcanology and mineral deposits, edited by J. Wood and H. Wallace, Ontario Geological Survey, Miscellaneous Paper 129, p. 62-68.

———in press. Precambrian geology of Lalibert Township, District of Algoma; Ontario Geological Survey, Geological Series, Preliminary Map, scale 1:15 840.

Sage, R.P., Rebic, Z., Abercrombie, S., Neale, K., MacMillan, D., England, D. and Calvert, T. 1982a. Precambrian geology of Chabanel Township, District of Algoma; Ontario Geological Survey, Geological Series, Preliminary Map P.2439, scale 1:15 840.

Sage, R.P., Rebic, Z., Abercrombie, S., Neale, K., MacMillan, D. and Calvert, T. 1982b. Precambrian geology of Esquega Township, Wawa area, District of Algoma; Ontario Geological Survey, Geological Series, Preliminary Map P.2440, scale 1:15 840.

Sage, R.P., Sawitsky, E., Turner, J., Leeselleuer, P. and Sagle, E. 1982c. Precambrian geology of McMurray Township, Wawa area, District of Algoma; Ontario Geological Survey, Geological Series, Preliminary Map P.2441, scale 1:15 840.

———1982d. Precambrian geology of Lastheels Township, Wawa area, District of Algoma; Ontario Geological Survey, Geological Series, Preliminary Map P.2442, scale 1:15 840.

Sage, R.P., England, D., Calvert, T., Oudkerk, G., Worona, R. and Kosciusko, K. 1982e. Precambrian geology of Musquash Township, District of Algoma; Ontario Geological Survey, Geological Series, Preliminary Map P.2569, scale 1:15 840.

Sage, R.P., Calvert, T., Epstein, R., England, D., Kosciusko, K., Worona, R., Oudkerk, J., Inasi, J., Lockwood, M. and Thomas, D. 1984. Precambrian geology of Corbiere Township, District of Algoma; Ontario Geological Survey, Geological Series, Preliminary Map P.2607, scale 1:15 840.

Sage, R.P., Thorpe, R. and Berdusco, E. 1987. Field trip guidebook—geology and stratigraphy of the Michipicoten iron formation; Institute on Lake Superior Geology, 33rd Annual Meeting, Wawa, Ontario, May, v.33, pt.3, 93 p.

Shrady, C.H. 1988. Structural interpretation of the Michipicoten greenstone belt, Ontario; Geological Association of Canada–Mineralogical Association of Canada, Joint Annual Meeting, Program with Abstracts, v.13, p.112.

Sullivan, R.W., Sage, R.P. and Card, K.D. 1985. U-Pb zircon age of the Jubilee stock in the Michipicoten greenstone belt near Wawa, Ontario; *in* Current research, pt.B, Geological Survey of Canada, Paper 85-1B, p.361-365.

Turek, A., Smith, P.E. and Van Schmus, W.R. 1982. Rb-Sr and U-Pb ages of volcanism and granite emplacement in the Michipicoten belt—Wawa, Ontario; Canadian Journal of Earth Sciences, v.19, p.1608–1626.

———1984. U-Pb zircon ages and the evolution of the Michipicoten plutonic-volcanic terrane of the Superior Province, Ontario; Canadian Journal of Earth Sciences, v.21, p.457-464.

Turek, A., Van Schmus, W.R. and Sage, R.P. 1988. Extended volcanism in the Michipicoten greenstone belt, Wawa, Ontario; Geological Association of Canada–Mineralogical Association of Canada, Joint Annual Meeting, Program with Abstracts, v.13, p.127.

Grant 353 Diagenetic History of Dolomitized Ordovician and Devonian Oil and Gas Reservoirs in Southwestern Ontario. Part A: Styles of Reservoir Development in the Middle Devonian of Southwestern Ontario

G.D. Hamilton and M. Coniglio

Department of Earth Sciences, University of Waterloo, Waterloo

ABSTRACT

Recent investigation of the Middle Devonian Lucas and Dundee formations has shown that the oil reservoirs present in this interval can be classified into 5 major types: 1) dolomitized siliciclastic-rich limestones, 2) fractured limestones with dissolution and microporosity, 3) microcrystalline dolostones, 4) fractured limestones and 5) calcareous sandstones. This classification scheme is based on both the stratigraphic position of each of the reservoirs (Lucas Formation or Dundee Formation) and petrophysical properties that make them distinct. In a given area, more than one type of reservoir may be present. Reservoirs types 1, 2 and 4 are exclusive to the Dundee Formation, whereas types 3 and 5 are found in the Lucas Formation. The styles of reservoir development in the Middle Devonian of southwestern Ontario reflect control by a unique set of diagenetic, tectonic and sedimentologic factors. Understanding these controls is necessary for establishing an effective exploration strategy specific to the various reservoir types present.

INTRODUCTION

The Middle Devonian Lucas and Dundee formations of southwestern Ontario have produced significant quantities of oil over the past 132 years since oil was first discovered in Petrolia in 1858. Early exploration efforts were directed to the drilling of hydrocarbon seeps and large, structurally closed highs. In more recent times exploration success has been very poor, and clearly a much better understanding of the Middle Devonian sedimentology and diagenesis is required to improve upon this lack of success.

The Middle Devonian Lucas and Dundee formations of southwestern Ontario play host to a number of significant hydrocarbon reservoirs. These reservoirs can be classified into 5 major types. The purpose of this report is to examine a selection of oil fields that typify each of the major styles of reservoir development. This study is based on core and geophysical records. Cores were studied by examination of petrographic thin sections via transmitted light and cathodoluminescence microscopy and scanning electron microscopy (SEM).

MIDDLE DEVONIAN STRATIGRAPHY

The Middle Devonian strata of southwestern Ontario have been divided in ascending order into the Bois Blanc Formation, Detroit River Group, Dundee Formation and Hamilton Group (Figure 353A.1). The Bois Blanc Formation has been correlated into Michigan but is not recognized in Ohio and New York. The Detroit River Group overlies the Bois Blanc Formation and has been subdivided into the Sylvania Sandstone, Amherstburg Formation and Lucas Formation. The Sylvania Sandstone is absent in the subsurface of most of southwestern Ontario, but where present it is found underlying the Amherstburg Formation. The Amherstburg Formation is conformably overlain by the Lucas Formation. Regionally, the Detroit River Group is recognized in Michigan and Indiana and is correlatable with the Columbus Formation of Ohio and in part with the Onondaga Formation of New York. The Detroit River Group is unconformably overlain by the Dundee Formation. The Dundee of Ontario and Michigan has been correlated with the Delaware Formation of Ohio and the Onondaga Formation of western New York. The Dundee is unconformably overlain by the Hamilton Group, which is correlatable with the Traverse Group in Michigan and the Marcellus Formation of western New York.

GEOLOGICAL SETTING

During the Middle Devonian in southwestern Ontario, shallow-marine seas onlapped the Algonquin Arch from the southeast in the Appalachian Basin and from the northwest in the Michigan Basin. During much of Detroit River time, the Algonquin Arch was periodically exposed and both basins were partially separated, with some communication interpreted as existing in the Chatham Sag area. Sea level was relatively stable throughout this time interval, with minor transgressive and regressive phases recorded in the Lucas Formation.

In southwestern Ontario, mixed carbonates and siliciclastics of the Lucas Formation were deposited in a variety of subtidal to supratidal settings. In the cores examined, the upper Lucas is composed of 3 or more shallowing-upward cycles. Three dominant facies are present: 1) stromatoporoid-rich floatstones to local

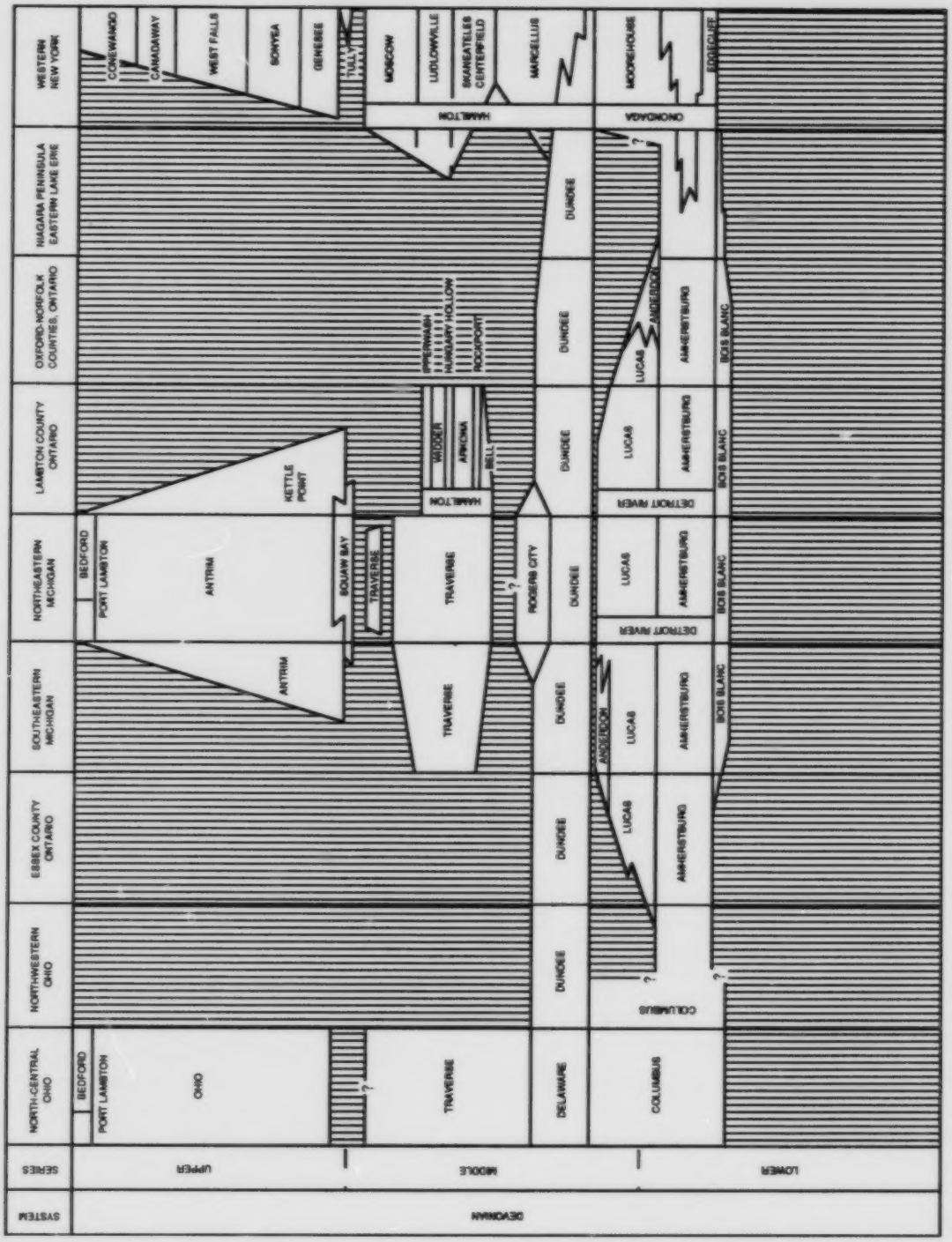

Figure 353A.1. Stratigraphic correlation of the Devonian sequence in southwestern Ontario and adjacent areas (*modified after* Uyeno et al. 1982).

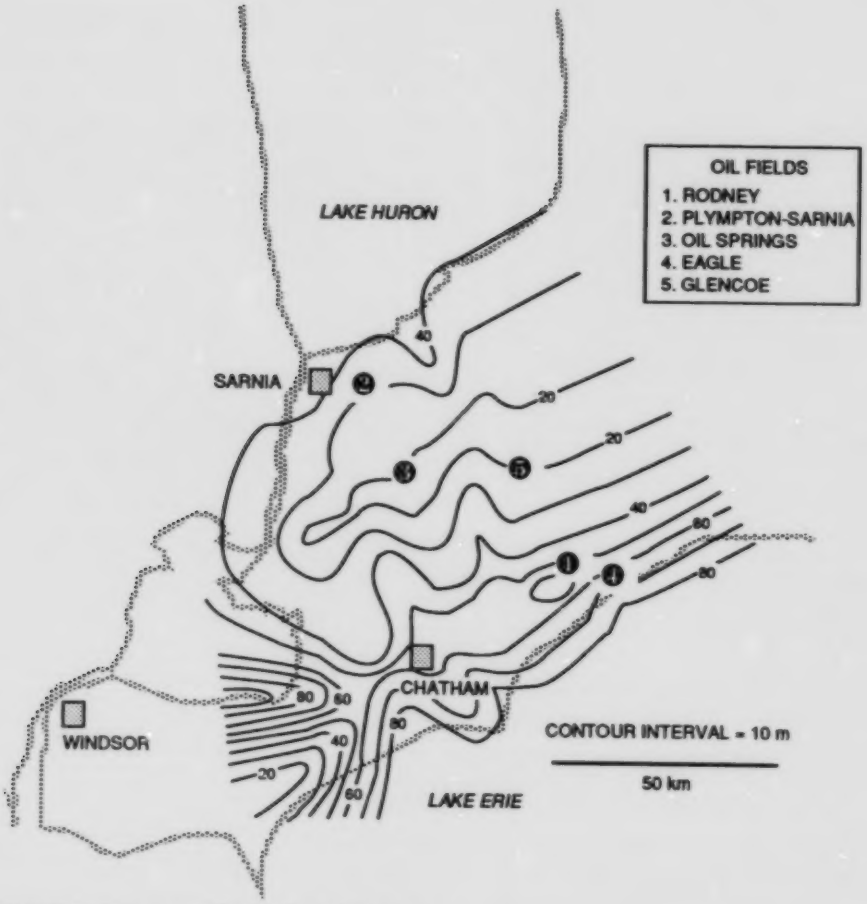

Figure 353A.2. Oil field location map and Dundee Formation isopach.

boundstones; 2) peloidal grainstones to sandy dolostones; and 3) stromatolitic lime mudstones locally containing pebble-chip breccia, mud cracks, fenestral pores and gypsum casts. This third facies usually caps the shallowing-upward cycles, which, however, are typically incomplete. Thick beds of microcrystalline dolostone are locally siliciclastic sand-rich and form one of the major reservoir types in the Lucas Formation.

The contact between the Lucas and Dundee formations is erosional. Clasts of Lucas Formation are commonly present in basal Dundee strata. The Dundee Formation in the Michigan Basin consists of 3 facies: 1) a lowermost bryozoan-rich, locally siliciclastic-rich, bioclastic packstone containing grainstone lenses; 2) an overlying section of interbedded lime mudstones and wackestones with thin packstone lenses; and 3) an uppermost rugose coral and crinoid-rich, bioclastic packstone with grainstone lenses. This vertical sequence is interpreted as representing a transgressive stacking of 3 environments: a shallow, subtidal, partially sheltered lagoon (lower Dundee); a slightly deeper water subtidal shelf (middle Dundee); and a shelf-marginal setting (upper Dundee). This primary subdivision of the Dundee Formation is supported by Ferrigno's (1971) interpretation based on conodonts in the Dundee section exposed at St. Marys, Ontario.

The Dundee Formation of the Appalachian Basin is largely a monotonous package of chert-rich, often shaly, lime mudstones and crinoidal wackestones. Higher energy packstones and grainstones in the basal section occur on the immediate southern flank of the Algonquin Arch. This lowermost Dundee interval may contain a siliciclastic-rich, dolomitized unit that forms an economically important reservoir (Rodney field).

The Dundee Formation is overlain unconformably by bioclast-rich shales of the Hamilton Group. The contact is sharp and erosive, proximal to the Algonquin Arch, and gradational in more basinal areas. The Hamilton Group represents a major episode of deposition of terrigenous clastics, shed from the Appalachians following the Acadian Orogeny.

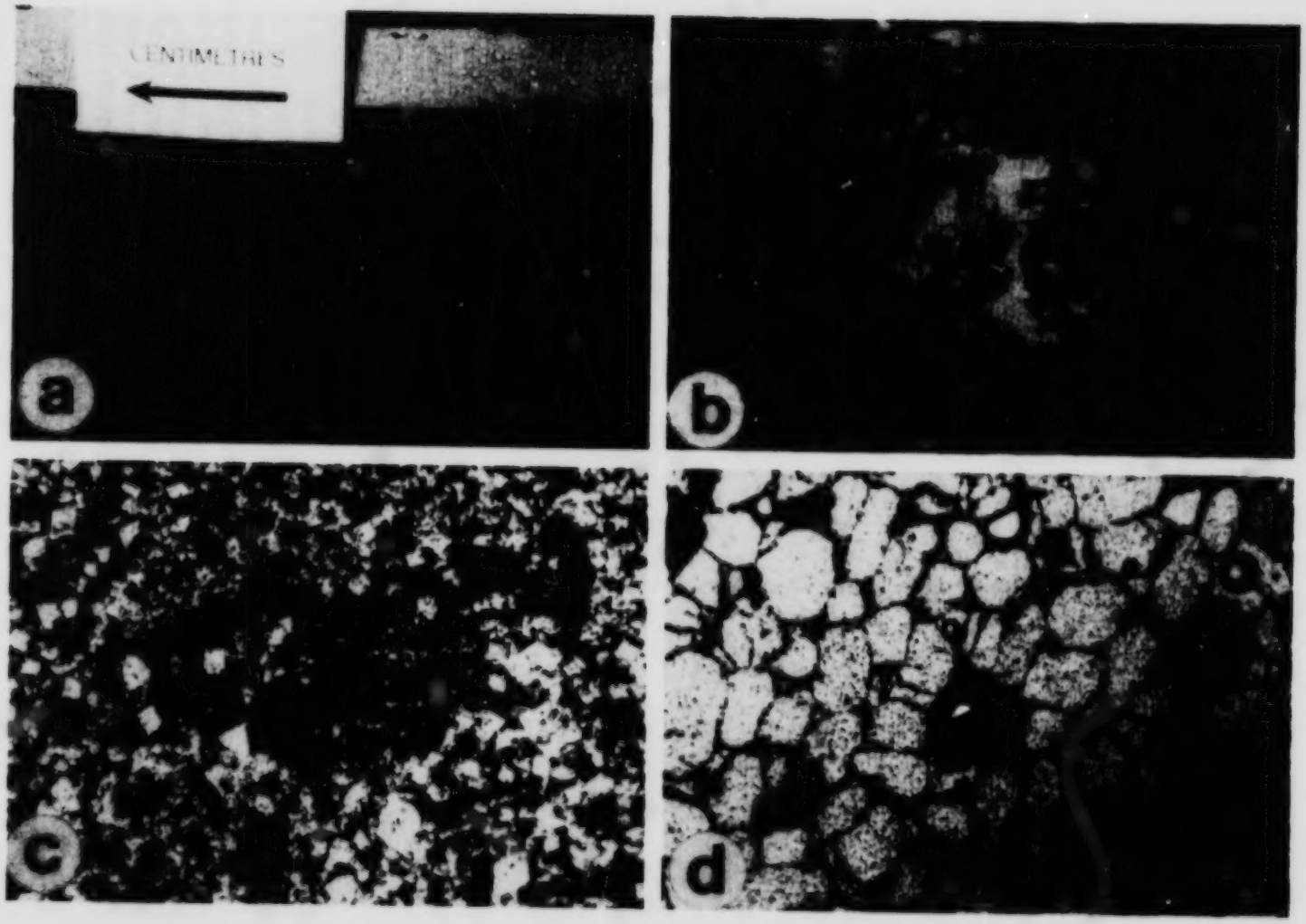

Photo 353A.1. Rodney field. **a)** Cored section of siliciclastic-rich dolostones. Core analysis indicates 26% porosity and 1300 mD permeability. **b)** Thin-section photomicrograph of dolostones. Note scattered fine- to medium-grained, rounded quartz grains and abundant intercrystalline porosity. Scale bar is 150 μm. **c)** Thin-section photomicrograph of dolostone showing partially dolomitized crinoid fragment in a matrix of finely crystalline dolomite. Scale bar is 150 μm. **d)** Thin-section photomicrograph of a siliciclastic-rich sample. Quartz grains are well rounded, well sorted and fine grained. Minor primary intergranular porosity is preserved. Scale bar is 150 μm.

TECTONIC SETTING

Southwestern Ontario has been subjected to multiple phases of faulting throughout much of its geological history (Sanford et al. 1985). Deep-seated faults have been reactivated from Cambrian through to Late Devonian times. These faults provided conduits for diagenetic fluids that were responsible for the dissolution of thick sequences of Silurian evaporites and in particular the Salina B, D, F and G salts. The source of the corrosive fluids remains unclear. Salt dissolution caused extensive reactivation of the Devonian section and resulted in the formation of large-scale anticlinal structures and faulting along the salt-dissolution margins. Faults provided pathways for the migration of hydrocarbons and corrosive fluids, which caused partial later dissolution of the Dundee section.

Evaporite dissolution may have taken place in many stages, resulting in multiple phases of post–Dundee fracturing. Dutton (1985) speculated that salt-dissolution-generated structures may have been present as paleohighs during deposition of the Middle Devonian sediments and locally influenced carbonate and siliciclastic accumulation. To a lesser extent, drape over underlying Silurian pinnacle reefs affected reservoir development by providing small structural traps.

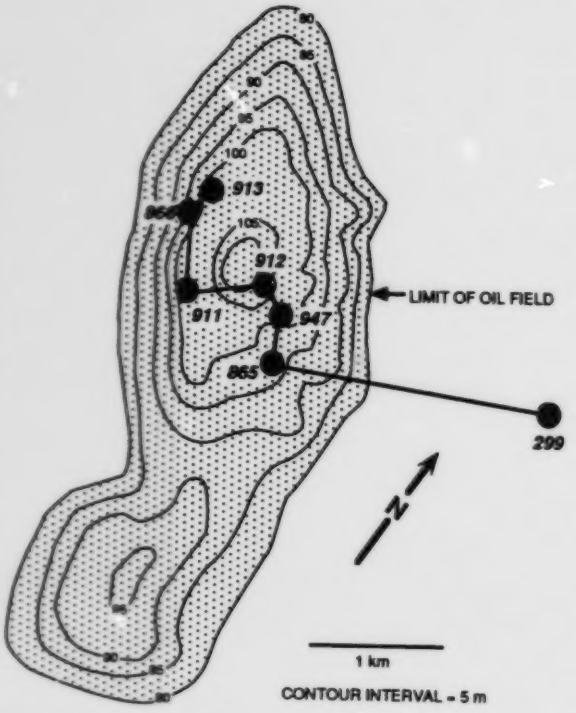

Figure 353A.3. Structural top of the lower Dundee reservoir in the Rodney field (*modified after* Bailey and Cochrane 1985).

STYLES OF RESERVOIR DEVELOPMENT

Type 1. Dolomitized Siliciclastic-rich Limestones

CASE STUDY: RODNEY FIELD, ALDBOROUGH TOWNSHIP, ELGIN COUNTY

Introduction

The Rodney field is located in the southwest portion of Aldborough Township and came into production in 1949 (Figure 353A.2). Initial production was in the range of 2 to 70 barrels (1 US barrel = 0.158 987 3 m^3) of oil per day (Sanford 1955). To date the cumulative production is in excess of 8.65 million barrels (Bailey and Cochrane 1985), and the field is presently undergoing secondary waterflood recovery. The 1988 production was approximately 114 000 barrels.

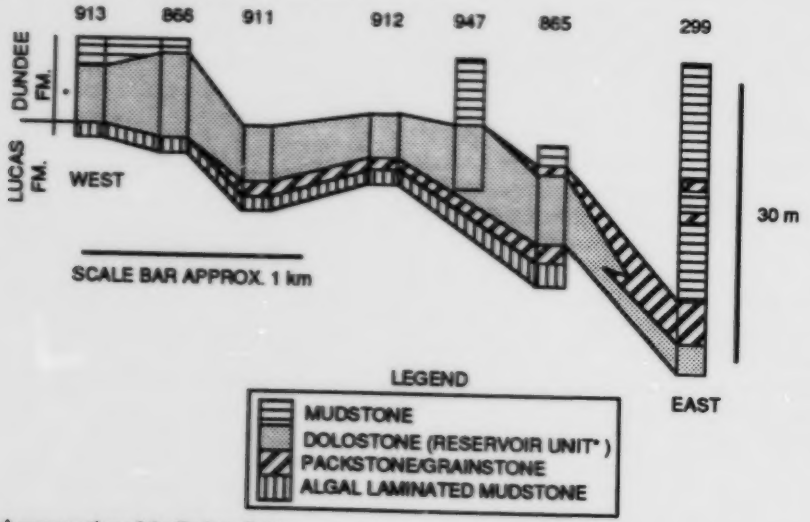

Figure 353A.4. Structural cross section of the Rodney field.

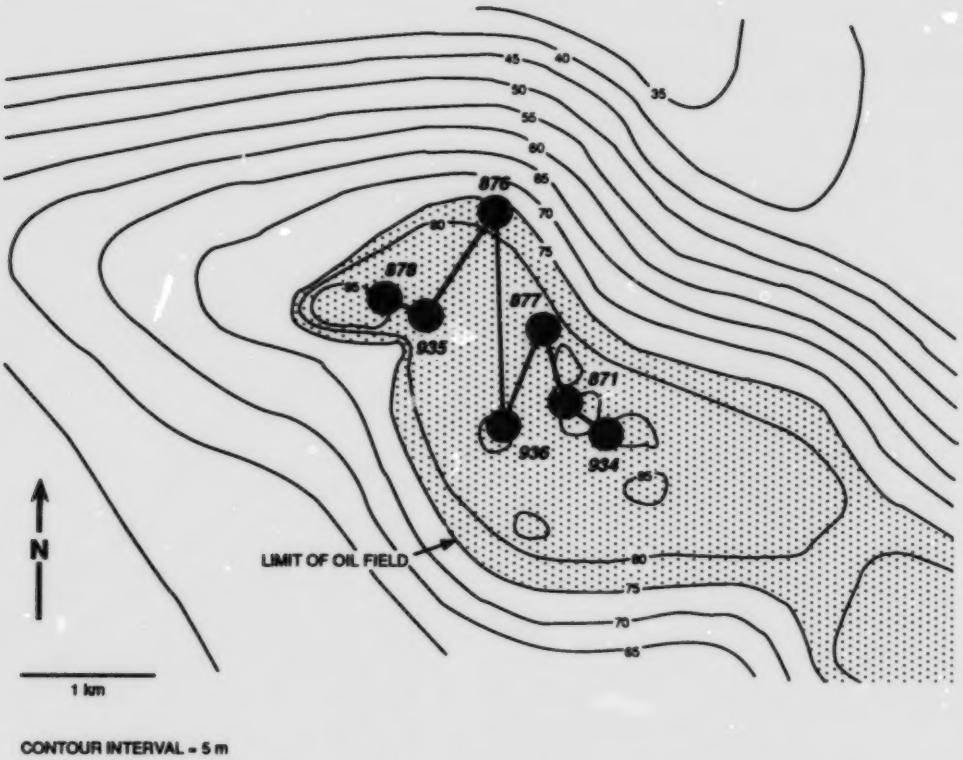

Figure 353A.5. Structural top of the Dundee Formation in the Plympton–Sarnia field (*modified after* Bailey and Cochrane 1985).

Core analyses indicate that reservoir porosity is commonly in the range of 10 to 27% and that permeability may exceed 1300 mD (1 darcy = 0.986 923 3 μm^2). Porosity is dominantly intercrystalline (Photos 353A.1a and 353A.1b), with minor amounts of vuggy and primary intergranular pores. Net pay values range from 3 to 10 m.

Sedimentology

The reservoir is developed near the base of the Dundee Formation in dolomitized siliciclastic-rich limestones and is overlain by nodular bioclastic mudstones and underlain by skeletal packstones and grainstones. The unit is apparently massively bedded, with local development of pure quartz sandstone lenses 5 to 10 cm in size. Bioclastic debris is dominated by crinoid fragments and has lesser amounts of rugose corals, bryozoans and brachiopods.

Examination of the 7 available cores in the field indicates the reservoir is extremely variable in lithology. Dolomite occurs as finely crystalline, zoned rhombs and may constitute from 0 to 100% of the reservoir (Photo 353A.1b). Partially dolomitized crinoid debris is present in varying amounts up to 30% of the rock (Photo 353A.1c). Quartz sand content ranges from 0 to >70% of the reservoir rock. The quartz sands are fine to medium grained and well rounded, tend to have a bimodal size distribution and display pitting suggestive of an eolian influence (Photo 353A.1d; *see also* Dutton 1985).

A structural cross section through the Rodney field demonstrates that the reservoir unit thickens over a structural high that dominates the area (Figures 353A.3 and 353A.4). The field is flanked by anomalously thick Dundee sediments, which may represent increased sedimentation in pre–Dundee salt-dissolution-generated lows.

This sequence was deposited in a shallow-water subtidal environment on the southern flank of the Algonquin Arch during the initial stages of a widespread transgression of the Middle Devonian seas.

Diagenesis

With burial and compaction much of the original primary porosity was lost, but there was some preservation in the more quartz sand-rich layers. Dolomitization appears to have occurred preferentially in proximity to the sandy beds and is not always pervasive. The incomplete nature of the dolomitization may reflect a short-lived diagenetic fluid source. Saddle dolomite is present in very minor amounts

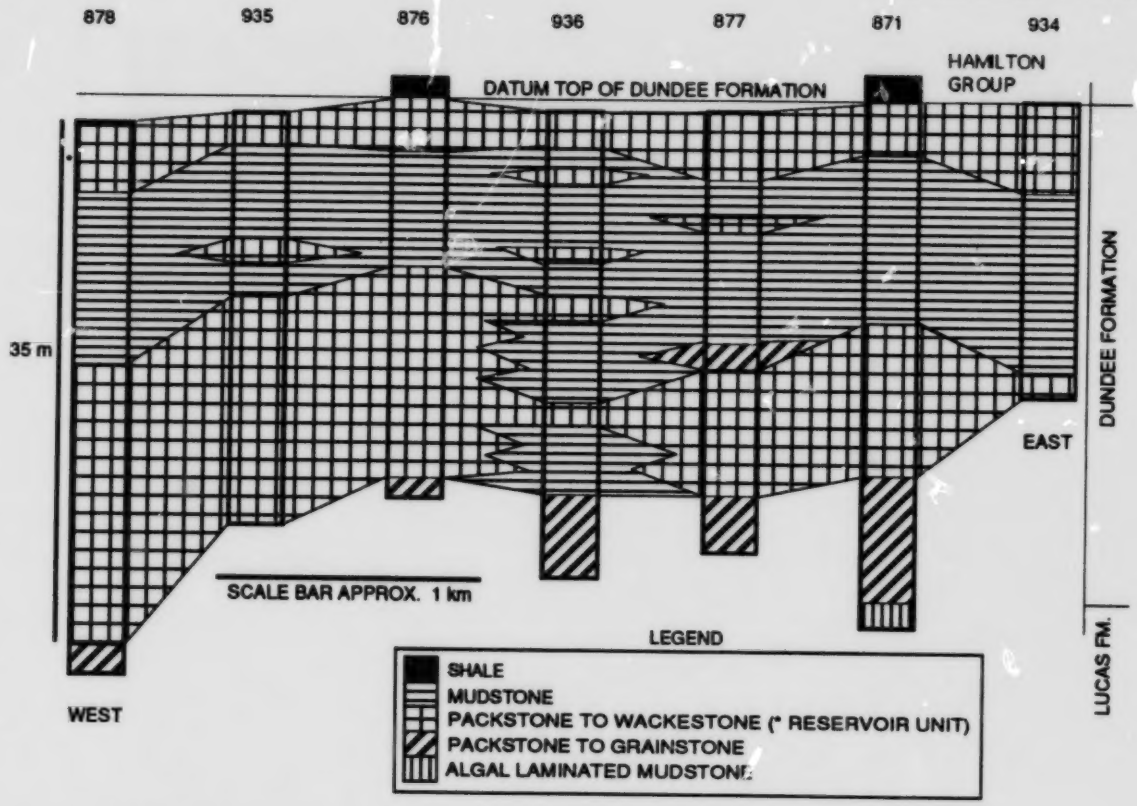

Figure 353A.6. Stratigraphic cross section of the Plympton–Sarnia field.

and may be indicative of high-temperature fluids during deeper burial. The Rodney field is in close proximity to a major fault that lies to the east. The fault may have provided the conduit for the diagenetic fluids that passed along the sand-rich layers and dolomitized the immediately overlying and underlying beds.

Type 2. Fractured Reservoirs with Associated Dissolution and Microporosity

CASE STUDY: PLYMPTON–SARNIA FIELD, SARNIA TOWNSHIP, LAMBTON COUNTY

Introduction

The Plympton–Sarnia field is located approximately 9.5 km to the east of Sarnia (Figure 353A.2) and was discovered in the late 1800s (Bailey and Cochrane 1985). Cumulative oil production to date is listed at only 11 840 barrels, but this is due in part to the fact that the bulk of the early production was not recorded. The field was subject to an unsuccessful enhanced oil-recovery scheme by Devran Petroleum between 1987 and 1988. Horizontal shafts were bored into the Middle Devonian carbonates with the hope of extracting the hydrocarbons by gravity drainage.

The Plympton–Sarnia field is located on the crest of a large structural nose (Figures 353A.5 and 353A.6). The field apparently produced from 2 separate reservoirs: the Lucas microcrystalline dolostones (*see* below) and the fractured Dundee limestones with associated dissolution and microporosity. Core analyses indicate that biomoldic and vuggy porosity and microporosity may range up to 18% and provide permeabilities in excess of 50 mD.

Sedimentology

In the Dundee section the reservoir is largely confined to an upper and lower bioclastic packstone unit. Areas of intense fracturing provided potential communication throughout the entire section. Examination of the reservoir units with SEM has indicated significant microporosity developed in the matrix of packstones (Photos 353A.2a and 353A.2b). The microporosity is largely intercrystalline and is optimally developed in the upper Dundee packstones (Photos 353A.3a to 353A.3c). Biomoldic and vuggy porosity are also present in variable amounts in the upper Dundee section and significantly enhance reservoir permeability.

Fractures are mainly vertical and range from open to completely filled with calcite and/or bitumen. The variable nature of the fracture fills may be indicative of multiple phases of fracture generation. Horizontal fractures have been documented in a few locations.

The microporous skeletal packstones that provide a reservoir in the Plympton–Sarnia field were deposited in a

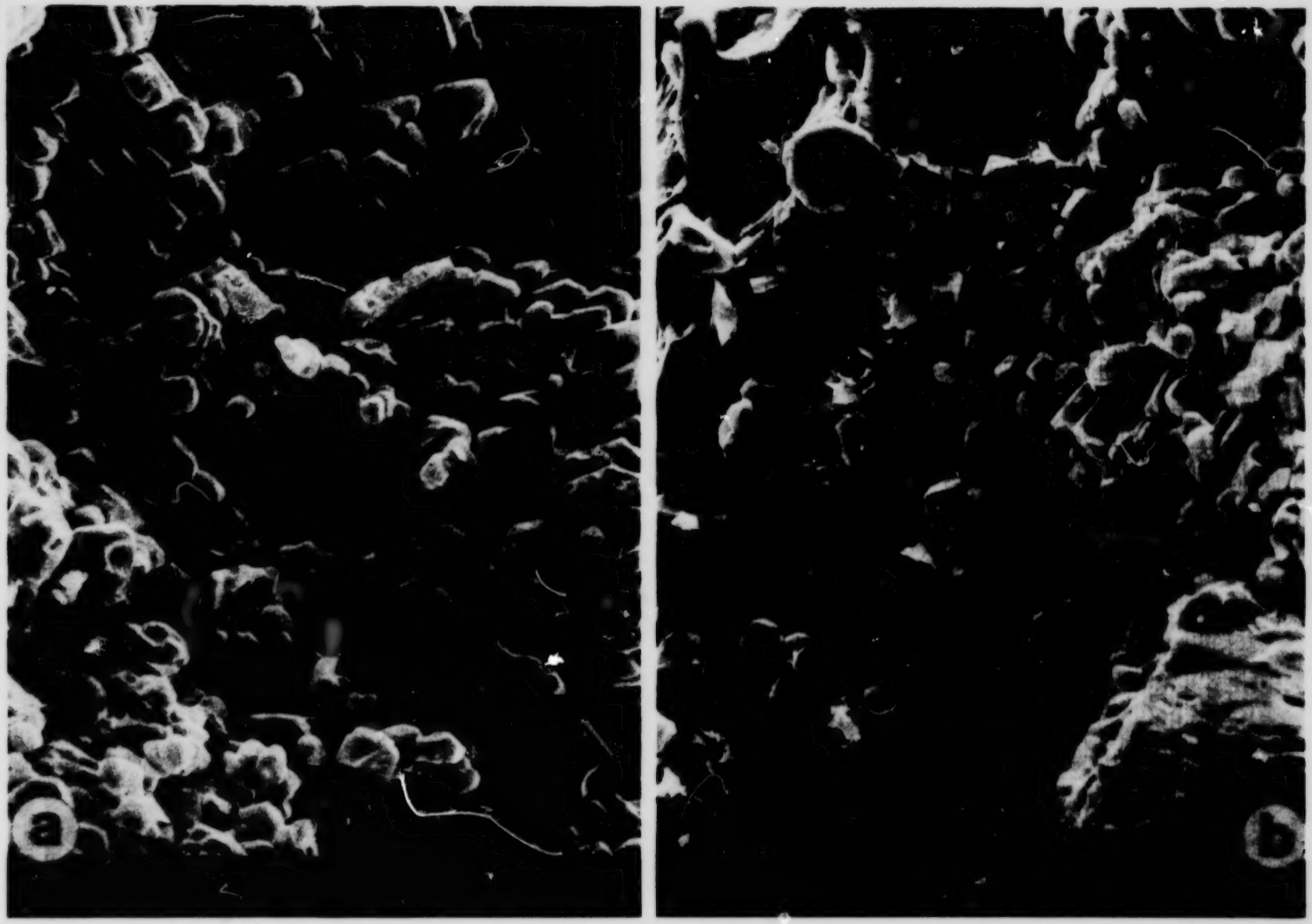

Photo 353A.2. SEM photomicrographs, Plympton–Sarnia Field. **a)** Abundant framework intercrystalline microporosity between predominantly euhedral calcite crystals. **b)** Abundant matrix intercrystalline microporosity. Note allochem fragments in the upper left and lower right corners of photo.

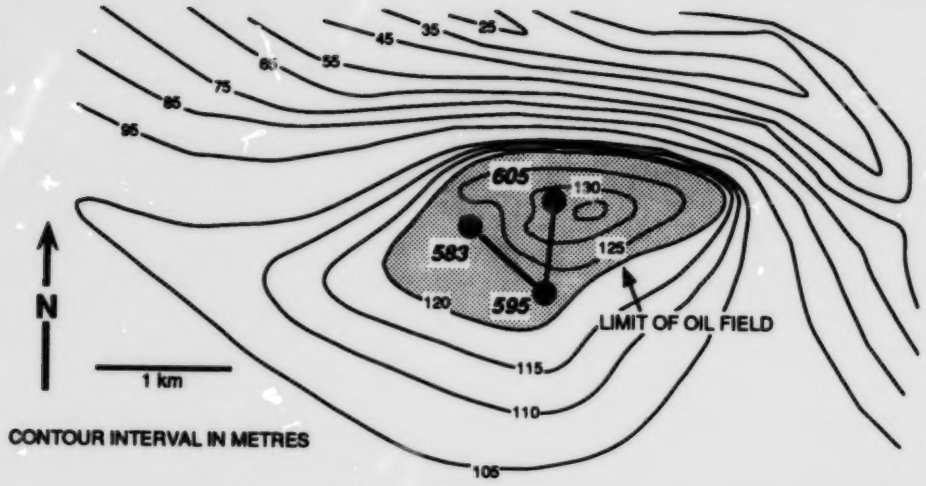

Figure 353A.7. Structural top of the Lucas Formation in the Oil Springs field (*modified after* Bailey and Cochrane 1985).

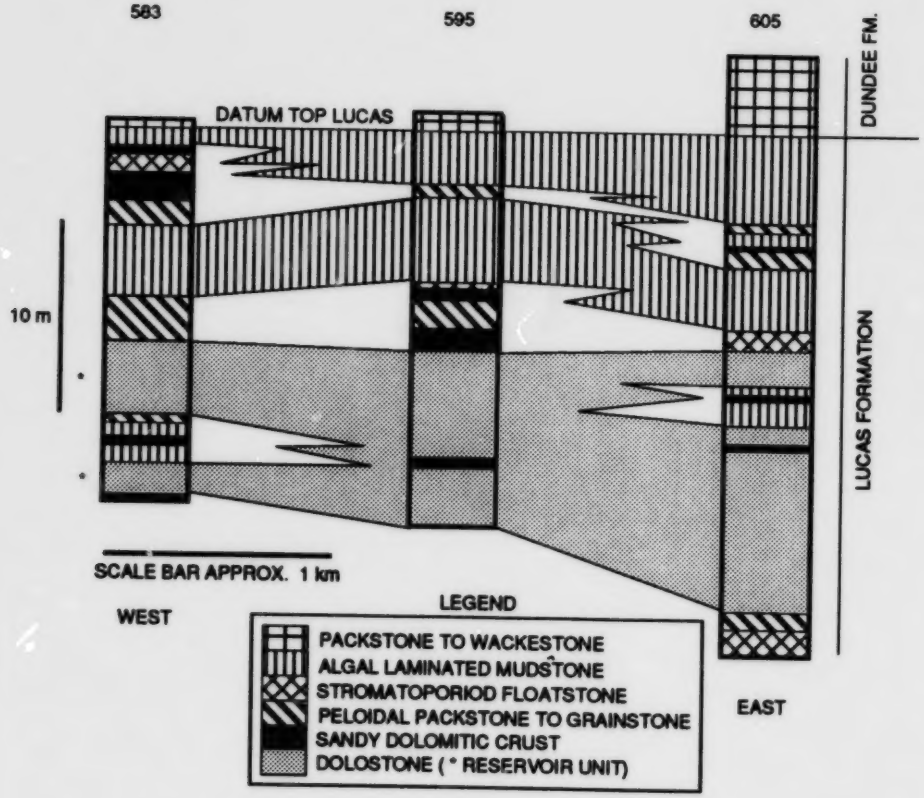

Figure 353A.8. Stratigraphic cross section of the Oil Springs field.

sheltered lagoon (lower Dundee) to shelf-marginal setting (upper Dundee). Local higher energy conditions are indicated by a decrease in micrite and an increase in the number of grainstone lenses. The middle Dundee mudstones to wackestones represent deposition in predominantly quiet-water conditions. Microporosity is apparently absent in this unit, but minor biomoldic porosity is developed in scattered coral fragments.

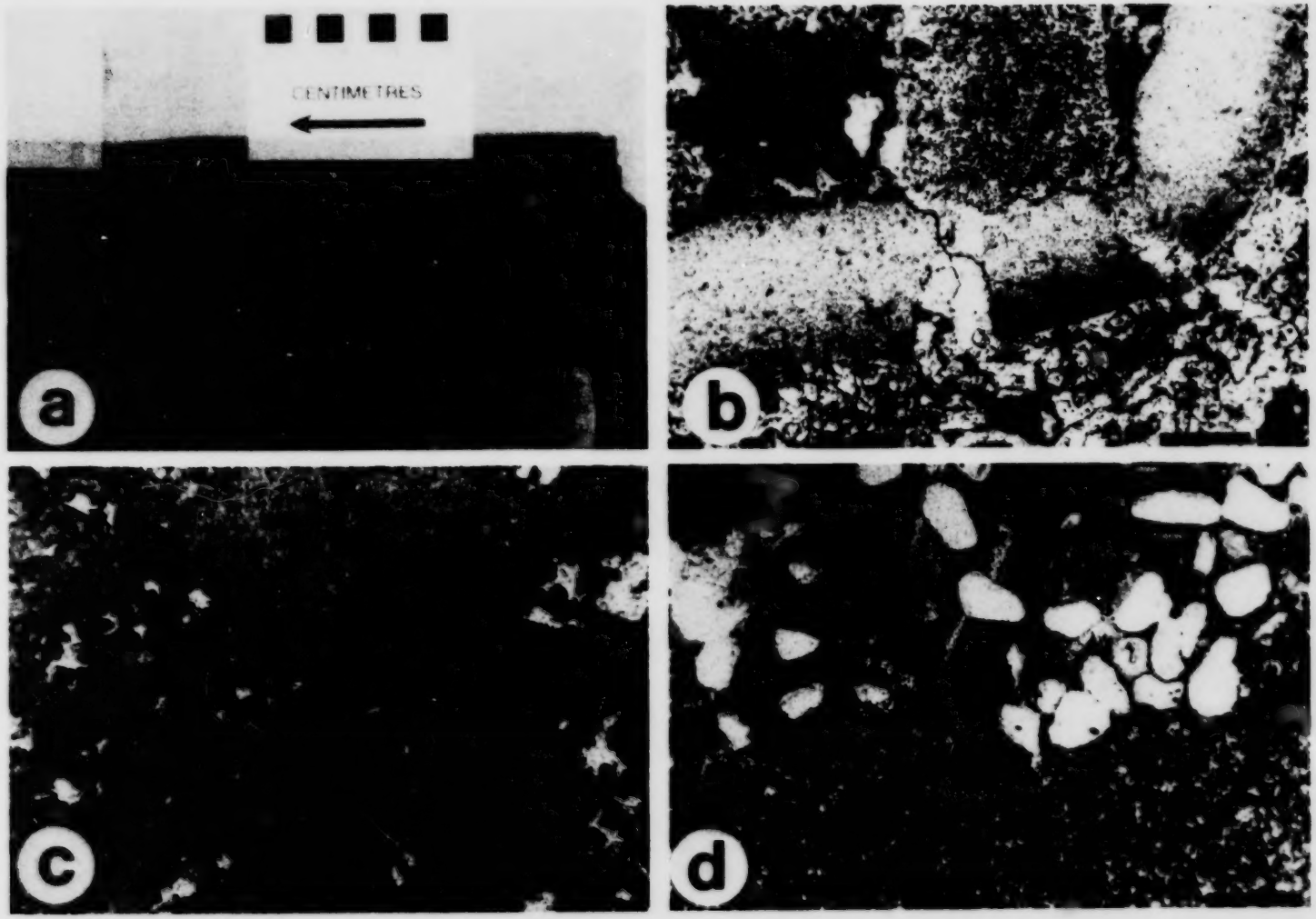

Photo 353A.3. Plympton–Sarnia field and Oil Springs field. **a)** Core sample. Note fracture at base and vuggy, porous nature of this packstone unit. (Plympton-Sarnia field.) **b)** Thin-section photomicrograph of the upper packstone unit showing minor grain interpenetration between crinoid (upper) and trilobite (lower) fragments and fracturing of the trilobite fragment. Scale bar is 150 μm. (Plympton-Sarnia field.) **c)** Thin-section photomicrograph of the upper crinoid-rich packstone unit showing extensive dissolution of matrix. Large crinoid fragment (left centre of photo) is 500 μm in diameter. Scale bar is 150 μm. (Plympton-Sarnia field.) **d)** Thin-section photomicrograph of siliciclastic-rich dolostone from the Oil Springs field. Note 2 types of dolomite: the lowermost microcrystalline phase (10 to 20 μm) with excellent intercrystalline porosity and a finely crystalline phase (100 to 150 μm) in the calcite-cemented, quartz sand-rich upper layer. Sand grains are well rounded. Scale bar is 150 μm.

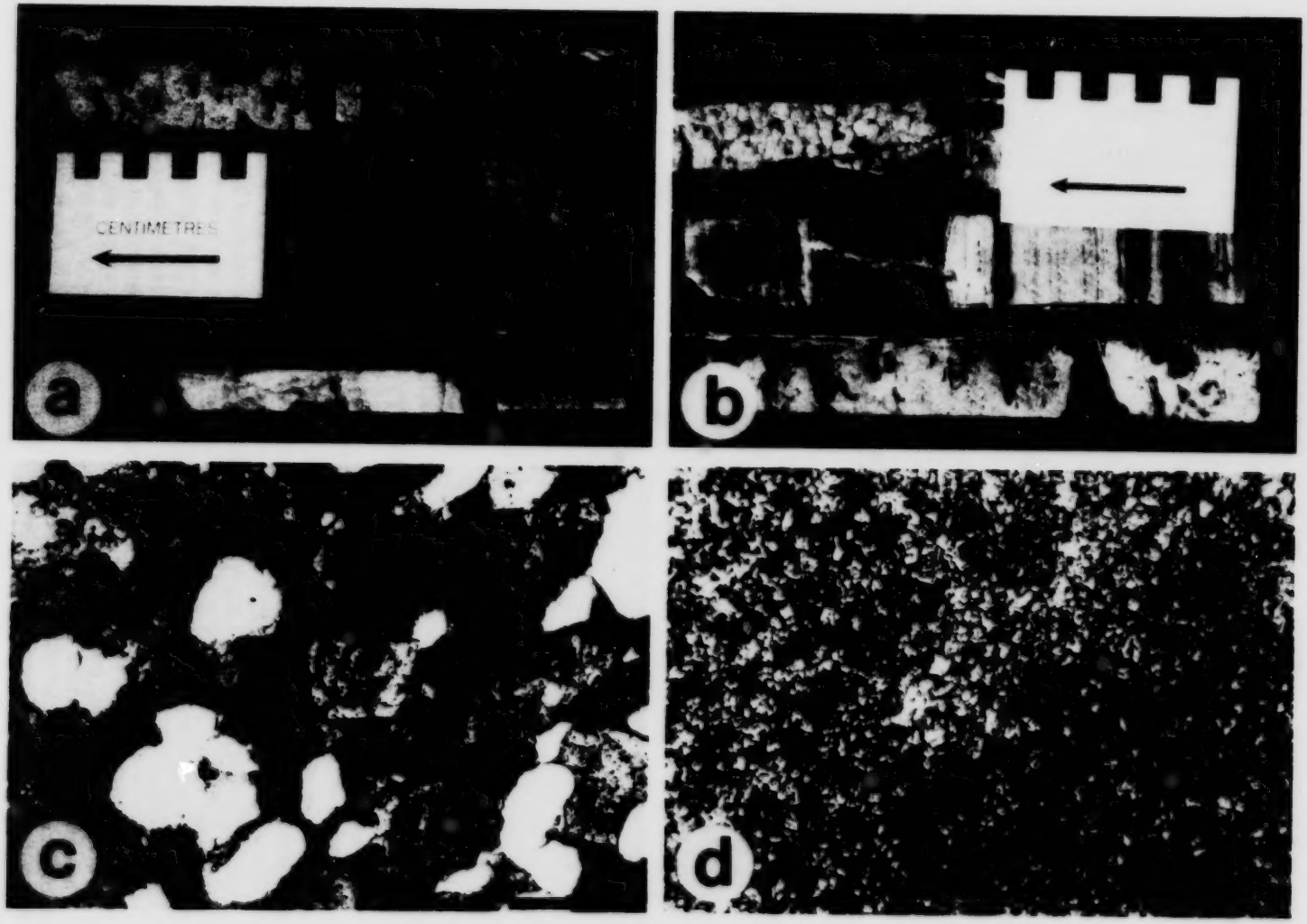

Photo 353A.4. Oil Springs field. **a)** Cored section of the Lucas Formation showing pebble-chip breccia, stromatolitic lime mudstone and stromatoporoid floatstone. **b)** Cored section of the Lucas Formation showing mud-cracked mudstone, stromatoporoid wackestone and floatstone. **c)** Thin-section photomicrograph of partially dolomitized, quartz sand-rich grainstone. Scale bar is 150 μm. **d)** Thin-section photomicrograph of microcrystalline dolostone containing abundant intercrystalline porosity filled with bitumen. Scale bar is 150 μm.

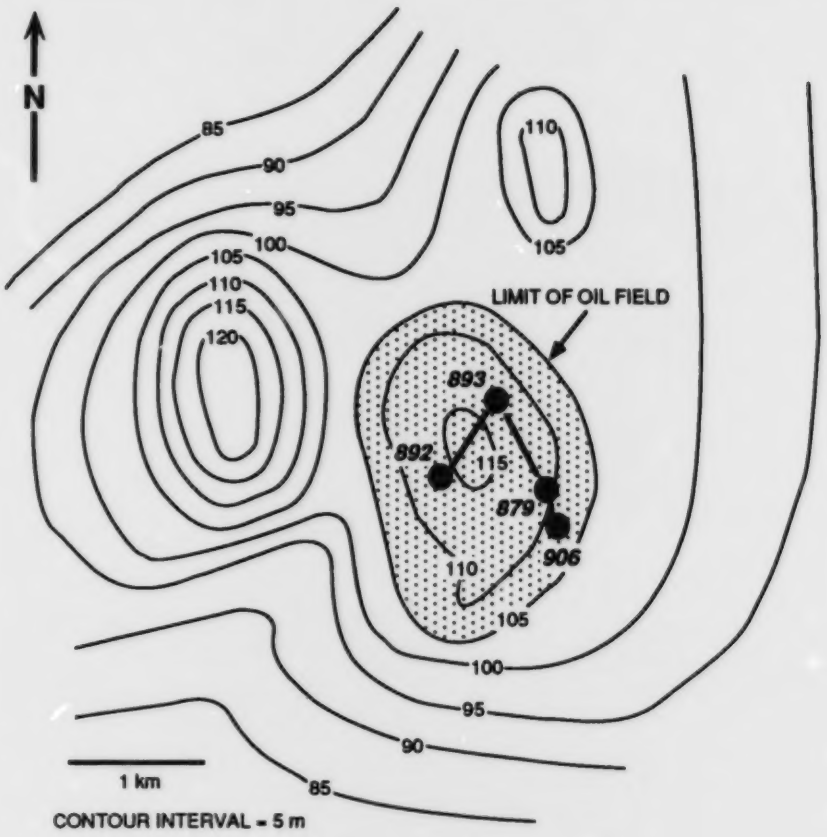

Figure 353A.9. Structural top of the Dundee Formation in the Eagle field.

Diagenesis

This reservoir type has a complex diagenetic history. Microporosity is interpreted as an early diagenetic event and is succeeded by stylolitization, fracturing, dissolution, late calcite cementation, hydrocarbon migration and minor late pyrite precipitation. Dolomite is a minor diagenetic constituent and is present as disseminated microcrystalline rhombs. Optimal porosity development is restricted to the upper and lower packstone facies and is therefore facies specific. The lower packstone unit was highly altered by pressure solution and has a higher dolomite content in the range of 10 to 15%.

Microporosity is apparently a recrystallization product of the original lime mud matrix. Microporosity is poorly developed where there is a marked decrease in micrite and an increase in matrix cement.

Following stylolitization, salt-dissolution-generated tectonic events were responsible for multiple phases of fracturing. These fractures provided pathways for diagenetic fluids, which caused dissolution in the upper Dundee section and enhanced matrix permeability. A late phase of calcite cementation partially occluded fracture, biomoldic and vuggy porosity and microporosity. The presence of thick bitumen along the fracture seams and late calcite cements indicates that hydrocarbon migration was a late event.

Type 3. Microcrystalline Dolostones

CASE STUDY: OIL SPRINGS, ENNISKILLEN TOWNSHIP, LAMBTON COUNTY

Introduction

The Oil Springs field is located below the town of Oil Springs and is situated 28 km southeast of Sarnia (Figures 353A.2 and 353A.7). The field was discovered in 1858 and to date has produced in excess of 9.5 million barrels of oil. Unfortunately there are only limited core and reservoir data on this very prolific reservoir type.

The reservoir is predominantly a brown to medium-grey microcrystalline to very finely crystalline dolostone with varying amounts of fine- to medium-grained, well-rounded, poorly sorted quartz sand. Porosity values are typically 12 to 30%, and permeabilities are in the range of 5 to 433 mD.

Sedimentology

These porous dolostones in the Lucas Formation are commonly found in close association with undolomitized stromatolitic lime mudstones, stromatoporoid floatstones

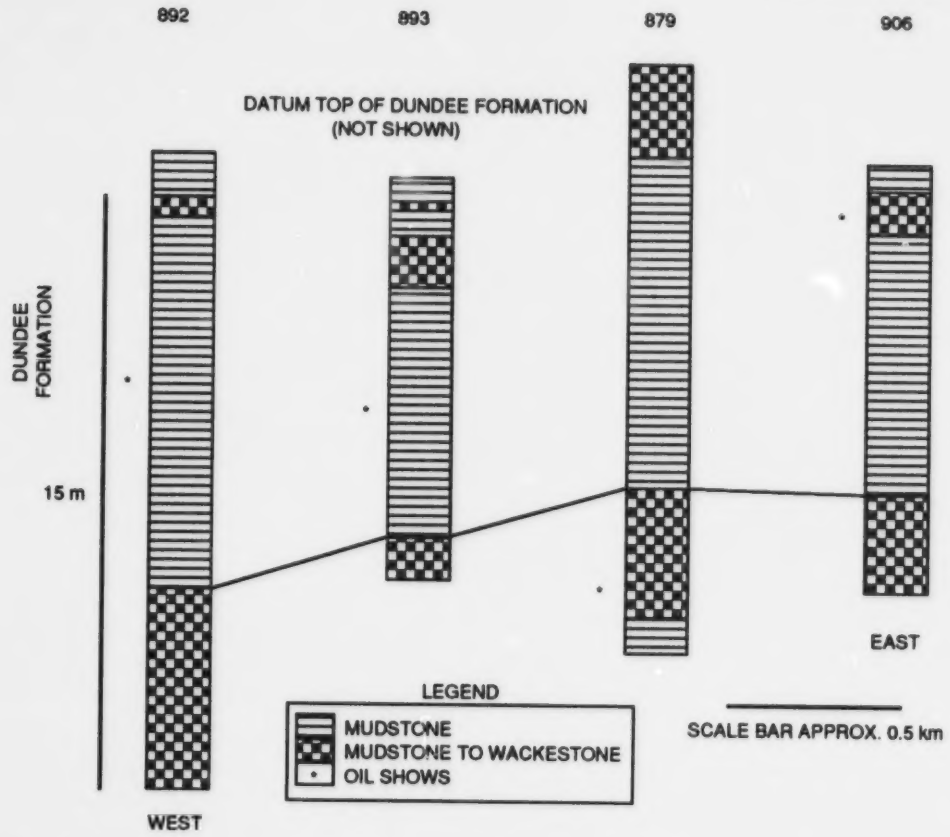

Figure 353A.10. Stratigraphic cross section of the Eagle field.

and sandy peloidal grainstones (Figure 353A.8 and Photo 353A.3d). The dolostones are distinctly bedded, tend to overlie the stromatoporoid floatstones and are overlain by the stromatolitic lime mudstones that commonly contain rip-up clast horizons, desiccation cracks filled with quartz sand and minor gypsum-dissolution molds (Photos 353A.4a and 353A.4b). These features are indicative of very shallow water and periodic subaerial exposure. Peloidal packstones and grainstones are commonly present instead of the dolostones. In the cores examined, it is apparent that there are several incomplete shallowing-upward cycles usually capped by stromatolitic lime mudstones. These cycles record minor transgressive and regressive phases during deposition of the Lucas Formation.

Diagenesis

The dolostones contain 2 distinct types of dolomite: a microcrystalline phase and a finely crystalline phase (Photo 353A.3d). The finely crystalline dolomite contains ghosts of peloidal allochems and is of minor overall importance (Photo 353A.4c). In contrast, microcrystalline dolomite, with its excellent intercrystalline porosity, constitutes the bulk of the reservoir rock (Photo 353A.4d). These dolostones are conspicuously interbedded with floatstones to packstones and lime mudstones, suggesting some facies control on dolomitization. The microcrystalline dolostones also display relics of peloids, indicating they are dolomitized peloidal packstones and grainstones.

Type 4. Fractured Limestones

CASE STUDY: EAGLE FIELD, ALDBOROUGH TOWNSHIP, ELGIN COUNTY

Introduction

The Eagle field is located approximately 10 km to the southeast of West Lorne and was discovered by the Consumers Gas Company Ltd. in 1984. Consumers drilled a total of 6 wells into what was recognized as a small structural high delineated by seismic work (Figure 353A.9). Only one of the wells encountered significant oil shows; it produced a total of 2191.4 m^3 of oil (13 782 barrels) prior to its abandonment in 1987. Excellent core control exists in the field, and it is apparent that the oil production was from fractures in the Dundee Formation (Figure 353A.10).

Sedimentology

The Dundee Formation in the Eagle field is interpreted as having been deposited on the Appalachian Basin side of the Algonquin Arch. The Dundee section is dominantly composed of thinly bedded, medium-grey to tan grey, lime mudstones with thin beds of medium-grey, bioclastic wackestone. The mudstones are bioturbated, contain thin bands of black shale, commonly have a nodular fabric and

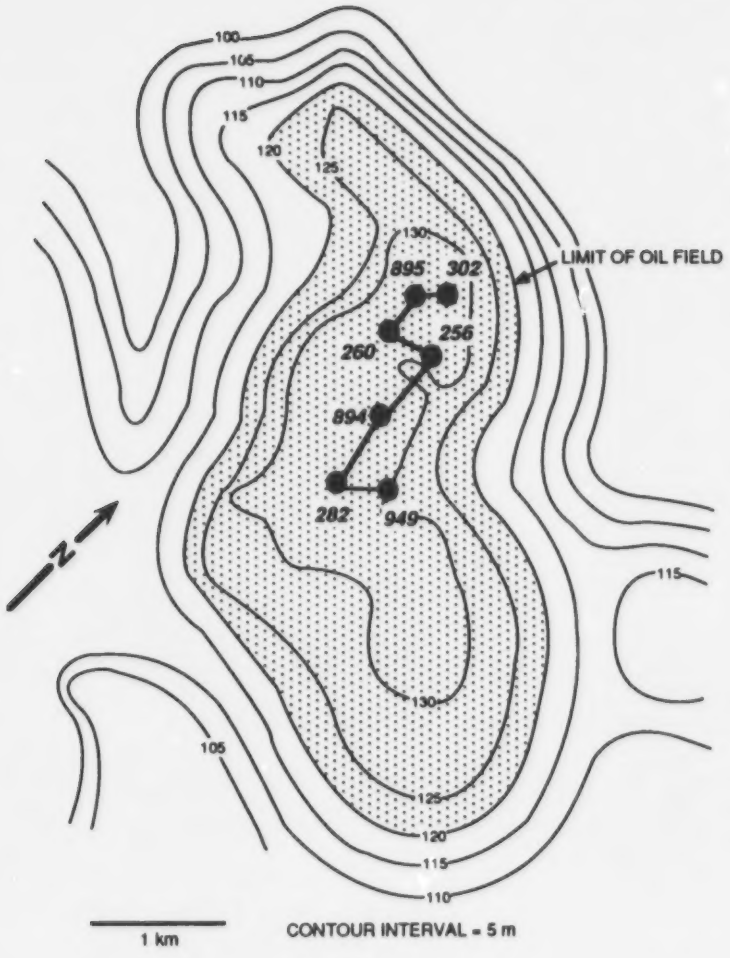

Figure 353A.11. Structural top of the Dundee Formation in the Glencoe field (*modified after* Bailey and Cochrane 1985).

locally contain bivalve and crinoid fragments. The wackestones also contain abundant crinoid fragments and host lesser amounts of stromatoporoid, bivalve and trilobite debris. Subvertical fractures are recognized in some of the mudstone beds but in general are rarely encountered in the cores examined.

In contrast to the shallow subtidal depositional environment in the Michigan Basin, Dundee sediments in the Appalachian Basin represent much lower energy conditions, possibly indicative of deeper water. The paleobathymetry for the Appalachian Basin in this area may have had a much steeper gradient than on the Michigan Basin side of the Algonquin Arch. This would indicate that there was no significant shelf developed on the northern edge of the Appalachian Basin and therefore limited opportunity for the production and trapping of higher energy sediments.

Diagenesis

The Dundee Formation in the Eagle field consists predominantly of nonporous lime mudstones and wackestones that have undergone significant compaction, as evidenced by extensive stylolitization throughout the interval. Minor leached bivalve fragments are filled with late calcite cement. A late stage of fracturing produced a network of vertical to subvertical fractures, which provided the only reservoir for the short-lived field.

Type 5. Calcareous Sandstones

CASE STUDY: GLENCOE FIELD, MOSA TOWNSHIP, MIDDLESEX COUNTY

Introduction

The Glencoe field is located 6.5 km to the north of the town of Glencoe and was discovered in 1904 (Bailey and Cochrane 1985). The Glencoe field has produced in excess of 177 200 m^3 (937 500 barrels) of oil. Most of this production is from the calcareous sandstones of the Lucas Formation, but oil has also been recovered from the overlying fractured Dundee limestones and a thin limestone unit within the Hamilton Shale. The pool is located on the crest of a large domal structure (Figure 353A.11). A total of

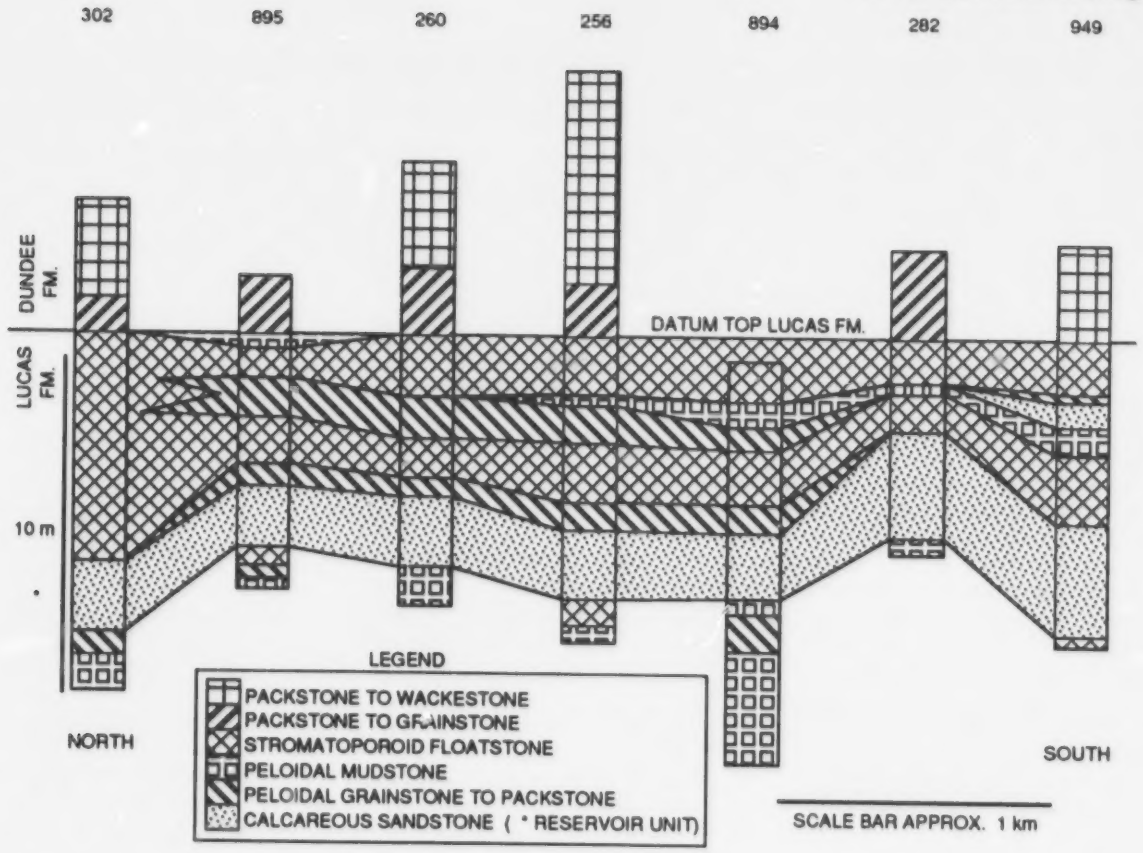

Figure 353A.12. Stratigraphic cross section of the Glencoe field.

8 cores have penetrated the Dundee and Lucas formations. Core analysis indicates that porosity ranges from 10 to 21%, with permeabilities commonly in the range of 50 to 200 mD, rarely reaching up to 665 mD. The pool is presently undergoing secondary waterflood recovery.

Sedimentology

Most of the production in the Glencoe field is from calcareous sandstones considered by Sanford (1968) as the sandy Anderdon Member of the upper Lucas Formation. This sandstone unit is invariably present at the top of the Lucas Formation or occurs as interbeds throughout the upper 10 to 15 m of the formation.

The sandstones in the Glencoe field are tan to medium brown, fine to medium grained and well sorted and range from 0.7 to 3.2 m in thickness. Sedimentary structures range from massive beds to parallel laminae to low-angle (10 to 15°), planar cross-beds. Quartz grains are well rounded and display microtextures indicative of a strong eolian influence (V-shaped grooves and dish-shaped impact features: Dutton 1985). In the cores examined the sandstone units are commonly overlain by sandy peloidal grainstones and stromatoporoid floatstones and underlain by stromatoporoid floatstones, peloidal grainstones and lime mudstones (Figure 353A.12). The lime mudstones are very finely laminated with vertical fractures (mud cracks?) filled with quartz sand. Grainstones commonly contain rip-up clasts of lime mudstone. Thin, sandy, lime mudstone and stromatoporoid floatstone interbeds are common in the basal portions of the sandstone unit. These features indicate that the sandstones were deposited in a shallow subtidal to intertidal setting.

On a more regional scale, the sandstones appear to be widespread and distributed preferentially along the top of the Algonquin Arch. The Florence–Oakdale field of Dawn Township in Lambton County is located approximately 45 km to the southwest of the Glencoe field along the crest of the Algonquin Arch. This field produced oil from the same upper Lucas sandstone.

Diagenesis

Most of the porosity in the upper Lucas sandstones is secondary. Early calcite cementation of the sandstones and subsequent compaction during burial resulted in preservation of only minor primary porosity. A late phase of dissolution removed much of the early cement and provided significant secondary porosity (pinpoint, vuggy and intergranular) and permeability. A later phase of dissolution of Silurian salt caused the formation of a large domal structure, which provided the hydrocarbon trap for the Glencoe field.

CONCLUSIONS

The Middle Devonian carbonate section of southwestern Ontario contains several economically important reservoir types. Type 1 (Rodney) and type 3 (Oil Springs) reservoirs are the most economically important. Type 1 reservoirs are confined close to the southern flank of the Algonquin Arch. Reservoir types 2 (Plympton–Sarnia) and 3 are situated on the northern flank of the Algonquin Arch in the Michigan Basin. Type 4 (Eagle) fractured reservoirs may produce oil for short periods and are overall a poor exploration target. Type 5 (Glencoe) calcareous sandstone reservoirs are mappable along the crest of the Algonquin Arch, and where they have been modified structurally into closed highs by Silurian salt dissolution, they present an excellent exploration play.

Understanding the development of these reservoirs in light of sedimentologic, diagenetic and tectonic controls will assist in developing exploration strategies for similar Devonian reservoirs. In addition, knowledge of the types and abundance of porosity in similar rock types is important, as they have been used extensively for the disposal of hazardous wastes.

ACKNOWLEDGMENTS

This research forms part of Hamilton's MSc thesis, which is supported by Ontario Geoscience Research Grant 353 to M. Coniglio and S.K. Frape and by Natural Sciences and Engineering Research Council of Canada funding to MC. The authors thank T.R. Carter (Ontario Ministry of Natural Resources) and R. Trevail (Telesis Oil and Gas) for their assistance in this study.

REFERENCES

Bailey, B. and Cochrane, R.O. 1985. Evaluation of the conventional and potential oil and gas reserves of the Devonian of Ontario; Ontario Geological Survey, Open File Report 5555, 178p.

Dutton, B.C. 1985. Sedimentology and diagenesis of the Middle Devonian Dundee Formation in south Lambton and west Middlesex counties, southwestern Ontario, Canada; unpublished MSc thesis, University of Toronto, Toronto, Ontario, 193p.

Ferrigno, K.F. 1971. Environmental influences on the distribution and abundance of conodonts from the Dundee Limestone (Devonian), St. Marys, Ontario; Canadian Journal of Earth Sciences, v.8, p.378-386.

Sanford, B.V. 1955. The Rodney oil field. Ontario Fuel Board, 2nd Annual Report, p.36-39.

———1968. Devonian of Ontario and Michigan; International Symposium on the Devonian System, p.973-999.

Sanford, B.V., Thompson, F.J. and McFall, G.H. 1985. Plate tectonics—a possible controlling mechanism in the development of hydrocarbon traps in southwestern Ontario. Bulletin of Canadian Petroleum Geology, v.33, p.52-71.

Uyeno, T.T., Telford, P.G. and Sanford, B.V. 1982. Devonian conodonts and stratigraphy of southwestern Ontario. Geological Survey of Canada, Bulletin 332, 55p.

Grant 353 Diagenetic History of Dolomitized Ordovician and Devonian Oil and Gas Reservoirs in Southwestern Ontario. Part B: Fracture-related Diagenesis of Middle Ordovician Carbonate Reservoirs, Southwestern Ontario

K. Middleton, M. Coniglio and S.K. Frape

Department of Earth Sciences, University of Waterloo, Waterloo

ABSTRACT

Oil and gas production from strata of the Middle Ordovician Trenton and Black River groups of the Michigan Basin occurs where the limestones have been fractured, made porous by dissolution and locally dolomitized. Reservoir seals are provided by the overlying shales of the Blue Mountain Formation and by interbedded, nonporous limestones and dolostones.

Crosscutting relations between stylolites and fractures indicate that fracturing occurred at depth following pressure solution. Two types of porosity are recognized in the dolomitized units: 1) facies-independent fracture porosity; and 2) facies-controlled, pinpoint to vuggy porosity developed in grainstone interbeds. Production generally occurs from facies-controlled porosity.

Three types of dolomite are present: 1) cap dolomite located in the upper few metres of the Trenton sequence, 2) massive replacement dolomite in the vicinity of fractures and 3) saddle-dolomite cement that partially occludes secondary pore space. The fracture-related replacement dolomite is porous in grainstone interbeds and along fractures but nonporous elsewhere. In hand sample dolomitized grainstone beds display partial preservation of original fabric or are sucrosic with the original fabric completely obscured.

Petrographic and geochemical (stable C and O isotopes, trace elements) evidence indicates that 1) the cap dolomite is distinctly different from the fracture-related dolomite; 2) cap dolomitization preceded fracture dolomitization; 3) where fractures transect the upper few metres of the Trenton, the cap dolomite is overprinted by fracture-related dolomitization; and 4) the fracture-related dolomite and saddle-dolomite cement have the same stable isotope signature, indicating a continuum of replacement followed by precipitation.

Fracture-occluding precipitates following saddle dolomite include sulphides, sparry calcite and anhydrite, commonly in this order. This paragenetic sequence of minerals is typical of Mississippi Valley-type deposits. The difference in this case is the abundance of hydrocarbons rather than sulphides.

INTRODUCTION

During the 1980s Ordovician oil production increased from a low of 3.6% of total Ontario production to 72.7% in 1989, during which time the total Ordovician oil production was 177 188 m^3 (T. Carter, Ontario Ministry of Natural Resources, personal communication, 1990). The rise in production resulted from the discovery of the Hillman, Renwick, Wheatley and Dover 7-5-VE pools in Essex and Kent counties (Figure 353B.1). Ordovician gas production reached a high of 5.6% of Ontario's total production in 1989 and is confined to the northern pools such as Dover and Lambton. Gas production is expected to increase as more gas plants are constructed in oil pools and as drilling expands to the north (T. Carter, personal communication, 1990).

Oil pools in the southwest part of the study area, such as Hillman, Wheatley and Renwick, are located in the vicinity of the Findlay Arch and produce from the middle to upper Trenton sequence. In contrast, the Dover pool to the north, located in the vicinity of the Algonquin Arch, produces from lower Trenton and upper Black River strata. Production from these reservoirs occurs where the usually nonporous Trenton and Black River limestones have been fractured, dissolution enhanced and dolomitized. Dissolution enhancement is confined to fractures and grainstone beds. Fracturing alone, without accompanying dissolution enhancement and dolomitization, did not provide the porosity necessary for hydrocarbon entrapment.

DOLOMITIZATION (PREVIOUS WORK)

A variety of dolomite types are found in the Ordovician sequence of the Michigan Basin. These include 1) cap dolomite, developed in the upper few metres of the Trenton directly beneath the shales of the Blue Mountain Formation (and correlative units); 2) fracture-related massive replacement dolomite located in the vicinity of fractures; and 3) fracture-occluding saddle-dolomite cement. In addition, this sequence in the extreme south and west portion of the Michigan Basin in Michigan and Indiana is massively dolomitized ("regional dolomite"). The

Figure 353B.1. Location of Middle Ordovician oil and gas pools in the study area (southwestern Ontario) as well as the Albion–Scipio field in Michigan. The location of the OGS 82-2 core that was examined for the study of pre-fracture diagenesis is also shown. Cross section A–A′ is the Renwick South pool (discussed in text).

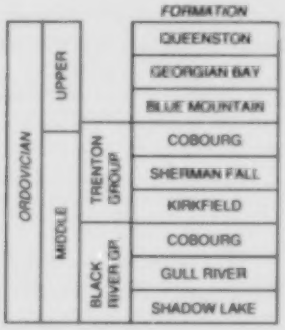

Figure 353B.2. Stratigraphic nomenclature for the subsurface of southwestern Ontario (*after* Trevail et al. 1989).

diagenesis in Michigan, Indiana and Ohio has been described by Shaw (1975), Taylor and Sibley (1986), Keith (1986, 1988), Budai and Wilson (1988), DeHaas and Jones (1988), Fara and Keith (1988), Haefner et al. (1988) and Prouty (1988). In southwestern Ontario the same dolomite types have only recently been investigated (Bailey Geological Services Ltd. and Cochrane 1983; Dollar 1988; Trevail 1988a, 1988b; Colquoun and Brand 1989a, 1989b; Middleton et al. 1989, 1990a).

Taylor and Sibley (1986) explained formation of the cap dolomite from magnesium- and iron-rich waters expelled during dewatering of the overlying Blue Mountain Formation shales. Prouty (1988) interpreted the fracture-related dolomite as having resulted from upward migration of brines that become pooled beneath the impermeable Blue Mountain-equivalent shales. The source of these brines remains unclear at this time.

Recently, similarities in style of hydrocarbon trap have been noted between the Middle Ordovician of the Michigan Basin and the Upper Devonian Wabamun Group in the Peace River Arch area of northwestern Alberta (Churcher and Majid 1989). This style of fracturing with the accompanying dolomitization and paragenetic suite of fracture-occluding precipitates is also typical of Mississippi Valley-type sulphide deposits, except there is a lack of sulphides in southwestern Ontario (and in the Wabamun Group) and, instead, an abundance of hydrocarbons. Based on fluid-inclusion evidence, Shaw (1975) determined hydrocarbon migration in the Albion–Scipio field occurred during saddle-dolomite precipitation. In northwestern Ohio, a noneconomic Mississippi Valley-type deposit is located within the Middle Ordovician sequence (Haefner et al. 1988).

METHODOLOGY

This study is based on cores representative of Middle Ordovician oil and gas pools as well as cores located outside the pools. Approximetely 350 petrographic thin sections were produced and stained with potassium ferricyanide and Alizaran Red-S to differentiate calcite from dolomite and ferroan carbonate from nonferroan carbonate. We examined the thin sections using standard transmitted light and cathodoluminescence microscopy. Fractured samples were observed with scanning electron microscopy (SEM).

Fifty samples were drilled for analysis of stable carbon and oxygen isotopes. We analyzed the samples at the University of Waterloo using standard procedures. The $\delta^{18}O$ and $\delta^{13}C$ values are reported relative to the Peedee belemnite (PDB) standard. Microprobe analyses were carried out at The University of Western Ontario on a Jeol JXA-8600 Superprobe with Tracor Northern TN500 automation, using a zero alignment feature (ZAF) correction routine.

Operating conditions were 15 kV, 10 nA, 10 μm wide beam and 20 s counting time. Smithsonian Institute carbonate standards were used for Ca, Mg, Fe and Sr analyses, and an in-house rhodonite standard was used to analyze for Mn. Thirteen samples were examined, and traverses of up to 13 spots were done across pore-filling cements; otherwise 6 to 10 spots were analyzed per thin section.

STRATIGRAPHY

The Middle Ordovician succession consists of the Trenton and Black River groups, which together range up to 280 m in thickness (Figure 353B.2). The depth of the top of the Trenton varies from 665 m in the extreme southwest (Malden field) to 950 m in Lambton County, just northeast of Lake St. Clair. Lower Ordovician strata are absent in the subsurface, and Black River strata rest disconformably on Cambrian sandstones.

The Trenton Group in the subsurface of southwestern Ontario exhibits a sharp, irregular contact with overlying deeper water shales of the Blue Mountain Formation (Utica Shale equivalent). The contact is readily picked in core and gamma ray log as a rapid change from limestone to shale. The upper few metres of the Trenton Group in southwestern Ontario is marked by an increase in phosphate and pyrite and is dolomitized ("cap dolomite"). The signficance of the phosphate and pyrite mineralization at this contact is uncertain. Similar contacts have been reported from Indiana (Keith 1986, 1988), northwestern Ohio (Haefner et al. 1988) and Michigan (Taylor and Sibley 1986).

Rooney (1966) suggested an unconformity origin for the sharp contact between the Trenton sequence and the overlying shales. DeHaas and Jones (1988) offered meteoric karstification as an explanation that accounted for the development of cavernous porosity in oil and gas fields of central southern Michigan. Trevail (1988a, 1988b) suggested a similar explanation for southwestern Ontario. Fara and Keith (1988), however, indicated that the nature of the erosional surface, as well as the presence of phosphate and pyrite, represents extensive submarine exposure and the development of a hardground surface.

In contrast to the above, north of the study area there is a gradual transition from the Trenton sequence to the overlying shale succession that is due to the presence of the Collingwood Member, a sequence of interbedded calcareous black shale and bioclastic limestone (Russell and Telford 1983; Churcher 1985). Graptolite evidence suggests that the Collingwood is equivalent to basal shales of the Blue Mountain Formation elsewhere (M. Melchin, University of Waterloo, personal communication, 1990). If this is the case, there is a facies change in the northeastern section of the basin, rather than erosion of the Collingwood to the south as has been suggested by Churcher (1985) and DeHaas and Jones (1988). Taylor and Sibley (1986) reported a sharp Trenton–Blue Mountain contact throughout Michigan except in the northeast (centre of the Michigan Basin), where the contact is more gradational.

FACIES

The 200 to 300 m thick Trenton and Black River groups include supratidal through shallow subtidal lithofacies. The Black River Group consists of monotonous brown or grey and rare black carbonate mudstones that are generally bioturbated (Photo 353B.1a). Bioclasts and the central portion of the burrows are commonly replaced by sparry calcite. Near the base of the Black River sequence there is sandy, glauconitic dolomite. Argillaceous partings and bioclastic packstone and grainstone beds are dispersed throughout, becoming volumetrically more important toward the top of the Black River sequence.

The Trenton Group is characterized by grey or brown, interbedded or nodular, argillaceous, fossiliferous carbonates, which exhibit the following features: 1) sharp, irregular-based grainstone fining upward to carbonate mudstone with a sharp upper contact, commonly overlain by another fining-upward sequence (Photo 353B.1b); 2) grainstone interbedded with wackestone or carbonate mudstone, again with sharp upper and lower contacts (Photo 353B.1c); and 3) packstone or grainstone nodules surrounded by argillaceous seams within carbonate mudstone or wackestone (Photo 353B.1d).

The grainstone interbeds, important because of their preferential development of secondary porosity, have the following characteristics: 1) a lighter grey or tan colour, in contrast to the surrounding darker grey or brown lithology; 2) a thickness up to 50 cm; and 3) an increase in abundance toward the upper middle Trenton Group and the upper Black River Group. Bioclasts include echinoderms, brachiopods, bryozoans and, to a lesser extent, trilobites, nautiloids, corals, gastropods and bivalves.

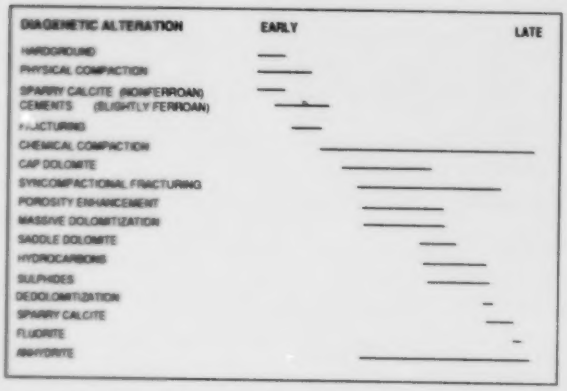

Figure 353B.3. Relative timing of the major diagenetic alterations in carbonates of the Trenton and Black River groups in southwestern Ontario.

DIAGENESIS

Diagenetic alterations have been divided into the following categories: seafloor to shallow burial, chemical compaction and syncompactional fracturing, fracture-related porosity development and dolomitization, and porosity-occluding precipitates. The relative order of diagenetic alterations is depicted in Figure 353B.3.

SEAFLOOR TO SHALLOW BURIAL

Hardgrounds are present throughout the Trenton and Black River groups. A prominent example is the contact between

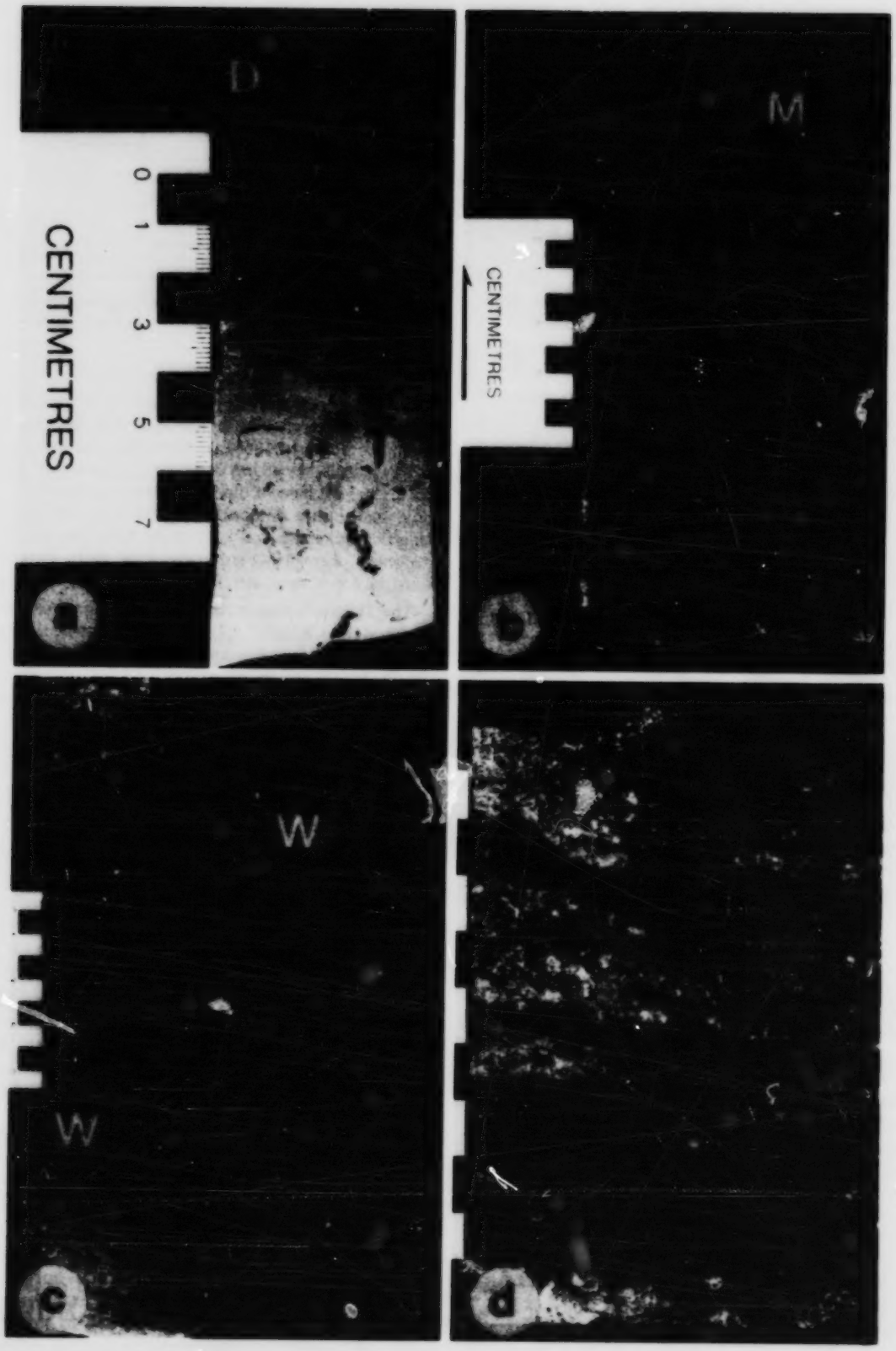
D
0 1 3 5 7
CENTIMETRES
M
CENTIMETRES
W
W

the Trenton Group and the Blue Mountain Formation. According to the classification scheme of Brett and Brookfield (1984), the highly pyritized and phosphatized Trenton–Blue Mountain contact illustrated in Photo 353B.2 is an undercut hardground.

The earliest calcite cements occur as isopachous, equant sparry rims around brachiopods, bryozoans, corals and trilobites and as syntaxial overgrowths on echinoderm fragments. Equant sparry cement occludes remaining pore space. Sparry cementation is not always complete and may leave minor pore space, which may be important in later dissolution enhancement. Microprobe analyses indicate that sparry cement is nonferroan and is commonly followed by a slightly ferroan phase (0.25 to 0.35 mol % $FeCO_3$). The slightly ferroan sparry calcite is more significant towards the top of the Trenton and decreases in abundance downward. Near the base of the Black River Group, ferroan sparry calcite is absent.

An early set of minute fractures filled with slightly ferroan sparry-calcite cement postdates calcite cementation and predates stylolites. The $\delta^{18}O$ values for early sparry calcite range from –6.1 to –5.9‰, and $\delta^{13}C$ values vary between –2.2 and 0.2‰.

CHEMICAL COMPACTION AND SYNCOMPACTIONAL FRACTURING

Stylolites located throughout the Trenton and Black River groups have stylocumulates of less than 1 mm in thickness and suture amplitudes of less than 2 mm. They are rare to absent in grainstones, becoming more numerous in other lithologies.

Fractures and breccia display an interesting relationship with stylolites indicating fracturing occurred during burial. The most obvious evidence for fracturing at depth can be seen in breccia fragments that contain stylolites or fracture-occluding cement that contains "clasts" of stylocumulate. For example, Cons et al. 33825 Mersea 7-14-A is brecciated throughout the producing zone, and the breccia fragments contain stylolites (Photo 353B.3a). Upon closer inspection in thin section, these stylolites are found to be poorly developed (Photo 353B.3b). This indicates fracturing occurred during burial but before the maximum burial depth was attained, as there are more prominently developed stylolites elsewhere in the section.

Syncompactional fractures are nearly vertical with irregular edges. The margins of the fractures do not always coincide, indicating some dissolution enhancement. Fractures may be closely spaced, creating an *in situ* crackle breccia in which the fragments are not rotated. In available core there is no evidence of more intense brecciation such as rock-matrix brecciation described in the Wabamun Group of the Peace River Arch area of northwestern Alberta (Packard et al. 1990). Brecciated intervals are cementation reduced by saddle dolomite or anhydrite and to a lesser extent sparry calcite and sulphides.

Photo 353B.2. Undercut hardground contact between the black shales of the Blue Mountain Formation and the bioclastic "cap dolomite" of the Trenton Group. Black arrow points to the contact. There is an increase in pyrite and phosphate at the contact. DPY, disseminated pyrite; SH, Blue Mountain shale; DSC, dolomitized sparry calcite; DGS, dolomitized geopetal sediment. (Cons et al. 33823 Mersea 1-12-A, 764.6 m depth.)

FRACTURE-RELATED POROSITY DEVELOPMENT AND DOLOMITIZATION

Migration of fluids undersaturated with respect to calcite along fractures resulted in 2 types of pore space:

Photo 353B.1. a) Bioturbated carbonate mudstone in the Gull River Formation of the Black River Group. Burrow centres (1) and formerly aragonitic bioclasts (2) have been replaced by sparry calcite. The lower carbonate mudstone (L) is tan with an overlying medium-brown carbonate mudstone (M), which is in turn overlain by dark brown carbonate mudstone (D). This sample is not dolomitized. (OGS 82-2 Chatham Harwich 25-IECR, 1159 m depth.) b) Overlying a carbonate mudstone is a fining-upward sequence beginning with a grainstone (G) at the base, followed by a carbonate mudstone (M), which in turn is overlain by another sharp-based grainstone. This sequence most likely represents a storm deposit. This sample is not dolomitized. (OGS 82-2 Chatham Harwich 25-IECR, 992 m depth.) c) Grainstone (G) interbedded with wackestone (W). This sample, located just below the oil-producing horizon, is dolomitized. (Cons et al. 34345 Romney 8-13-3, 848 m depth.) d) Dolomitized, nodular, bioclastic limestone with sucrosic dolomite developed in the former packstone-grainstone nodules. Porosity is pinpoint intercrystalline to vuggy, with minor saddle-dolomite cement and a few scattered sparry-calcite crystals. Arrow points to sparry-calcite crystal. (Cons et al. 33821 Mersea 3-12-I, 791 m depth.)

Photo 353B.3. **a)** Crackle breccia located in the oil-producing zone. Fragments are cemented together by anhydrite and contain stylolites in the early stages of development. (Cons et al. 33825 Mersea 7-14-A, 770 m depth.) **b)** Thin-section photomicrograph of a poorly developed stylolite (arrow) in a breccia fragment. The breccia fragment is cemented by a highly corroded rim of saddle dolomite (SD); the remainder of the pore space is occluded by anhydrite (A). (Cons et al. 33825 Mersea 7-14-A, 770 m depth.) Scale bar in lower left corner is 500 µm.

1) dissolution-enhanced fracture porosity (Photo 353B.4a) and 2) pinpoint intercrystalline to vuggy porosity in grainstone beds (Photo 353B.4b). Preferential dissolution of grainstone beds or nodules may be due either to incomplete primary cementation of the grainstone or to microporosity remaining along sparry-calcite crystal boundaries and creating natural pathways for migration of calcium carbonate undersaturated solutions. Dissolution varies from a minor amount at the edges of sparry crystals, creating intercrystalline porosity, to dissolution of sparry-calcite cement and bioclasts, creating vuggy to cavernous porosity.

Middle Ordovician oil pools in southwestern Ontario form linear trends up to 6 km by 1 km. The cross section of Renwick South (Figure 353B.4) depicts the following features: 1) cap dolomite; 2) fractured cap dolomite resulting from fractures transecting the upper few metres of the cap dolomite; 3) the remainder of the dolomite, referred to as "fracture-related massive dolomite"; 4) the abrupt change between wells from limestone to fracture-related dolomite; and 5) the presence of hydrocarbons only in the dolomitized section. In this example the hydrocarbon seal is the overlying nonporous Trenton limestones, but in other pools the shales of the Blue Mountain Formation or nonporous limestones of the Black River Group may be the seal. All wells in this cross section are approximately 500 m apart.

Three major types of dolomite have been identified: 1) cap dolomite, located in the upper few metres of the Trenton; 2) fracture-related dolomite, locally developed in the vicinity of fractures; and 3) saddle-dolomite cement, also fracture related, partially occluding both types of porosity (Figure 353B.5). Cap dolomite may be unaltered away from the fractures or is fractured cap dolomite where the upper few metres of the Trenton is cut by fractures.

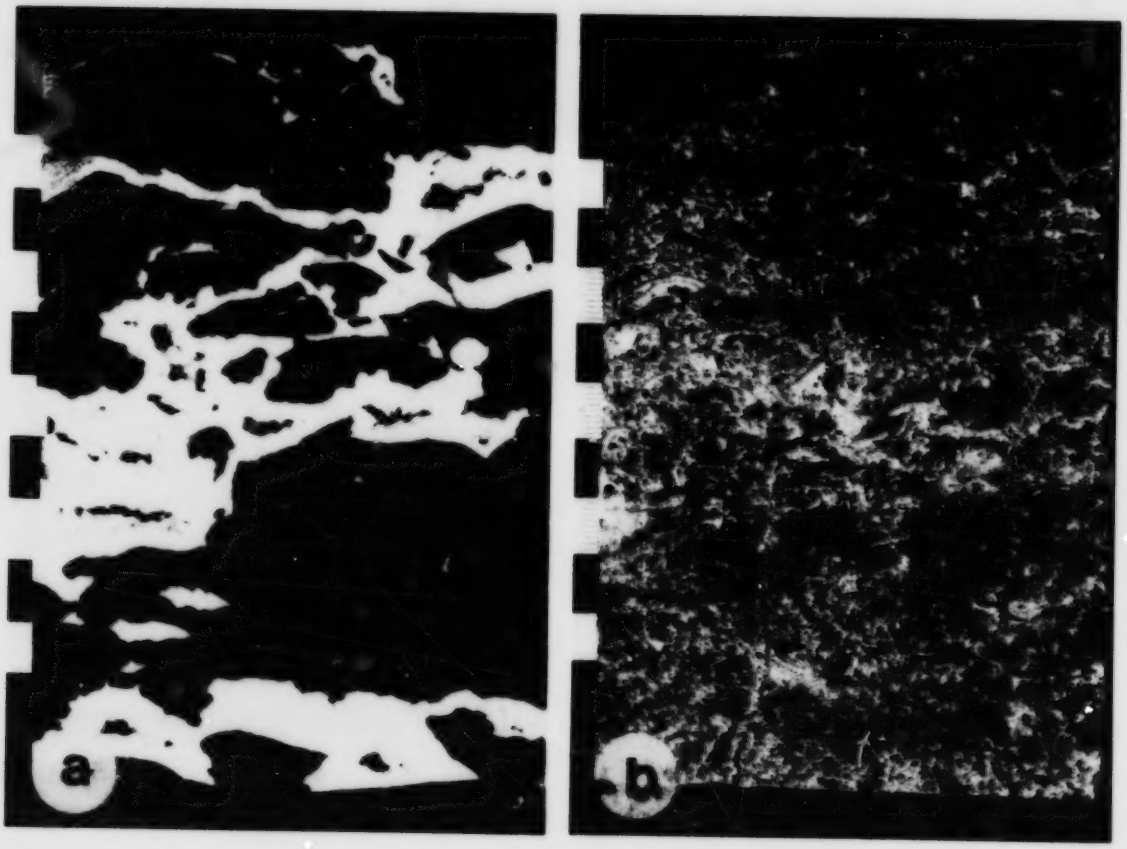

Photo 353B.4. a) Dolomitized breccia with stromatactis-like cavities incompletely cemented by saddle dolomite (white). (Cons et al. 33821 Mersea 3-12-1, 957 m depth.) **b)** Dolomitized grainstone with moderately well-preserved bioclasts. Pinpoint to vuggy intercrystalline porosity has been partially occluded by saddle dolomite and anhydrite. (Cons et al. 33823 Mersea 1-12-A, 780 m depth.)

Fracture-related dolomite may, in turn, be divided into 3 types based on porosity and nature of fabric preservation: 1) nonporous dolomite; 2) porous dolomite developed in grainstone with partial preservation of the original bioclasts; and 3) porous sucrosic dolomite in which all traces of original lithology have been destroyed, also developed in grainstone.

The 3 major types of dolomite (cap, fracture related and saddle) are also found as individual crystals throughout the limestone, decreasing in abundance with distance from massively dolomitized areas. In cathodoluminescence all massive dolomite is nonluminescent, but it becomes luminescent (red) with intricate zonation where disseminated in limestone. The increase in luminescence indicates a decrease in the iron content of the brines with distance travelled away from massively dolomitized areas and/or time. For all dolomite types the $\delta^{13}C$ values vary between –1.1 and +1.6‰ (Figure 353B.6).

Cap Dolomite

The cap dolomite is a nonporous, ferroan mosaic of xenotopic dolomite with cloudy cores, clear rims and undulose extinction. Undulose extinction is more easily detected in the larger crystals. Dolomite that has grown into phosphatized matrix or clays is hypidiotopic. The cap is typically more finely crystalline than the fracture-related massive dolomite. Crystal size in the cap dolomite is at least partially controlled by the original lithology: a dolomitized wackestone is more finely crystalline than a dolomitized grainstone. The only recognizable replaced bioclasts are echinoderm fragments preserved as an outline of relict inclusions within a larger dolomite crystal.

The $\delta^{18}O$ values are –8.3 to –7.3‰, with the most ^{18}O-enriched dolomite values encountered in massively dolomitized areas. The cap is the most ferroan of the dolomite types, with values between 3.2 and 11.4 mol % $FeCO_3$ (Figure 353B.7). In fact, dolomite directly adjacent to anhydrite-filled vugs within the cap is ankeritic. Compared with cap dolomite, the fractured cap dolomite has a lowered ferroan content of 2.1 to 4.5, with 2 ankeritic values of 9.5 and 10.1 mol % $FeCO_3$. The $\delta^{18}O$ of the fractured cap dolomite is –9.75 to –8.7‰.

Fracture-Related Dolomite

Fracture-related dolomite is porous in grainstone beds and nodules and nonporous elsewhere. In hand sample, nonporous massive dolomite displays excellent preservation of original texture. In contrast, porous

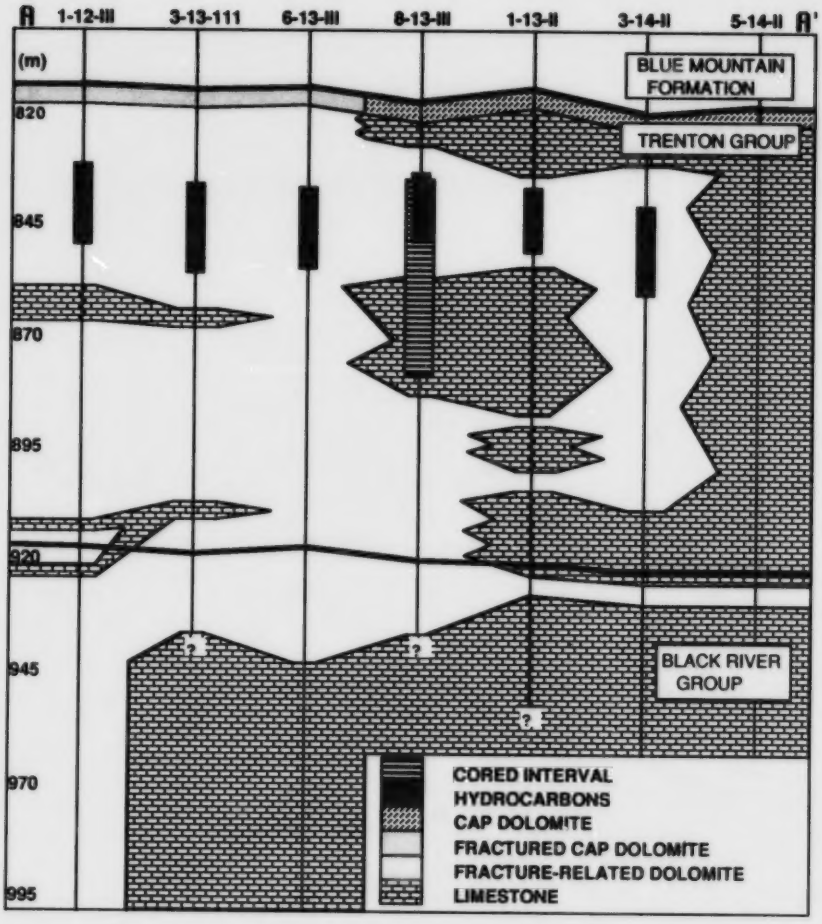

Figure 353B.4. Cross section of the Renwick South pool (A–A' in Figure 353B.1). In this example the cap dolomite can be distinguished from the fracture-related massive dolomite. There is no oil production in Cons et al. 34344 Romney 5-14-II, which has not been dolomitized. The wells are approximately 500 m apart.

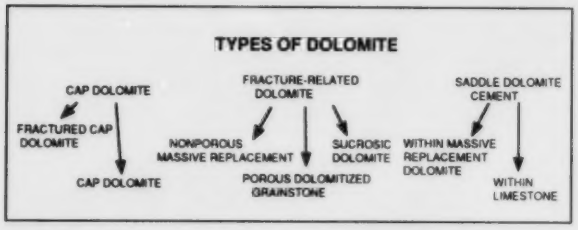

Figure 353B.5. Types of dolomite encountered in this study.

dolomitized grainstone is either sucrosic with original texture completely obscured or displays partial preservation of original texture.

All fracture-related massive dolomite types form a mosaic of xenotopic crystals with brown, inclusion-rich cores and undulose extinction. The exception is dolomitized echinoderm fragments, which do not have undulose extinction. Although, the nonporous dolomite and the porous, partially preserved grainstone dolomite display fair preservation of original texture in hand sample, in thin section the original depositional texture is barely discernible. In rare cases, a single dolomite crystal will replace an echinoderm fragment and retain the original shape of the fragment, or the outline of the original echinoderm will be preserved as relict inclusions.

The $\delta^{18}O$ for all fracture-related massive dolomite types varies between –11.2 and –8.5‰. The brown cloudy cores are more ferroan (2.8 to 4.1 mol % $FeCO_3$) than the crystal edges (1.7 mol % $FeCO_3$). This more to less ferroan trend of individual crystals is the opposite of that observed in the cap dolomite.

Sucrosic dolomite may remain as a friable mass of brown crystals (Photo 353B.5a), or intercrystalline pore space may be partially occluded by saddle dolomite, imparting a characteristic mottled brown-white colour in hand sample (Photo 353B.5b).

Saddle Dolomite

Volumetrically, saddle dolomite is the most abundant porosity-occluding precipitate. Saddle dolomite partially to completely occludes both fracture porosity and pinpoint to vuggy grainstone porosity. Saddle dolomite typically appears as pearly white (in hand sample), hypidiotopic crystals with curved faces and is up to 3 mm in size. As is

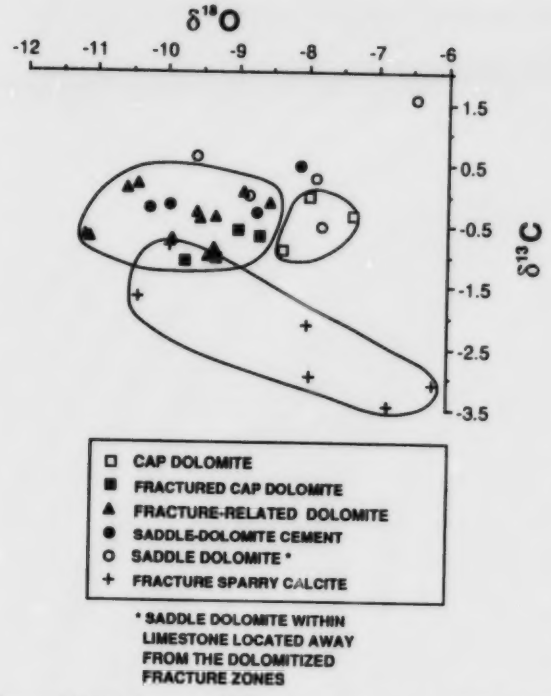

Figure 353B.6. Graph of $\delta^{18}O$ versus $\delta^{13}C$ (in per mil PDB) for dolomite and fracture calcite sampled in this study.

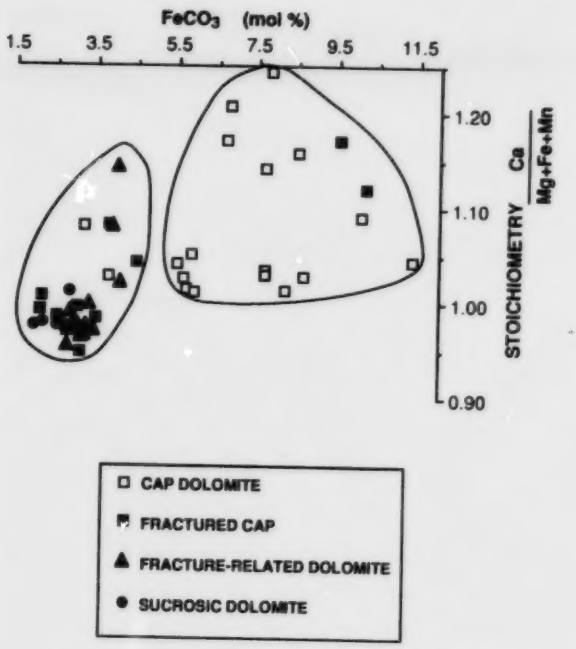

Figure 353B.7. Graph of $FeCO_3$ versus stoichiometry for the various types of dolomite.

characteristic of saddle dolomite, extinction is distinctly undulose. Most saddle-dolomite crystal faces appear smooth, but some may have corroded terminations in contact with either later sparry calcite or anhydrite. In stained thin sections, the pore-filling saddle dolomite exhibits 1 or 2 zones, each of which becomes more ferroan with progressive precipitation. Generally, only 1 zone is apparent in dolomite-cement-occluding grainstone porosity, and 2 zones can be seen in larger pore spaces such as fractures and vugs in grainstone. Lack of saddle-dolomite cement leaves a friable mass of sucrosic dolomite crystals. In contrast, partial occlusion of pore space imparts a slightly mottled, brown-white colour. Complete occlusion of pore space results in the mottled brown-white colour imparting a pseudo-brecciated appearance. The $\delta^{18}O$ values are the same as those of the fracture-related massive dolomite.

Saddle dolomite that has precipitated away from fracture-related massive dolomite replaces original sparry-calcite cement, especially in intraparticle pore spaces such as nautiloid chambers. Away from fracture-related massive dolomite, these crystals may exhibit intricately zoned red luminescence, suggesting a lower iron content, and $\delta^{18}O$ values may be as heavy as –6.5‰, the most ^{18}O-enriched dolomite values outside massively dolomitized areas. This suggests that the ferroan content and temperature of the brines or water/rock ratio decreased with distance from the main fracture system.

OTHER POROSITY-OCCLUDING PRECIPITATES

Following saddle-dolomite precipitation, remaining porosity was partially to completely occluded by sulphides, sparry calcite and anhydrite. The most common situation is saddle dolomite followed by either sparry calcite or anhydrite, but in rare cases sulphides follow saddle dolomite. Cons et al. 33825 Mersea 7-14-A, for example, has saddle dolomite followed by anhydrite in the upper Trenton sequence and saddle dolomite followed by sparry calcite in the middle Trenton. Sulphides, including pyrite and minor sphalerite, may coat or partially replace saddle dolomite. The sulphide coating may be followed by sparry calcite or anhydrite. Generally, the sulphides are absent or volumetrically unimportant with the exception of Cons et al. 34160 Romney 5-8-II, which contains a fracture system occluded by saddle dolomite and a larger than usual amount of sulphides. In some cases there is replacement of more ferroan zones within dolomite by sparry calcite or "dedolomite" (Middleton et al. 1990b).

Sparry-calcite crystals are up to 2 cm in diameter and are uniformly bright orange in cathodoluminescence, in contrast to typically nonluminescent saddle dolomite. The $\delta^{18}O$ values vary between –10.4 and –6.2‰, similar to those of other fracture-related carbonate precipitates. The $\delta^{13}C$ values include the lowest values encountered in this study (–3.5 to –0.8‰). The $MnCO_3$ content (0.01 to 1.18 mol %) is higher than any of the dolomite or earlier types of calcite, explaining the bright luminescence.

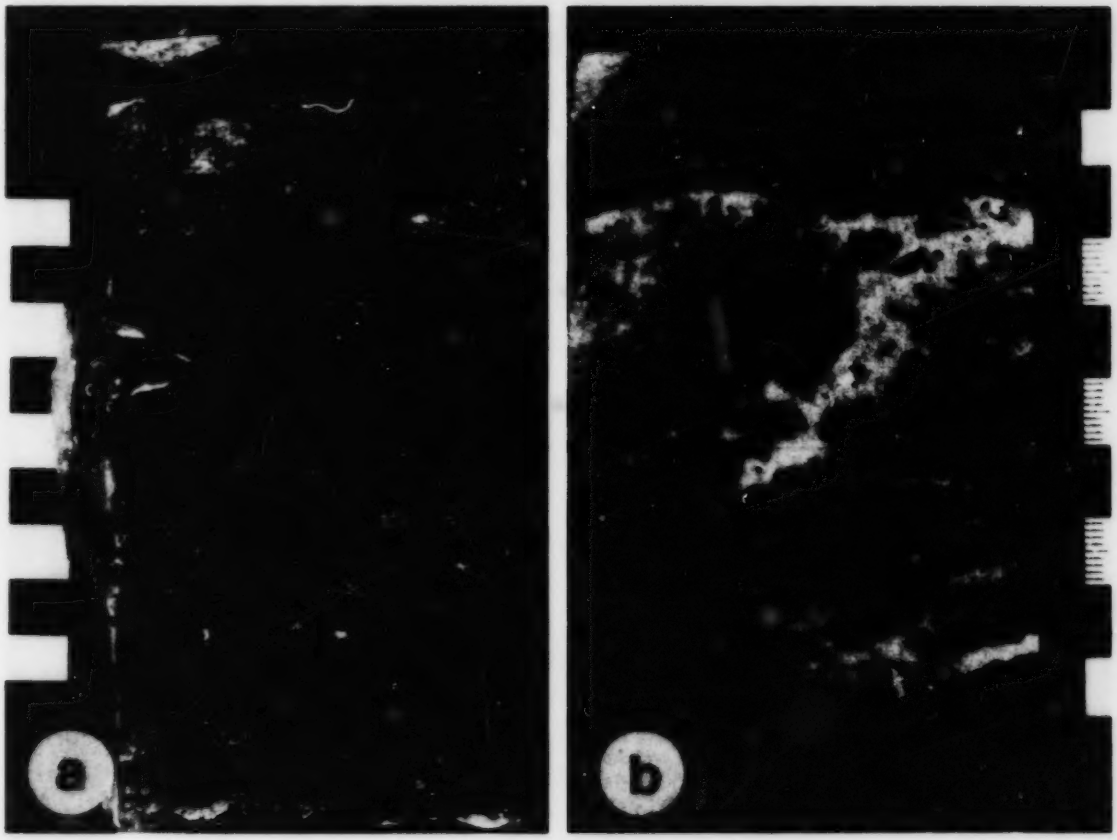

Photo 353B-5. a) This dolomitized nodular limestone has sucrosic dolomite and vuggy porosity developed in the packstone-grainstone nodules. In this sample there are a few scattered sparry-calcite crystals but no porosity reduction from saddle-dolomite cement. (Cons et al. 33823 Mersea 1-12-A, 787 m depth.) b) Porosity is nearly completely occluded by saddle-dolomite cement (white) imparting a white-brown mottling. A minor amount of porosity is seen in the upper right corner (arrow). (Cons et al. 33822 Mersea 5-11-I, 764 m depth.)

SUMMARY AND CONCLUSIONS

In summarizing some of the more important observations the following conclusions may be drawn:

1. Fracture-stylolite relationships indicate fracturing during burial following the onset of chemical compaction.
2. Solution enhancement along fractures increased fracture porosity, whereas dissolution along laterally extensive grainstone interbeds adjacent to the fractures resulted in pinpoint intercrystalline to vuggy porosity; both types of porosity are cement reduced.
3. Porosity enhancement may have preceded or been penecontemporaneous with dolomitization. There is no petrographic evidence to indicate either.
4. Compared with fracture-related dolomite, the cap dolomite is more ferroan and has slightly more positive $\delta^{18}O$ values. Where the cap is intersected by fractures, the $\delta^{18}O$ values become more negative and iron content is diminished, with values similar to those encountered in fracture-related massive dolomite. The cap and fracture-related dolomite do not have the same geochemistry, and the fractured cap is more similar in geochemistry to fracture-related dolomite. The decrease in $\delta^{18}O$ values from the cap to the fracture-related dolomite indicates that cap dolomitization occurred first, probably as a result of to dewatering and illitization of the Blue Mountain shale, as Taylor and Sibley (1986) suggested, followed by fracture-related dolomitization at increasing temperatures accompanying progressive burial.
5. The fracture-related massive dolomite and the saddle dolomite cement have the same range of $\delta^{18}O$ values and similar iron contents, indicating that fracture-related dolomitization and saddle-dolomite precipitation resulted from the same brine.

According to Radke and Mathis (1980) and Machel (1987), saddle dolomite precipitates from hypersaline brines at temperatures between 60° and 150°C. Both fracture-related replacement dolomite and saddle-dolomite cement are thus presumed to have been precipitated from hypersaline brines. However, it is unclear whether these brines were hydrothermal (i.e., characterized by anomalously high temperature for the burial depth of the sediment). In a study of the thermal history of the southern section of the Michigan Basin, Cercone (1984) suggested 1000 m of sediment was removed during post–Pennsylvanian erosion. Her study also indicated that a

higher geothermal gradient was present during basin subsidence (35° to 45°C/km). Hogarth and Sibley (1985) calculated a slightly lower geothermal gradient of 31°C/km. With 1000 m of sediment removed, the maximum burial depth of the top of the Trenton Group in southwestern Ontario before the post–Pennsylvanian unconformity was 1700 to 1900 m. If a generous 35°C/km geothermal gradient is assumed, the temperature at the maximum burial depth during the Mississippian would have been 80° to 87°C. This figure is in agreement with a temperature of 60° to 90°C determined by Legall et al. (1981) for Middle Ordovician sediments in southwestern Ontario. Therefore, it is possible that the brines responsible for dolomitization were not at an anomalously high temperature. However, the temperatures suggested above are at the low end of the 60° to 150°C range for saddle-dolomite precipitation. The migration of hydrothermal brines upward from below, therefore, remains a distinct possibility, although evidence for this is currently lacking. Underlying porous Cambrian sandstones could readily provide an aquifer for brine migration.

ACKNOWLEDGMENTS

This research forms part of Middleton's MSc thesis, which is supported by Natural Sciences and Engineering Research Council of Canada (NSERC) and Ontario Geoscience Research grants to M. Coniglio and S.K. Frape. The authors thank R. Trevail (Telesis Oil and Gas) and T.R. Carter (Ontario Ministry of Natural Resources) for their assistance in this study.

REFERENCES

Bailey Geological Services Ltd. and Cochrane, R.O. 1983. Evaluation of the conventional and potential oil and gas reserves of the Ordovician of Ontario; Ontario Geological Survey, Open File Report 5498, 77p.

Brett, C.E. and Brookfield, M.E. 1984. Morphology, faunas and genesis of Ordovician hardgrounds from southern Ontario, Canada; Palaeogeography, Palaeoclimatology, Palaeoecology, v.46, p.233-290.

Budai, J.M. and Wilson, W.L. 1988. Diagenetic history of the Trenton–Black River formations in the Michigan Basin; Proceedings of the Ontario Petroleum Institute, 27th Annual Conference, London, Ontario, October 23–25, Technical Paper, 1p.

Cercone, K.R. 1984. Thermal history of Michigan Basin; American Association of Petroleum Geologists Bulletin, v.68, p.130-136.

Churcher, P.L. 1985. Diagenesis and nature of the geological contacts in the Middle to early Upper Ordovician rocks in southwestern Ontario; unpublished BSc thesis, University of Waterloo, Waterloo, Ontario, 25p.

Churcher, P.L. and Majid, A.H. 1989. Similarities between the Tangent–Wabamun type play of the Alberta Basin and the Albion–Scipio type play of the Michigan Basin; Bulletin of Canadian Petroleum Geology, v.37, p.241-245.

Colquoun, I. and Brand, U. 1989a. Burial diagenesis, dolomitization and thermal maturation of the Ordovician Trenton Group carbonates, southwestern Ontario; Geological Association of Canada–Mineralogical Association of Canada, Program with Abstracts, v.14, p.A65.

———1989b. Paragenetic history of the Ordovician Trenton Group carbonates, southwestern Ontario; American Association of Petroleum Geologists, Annual Meeting, Program with Abstracts, v.14, p.A79.

DeHaas, R.J. and Jones M.W. 1988. Cave levels of the Trenton–Black River, in central southern Michigan; *in* The Trenton Group (Upper Ordovician Series) of eastern North America, edited by B.D. Keith, American Association of Petroleum Geologists, Studies in Geology no.29, p.237-242.

Dollar, P.S. 1988. Geochemistry of formation waters, southwestern Ontario, Canada and southern Michigan, U.S.A.—implications for origin and evolution; unpublished MSc thesis, University of Waterloo, Waterloo, Ontario, 129p.

Fara, D.R. and Keith, B.D. 1988. Depositional facies and diagenetic history of the Trenton Limestone in northern Indiana; *in* The Trenton Group (Upper Ordovician Series) of eastern North America, edited by B.D. Keith, American Association of Petroleum Geologists, Studies in Geology no.29, p.277-298.

Haefner, R.J., Mancuso, J.J., Frizado, J.P., Shelton, K.L. and Gregg, J.M. 1988. Crystallization temperature and stable isotope composition of Mississippi Valley-type carbonates and sulfides of the Trenton Limestone, Wyandot County, Ohio; Economic Geology, v.83, p.1061-1069.

Hogarth, C.G. and Sibley, D.F. 1985. Thermal history of the Michigan Basin: evidence from conodont coloration index; *in* Ordovician and Silurian rocks of the Michigan Basin and its margins, edited by K.R. Cercone and J.M. Budai, Michigan Basin Geological Society, Special Paper 4, p.45-58.

Keith, B.D. 1986. Reservoirs resulting from facies-independent dolomitization: case histories from the Trenton and Black River carbonate rocks of the Great Lakes area; Carbonates and Evaporites, v.1, p.74-82.

———1988. Regional facies of the Upper Ordovician Series of eastern North America; *in* The Trenton Group (Upper Ordovician Series) of eastern North America, edited by B.D. Keith, American Association of Petroleum Geologists, Studies in Geology no.29, p.1-16.

Legall, F. D, Barnes, C.R. and Macqueen, R.W. 1981. Thermal maturation, burial history and hotspot development in Paleozoic strata of southern Ontario–Quebec, from conodont and acritarch colour alteration studies; Bulletin of Canadian Petroleum Geology, v.29, p.492-539.

Machel, H.G. 1987. Saddle dolomite as a by-product of chemical compaction and thermochemical sulfate reduction; Geology, v.15, p.936-940.

Middleton, K., Coniglio, M. and Frape, S.K. 1989. Diagenesis of Middle Ordovician carbonate reservoirs, southwestern Ontario; Ontario Mines and Minerals Symposium, Geoscience Research Seminar, Toronto, Ontario, December 11–13, p.20.

———1990a. Fracture-related diagenesis as a control on Middle Ordovician carbonate reservoirs, southwestern Ontario. Bulletin of Canadian Petroleum Geology, v.38, p.173.

———1990b. Burial dedolomitization, Middle Ordovician carbonates, southwestern Ontario; American Association of Petroleum Geologists, Eastern Section Meeting, Program with Abstracts.

Packard, J.J., Pellegrin, G.J., Al-Aasm, I.S., Samson, I. and Gagnon, J. 1990. Diagenesis and dolomitization associated with hydrothermal karst in Famennian upper Wabamun ramp sediments, northwest Alberta; *in* The development of porosity in carbonate reservoirs, edited by G.R. Bloy and M.G. Hadley, Canadian Society of Petroleum Geologists, Continuing Education Short Course, p.9-1–9-20.

Prouty, C.E. 1988. Trenton exploration and wrenching tectonics—Michigan Basin and environs; *in* The Trenton

Group (Upper Ordovician Series) of eastern North America, edited by B.D. Keith, American Association of Petroleum Geologists, Studies in Geology no.29, p.207-236.

Radke, B.M. and Mathis, R.L. 1980. On the formation and occurrence of saddle dolomite; Journal of Sedimentary Petrology, v.50, p.1149-1168.

Rooney, L.F. 1966. Evidence of unconformity at top of Trenton Limestone in Indiana and adjacent states; American Association of Petroleum Geologists Bulletin, v.50, p.533-548.

Russell, D.J. and Telford, P.G. 1983. Revisions to the stratigraphy of the Upper Ordovician Collingwood beds of Ontario—a potential oil shale; Canadian Journal of Earth Sciences, v.20, p.1780-1790.

Shaw, B. 1975. Geology of the Albion–Scipio trend, southern Michigan; unpublished MSc thesis, University of Michigan, Ann Arbor, Michigan, 69p.

Sibley, D.F. 1982. The origin of common dolomite fabrics: clues from the Pliocene; Journal of Sedimentary Petrology, v.52, p.1087-1100.

Taylor, T.R. and Sibley D.F. 1986. Petrography and origin of ferroan dolomite in the Trenton Formation, Ordovician, Michigan Basin, USA; Sedimentology, v.33, p.61-86.

Trevail, R.A. 1988a. Tectonic and diagenetic controls on development of the Hillman pool, Trenton Group, southwestern Ontario; Geological Association of Canada–Mineralogical Association of Canada–Canadian Society of Petroleum Geologists, Joint Annual Meeting, Program with Abstracts, v.13, p.A126.

———1988b. The enigma of karst features in the Trenton and Black River groups of southwestern Ontario: fact or fantasy? Proceedings of the Ontario Petroleum Institute, 27th Annual Conference, London, Ontario, October 23–25, Technical Paper 14, 2p.

Trevail, R.A., Pakvis, P.J. and Brown, S. 1989. Oil and gas exploration drilling and production summary, 1984; Ontario Ministry of Natural Resources, Oil and Gas Paper 7, 190p.

Grant 357 Diagenetic Evolution of Cambro-Ordovician Clastic Sedimentary Rocks, Southwestern Ontario

F.J. Longstaffe[1], M.A. Wadleigh[1], S.K. Frape[2] and R.H. McNutt[3]

[1]Department of Geology, The University of Western Ontario, London
[2]Department of Earth Sciences, University of Waterloo, Waterloo
[3]Department of Geology, McMaster University, Hamilton

ABSTRACT

Cambrian Mt. Simon Formation–Eau Claire Formation interbedded sandstones and sandy dolostones and Ordovician Shadow Lake Formation argillaceous sandstones are stratigraphically situated on Precambrian basement at the interface between the Appalachian and Michigan basins. This unique location provides an opportunity to examine diagenetic effects resulting from water-rock interaction involving multiple fluid sources, possibly including Precambrian basement brines.

A striking feature of these sandstones is the abundance of K-feldspar to the virtual exclusion of other feldspars. K-feldspar occurs as detrital grains, overgrowths and euhedral, authigenic crystals. Diagenetic phases are enriched in K and depleted of Na and Ba relative to their detrital equivalents. Widespread potassic alteration has been recognized elsewhere in midcontinental North America. Similar, if not the same, type of alteration may have affected the Cambrian section in southwestern Ontario. The present formation waters, however, consist of Na-(Ca)-Cl-rich brines thought to be a mixture of 2 end-member fluids.

A variety of other diagenetic minerals are observed. Early diagenetic glauconite of intermediate composition is found near the top of the Cambrian section and within the Ordovician sandstones. Fine-grained clay, mostly illite ± chlorite, partially fills pores between detrital quartz and feldspar grains. It appears to predate dolomite and calcite cements and perhaps some quartz overgrowths.

Dolomite is the most common carbonate cement. It occurs as euhedral rhombs within pores, partially replacing K-feldspar, and as a massive pore filler. Some varieties exhibit regular chemical zonation of iron and manganese; others display complex intergrowths of Fe-Mn-rich and Fe-Mn-poor phases. Dolomite crystallization appears to postdate formation of diagenetic pyrite, matrix illite and most calcite cement. Calcite occurs as scattered inclusions within dolomite, as cores to dolomite rhombs and as a massive pore filler.

The diagenetic mineralogy of the sandy dolostones is similar to that of the sandstones except that a minor amount of smectitic clay occurs together with illite in the <2 μm size fraction. The preservation of smectitic clay in the sandy dolostone suggests isolation of that portion of the pore system during subsequent major diagenetic episodes.

INTRODUCTION

Chemical and isotopic compositions of formation waters reflect a variety of physical and chemical processes that occur during deposition and diagenesis (Clayton et al. 1966; Hitchon and Friedman 1969). McNutt et al. (1987) and Dollar et al. (1988) illustrated this point for pore waters from the Michigan and Appalachian basins. The oxygen and hydrogen isotopic compositions of these brines plot below the meteoric waterline (Craig 1961), with Cambrian and Ordovician samples plotting closest to the line. For some samples, mixing of brines and surficially derived waters is indicated, but other more concentrated brines from each stratigraphic unit display a very narrow spread in isotopic composition. Ordovician brines, in particular, show such a narrow range in Sr, O, and H isotopic composition over at least 200 km that extensive lateral migration and/or homogenization of present pore waters is indicated. McNutt et al. (1987) demonstrated that the $^{87}Sr/^{86}Sr$ of brine samples varies from 0.708 to 0.711. With the exception of the Silurian Salina Formation evaporites, most values are greater than that of seawater for the geologic period in question, indicating a high degree of water-mineral interaction. The source of the radiogenic strontium, however, remains unidentified. Strontium in the formation waters has not equilibrated isotopically with its host minerals, except for certain very late-stage phases, such as dolomite, calcite and anhydrite.

These data indicate that the present formation-water compositions are the end product of a myriad of fluid mixing and water-rock interactions. McNutt et al. (1987) suggested that this evolution may have involved components of deep (Precambrian) fluids (source of the excess radiogenic strontium?) and downward-migrating freshwaters (during Pleistocene and more recent time?). By comparison, Steuber et al. (1987) argued that the Sr isotopic signature of Illinois Basin brines reflected that of shale units within the basin.

Cambrian and Ordovician sandstones in southwestern Ontario should have experienced intense interaction with putative Precambrian-derived or transported brines. Diagenetic minerals from these units may preserve a geochemical record of such water-rock interaction. Schwartz and Longstaffe (1988) reviewed the effects of fluid-controlled mass transport on clastic diagenesis. Diagenetic minerals formed in equilibrium with pore waters obtain chemical and isotopic signatures characteristic of that pore water. These compositions can be used to reconstruct

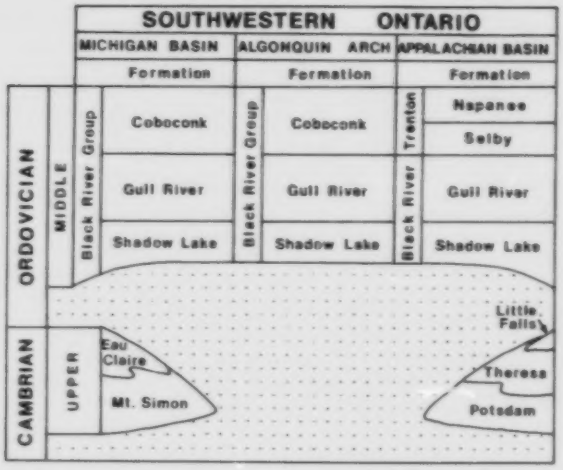

Figure 357.1. Stratigraphic section of lower Paleozoic sequence in southwestern Ontario. Shaded area represents a presumed hiatus (*after* Winder and Sanford 1972).

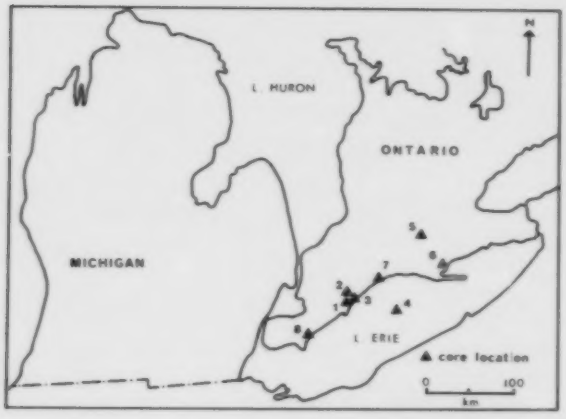

Figure 357.2. Location map of study area and sampled drill cores. 1) Imperial 829 Buch 1; 2) Canadian Kewanee Downie #101; 3) Canadian Delhi; 4) Consumers Pan-Am; 5) McMaster #31 Gobles 20; 6) U.S. Steel-DDH1; 7) OGS-82-3; 8) Imperial Oil #616.

pore-water evolution throughout diagenesis, provided that the prerequisite information on mineralogy, mineral chemistry and paragenesis of the units has been obtained (Longstaffe 1987, 1988, 1989). This approach has been successfully applied to the western Canada sedimentary basin (Longstaffe and Ayalon 1987; Ayalon and Longstaffe 1988; Longstaffe 1983, 1984, 1986; Tilley and Longstaffe 1989; Tilley et al. 1989). With the exception of a few isotopic analyses of carbonate and sulphate minerals (McNutt et al. 1987; Fritz et al. 1988; O'Shea et al. 1988), no isotopic data for diagenetic minerals from southwestern Ontario are available in the literature.

REGIONAL STRATIGRAPHY

Upper Cambrian and Lower Ordovician strata in southwestern Ontario are primarily confined to the subsurface. Basal Cambrian strata (Figure 357.1) are arkosic conglomerates and red, white and grey arenitic sandstones of the Mt. Simon (Potsdam) Formation. These grade upward into alternating sandstones and grey or grey-tan, finely crystalline oolitic dolostones and grey, argillaceous and glauconitic dolostones of the Eau Claire (Theresa) Formation. The youngest Cambrian strata (Trempealeau (Little Falls) Formation) are tan and light brown, fine to medium crystalline dolostones. These 3 subdivisions can be traced along the southern flank of the Algonquin Arch in Ontario but become diachronous as they enter the Appalachian Basin (Winder and Sanford 1972).

The Black River Group represents the oldest Ordovician rocks in southwestern Ontario. It consists of the Shadow Lake, Gull River and Coboconk formations (Figure 357.1). The Shadow Lake Formation is composed of maroon, red and green, silty and calcareous shales and siltstones alternating with argillaceous, dolomitic limestones.

OBJECTIVES

The Cambrian Mt. Simon and Eau Claire formations and the Ordovician Shadow Lake Formation are located in an area that forms a critical boundary between the Michigan and Appalachian basins. They therefore provide an opportunity for one to examine the diagenetic influence of a number of potential fluid reservoirs including 1) brines from the Precambrian basement, 2) carbonate-equilibrated basin brines (from intercalated carbonate-rich units), 3) connate waters associated with evaporite deposits (e.g., Silurian Salina Formation), 4) shale-derived pore waters (e.g., moving outwards from Ordovician shales or downwards from Silurian shale (Medina)), 5) surface-derived meteoric water and 6) interbasinal fluid transport and mixing. Of particular interest is whether these rocks have participated in the major episode of potassic diagenesis recognized elsewhere in midcontinental North America (e.g., Duffin 1989; Duffin et al. 1989).

SAMPLING AND ANALYTICAL

Seventy-one samples of sandstone and dolostone from Cambro-Ordovician strata have been collected from the following 8 drill cores (Figure 357.2): 1) Imperial 829 Buch 1 (Kent Co., Orford Tp., Lot 52, Conc. NTR); 2) Canadian Kewanee Downie #101 (Elgin Co., Aldborough Tp., Lot 1, Conc. Gore); 3) Canadian Delhi (Elgin Co., Aldborough Tp., Lot 8, Conc. X); 4) Consumers Pan-Am (Elgin Co., Lake Erie, #13039); 5) McMaster #31 Gobles 20 (Brant Co., Burford Tp., Lot 15, Conc. I); 6) U.S. Steel-DDH1 (Norfolk Co., Charlotteville Tp., Lot 21, Conc. I); 7) OGS-82-3 (Elgin Co., Yarmouth Tp., Lot 9, Conc. 1); 8) Imperial Oil #616 (Kent Co., Romney Tp., Lot A, Conc. Gore). Ten additional cores have been logged, and sampling is in progress.

Samples from the first 8 wells include green sandstones from the Shadow Lake Formation (Middle Ordovician), oolitic stringers from the Trempealeau Formation (Upper Cambrian), fine-grained dolomitic sandstones and sandy dolostones from the Eau Claire Formation (Upper Cambrian) and well-sorted, coarse-grained sandstones from

the Mt. Simon Formation (Upper Cambrian). A few samples of the Cambrian-Precambrian contact have also been obtained.

Identification of diagenetic phases has utilized X-ray diffraction (XRD), scanning electron microscopy (SEM), energy-dispersive X-ray analysis (EDX), petrography, cathodoluminescence, backscattered electron imaging (BEI) and the electron microprobe.

RESULTS

Bulk Mineralogy

Detailed point counting (over 500 points) and XRD analysis of representative samples have enabled classification of the rocks into 4 major types: quartz arenites, dolomitic quartz sandstones, dolomitic arkoses and sandy dolostones.

The abundance of 10 Å phyllosilicates (micas, illitic clays) increases relative to the bulk sample in the 2 to 20 μm fraction from all rock types. In the same size fraction from sandy dolostones, the abundance of quartz also increases.

Clay Mineralogy

Preliminary examination of the <2 μm (clay) size fraction from the 4 major rock types has revealed 2 somewhat distinct assemblages. The dolomite-poor sandstones contain a significant fraction of K-feldspar, 10 Å clay minerals (illitic clays ± mica) and minor amounts of 14 Å clay (chlorite group) (Figure 357.3a). No smectite-group clay minerals have been detected; the occurrence of kaolin-group minerals is as yet unproven. In dolomite-rich samples, the <2 μm material is dominated by calcite but also contains K-feldspar and a smectite-group clay mineral (at approximately 17 Å, Ca-glycol treatment) ± 10 Å (illitic) clays (Figure 357.3b). Kaolin-group minerals have not been detected. Whether the smectitic clay minerals are detrital or diagenetic is unclear at present. The occurrence of calcite and smectitic clays in these samples is of special interest: the reaction dolomite + quartz + H_2O = smectite + calcite + CO_2 is characteristic of low-temperature, hydrothermal alteration of such rock types (e.g., Hebner et al. 1986; Kirk et al. 1987).

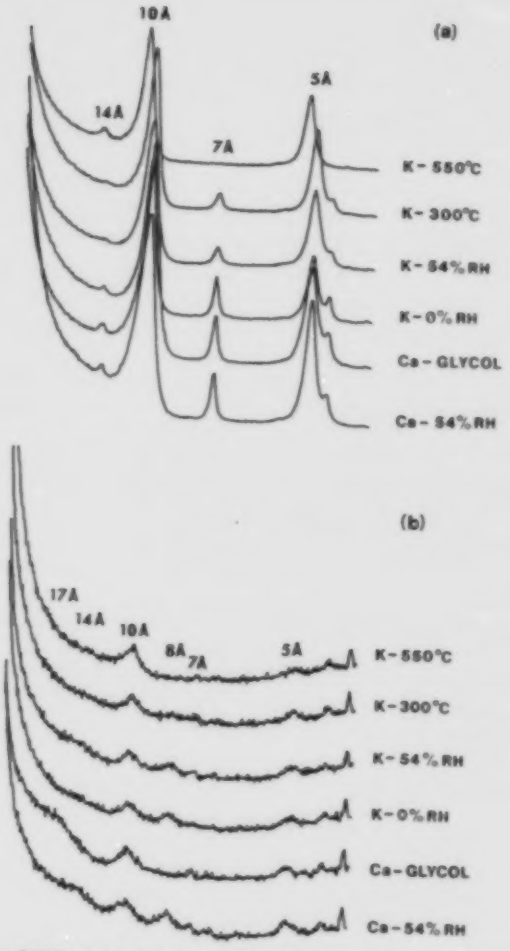

Figure 357.3. a) A set of 6 typical X-ray diffractograms for the <2 μm size fraction obtained from a dolomite-poor sandstone: Ca-saturated at 54% relative humididty (RH); Ca-glycol solvated; K-saturated at 0% RH; K-saturated at 300°C; and K-saturated at 550°C. Peaks: 14 Å, chlorite (001); 10 Å, illite (001); 7 Å, chlorite (002) ± kaolinite (001); 5 Å, illite (002). b) A set of 6 typical X-ray diffractograms for the <2 μm size fraction obtained from a dolomite-rich sandstone. Treatments as described in (a). Peaks: 17 Å, glycol smectite (001); other interpretations as in (a).

Chemical Characterization

We obtained 450 quantitative chemical analyses of detrital and diagenetic minerals, as well as matrix clays of uncertain origin (e.g., neoformed, transformed, detrital), using a JEOL 8600 electron microprobe and appropriate standards. Analyses of clays, carbonates and feldspars were performed at an accelerating voltage of 15 kV, a sample current of 10 Na, a beam diameter of 1 to 5 μm and counting times of 20 s.

GLAUCONITE

Rounded grains of glauconite are observed in samples located near the top of the Cambrian section and in the Ordovician sandstones. The glauconite comprises mostly 10 Å clay minerals; its average chemical composition lies midway in the range for glauconite (Velde and Meunier 1987) (Table 357.1). Glauconite formation is typical of slow, shallow-marine sedimentation and is particularly abundant in Cambro-Ordovician rocks on a worldwide basis, perhaps reflecting a major episode of global sea-level rise.

PHYLLOSILICATES

Fine-grained clay matrix is most abundant filling pores between detrital quartz and feldspar grains. It predates formation of most quartz and K-feldspar overgrowths and, apparently, crystallization of dolomitic and calcitic cements (Photo 357.1a). Clay is less commonly associated with K-feldspar alteration. Other clay occurrences are intermixed with pyrite and may be related to glauconite destabilization reactions. Both XRD and chemical data confirm that this

Table 357.1 Summary of average chemical compositions (weight percents) of clay minerals.

Sample no.	SiO_2	Al_2O_3	Na_2O	K_2O	CaO	MgO	BaO	MnO	FeO	TiO_2	Cr_2O_3	F	Cl	Total
						Glauconite								
(*n*=36)	52.37	11.53	0.04	8.19	0.21	5.63	0.16	0.02	13.75	0.41	0.02	0.67	0.07	92.56
						Matrix clay								
OGS-10 (*n*=9)	49.42	23.19	0.10	7.96	1.05	4.07	0.05	0.03	3.81	0.51	0.00	0.14	0.01	90.34
OGS-14 (*n*=9)	52.83	21.25	0.11	8.97	1.19	3.26	0.09	0.04	2.85	0.56	0.00	0.00	0.00	91.15
OGS-25 (*n*=5)	53.98	22.50	0.08	7.82	0.38	3.28	0.00	0.00	3.36	1.48	0.03	0.03	0.03	92.88
OGS-32 (*n*=8)	44.90	21.65	0.06	6.51	0.32	4.32	0.01	0.00	4.32	0.27	0.00	0.06	0.14	82.56
OGS-33 (*n*=4)	50.47	25.35	0.04	6.05	0.26	3.59	0.00	0.00	3.51	0.00	0.00	0.00	0.09	89.36
						Fe-Mg-rich clay								
OGS-32 (*n*=3)	26.54	22.70	0.05	0.10	0.04	12.29	0.00	0.00	22.71	0.00	0.00	0.10	0.01	84.54
OGS-33 (*n*=2)	26.07	21.56	0.00	0.07	0.00	11.95	0.00	0.00	27.86	0.02	0.00	0.28	0.00	87.81
OGS-51 (*n*=2)	27.33	21.91	0.03	0.13	0.19	15.31	0.00	0.07	20.29	0.01	0.02	0.18	0.04	85.51

material is illitic (Newman and Brown 1987) (Table 357.1). SEM, mineral separation and stable isotope studies are in progress to determine whether this clay is detrital, transformed or neoformed; this characterization is a prerequisite to radiogenic isotope measurements.

QUARTZ

Quartz occurs as well-rounded grains and as overgrowths. The continuity of some quartz overgrowths is disrupted by K-feldspar crystals or illitic clay matrix (Photo 357.1a). Overgrowth formation appears to predate carbonate cementation.

K-FELDSPAR

The high abundance of K-feldspar, to the virtual exclusion of other feldspars, is a striking feature of these rocks. It is most common as detrital grains upon which abundant K-feldspar overgrowths have developed (Photos 357.1a and 357.1b). The K-feldspar overgrowths have a "purer" chemical composition, being enriched in K and depleted of Ba and Na relative to their detrital substrates (Table 357.2); low Ba contents appear to be particularly diagnostic of overgrowths. In one sample, "pits" in the detrital grains were filled with barite. The samples also contain euhedral K-feldspar crystals in pore space (Photo 357.1a), K-feldspar-rich fine-grained matrix and K-feldspar partially altered to illite or replaced by dolomite. The chemical compositions of these types are most similar to those of the K-feldspar overgrowths, except for somewhat higher Na and K contents (Table 357.2). Some K-feldspar grains and overgrowths appear chemically corroded (Photo 357.1c).

DOLOMITE

Dolomite cement is common in some samples and entirely absent in others. Five textural varieties can be recognized (Table 357.3): 1) dolomite replacement of K-feldspar (and perhaps quartz?), generally Fe poor (FeO < 2.5%); 2) zoned, rhombic crystals—alternating Fe-Mn-rich and Fe-Mn-poor bands on a micrometre scale—that have grown in pore space and can interrupt K-feldspar overgrowth development (Photo 357.1d); 3) pore-filling, mottled (in backscattered electron image) dolomite, with irregular distribution of high and low Fe-Mn contents on a micrometre scale; 4) dolomite rims of variable Fe-Mn content with calcite cores; and 5) pore-filling dolomite containing irregularly shaped inclusions of calcite (Photo 357.1c). Dolomite appears to postdate formation of diagenetic pyrite, matrix illite and most calcite cement. It also appears to postdate most K-feldspar and quartz overgrowths.

CALCITE

Calcite is less common than dolomite, but in some samples it is the only pore-filling carbonate present. Three textural varieties have been identified: 1) calcite included within pore-filling dolomite (poikilotopic?) (Photo 357.1c), 2) massive pore-filling calcite (Photo 357.1c) and 3) calcite cores to dolomite rhombs. The Fe, Mn and Mg contents of all varieties are low (<2.5%) (Table 357.3).

ACCESSORY MINERALS

Other minerals have been observed in minor to trace quantities. Most significant in abundance is pyrite, which occurs as euhedral, diagenetic crystals that are commonly intergrown with illitic clay matrix or nucleated along the edges of K-feldspar crystals, including overgrowths. Detrital rutile, zircon and sphene are also present. Locally abundant apatite and fluorite of uncertain origin have been documented, and vugs filled with anhydrite are present in some samples.

Paragenetic Sequence

Based on petrographic and electron microprobe observations, the following preliminary paragenetic sequence is suggested: K-feldspar overgrowths (± authigenic K-feldspar, ± glauconite); quartz overgrowths (+ some authigenic K-feldspar); grain-coating (illitic) clay; pyrite (?); early calcite; dolomite; late calcite. As SEM work proceeds, many of the details will be clarified.

Table 357.2 Summary of average chemical compositions (weight percents) of K-feldspars.

Sample no.	SiO_2	Al_2O_3	Na_2O	K_2O	CaO	BaO	SrO	Total
Detrital K-feldspar								
OGS-2 (n=8)	63.58	18.21	1.09	14.65	0.00	1.63	0.20	99.36
OGS-8 (n=3)	64.25	18.77	1.25	14.46	0.04	1.38	0.28	100.43
OGS-10 (n=17)	65.51	18.29	0.66	15.54	0.03	0.38	0.17	100.57
OGS-14 (n=6)	64.22	18.60	1.14	14.99	0.06	1.04	0.00	100.03
OGS-18 (n=3)	62.66	19.11	1.40	13.65	0.00	3.49	0.13	100.47
OGS-21 (n=5)	64.14	18.72	0.93	15.05	0.03	1.75	0.04	100.65
OGS-22 (n=8)	63.14	19.59	1.03	14.83	0.03	0.89	0.06	99.51
OGS-25 (n=15)	66.51	18.58	0.73	14.92	0.00	0.27	0.26	100.28
OGS-31 (n=4)	65.05	18.76	0.71	15.58	0.00	0.35	0.00	100.45
OGS-32 (n=4)	65.96	18.37	0.44	14.62	0.02	0.26	0.00	99.67
OGS-33 (n=4)	64.50	18.35	0.34	15.70	0.00	0.57	0.00	99.46
OGS-40 (n=5)	65.87	18.48	0.82	14.67	0.03	0.88	0.00	100.75
OGS-46 (n=5)	65.18	18.18	1.14	14.45	0.07	0.28	0.00	99.30
OGS-63 (n=8)	63.24	18.17	0.61	17.12	0.01	0.61	0.00	99.76
K-feldspar overgrowths								
OGS-2 (n=4)	65.59	17.95	0.11	16.76	0.00	0.02	0.11	100.34
OGS-8 (n=2)	66.27	18.22	0.00	16.52	0.00	0.03	0.29	101.22
OGS-18 (n=3)	64.83	18.29	0.04	16.64	0.12	0.02	0.10	100.03
OGS-21 (n=2)	66.14	18.24	0.05	16.88	0.02	0.01	0.00	101.32
OGS-22 (n=6)	64.65	18.93	0.05	16.20	0.05	0.02	0.02	99.91
OGS-31 (n=5)	66.11	18.51	0.03	15.01	0.02	0.00	0.00	99.68
OGS-46 (n=2)	65.81	17.69	0.04	15.07	0.04	0.00	0.00	98.65
OGS-63 (n=2)	65.36	18.04	0.02	19.11	0.00	0.04	0.00	102.57
Euhedral K-feldspar								
OGS-8 (n=3)	65.99	18.21	0.03	16.10	0.01	0.00	0.01	100.35
OGS-18 (n=3)	64.98	18.31	0.67	15.11	0.04	0.40	0.26	99.77
OGS-22 (n=11)	63.97	19.13	0.57	15.86	0.03	0.23	0.01	99.81
Altered K-feldspar								
OGS-14 (n=5)	65.35	18.68	0.63	15.96	0.05	0.26	0.00	100.92
OGS-21 (n=12)	65.29	18.48	0.36	15.86	0.02	0.13	0.00	100.13
OGS-22 (n=4)	63.00	19.23	0.40	16.00	0.02	0.17	0.02	98.83
OGS-32 (n=2)	66.44	17.14	0.67	12.99	0.00	0.00	0.00	97.24
OGS-33 (n=5)	64.24	19.01	0.15	13.86	0.09	0.12	0.00	97.47
OGS-40 (n=10)	67.30	18.24	0.09	14.93	0.06	0.08	0.00	100.70
OGS-63 (n=5)	64.15	17.88	0.32	19.45	0.01	0.07	0.00	101.88
Matrix K-feldspar								
OGS-8 (n=3)	66.68	18.52	0.49	13.62	0.08	0.15	0.01	99.54

Formation-fluid Geochemistry

Cambro-Ordovician formation waters were sampled from 10 wells throughout southwestern Ontario, in particular along the north shore of Lake Erie, and their chemical and isotopic compositions (O, H, Sr) determined. The results were integrated with the data of Dollar et al. (1988) and plotted in Figures 357.4 and 357.5. The major observation is that interbasinal mixing appears to be an important control on the formation-fluid chemistry.

In a recent discussion of brines from Silurian age strata in Ohio, Lowry et al. (1988) concluded that many samples are mixtures of 2 end-member fluids: a Ca-rich water derived from the Appalachian Basin and a Na-rich water that probably originated in the Michigan Salina Formation. Such a concept can be applied to explain the compositions of Cambro-Ordovician formation waters within southwestern Ontario. A plot of Ca/Na ratios for the formation waters (Figure 357.4) suggests that a relatively dilute

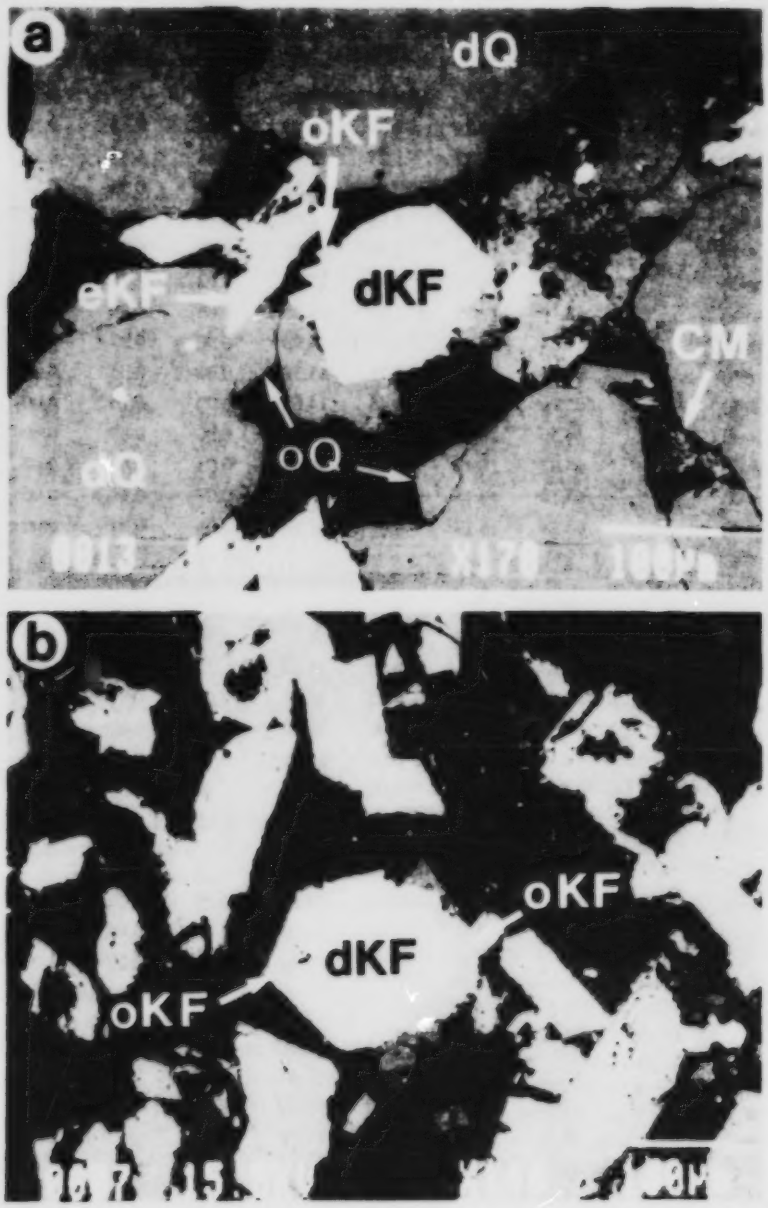

Photo 357.1. a) Backscattered electron image (BEI) of dolomitic arkosic sandstone. CM, clay matrix; d, detrital; eKF, euhedral K-feldspar; KF, K-feldspar; o, overgrowth; Q, quartz. b) BEI of arkosic sandstone. Symbols as in (a).

Na-(Ca)-Cl-rich brine (total dissolved solids (TDS) <150 g L^{-1}) migrated into the study area from the south-southwest. A plot of TDS throughout southwestern Ontario (Figure 357.5) confirms this observation. The exact nature and extent of fluid movement are still uncertain because of the limitations on sampling to the northeast and the paucity of published data for formation waters located farther south. However, it appears that dilute Na-(Ca)-Cl brines moving into southwestern Ontario mixed with pre-existing formation waters across most units, beginning with the Ordovician carbonate sequence to the southwest, moving through Cambrian and Silurian sandstones and into Silurian carbonate reefs near Lake Huron. Silurian sandstones in the vicinity of eastern Lake Erie appear to have been recharged by a separate tongue of this dilute Na-(Ca)-Cl brine, as were Cambrian sediments located in the same area. Diagenesis of the Cambro-Ordovician section should have been particularly strongly influenced by infiltration of this Na-(Ca)-Cl brine.

Structural and tectonic features may have facilitated fluid movement. The Algonquin Arch, trending in a southwest direction beneath southern Ontario, forms a broad, positive, basement lineament from which overlying Paleozoic strata either dip westward into the Michigan

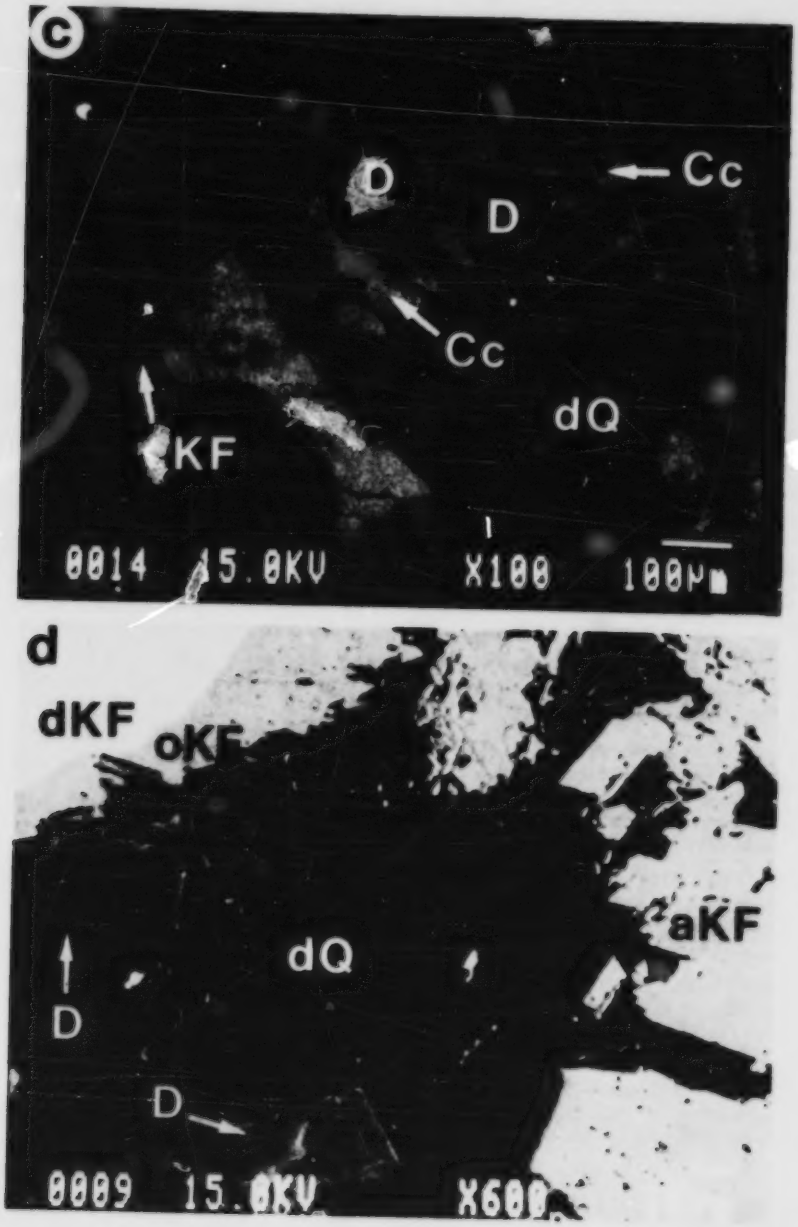

Photo 357.1 (concluded). **c)** BEI of dolomitic arkosic sandstone. Cc, calcite; cKF, corroded K-feldspar; D, dolomite; dQ, detrital quartz. **d)** BEI of arkosic sandstone. Symbols as in (a), (b) and (c).

Basin or southward into the Appalachian Basin (Winder and Sanford 1972). The location of arches and the maximum density of putative fractures appear to correspond to the major western expression of brine incursion into these sediments. The implication is that the Na-(Ca)-Cl brine entered both the Appalachian and Michigan basins, using large fracture systems and/or basement highs as conduits. Such fluid movement would be focussed in the Precambrian, Cambrian and Ordovician interface in southwestern Ontario. Depending on the age and extent of this migration event, it should have imparted a significant diagenetic signature to these rocks. The origin of the waters remains uncertain; dissolution of Salina salt beds is one possibility, but a source farther to the south, perhaps near the termination of the Findlay Arch (in the Illinois Basin?), is equally plausible.

SUMMARY

Mineralogical, geochemical and isotopic studies of Cambro-Ordovician clastic rocks from southwestern Ontario are underway to elucidate the area's diagenetic history. The general objectives are 1) to deduce the nature of fluids and temperatures involved in mineral reactions;

Table 357.3 Summary of average chemical compositions (weight percents) of diagenetic carbonates.

Description	CaO	MgO	BaO	SrO	MnO	FeO	Total
			Dolomite				
Zoned rhombs							
Bands >2.5% FeO (n=17)	30.02	18.90	0.00	0.00	0.67	3.39	52.98
Bands <2.5% FeO (n=22)	30.42	20.67	0.00	0.01	0.30	1.31	52.71
Mottled pore filler							
High-Fe areas (n=18)	29.05	18.48	0.01	0.02	0.98	4.96	53.50
Low-Fe areas (n=16)	29.99	22.33	0.01	0.00	0.17	0.91	53.41
Replacing K-feldspar (n=6)	30.95	19.26	0.00	0.00	0.33	2.11	52.66
Rim on calcite cement (n=3)	30.35	18.69	0.00	0.00	0.92	3.41	53.37
			Calcite				
Pore filler (n=24)	54.17	0.54	0.01	0.01	0.64	0.43	55.80
Inclusions in dolomite (n=4)	55.99	0.79	0.02	0.10	0.58	0.61	58.09
Cores to dolomite rhombs (n=4)	55.64	0.73	0.00	0.02	0.30	0.20	56.89

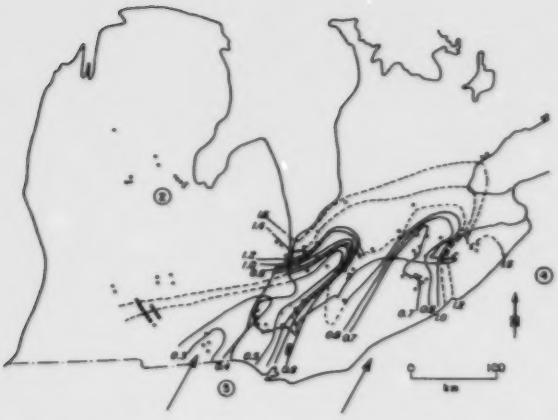

Figure 357.4. Contour diagram of Ca/Na weight ratio showing the distribution of low-Na, low-TDS brines. Dot, sample location; 2) brine from 1200 m depth in the Michigan Basin (Ca-Na-Cl; TDS < 300 g L^{-1}); 4) inferred Ca-Na-Cl brine whose probable origin is the Appalachian Basin; 5) Na-Ca-Cl brine (TDS < 150 g L^{-1}) entering the study area from the south.

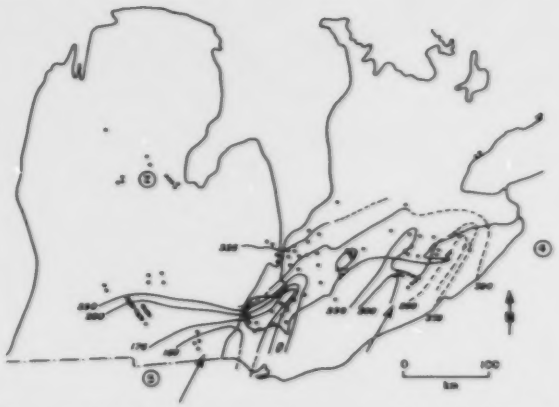

Figure 357.5. Contour diagram showing distribution of TDS in existing formation waters. Symbols as in Figure 357.4.

and 2) to relate chemical and isotopic variations in diagenetic minerals to basin-wide phenomena such as changing fluid fluxes, mass transport, burial history, detrital mineralogy and sedimentary facies variations.

The first year of this research has focussed on 2 principal areas: 1) mineralogical and geochemical characterization of typical porous and permeable Cambro-Ordovician sandy units; and 2) evaluation of the formation-water chemistry of these units and the role of the Precambrian-Cambro-Ordovician interface as a fluid conduit. The immediate product of this research is a substantially larger and more comprehensive data base on the geochemistry, mineralogy and diagenesis of southwestern Ontario's lower Paleozoic sequence. Four major rock types were identified containing complex assemblages of diagenetic glauconite, illite, pyrite, K-feldspar, quartz, calcite and dolomite. The most striking observation in bulk mineralogy is that K-feldspar is virtually the only feldspar present in these rocks, suggesting a possible genetic link with other recognized episodes of potassic alteration. Diagenetic mineralogy of all rock types is similar, with the exception of a smectitic component identified in the <2 μm size fraction of dolomite-rich samples. This suggests that the pore system in this rock type

was isolated during subsequent diagenesis. Also, new chemical data for the Cambro-Ordovician pore waters have been integrated with earlier information, and a working hypothesis has been developed indicating widespread (interbasin) migration during at least one major stage of fluid flux.

FUTURE WORK

Additional work planned or in progress includes the following: 1) separation of glauconite for detailed stable and radiogenic isotope studies (its stable isotopic composition should provide information on early diagenetic pore waters; if glauconite remained closed to subsequent diagenesis, radiogenic isotope dating of this early diagenesis may be possible); 2) separation of both quartz and K-feldspar overgrowths for isotopic study (dating, thermal history, fluid composition); and 3) separation of calcite and dolomite for O, C and Sr isotopic analysis. These data should provide important constraints on pore-fluid evolution during dolomitization and predolomitization events.

REFERENCES

Ayalon, A. and Longstaffe, F.J. 1988. Oxygen-isotope studies of diagenesis and porewater evolution in the western Canada sedimentary basin: evidence from the Upper Cretaceous basal Belly River sandstone, Alberta; Journal of Sedimentary Petrology, v.58, p.489-505.

Clayton, R.N., Friedman, I., Graf, D.L., Meents, W.F. and Shimp, N.F. 1966. The origin of saline formation waters: 1. Isotopic composition; Journal of Geophysical Research, v.71, p.3869-3882.

Craig, H. 1961. Isotopic variations in meteoric waters; Science, v.133, p.1702-1703.

Dollar, P.S., Frape, S.K. and McNutt, R.H. 1988. Geochemistry of formation waters, southwestern Ontario, Canada and southern Michigan, U.S.A.—implications for origin and evolution; Ontario Geological Survey, Open File Report.

Duffin, M.E. 1989. Nature and origin of authigenic K-feldspar in Precambrian basement rocks of the North American midcontinent; Geology, v.17, p.765-768.

Duffin, M.E., Lee, M., Klein, G.DeV. and Hay, R.L. 1989. Potassic diagenesis of Cambrian sandstones and Precambrian granitic basement in UPH-3 deep hole, upper Mississippi Valley, U.S.A.; Journal of Sedimentary Petrology, v.59, p.848-861.

Fritz, P., Lapcevic, P.A., Miles, M., Frape, S.K., Lawson, D.E. and O'Shea, K.J. 1988. Stable isotopes in sulphate minerals from the Salina formation in southwestern Ontario; Canadian Journal of Earth Sciences, v.25, p.195-205.

Hebner, B.A., Bird, G.W. and Longstaffe, F.J. 1986. Fluid/pore-mineral transformations during simulated steam injection: implications for reduced permeability damage; The Journal of Canadian Petroleum Technology, v.25, p.68-73.

Hitchon, B. and Friedman, I. 1969. Geochemistry and origin of formation waters in the western Canada sedimentary basin: I. Stable isotopes of hydrogen and oxygen; Geochimica et Cosmochimica Acta, v.33, p.1321-1349.

Kirk, J.S., Bird, G.W. and Longstaffe, F.J. 1987. Laboratory study of the effects of steam-condensate flooding in the Clearwater Formation: high temperature flow experiment; Bulletin of Canadian Petroleum Geology, v.35, p.34-47.

Longstaffe, F.J. 1983. Stable isotope studies of diagenesis in clastic rocks; Geoscience Canada, v.10, p.43-58.

———1984. The role of meteoric water in diagenesis of shallow sandstones: stable isotope studies of the Milk River aquifer and gas pool, southeastern Alberta; *in* Clastic diagenesis, edited by D.A. McDonald and R.C. Surdam, American Association of Petroleum Geologists, Memoir 37, p.81-98.

———1986. Oxygen-isotope studies of diagenesis in the basal Belly River sandstone, Pembina-I pool, Alberta; Journal of Sedimentary Petrology, v.56, p.78-88.

———1987. Stable isotope studies of diagenetic processes; *in* Stable isotope geochemistry of low temperature fluids, edited by T.K. Kyser, Mineralogical Association of Canada, Short Course no.13, p.187-257.

———1988. Mineralogical and oxygen-isotope studies of clastic diagenesis: implications for fluid flow in sedimentary basins; *in* Hydrogeology of sedimentary basins, edited by B. Hitchon, S. Bachu and C.M. Sauveplane, Proceedings of the 3rd Annual Canadian–American Conference on Hydrogeology, Banff, Alberta, June 1986, p.204-220.

———1989. Stable isotopes as tracers in clastic diagenesis; *in* Clastic diagenesis, edited by I. Hutcheon, Mineralogical Association of Canada, Short Course no.15, p.201-277.

Longstaffe, F.J. and Ayalon, A. 1987. Oxygen-isotope studies of clastic diagenesis in the Lower Cretaceous Viking Formation, Alberta: implications for the role of meteoric water; *in* Diagenesis of sedimentary sequences, edited by J.D. Marshall, Geological Society, Special Publication 36, p.277-296.

Lowry, R.M., Faure, G., Mullet, D.I. and Jones, L.M. 1988. Interpretation of chemical and isotopic compositions of brines based on mixing and dilution, "Clinton" sandstones, eastern Ohio, U.S.A.; Applied Geochemistry, v.3, p.177-184.

McNutt, R.H., Frape, S.K. and Dollar, P. 1987. A strontium, oxygen and hydrogen isotopic composition of brines, Michigan and Appalachian basins, Ontario and Michigan; Applied Geochemistry, v.2, p.495-506.

Newman, A.C.D. and Brown, G. 1987. The chemical constitution of clays; *in* Chemistry of clays and clay minerals, edited by A.C.D. Newman, Mineralogical Society, Monograph 6, p.1-28.

O'Shea, K.J., Miles, M.C., Fritz, P., Frape, S.K. and Lawson, D.E. 1988. Oxygen-18 and carbon-13 in the carbonates of the Salina formation of southwestern Ontario; Canadian Journal of Earth Sciences, v.25, p.182-194.

Schwartz, F.W. and Longstaffe, F.J. 1988. Groundwater and clastic diagenesis; *in* Hydrogeology, edited by W. Back, J.S. Rosenshein and P.R. Seaber, Geological Society of America, Boulder, Colorado, The Geology of North America, v.O-2, p. 413-434.

Stueber, A.M., Pushkar, P. and Hetherington, E.A. 1987. A strontium isotopic study of formation waters from the Illinois Basin, U.S.A.; Applied Geochemistry, v.2, p.477-494.

Tilley, B.J. and Longstaffe, F.J. 1989. Diagenesis and isotopic evolution of porewaters in the Alberta Deep Basin: Part I—Fahler Member and Cadomin Formation; Geochimica et Cosmochimica Acta, v.53, p.2529-2546.

Tilley, B.J., Nesbitt, B.E. and Longstaffe, F.J. 1989. Thermal history of Alberta Deep Basin: comparative study of fluid inclusion and vitrinite reflectance data; American Association of Petroleum Geologists Bulletin, v.73, p.1206-1222.

Velde, B. and Meunier, A. 1987. Petrological phase equilibria in natural clay systems; *in* Chemistry of clays and clay minerals, edited by A.C.D. Newman, Mineralogical Society, Monograph 6, p.423-458.

Winder, C.G. and Sanford, B.V. 1972. Stratigraphy and paleontology of the Paleozoic rocks of southern Ontario; International Geological Congress, 24th Session, Field Excursion A45-C45, 74p.

Grant 359 Structural Geology of the Midlothian Lake–Peterlong Lake Area, Abitibi Greenstone Belt, Superior Province

R.B. Hrabi and H. Helmstaedt

Department of Geological Sciences, Queen's University, Kingston

ABSTRACT

The ultimate objectives of the project are to understand the structural evolution of the Midlothian Lake–Peterlong Lake area of the southwest Abitibi greenstone belt and to evaluate the structural setting of gold mineralization in the project area.

The field area was divided into 3 domains:

Domain I is in the northeast part of the field area and is remote from the Kenogamissi dome, a large composite batholith, and the inferred extension of the Cadillac–Larder Lake Break (CLLB). Early east- to northeast-trending folds have no axial-planar foliation and are overprinted by a later foliation, striking east-northeast to northeast, which cuts adjacent limbs of the folds. A zone of high strain is coincident with the contact between the metavolcanic rocks of the Deloro and Tisdale groups at the nose of a regional northeast-trending syncline. At present it is still uncertain whether this zone predates or postdates the upright folds. At the high-strain zone, rocks of the Tisdale Group structurally overlie rocks of the Deloro Group. Pillow facing directions on the northwest limb of the fold show that both groups face southeast, indicating that the younger Tisdale Group is in the correct inferred stratigraphic position. Although the high-strain zone suggests tectonic movement between the 2 groups, a large displacement is not required. However, to the south, at the northern margin of the Halliday dome, rocks of the Tisdale Group young southward into rocks of the Deloro Group, suggesting either tectonic juxtaposition or problems with the existing stratigraphic correlation.

Domain II is dominated by fabrics related to the intrusion of different phases of the Kenogamissi dome. No fabrics predating the syn-intrusion foliation were observed in the metavolcanic country rocks. Strong foliations were developed in older phases of the intrusive complex along the contacts with younger phases. At the southern margin of the batholith is a wide zone of strong foliation, which may have been caused by intrusion of a younger intrusive phase. Alternatively, the foliation may be related to zones of strong, east-trending high strain immediately to the northeast in the metavolcanic rocks, which are tentatively correlated with deformation along the CLLB.

Domain III is in the southwest corner of the field area and includes a sequence of Timiskaming-type sedimentary rocks. Folds in the metasedimentary rocks do not appear to have an axial-planar foliation. A weak foliation with orientation nearly parallel to bedding cuts opposing limbs of these folds. A series of strong, northeast-striking high-strain zones and a strongly developed, contact-parallel planar fabric are localized at the Timiskaming contact.

INTRODUCTION

The Midlothian Lake–Peterlong Lake area is located in the southwest corner of the Abitibi greenstone belt, approximately 50 km south of Timmins and 95 km west-southwest of Kirkland Lake (Figure 359.1). The area lies to the northwest of the Cobalt embayment and includes the contact between Archean metavolcanic rocks and a large composite batholith, the Kenogamissi dome. The southeastern corner of the field area lies approximately along strike of the CLLB and includes a significant section of Timiskaming-type metasedimentary rocks.

The main objectives of the project are to map the structural elements of the field area and to determine the sequence of deformation for this portion of the Abitibi greenstone belt. Special attention during the 1989 field season was paid to the relationships between 1) major packages of metavolcanic rocks, 2) metavolcanic rocks and the Timiskaming-type metasedimentary rocks and 3) metavolcanic rocks and the margin of the Kenogamissi dome. The ultimate aim is to understand the structural evolution of the Midlothian Lake–Peterlong Lake area of the Abitibi greenstone belt and the relationship between the deformation history and gold mineralization in the project area.

This paper describes the results of field work conducted during the summer of 1989. Reconnaissance mapping (1:50 000 scale) of the entire field area, consisting of approximately 12 townships (Figure 359.2), was completed.

GEOLOGICAL SETTING

General Geology

The existing geological data base was assembled by the Ontario Geological Survey and its predecessors from 1926 to 1984 (Gledhill 1926; Rickaby 1932; Marshall 1947; Abraham 1954; Bright 1970, 1984; Pyke 1978). The area is also included on 2 compilation maps (Pyke et al. 1973; MERQ–OGS 1983).

Table 359.1 summarizes the stratigraphy of the metavolcanic rocks defined by Jensen and Langford (1985) for the Kirkland Lake area, and the correlative stratigraphy for the Timmins area (Pyke 1982) as well as the

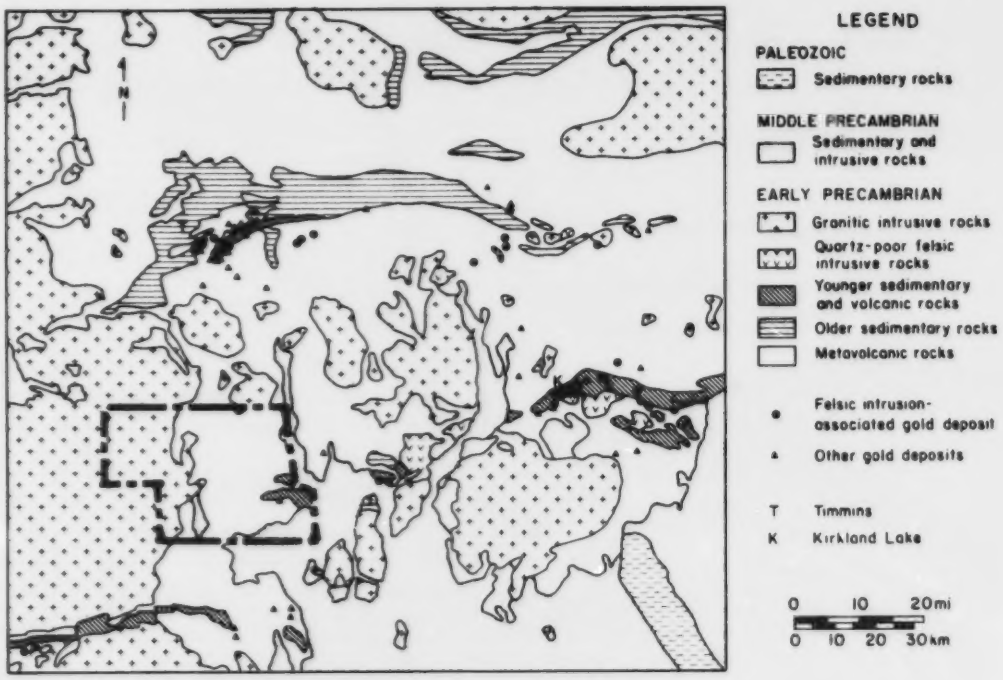

Figure 359.1. Location of study area (outlined area). *Modified from* Cherry (1983, Figure 1).

high-precision U-Pb dating of the metavolcanic rocks (Corfu et al. 1989). The metavolcanic rocks have been divided into 3 cycles (Jensen and Langford 1985; Pyke 1982). Each cycle has a komatiitic and Mg-rich tholeiitic base, followed by a package of Mg-rich tholeiite and Fe-rich tholeiitic basalt, which in turn is overlain by a package of calc-alkalic basalt to rhyolite.

In the northwest portion of the field area, mafic to felsic calc-alkalic rocks of the "Upper Formation" of the Deloro Group (cycle II) form a southeast-facing homocline (northeast corner of Figure 359.3 in English Township). The south part of the field area is underlain by intermediate to felsic calc-alkalic rocks of the same group, forming a large anticline that has been called the Halliday dome (Figure 359.3). The area between the Halliday dome and the homocline is underlain predominantly by the "Lower Formation" of the Tisdale Group (cycle III). In the southeastern corner of the area is a sequence of Timiskaming-type conglomerates, sandstones and siltstones (Bright 1970). The west half of the field area is underlain by the Kenogamissi dome, a composite batholith composed of trondhjemite, leucocratic granodiorite and diorite (Pyke 1978).

Absolute ages of the rocks can only be inferred from U-Pb dating of the uppermost felsic members of each cycle in the Timmins area (Corfu et al. 1989). The dating supports the overall stratigraphic sequence established for the area south of Timmins (Table 359.1). Problems exist, however, with the stratigraphy established in the Kirkland Lake and Lake Abitibi areas and with the correlation of cycles between areas. A date of 2727 ± 1.5 Ma was obtained from a tuff of the "Upper Formation" of the Deloro Group, just north of the field area, in central Bartlett Township. This unit continues into the field area, forming part of the southeast-facing homoclinal sequence of felsic calc-alkalic rocks in Beemer and English townships.

Previous Structural and Tectonic Studies

Pyke (1978) and Bright (1984) outlined major upright, east- to north-northeast-trending, shallowly east-plunging folds. The southeast- to east-facing homoclinal sequence of volcanic rocks in the northeast part of the field area forms the south limb of a syncline north of the field area. The anticline forming the Halliday dome belongs to the same set of folds. Bright (1984) interpreted the Timiskaming section in Midlothian Township as a north-facing homoclinal sequence. The Timiskaming rocks form the south limb of a syncline whose axial trace is situated in metavolcanic rocks separating the main Timiskaming section from a second, equivalent section to the north (Pyke et al. 1973). Cross folding of the metavolcanic rocks in western English Township and eastern Zavitz Township was attributed by Bright (1984) to the intrusion of the granodioritic phase of the Kenogamissi dome and an underlying granitoid, respectively.

Both Pyke (1978) and Bright (1984) mapped 2 sets of relatively late north- and northwest-striking faults, with left-lateral strike separations of up to 6.1 km. These faults appear to have been reactivated, as Proterozoic dikes are displaced less than contacts within the Archean metavolcanic rocks. Pyke (1978) interpreted the north-striking faults as part of the Onaping lineament, the

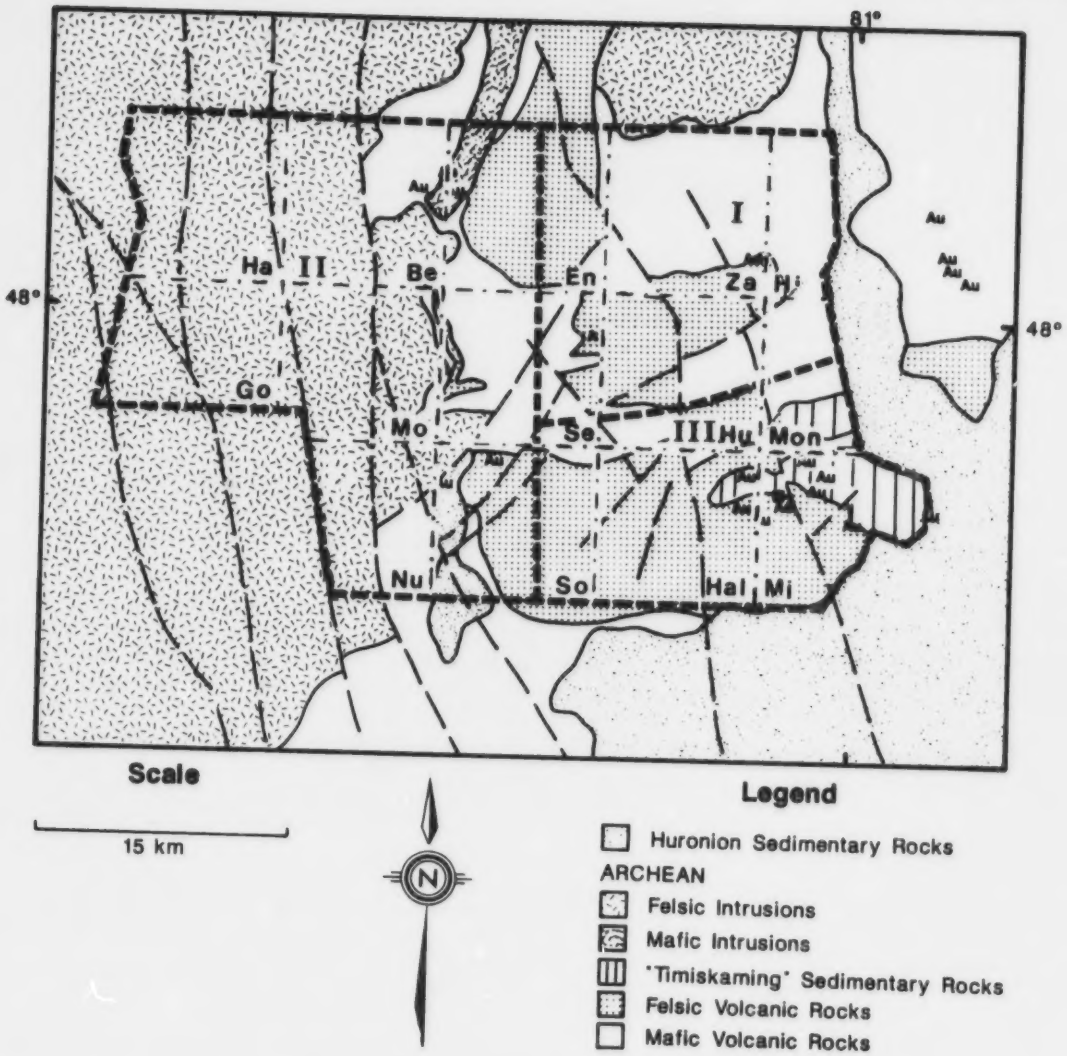

Figure 359.2. Geological map of study area, with initial domain boundaries outlined. Geology *from* Pyke et al. (1973). Township legend: Ha, Hassard; Go, Gouin; Be, Beemer; Mo, Moher; Nu, Nursey; En, English; Se, Semple; So, Sothman; Za, Zavitz; Hu, Hutt; Hal, Halliday; Hi, Hincks; Mon, Montrose; Mi, Midlothian.

westernmost expression of the Cobalt graben. Bright (1970, 1984) also mapped a series of northeast-oriented faults in Halliday and Semple townships that have minor right-lateral strike separation and are truncated by the north-striking fault set. In Halliday and Midlothian townships, Bright (1970) mapped a series of northeast-oriented shear zones, based on strong development of schistosity.

Detailed structural analyses have not been undertaken in the project area, but such studies in the Timmins area (Piroshco and Kettles 1988) and the Kirkland Lake area (Hodgson and Hamilton 1989) have implications for the present study.

In the Timmins area, Piroshco and Kettles (1988) outlined 4 Archean deformation events: 1) folding of the metavolcanic rocks and older metasedimentary rocks before deposition of the younger Timiskaming-type sedimentary rocks; 2) juxtaposition of strata along northeast-striking reverse faults; 3) development of northwest-oriented folds with a strong axial-planar cleavage; and 4) formation of a strong east-northeast-striking fabric, with S-shaped minor folds and gently dipping extension veins indicating left-handed reverse movement along northeast-striking shears. A later, bedding-parallel, northeast-striking planar fabric with dextral slip is also attributed to this deformation event.

Three Archean deformation events have been interpreted in the Kirkland Lake area (Hodgson and Hamilton 1989). D_0 includes early folding and faulting, without any associated foliation development. D_1 was the first foliation-forming event, which resulted in west-northwest- to west-trending folds with a subvertical to moderately dipping axial-planar foliation. A number of prominent shear zones approximately parallel the D_1 foliation and have been included in the same event. Hodgson and Hamilton (1989) suggested the CLLB was

Table 359.1. Stratigraphic subdivision of the southwestern Abitibi belt.

Domain	Timmins area	Lake Abitibi area	Kirkland Lake area
III	"Upper Fm." of Tisdale Gp. (2698 ± 4 Ma 2703 ± 1.5 Ma)	Blake River Gp. (2701 ± 2 Ma)	
	"Middle Fm." of Tisdale Gp.	Kinojévis Gp.	
	"Lower Fm." of Tisdale Gp.	Stoughton–Roquemaure Gp. (2714 ± 2 Ma)	Larder Lake Gp. (2705 ± 2 Ma)
II	"Upper Fm." of Deloro Gp. (2727 ± 1.5 Ma)	Hunter Mine Gp. (2713 ± 2 Ma 2730 ± 1.5 Ma)	Skead Gp. (2701^{+3}_{-2} Ma)
	"Middle Fm." of Deloro Gp.		Catherine Gp.
	"Lower Fm." of Deloro Gp.		Wabewawa Gp.
I			Pacaud Gp. (2747 ± 2 Ma)

Note: Modified from *Corfu et al. (1989, Table 1).*

initiated as an early growth fault and reactivated as a thrust fault during D_1. The rotation of D_1 foliation and small-scale folds into the CLLB, however, suggests that movement along the break continued after formation of the folds and foliation. D_2 structures include folds in bedding with an axial-planar cleavage and a group of shear zones with an east-northeast to northeast strike.

STRUCTURAL GEOLOGY

The approach taken during the present project was to divide the area into 3 domains (Figure 359.2). Domain I, centred on English, Zavitz and northern Semple and Hutt townships in the northeast corner of the field area, is distant from both the Kenogamissi dome and the CLLB and was chosen to outline the deformation as far away from the influence of these features as possible. Domain II consists of the western part of the area and includes the Kenogamissi dome and its contact with the metavolcanic rocks. This domain was chosen to highlight the deformation associated with the intrusion of the batholith. Domain III is in the southeastern portion of the field area and includes the section of Timiskaming-type metasedimentary rocks. This area is along strike of the inferred extension of the CLLB, which has been traced through the Huronian cover to Matachewan (Powell et al. 1989). Timiskaming-type metasedimentary rocks show a strong spatial correlation with regional deformation zones, such as the CLLB (Colvine et al. 1988). The combination of these facts made domain III the likely area for us to document deformation associated with the CLLB.

Domain I: English–Zavitz–Semple–Hutt Townships

The most obvious structural elements are large map-scale folds defined by reversals in younging direction based on pillow top determinations. These F_n folds are upright, have axial traces trending east or northeast and plunge moderately to the east or northeast (Figure 359.3). A weak foliation is commonly observed, but it is not axial planar to the folds. Generally it maintains the same relationship to bedding on opposing limbs of the folds. The foliation is therefore believed to be later than the development of the folds (S_{n+1}). No folds of intermediate scale were outlined in this domain because bedding in the metavolcanic rocks is difficult to measure.

Discrete zones of high strain are oriented west and northwest. They contain a strongly developed, anastomosing, steeply dipping schistosity and are generally outlined by strong iron carbonate alteration. No crosscutting relationship between these zones was observed, but because they were seen to overprint the weak S_{n+1} foliation and are believed to postdate it, these foliations, related to the high-strain zones, are tentatively grouped together as S_{n+2}. To date, no reliable kinematic indicators have been observed along these zones.

A laterally extensive zone of anomalously high strain is located at the nose of a regional northeast-trending F_n syncline (near the English–Semple township boundary, Figure 359.3) and is coincident with the contact between the "Upper Formation" of the Deloro Group and the "Lower Formation" of the Tisdale Group (MERQ–OGS 1983). The contact is locally marked by a unit of heterolithic, poorly sorted conglomerate that has been highly strained. The foliation strikes northwest and dips gently to the northeast (Photo 359.1), with a chlorite mineral elongation oriented approximately downdip. The relationship to the other early foliations is presently uncertain and will be the object of detailed study during the 1990 field season. This zone of high strain has been overprinted by a well-developed, north-striking crenulation cleavage (Photo 359.2). The cause of this cleavage is unknown, but its orientation is consistent with shortening caused by the intrusion of the Kenogamissi dome.

No apparent stratigraphic reversals are seen in this high-strain zone. Top determinations from pillows indicate that calc-alkalic intermediate to felsic rocks of the "Upper Formation" of the Deloro Group sit structurally below the tholeiitic basalts of the "Lower Formation" of the Tisdale

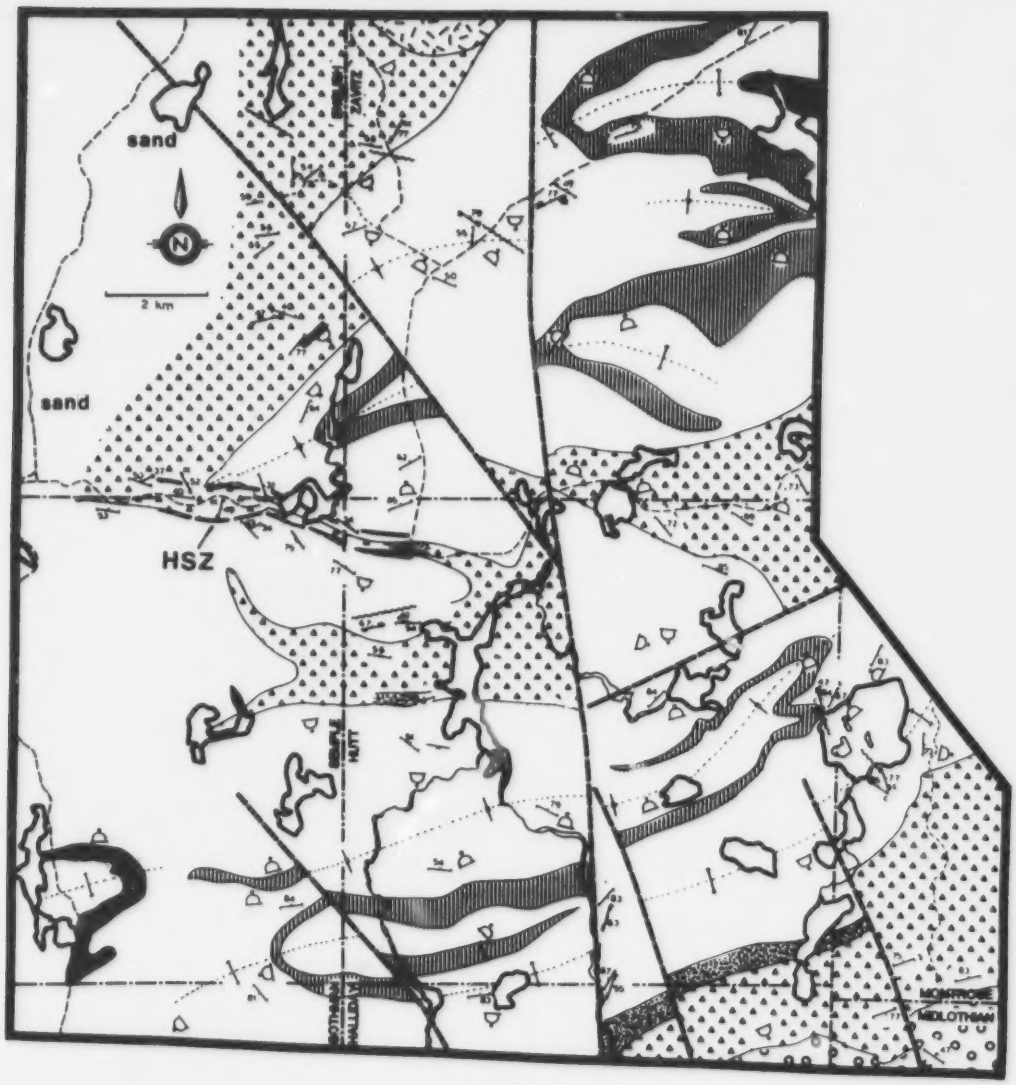

LEGEND

Archean

- Granodiorite Intrusions
- Ultramafic to Mafic Intrusive Rocks and Ultramafic Extrusive Rocks
- Timiskaming Sedimentary Rocks
- Heterolithic Conglomerate and Associated Sediments
- White-weathering, dark to pale green basalt to rhyolite (Calc-alkalic Volcanic Rocks)
- Light green-weathering, pale grey-green basalt (Mg-rich Tholeiitic Basalt)
- Light green-weathering, dark green basalt (Fe-rich Tholeiitic Basalt)

- Bedding, top unknown (inclined)
- Bedding, (inclined, overturned)
- Pillowed lava flow (top from pillow shape/packing)
- Foliation (S_{n+1}, S_{n+2}, S_{n+3}, crenulation cleavage)
- Lineation
- Fault
- Minor shear zone
- Fold-axial trace (anticline, syncline)

Figure 359.3. Geological map of domain I (English–Zavitz–Semple–Hutt area). Geology *modified from* Bright (1970, 1984), Pyke (1978) and MERQ–OGS (1983). HSZ, high-strain zone coincident with the contact of the Tisdale and Deloro groups. The "Upper Formation" of the Deloro Group is represented by the white-weathering, dark to pale green basalt to rhyolite unit. The "Lower Formation" and "Middle Formation" of the Tisdale Group are represented by the light green-weathering, pale grey-green and dark green basalt units. Most of the Halliday dome is located to the south of this figure, with the northern contact of the dome approximately at the unit referred to as "Heterolithic Conglomerate and Associated Sediments".

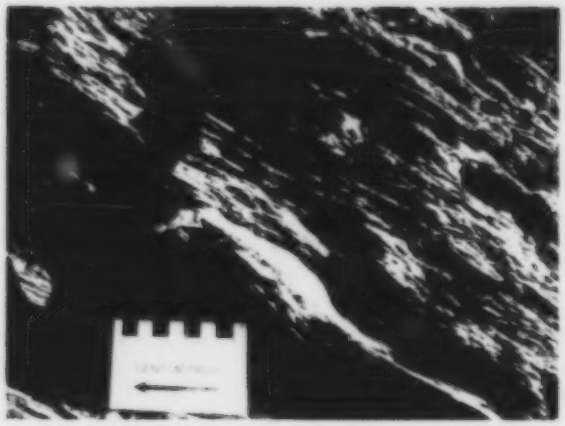

Photo 359.1. Vertical face of an outcrop of metavolcanic rock at the contact between the "Upper Formation" of the Deloro Group and the "Lower Formation" of the Tisdale Group. Well-developed foliation dips gently to northeast. Photo taken along Papakomeka Road at the English–Semple township boundary.

Photo 359.2. Approximately north-striking crenulation cleavage (parallel to pencil) overprinting the gently dipping, well-developed foliation in an outcrop of felsic metavolcanic rock. Photo taken just west of Photo 359.1, along Papakomeka Road.

Group. This corresponds to the interpreted stratigraphic relationship (Pyke1982). Therefore, although the high-strain zone suggests tectonic movement between the 2 formations, it is not a requirement. The geometry of the metavolcanic and metasedimentary rock units to the south of this zone appears to be complex and could not be defined properly during the reconnaissance mapping. At the northern margin of the Halliday dome, stratigraphic facing directions indicate that the rocks of the Deloro Group overlie the Tisdale Group (southeast corner of Figure 359.3). One of 2 explanations is possible: 1) the stratigraphic section is not as simple as previously interpreted or 2) the rock packages have been structurally juxtaposed.

Along the north-striking, late fault set (Bright 1984; Pyke 1978) a northeast-oriented axial-planar cleavage (S_{n+3}) developed in decimetre-scale, upright, steeply plunging minor folds. This is consistent with the left-lateral strike separation observed along metavolcanic contacts and dikes. These faults, folds and crenulation cleavage are therefore grouped together as a late D_{n+3} deformation event. One of these north-trending faults is the southerly extension of the Burrows–Benedict fault, which in Timmins is marked only by a narrow fault gouge and subhorizontal lineations (Piroshco and Kettles 1988). The reason for this difference is not known.

Domain II: Peterlong Lake–Grassy River Area

A wide variety of rock types is present in the Kenogamissi dome (Pyke 1978), but the 2 dominant phases are a white-weathering, biotite or hornblende tonalite, found in the north half of the field area, and a pink-weathering, leucocratic granodiorite, found in the south half (Figure 359.4). Both phases have caused a wide metamorphic and strain aureole within the metavolcanic country rocks. In outcrops as far as 3 km from the intrusion, a strong contact-parallel foliation or finely banded gneissosity (S_{n+1}) can be recognized in the metavolcanic rocks (Photo 359.3). It was not possible to distinguish between the effect of each of the intrusive phases in the metavolcanic rocks at the batholith margin. Some primary structures such as strongly flattened pillows were recognizable in the metavolcanic rocks near this contact, but a penetrative fabric predating the syn-intrusion fabric was not observed within the contact aureole. Only a few weak foliations (S_{n+1}) parallel to the intrusive contact were observed in the granodiorite. At the contact between the 2 main phases, the tonalite has a 500 m wide zone of high strain, which is not found in the granodiorite. The tonalite is therefore interpreted as the older phase. In the tonalite a weak, approximately east-trending fabric is defined by a poor alignment of mafic minerals. Narrow, east-striking, discrete shear zones with a dominantly left-lateral strike-slip motion were also found in the tonalite but not in the granodiorite.

Isolated areas in the metavolcanic country rocks were found with east-oriented zones of high strain, but these could not be correlated between outcrops because of extremely poor exposure immediately to the east of the batholith. The widest zone found, on the northeast side of Sinclair Lake, is expressed by strong carbonate alteration and high strain in the metavolcanic rocks. This zone is approximately along strike (although offset by a north-northwest-striking fault) with a kilometre-wide, northeast-striking zone of high strain (S_{n+2}) in the Kenogamissi dome, on the southeast side of Sinclair Lake, that is characterized by a spaced mica-chlorite foliation and flattening of quartz grains (Photo 359.4). Three explanations are possible: 1) The fabric is intrusion related, a result of the intrusion of the granodiorite as a solid-state diapir. The wide metamorphic aureole in the metavolcanic country rocks and the lack of similar fabrics anywhere else along the margin of the granodiorite are evidence against this hypothesis. 2) There is another, younger intrusion not recognized during the reconnaissance mapping that imposes a strong flattening fabric on the granodiorite. 3) The

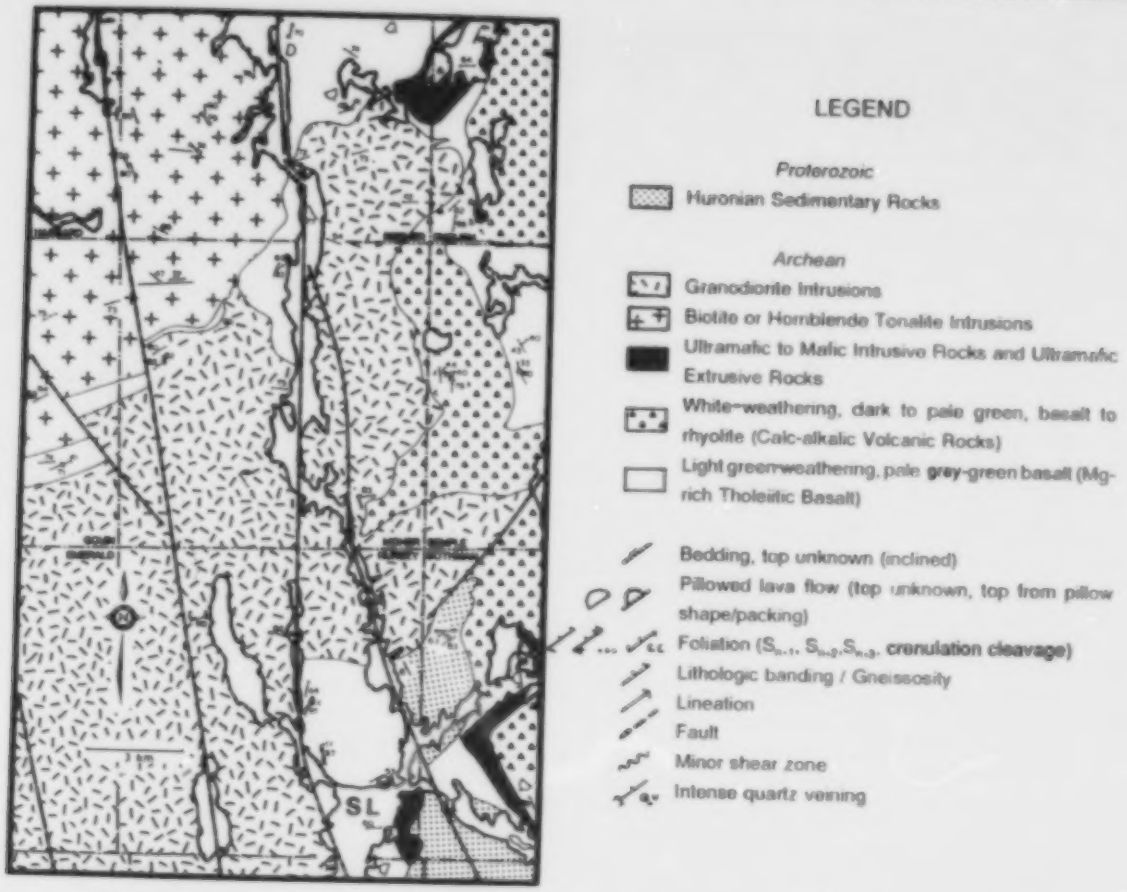
LEGEND
Proterozoic
Huronian Sedimentary Rocks
Archean
Granodiorite Intrusions
Biotite or Hornblende Tonalite Intrusions
Ultramafic to Mafic Intrusive Rocks and Ultramafic Extrusive Rocks
White-weathering, dark to pale green, basalt to rhyolite (Calc-alkalic Volcanic Rocks)
Light green-weathering, pale grey-green basalt (Mg-rich Tholeiitic Basalt)
Bedding, top unknown (inclined)
Pillowed lava flow (top unknown, top from pillow shape/packing)
Foliation (S_{n-1}, S_{n-2},S_{n-3}, crenulation cleavage)
Lithologic banding / Gneissosity
Lineation
Fault
Minor shear zone
Intense quartz veining
SL

Figure 359.4. Geological map of domain II (Peterlong Lake–Grassy River area). Geology *modified from* Bright (1984), Pyke (1978) and MERQ–OGS (1983). SL, Sinclair Lake.

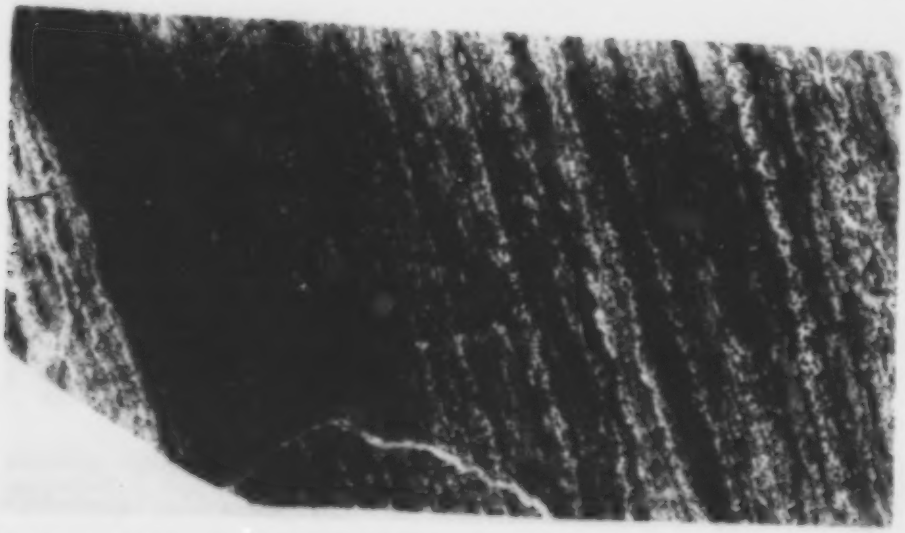

Photo 359.3. Photomicrograph of well-developed, contact-parallel schistosity (S_{n-1}) in mafic metavolcanic rocks at the contact of the Kenogamissi dome. Sample from unnamed lake in central Nursey Township.

foliation is a postintrusion fabric and, possibly, is an indication of deformation related to the CLLB within the Kenogamissi dome.

Both phases of the intrusion and the surrounding metavolcanic rocks show left-lateral strike separation of up to 6 km along north-striking faults that are equivalent to

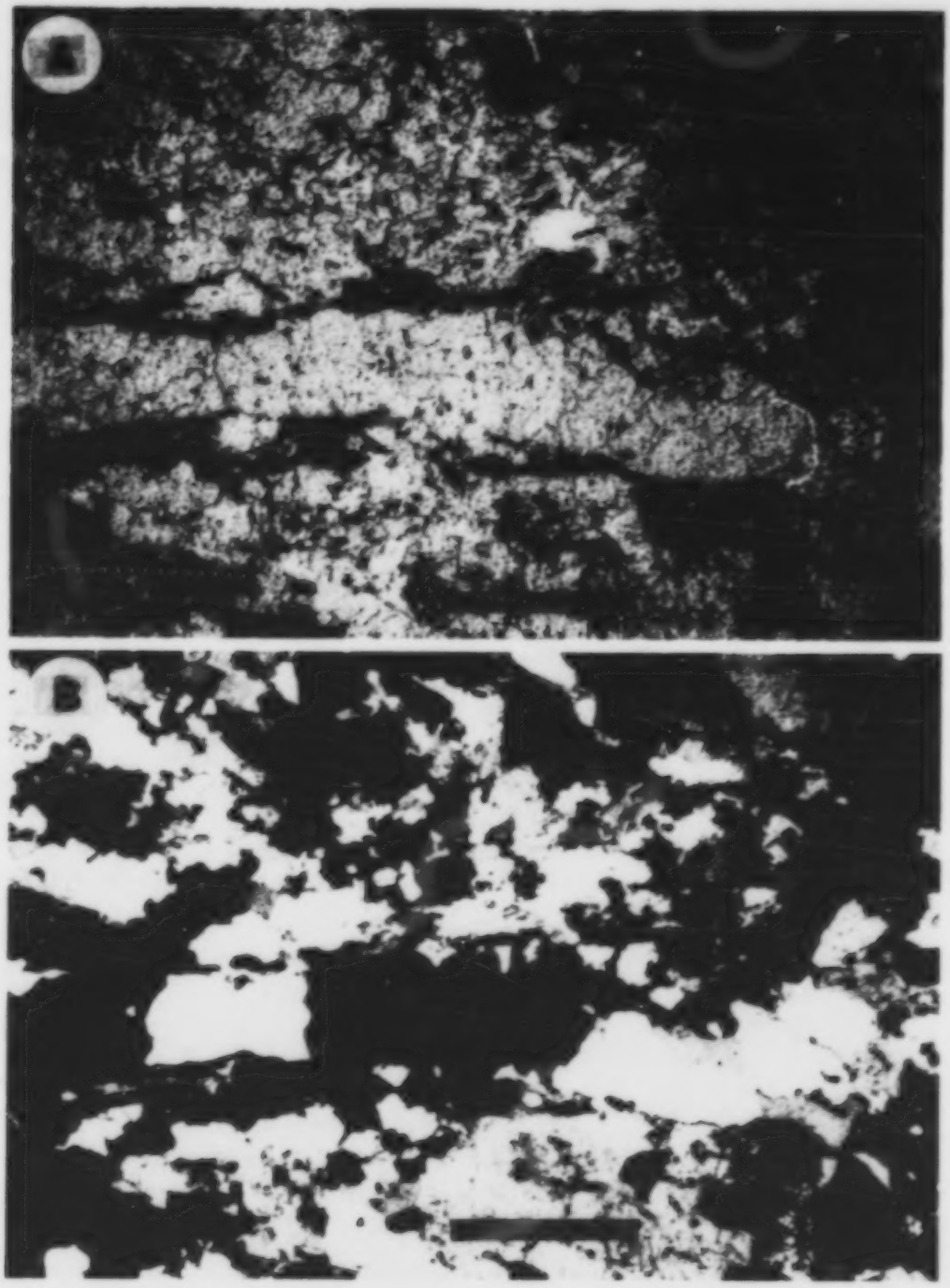

Photo 359.4. Northeast-striking foliation developed at the margin of the granodiorite, expressed by the alignment of mafic minerals, particularly biotite, and the flattening of quartz grains. A) Photomicrograph taken under plane-polarized light. B) Photomicrograph taken under cross-polarized light. Scale bars are 1 mm. Sample from southeast side of Sinclair Lake at southern Nursey Township boundary.

those found in domain I. In the batholith these faults only rotate the weak east-oriented foliation found in the tonalite. Within the highly strained metavolcanic rocks at the batholith margin, adjacent to these faults, the gneissosity or strong schistosity has been folded in moderately plunging and moderately inclined folds trending north-northeast to

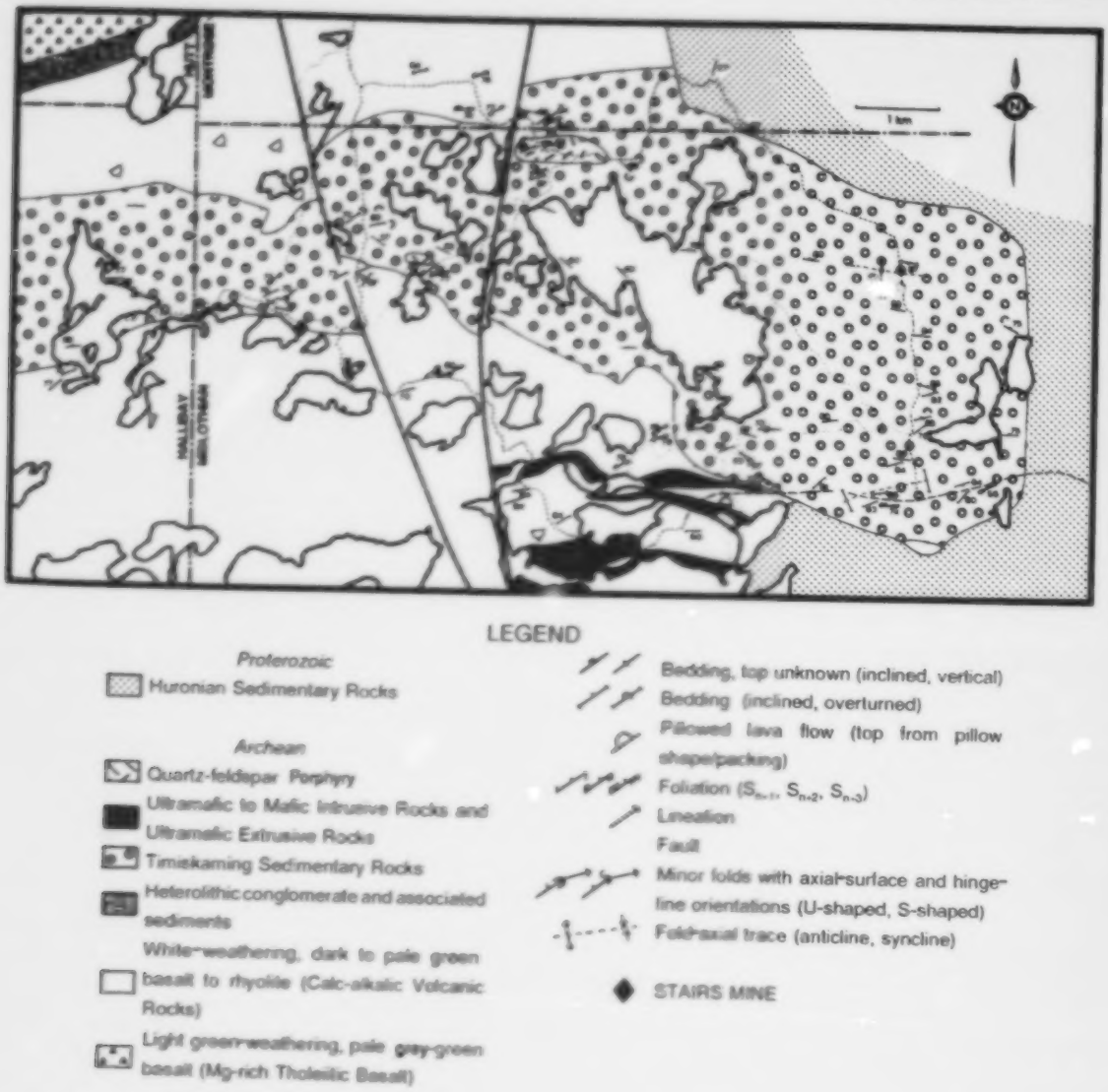
1 km
N
LEGEND
Proterozoic
Huronian Sedimentary Rocks
Archean
Quartz-feldspar Porphyry
Ultramafic to Mafic Intrusive Rocks and Ultramafic Extrusive Rocks
Timiskaming Sedimentary Rocks
Heterolithic conglomerate and associated sediments
White-weathering, dark to pale green basalt to rhyolite (Calc-alkalic Volcanic Rocks)
Light green-weathering, pale grey-green basalt (Mg-rich Tholeiitic Basalt)
Bedding, top unknown (inclined, vertical)
Bedding (inclined, overturned)
Pillowed lava flow (top from pillow shape/packing)
Foliation (S_{n-1}, S_{n-2}, S_{n-3})
Lineation
Fault
Minor folds with axial-surface and hinge-line orientations (U-shaped, S-shaped)
Fold-axial trace (anticline, syncline)
STAIRS MINE

Figure 359.5. Geological map of domain III (Campbell Lake—Midlothian Lake area). Geology *modified from* Bright (1970) and MERQ–OGS (1983).

northeast with an axial-planar schistosity (S_{n-3}). These folds are believed to be equivalent to the late deformation features found in domain I.

Domain III: Campbell–Midlothian Lakes Area

We investigated the third domain to see whether the CLLB extends into this area and to determine the time relationships between the break and other structures. Most of the metasedimentary rocks face north, but a map-scale bedding reversal near the northern margin of the Timiskaming section (Figure 359.5) and outcrop-scale, upright, steeply plunging folds (F_n) (Photo 359.5) were observed. No axial-planar foliation is present in these folds.

The earliest planar fabric (S_{n+1}) recognized is a weak to moderately developed, closely spaced foliation that in most of the area is oriented 10° to 20° counterclockwise from bedding and is locally bedding parallel. This foliation cuts across opposing limbs of the map-scale fold with the same relationship to bedding, indicating that this foliation developed after the folds. This cleavage is found in both the metavolcanic rocks and the younger Timiskaming-type metasedimentary rocks.

The second planar fabric (S_{n+2}) recognized is a very strong, northeast-oriented, closely spaced, anastomosing cleavage. It is found in wide northeast-striking zones of high strain predominantly near the Timiskaming contacts. In a few places this fabric was found to be axial planar to small, steeply plunging, upright folds (F_{n+2}).

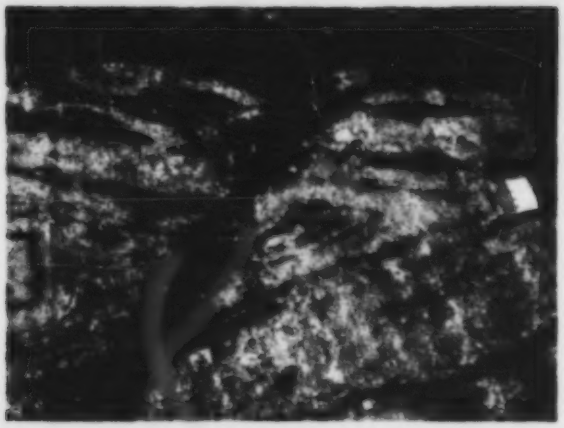

Photo 359.5. Upright, steeply plunging fold with axial trace trending east in Timiskaming interbedded sandstones and siltstones. A weak foliation, not visible in the photo, cuts obliquely across the axial surface. Photo from outcrop just to south of southeast tip of Midlothian Lake, Midlothian Township.

Photo 359.6. Well-developed, spaced, sericitic cleavage in quartz-feldspar porphyry at northern contact of the Timiskaming-type metasedimentary rocks. Arrow is approximately 5 cm. Photo taken along old logging road approximately at the midpoint of the Midlothian–Montrose township boundary.

Table 359.2. Tentative correlation of structural features in the Midlothian Lake–Peterlong Lake area.

	Domain I		Domain II	Domain III
Pre-pluton	? ? E-trending, open, upright folds	Strong, gently dipping planar fabric	Not recognized	? E-trending, open, upright folds ?
	Crosscutting, weak planar fabric			? Crosscutting, weak planar fabric ?
	? ?			
Syn-pluton	? Crenulation cleavage overprinting gently dipping planar fabric ?		Contact-parallel planar fabric in metavolcanic country rocks Contact-parallel, planar fabric in tonalite	Not recognized
Post-pluton			? NE-striking zone of strong, planar fabric in granodiorite ?	? NE-striking planar fabric ? Strongly developed, spaced planar fabric at Timiskaming contact
	NNW- and N-striking faults*, minor folds and crenulation cleavage		NNW- and N-striking faults*, minor folds and crenulation cleavage	NNW-and N-striking faults*
			* Reactivated in the Proterozoic	

Note: Question marks bracketing some structural features indicate uncertainty in the time of formation of the structure or its correlation with other structures.

A strong sericitic alteration occurs along fractures with numerous orientations in felsic extrusive rocks and small, felsic intrusions near the northern Timiskaming contact. This sericitic alteration may be earlier than the initiation of the S_{so1} and S_{so2} foliations, since these foliations refract into the altered fractures. The strong, preferred east- to east-southeast-trending orientation of many sericitic bands and the local, strong reorientation of earlier fabrics within these sericitic bands suggest that a later foliation, S_{so3}, is preferentially localized along the sericitic alteration, resulting in a spaced, sericitic cleavage (Photo 359.6). A similar, spaced cleavage defined by chlorite was found in

the Timiskaming-type metasedimentary rocks near the south contact with the metavolcanic rocks. The cleavage overprints S_{n+1} but was not found in the same outcrop with S_{n+2}. It is interpreted as having the same relative timing as the spaced, sericitic cleavage (S_{n+3}). The strong, spaced cleavages along the contacts between the metavolcanic rocks and the Timiskaming-type metasedimentary rocks are presently interpreted as expressions of the CLLB and associated structures in this area.

Late, north- to north-northwest-trending faults with left-lateral strike separation cut both the metavolcanic rocks and the Timiskaming-type rocks. These are interpreted as equivalent to the late, left-lateral faults in domains I and II. Very open, north-south-trending folds affect bedding in the Timiskaming-type metasedimentary rocks and all of the fabrics observed. These structures are considered the latest deformation features in the Midlothian area.

DISCUSSION

Table 359.2 summarizes the correlation of structural features made to date. Question marks bracketing the structural feature indicate uncertainty in the time of formation of the structure or its correlation with other structures. Significant problems still exist with the correlation of early structures recognized in Timiskaming-type rocks in domain III with early structures in domain I.

No attempt was made to correlate the minor shear zones. The timing of the high strain in domain I between the "Upper Formation" of the Deloro Group and the "Lower Formation" of the Tisdale Group in the southeast corner of English Township is still uncertain. If the crenulation cleavage that deforms this zone is correlative with the strong foliation at the contact of the Kenogamissi dome, then the gently dipping planar fabric at the contact between the packages of metavolcanic rocks must be a very early feature. Field work during 1990 will include detailed mapping of this contact to better define the geometric relationships of the metavolcanic rock units. Additional detailed mapping will be conducted at the contact between the "Upper Formation" of the Deloro Group and the "Lower Formation" of the Tisdale Group at the northern margin of the Halliday dome. This is intended to resolve the apparent reversal of the stratigraphic position of the metavolcanic rock formations at this contact.

Detailed mapping in Midlothian Township in 1990 will concentrate on the area near the metavolcanic–Timiskaming contacts. Objectives include further evaluation of the early folding of the metavolcanic rocks, confirmation of the tentative structural chronology and resolution of the problem of face to face younging directions at the northern Timiskaming contact.

ACKNOWLEDGMENTS

We would like to thank Andy Fyon (Ontario Geological Survey, Toronto) and Pamela Sangster (Staff Geologist, Ministry of Northern Development and Mines, Timmins) for their assistance and interest; Steve Jackson (Ontario Geological Survey, Toronto) and Wayne Powell (Queen's University, Kingston) for informative field trips during the summer; and Hugh Jennings for able field assistance.

REFERENCES

Abraham, E.M. 1954. Geology of Sothman Township, District of Sudbury; Ontario Department of Mines, v.62, pt.6, 36p.

Bright, E.G. 1970. Geology of Halliday and Midlothian townships, districts of Sudbury and Timiskaming; Ontario Department of Mines, Geological Report 79, 33p.

———1984. Geology of the Ferrier Lake–Canoeshed Lake area, District of Sudbury; Ontario Geological Survey, Report 231, 60p.

Cherry, M.E. 1983. The association of gold and felsic intrusions—examples from the Abitibi belt; *in* The geology of gold in Ontario, edited by A.C. Colvine, Ontario Geological Survey, Miscellaneous Paper 110, p.48-55.

Colvine, A.C., Fyon, J.A., Heather, K.B., Marmont, S., Smith, P.M. and Troop, D.G. 1988. Archean lode gold deposits in Ontario; Ontario Geological Survey, Miscellaneous Paper 139, 136p.

Corfu, F., Krogh, T.E., Kwok, Y.Y. and Jensen, L.S. 1989. U-Pb zircon geochronology in the southwestern Abitibi greenstone belt, Superior Province; Canadian Journal of Earth Sciences, v.26, p.1747-1763.

Gledhill, T.L. 1926. Grassy River area, District of Sudbury; Ontario Department of Mines, Annual Report, v.35, pt.6, p.57-76.

Hodgson, C.J. and Hamilton, J.V. 1989. Gold mineralization in the Abitibi greenstone belt: end-stage result of Archean collisional tectonics; *in* The geology of gold deposits: the perspective in 1988, edited by R.R. Keays and B.J. Skinner, Economic Geology, Monograph 6, p.86-100.

Jensen, L.S and Langford, F.F. 1985. Geology and petrogenesis of the Archean Abitibi belt in the Kirkland Lake area, Ontario; Ontario Geological Survey, Miscellaneous Paper 123, 130p.

Marshall, H.I. 1947. Geology of Midlothian Township, District of Timiskaming; Ontario Department of Mines, Annual Report, v.56, pt.5, 24p.

MERQ–OGS 1983. Lithostratigraphic map of the Abitibi Subprovince; Ministère de l'Énergie et des Ressources du Québec–Ontario Geological Survey, MERQ DV 83-16, OGS Map 2484, scale 1:500 000.

Piroshco, D. and Kettles, K. 1988. Geology of Tisdale and north Whitney townships, District of Cochrane; *in* Summary of field work and other activities 1988, Ontario Geological Survey, Miscellaneous Paper 141, p.197-205.

Powell, W.G., Hodgson, C.J. and Hanes, J.A. 1989. The expression of the Larder Lake Break in the Matachewan area; *in* Geoscience Research Grant Program, summary of research 1988–1989, Ontario Geological Survey, Miscellaneous Paper 143, p.125-132.

Pyke, D.R. 1978. Geology of the Peterlong Lake area, districts of Timiskaming and Sudbury; Ontario Geological Survey, Report 171, 53p.

———1982. Geology of the Timmins area, District of Cochrane; Ontario Geological Survey, Report 219, 141p.

Pyke, D.R., Ayre, L.D. and Innes, D.G. 1973. Timmins–Kirkland Lake sheet, Cochrane, Sudbury and Timiskaming districts; Ontario Division of Mines, Geological Compilation Series, Map 2205, scale 1:253 440.

Rickaby, H.C. 1932. Bannockburn gold area, District of Timiskaming; Ontario Department of Mines, Annual Report, v.41, pt.2, p.1-24.

Grant 363 A Seismotectonic Study of the Western Lake Ontario Region. Phase 1: A Background-noise Survey and Further Testing of Two Microearthquake Recording Sites

A.A. Mohajer and H.C. Halls

Department of Geology, University of Toronto, Erindale Campus, Mississauga

ABSTRACT

Southwestern Ontario has been seismically quiescent in recent decades with the exception of a series of small-magnitude ($M \leq 3.5$) events around Burlington in the mid-1970s, an earthquake of $M = 3.4$ in July 1987 and 2 recent ones of $M = 3.3$ and 2.2 that occurred beneath Lake Ontario, south of Burlington, in August 1989. More than 30 earthquakes ($M \leq 5$) have been reported in the southwestern Ontario region during the 19th and first half of the 20th centuries.

The objectives of our study are to gain insight into the distribution of microearthquakes in southwestern Ontario, their frequency as a function of magnitude and their geological cause. These objectives, which are vital to the accurate assessment of seismic risk, cannot be attained with presently existing seismographic coverage, detection thresholds and errors in hypocentral location. As a prelude to earthquake monitoring, a background-noise survey was carried out in the western Lake Ontario region. Thirty sites were occupied for periods ranging from 24 to 48 h. It was found that sites had to be about 3 km from railways and about 2 km from main roads before traffic noise was satisfactorily suppressed. Most sites received signals from quarry blasts, which will be used ultimately to improve the interpretation of the local velocity structure and hence the accuracy of hypocentre location.

Eight locations were found where noise amplitude may be sufficiently low for local earthquakes to be recorded down to $M = 1$. At these stations the noise levels ranged between 150 and 250 nm/s for frequencies of 5 to 15 Hz, the interest range for local earthquakes. Three of the best sites were selected for continuous monitoring during 1990. Approximately 90 events were recorded during the first 3 months of monitoring at Mount Nemo Conservation Park, about 10 km north of Burlington. More than 70% of the recorded events were quarry blasts, and 20% showed characteristics of other cultural activities; the origin of the remainder is under investigation.

1. INTRODUCTION

1.1 Regional Seismicity

Earthquake activity in southern Ontario and adjacent areas is not uncommon, but lack of understanding of the features that cause earthquakes there has resulted in earthquake-hazard assessments with inherently large uncertainties. The largest documented earthquakes around Lake Ontario are those of $M = 5$ near Welland in 1873; $M = 5.7$ near Attica in 1929; $M = 5.7$ near Cornwall-Massena in 1944; $M = 3$ to 3.5 near Burlington (11 events from 1975 to 1980); $M = 3.3$ on Toronto Island in 1987; and $M = 3.4$ near Hamilton in 1989. These earthquakes and more than 55 felt tremors or recorded microearthquakes since 1970 appear within the same seismotectonic environment, but their possible association with specific geological structures has yet to be established. Nevertheless, the spatial relation of the above earthquakes to the Clarendon–Linden fault, the St. Lawrence Paleozoic rift-fault system and the Toronto–Burlington aeromagnetic lineament is very suggestive (Figures 363.1 and 363.2).

Identification of seismic sources and in-depth seismotectonic interpretations are important to earthquake-hazard assessment and safety evaluation at sites of existing and future critical facilities. It is therefore important to utilize all available means to determine precisely the location of earthquakes and their relationship, if any, to possible faults. This will improve the seismotectonic data base and should help to reduce the uncertainties associated with estimating seismic design parameters. Relevant work has already begun, in recent years, by recomputation of earthquake locations (Mohajer 1987), redefinition of the attenuation of ground motion (Boore and Atkinson 1987) and seismic source modelling (Adams and Basham 1989). Furthermore, the work of Parrish (1989) and Mohajer (1989) has shown that earthquakes may be related to magnetic and topographic lineaments in Ohio and western Quebec. The next necessary step is deployment of a local seismic network, designed to locate the foci of microearthquakes ($M_L < 3$), which occur more frequently than macroearthquakes and, therefore, may be useful in defining linear zones of seismic activity. Examples of microseismic networks used to delineate seismic sources in eastern North America are from the New Madrid (Stauder 1982) and Giles County, Virginia, areas (Bollinger and Wheeler 1988).

1.2 Objectives

The main purpose of this study is to determine the distribution, frequency and source mechanism of microearthquakes in the western Lake Ontario region and their relation to local and regional geology. More specific

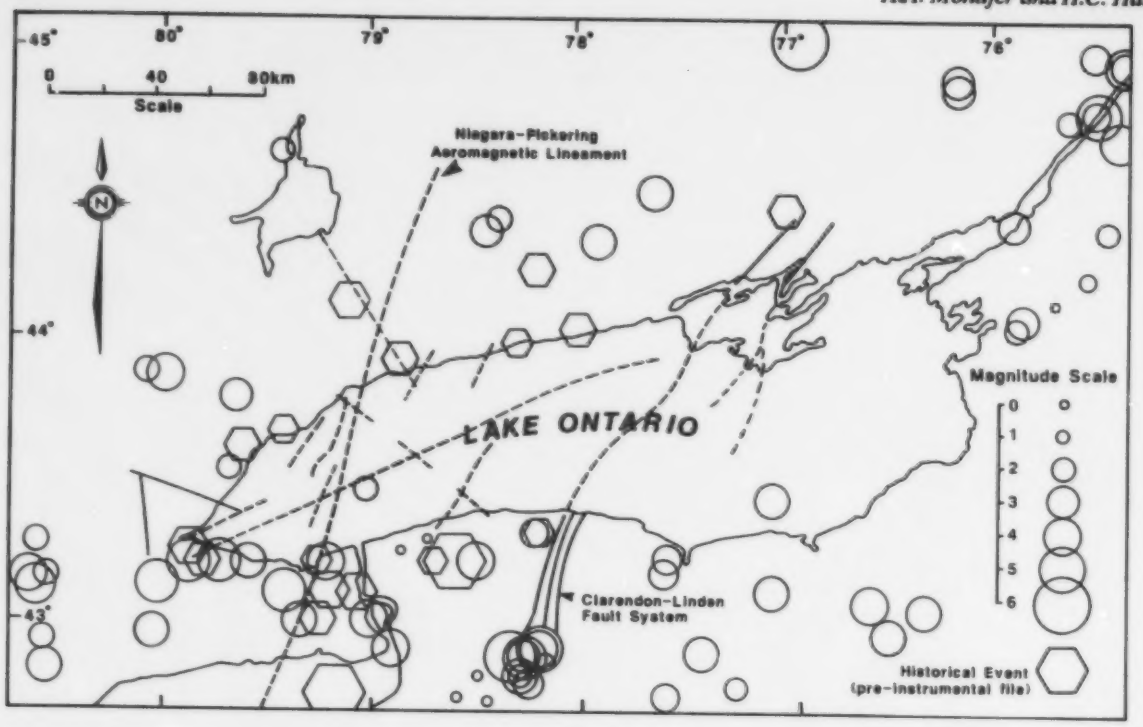

Figure 363.1. Seismicity and structural framework of southern Ontario. Historical and instrumental seismic data extend from 1700 to 1970 (compilation is based on Smith 1962; Mohajer 1987; Geological Survey of Canada and the Lamont–Doherty Geological Observatory bulletins). Solid lines denote known geological structures, and dashed lines are prominent geophysical lineaments (compilation based on Forsyth et al. 1987; Mohajer and Thomas 1988; McFall and Allam 1989; Wallach and Mohajer 1990).

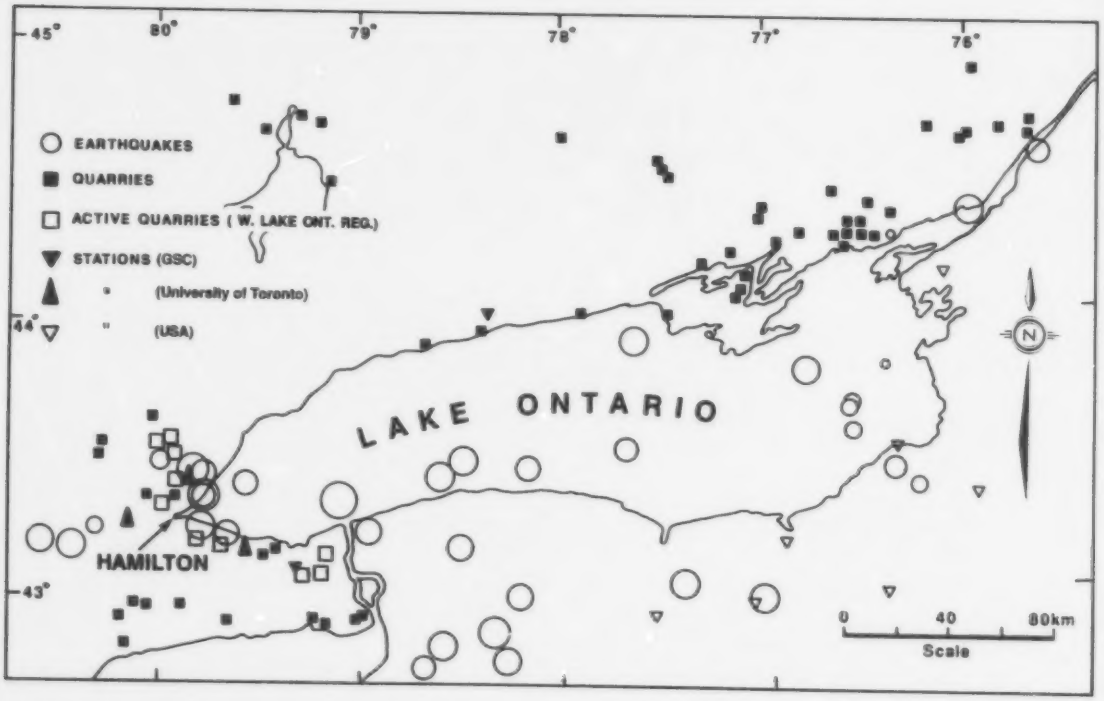

Figure 363.2. Recent earthquake activity (1971–1989), quarry locations (open squares show active ones with scheduled blasts in the western Lake Ontario region) and seismographic stations in southern Ontario. The locations of our proposed stations are shown by the larger solid triangles.

Table 363.1 Data summary of background-noise survey.

Record no.	Date on/off	Site location	Elevation (m)	Site foundation	Lat. (N)	Long. (W)	Gain (dB)	Duration of record (h)	% of LTA >1 mm	Comments
1	Jun 27/Jun 28	Terra Cotta	330	Bedrock	43°43.3′	79°57.6′	72	24	4	Quiet*
2	Jun 28/Jun 29	Terra Cotta	330	Bedrock	43°43.3′	79°57.6′	72	24	2	Quiet
3	Jun 28/Jun 29	Maple L. Rock	240	Overb'dn	43°35.3′	79°52.7′	66	12	92	Unacceptable
4	Jun 30/Jul 4	Terra Cotta	330	Bedrock	43°43.3′	79°57.6′	72	48	4	Acceptable
5	Jun 30/Jul 4	Cred. Val. Cons. Area	180	Overb'dn	43°37.5′	79°44.2′	66	48	3	Quiet
6	Jul 4/Jul 5	Terra Cotta	330	Bedrock	43°43.3′	79°57.6′	72	19	11	Quiet
7	Jul 4/Jul 6	Cred. Val. Cons. Area	180	Overb'dn	43°37.5′	79°44.2′	60	48	42	Unacceptable
8	Jul 6/Jul 7	Heart L. Cons. Area	250	Overb'dn	43°44.5′	79°47.5′	72	24	6	Acceptable*
9	Jul 6/Jul 8	Heart L. Cons. Area	250	Overb'dn	43°44.5′	79°47.5′	60	48	44	Unacceptable
10	Jul 10/Jul 12	Early Farm	230	Overb'dn	43°37.5′	79°51.0′	72	48	31	Unacceptable
11	Jul 10/Jul 14	Hume Farm	250	Overb'dn	43°34.5′	79°50.0′	66	48	42	Unacceptable
12	Jul 17/Jul 19	Conlin Farm	330	Overb'dn	43°34.5′	79°58.7′	66	48	3	Quiet
13	Jul 17/Jul 19	Hilton Falls Cons. Area	320	Bedrock	43°30.6′	79°59.6′	66	8	2	Quiet
14	Jul 19/Jul 21	Hilton Falls Cons. Area	320	Bedrock	43°30.6′	79°59.6′	66	18	11	Unacceptable
15	Jul 20/Jul 21	Hilton Cons. Park	300	Bedrock	43°30.3′	79°58.5′	66	0	0	No data
16	Jul 22/Jul 23	Croatian Park	180	Overb'dn	43°29.2′	79°48.7′	66	0	0	No data
17	Jul 22/Jul 23	Martin Farm	185	Overb'dn	43°28.5′	79°50.3′	66	24	25	Unacceptable
18	Jul 24/Jul 25	Croatian Park	180	Overb'dn	43°28.2′	79°48.7′	72	11	5	Acceptable*
19	Jul 26/Jul 27	Brunham & Tremaine	170	Overb'dn	43°26.0′	79°48.6′	66	0	0	Unacceptable
20	Jul 27/Jul 28	Moodie Farm	160	Bedrock	43°27.6′	79°47.0′	66	24	8	Unacceptable
21	Jul 29/Jul 30	Bronte Park	140	Overb'dn	43°25.2′	79°45.8′	66	24	0	Unacceptable
22	Jul 29/Jul 30	Mt. Nemo	290	Bedrock	43°25.3′	79°52.6′	72	24	0	Very quiet†
23	Jul 31/Aug 1	Robinson Farm	270	Overb'dn	43°22.7′	79°58.7′	72	23	4	Acceptable
24	Jul 31/Aug 1	Josling Farm 2	280	Overb'dn	43°23.5′	79°55.3′	72	24	1	Acceptable
25	Aug 2/Aug 3	Josling Farm 2	280	Overb'dn	43°23.5′	79°55.3′	72	24	17	Unacceptable
26	Aug 2/Aug 3	Bennett Mftg.	255	Overb'dn	43°20.6′	79°59.0′	60	24	17	Unacceptable
27	Aug 28/Aug 29	Lauren Farm	250	Overb'dn	43°20.5′	79°52.5′	66	12	8	Unacceptable
28	Sep 3/Sep 4	Terra Cotta	330	Bedrock	43°43.3′	79°57.6′	72	24	2	Acceptable
29	Sep 3/Sep 4	Croatian Park	180	Overb'dn	43°29.2′	79°48.7′	72	25	25	Unacceptable
30	Sep 4/Sep 5	Early Farm	230	Overb'dn	43°37.5′	79°51.0′	72	24	50	Unacceptable
31	Sep 5/Sep 6	Conlin Farm	330	Overb'dn	43°34.5′	79°58.7′	72	14	21	Unacceptable
32	Sep 9/Sep 10	Sundance Resort	280	Bedrock	43°26.0′	80°05.0′	78	24	2	Very quiet†
33	Sep 14/Sep 15	Wasser Farm	230	Overb'dn	43°17.5′	80°09.3′	78	24	2	Very quiet*
34	Sep 21/Sep 22	Valens Cons. Area	270	Bedrock	43°23.3′	80°08.3′	78	24	25	Unacceptable
35	Sep 27/Sep 28	Hall Pike	210	Overb'dn	43°08.0′	79°58.5′	72	24	42	Unacceptable
36	Oct 1/Oct 2	Workman	210	Overb'dn	43°08.6′	80°04.0′	72	12	25	Unacceptable
37	Oct 11/Oct 12	Binbrook	200	Overb'dn	43°05.0′	79°49.5′	72	24	79	Unacceptable
38	Oct 21/Oct 22	Fulton	190	Bedrock	43°06.6′	79°35.7′	72	23	5	Unacceptable
39	Oct 21/Oct 22	Grimsby	190	Bedrock	43°09.5′	79°32.8′	72	23	5	Acceptable†

* *Quiet site, acceptable station.*

† *Selected site for microearthquake monitoring.*

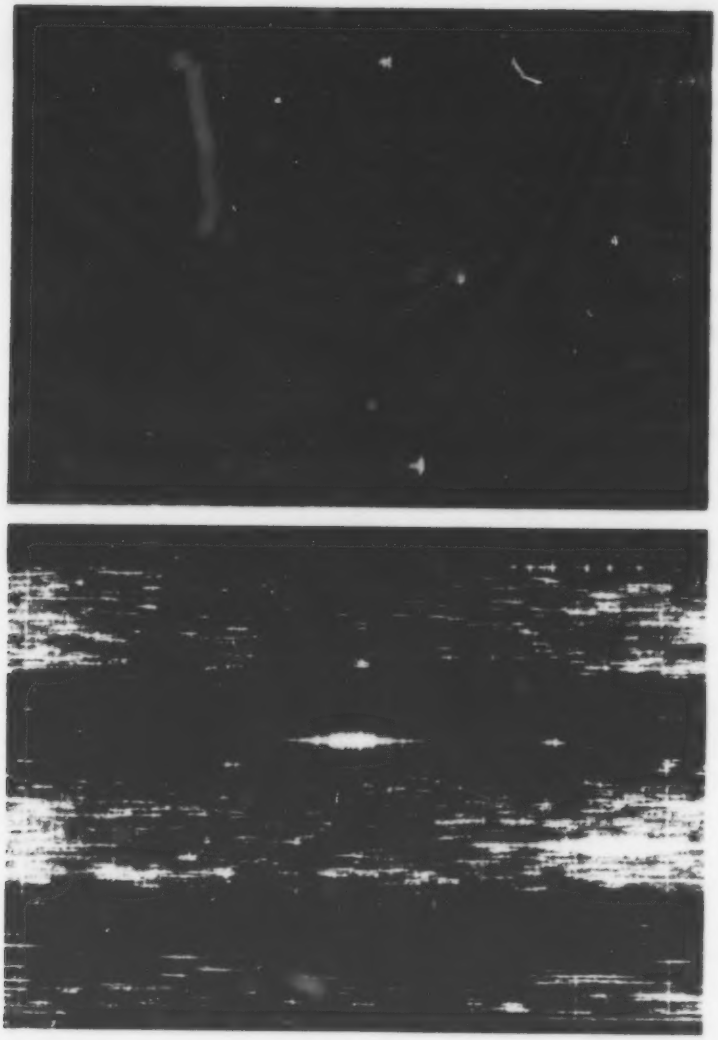

Photo 363.1. Two MEQ-800 records of 48 h duration from a noisy site (a) and a relatively quiet site (b), demonstrating the daytime increase in cultural noise level. **a)** Credit Valley Conservation Area; gain 60 dB; large event is a passing train. **b)** Conlin Farm; gain 66 dB; possible distant trains; the 3 large events are quarry blasts.

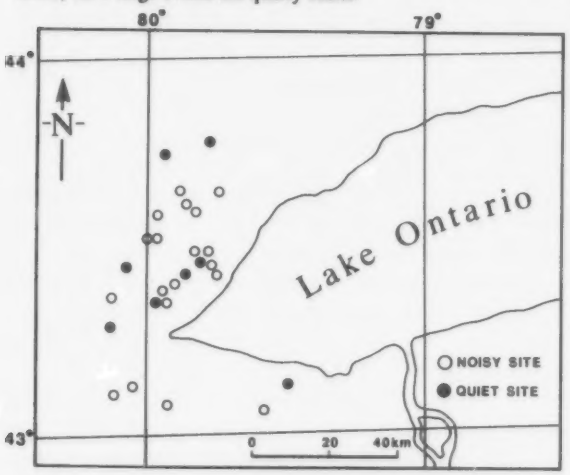

Figure 363.3. Recording sites occupied during a background-noise survey in the western Lake Ontario region. The black dots are those sites of relatively low noise level that are suitable for microearthquake monitoring.

objectives are 1) to increase the detection threshold to lower magnitude events, which may be more frequent but go unrecorded by the current national and regional networks (Mohajer 1987); 2) to increase the accuracy of earthquake location by using quarry blasts to obtain the local subsurface velocity structure; and 3) to search for surface and subsurface features that may be indicative of neotectonic activity.

The first phase of the study, reported herein, consists of a background-noise survey, selection of possible sites for deployment of seismograph stations, comparision of site noise levels and assessment of the equipment used.

This year we intend to set up and test 3 sites for semipermanent operation, and using this array we will be able to locate earthquakes in the Burlington–Hamilton area. We then intend to use quarry blasts of known position to increase the accuracy of subsequent earthquake locations.

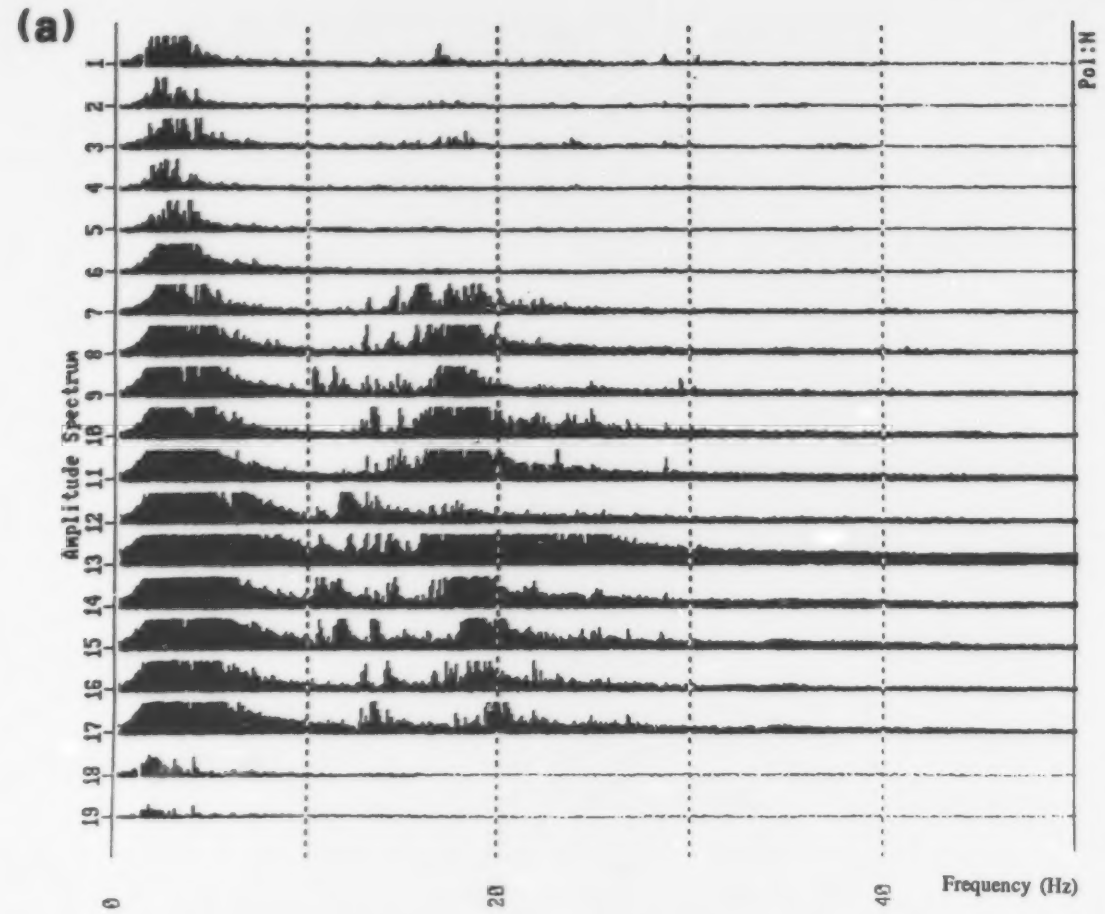

Figure 363.4. Amplitude-frequency spectra derived from PRS-4 recordings. **a)** From a noisy site.

In the final phase of the project, during the time that microearthquakes are being located by our array, we will begin a detailed search for geological signs of postglacial tectonic activity.

2. BACKGROUND

2.1 Rationale for Microearthquake Monitoring

The fact that there are more small earthquakes than large ones was originally quantified by Gutenberg and Richter (1956). They found a logarithmic relationship between the number and magnitude of relatively large earthquakes. Basically, a tenfold increase of earthquake occurrence is predicted for each unit decrease in magnitude.

In the late 1950s, researchers began to investigate the characteristics of smaller magnitude ($M < 3$) earthquakes. These shocks were termed microearthquakes and even ultra-microearthquakes (which have magnitudes as small as zero or less). Microearthquake studies in the past 3 decades have shown generally that 1) the physical mechanism of microearthquakes is the same as for larger events except for scale, i.e., it is related to fault movements; 2) the frequency of microearthquakes increases as magnitude decreases down to the smallest detectable events of about $M_L = -2$; 3) foreshocks, aftershocks and swarms of microearthquakes occur, similar to the situation with larger earthquakes; and 4) the spatial distribution of microearthquakes generally correlates with historical seismicity and with known faults.

Exceptions to these generalizations occur, and some controversy exists concerning the implications of microearthquake activity for earthquake-hazard potential. Nonetheless, it is widely held by seismologists that microearthquakes can be used to investigate seismicity and tectonics in regions of both major and minor seismicity. It is also believed that with precision surveys it is possible to identify specific faults on which strain release is taking place through active faulting.

Discovery of several aeromagnetic lineaments in the western Lake Ontario region (Forsyth et al. 1987; Mohajer and Thomas 1988; McFall and Allam 1990) and frequent reporting of microearthquakes in the region have renewed concern about the reliability of seismic hazard estimates for critical facilities. It is now generally recognized by the seismological community that earthquakes below the

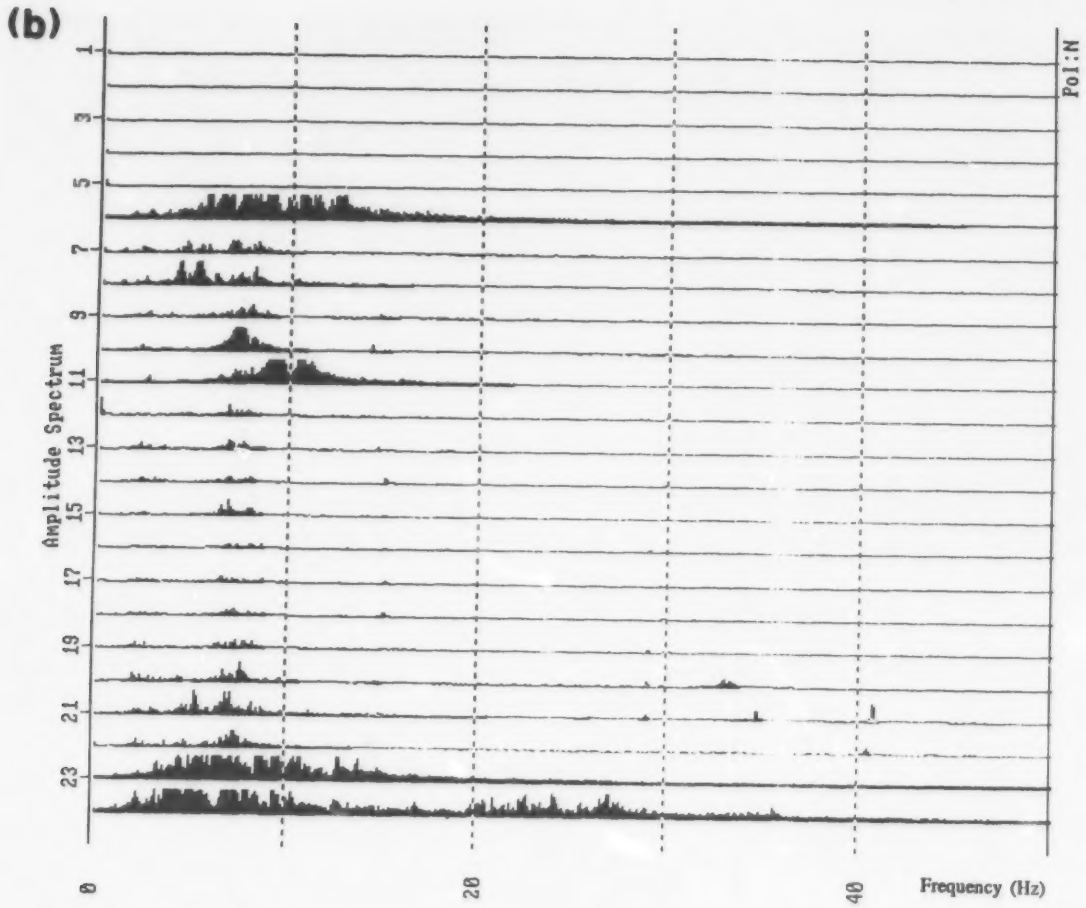

Figure 363.4 (concluded). **b)** From a relatively quiet site.

detection threshold of regional seismic networks are just as important as larger ones in defining the local stress field and the nature of the active faults, both large and small. This knowledge, coupled with the availibility of more sensitive instrumentation, opens a wide range of applications for precise monitoring of microearthquakes. These include 1) the definition of the location, geometry and sense of motion of active faults, 2) the testing of theoretical models of the earthquake process, 3) the mapping of tectonic stress patterns from the regional variation in fault parameters and stress drops and 4) the siting of new critical facilities and the safety review of old ones based on improved seismic hazard analysis.

2.2 Instrumentation

Microearthquakes represent low vibration-energy levels rich in high frequencies. These characteristics dictate the basic design principles for monitoring instruments with high sensitivity and high frequency response. In addition, many applications impose the added requirements of portability and low power consumption for remote operation. The low signal levels of microearthquakes are easily masked by cultural and natural ground vibrations. Some sites are thus ruled out unless deep borehole installations are possible. In the quietest terrestrial environments, a microearthquake with equivalent Richter magnitude of about –2 can be monitored with surface stations a few kilometres from the epicentre.

In addition, successful data analysis requires an accurate, synchronizable chronometer and provision for easy instrument calibration. For time-domain studies (event detection, hypocentre location, magnitude and recurrence-rate estimates, focal-mechanism determination, etc.), portable analogue or digital recorders at variable recording rates offer the simplest, cheapest and most cost-effective approach. For frequency-domain studies (source spectra, stress drops, source-time functions, spatial source-dimension estimates, etc.), digital recording is necessary. Two types of seismographic instruments are readily available for monitoring local microearthquakes. One approach is through continuous data transmission to a recording centre. An alternative method, used in this study, is to record the seismic motions at each station by either analogue or digital means and then to retrieve the

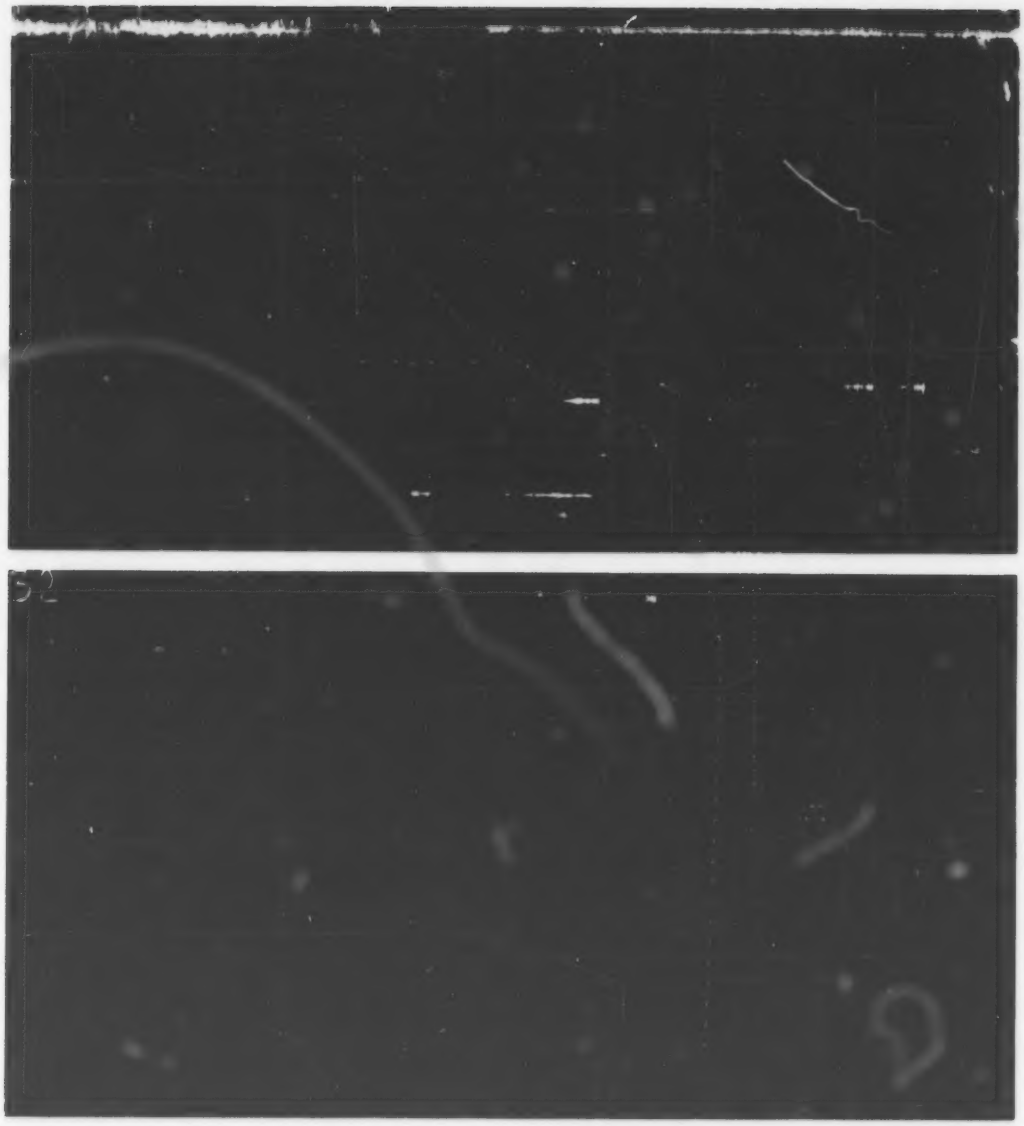

Photo 363.2. Analogue 24 h records from 3 sites forming the planned microseismic network. **a)** Grimsby: gain 72 dB; diurnal variation in cultural noise is apparent; **b)** Cambridge: gain 78 dB; possible tractor activity.

information at a later time for further processing. Instruments typically used in the latter technique are the classic portable smoked-paper seismographs, such as the Sprengnether MEQ-800, and a modern version of digital recording devices, such as the Scintrex PRS-4, which provides remarkable flexibility when a reconnaissance survey of background noise or an indication of the level of local earthquake activity is required.

3. EXPERIMENTAL PROCEDURE

A background-noise survey was carried out in the Hamilton–Burlington area between June and October 1989. Thirty sites (Figure 363.3) covering an area of >4000 km^2 were occupied. Several stations were visited more than once, so that a total of 39 deployments was made (Table 363.1). Three recording instruments were used: two MEQ-800 smoked-paper analogue recorders and one PRS-4 digital system. The advantage of analogue recording is that an immediate appreciation of the noise amplitude and character can be obtained in the field, whereas digital recording allows subsequent spectral and other analyses to be performed on the wave form.

The PRS-4 device is the instrument that we selected for long-term monitoring of earthquakes because it records only when triggered by an incoming signal whose amplitude exceeds a certain preset threshold. It is thus an ideal instrument for capturing relatively rare events; after several

Photo 363.2 (concluded). c) Mount Nemo: gain 78 dB; the record includes a teleseismic event.

weeks of recording, an immediate scan of all events can be obtained using a laptop or transportable field computer. However, the instrument can be used in a nontriggering (real-time) mode whereby the site response can be monitored for prescribed periods of time. During the noise survey we used this instrument in the nontriggering mode and tested it in the field by leaving it alongside one of the smoked-paper recorders for comparison purposes.

For all stations the seismometer was placed on bedrock unless drift thickness was prohibitive. Often the siting of stations was determined by the location of active farm lands, co-operation of property owners and our concern for instrument security. Despite these restrictions an attempt was made to obtain an even coverage of the area.

Instruments were left in the field for periods of 24 to 48 h. The PRS-4 was preset to sample the background noise in 90 s windows every hour. Depending upon the noise level, the gain settings on the MEQ-800 instruments ranged from 60 to 78 dB, where 60 dB corresponds to 1000 times magnification and each increment of 6 dB doubles the amplification.

We retrieved the data from the stations and displayed them using a Toshiba 1600 laptop computer and a multipurpose seismic program LITHOSEIS written by the Geological Survey of Canada (GSC). We computed power spectra using the commercially available digital signal-processing code VISTA. The frequency of site visits was once a day for time-mode operation used in the background-noise survey. Site visits varied from once a week to every 10 days for the triggered-mode operation. We are presently exploring the feasibility of installing modem telephone and power services at the sites that would convert data retrieval to an on-line, remote-control system.

4. RESULTS

The results of the noise survey showed that sites less than 3 km from railways and about 2 km from main roads are too noisy for microearthquake monitoring as they required gain settings of about 60 to 66 dB in order to maintain the long-term average (LTA) trace amplitude to about a millimetre (Table 363.1). However, 8 sites (Figure 363.3) where gain levels could be increased to the 72 to 78 dB range are suitable for more permanent seismograph stations. For all stations the average background noise increased during the daylight hours, corresponding to increased cultural activity. This behaviour is well shown for both noisy and quiet sites in MEQ-800 analogue records (Photo 363.1), which also illustrate the character of train and quarry-blast events.

PRS-4 records were obtained for each of the 8 stations and showed that the average noise level over a 24 h period varied between 150 and 250 nm/s for frequencies of 5 to 15 Hz, the range of interest for local earthquakes. This is an acceptable noise level for recording microearthquakes of $M_L \geq 1$ that occur within about 50 km of the station. Amplitude-response spectra for a noisy and quiet site (Figures 363.4a and 363.4b, respectively) show peaks at about 3 and 18 Hz, the latter being suppressed in the quiet site. Fortunately, in the expected earthquake-frequency band, the cultural noise is relatively low.

During the noise survey a local earthquake of $M = 3.3$ occurred on August 5, 1989, and was extensively felt over a large area between Mississuaga and Burlington. The epicentral location given by the GSC for this shock was at lat. 43.29°N, long. 79.76°W (about 10 km east of Hamilton), which is puzzling in view of the lack of felt reports in the Hamilton–Niagara area. An aftershock of $M = 2.2$ on August 9, 1989, triggered our PRS-4 instrument at a 60 km distance, but we could not obtain its location because only

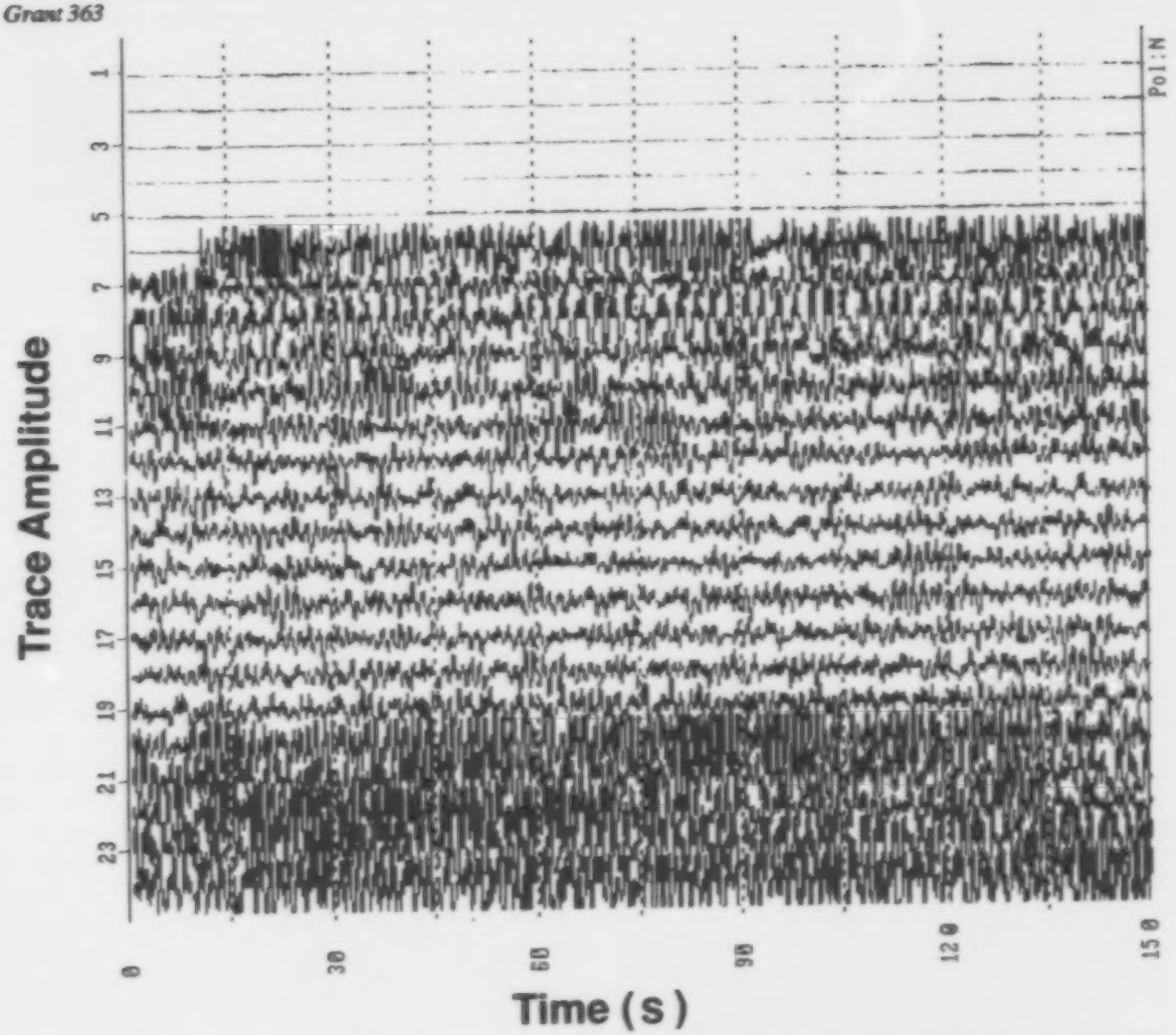

Figure 363.5. A seismogram of 24 samples, each of 90 s duration, taken at hourly intervals with a PRS-4 digital recorder at Mount Nemo. For the top 5 traces the seismometer was disconnected to record internal instrument noise.

a single station was in operation at the time. Nevertheless, the occurrence of such events in the western Lake Ontario region emphasizes the necessity for a comprehensive microearthquake-monitoring program in this region.

5. FURTHER DEVELOPMENTS

Since completion of the noise survey, we selected 3 sites for our seismograph stations (Figure 363.2). The choice represents a compromise between low noise levels and the optimum configuration and position of the seismic network. The 3 stations, for which analogue records are shown in Photo 363.2, are at Mount Nemo Conservation Park (lat. 43°25.3′N, long. 79°52.5′W, elevation 290 m), on a farm 12 km east of Cambridge (lat. 43°17.75′N, long. 80°9.4′W, elevation 250 m) and near Grimsby on the Niagara Peninsula (lat. 43°9.5′N, long. 79°32.8′W, elevation 190 m).

Extended recording using two PRS-4 instruments is currently underway at the Mount Nemo and Cambridge sites. The 2 stations were synchronized with Universal Standard Time through a Nanometrics 501F field clock. At both stations the seismometer is anchored on bedrock, and mean background-noise levels are exceptionally low (78 dB gain possible on MEQ-800 records). A representative digital recording from the Mount Nemo site (Figure 363.5) reaffirms the excellent response at this station. The Cambridge site is protected by electrical fencing and has a solar cell to maintain battery levels. The third station at Grimsby will be tested initally with an MEQ-800 recorder and later with a PRS-4 instrument on temporary loan from the GSC. At that time all 3 stations will be operating, and thus earthquakes and other events can be located. We will also use the network to locate quarry blasts of known position and to use the residual between actual and computed position to refine earthquake locations. Although many quarries exist in the vicinity of western Lake Ontario, only 10 are presently active (Figure 363.2).

Table 363.2. Location and blast schedule of active quarries around western Lake Ontario.

Quarry	Lat. (N)	Long. (W)	Altitude (feet)	Approx. blast window*
Nelson Aggregates, Lincoln	43°10'36"	79°40'00"	650	Every day, 4:00–5:00 p.m.
Nelson Aggregates, Burlington	43°24'24"	79°53'14"	910	Fridays, 9:00 a.m. (as many as 5 blasts)
Walker Bros., Stanford	43°07'53"	79°10'49"	600	Every day, 12:00–12:30 p.m. (1 blast but sometimes 2)
Walker Bros., Vineland	43°07'30"	79°14'25"	580	No specific time (1 blast)
Steetly Industries, Queenston	43°09'08"	79°05'00"	619	No specific time (1 blast)
Steetly Industries, Dundas	43°17'30"	79°59'32"	550	Every day between 11:30 a.m. and 12:30 p.m. and 3:30–4:30 p.m. (up to 2 blasts per day)
Taro Aggregates, Hamilton	43°11'31"	79°46'28"	660	No specific time (1 blast)
Dufferin Aggregates, Downsview	43°31'25"	79°57'53"	1040	Every day, 4:00–4:30 p.m. (1 blast)
Halton Crushed Stone, Halton	43°32'30"	79°57'30"	1020	Every day, 12:00–12:15 p.m. (uncertain)
United Aggregates, Acton	93°30'23"	79°55'00"	1050	Weekdays, at 12:00 p.m. (1 blast); may blast at 10:30 a.m. or 2:30 p.m.

* *Note: May or may not blast on schedule.*

Approximately 90 events have been recorded at Mount Nemo, with an average of 20 events per week. Seventy percent of the data are known quarry blasts as determined from blasting schedules (Table 363.2). Twenty percent are incidentally triggered events caused by heavy machinery and animal activity. The latter group of events can easily be identified on the basis of their wave form. Nevertheless, about 10% of the events are not readily identifiable; they could be natural events, and their origin needs further investigation.

6. CONCLUSIONS

A background seismic noise survey, preparatory to the establishment of a three-station network for microearthquake monitoring, was carried out at 30 sites in the western Lake Ontario region. This area was selected because its seismicity, in the context of southwestern Ontario, is relatively high. The purpose of our investigation is to understand the geological cause of the earthquakes, which in turn may help to increase the reliability of earthquake-hazard assessment in an industrially sensitive part of Canada.

High levels of cultural noise, produced mainly by rail and road vehicles, quarry blasts and farm-related activities, rendered all but 8 of the occupied sites unsuitable for permanent microearthquake monitoring. Continuous recording over a period of several weeks at 2 of the quietest sites, near Burlington and Cambridge, suggests that high-fidelity records of local microearthquakes ($M_L \sim 1$) within a distance of about 60 km from the array can be obtained.

ACKNOWLEDGMENTS

This work has been supported by the Ontario Geological Survey through the Geoscience Research Grant Program. The GSC loaned two MEQ-800 seismographs. Gordon West (Geophysics Laboratory, University of Toronto) provided seismometers and much helpful advice. Bert Ellison, Rebecca Irving, Dennis Carlos, Peter Hurley and Robert McGrory assisted with field work and data reduction.

REFERENCES

Adams, J. and Basham, P. 1989. The seismicity and tectonics of eastern Canada; *in* Neotectonics of North America, Geological Society of America, v.CSMV-1, p.127-142.

Bollinger, G.A. and Wheeler, R.L. 1988. The Giles County, Virginia seismic zone: seismological results and geological interpretation; United States Geological Survey, Professional Paper 1355.

Boore, D. M. and Atkinson, G. 1987. Stochastic prediction of ground motion and spectral response parameters at hard rock sites in eastern North America; Bulletin of the Seismological Society of America, v.77, p.440-467.

Forsyth, D.A., Thomas, M.D., Real, D., Abinett, D., Broome, J. and Halpenny, J. 1987. Geophysical investigations of the Central metasedimentary belt, Grenville Province: Quebec to northern New York State; Proceedings, 7th International Conference on Basement Tectonics.

Gutenberg, B. and Richter, C.F. 1956. Earthquake magnitude, intensity, energy, and acceleration; Bulletin of the Seismological Society of America, v.46, p.104-145.

McFall, G. H. and Allam, A. 1989. Neotectonic investigations in southern Ontario: Prince Edward County—phase I; Atomic Energy Control Board, Open File Report 3.131.1.

Mohajer, A.A. 1987. Relocation of earthquakes and delineation of seismic trends in western Quebec and southern Ontario; Atomic Energy Control Board, MAGNEC Contribution 87-01.

———1989. Seismotectonic framework of western Quebec: relocation of seismic events, phase 2; unpublished report for the Safety and Safeguards Section, Atomic Energy Control Board.

Mohajer A.A. and Halls, H.C. 1989. A seismotectonic study of the western Lake Ontario region. Phase 1: A background noise survey; poster, Ontario Geological Survey, Annual Open House, Toronto, Ontario, December 1989.

Mohajer, A.A. and Thomas, R.L. 1988. Seismicity pattern and neotectonic features in the Lake Ontario region; *in* Seismological research letters, Proceedings, Seismological Society of America, Eastern Section, 60th Annual Meeting.

Parrish, J.B. 1989. The seismicity of Ohio and its relationship to potential field and remote sensing lineaments; lecture, Geological Association of Canada, Annual Meeting, Montréal, Quebec, May 15–17.

Smith, W.E.T. 1962. Earthquakes of eastern Canada and adjacent areas, 1534–1927; Dominion Observatory (Canada) Publication, v.26, no.5.

Stauder, W. 1982. Present-day seismicity and identification of active faults in the New Madrid seismic zone; United States Geological Survey, Professional Paper 1236-C, p.21-30.

Wallach, J.L. and Mohajer, A.A. 1990. Integrated geoscientific data relevant to assessing seismic hazard in the vicinity of the Darlington and Pickering nuclear power plants; Proceedings, Canadian Geotechnical Conference, Québec, Quebec, October.

Grant 364 The Kerr Addison–Chesterville Archean Gold-Quartz Vein System, Virginiatown: Time Sequence and Associated Mafic "Albitite" Dike Swarm

J.P. Smith[1], E.T.C. Spooner[1], D.W. Broughton[2] and F.R. Ploeger[3]

[1] Department of Geology, Earth Sciences Centre, University of Toronto, Toronto
[2] Golden Shield Resources, Kerr Mine, Virginiatown, Ontario
[3] GSR Mining / Desk Resources Ltd., Kerr Mine, Virginiatown, Ontario

ABSTRACT

The combined Kerr Addison–Chesterville mines (~335 t Au) comprise Canada's fifth largest Archean gold-quartz vein-disseminated ore system. The deposit is a structurally controlled vein system that is syndeformational and, unusually, located *within* a ~300 km long first-order structure, the Larder Lake–Cadillac Break. The break is interpreted as a south-over-north, flattened and steepened thrust, localized along a thin, incompetent, ultramafic horizon (strong foliation developed over ~50 to 150 m width). Mine host lithologies comprise deformed and altered ultramafic spinifex-textured komatiites, Fe-tholeiite pillow lavas, mafic "albitite" intrusions and graphitic metasediments. The gold-quartz vein system is contained within a flat, funnel-shaped hydrothermal alteration envelope, plunging ~70°E to a deep focal (≥4 km) fluid source. Based on mapped crosscutting relationships in over 50 areas of the mine, a detailed relative time sequence has been built up comprising 10 stages of veining and 4 episodes of igneous intrusion. A significant finding of this study has been that the gold-quartz vein system and associated hydrothermal alteration were developed cospatially, costructurally and significantly overlapping in time with 3 major plugs and an intense swarm of more than 5000 mafic "albitite" dikes. The significant closeness (space, structure, time) between intrusions and mineralization suggests that gold mineralization may have been magmatically derived from a parent intrusive body at ≥4 km depth.

INTRODUCTION

The Kerr Addison–Chesterville Archean gold-quartz vein-disseminated ore system, located near Virginiatown and Kearns, ~500 km north of Toronto, 2 km west of the Quebec border, is significant because of its size (~335 t Au) and unusual location *within* the Larder Lake–Cadillac Break, a major tectonic structure ~300 km long, which to the east of Kearns defines the Pontiac–Abitibi subprovince boundary (e.g., Robert 1989); to the west, the break lies within the Abitibi greenstone belt (*see* Figure 364.1).

A narrow, ~10 km wide structural corridor along the break constitutes a very significant gold-producing zone, with total production plus reserves of ~1900 t Au from ~75 mines (*see* Figure 364.1). However, most of the mines are located on subsidiary structures rather than in the break itself (e.g., Colvine et al. 1988). Thus, the large Kerr Addison–Chesterville system is unusual because of its location within the main break structure, where it is syndeformationally contained within a 150 m wide zone of foliation intensification and is crosscut by the later, brittle Kerr fault.

As the data in Table 364.1 show, the combined Kerr Addison (34.93 Mt at 9.3 g/t Au)–Chesterville (2.96 Mt at 3.8 g/t Au) mines comprise the fifth largest known (~335 t Au) Archean gold-quartz vein ore system in the Superior Province, after Hollinger–McIntyre (~995 t Au), the 7 Kirkland Lake mines that define a single system (~715 t Au), Campbell–Dickinson in the Red Lake area (~460 t Au) and the Dome Mine (~390 t Au). In common with many other Archean gold-quartz vein systems (e.g., Hollinger–McIntyre, Lamaque–Sigma) the Kerr Addison–Chesterville gold system is locally enriched in W (e.g., 1533 t at 0.5 to 0.7% WO_3 produced in 1942; reserves defined at that time of 46 300 t at 0.085% WO_3).

The principal objectives of this report are 1) to describe and interpret the relative sequence of deformation, hydrothermal veining and mineralization, and igneous intrusive events in the Kerr Addison–Chesterville system; and 2) to document and discuss the significance of a mafic "albitite" dike swarm-intrusive plug system spatially, structurally and temporally associated with gold mineralization.

This research is based on ~21 person-months of field work over 3 years, including ~18 person-months of underground mapping and observations in over 50 areas of the Kerr Addison Mine, correlation of over 6000 drill holes towards complete geological reconstruction of 27 of the 31 Kerr Addison mine levels (J.P.S.), addition of all available data on Chesterville, 12 person-weeks of surface mapping at a scale of 1:10 000 along the break in the Virginiatown area (1989) and compilation of previous published and unpublished literature on the 2 mines.

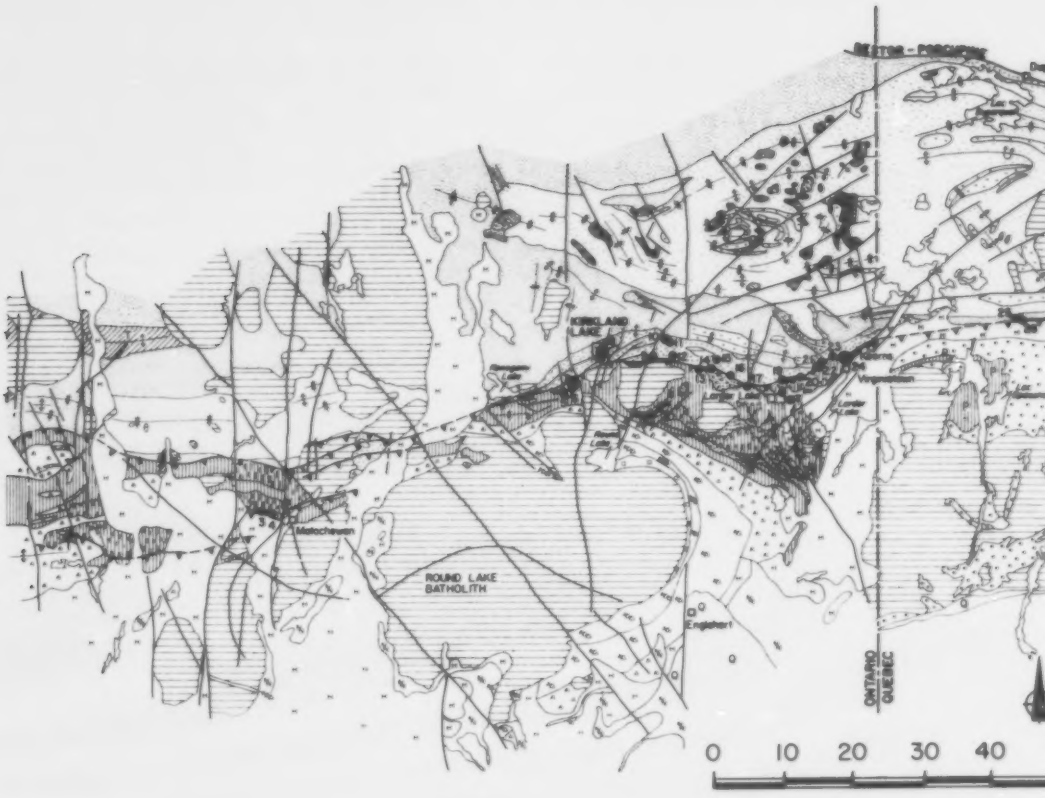

Figure 364.1. Structural and stratigraphic compilation map showing the Larder Lake–Cadillac Break and its close spatial association with 75 presently or past-producing gold mines and some recent exploration projects (OGS–MERQ 1983; W. Powell, Queen's University, personal communication, 1989). For stratigraphic units refer to OGS–MERQ (1983). The mines are numbered as follows: 1) Stairs; 2) Ashley; 3) Young–Davidson; 4) Matachewan Consolidated; 5) Crescent Kirkland; 6) Golden Gate; 7) Lucky Cross; 8) Kirkland Lake Camp (8 mines): Macassa, Kirkland Gold, Teck–Hughes, Lakeshore, Wright–Hargreaves, Sylvanite, Toburn, Kirkland Townsite; 9) Pawnee; 10) Bidgood; 11) Moffat–Hall; 12) Morris Kirkland; 13) Upper Canada; 14) Anoki; 15) McBean (Queenston); 16) Princeton/Ritoria/Olivet; 17) Misema River; 18) Raven River; 19) Omega; 20) Fernland; 21) Cheminis; 22) Barber–Larder; 23) Armistice (Arjon); 24) KERR ADDISON–CHESTERVILLE; 25) Francoeur; 26) Arntfield; 27) Wakeko; 28) Bazooka; 29) Durban; 30) Cinderella; 31) Granada; 32) Plexore; 33) McWatters; 34) Rouyn Merger; 35) Heva Cadillac; 36) Hosco; 37) Odyno (Calder Bousquet); 38) Norgold; 39) Doreva; 40) Mic Mac; 41) Mooshla; 42) Doyon (Silverstack); 43) Westwood–Warrenmac; 44) Bousquet; 45) Dumagami; 46) Bouscadillac; 47) New Alger (Thompson Cadillac); 48) Darius (O'Brien); 49) Kewagama; 50) Consolidated Central Cadillac; 51) Wood Cadillac; 52) Lapaska (?Lara); 53) Pan Canadian; 54) West Malartic; 55) Canadian Malartic; 56) Sladen Malartic; 57) East Malartic; 58) Malartic Goldfields; 59) Camflo/Malartic Hygrade; 60) Aur (1st Canadian); 61) Malartic Goldfields; 62) Kiena; 63) Lamaque; 64) Sigma; 65) Bramineo (#4); 66) Sigma-2.

HOST LITHOLOGIES

Ultramafic Horizon (Base of Larder Lake Group)

Throughout McGarry Township along strike from the Kerr Addison–Chesterville gold system a thin (usually <30 m), laterally extensive horizon of altered ultramafic, komatiitic flows occurs spatially related to, and on the south side of, the Larder Lake–Cadillac Break (Figure 364.2; *see also* Downes 1980, 1981). The Kerr Addison–Chesterville gold system is characterized by a thick lens (~100 to 150 m) of these incompetent ultramafic rocks, which narrow or pinch out both to the west of Kerr Addison and to the east of Chesterville (*see* Figure 364.3). The komatiites locally show well-preserved pseudomorphed spinifex textures in all stages of deformation and alteration (e.g., Tihor and Crocket 1977).

Ultramafic breccias are not seen along this horizon, which appears to consist of altered flows. The ultramafic rocks have been traced for >1 km east of Kearns by drilling underneath the unconformable Proterozoic Huronian sediments and probably correlate farther east with the Piché Group volcanics (~50 to 1000 m thick) in Quebec. They are also traceable as a semicontinuous horizon for >50 km to the west along the break as far as Kenogami Lake (Tihor and Crocket 1977).

South of the Ultramafic Horizon (Larder Lake Group)

In the vicinity of Kearns and Virginiatown, the area immediately south of the ultramafic break horizon (*see* Figure 364.1) comprises a ~400 m thick mixed assemblage of predominantly Fe-tholeiitic pillow lavas, with lesser ultramafic rocks, tuffs, agglomerates and sediments. A major ~300 m wide zone of ultramafic flows occurs underneath the northeast arm of Larder Lake and outcrops on its north shore. South of this, underground drilling from the Kerr Addison Mine has detected significant widths of greywackes under the Huronian sediments. Within the Kerr Addison–Chesterville gold system, the Fe-tholeiite pillow

lavas are mineralized to form the "flow ore" type (e.g., #21 and #16 orebodies). The #21 to #16 flows (*see* Figures 364.3, 364.4a, 364.4b) appear to be a stratigraphically isolated inclusion of mafic volcanics within ultramafic to transitional mafic-ultramafic flows and are not continuous with mafic volcanics south of the Kerr fault. Graphitic interflow sediments occur within the mafic volcanics and have localized post-ore faults (e.g., Kerr fault, which displaces part of the #21 orebody; graphitic faults south of the Barber and Omega deposits). More ultramafic rocks, including conglomerates and breccias with spinifex-bearing ultramafic fragments, are exposed in a cliff southeast of the Kerr Addison tailings pond (e.g., Downes 1980).

Farther to the west, a large area extending down to the shore of Larder Lake comprises fine-grained, thinly bedded distal turbidites. Near the break, between these sediments and the ultramafic rocks, lies a thin pillowed mafic flow-hyaloclastite horizon, which is mineralized to form the ore in the Barber Pit and the Cheminis Mine. Evidence from graded bedding in the vertically dipping Larder Lake Group sediments in the south wall of the Barber Pit indicates that local facing is to the south (1989 observations; J.P.S. and E.T.C.S.). There is no evidence for major discontinuities in the above sequence. Hence, the Larder Lake Group is interpreted as a south-facing succession of ultramafic and tholeiitic volcanics, volcaniclastic breccias and distal turbiditic sediments, north dipping (i.e., overturned) in the vicinity of the Kerr Addison Mine.

Table 364.1. Historic production figures plus proven reserves (t Au) for the 8 largest gold-quartz vein systems in the Superior Province.

Ranking	Au (t)
1. Hollinger–McIntyre	~995
2. Kirkland Lake (7 mines)	~715
3. Campbell–Dickenson (Red Lake)	~460
4. Dome	~390
5. Kerr Addison–Chesterville	~335
6. Lamaque–Sigma	~254
7. Doyon–Bousquet–Dumagami	~245
8. Pamour #1	~101

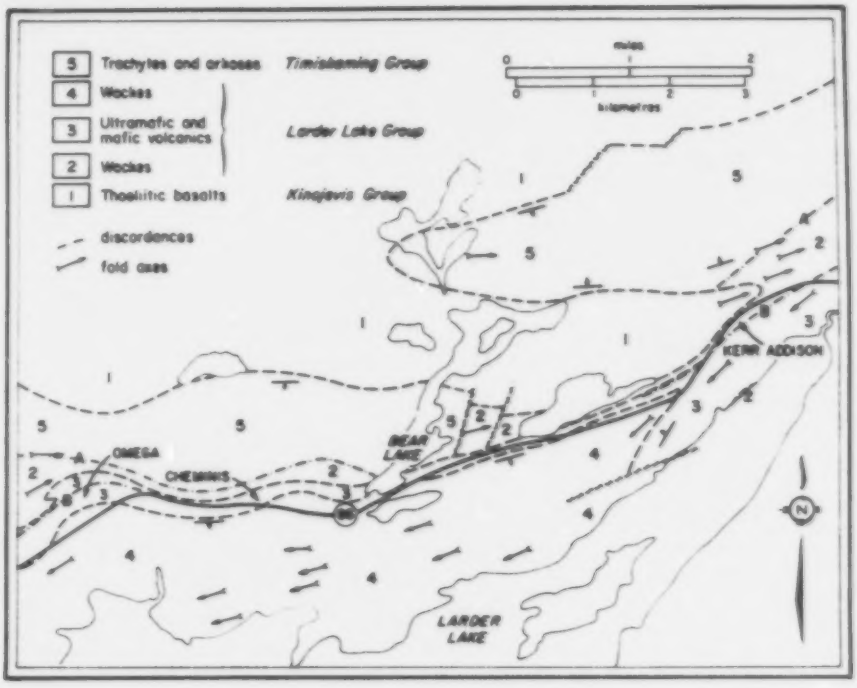

Figure 364.2. Geological map of McGarry Township (*from* Downes 1981) showing structural discordances "A" and "B" and opposing plunges of fold axes either side of the break.

North of the Ultramafic Horizon (Timiskaming and Kinojévis Groups)

In the northern part of McGarry Township is a series of north-facing, alternating Mg- and Fe-tholeiitic basalt flows assigned to the Kinojévis Group. Scattered outcrops of fine-grained, massive or brecciated rhyolite are also present. The older volcanics are overlain with angular unconformity (Thomson 1946; Jackson 1988) by opposite- (south-) facing coarse basal conglomerates of the Timiskaming Group. The conglomerates are polymictic, clast supported and interbedded with thick lenses of fluvial trough cross-bedded sandstones (Hyde 1978). Stratigraphically above these, the sequence is dominated by feldspar-porphyritic, trachytic agglomerates and flow breccias, with narrow, interbedded conglomerate horizons. The trachytes are cut on their south side, north of Virginiatown, by structural discordance "A" of Downes (1980, 1981) (*see* Figure 364.2). South of the discordance are thin-bedded, fine- to medium-grained proximal turbidites with background black argillites (Hyde 1978). These are again south facing. Across a further discordance to the south are thicker bedded, coarser grained turbidites with increased sand contents (Hamilton 1986). These become tightly folded at the nose of the Spectacle Lake anticline, and a thin (<30 m) south limb of schistose, fine-grained sediments continues adjacent to the break, just north of the Kerr Addison Mine, and connects through to a thicker section of Timiskaming sediments north of the Armistice and Barber–Larder deposits.

It has been considered (e.g., Ridler 1970, 1976; Hyde 1980) that the sediments south of the Larder Lake Break can be correlated with the Timiskaming succession because of their lithological similarities. However, it has been shown (e.g., J.E. Thomson 1943; Jensen 1985; Hamilton 1986; Toogood and Hodgson 1986) that marked differences in clast contents exist between conglomerates of the 2 sediment types. For example, the Timiskaming succession contains abundant distinctive trachyte (locally derived from volcanics), jasper (unknown distal source) and only occasional ultramafic clasts, whereas the Larder Lake Group generally has no trachyte or jasper and has abundant locally derived, intraformational ultramafic-mafic and banded iron formation clasts. Recent precise U-Pb geochronology (F. Corfu, Royal Ontario Museum, unpublished data, 1990) and trace-element geochemistry of the 2 sedimentary types (Feng and Kerrich 1990) show that they are of widely different ages (~2705 Ma for the Larder Lake Group versus ~2680 Ma for the Timiskaming), were derived from compositionally different source areas and were tectonically juxtaposed across the break.

STRUCTURAL DEVELOPMENT OF THE LOCAL AREA

External to the Kerr Addison–Chesterville Gold System

The Larder Lake Group ultramafic–Timiskaming sediment contact is interpreted as having been a south-over-north thrust for the following reasons: 1) way-up determinations from normal grading and trough cross-bedding in sediments on either side of the contact indicate that both units are south

facing, although locally they are overturned and north dipping; 2) south-over-north kinematics based on asymmetrically folded fabrics was described by Hamilton (1986); 3) a subvertical to steeply east-plunging lineation defined by elongation of clasts and/or intersection of cleavages occurs within the plane of the foliation; 4) associated early F_1 folds have vertical to northeast-verging axial planes; 5) strain intensity increases symmetrically into the contact; 6) evidence exists for a possible southward shallowing at depth (listric geometry to the break) from underground development and drilling at the Cheminis, Omega and McBean–Anoki mines (J.E. Thomson 1943; Hamilton 1986; Queenston Mining Ltd., Kirkland Lake, personal communication, 1989); 7) U-Pb geochronology (Corfu et al. 1989; F. Corfu, Royal Ontario Museum, unpublished data, 1990) indicates that older Larder Lake units thus structurally overlie the younger Timiskaming units. A thrust origin for the break is in agreement with ideas suggested by J.E. Thomson (1943, 1948) and Hamilton (1986). High-angle north- or northeast-trending shear-zone structures also intersect the break from the south, notably at Misema River, Larder Lake (e.g., Raven River Mine) and the northeast arm of Larder Lake, in each case corresponding to a change in the dip and strike of the break.

In McGarry Township, the break is characterized by intense development of a flattening foliation over a width of ~50 to 150 m, within a wider zone of moderate fabric development. Fabric intensity is closely related to lithology (especially in ultramafic host rocks) and proximity to the ultramafic-greywacke contact. Evidence for flattening deformation is from aspect ratios (e.g., 5:5:1, J.P.S. measurements) of finite-strain markers (e.g., pillows, varioles and polyhedral vein networks). Lineations are poorly developed or absent in the ultramafic rocks. In the pillowed mafic volcanics, deformed varioles are flattened perpendicular to the foliation and, rarely, define a steeply plunging lineation.

Based on detailed field mapping between Larder Lake and Kearns, Hamilton (1986) divided the Larder Lake–Virginiatown area into coherent lithostructural domains and subdomains, separated by structural discontinuities. The Larder Lake–Cadillac Break and associated structures were considered as defining an east-trending deformation zone several kilometres wide. Within this zone, strain is heterogeneously developed as small (tens of metres wide), high-strain zones, subparallel to or splaying off the break and anastamosing around lozenge-shaped lower strain areas. In contrast to Jensen and Langford (1985), Hamilton (1986) was able to demonstrate that fabrics are pervasively developed throughout the area and that overprinting of fabrics of different orientations does occur.

Internal to the Kerr Addison–Chesterville Gold System

Lithological units (*see* Figures 364.3, 364.4a and 364.4b) strike ~060° and dip ~78°NW conformably with the foliation and appear to be overturned and facing south. Ductile flattening deformation along the break is heterogeneously developed within all the units shown. Underground measurements indicate that the predominant foliation in both ore types strikes ~057° and dips ~78°NW (*see* Figures 364.5a and 364.5b). Two measurements have also been made of a steeply plunging lineation defined by elongated, flattened varioles in the flow ore (e.g., 1117-63 stope). This is in agreement with observations farther along the break by Hamilton (1986) and Jackson (1988). No lineations were observed in the ultramafic host rocks, where the fabric is dominated by intense flattening. Previous workers (e.g., J.E. Thomson 1943; Buffam and Allen 1948) noted a steep, east-plunging, S-shaped fold within the Chesterville Mine, which they interpreted as a drag fold caused by movement on the break. The Kerr Addison–Chesterville gold system and the blind Chesterville East orebody (see below) both plunge ~70°E within the plane of the break. No evidence has been found to suggest that the Kerr Addison Mine is located in an anticlinal fold structure, as suggested by Downes (1980, 1981) and Charteris (1984). There is a general lack of stratigraphic marker units within the komatiite lithologies.

Kinematic observations from underground mapping indicate progressive development of a ductile flattening fabric with boudinage and folding of synkinematic veins and dikes, especially if emplaced at a high angle to fabric. Some of the late "mylonitic" faults show shallow, south-dipping, sigmoidal tension gash veins indicative of late north-side-up fault movement and reorientation of the break to a northwest dip.

DISTRIBUTION AND CHARACTERISTICS OF PRINCIPAL ORE TYPES

Principal Ore Types

The main Kerr Addison–Chesterville gold system comprises 4 main ore types: "flow ore", "green carbonate or siliceous break ore", "albitite ore" and "graphitic ore", distributed among 19 (Kerr Addison) and 8 (Chesterville) orebodies. ("Siliceous break" or "sil break" is a local mine term for a quartz-dominated often gold-mineralized vein, or fault structure, with included wall-rock fragments; these have widths of ~1 to ~10 m and mapped strike lengths of <10 to >100 m.) The grade-depth variations of the flow ore (Kerr Addison: 21.08 Mt at 11.2 g/t Au, including graphitic ore) and green carbonate ore (Kerr Addison: 13.29 Mt at 8.0 g/t Au) are shown in Figure 364.6.

The Kerr Addison–Chesterville ore zones are developed principally within strained and altered ultramafic komatiite, Fe-tholeiite pillow lava, mafic "albitite" dike and graphitic metasedimentary lithologies over a 900 m strike length near surface, which shortens to ~600 m at the 3850-foot level, and over widths of ~150 to 200 m. Individual orebodies within the ultramafic-hosted green carbonate or siliceous break ore are contained within a hydrothermal alteration envelope, defined by the maximum extent of emerald-green, fuchsitic (Cr-mica) alteration and recording gold-related K-, SiO_2- and CO_2-metasomatism overprinting early, barren, pervasive carbonate (+ talc, chlorite) alteration. The green carbonate envelope has a strike length of ~900 m on surface, decreasing to ~300 m at the 5600-foot level, and a maximum width of up to 150 m.

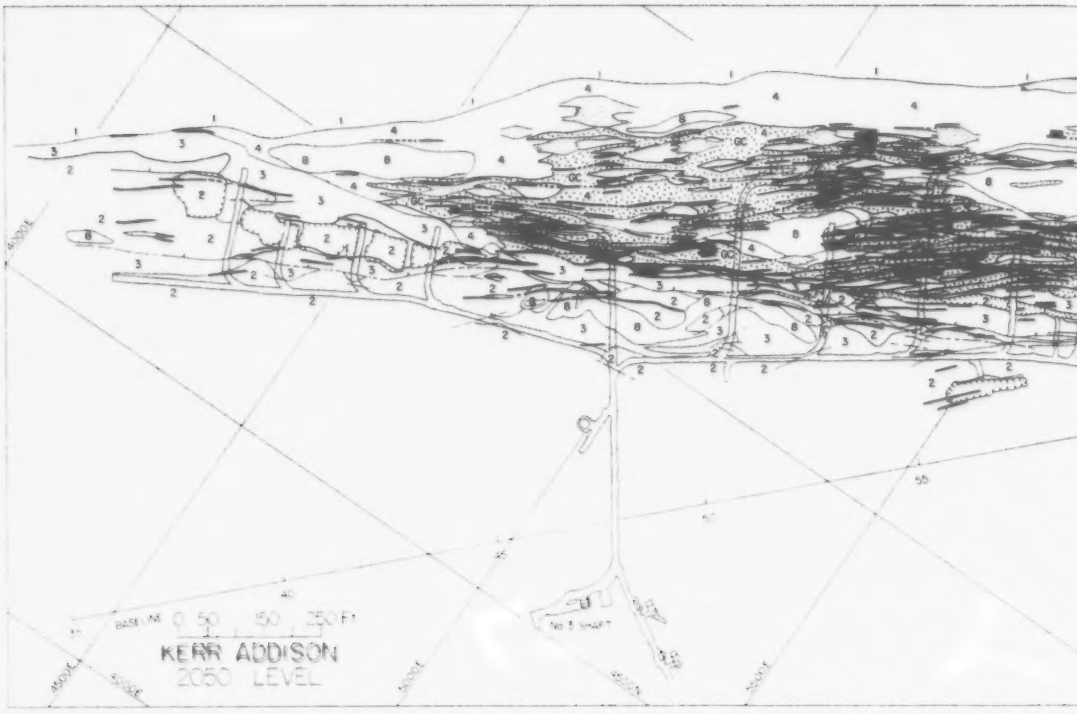

Figure 364.3. Combined Kerr Addison 2050-foot level–Chesterville 2037-foot level geological plan, reconstructed from drift mapping and closely spaced diamond drilling (sections ~11 m apart). The figure shows the principal geological units and the distribution of "green carbonate" alteration versus areas of barren, precursor, talcose ultramafic host rock.

At Kerr Addison, minor tungsten was also produced (1533 t at 0.5 to 0.7% WO_3) in 1942 from low-grade disseminated scheelite ore (proven reserves: 46 300 t at 0.085% WO_3). The scheelite was reported to occur as millimetre-scale, white crystals (R.E. Folinsbee, Geological Survey of Canada, personal communication, 1989) disseminated particularly in the transitional mafic-ultramafic host rocks to the north of the #21 flow orebody (Folinsbee 1943).

Ore Distribution Relative to Level-plan Geology

Representative level plans (2050-, 2650- and 2800-foot levels) are shown in Figures 364.3, 364.4a and 364.4b and exhibit the following features: 1) the break contact with Timiskaming sediments to the north; 2) the lens shape of the ultramafic host rocks, narrowing down or pinched out to the west and the east; 3) the isolated sliver of mafic flows hosting the #21 and #6/#8 orebodies; 4) a narrow zone of transitional mafic to ultramafic rocks between the 2 main lithologies; 5) a package of dominantly mafic flows and agglomerates to the south, with lesser tuffs and sediments; 6) repetition of units and orebodies across the late, graphitic post-ore Kerr fault; 7) major mafic plugs and an intense swarm of mafic "albitite" dikes, confined mainly to the ultramafic unit and coextensive with the limits of ore and green carbonate alteration; 8) a swarm of "siliceous break" main-stage gold-quartz veins, especially in the green carbonate ore; and 9) barren "horses" of talc-chlorite-carbonate rocks representing relict ultramafic precursors not overprinted by later gold-related alteration. The orebodies are contained largely within the mafic and ultramafic units, with the transitional volcanics less favourable to mineralization. No ore occurs north of the sediment contact.

Ore Distribution Relative to Longitudinal Sections

Figures 364.7a and 364.7b show vertical longitudinal projections of the Kerr Addison–Chesterville gold system, within the plane of the break, for the green carbonate and

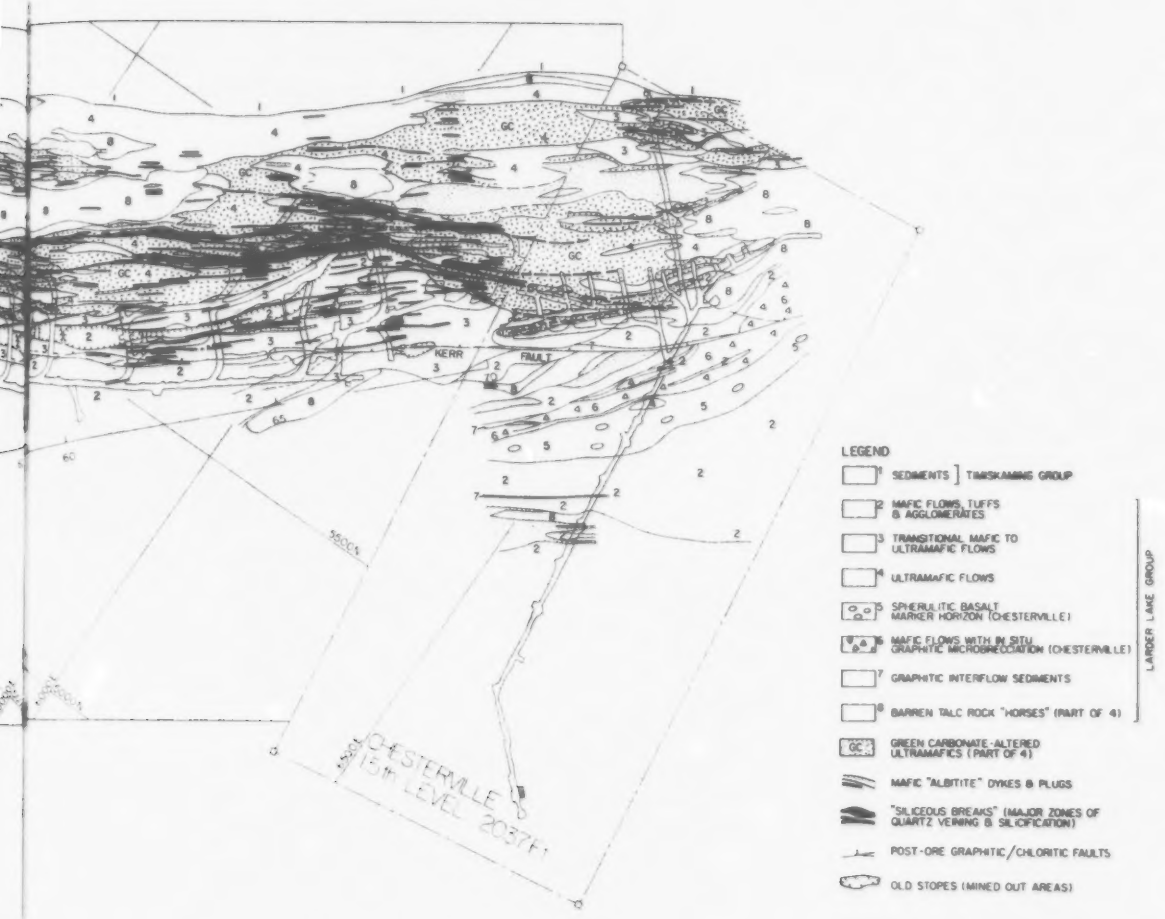
KERR
FAULT
CHESTERVILLE
5150m LEVEL 2037Ft
LEGEND
SEDIMENTS] TIMISKAMING GROUP
MAFIC FLOWS, TUFFS & AGGLOMERATES
TRANSITIONAL MAFIC TO ULTRAMAFIC FLOWS
ULTRAMAFIC FLOWS
SPHERULITIC BASALT MARKER HORIZON (CHESTERVILLE)
MAFIC FLOWS WITH IN SITU GRAPHITIC MICROBRECCIATION (CHESTERVILLE)
GRAPHITIC INTERFLOW SEDIMENTS
BARREN TALC ROCK "HORSES" (PART OF 4)
LARDER LAKE GROUP
GREEN CARBONATE-ALTERED ULTRAMAFICS (PART OF 4)
MAFIC "ALBITITE" DYKES & PLUGS
"SILICEOUS BREAKS" (MAJOR ZONES OF QUARTZ VEINING & SILICIFICATION)
POST-ORE GRAPHITIC/CHLORITIC FAULTS
OLD STOPES (MINED OUT AREAS)

flow ores, respectively. The main features shown are as follows: 1) the ultramafic-hosted ore is contained within a funnel-shaped, green carbonate alteration envelope plunging ~70°E to a deep focal fluid source at ≥4 km depth; 2) stoped green carbonate and dike ores within the overall envelope begin at 3 "root-zone" localities on the 4000-foot level and expand considerably upwards; 3) one major and 2 subsidiary mafic "albitite" plugs (cf. 2050-foot-level geology plan; *see* Figure 364.3) have been identified within the green carbonate ore system: in the #15W and #15 orebodies, the plugs were individually stoped as "albitite" ore; 4) the alteration system converges on the larger mafic plug with depth: deep drilling indicates that this plug is the only significantly mineralized unit from below the bottom of the green carbonate ore at the 4000-foot level (~1250 m) to >2000 m depth; 5) the Chesterville East zone (cf. 2650-foot level, *see* Figure 364.4a) is a *separate*, blind, green carbonate-dike potential ore target that plunges subparallel to the main Kerr Addison–Chesterville system; 6) the flow ores coincide with, but are asymmetrical to, the adjacent green carbonate envelope; 7) stoped flow ore extends down to the 4600-foot level; its host rock pinches out stratigraphically downwards and to the east; and 8) present flow ore distribution is partly due to later displacement by post-ore faults, e.g., the graphitic Kerr fault and its branches.

Ore Distribution Relative to a True-scale Cross Section

Figure 364.8 shows a true-scale cross section of the Kerr Addison Mine from surface to the 4800-foot level and emphasizes the following: 1) the tabular nature of the overall ore zone, confined within the break, and extreme downdip continuity relative to its width; 2) the massive feeder quartz vein system within the green carbonate ore; e.g., major "sil break" quartz veins of the #14 orebody, which were individually stoped over widths of up to 10 m and vertical distances of over *700 m*; 3) the concentration of stoped ore on either side of the footwall contact of the ultramafic and mafic host rocks within the north-dipping break zone; and 4) the V-shaped alteration "nick" point into the talcose ultramafic host rock below the deposit, caused by the eastward plunge of the system.

Figure 364.4. a) Combined Kerr Addison 2650-foot level–Chesterville 2589-foot level geological plan, reconstructed from drift mapping and closely spaced diamond drilling (sections ~11 m apart). The figure shows the principal geological units and the distribution of "green carbonate" alteration versus areas of barren, precursor, talcose ultramafic host rock.

TIME SEQUENCE OF DEFORMATION, HYDROTHERMAL ALTERATION AND MINERALIZATION, AND IGNEOUS INTRUSIVE EVENTS

A relative time sequence of deformation, veining, alteration and mineralization, and mafic "albitite" dike intrusion has been determined from mapped crosscutting relationships in over 50 areas of the mine. The areas mapped (~18 person-months between 1987 and 1989), representing 14 of the 19 Kerr Addison orebodies and 24 of the 28 levels developed in ore, range in depth from 90 to 1250 m below surface. The results are summarized in Figure 364.9. The most important points shown by this diagram are the following:

1. The interval of ductile deformation represented by the break contains the episode of gold-quartz vein mineralization.
2. Physical correlation, through mapping in 3 different localities, has been made between main-stage gold mineralization in the green carbonate ore and that in the flow ore.
3. Mafic "albitite" dike intrusion (4 generations, A_1 to A_4) is partly cotemporal with the main interval of gold mineralization.
4. Green carbonate ore shows 10 distinct stages of quartz-carbonate veining and associated alteration, 5 of which are gold related. These can be grouped approximately as follows: 4a) (stage 1) early, barren, magnesite-dolomite veining and alteration; 4b) (stages 2 to 6) gold-related quartz-ferroan dolomite and ankerite veining with associated fuchsitic green carbonate alteration; and 4c) (stages 7 to 10) later quartz-dolomite, dolomite and calcite veining, faulting and apparent gold remobilization.

We will now present the observational basis for these points by going through each major ore type in detail, discussing crosscutting relationships and characterizing the nature, abundance and distribution of each distinct vein event and its relationship to deformation and ore.

Kerr Addison—Green Carbonate Ore Vein Stages

STAGE 1: POLYGONAL CARBONATE VEINS (PHOTO 364.1)

These ubiquitous, early, barren, polygonal carbonate veins form networks only within the ultramafic host rocks (including the talc areas), where they constitute ~30% of the volume. Where observed in rare unstrained lithons, the veins define equant polygons ~5 to 15 cm across; individual veins are ~0.5 cm in width and may have followed previous polysuture cooling fractures in the komatiitic ultramafic rocks. They cause coarse carbonate replacement and

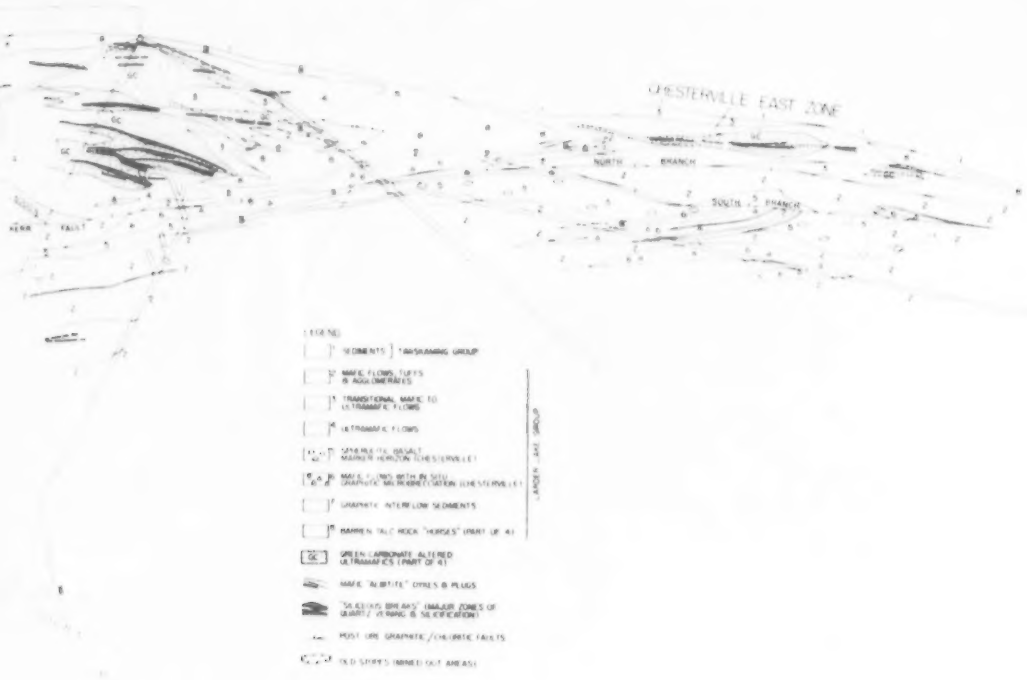

compositional zoning of the ultramafic host rock inside the polygons. Veins consist of "lumpy", diffuse grey to white carbonate (~60/40 magnesite/dolomite) + chlorite. Geochemical analysis indicates that the polygonal veins and associated early carbonate alteration are barren of Au (<1 ppb detection limit: $n = 4$). The veins appear to represent preductile deformation and carbonate alteration in a neutral stress regime. Within the Kerr Addison–Chesterville gold system, the polygonal carbonate veins are subsequent finite-strain markers of ductile flattening deformation and generally occur as background veins parallel to and defining the schistosity while still maintaining low-angle contacts with each other.

STAGE 2: LOCAL CARBONATE STOCKWORKS AND PODS

These are early syn-ductile-deformation carbonate stockworks and pods that locally cut and overprint fabric (defined by deformed polygonal stage 1 veins) in pre-existing talc-chlorite-carbonate host rocks. They show patchy spatial preservation and appear to be restricted to higher strain zones. The stage 2 veins consist of ~1 to 2 cm wide stockwork or polygonal to deformed "shredded" veins with grey-brown to weak green alteration at vein margins. Mineralogy consists of milky white carbonate (ferroan dolomite) and albite, with minor quartz and pyrite. Sampled veins show Au enrichment (~9 ppb: $n = 2$); a grab sample of an early, folded carbonate-pyrite pod from the 1719-74 stope assayed 1.7 g/t Au (J.P.S., 1989).

STAGE 3: "CHERTY SILICEOUS BREAK" FAULTS (PHOTO 364.2)

These are syndeformational, fine-grained SiO_2 "cherty" structures that cut and overprint the fabric and deformed stage 1 and stage 2 veins. They range from quartz-replaced, narrow (~5 to 50 cm) shear zones to thin (~5 to 15 cm), subtle "weak" fractures with silicified grey-green fault gouge, defining an open-intersected, curvilinear branching framework within the green carbonate altered ultramafic rocks. These "cherty siliceous break" faults have steep north-south to northwest-southeast dips (*see* Figure 364.10a) and mostly strike at low angles (±30°) to the break fabric. They crosscut from high- to low-strain areas (e.g., 3214-65 sill) and are not closely related to ductile deformation. Offset of lithological markers (e.g., spinifex horizons and some dikes) across the faults indicates a possible dextral, south-over-north sense of motion. The veins contain mostly cherty grey-green quartz (due to grain-size reduction by local deformation and dynamic recrystallization), with minor carbonate (ferroan dolomite or ankerite). They are surrounded by ~30 to 60 cm halos of weak green carbonate alteration and silicification. Visible gold is occasionally well developed along the "cherty" veins, but overall the veins form only ~10% of the green carbonate ore. Millimetre-scale, grey network quartz-pyrite "crackle" veins (+ gold) internal to the A_1 "albitite" dikes (*see* below) appear to be related through branching to the "cherty siliceous break" vein generation outside the dikes. The "cherty siliceous break" faults formed loci for

Figure 364.4 (concluded). **b)** Combined Kerr Addison 2800-foot level–Chesterville 2739-foot level geological plan, reconstructed from drift mapping and closely spaced diamond drilling (sections ~11 m apart).

subsequent main-stage Au-fluid flow and acted as "stress guides" for vein dilatancy and green carbonate alteration (*see* below).

STAGE 4: MAIN-STAGE, MASSIVE, MILKY GOLD-QUARTZ VEINS (PHOTOS 364.3, 364.4)

The "cherty siliceous break" veins are crosscut and massively dilated by main-stage gold-quartz veins, which occupy pinch-and-swell zones of dilatancy along, and branching between, the guiding fault structures. The gold-quartz veins are brittle fractures synkinematic to overall ductile deformation and may be strongly folded, especially where they crosscut fabric at a high angle. There are up to 4 different preferred vein orientations, ranging from steep to shallow in dip (*see* Figure 364.10a), although the majority are steep. Main-stage gold-quartz vein style and geometry are characterized by branching, steep, irregular, mutually open-intersected vein systems (*see* Figure 364.11), hydraulic brecciation, high-pressure fluid "spurs" and intense "breakout" stockwork veining, often on one side (e.g., hanging wall) of planar "siliceous break" structures or at their intersections. Individual veins and vein zones range from <0.3 to >15 m in width. Vein minerals are massive, milky white quartz, zoned with fringes of delicate, wedge-shaped carbonate (ferroan dolomite or ankerite) crystals, coarse visible native gold, particularly in the quartz, and occasional vein albite. The gold is clearly depositional within the quartz veins and contemporary with vein formation, although where narrow quartz stringers at a high angle to fabric have been folded, gold has been locally remobilized into axial-planar fractures (D. McCormick, Kerr Mine, personal communication, 1989). Minor pyrite, galena, chalcopyrite, arsenopyrite and millerite (NiS) have also been reported from the ore (E. Thomson 1941). The veins are surrounded by intense emerald-green fuchsite-bearing carbonate alteration selvages, with little or no pyrite. Compressed stylolytic inclusions of green carbonate wall rock, possibly indicating repeated vein opening, and comminuted vein fragments are found in the larger veins. The main-stage gold-quartz veins host the bulk (~70%) of the gold mineralization and are ubiquitous in all the green carbonate ore zones. Main-stage gold-quartz veins also cut A_1 "albitite" dikes (*see* below) and produce disseminated pyrite mineralization in the dike wall rock. Such dike-hosted veins locally contain visible gold.

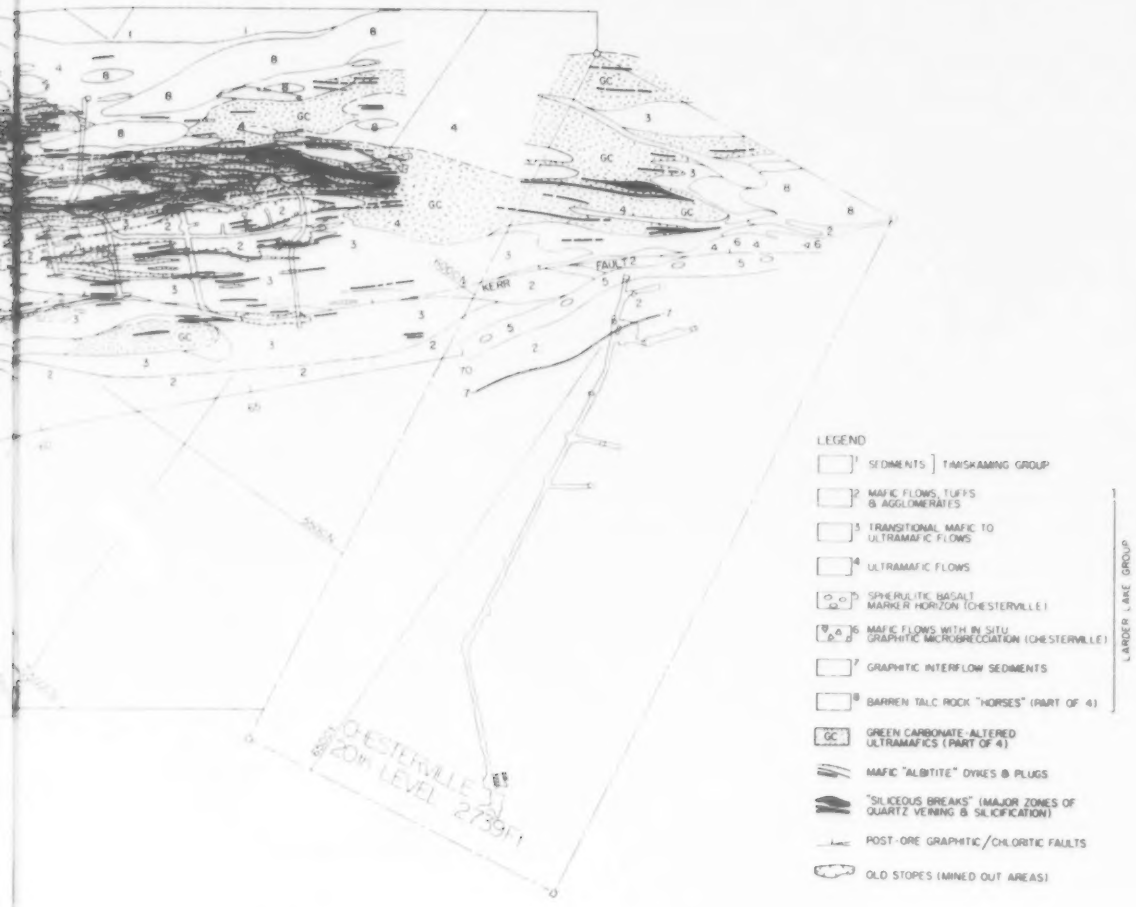
FAULT?
KERR
CHESTERVILLE
ZONE
LEVEL 2730ft
LEGEND
1 SEDIMENTS] TAMISKAMING GROUP
2 MAFIC FLOWS, TUFFS & AGGLOMERATES
3 TRANSITIONAL MAFIC TO ULTRAMAFIC FLOWS
4 ULTRAMAFIC FLOWS
5 SPHERULITIC BASALT MARKER HORIZON (CHESTERVILLE)
6 MAFIC FLOWS WITH IN SITU GRAPHITIC MICROBRECCIATION (CHESTERVILLE)
7 GRAPHITIC INTERFLOW SEDIMENTS
8 BARREN TALC ROCK "HORSES" (PART OF 4)
LARDER LAKE GROUP
GC GREEN CARBONATE-ALTERED ULTRAMAFICS (PART OF 4)
MAFIC "ALBITITE" DYKES & PLUGS
"SILICEOUS BREAKS" (MAJOR ZONES OF QUARTZ VEINING & SILICIFICATION)
POST-ORE GRAPHITIC/CHLORITIC FAULTS
OLD STOPES (MINED OUT AREAS)

STAGE 5: LATE, MINOR QUARTZ STRINGERS

These comprise late syndeformational, volumetrically minor vein stringers that postdate deformed main-stage gold-quartz veins and all dikes. Locally, in the #10 orebody (e.g., 1910-26, 1710-26 and 1610-26 stopes), these veins form a predominant 020°-trending vein set hosting most of the ore. The veins are steeply dipping, <30 cm in width, extremely planar and most recognizable when cutting at a high angle across the fabric and earlier, more-deformed, main-stage milky gold-quartz veins. Vein mineralogy consists of milky to lime-green quartz, zoned with carbonate (ferroan dolomite) crystals at vein margins, and locally abundant galena, pyrite and sphalerite in the areas of ore outlined above. Green carbonate alteration at the vein margins occurs in the ultramafic rocks; the veins also have bleached carbonate-pyrite alteration halos where cutting the later, less-altered mafic "albitite" dikes (A_2 to A_4).

STAGE 6: VEIN FRAGMENTATION, SILICIFIED FAULT BRECCIAS AND "MYLONITIC" ZONES

These steep, post-ductile-deformation fault structures, characterized by vein fragmentation zones and silicified fault breccias, cut fabric and offset the green carbonate ore zones. Faults vary from <0.3 to 4 m wide, and the largest are traceable vertically for several levels (e.g., 2015-64 sill, 1915-69 exploration drift, 1715-66 exploration drift). The faults usually form north-dipping sets, parallel to the break, and rarely crosscut fabric at higher angles. Where adjacent to previous siliceous break and gold-quartz vein zones, the faults incorporate fragments of the earlier veins. The sense of drag of units into the faults—and sigmoidal, *en échelon* subhorizontal to south-dipping extension veins cutting them (*see* below, stage 8)—indicates late sinistral, north-over-south motion. Alteration associated with this event consists of intense grey fault-gouge silicification and disseminated pyrite mineralization, resulting from abundant, centimetre-scale, irregular, grey-green to black cherty quartz "jigsaw" vein breccias. Disseminated pyrite mineralization in dikes (one grab sample from 1915-69

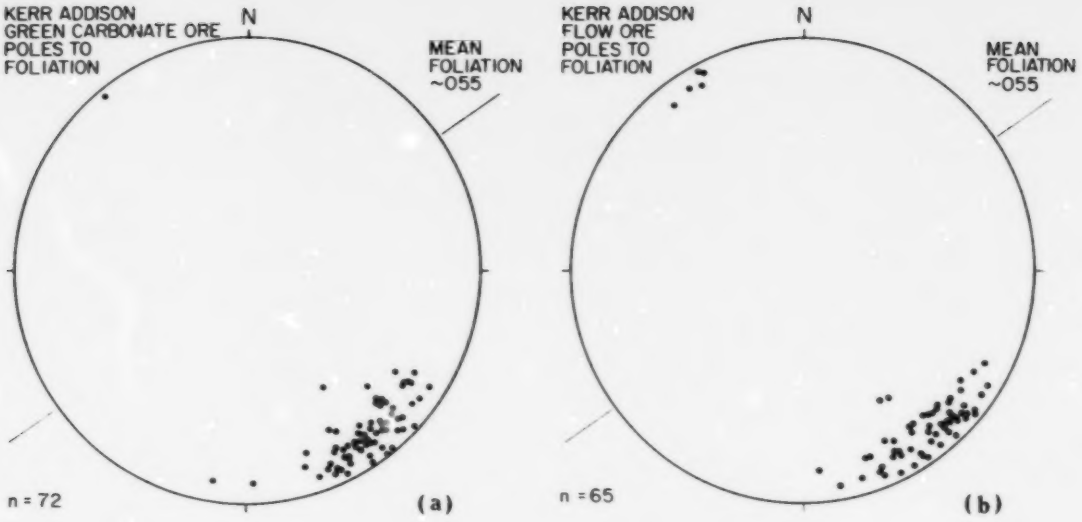

Figure 364.5. a) Equal-area stereographic projection of poles to foliation, green carbonate ore; data from underground mapping (D.W.B., J.P.S.). **b)** Equal-area stereographic projection of poles to foliation, flow ore; data from underground mapping (D.W.B., J.P.S.).

exploration drift assayed 4.8 g/t Au) and intense yellow alteration of green carbonate are noticeable adjacent to such veins. Close examination reveals that the fragmentation appears to be mostly *in situ*, fluid-caused vein brecciation, without significant tectonic movement. Visible gold occurs locally in cherty, recrystallized, "mylonitic" quartz veins (e.g., 1014-52 drift) and may have been remobilized. In places, for example the 1715-66 exploration drift at the east end of Kerr Addison, these fault gouges contain 3 to 5% disseminated pyrite and form potential mineralized targets or were even stoped as ore (part of Chesterville "F" orebody).

STAGE 7: LOCAL, IRREGULAR, STEEP VEINS CUTTING SILICIFIED FAULT BRECCIAS

These local, steep, irregular veins were only observed in one locality (2015-64 sill), along and crosscutting a silicified fault breccia containing fragmented quartz veins. Two open-intersected orientations of the steep veins, forming a conjugate set, were themselves cut by shallow "flats" (stage 8) at this locality. The veins are slightly irregular and deformed across the fault structure, have a maximum width of ~10 cm, and consist of quartz and carbonate (dolomite). No Au values or significant alteration is associated with these veins.

STAGE 8: SIGMOIDAL, *EN ÉCHELON*, SHALLOW-DIPPING "FLAT" VEINS

A set of *en échelon*, shallow-dipping "flat" veins occurs throughout the mine, particularly localized by competent structures such as silicified fault gouges, major "sil break" quartz veins and silicified dikes. The flat veins are not observed to be folded; they sharply crosscut even the most intense high-strain zones. They define a set of shallow, *en échelon* gash vein fractures and hydraulic "spurs", locally intersected with steep quartz veins in a ladder fashion. The flat veins can reach maximum widths of ~30 cm (e.g., 1715-66 exploration drift) and may extend more than 5 m to either side of the generating structure. Their vein mineralogy ranges from milky white quartz-carbonate to brown-white, coarse carbonate (dolomite); patches of grey tetrahedrite (and minor chalcopyrite) are common within the flat veins, but they are barren of gold and do not have visible alteration halos.

STAGE 9: LATE CHLORITIC FAULTS AND SLIPS

A variety of orientations of late chloritic faults and slips cuts all units in the green carbonate ore. Clean white carbonate (dolomite) veins up to ~5 to 10 cm in width are occasionally developed along these slips.

STAGE 10: LATE CALCITE-HEMATITE FISSURES

These are narrow northwest-trending fissures normal to the break, across which there has been no significant offset (e.g., 1719-74 sill). The fissures are coated by specular hematite at the margins and infilled by translucent, coarse, vuggy calcite.

Kerr Addison—Flow Ore Vein Stages

EARLY, LOW-GRADE, DISSEMINATED PYRITE MINERALIZATION

Mapping in several flow ore stopes has defined early, low-grade (~1.0 to 1.7 g/t Au) disseminated pyrite mineralization, rarely observed outside areas of subsequent ore. This early, purple-brown alteration occurs preferentially at pillow and variole margins, at flow contacts and within tuffaceous units and is characterized by millimetre-scale pyritic microveining. The accompanying

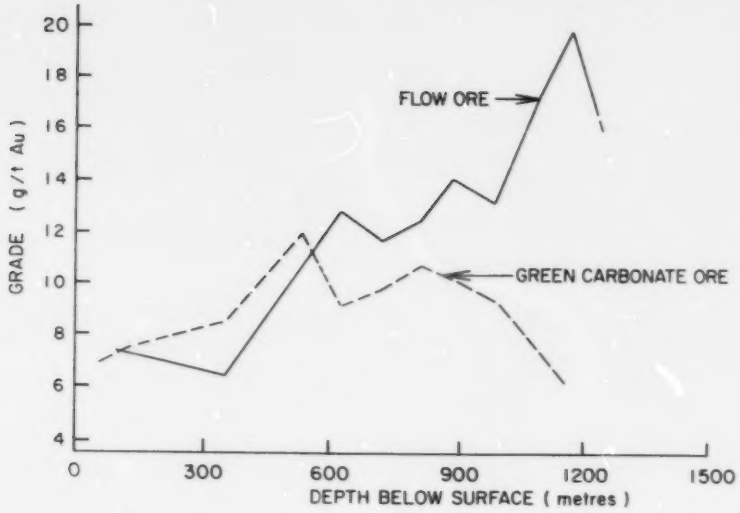

Figure 364.6. Variation of historical production grade with depth in the 2 principal ore types (flow and green carbonate), Kerr Addison Mine (*from* Lowrie and Wilton 1986).

silicification appears to increase locally the competency of the host tholeiitic flows, making them more favourable to subsequent overprinting by main-stage gold brittle fractures. Main-stage ore veins occur in close proximity to areas of earlier disseminated low-grade gold.

MAIN-STAGE GOLD-QUARTZ VEINS, STRINGERS AND HEALED PYRITIC FRACTURES

These are brittle fractures developed within the mafic Fe-tholeiitic host rocks (*see* Figure 364.12), synkinematic to a strong ductile flattening fabric (*see* Figure 364.5b) and subvertical extension lineation defined by deformed pillows and varioles. Fractures are filled by gash-type, single-opening veins, ranging from ~30 to 60 cm maximum width and ~15 m maximum length down to <2 to 5 cm wide veins; healed fractures have pyritic alteration halos. Irregular stockwork-type veining also occurs locally. Main-stage gold-quartz veins are strongly folded where they crosscut the fabric at a high angle. There are 4 to 5 different preferred vein orientations (not simultaneous), ranging in dip from steep to shallow (*see* Figure 364.10b), although the majority are steep dipping. Veins are observed to be mutually open intersected. Mineralogy in the larger veins consists of massive black smoky quartz, especially if near graphitic horizons or where compressed and folded at a high angle to the fabric. Stringer veins consist of zoned, glassy grey to milky white quartz with margins of delicate, wedge-shaped carbonate (ankerite) crystals. Occasional coarse visible native gold occurs within the quartz and, rarely, vein albite. Minor chalcopyrite, sphalerite, arsenopyrite and galena have also been reported from the ore (E. Thomson 1941). The veins are surrounded by beige-purple, bleached pyrite-carbonate-quartz alteration selvages up to 5 or 6 times greater in width than the veins. These main-stage gold-quartz veins and their disseminated pyrite wall-rock selvages host most (95%) of the gold mineralization.

BARREN, POST-ORE, STEEP OR FLAT VEINS RELATED TO LATE FAULTS

These occur as late, steep, occasionally flat, open-intersected ladder veins and breccias within or adjacent to post-ore graphitic faults. The late veins cut across main-stage gold-quartz veins and also occur as tension fractures across the larger smoky quartz veins, perpendicular to their contacts. The veins are volumetrically minor, usually less than 10 cm in width, and are developed over maximum lengths of up to 4 to 5 m. They may be oriented perpendicular or even parallel to the flow ore zones and have rarely been observed to reopen previous gold-quartz vein fractures. The late veins are infilled by granular, milky carbonate ± quartz, do not have bleached pyritic alteration halos and are barren of gold.

Kerr Addison—Graphitic Ore Timing Relations

SYN-ORE, DEXTRAL MOVEMENT ON GRAPHITIC FAULTS

The graphitic ore (1.81 Mt at 7.9 g/t Au) presents a special case of the flow ore because of the complicating presence of interflow graphitic metasedimentary horizons along which syn- and post-ore faults have developed. Detailed mapping of the 2016-65 and 2016-67½ sills shows a close correlation between ore and proximity to the graphitic Kerr fault and its branches. Detailed examination indicates that a network of pyrite-mineralized fractures, containing mechanically remobilized graphite, is adjacent to the faults. The sense of swing of foliation into the graphitic faults is interpreted as reflecting a syn-ore, dextral component of motion.

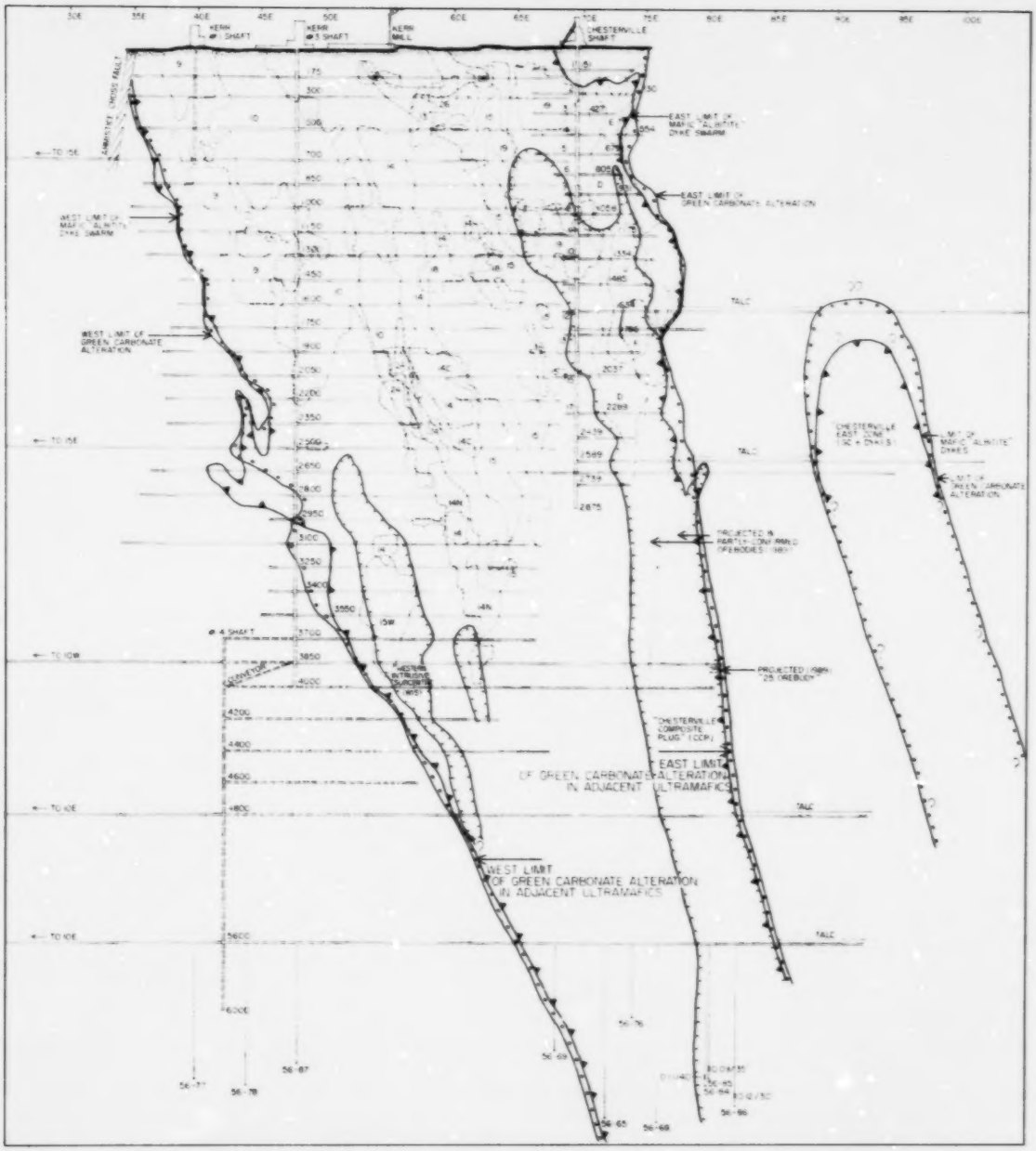
KERR #1 SHAFT
KERR #3 SHAFT
KERR MILL
CHESTERVILLE SHAFT
EAST LIMIT OF MAFIC "ALBITITE" DYKE SWARM
EAST LIMIT OF GREEN CARBONATE ALTERATION
WEST LIMIT OF MAFIC "ALBITITE" DYKE SWARM
WEST LIMIT OF GREEN CARBONATE ALTERATION
TALC
CHESTERVILLE EAST LOBE (SC + CHAIS)
LIMIT OF MAFIC "ALBITITE" DYKES
LIMIT OF GREEN CARBONATE ALTERATION
PROJECTED (50m) 25 OREBODY
CHESTERVILLE COMPOSITE PLUG (CCP)
EAST LIMIT OF GREEN CARBONATE ALTERATION IN ADJACENT ULTRAMAFICS
WEST LIMIT OF GREEN CARBONATE ALTERATION IN ADJACENT ULTRAMAFICS
#4 SHAFT

Figure 364.7. a) True-scale vertical longitudinal projection of green carbonate-dike orebodies, in the plane of the break, looking north-northwest. Scale is shown by the depths of the mine levels (in feet). Note the similarity in outline of the green carbonate alteration and mafic "albitite" dike swarm envelopes.

POST-ORE, SINISTRAL, REVERSE NORTH-OVER-SOUTH FAULT MOVEMENT

The above kinematics are in contrast with the more obvious post-ore, sinistral, reverse north-over-south motion on the Kerr fault, which displaced the flow orebodies. Fragments and lenses of mineralized flow material and broken quartz veins from the adjacent #21 and #16 flow orebodies were incorporated into the graphitic fault gouge, which is locally stoped as ore.

Kerr Addison—"Albitite" Ore Timing Relations

There were 4 episodes of mafic "albitite" intrusion within the green carbonate ore, based on mapped crosscutting relationships confirmed throughout the mine (*see* Figure 364.9). Parts of the larger altered mafic plugs were individually stoped as ore (e.g., #15W and #15 orebodies). "Albitite" dikes are spatially coincident, costructural (similar dips and strikes) and significantly overlapping in time with main-stage gold "siliceous break" veining (*see*

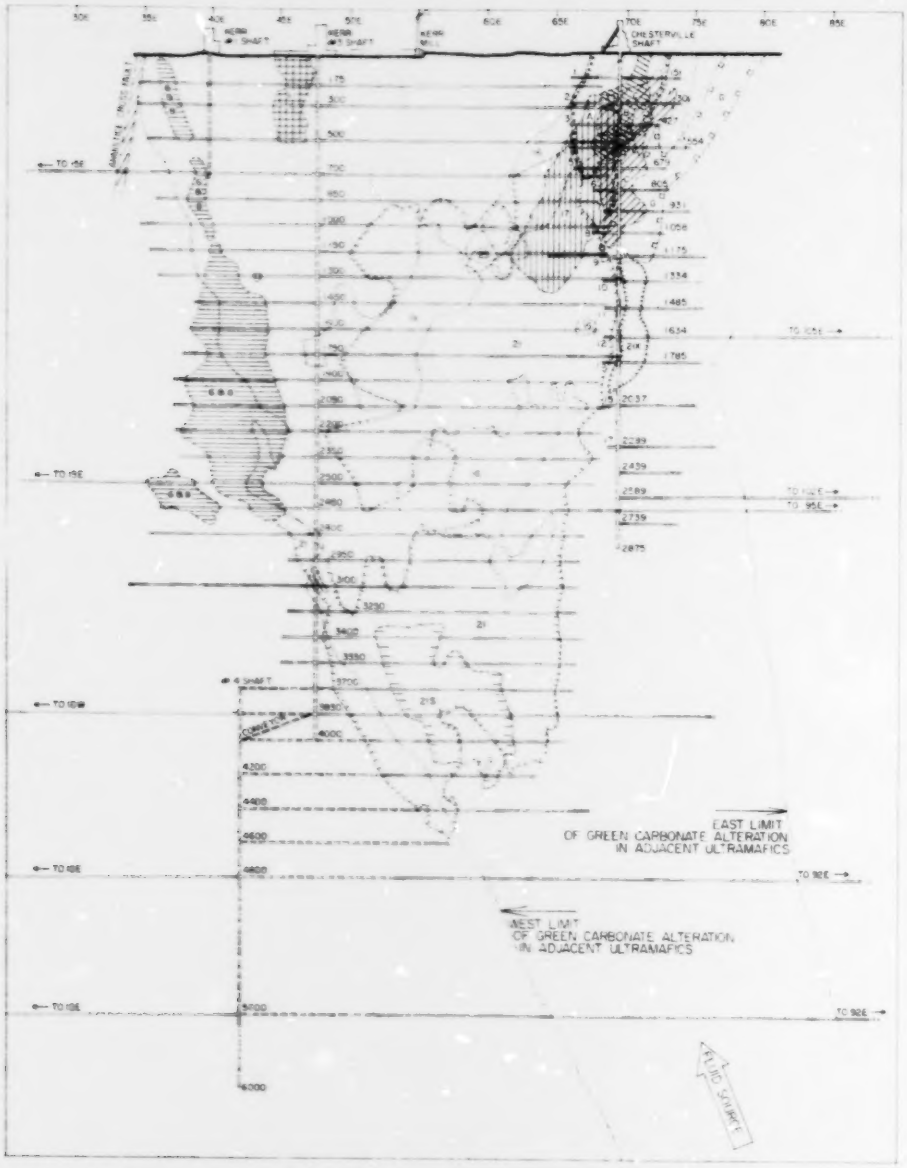
CHESTERVILLE SHAFT
EAST LIMIT OF GREEN CARBONATE ALTERATION IN ADJACENT ULTRAMAFICS
WEST LIMIT OF GREEN CARBONATE ALTERATION IN ADJACENT ULTRAMAFICS
FLIN SHAFT

Figure 364.7 (concluded). b) True-scale vertical longitudinal projection of flow orebodies, in the plane of the break, looking north-northwest. Scale is shown by the depths of the mine levels (in feet). The green carbonate alteration envelope in adjacent ultramafic host rocks is superimposed for reference to Figure 364.7a.

Figures 364.3, 364.4a, 364.4b, 364.9 and 364.13) and constitute ~15 to 20% of the green carbonate ore. Detailed timing relationships of mafic "albitite" intrusive events relative to the above vein stages and alteration in the green carbonate ore are discussed below.

Discussion of Timing Relationships; Correlation of Ore Types

Physical correlation through mapping in 3 different localities (3821-63 rib; 866 south crosscut; 1610-25½ sill) has been made between the main-stage gold mineralization in the green carbonate ore (vein stage 4) and that in the flow ore. This correlation is further reinforced by similar Au/Ag ratios of ~18:1 in both ore types (James et al. 1961). Mapping and structural measurements (*see* Figures 364.5a, 364.5b, 364.10a and 364.10b) also indicate that there are similar orientations of foliation and of main-stage gold-quartz veins in both the green carbonate and the flow ore types. The veins also exhibit comparable strain states and geometries in both ore types; thus, there is no evidence to suggest that ductile deformation and development of a progressive flattening fabric were not approximately synchronous in both host rocks. There are, however, fewer vein stages recorded in the flow ore, possibly because of its higher competency.

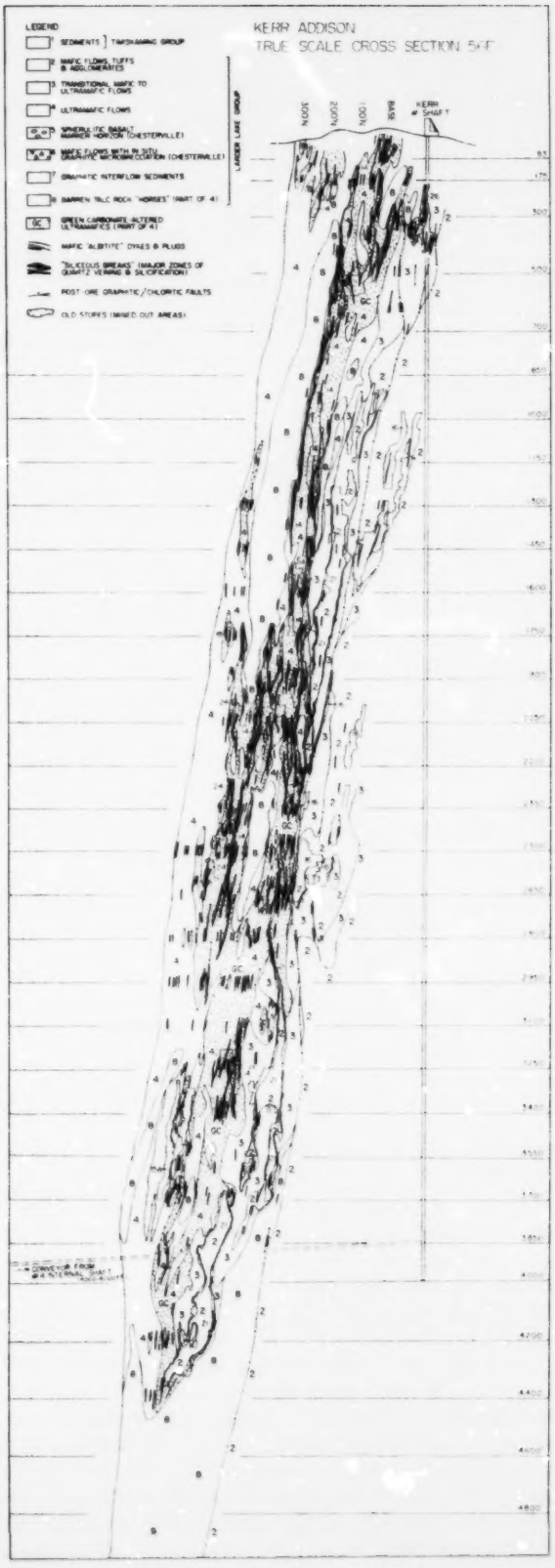

Figure 364.8. True-scale cross section of the Kerr Addison gold system at mine section 56E, looking east along the break. The figure shows the close association of green carbonate ore in the ultramafic host rocks with an intense feeder gold-quartz vein system and abundant mafic "albitite" dikes.

Tentative correlation is made here between the "cherty siliceous break" vein stage in the green carbonate ore and the early, low-grade gold-disseminated-pyrite event in the flow ore, based on the facts that they both predate main-stage gold and contain some gold. The microvein-controlled early mineralization in the flows is also extremely similar in style and geometry to the grey network quartz-pyrite "crackle" veins (+ gold) internal to the A_1 "albitite" dikes, which are related through branching to the "cherty siliceous break" vein generation.

The post-ore, silicified, "mylonitic" fault gouges in the green carbonate ore and the graphitic faults in the flow ore appear to share common similarities in relative timing, orientation and north-over-south (sinistral) kinematics and have also been tentatively correlated. However, both ductile strain and later faulting appear to have continued for a longer period, and with greater magnitude, along the incompetent graphitic horizons (*see* above).

MAFIC "ALBITITE" DIKE SWARM-INTRUSIVE PLUG IGNEOUS SYSTEM

A significant finding of this study has been that the Kerr Addison–Chesterville ore system is characterized by 3 major plugs and an intense swarm of more than 5000 mafic "albitite" dikes (Photo 364.5), intruded preferentially (>90% by volume) into the least-competent ultramafic host rock and constituting ~10% of its volume. Part (<10% by volume) of the dike swarm also occurs within the transitional mafic-ultramafic lithology north and south of the #21 orebody. However, virtually no dikes have been reported in the flow ores, possibly because of their greater competency. The petrography and preliminary geochemistry of the intrusions (Smith and Spooner 1990) indicate that they were originally mafic, alkaline and possibly shoshonitic in composition, before variable sodic alteration to "albitites" consisting of secondary albite + quartz + carbonate + pyrite (+ gold) + mica + rutile. The intrusive dike-plug swarm shows the following principal geometric features relative to the green carbonate ore (*see* Figures 364.3, 364.4a, 364.4b, 364.7a and 364.8):

1. The swarm is volumetrically coextensive with the same green carbonate hydrothermal alteration envelope that contains the individual orebodies.

2. Major and subsidiary plugs are located as follows (*see* Figure 364.7a): 2a) The Chesterville plug occurs near the east edge of the green carbonate alteration envelope and extends from below the deepest drilled depth of ~2000 to ~180 m below the surface. 2b) A second, subsidiary plug occurs near the west edge of the alteration envelope between the 4800-foot and 3100-foot levels. 2c) A smaller plug occurs central to

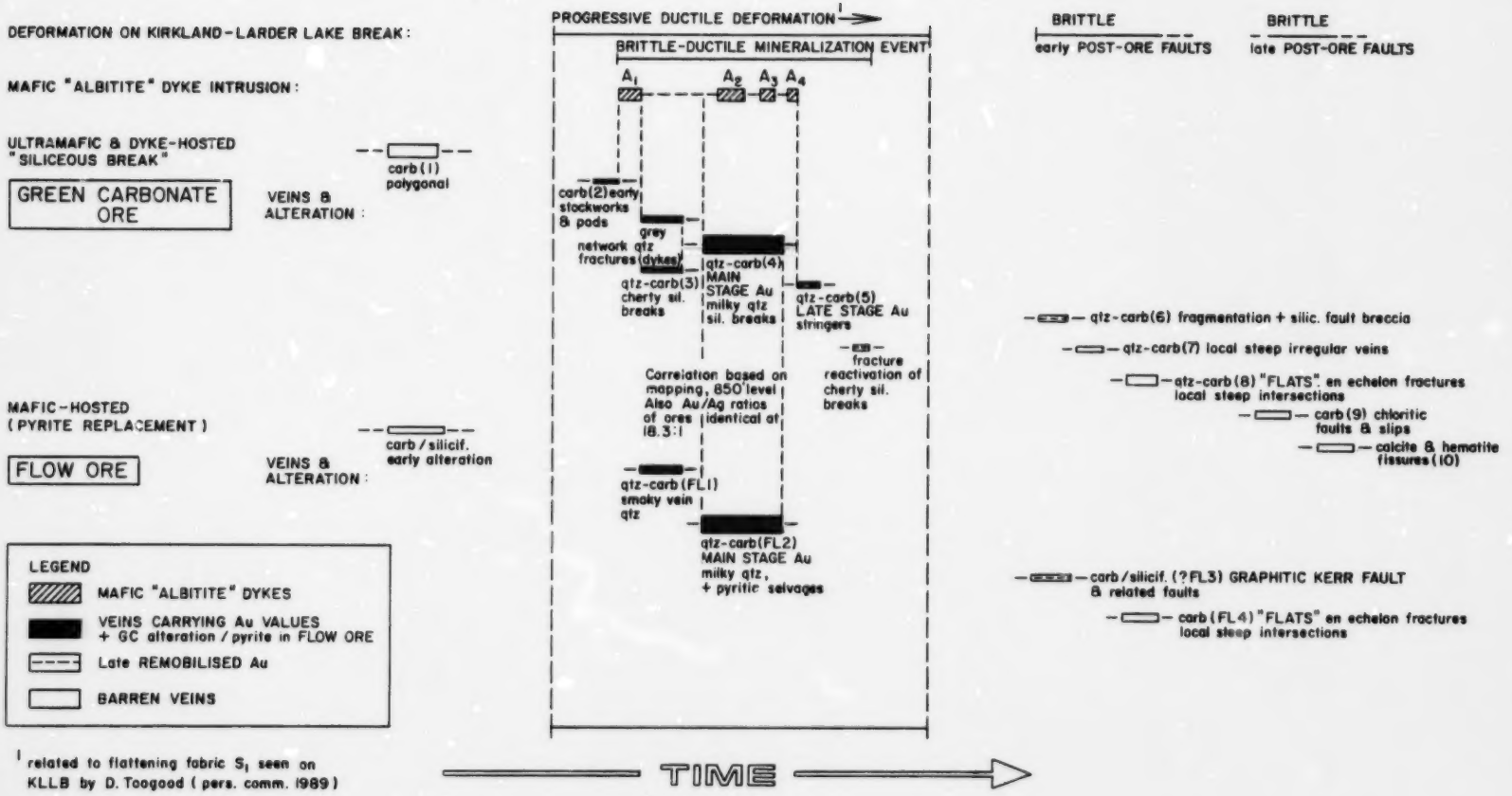
DEFORMATION ON KIRKLAND-LARDER LAKE BREAK:
MAFIC "ALBITITE" DYKE INTRUSION:
ULTRAMAFIC & DYKE-HOSTED "SILICEOUS BREAK"
carb(1) polygonal
GREEN CARBONATE ORE
VEINS & ALTERATION:
MAFIC-HOSTED (PYRITE REPLACEMENT)
carb / silicif. early alteration
FLOW ORE
VEINS & ALTERATION:
LEGEND
MAFIC "ALBITITE" DYKES
VEINS CARRYING Au VALUES + GC alteration / pyrite in FLOW ORE
Late REMOBILISED Au
BARREN VEINS
[1] related to flattening fabric S1 seen on KLLB by D. Toogood (pers. comm. 1989)
PROGRESSIVE DUCTILE DEFORMATION
BRITTLE-DUCTILE MINERALIZATION EVENT
A1 A2 A3 A4
carb(2) early stockworks & pods
grey network qtz fractures (dykes)
qtz-carb(3) cherty sil. breaks
qtz-carb(4) MAIN STAGE Au milky qtz sil. breaks
qtz-carb(5) LATE STAGE Au stringers
fracture reactivation of cherty sil. breaks
Correlation based on mapping, 850' level Also Au/Ag ratios of ores identical at 18.3:1
qtz-carb (FL1) smoky vein qtz
qtz-carb(FL2) MAIN STAGE Au milky qtz, + pyritic selvages
TIME
BRITTLE
early POST-ORE FAULTS
BRITTLE
late POST-ORE FAULTS
qtz-carb(6) fragmentation + silic. fault breccia
qtz-carb(7) local steep irregular veins
qtz-carb(8) "FLATS" en echelon fractures local steep intersections
carb(9) chloritic faults & slips
calcite & hematite fissures(10)
carb/silicif. (?FL3) GRAPHITIC KERR FAULT & related faults
carb(FL4) "FLATS" en echelon fractures local steep intersections

Figure 364.9. Diagram showing the relative time sequence of foliation development, quartz-carbonate veins and mafic "albitite" dike intrusions; based on mapped crosscutting relationships confirmed throughout the Kerr Addison Mine. The figure also shows where physical correlation between vein stages in the flow and green carbonate ore types has been made possible through mapping across their mutual contacts (D.W.B., J.P.S.).

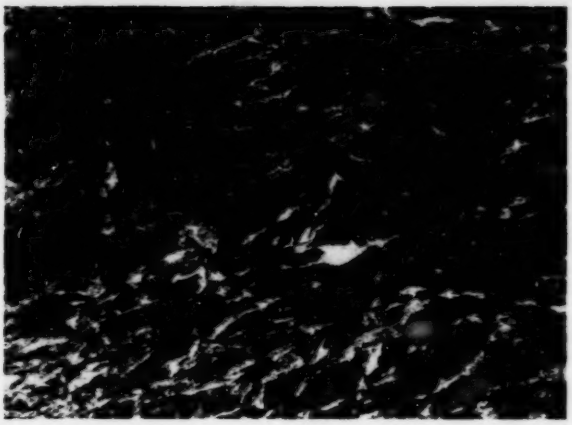

Photo 364.1. Early, barren carbonate veining and replacement of polyhedral fractured ultramafic host rocks at Kerr Addison and along the break (3850-foot level). These early polygonal veins predate ductile deformation and gold mineralization with associated "green carbonate" alteration and are good subsequent strain indicators.

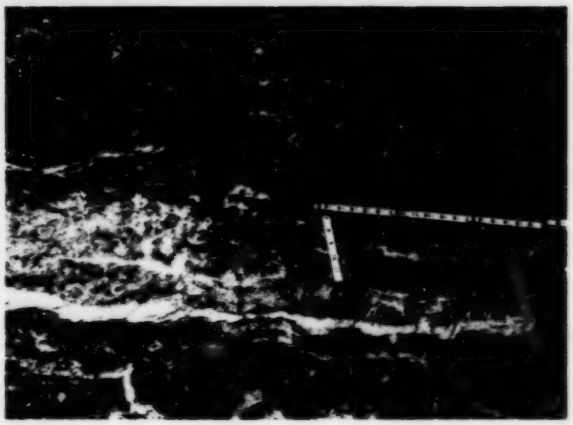

Photo 364.2. Cherty green-grey "siliceous break" fault and narrow shear zone structure cut by later main-stage milky gold-quartz vein; 814-61 sill.

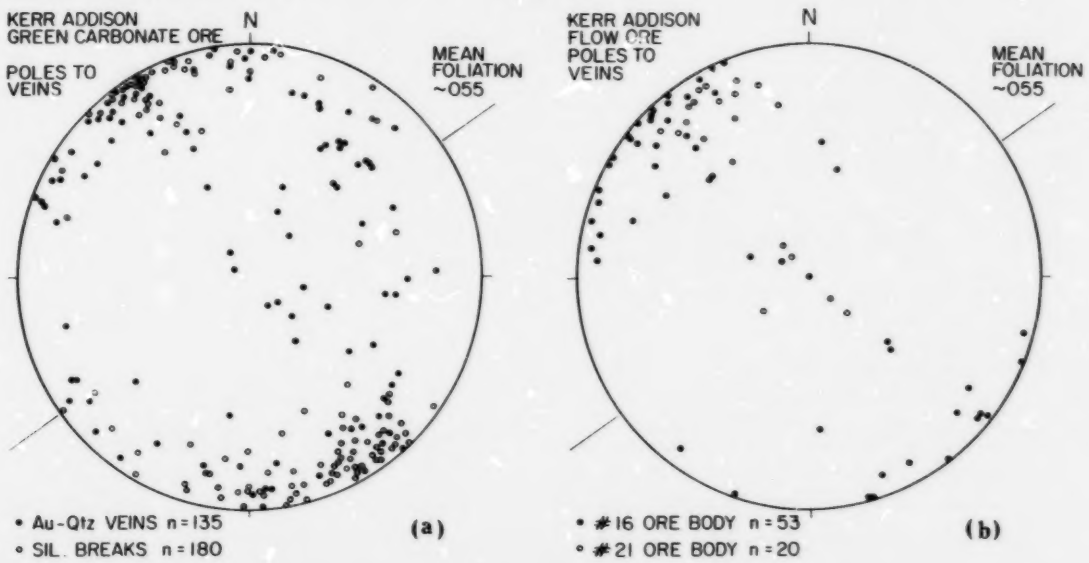

Figure 364.10. a) Equal-area stereographic projection of poles to gold-quartz veins, green carbonate ore; data from underground mapping. A distinction has been made here between major "siliceous break" vein structures and smaller gold-quartz veins (D.W.B., J.P.S.). **b)** Equal-area stereographic projection of poles to gold-quartz veins, flow ore; data from underground mapping. A distinction has been made here between gold-quartz veins of the #21 and #16 flow orebodies (because of possible reorientation and rotation of the #16 orebody caused by displacement by the post-ore graphitic Kerr fault) (D.W.B., J.P.S.).

the gold system from below the 4000-foot level to the 3700-foot level. Dikes coalesce and thicken laterally towards these and other smaller plugs.

3. The dike swarm has an overall strike length near surface of ~900 m and an average width of ~50 to 60 m, decreasing to a ~300 m strike length and a width of ~25 m at the 5600-foot level. The swarm is made up of mappable dike segments estimated to be 12 to 25 m in average length.

4. Dike-plug intersection widths (measured perpendicular to the strike of the orebody) range from <0.3 to 40 m. The width distribution is strongly positively skewed,

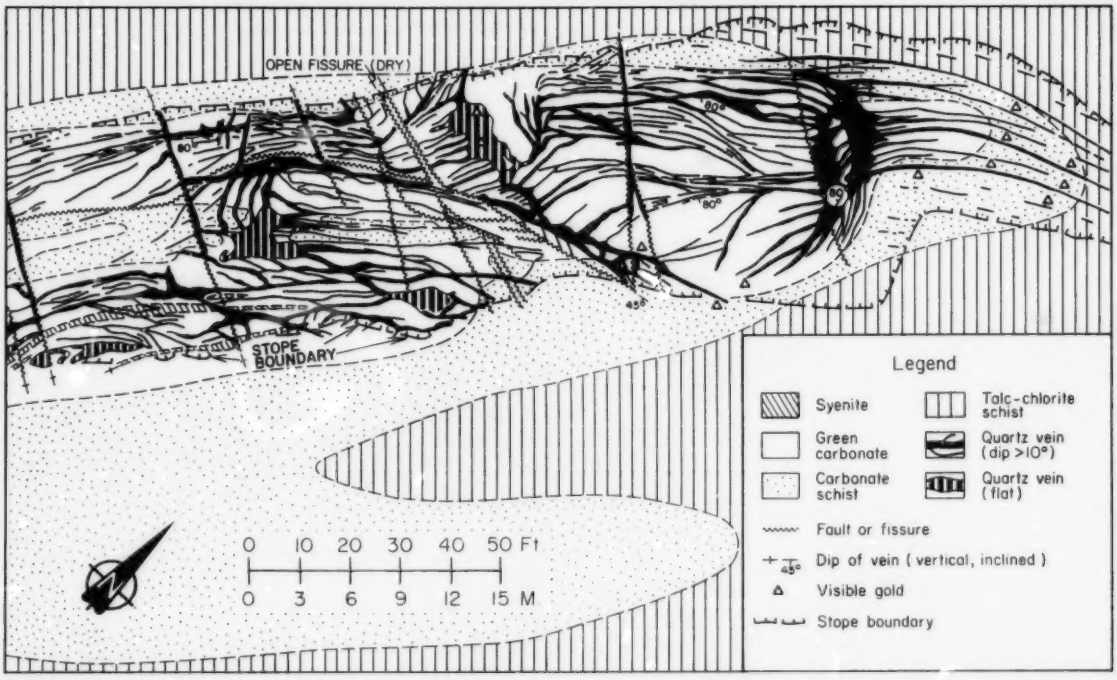

Figure 364.11. Geological stope map of the Chesterville 9D1 green carbonate orebody (*from* Buffam and Allen 1948), showing the extremely irregular gold-quartz vein structures.

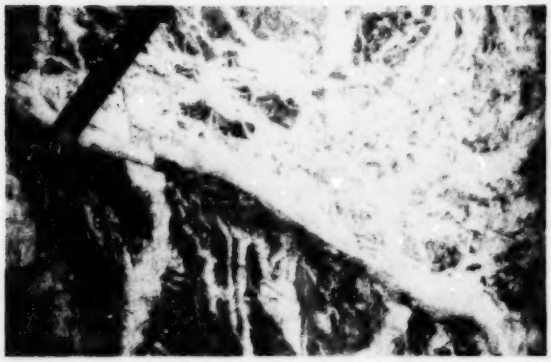

Photo 364.3. Intense high-pressure fluid "breakout" veining on one side of a planar "siliceous break" fault; typical of stage 4 (main-stage) mineralization; 3815-73 stope.

Photo 364.4. Major "siliceous break" milky quartz vein with green carbonate wall-rock fragments; from the "root zone" of the green carbonate ore, 4014-63½ stope.

with a mean of 2.0 m and a mode of 0.3 m. Underground mapping and observations further indicate that the frequency of occurrence of narrow dikelets (<0.3 m width) is comparable to that of measured dikes of >0.3 m width.

5. Statistics (volume, frequency, average width) of dike distribution within the swarm show the following trends with depth in the gold system: 5a) Volume percent (of ultramafic host rock) data show 2 peaks at ~14% each on the 3550-foot and 1150-foot levels and strong decreases both at surface and below the 4000-foot level. 5b) Total-volume data tend to mirror the above trend in (5a). 5c) Average intersection width is greatest (~3.9 m) around the 3550- to 3700-foot levels of Kerr Addison, with a subsidiary peak (~2.9 m) at the 850-foot level. Pronounced minima in dike widths (~1.3 m) are noted in the midlevels of the mine (3100- to 1750-foot levels) and on the 4400-foot level. 5d) Dike frequency is greatest in the middle to upper levels of the mine (2050- to 1000-foot levels), decreasing with depth and dying off near the surface.

6. Measured orientations of dike contacts (n = 63) are shown in Figure 364.13. Dikes mostly strike subparallel or at a low angle (±30°) to the mean foliation and exhibit steep northwest or southeast dips.

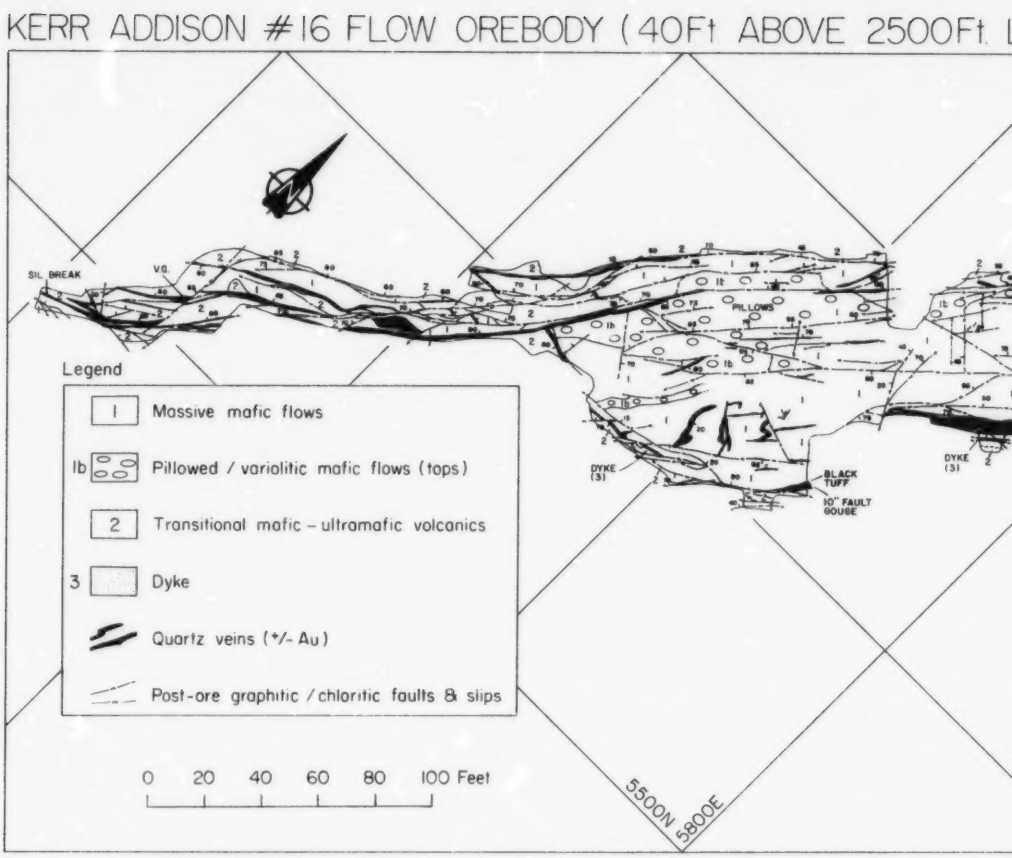

Figure 364.12. Geological map of several combined stopes in the #16 flow orebody on the 2500-foot level of the Kerr Addison Mine (*from* Kerr Addison Mine Geological Staff, ca.1952; reproduced by permission of Deak Resources Ltd.), showing variolitic pillow horizons (flow tops?) and major bordering quartz veins, which cause silicification and disseminated pyrite mineralization of the mafic flows.

Intrusive Time Sequence Relative to Deformation, Veining and Gold Introduction

Based on mapped crosscutting relationships (*see* above), 4 distinct generations of mafic "albitite" dike intrusion have been distinguished within the ultramafic-hosted green carbonate ore (*see* Figure 364.9). The nature, abundance and distribution of each intrusive episode are listed here in detail, and the observational evidence for its timing with respect to deformation, hydrothermal alteration, veining and mineralization, based on crosscutting relationships (*see* Figure 364.9), is presented below.

STAGE A_1: MINERALIZED AND SILICIFIED DIKES CUT BY MULTIPLE GOLD-QUARTZ VEIN GENERATIONS

Based on mapping and drill data, these constitute an estimated 50% by volume of the mafic "albitite" intrusive material, including parts of the 3 major plugs. The A_1 dikes are early synkinematic relative to ductile deformation. Their locally irregular intrusive contacts cut fabric defined by deformed, flattened stage 1 polygonal veins and deformed stage 2 veins. However, the dikes are commonly podiform and boudinaged. The dikes are massive (silicified) and pale grey to beige, have abundant (~2 to 5%) disseminated pyrite and are not observably xenolithic. They are crosscut by multiple quartz vein generations (stages 3, 4, 5 etc.) and are the only intrusive phase to contain millimetre-scale, irregular networks of quartz-pyrite "crackle" veins (+ gold). These veins are internal to the A_1 dikes and appear to be related via branching to the cherty "sil break" (stage 3) vein generation outside the dikes. They are also the only dikes to be cut by irregular, main-stage gold-milky quartz veins (stage 4), which have dark pyritic alteration selvages and locally contain visible gold. The A_1 dikes comprise the highest grade, most consistent "albitite" ore (up to ~10 g/t Au).

STAGE A_2: WEAKLY MINERALIZED, FOLIATED, MIXED XENOLITHIC DIKES (PHOTOS 364.6, 364.7, 364.8)

These constitute an estimated 35% by volume of the mafic "albitites". The A_2 dikes are late synkinematic relative to ductile deformation and have extremely irregular intrusive contacts crosscutting fabric. They form lens-shaped and locally boudinaged bodies, which clearly crosscut earlier, more podiform A_1 dikes and their contained vein sets (stages 3 and 4, with visible gold). Texturally, the A_2 dikes are foliated, rarely silicified and mustard beige to yellow and

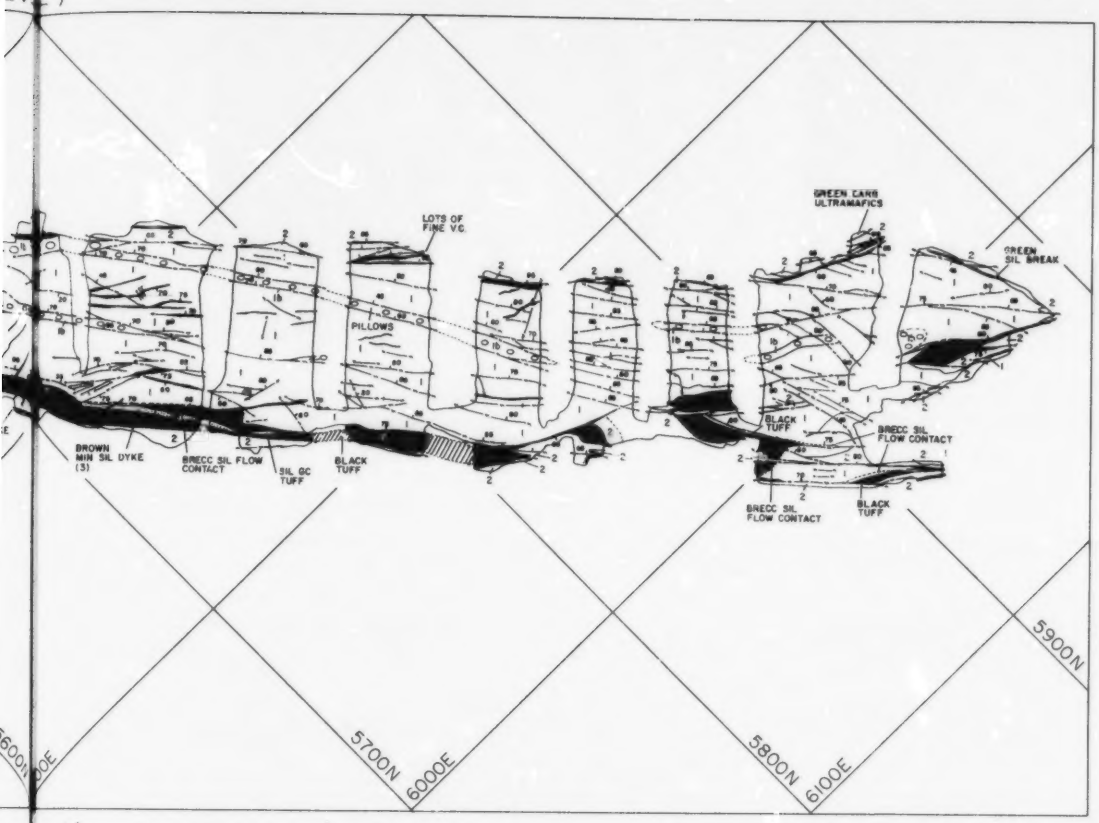

have variable amounts of disseminated pyrite. The dikes are particularly characterized by a mixed xenolith suite, including 1) mineralized A_1 dike fragments; 2) mineralized quartz-pyrite and carbonate-pyrite vein fragments; 3) green carbonate (schistose) with stage 2 carbonate veins and fuchsite flakes (disaggregated green carbonate wall rock); 4) talc-chlorite-carbonate schist fragments; 5) yellow-green and black altered ultramafic(?) fragments. Mineralized xenoliths of (1) and (2) were carefully sampled and assayed (J.P.S., 1989) and were found to contain up to 2.8 g/t Au. The A_2 dikes are crosscut by weak, late stage 4 and 5 deformed quartz stringers with bleached pyritic hydrothermal alteration selvages and minor gold. These dikes usually form lower grade, subeconomic dike ore (~2 to 4 g/t Au).

STAGE A_3: MAFIC, FOLIATED, SIMPLE MAFIC XENOLITHIC SUITE

These form an estimated 10 to 15% by volume of the mafic "albitites". The A_3 dikes are late synkinematic relative to ductile deformation and have extremely irregular intrusive contacts crosscutting fabric, earlier silicified A_1 dikes containing stage 3 and 4 gold-quartz veins, and A_2 dikes. They are lens shaped or boudinaged to planar in geometry. They are less foliated than A_2 dikes where both are in mutual contact. The A_3 dikes have a mafic, crystalline "bitty" texture with pinker matrix patches and schlieren. In contrast with the A_2 dikes, they have a simple xenolith suite of mainly mafic-ultramafic fragments. The dikes are crosscut by

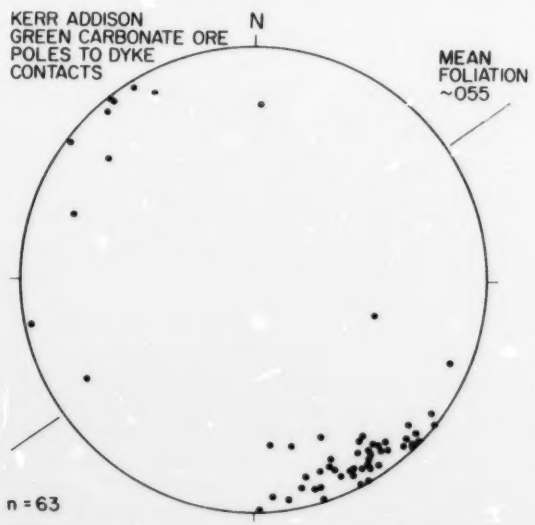

Figure 364.13. Equal-area stereographic projection of poles to dike contacts, green carbonate ore; data from underground mapping (J.P.S.).

Photo 364.5. Altered (originally mafic) "albitite" dike with irregular intrusive contacts cutting a steep fabric in the green carbonate ore; 2614-57½ stope.

Photo 364.6. Silicified and heavily veined A_1 "albitite" dike cut by later, less-altered and veined A_3 "albitite" dike showing darker grey, unaltered mafic remnant patches; 3815-79 stope.

several quartz-carbonate stringers (stage 5 vein set) with bleached, pyritic alteration halos. Individual dikes are often zoned from pale beige, altered margins to mafic dark grey-green, less altered centres. The A_3 dikes do not contain significant gold.

STAGE A_4: MINOR, IRREGULAR, SILICIFIED PYRITIC, NONXENOLITHIC DIKES

Only one example of this volumetrically minor phase (<2% by volume of mafic "albitite" intrusions) has been observed to date: a small, irregular dike patch intersected along the 1715-66 exploration drift. This appears to be very late relative to deformation, with irregular contacts crosscutting fabric and an A_2-A_3 dike contact in a "triple-junction" arrangement. The A_4 intrusive phase is fine grained, massive, flinty, silicified and brown to pink with ~1% disseminated pyrite. No xenoliths were observed. The dike is crosscut by very minor quartz-carbonate stringers of the stage 5 vein and does not attain ore grade.

Discussion—Significance of Mafic "Albitite" Intrusions

On each mining level of the Kerr Addison–Chesterville gold system, the mafic "albitite" dike swarm is approximately coextensive with the limits of main-stage gold-related alteration, characterized particularly by the green carbonate alteration of the ultramafic host rock. In longitudinal projection, the limits of dike occurrence coincide closely with the funnel-shaped green carbonate alteration envelope. Extensive drilling over a 2 km strike length of the break has demonstrated that these dikes do not occur outside the ore system. The boundaries of the dike swarm expand upward in an identical manner to the rapid areal expansion of the green carbonate alteration. Furthermore, within the limits of the deposit, intrusions are an order of magnitude more abundant (~11% per unit volume) in areas of gold-related hydrothermal alteration overprinting the precursor talc-carbonate rocks than in the barren talc "horses" (~1% per unit volume). Such a spatial distribution suggests a close connection between intrusions and hydrothermal alteration and is not what would be expected if gold mineralization were overprinting a homogeneously distributed dike swarm.

Structural data show that dike orientations are similar to the orientations of major "sil break" quartz veins, indicating that both may be costructural. Exact comparison is difficult because of the probably different natures of emplacement of the quartz veins and dikes: the latter possess much more irregular local intrusive contacts.

Crosscutting relationships indicate that mafic "albitite" dike intrusion significantly overlapped in time the main-stage gold mineralization. Later dikes contain fewer vein stages and have been less altered and mineralized than earlier, higher grade dikes, which they crosscut. For example, in the 3815-79 stope, an earlier silicified and veined plug (A_1) carries high-grade values at ~10.3 g/t Au. This plug is cut by 2 generations of later dikes (A_2, A_3) carrying grades of <3.5 and <0.4 g/t Au, respectively. Xenoliths of earlier gold-mineralized dikes, mineralized quartz veins and schistose green carbonate wall rock with carbonate veins are also contained in the later dikes.

PRINCIPAL CONCLUSIONS

1. The Kerr Addison–Chesterville gold deposit is a structurally controlled, quartz-carbonate vein-related Archean gold system with distinct similarities to other examples of the same type (e.g., Colvine et al. 1988). It is not syngenetic, since time sequence analysis shows that Au was not introduced by externally derived hydrothermal fluids until late in the history of ductile deformation and development of a flattening fabric. The carbonate-rich host lithologies to the green carbonate ore have been shown to be metasomatized, spinifex-textured komatiitic flows (Tihor and Crocket 1977).
2. The deposit is located within the Larder Lake–Cadillac Break, a major 150 to 500 m wide high-strain zone in this area, that to the east defines the Abitibi–Pontiac subprovince boundary (e.g., Robert 1989). This mode of occurrence in a major first-order structure, rather than in subsidiary structures, is relatively uncommon

Photo 364.7. Narrow A_3 dikes cutting earlier A_1 veined and silicified dike; 3815-79 stope.

Photo 364.8. Mineralized xenolith of earlier A_1 "albitite" dike in later, crosscutting A_2 "albitite" dike (shows a mixed xenolith suite, including here abundant mafic xenoliths); 3815-79 stope.

along the ~300 km strike length of the break but is also shown by the McBean, Omega, Cheminis, Fernland and Barber–Larder deposits to the west and by the McWatters and Astoria deposits to the east in Quebec (~75 km strike length). Hence, mineralization is shear-zone related but occurs in a zone characterized predominantly by pure shear (flattening) on this particular 060°-striking segment of the break (perpendicular to inferred north-northwest to south-southeast D_2 compression; Hamilton 1986).

3. The Larder Lake–Cadillac Break in this area is interpreted as a flattened and steepened thrust, with the south-facing Larder Lake Group ultramafic komatiite-pillowed Fe-tholeiite-greywacke sequence originally thrust over the Timiskaming sediments to the north. The Kerr Addison–Chesterville gold-quartz vein system is developed in a thick lens of ultramafic komatiites directly adjacent to the south of this major discontinuity.

4. Gold mineralization developed synkinematically relative to ductile deformation (mainly flattening) in the break and is hence post–Timiskaming (~2680 Ma) but syn-"albitite" intrusion in age. This constraint is in agreement with the observed late timing of gold mineralization elsewhere in the southwest Abitibi Subprovince, e.g., postdating intrusion of the Hollinger–McIntyre "albitites" at 2673 $\pm_2$ Ma (Corfu et al. 1989).

5. A flat, funnel-shaped, hydrothermal alteration envelope, with a strike length of ~900 m on surface decreasing to ~300 m at the 5600-foot level and a maximum width of up to 120 m in the ultramafic host rocks and 50 m in the adjacent mafic volcanics, defines the limits of the composite hydrothermal-igneous system. In longitudinal section, the alteration envelope plunges 70°E to a deep focal (≥4 km) fluid source. Green carbonate ore expands upwards from a narrow root zone (~50 by 10 m) controlled by major "siliceous break" vein structures.

6. The gold-quartz vein system and associated hydrothermal alteration developed costructurally, cospatially and overlapping in time with a mafic "albitite" dike swarm-igneous intrusive plug system. The latter finding is based on observational evidence in the form of crosscutting relations and xenoliths of mineralization in dikes and quartz veins. Later dikes in the relative time sequence contain fewer gold-quartz vein stages and have been less altered and mineralized than earlier, higher grade dikes that they crosscut.

7. The significant closeness in space, structure and time between intrusions and mineralization suggests a related origin of main-stage gold mineralization and dike intrusion to a parent intrusive body at an inferred depth of ≥4 km below the present land surface. This relationship is compatible with other evidence for a magmatic origin for Archean gold deposits (e.g., Burrows et al. 1986; Burrows and Spooner 1987, 1989; Spooner 1990, Spooner and Bray 1990).

ACKNOWLEDGMENTS

The authors wish to thank GSR Mining and Deak Resources Ltd. for permission to publish this article and Golden Shield Resources, particularly mine managers D. Douglass and R. Doran, for initial underground access at the Kerr Addison Mine and the employment of J.P.S. during the summers of 1988 and 1989. The careful geological records kept by Kerr Addison Mines Ltd. proved invaluable. Particular thanks go to Golden Shield geological staff: R. Milot, D. McCormick, M. Croteau, J. Butler, G. Knieremen and K. Calberry; Kirkland Lake Resident Geologists: G. Meyer and G. Grabowski; and officials W. McGinty and D. Toogood of Queenston Mining Ltd. for support and contributory discussions. W. Powell of Queen's University is thanked for permission to use his preliminary MSc thesis map as part of Figure 364.1. We would particularly like to thank Subhash Shanbhag for drafting the figures, Karyn Gorra for preparing the photographs, George Taylor and Sean McConville for preparing thin sections, and Claudio Cermignani for the instruction of J.P.S. in the use of X-ray diffraction apparatus. This research was started with funding from Natural Sciences and Engineering Research Council of Canada strategic grant G1862 (E.T.C.S.), receipt

of which is acknowledged with appreciation. Continued financial support by the Ontario Geoscience Research Grant Program (Grant 364) and the receipt of a University of Toronto Fellowship (by J.P.S.) are likewise acknowledged with appreciation.

REFERENCES

Buffam, S.W. and Allen, R.B. 1948. Chesterville Mine; *in* Structural geology of Canadian ore deposits; Canadian Institute of Mining and Metallurgy, Jubilee Symposium Volume, p.662-671.

Burrows, D.R. and Spooner, E.T.C. 1987. Generation of a magmatic H_2O-CO_2 fluid enriched in Mo, Au and W within an Archean sodic granodiorite stock, Mink Lake, northwestern Ontario; Economic Geology, v.82, p.1931-1957.

———1989. Relationships between Archean gold quartz vein-shear zone mineralization and igneous intrusions in the Val-d'Or and Timmins areas, Abitibi Subprovince, Canada; *in* The geology of gold deposits: the perspective in 1988, edited by R.R. Keays et al., Economic Geology, Monograph 6, p.424-444.

Burrows, D.R., Wood, P.C. and Spooner, E.T.C. 1986. Carbon isotope evidence for a magmatic origin for Archean gold-quartz vein ore deposits; Nature (London), v.321, p.851-854.

Charteris, S.N. 1984. Evaluation of the ore potential of the Kerr Addison Mine, Virginiatown, Ontario; unpublished Mine Consultant's report, 12p.

Colvine, A.C., Fyon, J.A., Heather, K.B., Marmont, S., Smith, P.M. and Troop, D.G. 1988. Archean lode gold deposits in Ontario; Ontario Geological Survey, Miscellaneous Paper 139, 210p.

Corfu, F., Krogh, T.E., Kwok, Y.Y. and Jensen, L.S. 1989. U-Pb geochronology in the southwestern Abitibi greenstone belt, Superior Province; Canadian Journal of Earth Sciences, v.26, p.1747-1763.

Downes, M.J. 1980. Structural and stratigraphic aspects of gold mineralization in the Larder Lake area, Ontario; *in* Genesis of Archean, volcanic-hosted gold deposits, edited by R.G. Roberts, Ontario Geological Survey, Open File Report 5293, p.92-103.

———1981. Structural and stratigraphic aspects of gold mineralization in the Larder Lake area, Ontario; *in* Genesis of Archean, volcanic-hosted gold deposits, edited by E.G. Pye and R.G. Roberts, Ontario Geological Survey, Miscellaneous Paper 97, p.66-70.

Feng, R. and Kerrich, R. 1990. Geochemistry of fine-grained clastic sediments in the Archean Abitibi greenstone belt, Canada: implications for provenance and tectonic setting; Geochimica et Cosmochimica Acta, v.54, p.1061-1081.

Folinsbee, R.E. 1943. Scheelite at Kerr Addison Gold Mines Limited; Geological Survey of Canada, unpublished report, 3p.

Hamilton, J.V. 1986. The structural and stratigraphic setting of gold mineralization in the vicinity of Larder Lake, south-central Abitibi greenstone belt, northeastern Ontario; unpublished MSc thesis, Queen's University, Kingston, Ontario, 156p.

Hyde, R.S. 1978. Sedimentology, volcanology, stratigraphy and tectonic setting of the Archaean Timiskaming Group, Abitibi greenstone belt, N.E. Ontario, Canada; unpublished PhD thesis, McMaster University, Hamilton, Ontario, 422p.

———1980. Sedimentary facies in the Archean Timiskaming Group, and their tectonic implications, Abitibi greenstone belt, northeastern Ontario, Canada; Precambrian Research, v.12, p.161-195.

Jackson, S.L. 1988. The Abitibi greenstone belt near Larder Lake: structural and stratigraphic studies; *in* Summary of field work and other activities, 1988, Ontario Geological Survey, Miscellaneous Paper 141, p.206-211.

James, W.F., Buffam, B.S.W. and Cooper, M.A. 1961. Report on the geology and future exploration of Kerr Addison Gold Mines Ltd., McGarry Township, Ontario; unpublished Mine Consultants' report, 37p.

Jensen, L.S. 1985. Stratigraphy and petrogenesis of Archean metavolcanic sequences, southwestern Abitibi Subprovince, Ontario; *in* Evolution of Archean supracrustal sequences, edited by L.D. Ayres, P.C. Thurston, K.D. Card and W. Weber, Geological Association of Canada, Special Paper 28, p.65-87.

Jensen, L.S. and Langford, F.F. 1985. Geology and petrogenesis of the Archean Abitibi belt in the Kirkland Lake area; Ontario Geological Survey, Miscellaneous Paper 123, 130p.

Lowrie, D.A. and Wilton, C.K. 1986. Geology of the Kerr Addison Mine—a review; unpublished Mine Consultants' report, 8p.

MERQ–OGS 1983. Lithostratigraphic map of the Abitibi Subprovince; Ministère de l'Énergie et des Ressources du Québec–Ontario Geological Survey, MERQ Map D.V. 83-16, OGS Map 2484, scale 1:500 000.

Ridler, R.H. 1970. Relationship of mineralization to volcanic stratigraphy in the Kirkland Lake–Larder Lake area, Ontario; Geological Association of Canada, Proceedings, v.21, p.33-42.

———1976. Stratigraphic keys to the gold mineralization of the Abitibi belt; Canadian Mining Journal, v.97, no.6, p.81-90.

Robert, F. 1989. Internal structure of the Cadillac tectonic zone southeast of Val-d'Or, Abitibi greenstone belt, Quebec; Canadian Journal of Earth Sciences, v.26, p.2661-2675.

Smith, J.P. and Spooner, E.T.C. 1990. Evidence for a mafic "albitite" intrusion/Archean Au structure-time association, Kerr Addison–Chesterville mines, N. Ontario, Canada; 8th IAGOD Symposium, Ottawa, Ontario, August, Program with Abstracts, p.A74.

Spooner, E.T.C. 1990. Archaean intrusion-hosted, stockwork Au-quartz vein mineralization, Lamaque Mine, Val-d'Or, Quebec: part II. Light stable isotope (H, O, C and S) characteristics and enriched calc-alkaline/shoshonitic igneous geochemistry; *in* Greenstone gold and crustal evolution, Geological Association of Canada NUNA–SEG Conference, Val-d'Or, Quebec, May 24–27, Abstracts and Proceedings.

Spooner, E.T.C. and Bray, C.J. 1990. The fluid inclusion volatile geochemistry of Archean Au/W enriched mineralization, Mink Lake stock, N.W. Ontario and Archean Au-quartz vein mineralization, Barberton greenstone belt, southern Africa; 3rd Biennial Pan-American Conference on Research on Fluid Inclusions, Toronto, Ontario, May 20–22, Program and Abstracts, p.83-86.

Thomson, E. 1941. The mineralogy of the Kerr Addison ore, Larder Lake, Ontario; *in* Contributions to Canadian mineralogy, 1941, University of Toronto, Geological Series no.46, p.141-147.

Thomson, J.E. 1943. Geology of McGarry and McVittie townships, Larder Lake area; Ontario Department of Mines, Annual Report, v.50, pt.7, 99p.

———1946. The Keewatin–Timiskaming unconformity in the Kirkland Lake District; Transactions of the Royal Society of Canada, sect.IV, ser.3, v.40, p.113-122.

———1948. Regional structure of the Kirkland Lake–Larder Lake area; *in* Structural geology of Canadian ore deposits, Canadian Institute of Mining and Metallurgy, Jubilee Symposium Volume, p.627-632.

Tihor, L.A. and Crocket, J.H. 1977. Gold distribution in the Kirkland Lake–Larder Lake area, with emphasis on Kerr Addison-type ore deposits—a progress report; *in* Report of activities, pt.A, Geological Survey of Canada, Paper 1977-1A, p.363-369.

Toogood, D.J. and Hodgson, C.J. 1986. Relationship between gold deposits and the tectonic framework of the Abitibi greenstone belt in the Kirkland Lake–Larder Lake area; *in* Ontario Geoscience Research Grant Program, summary of research 1985–1986, Ontario Geological Survey, Miscellaneous Paper 130, p.79-86.

Grant 370 Tectonic Relations among Parry Sound Domain and Seguin and Rosseau Subdomains

R.I. Macfie and J.M. Dixon

Department of Geological Sciences, Queen's University, Kingston

ABSTRACT

Near Orrville, in the southwestern part of the Central gneiss belt of the Grenville Province, there is a triple junction between 3 lithotectonic domains thought to be remnants of crustal slices thrust northwestward during tectonic activity associated with the Grenville Orogeny. In this area granulite-facies gneisses of Parry Sound domain lie sandwiched between amphibolite-facies gneisses of Seguin and Rosseau subdomains. The objectives of this project are to test the model of northwest-directed thrusting in a structurally intriguing and well-exposed area, to investigate mechanisms of deformation in these deep-crustal, high-grade rocks and to evaluate the economic potential of the area.

A variety of kinematic indicators shows that rocks of Parry Sound domain have been thrust westward to northwestward over a structural basement represented by highly migmatitic orthogneiss of Rosseau subdomain. Rocks of Seguin subdomain were subsequently thrust northwestward over Parry Sound domain.

An extensive unit of distinctive calc-silicate gneiss may be of volcaniclastic origin. It contains several gold anomalies and should be investigated further. New areas underlain by marble and graphite-bearing metapelite have been discovered.

INTRODUCTION

This project involves geological mapping (at 1:15 000 scale) of a portion of the Central gneiss belt of the Grenville Province (Figure 370.1). The study area includes part of a region in which several lithotectonic domains (Parry Sound domain, Seguin subdomain and Rosseau subdomain), characterized by contrasting rock types and metamorphic grade, may have been juxtaposed by displacement on ductile thrust faults (Davidson et al. 1982). The complex geological pattern observed is suggestive of mid- or deep-crustal sandwiching of a granulite-grade domain between amphibolite-grade domains, but the significance of the domains and the mechanisms of their emplacement have remained obscure.

The goals of the study include the elucidation of the tectonic history of the area and the evaluation of its economic potential. The area includes part of Parry Sound domain, within which numerous mineral occurrences of potential economic interest have been identified (Hewitt 1967). Metamorphosed supracrustal rocks, including rocks of possible volcanic origin, are known to be present in the area, and their extent, composition, mineralization and structural geology are important aspects of the project.

This report presents results of 3 months of field work (1989) and subsequent laboratory study. The project constitutes the PhD project of the first author.

PREVIOUS WORK

The area was included in the region mapped at 1:126 720 scale by Hewitt (1967), although very few data for the area were obtained.The area was later included in a reconnaissance study of the southwestern Central gneiss belt by Davidson and Morgan (1980) and Davidson et al. (1982). Part of the western sixth of the map area was mapped at 1:15 000 scale by McRoberts et al. (1988) and Macfie (1988).

TECTONIC SIGNIFICANCE AND SETTING OF THE STUDY AREA

The mechanisms of thrusting in deep-level continental crust continue to be poorly understood. Whereas upper-crustal portions of major thrust systems are exposed in many areas and have been well studied, deeper level parts of continental thrusts are more rarely exposed and are relatively little studied (Hanmer 1988). In the Cordillera of North America, for example, thin-skinned, upper-crustal tectonic processes have been worked out in detail (e.g., Price 1981), but deformation of deeper level crystalline rocks (e.g., Omineca belt and Coast plutonic complex) is less well understood (e.g., Monger et al. 1982). The same is true of the Alps (Ramsay 1981). It may be that mechanisms of thin-skinned thrusting are inapplicable below the brittle-plastic transition (e.g., Davis et al. 1983).

Processes similar to those operating during the evolution of the Cordillera and the Alps may have been involved during the assembly of the Central gneiss belt of the Grenville Province. Deep-level thrust zones believed to be in the southwestern part of the Central gneiss belt may bound allochthonous terranes assembled during orogenesis occurring about 1.2 to 1.0 Ga ago (Davidson 1986; van Breemen et al. 1986) or slices of basement that have been telescoped into a crustal-scale duplex structure (e.g., Journeay 1986).

Tectonic Models for the Central Gneiss Belt

The Grenville Province forms a coherent structural and geochronological province (Wynne-Edwards 1972), characterized by nearly ubiquitous tectonites with predominant southeast-trending stretching lineations and

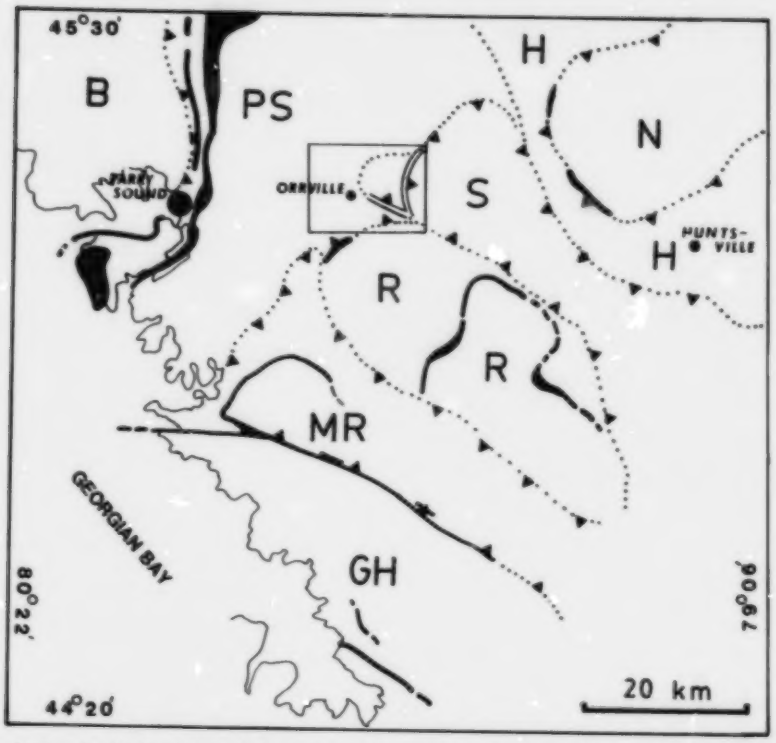

Figure 370.1. Lithotectonic domains in the vicinity of the study area (rectangle), *after* A. Davidson and co-workers. Adjusted boundary of Seguin subdomain (this study) and possible splay rooted in Seguin subdomain boundary zone indicated by double curved line segments. Barbs indicate dip direction. Anorthosite outside of study area shown in black. B, Britt domain; PS, Parry Sound domain. Subdomains of Muskoka domain as follows: GH, Go Home; MR, Moon River; R, Rosseau; S, Seguin. Subdomains of Algonquin domain as follows: H, Huntsville; N, Novar.

mainly Mesoproterozoic radiometric ages. In the recent past it has been viewed as an area of extensive basement gneiss (including the Central gneiss belt) capped by erosional remnants of an in-folded, metamorphosed sedimentary sequence (including the Central metasedimentary belt and Parry Sound domain) (Wynne-Edwards 1972) or as a heterogeneous product of various plate-tectonic processes (e.g., Brown et al. 1975; Baer 1981).

Davidson et al. (1982) and Culshaw et al. (1983) identified within the Central gneiss belt a number of distinct "lithotectonic regions" (Davidson 1986, p. 63). They referred to them as "domains" and "subdomains" (*see* Figure 370.1) and distinguished them on the basis of lithology, internal structure, metamorphic grade and geophysical signatures. Bounding deformation zones were outlined, mainly on the basis of topographic and magnetic-anomaly expressions, and "northwest-directed stacking of large blocks and slices along inclined ductile shear zones" (Davidson 1986, p. 61) was proposed. In the general region of the study area of this project, Davidson et al. (1982) proposed that the granulite-grade Parry Sound domain is bounded to the southeast by the amphibolite-grade Go Home, Moon River, Rosseau and Seguin subdomains (Figure 370.1) of Muskoka domain. Together, these lithotectonic domains appear to represent 3 lithological packages: the structurally lowest, represented by Rosseau and Go Home subdomains; an overlying one, represented by Parry Sound domain; and the structurally uppermost one, the erosional remnants of a migmatite terrane represented by Moon River and Seguin subdomains. Parry Sound domain is postulated to have been thrust northwestward over a structural basement represented by Rosseau subdomain, and the Seguin–Moon River thrust sheet is thought to have been similarly thrust over both.

The tectonic model of Davidson et al. (1982) has been widely accepted and is becoming entrenched in the literature. However, it was based upon reconnaissance mapping and remains a hypothesis that requires testing (A. Davidson, Geological Survey of Canada, personal communication, 1989).

GEOLOGY OF THE STUDY AREA

Although Parry Sound domain, Seguin subdomain and Rosseau subdomain all consist mainly of high-grade tectonites, they differ sufficiently in detail to be distinguished in the field. General descriptions of the domains and subdomains are found in Davidson et al. (1982). With regard to the study area of this project, the descriptions below refer first to rock types, structures and important metamorphic features characteristic of each of the domains and subdomains and their boundaries; these are followed by descriptions of late- and posttectonic features of the area.

Although geochronological data are lacking for the study area of this project, intermediate orthogneiss of the western part of Parry Sound domain has an interpreted primary zircon U-Pb crystallization age of 1425 ± 75 Ma,

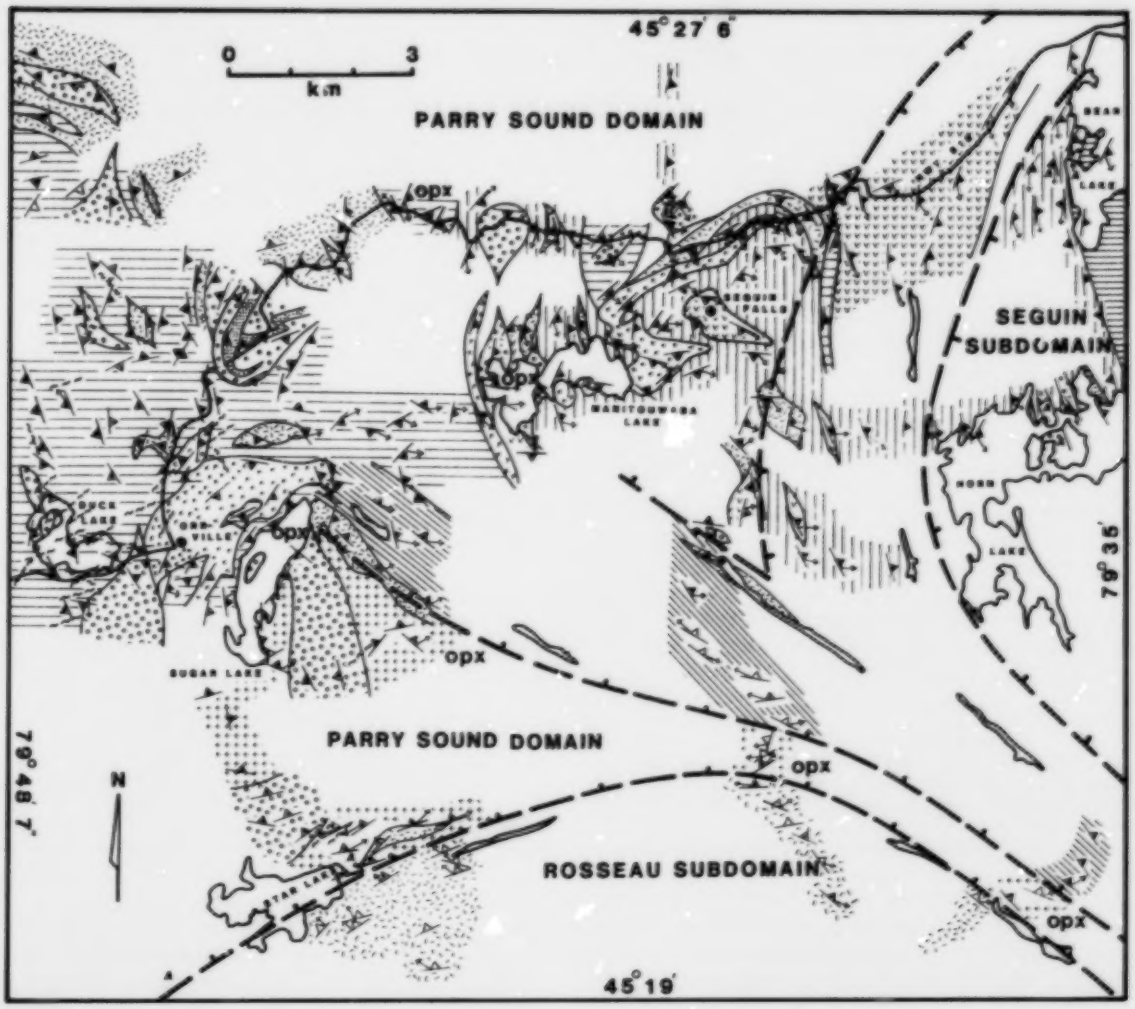

Figure 370.2. Geology of the study area. Legend on opposite page.

and ductile deformation in the basal shear zone (Parry Sound shear zone) at the western side of Parry Sound domain has been dated at 1159$^{+3}_{-2}$ Ma (van Breemen et al. 1986). The Parry Sound shear zone is probably continuous in the subsurface with the bounding shear zone between Parry Sound domain and Rosseau subdomain. Movements on the bounding shear zones of Seguin subdomain (sampled north of the study area of this project) and Moon River subdomain are coeval (within error) at approximately 1100 Ma (O. van Breemen, Geological Survey of Canada, personal commmunication, 1990). These shear zones are thought to be remnants of the basal thrust of a single sheet.

According to the thermobarometric work of Anovitz and Essene (1990), selected rocks (in all cases sampled outside the study area of this project) of Parry Sound domain equilibrated at 700° to 800°C, rocks of Seguin subdomain equilibrated at 680° to 770°C and rocks of Rosseau subdomain equilibrated at 500° to 780°C. Pressures obtained from rocks of all subdomains range from about 10 to 11 kbars (1 kbar = 100 MPa).

Parry Sound Domain

ROCK TYPES

Rocks of this domain are generally layered on a metre scale, although some large bodies of dioritic to tonalitic rock and some metagabbro bodies retain relatively massive central portions. Abundant high-strain ductile-deformation structures, including boudins, attenuated layering and rotational features, indicate a tectonic origin for the layering. Rock types include intermediate to mafic orthogneiss, metagabbro, intermediate and granitoid gneiss of indeterminate origin, paragneiss (semipelitic to quartzitic), marble and calc-silicate gneiss of possible volcaniclastic origin (Figure 370.2).

The dominant rock type is grey dioritic to tonalitic gneiss of probable plutonic origin. At Duck Lake a body of this gneiss, although strongly to moderately deformed, contains recognizable igneous xenoliths of variable composition, and such material is common in the

Tectonic layering and main foliation, with stretching lineation
Dip intervals
0-30°
31-50°
51-70°
71-90°
Minor shear zone
Boundary of major tectonite zone
Heterogeneous granitoid, intermediate and mafic gneiss protolith unknown
Heterogeneous migmatite gneiss, granitoid composition but protolith unknown
Granitoid gneiss, in part migmatitic
Heterogeneous grey gneiss, tonalitic and dioritic composition
Tonalitic and dioritic orthogneiss
Heterogeneous granulite gneiss, predominately mafic and intermediate in composition
Gabbro and related mafic gneiss
Gneiss of tonalitic composition, in part rich in calc-silicate minerals, with abundant calc-silicate lenses
Pink migmatite gneiss, in part >50% quartz
Marble
Quartzite and quartzofeldspathic gneiss; minor meta-semipelite
A Anorthosite occurrence
opx Easternmost orthopyroxene occurrences

Manitouwabing Lake map area to the west (McRoberts et al. 1988). Overall, this suite of gneisses contains from 10 to 30% biotite and/or hornblende and locally contains clinopyroxene. Microcline is a rare constituent. In places the gneiss contains orthopyroxene; this mineral is more common in the west and south and is absent adjacent to the boundary with the Seguin subdomain, except near the triple junction (*see* "Domain and Subdomain Boundaries"). The gneiss is often migmatitic, containing up to 10% leucosome of granitic composition. The leucosome is variably deformed, commonly showing evidence of at least 3 generations, some being transposed into parallellism with tectonic layering and some being completely disaggregated.

Mafic gneiss consisting predominantly of hornblende and plagioclase, in places with clinopyroxene, garnet, orthopyroxene, scapolite, actinolite and talc, forms metre- to kilometre-scale lenses and lobate bodies within the grey gneiss. Some exposures show layering that may be primary, but metamorphism has destroyed the primary mineral assemblage. Minor meta-anorthosite (An_{65-70}) is in part associated with mafic gneiss.

Metre- to kilometre-scale lenses of pink migmatitic gneiss of granitic composition underlie about 5% of the domain. They contain 2 to 5% biotite, and in places some contain more than 25% quartz. The latter may be derived from arkose, but in general the pink migmatitic gneisses resemble leucosome in the grey intermediate gneisses, from which they may be derived by partial melting.

Rocks of pelitic composition containing sillimanite and graphite are spatially associated with quartzofeldspathic gneiss containing up to 95% quartz in some layers, calc-silicate (epidote, titanite, apatite, scapolite and hornblende-rich) gneisses and white marble containing both calcite and dolomite. This supracrustal package occurs in isolated outcrops, which in places may form continuous or boudinaged units folded within the grey gneiss. North of Manitouwaba Lake, rock of this association has the appearance of a raft within a body of intermediate orthogneiss.

A unit consisting of grey gneiss containing centimetre- to metre-scale epidote-quartz-scapolite pods and layers is widespread in the area. In places the host gneiss is rich in epidote, titanite, apatite and scapolite. It may be of supracrustal, perhaps volcaniclastic, origin (*see* "Economic Geology").

STRUCTURE

Apart from areas immediately adjacent to the domain boundary (*see* "Domain and Subdomain Boundaries"), tectonic layering defined by contrasting composition and strain variation constitutes the major structural feature within Parry Sound domain. Although macroscopic evidence of ductile strain is very common, the gneisses are mostly annealed; they are medium grained and show such features as 120° grain-boundary intersections and quartz drops in coarser feldspar matrices (Hanmer 1984). Where present, grain-scale foliations, mainly defined by biotite and hornblende, are usually concordant with this layering. Average trend of layering is north, but at outcrop scale warping of layering is ubiquitous, and trend of layering varies by 45° or more from outcrop to outcrop. Trends of layering are suggestive of open to tight folding at map scale, but outcrop-scale fold closures are uncommon, and scarcity of traceable map units makes definition of folds difficult. Layering is less regularly disposed in the eastern part of the domain, towards the boundary with Seguin subdomain, and small-scale fold closures with southeast-plunging axes are more common in that area. In general, though, tectonic layering within the domain dips moderately to steeply eastward, and mineral-aggregate stretching lineations plunge to the southeast (Figure 370.3a).

In some places, weakly developed, steeply dipping biotite foliations having varied but generally east-southeasterly trends cut the above-mentioned layering. Associated fold closures are not observed.

In the western part of the map area the tectonic layering in annealed granulite gneisses is cut by metre-scale amphibolite-facies shear zones (Figure 370.2) with well-preserved fine grain sizes. These most commonly dip shallowly to moderately, with easterly to northeasterly strikes. They show subtle features such as C-S and shear-band fabrics, and stretching lineations are abundant. Rotated porphyroclasts (Photo 370.1) and other kinematic indicators reveal top-to-west transport sense.

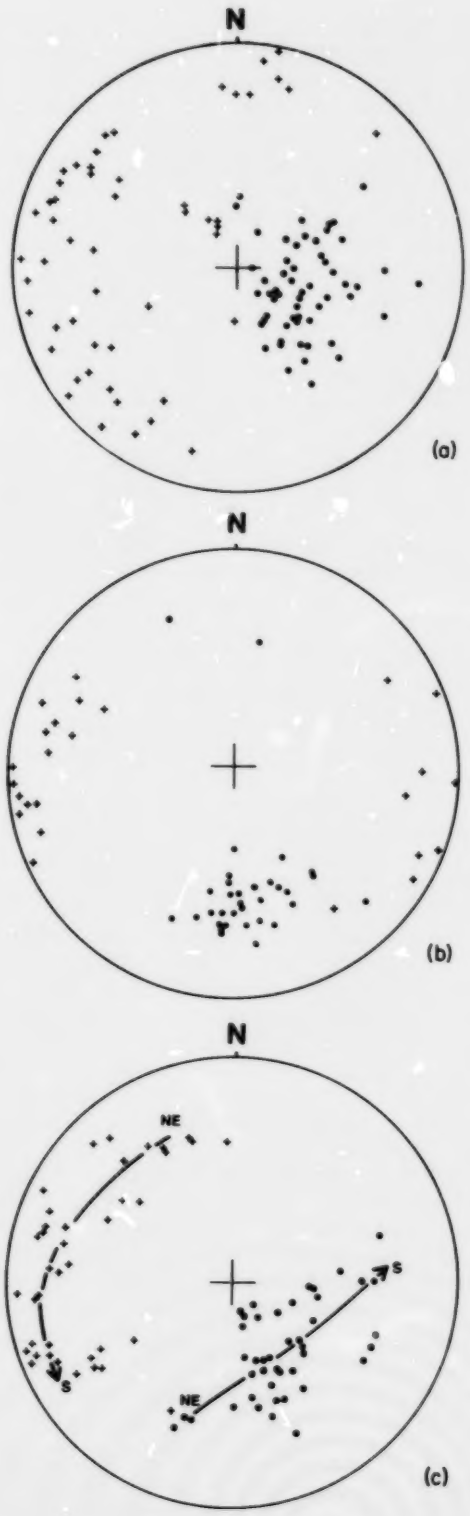

Figure 370.3. Equal-area plots of poles to main tectonic layering and main foliation (crosses) and stretching lineations (dots) from selected areas. a) Parry Sound domain north of possible splay; b) interior Seguin subdomain; c) western part of bounding high-strain zone of Seguin subdomain, showing regular variation of orientation of layering and lineations around the lobate margin of the subdomain.

METAMORPHISM

Metamorphism in Parry Sound domain reached granulite grade in at least the western and central parts of the map area, where metamorphic orthopyroxene is common. However, even here, preservation of granulite-facies assemblages is patchy: eastward-increasing retrogression is apparent (Macfie 1988). Within 3 km of the boundary with Seguin subdomain the rocks appear to be completely of amphibolite grade, although isolated occurrences of orthopyroxene visible in thin section attest to the one-time prevalence of granulite facies in at least some places. Along with the disappearance of orthopyroxene, the amount of leucosome in the rocks, particularly that cutting layering, increases towards Seguin subdomain, as does the amount of weakly deformed and posttectonic pegmatite.

Rocks containing sillimanite and potassium feldspar in the absence of muscovite, an assemblage indicative of temperatures in excess of 600°C, occur in 2 places. The presence of sillimanite reinforces Anovitz and Essene's (1990) tentative placement of an aluminosilicate isograd (kyanite to northwest, sillimanite to southeast) through central Parry Sound domain, although its significance remains unclear because of the paucity of data. In several places muscovite is present in quartz-rich metasediment. Meionitic scapolite occurs in a wide range of rock types, including calc-silicate gneiss and anorthosite, and suggests significant CO_2 pressure during metamorphism.

Seguin Subdomain

Rocks of Seguin subdomain consist almost entirely of felsic to intermediate quartzofeldspathic gneisses. Grey tonalitic and dioritic gneisses dominate the extreme southwesternmost part of the subdomain, and pinker granitoid-composition gneisses are found to the east (Figure 3/0.2). The gneisses contain up to 20% coarse leucosome. As in Parry Sound domain, evidence that layering is tectonic is abundant. In most cases, evidence of protolith is absent. However, some metagabbro is recognizable, in places showing possible deformed igneous layering. Minor quartzofeldspathic gneiss with >30% quartz may be of sedimentary origin. Metre- to 10 m scale pods of mafic material, in some cases clearly in the form of boudins, probably represent deformed mafic dikes. Meta-anorthosite occurs in association with metagabbro as well as in isolated outcrops.

Tectonic layering within Seguin subdomain is less warped than that in Parry Sound domain. Within the map area the layering is oriented approximately northerly, with steep easterly dips (Figure 370.3b). Stretching lineations plunge southeastward. Near the margin of the subdomain this layering swings asymptotically towards the bounding high-strain zone. Weakly developed biotite foliations cutting layering and resembling in nature and attitude the crosscutting foliations in Parry Sound domain occur in some rocks. Their strikes vary from southeast to south-southeast, and associated fold closures are not observed in outcrop (*see* "Discussion").

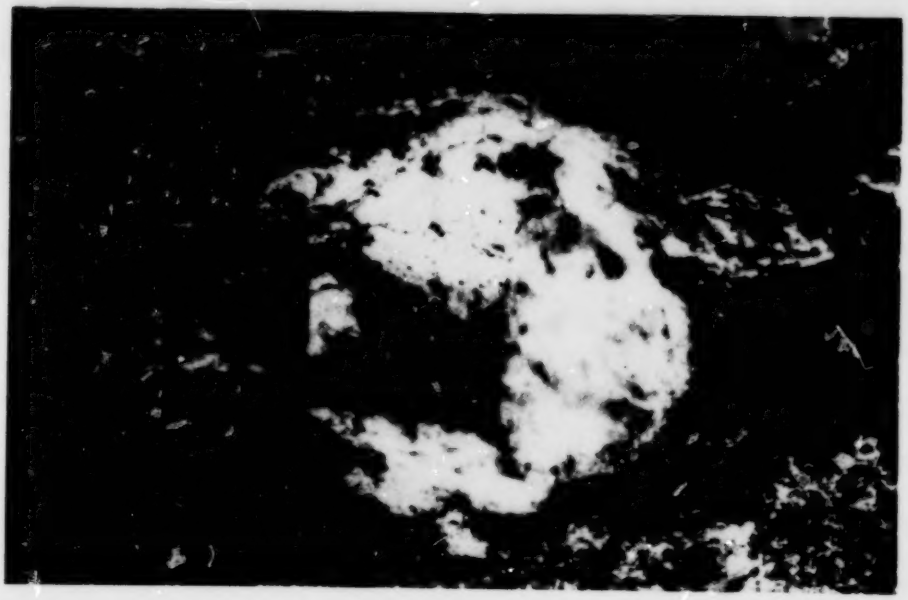

Photo 370.1. Rotated alkali-feldspar porphyroclast in minor shear zone within Parry Sound domain, indicating top-to-northwest transport. Outcrop near Star Lake. Area shown is 14 cm wide.

Photo 370.2. Typical migmatite gneiss of Rosseau subdomain. Fold of leucosome vein verges northwest, and delta-type asymmetric feldspar porphyroclast shows possible top-to-northwest rotation. Outcrop near Star Lake. Area shown is 35 cm wide.

Metamorphic grade is amphibolite facies. Rocks containing hornblende, clinopyroxene and almandine-rich garnet are common, but orthopyroxene is not observed. Aluminosilicate-bearing rocks have not been found.

Rosseau Subdomain

Rocks of Rosseau subdomain are relatively poorly layered, except near the margin of the subdomain. The main rock type is pink migmatitic gneiss of granitic to granodioritic composition, consisting of quartz, plagioclase, microcline, biotite, hornblende and minor garnet, with 10 to 20% leucosome veins typically 1 to 4 cm in width and consisting of quartz, plagioclase, microcline, biotite and conspicuous centimetre-scale hornblende porphyroblasts. This unit is remarkably homogeneous and is probably of plutonic origin. Minor rock types include amphibolite lenses and a single outcrop of distinctive orange marble.

Photo 370.3. Heterogeneous, highly strained tectonite with mafic boudins, truncated tectonic layering and several generations of leucosome, from boundary of Seguin subdomain. Outcrop on Highway 518 near Bear Lake. Area shown is approximately 2 m wide in foreground.

Photo 370.4. Sheath fold within highly strained tectonite from boundary of Seguin subdomain. Outcrop near northwest Horn Lake. Area shown is 50 cm wide in foreground.

As in Seguin subdomain, metamorphic grade reached the amphibolite facies, and aluminosilicate rocks have not been found.

Tectonic layering is relatively weakly developed except adjacent to the margin of the domain. Within the subdomain phlebitic leucosome veins are commonly folded with shallow-plunging, northeastward-trending fold axes (Photo 370.2). Most such folds verge to the northwest.

Photo 370.5. Photomicrograph of clinopyroxene (CPX) - orthopyroxene (OPX) - hornblende (H) - plagioclase (P) - quartz (Q) granulite of Parry Sound domain, from margin of apparent splay. See text for discussion. Sample taken from outcrop near Sugar Lake. Field of view 4 mm.

Photo 370.6. Porphyroclastic gneiss from boundary of Rosseau subdomain. Outcrop adjacent to Parry Sound domain in southeastern part of area. Area shown is 21 cm wide.

Domain and Subdomain Boundaries

Within the study area the boundary of Seguin subdomain is an east-concave, east-dipping, kilometre-wide zone of intense ductile strain (Photos 370.3 and 370.4) with tectonic layering that truncates, at an angle of about 25°, the tectonic layering of the interior of the subdomain. It also truncates the irregular tectonic layering in Parry Sound domain. The boundary zone appears to contain highly deformed and transposed rocks of both Parry Sound domain and Seguin subdomain. Placement of a sharp boundary is therefore not possible. Although annealing has resulted in pervasive medium grain sizes and has destroyed subtle grain fabrics within the boundary zone, preserved macroscopic kinematic indicators, primarily sigma-type rotated pophyroclasts

Photo 370.7. Football-shaped calc-silicate (epidote with minor quartz and scapolite) lenses in heterogeneously layered intermediate gneiss, perhaps of volcaniclastic origin. See text for discussion. Outcrop near Manitouwaba Lake. Area shown is approximately 1.1 m wide.

(Passchier and Simpson 1986), indicate northwest- to west-directed thrusting of Seguin subdomain over Parry Sound domain.

The otherwise simple, lobate Seguin–Parry Sound boundary zone (Figures 370.1 and 370.3c) is complicated in the central part of the map area by an apparent extension of the Seguin–Rosseau boundary zone, rooted in the triple junction and apparently imposed on Parry Sound domain (Figure 370.2). This straight, high-strain zone was originally considered part of the Seguin–Parry Sound boundary (Figure 370.1; *see also* Davidson et al. 1982), but it is enclosed by recognizable Parry Sound gneisses and ends abruptly within Parry Sound domain about 5 km from the triple junction. On the southwest side (at Sugar Lake), weakly retrogressed (Photo 370.5) granulite gneisses are caught up in the structure; to the north and northeast is the zone of apparently greater retrogression described above.

Small outcrops of anorthosite and a 300 m wide body of metagabbro with anorthositic zones are found within the marginal part of Seguin subdomain, adjacent to its boundary with Parry Sound domain.

The boundary between the Seguin and Rosseau subdomains is more readily mapped because strained but easily recognizable gneisses of Rosseau subdomain are separated from heterogeneous gneisses of Seguin subdomain by a septum or tongue of granulite gneiss (Figure 370.2). This granulite tongue is about 600 m wide and has been partially traced for 6 km from the triple junction, where it is continuous with granulites of Parry Sound domain.

The boundary between Parry Sound domain and Rosseau subdomain is also readily placed, as it juxtaposes heterogeneous Parry Sound granulites against highly porphyroclastic (Photo 370.6) amphibolite-grade migmatites of Rosseau subdomain. Delta- and sigma-type (Passchier and Simpson 1986) rotated porphyroclasts, shear-band foliation and oblique quartz-grain fabrics in the boundary zone and in shear zones in Parry Sound domain overlying the boundary indicate top-to-west transport of Parry Sound domain. Metre- to 50 m scale lenses of anorthosite are found within the margin of Parry Sound domain.

Late- and Posttectonic Features

A variety of lithological and structural features postdate the major episodes of deformation in the area. Weakly deformed late-tectonic and undeformed posttectonic pegmatite dikes are common in the boundary zones, particularly in Parry Sound domain adjacent to Seguin subdomain.

A 0.5 m wide probable metalamprophyre dike with a very weak foliation cuts tectonic layering in Parry Sound domain at the termination of the splay-like straight zone. It consists of 65% coarse-grained green biotite with minor green amphibole in a matrix of microcline and plagioclase, with minor quartz and abundant calcite, titanite, apatite and zircon. Titanite in biotite is surrounded by strong pleochroic halos. Some apophyses grade to plagioclase-microcline-quartz-biotite pegmatite.

Metre-scale brittle fault zones consisting of anastomosing millimetre-wide epidote veins, in places associated with pervasive hematite alteration, occur sporadically in the area. They are generally discordant to tectonic layering within major boundary zones, but they cannot be traced from outcrop to outcrop, and their large-scale distribution is not known. In general they have northeast strikes and steep southeast dips. Slickenside lineations have widely varying orientations. The senses of displacement on these zones are not known.

A narrow valley that to the west of the map area contains outcrops of an unaltered mafic dike (McRoberts et al. 1988), probably of the 575 Ma Grenville swarm (Fahrig and West 1986), continues into the map area, although no outcrop has been found within it.

ECONOMIC GEOLOGY

The area now known as Parry Sound domain contains a number of economically interesting mineral occurrences (*see* Hewitt 1967). It was once thought to include a large proportion of material of supracrustal origin (*see* Hewitt 1967), and the supposed supracrustal rocks of the Parry Sound "greenstone belt" (Villard 1980) were a target for mineral exploration. However, in recent years it has been demonstrated that virtually all layering in the area is tectonic, and no supracrustal protoliths are recognizable except in the case of carbonate-, quartz- and aluminum-rich metasediments (Davidson et al. 1982). Thus the discovery of a package of rocks of possible volcaniclastic origin in the study area of this project is of considerable interest.

The unit in question, informally named here the "Seguin Falls gneiss", consists of mesocratic plagioclase-hornblende-biotite-quartz-epidote gneisses layered on a 10 cm to 2 m scale. Like most rocks in the area, the gneisses are recrystallized, foliated and lineated, and in most places they are best described as tectonites having completely transposed layering. While rocks of this unit have similar mineralogy, colour index and general appearance, their most striking unifying characteristic is the presence of centimetre- to metre-scale layers and boudins of calc-silicate material (Photo 370.7), usually consisting of 80 to 95% epidote, that make up from <0.05 to 2% of the rock. At Seguin Falls these gneisses are exposed in a zone of relatively low strain, and the calc-silicate bodies lie predominantly along the contacts of layers within the gneiss. Furthermore, at this location the layering differs from that of typical transposed Grenville gneiss: layers, varying somewhat in grain size and colour index, have sharp contacts showing little evidence of tectonic modification. Layering in the low-strain zone resembles either bedding or a swarm of multiply intruded dikes.

A supracrustal protolith for the Seguin Falls gneiss is suggested by the presence of the calc-silicate bodies, for which 2 origins are considered possible. They may be fragments of metamorphosed carbonate interlayers in a bedded sequence of intermediate clastic sediments or tuffs, or they may be epidote-dominated open-space fillings in an epidotized volcanic sequence. The former explanation is considered the more likely, given the relative absence of epidote in the host rock. The least-strained of these gneisses greatly resemble a gneiss found near Actinolite, Ontario, which may be the metamorphosed equivalent of the Apsley Formation of the Elzevir terrane (R.M. Easton, Ontario Geological Survey, personal commmunication, 1989 and unpublished geochemical data). The Apsley Formation consists of andesitic to dacitic tuffaceous material resedimented in a turbiditic sequence with abundant limestone interlayers (Easton 1986), and its possible equivalent at Actinolite contains epidote-rich calc-silicate lenses macroscopically identical to those in the Seguin Falls gneiss. Like the Apsley Formation, the Seguin Falls gneiss is spatially associated with marble.

Easton (1986) suggested that the Apsley Formation represents pyroclastic turbidite fans derived from an andesitic to rhyolitic volcano, with gold and base metal mineralization being developed where proximal hydrothermal fluids were channelled through the porous fan deposits. He found anomalous concentrations of gold, copper, lead and zinc in gossans and recommended the Apsley Formation as a target for gold and base metal exploration. In the Seguin Falls gneiss a gold and base metals prospect has been assessed recently (Villard and Garland 1986), and several other gold anomalies are known from the area underlain by the gneiss (Hewitt 1967). These anomalies, combined with the distinctive appearance of the unit, make the Seguin Falls gneiss an interesting and extensive target for prospectors.

Other discoveries of potential economic interest include new outcrops of dolomitic and calcitic marble and graphite-bearing metapelite in Parry Sound domain (Figure 370.2). Marble within Parry Sound domain has been exploited commercially in Ferguson Township, and graphite is mined from metapelite at the Cal Graphite property in Butt Township, approximately 60 km from the study area of this project (Garland 1987). Graphite-bearing rocks of the area have also been recommended as targets for gold exploration (Villard and Garland 1985).

DISCUSSION

Previous skepticism (Macfie 1988) regarding the existence of the Parry Sound–Seguin boundary zone proposed near Orrville (Davidson et al. 1982) has been answered by the discovery that the true domain boundary lies approximately 10 km to the east (Figure 370.2). Furthermore, the general tectonic framework established by Davidson et al. (1982) has been shown to be correct. Their lithotectonic domains are recognizable, and for the most part the bounding deformation zones predicted by them lie in approximately the correct locations. These boundaries truncate the variably folded tectonic layering within the domains, but both older and younger tectonites have been recrystallized during annealing.

Anorthosite, known to occur along a number of major tectonic boundaries within the Central gneiss belt (Figure 370.1), has been found in several places along the margin of Parry Sound domain and Seguin subdomain (Figure 370.2).

Stretching lineations and kinematic indicators in the bounding high-strain zones indicate predominant west- to northwest-directed thrusting of Parry Sound domain over Rosseau subdomain and of Seguin subdomain over both (Figures 370.4 and 370.5). Subhorizontal stretching lineations in Parry Sound domain may be a result of approximately horizontal movement of the former, past (in the plane of the erosional surface) an irregularity on the structural basement represented by Rosseau subdomain (*see* Figure 370.5, section C). Similar movement sense is apparent on minor shear zones within Parry Sound domain. Northward-directed downdip movement in gneisses of adjacent Rosseau subdomain (Figure 370.5, section C) is

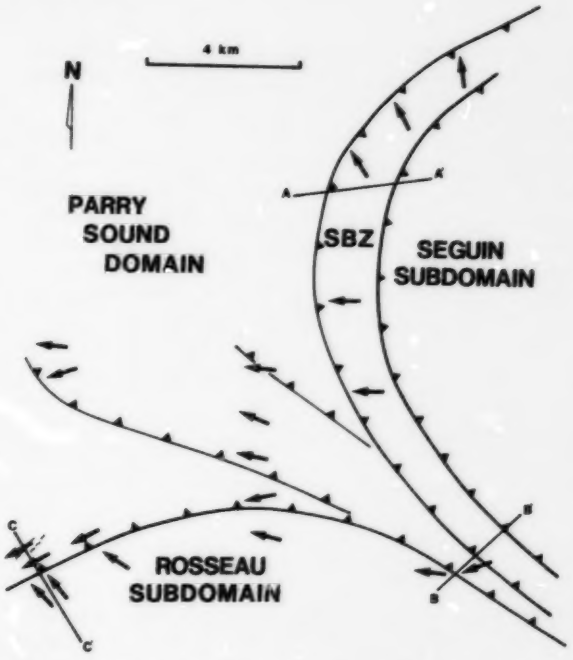

Figure 370.4. Sense of displacement along the boundaries of the lithotectonic domains. Direction and sense of movement inferred from stretching lineations, asymmetric porphyroclasts and boundins, C-S fabrics, shear bands and vergence of minor folds. Line segments correspond to cross sections in Figure 370.5. SBZ, Seguin subdomain boundary zone.

recorded by stretching lineations and rotated porphyroclasts, but its significance with regard to emplacement of Parry Sound domain is presently unknown. It may be a result of sagging of the plastic migmatitic rocks beneath the overriding domain or of analogous dragging during subsequent diapiric uprise of the migmatites, or it may predate emplacement of Parry Sound domain.

The internal tectonic layering of Parry Sound domain and Seguin subdomain is discordant to and predates the bounding deformation zones. It may have been formed, and subsequently folded, during transport of the thrust sheets to their present location. Amount of offset along the thrusts is presently unknown. Whereas juxtaposition of granulite-facies rocks against amphibolite-facies rocks southeast of the triple junction suggests significant offset along the relatively narrow basal shear zone of the Seguin–Moon River thrust sheet, the wider deformation zone (Figure 370.4, cf. sections A and B) at the front of Seguin subdomain might have accommodated movement on the basal shear zone without major vertical offset. Although Seguin subdomain has experienced some degree of northwestward movement over Parry Sound domain, there is no evidence, whether structural or lithological, available to allow proper evaluation of the amount of that movement. The few (for this area) pressure-temperature data of Anovitz and Essene (1990) are not supportive of major vertical offset between domains.

The narrow deformation zone at the base of Parry Sound domain may be contrasted with the wide boundary zone of Seguin subdomain. In general, deformation in the migmatitic Seguin and Rosseau subdomains is more pervasive, resulting in wide ductile mobile zones, whereas strain in the drier, and probably more rigid, Parry Sound domain is concentrated in the basal shear zone. Some strain related to emplacement of Parry Sound domain may also have been partitioned into the internal shear zones that are preserved in the less retrogressed part of the domain. However, deformation zones in all cases may be contrasted with the very narrow thrust surfaces observed in thin-skinned thrust belts. Clearly, wider zones of pervasive ductile deformation have developed in these deep-crustal rocks.

The apparent splay rooted in the triple Seguin subdomain boundary and cutting into Parry Sound domain may have been imposed as the Seguin–Moon River thrust sheet ramped (Figure 370.5, line A) over competent but brittle rocks of Parry Sound domain. The splay may have developed during incipient footwall collapse, forming a blind thrust with a north-plunging tip line. However, it too developed as a wide zone of ductile deformation and defies easy explanation.

The eastward increase in retrogression observed to the north and east of the apparent splay may be a result of hydration during the failure that led to the splay's development. In this area orthopyroxene is very rare, and an increase in the percentage of leucosome and pegmatite attests to an increase in fluid content. This situation must be contrasted with the common preservation of metamorphic orthopyroxene on the immediate southwest margin of the splay and within the granulite tongue extending into the Seguin–Rosseau boundary zone. Perhaps granulites of Parry Sound domain remained relatively impervious to hydrating fluids from the adjacent migmatitic, amphibolite-grade subdomains, except where affected by particular high-strain zones. Alternatively, the apparent splay may have developed within the zone of retrogression, where increased fluid pressure promoted recrystallization and rapid slip.

The presence of the 600 m wide tongue of Parry Sound granulite extending for at least 6 km along the Seguin–Rosseau boundary appears to confirm a previous suggestion, following a Bouguer gravity anomaly study, that Parry Sound domain continues eastward in the subsurface beneath Seguin subdomain (Lindia et al. 1983).

The sporadic, weakly developed biotite foliations seen in some rocks of Parry Sound domain and Seguin subdomain must record late northeast-southwest shortening of the region. However, folds related to these foliations are not observed, and the extent to which this late event may have affected the morphology of the lithotectonic domains (cf. Schwerdtner 1987) is difficult to evaluate. The consistent orientations of features such as strongly developed stretching lineations and minor fold axes parallel to those lineations in the boundary-zone gneisses give no indication of significant subsequent folding of the shear zones. The simplest explanation for the synformal morphology of Seguin subdomain, as well as that of the coeval Moon River subdomain, is that they are both parts of a single thrust sheet with an irregular, perhaps corrugated, basal thrust.

Because of the weakness of the late foliation it is not known whether it pre- or postdates the brittle,

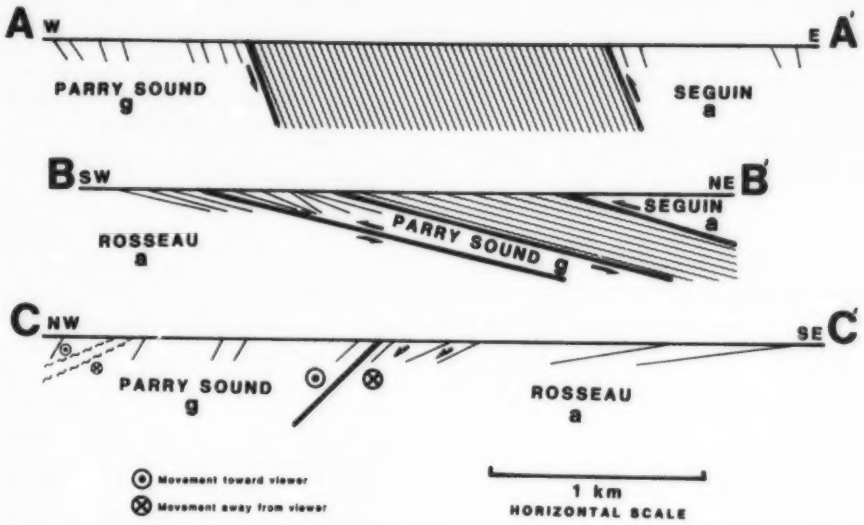

Figure 370.5. Cross sections of domain boundaries. Locations shown in Figure 370.4. Vertical scale schematic. Heavy lines indicate boundary between Parry Sound domain and Rosseau subdomain and margins of Seguin subdomain boundary zone (patterned). Light lines indicate dip of gneissosity along cross section. Abbreviations: a, amphibolite facies; g, predominantly granulite facies. See text for discussion.

greenschist-grade fault swarms. These may be a result of late extension in the southwestern Grenville Province, as has been recorded elsewhere (e.g., Carlson et al. 1990).

A second field season (1990) will complete the mapping. Planned U-Pb geochronological work and detailed thermobarometric studies will lead to an improved understanding of the timing and magnitute of displacements resulting in emplacement of the lithotectonic domains.

CONCLUSIONS

As it applies to the study area of this project, the model for the tectonic evolution of the southwestern Central gneiss belt proposed by Davidson et al. (1982) is confirmed in its major aspects. Their lithotectonic domains are recognizable and are bounded by major ductile-deformation zones retaining evidence of west- to northwest-directed transport. Granulite gneisses of Parry Sound domain are sandwiched between amphibolite-grade migmatitic gneisses of Seguin and Rosseau subdomains.

In contrast to thrusting in thin-skinned orogenic belts, thrusting in these deep-level, high-grade gneisses has been accomplished along wide, highly ductile shear zones showing pervasive recrystallization to medium grain size. At the same time, there is evidence that a process resembling ramping, followed by incipient footwall collapse, may have occurred locally as the Seguin–Moon River thrust sheet overrode a rigid structural basement represented by Parry Sound domain.

Finally, an intriguing gold-anomaly-bearing unit of probable supracrustal, and possible volcaniclastic, origin should be considered as a target for further evaluation.

ACKNOWLEDGMENTS

R.M. Easton (Ontario Geological Survey, Toronto) paid a very beneficial visit to the study area during the field season and later conducted the first author to a number of relevant areas in the Central metasedimentary belt, including the type outcrops of the Apsley Formation. A. Davidson (Geological Survey of Canada, Ottawa) directed our attention to a number of important features in and around the study area and provided invaluable advice. P. Fedirchuk provided cheerful field assistance.

REFERENCES

Anovitz, L. M. and Essene, E. J. 1990. Thermobarometry and pressure-temperature paths in the Grenville Province of Ontario; Journal of Petrology, v.31, p.197-241; Ontario Geological Survey, Miscellaneous Paper 132.

Baer, A.J. 1981. Two orogenies in the Grenville belt?; Nature (London), v.290, p.129-131.

Brown, R.L., Chappell, J.F., Moore, J.M., Jr., and Thompson, P.H. 1975. An ensimatic island arc and ocean closure in the Grenville Province of southeastern Ontario, Canada; Geoscience Canada, v.2, p.141-144.

Carlson, K.A., van der Pluijm, B.A. and Hanmer, S. 1990. Marble mylonites of the Bancroft shear zone: evidence for extension in the Canadian Grenville; Geological Society of America Bulletin, v.102, p.174-181.

Culshaw, N.G., Davidson, A. and Nadeau, L. 1983. Structural subdivisions of the Grenville Province in the Parry Sound–Algonquin region, Ontario; *in* Current research, pt.B, Geological Survey of Canada, Paper 83-1B, p.243-252.

Davidson, A. 1986. New interpretations in the southwestern Grenville Province; *in* The Grenville Province, edited by J.M. Moore, A. Davidson and A. Baer, Geological Association of Canada, Special Paper 31, p.61-74.

Davidson, A. and Morgan, W.C. 1981. Preliminary notes on the geology east of Georgian Bay, Grenville structural province, Ontario; *in* Current research, pt.A, Geological Survey of Canada, Paper 81-1A, p.291-298.

Davidson, A., Culshaw, N. and Nadeau, L. 1982. A tectono-metamorphic framework for part of the Grenville Province, Parry Sound region, Ontario; *in* Current research, pt.A, Geological Survey of Canada, Paper 82-1A, p.175-190.

Davis, D., Suppe, J. and Dahlen, F.A. 1983. Mechanics of fold-and-thrust belts and accretionary wedges; Journal of Geophysical Research, v.88, p.1153-1172.

Easton, R.M. 1986. Paleoenvironment and facies of the Apsley Formation, Peterborough County; *in* Summary of field work and other activities 1986, by the Ontario Geological Survey, Ontario Geological Survey, Miscellaneous Paper 132, p.141-151.

Fahrig, W.F. and West, T. 1986. Diabase dyke swarms of the Canadian Shield; Geological Survey of Canada, Map 1627A, scale 1:4 873 900.

Garland, M. 1987. Graphite in the Central gneiss belt of the Grenville Province of Ontario; Ontario Geological Survey, Open File Report 5649.

Hanmer, S. 1984. Strain-insensitive foliations in polymineralic rocks; Canadian Journal of Earth Sciences, v.21, p.1410-1414.

———1988. Ductile thrusting at mid-crustal level, southwestern Grenville Province; Canadian Journal of Earth Sciences, v.25, p.1049-1059.

Hewitt, D.F. 1967. Geology and mineral deposits of the Parry Sound–Huntsville area; Ontario Geological Survey, Geological Report 52, 65p.

Journeay, J.M. 1986. Stratigraphy, internal strain and thermo-tectonic evolution of northern Frenchman Cap Dome: an exhumed duplex structure, Omineca Hinterland, S.E. British Columbia; unpublished PhD thesis, Queen's University, Kingston, Ontario, 450p.

Lindia, F.M., Thomas, M.D. and Davidson, A. 1983. Geological significance of Bouguer gravity anomalies in the region of Parry Sound domain, Grenville Province, Ontario; *in* Current research, pt.B, Geological Survey of Canada, Paper 83-1B, p.261-266.

Macfie, R.I. 1988. Preliminary investigation of the Parry Sound–Seguin domain boundary; *in* Summary of field work and other activities 1988, by the Ontario Geological Survey, Ontario Geological Survey, Miscellaneous Paper 141, p.315-318.

McRoberts, G., Macfie, R.I. and Hammar, J. 1988. Geology of the Manitouwabing Lake area, District of Parry Sound; *in* Summary of field work and other activities 1988, by the Ontario Geological Survey, Ontario Geological Survey, Miscellaneous Paper 141, p.309-314.

Monger, J.W., Price, R.A. and Tempelman-Kluit, D.J. 1982. Tectonic accretion and the origin of the two major metamorphic plutonic welts in the Canadian Cordillera; Geology, v.10, p.70-75.

Passchier, C.W. and Simpson, C. 1986. Porphyroclast systems as kinematic indicators; Journal of Structural Geology, v.8, p.831-843.

Price, R.A. 1981. The Cordilleran foreland thrust and fold belt in the southern Canadian Rocky Mountains; *in* Thrust and nappe tectonics, edited by K. McClay and N. Price, Geological Society of London, Special Paper 9, p.427-448.

Ramsay, J.G. 1981. Tectonics of the Helvetica nappes; *in* Thrust and nappe tectonics, edited by K. McClay and N. Price, Geological Society of London, Special Paper 9, p.293-309.

Schwerdtner, W.M. 1987. Interplay between folding and ductile shearing in the Proterozoic crust of the Muskoka–Parry Sound region, central Ontario; Canadian Journal of Earth Sciences, v.24, p.1507-1525.

van Breemen, O., Davidson, A., Loveridge, W.D. and Sullivan, R.W. 1986. U-Pb zircon geochronology of Grenville tectonites, granulites and igneous precursors, Parry Sound, Ontario; *in* The Grenville Province, edited by J.M. Moore, A. Davidson and A. Baer, Geological Association of Canada, Special Paper 31, p.191-208.

Villard, D.J. 1980. 1979 report of the Algonquin Regional Mineral Resource Coordinator, *in* Annual report of the Regional and Resident Geologists 1979, edited by C.R. Kustra, Ontario Geological Survey, Miscellaneous Paper 91, p.117-112.

Villard, D.J. and Garland, M. 1985. Huntsville Resident Geologist area, Algonquin region; *in* Report of activities 1984, Regional and Resident Geologists, edited by C.R. Kustra, Ontario Geological Survey, Miscellaneous Paper 122, p.242-246.

———1986. Huntsville Resident Geologist area, Algonquin region; *in* Report of activities 1985, Regional and Resident Geologists, edited by C.R. Kustra, Ontario Geological Survey, Miscellaneous Paper 128, p.273-277.

Wynne-Edwards, H.R. 1972. The Grenville Province; *in* Variations in tectonic style in Canada, edited by R.A. Price and R.J.W. Douglas, Geological Association of Canada, Special Paper 11, p.263-334.